frontiers | Research Topics

Combination therapies in cancer treatment: enhancing efficacy and reducing resistance

Edited by
Xinyu Wang, Milica Pešić and Ana Podolski-Renic

Published in
Frontiers in Pharmacology
Frontiers in Oncology

ISSN 1664-8714
ISBN 978-2-8325-7383-9
DOI 10.3389/978-2-8325-7383-9

Generative AI statement
Any alternative text (Alt text) provided alongside figures in the articles in this ebook has been generated by Frontiers with the support of artificial intelligence and reasonable efforts have been made to ensure accuracy, including review by the authors wherever possible. If you identify any issues, please contact us.

About Frontiers

Frontiers is more than just an open access publisher of scholarly articles: it is a pioneering approach to the world of academia, radically improving the way scholarly research is managed. The grand vision of Frontiers is a world where all people have an equal opportunity to seek, share and generate knowledge. Frontiers provides immediate and permanent online open access to all its publications, but this alone is not enough to realize our grand goals.

Frontiers journal series

The Frontiers journal series is a multi-tier and interdisciplinary set of open-access, online journals, promising a paradigm shift from the current review, selection and dissemination processes in academic publishing. All Frontiers journals are driven by researchers for researchers; therefore, they constitute a service to the scholarly community. At the same time, the *Frontiers journal series* operates on a revolutionary invention, the tiered publishing system, initially addressing specific communities of scholars, and gradually climbing up to broader public understanding, thus serving the interests of the lay society, too.

Dedication to quality

Each Frontiers article is a landmark of the highest quality, thanks to genuinely collaborative interactions between authors and review editors, who include some of the world's best academicians. Research must be certified by peers before entering a stream of knowledge that may eventually reach the public - and shape society; therefore, Frontiers only applies the most rigorous and unbiased reviews. Frontiers revolutionizes research publishing by freely delivering the most outstanding research, evaluated with no bias from both the academic and social point of view. By applying the most advanced information technologies, Frontiers is catapulting scholarly publishing into a new generation.

What are Frontiers Research Topics?

Frontiers Research Topics are very popular trademarks of the *Frontiers journals series*: they are collections of at least ten articles, all centered on a particular subject. With their unique mix of varied contributions from Original Research to Review Articles, Frontiers Research Topics unify the most influential researchers, the latest key findings and historical advances in a hot research area.

Find out more on how to host your own Frontiers Research Topic or contribute to one as an author by contacting the Frontiers editorial office: frontiersin.org/about/contact

Combination therapies in cancer treatment: enhancing efficacy and reducing resistance

Topic editors

Xinyu Wang — Department of Bio-Medical Sciences, Philadelphia College of Osteopathic Medicine (PCOM), United States

Milica Pešić — University of Belgrade, Serbia

Ana Podolski-Renic — Institute for Biological Research "Siniša Stanković" – National Institute of Republic of Serbia, Serbia

Citation

Wang, X., Pešić, M., Podolski-Renic, A., eds. (2026). *Combination therapies in cancer treatment: enhancing efficacy and reducing resistance*. Lausanne: Frontiers Media SA. doi: 10.3389/978-2-8325-7383-9

Table of contents

frontiers | Frontiers in Pharmacology

TYPE Editorial
PUBLISHED 07 January 2026
DOI 10.3389/fphar.2025.1770248

OPEN ACCESS

EDITED AND REVIEWED BY
Olivier Feron,
Université catholique de Louvain, Belgium

*CORRESPONDENCE
Xinyu Wang,
xinyuwa@pcom.edu

RECEIVED 17 December 2025
REVISED 17 December 2025
ACCEPTED 29 December 2025
PUBLISHED 07 January 2026

CITATION
Wang X, Pešić M and Podolski-Renić A (2026) Editorial: Combination therapies in cancer treatment: enhancing efficacy and reducing resistance.
Front. Pharmacol. 16:1770248.
doi: 10.3389/fphar.2025.1770248

Editorial: Combination therapies in cancer treatment: enhancing efficacy and reducing resistance

Xinyu Wang[1]*, Milica Pešić[2] and Ana Podolski-Renić[2]

[1]Department of Biomedical Sciences, Philadelphia College of Osteopathic Medicine, Suwanee, GA, United States, [2]Department of Neurobiology, Institute for Biological Research "Siniša Stanković"- National Institute of Republic of Serbia, University of Belgrade, Belgrade, Serbia

KEYWORDS

antibody-drug conjugates (ADC), combination therapies, DNA damage response (DDR), drug resistance, ferroptosis, immunotherapy, STING pathway

Editorial on the Research Topic
Combination therapies in cancer treatment: enhancing efficacy and reducing resistance

1 Introduction

Cancer's complexity, including diverse cell types and drug resistance, hinders long-term patient survival. Single-agent therapies are often ineffective, prompting a move towards combination therapies that target multiple survival pathways in cancer cells. This strategy can prolong treatment responses, resensitize resistant tumors, and lower drug doses to reduce toxicity while preserving effectiveness.

This Research Topic includes 19 contributions on new pharmacological strategies for enhancing tumor elimination and minimizing resistance. It highlights the importance of rational, mechanism-based combinations adapted to each patient's unique molecular and immunological profile for effective cancer control.

2 Advancing immunotherapy and T-cell engagement

Immunotherapy has revolutionized cancer treatment, and much research is focused on combining immune checkpoint inhibitors (ICI) with other modalities, such as chemotherapy and targeted therapy, to overcome primary and acquired resistance. The core principle of this strategy involves leveraging chemotherapy to induce immunogenic cell death, thereby releasing tumor antigens and danger signals that effectively prime the immune system for attack. This mechanistic foundation is detailed in the review Li et al., which synthesizes preclinical and clinical evidence supporting rational scheduling and dosing of chemotherapy–ICI combinations.

The clinical potential of such immune-oncology doublets is exemplified by the meta-analysis Tang and Zhou. This study found that combining PD-1/PD-L1 inhibitors with tyrosine kinase inhibitors significantly improved progression-free survival and objective response rate in patients with unresectable hepatocellular carcinoma, particularly among

Asian patients and those infected with hepatitis B virus, without an unacceptable increase in severe adverse events. In a complementary real-world setting, Guo et al. showed that extending immunochemotherapy beyond first-line treatment can offer clinically meaningful benefit in recurrent small-cell lung cancer, highlighting how combination strategies may reshape treatment paradigms even in aggressive, traditionally chemo-sensitive malignancies.

A particularly notable contribution in this Research Topic is the work Choi et al. Soft-tissue sarcomas are prototypical "cold" tumors with sparse lymphocytic infiltrates and limited responsiveness to immunotherapy. By combining the DNA-damaging agent doxorubicin with deliberate activation of the STING (Stimulator of Interferon Genes) pathway, the authors demonstrate that chemotherapy-induced release of tumor DNA into the cytosol can be harnessed to trigger cGAS–STING signaling, type I interferon production, and enhanced recruitment and activation of effector immune cells. This dual-action approach not only amplifies the direct cytotoxicity of doxorubicin but also remodels the tumor microenvironment toward an inflamed, T cell–permissive state, providing a compelling blueprint for transforming immunologically "cold" sarcomas into "hot" tumors amenable to additional immunotherapeutic interventions.

Beyond systemic antibodies and innate immune modulators, innovative cell-based strategies aim to broaden and deepen antitumor immune responses. The article He et al. explored the vast potential of TCR-engineered T cells, which can recognize intracellularly derived peptide–MHC complexes and thus target a broader antigenic repertoire than chimeric antigen receptor T (CAR-T) cells. The review discusses combination strategies that integrate TCR-T cells with checkpoint inhibitors, oncolytic viruses, or targeted agents to overcome antigen heterogeneity, T-cell exhaustion, and immunosuppressive microenvironments. Complementing this immunoengineering perspective, Liu et al. introduced hybrid nanovesicles co-decorated with PD-1 and signaling regulatory protein alpha (SIRPα) receptors to simultaneously disrupt the "do not find me" (PD-1/PD-L1) and "do not eat me" (CD47/SIRPα) signals. In melanoma models, this combinatorial blockade translated into robust antitumor activity and illustrates how multi-receptor targeting on a single nanoplatform can synergistically amplify innate and adaptive immune responses.

3 Targeted DNA damage response (DDR) and cell cycle disruption

A second major theme centers on exploiting cancer-specific vulnerabilities in DNA repair and cell-cycle regulation. The review Qian et al. provides a comprehensive overview of how inhibitors of DNA-PK, ATM, ATR, Wee1 and other DDR kinases can be combined with DNA-damaging agents to induce synthetic lethality. The authors emphasize the importance of genomic and functional biomarkers, such as homologous recombination deficiency signatures, to select patients most likely to benefit from DDR inhibitor–based combinations and to avoid overlapping hematologic and gastrointestinal toxicities.

This conceptual framework is further strengthened by the data-driven clinical synthesis Fontenot et al. By systematically compiling clinical trial outcomes across tumor types, the review delineates where combinations of DDR inhibitors (DDRis) with DNA-damaging agents (DDAs) have achieved meaningful efficacy and where toxicity or lack of stratification has limited success. Together, these two reviews underscore that the future of DDR-based combination therapy lies in rational pairing of agents, careful dose optimization, and biomarker-guided patient selection.

Several mechanistic studies in this Research Topic provide concrete examples of these principles. In Li et al., inhibition of PCNA was shown to synergize with the PARP inhibitor olaparib by disrupting the PCNA/PARP1 axis, impairing DNA repair and suppressing proliferation and invasion of hepatocellular carcinoma cells. This work highlights a previously underappreciated node of vulnerability that could be exploited in combination with clinically available PARP inhibitors.

Similarly, Ma et al. investigated the role of the cyclin-dependent kinase CDK2 in radioresistance. The authors demonstrate that Milciclib induces G1 arrest, downregulates CDK2 and cyclin E1, and impairs Rad51-mediated DNA repair. When combined with ionizing radiation, Milciclib significantly enhances apoptosis and partially reverses radiation resistance in colorectal cancer cell lines, achieving significant sensitizer enhancement ratios in resistant models. These findings position CDK2 inhibition as a promising approach to resensitize tumors to radiotherapy and exemplify how modulation of cell-cycle checkpoints can be integrated with genotoxic therapies for maximal impact.

4 Combination of antibody- and toxin-based therapeutics

Antibody-based therapies, including antibody–drug conjugates (ADCs) and recombinant immunotoxins, leverage antigen specificity to improve the therapeutic index of potent cytotoxic payloads. The mini-review Shi et al. summarizes how pairing ADCs with immune checkpoint inhibitors, conventional chemotherapy (e.g., taxanes and platinum compounds), or targeted small molecules can overcome resistance mechanisms such as antigen heterogeneity, drug efflux, and adaptive signaling rewiring. The authors highlight emerging clinical evidence that such combinations can deepen responses and extend survival in breast, lung, and urothelial cancers, while underscoring the need for vigilant monitoring of overlapping myelosuppression and neuropathy.

In parallel, the review Rashad et al. focuses on recombinant immunotoxins, such as moxetumomab pasudotox and tagraxofusp, which fuse bacterial or plant-derived toxins to antibodies or cytokines that recognize hematologic malignancies. The article discusses combination strategies that incorporate these agents with chemotherapy or hypomethylating drugs to eradicate minimal residual disease, prevent antigen-negative relapse, and achieve deeper remissions in otherwise refractory leukemia and lymphoma.

Beyond protein–toxin fusions, innovative radiopharmaceutical combinations add another dimension to this theme. In Ling et al., the authors demonstrate that the radioisotope Iodine-131 not only causes classical radiogenic DNA damage but also triggers ferroptosis

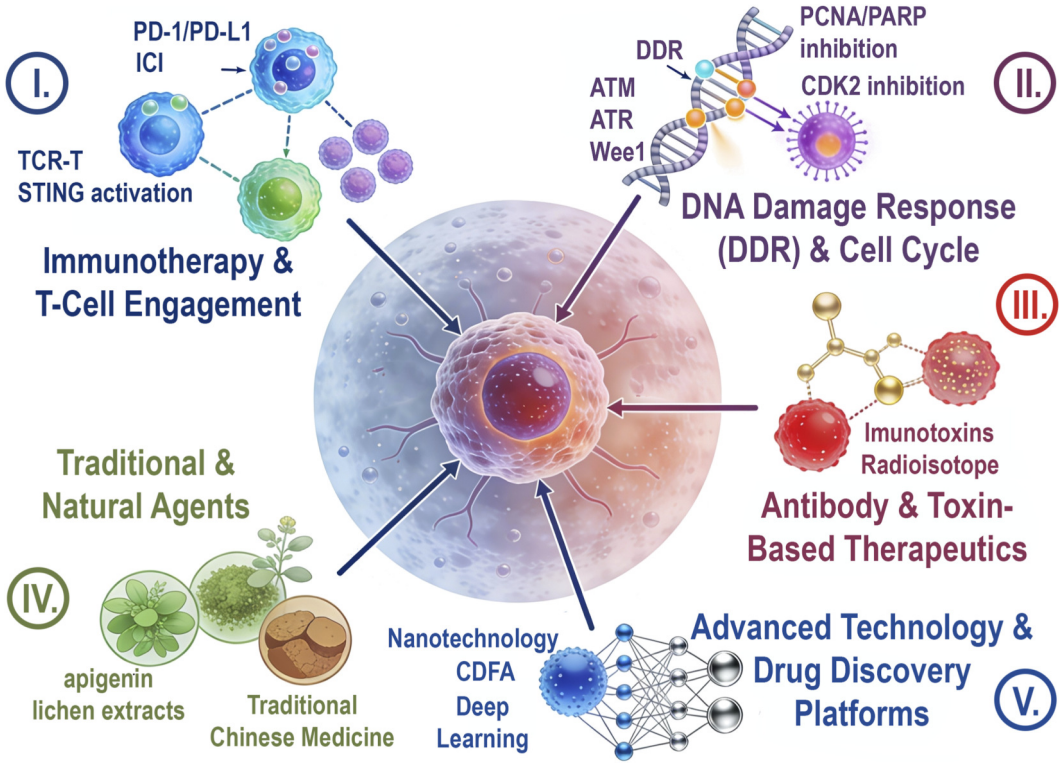

FIGURE 1
Diverse therapeutic strategies to enhance chemotherapy and radiotherapy, as well as innovative targeted and immunotherapy, presented in the Research Topic.

by downregulating the cystine transporter SLC7A11. When combined with the ferroptosis inducer sulfasalazine, Iodine-131 produces marked synergistic antitumor effects in thyroid cancer cells. This work illustrates how integrating radiotherapy with regulated cell-death modulators can expand the cytotoxic repertoire beyond apoptosis and necrosis.

5 Integration of traditional and natural agents

The incorporation of traditional medicine and naturally derived compounds into modern oncologic regimens provides a critical perspective on modulating both systemic and tumor-specific environments. The systematic review Chen et al. offers high-level evidence that adding Traditional Chinese Medicine formulations to transarterial chemoembolization (TACE) significantly improves overall response and disease control rates, prolongs overall survival, and reduces adverse events such as abdominal pain and nausea. Network pharmacology analyses further suggest that multi-component herbal preparations exert pleiotropic effects on angiogenesis, inflammation, and apoptosis, providing a mechanistic rationale for their combination with locoregional chemotherapy.

This concept of multi-target, low-toxicity modulation is also showed in the prospective cohort study Li et al. Here, the addition of Huaier granules to a backbone of targeted therapy plus immunotherapy significantly extended median progression-free survival in unresectable HCC without compromising safety, supporting the feasibility of integrating evidence-based traditional agents into complex systemic regimens.

Two research article contributions focus on natural products as chemosensitizers. Huseynova et al. shows that the flavonoid apigenin synergistically enhances the cytotoxic and pro-apoptotic effects of L-asparaginase in T-cell acute lymphoblastic leukemia cells. By modulating oxidative stress, mitochondrial integrity, and pro-survival signaling, apigenin may permit dose reduction of L-asparaginase and thereby alleviate its dose-limiting toxicities. In a solid tumor context, Shcherbakova et al. highlights that lichen-derived compounds such as evernic acid can restore temozolomide sensitivity in glioblastoma models, likely through modulation of the Wnt signaling pathway and drug efflux mechanisms. These studies collectively suggest that rational incorporation of phytochemicals into conventional chemotherapy regimens may offer a route to overcoming resistance while preserving or even improving tolerability.

6 Advanced technology and drug discovery platforms

Modern combination therapy development increasingly depends on innovative delivery platforms and computational tools. The review Zhou et al. emphasizes the growing role of local drug delivery systems in the postoperative setting. By implanting or spraying nanomedicine-loaded materials directly

into the surgical bed, these approaches can achieve sustained, localized release of chemotherapeutic agents, immune modulators, photothermal and photodynamic sensitizers, and even CAR-T cells. Such strategies have the potential to eradicate residual tumor cells, prevent local recurrence and distant metastasis, reduce systemic toxicity, and simultaneously manage postoperative inflammation and wound healing.

Complementing these physical platforms, Kang et al. introduces a sophisticated deep learning framework to address the vast combinatorial search space inherent to multi-drug regimens. By integrating molecular fingerprints of drug pairs with gene-expression–based representations of cancer cell lines and using transformer-based feature aggregation with uncertainty calibration, CDFA outperforms previous machine-learning and deep-learning models in predicting synergistic combinations. This work exemplifies how data-driven, AI-assisted pipelines can prioritize the most promising drug pairs for experimental validation, thereby accelerating the discovery of clinically actionable combinations and reducing the cost and time associated with empirical high-throughput screening.

7 Conclusion

This Research Topic emphasizes the shift in oncology towards rational combination therapies. The 19 contributions explore topics such as targeting DDR, inducing ferroptosis, activating the STING pathway, and advancements in nanotechnology, cell therapy, and AI-based drug screening, along with clinical studies on complex treatment regimens (Figure 1). Overcoming resistance requires combining agents with complementary mechanisms and incorporating biomarkers and advanced delivery systems. Key themes include reshaping the tumor microenvironment for immune response, targeting multiple survival pathways, and balancing efficacy with toxicity using natural agents. These efforts aim for durable cancer control, supported by interdisciplinary collaboration and emerging technologies in precision medicine.

Author contributions

XW: Writing – review and editing, Writing – original draft. MP: Writing – review and editing. AP-R: Writing – review and editing.

Funding

The author(s) declared that financial support was not received for this work and/or its publication.

Conflict of interest

The author(s) declared that this work was conducted in the absence of any commercial or financial relationships that could be construed as a potential conflict of interest.

Generative AI statement

The author(s) declared that generative AI was not used in the creation of this manuscript.

Any alternative text (alt text) provided alongside figures in this article has been generated by Frontiers with the support of artificial intelligence and reasonable efforts have been made to ensure accuracy, including review by the authors wherever possible. If you identify any issues, please contact us.

Publisher's note

frontiers | Frontiers in Pharmacology

TYPE Review
PUBLISHED 20 September 2024
DOI 10.3389/fphar.2024.1474337

OPEN ACCESS

EDITED BY
Xinyu Wang,
Philadelphia College of Osteopathic Medicine (PCOM), United States

REVIEWED BY
Michael Kemp,
Wright State University, United States
Dianzheng Zhang,
Philadelphia College of Osteopathic Medicine (PCOM), United States
Yuancheng Li,
Emory University, United States

*CORRESPONDENCE
Zhang Yang,
fjxh_zhang2021@163.com
Chun Chen,
chenchun0209@fjmu.edu.cn
Bin Zheng,
lacustrian@163.com

†These authors have contributed equally to this work and share first authorship

RECEIVED 01 August 2024
ACCEPTED 10 September 2024
PUBLISHED 20 September 2024

CITATION
Qian J, Liao G, Chen M, Peng R-W, Yan X, Du J, Huang R, Pan M, Lin Y, Gong X, Xu G, Zheng B, Chen C and Yang Z (2024) Advancing cancer therapy: new frontiers in targeting DNA damage response.
Front. Pharmacol. 15:1474337.
doi: 10.3389/fphar.2024.1474337

Advancing cancer therapy: new frontiers in targeting DNA damage response

Jiekun Qian[1,2†], Guoliang Liao[1,3†], Maohui Chen[1,3], Ren-Wang Peng[4], Xin Yan[5], Jianting Du[2,3], Renjie Huang[2,3], Maojie Pan[2,3], Yuxing Lin[2,3], Xian Gong[1,3], Guobing Xu[1,3], Bin Zheng[1,2*], Chun Chen[1,3*] and Zhang Yang[1,3*]

[1]Department of Thoracic Surgery, Fujian Medical University Union Hospital, Fuzhou, China, [2]Fujian Key Laboratory of Cardiothoracic Surgery, Fujian Medical University, Fuzhou, China, [3]Clinical Research Center for Thoracic Tumors of Fujian Province, Fuzhou, China, [4]Division of General Thoracic Surgery, Department of BioMedical Research (DBMR), Inselspital, Bern University Hospital, University of Bern, Bern, Switzerland, [5]Department of Cardiac Medical Center Nursing, Fujian Medical University Union Hospital, Fuzhou, China

Genomic instability is a core characteristic of cancer, often stemming from defects in DNA damage response (DDR) or increased replication stress. DDR defects can lead to significant genetic alterations, including changes in gene copy numbers, gene rearrangements, and mutations, which accumulate over time and drive the clonal evolution of cancer cells. However, these vulnerabilities also present opportunities for targeted therapies that exploit DDR deficiencies, potentially improving treatment efficacy and patient outcomes. The development of PARP inhibitors like Olaparib has significantly improved the treatment of cancers with DDR defects (e.g., BRCA1 or BRCA2 mutations) based on synthetic lethality. This achievement has spurred further research into identifying additional therapeutic targets within the DDR pathway. Recent progress includes the development of inhibitors targeting other key DDR components such as DNA-PK, ATM, ATR, Chk1, Chk2, and Wee1 kinases. Current research is focused on optimizing these therapies by developing predictive biomarkers for treatment response, analyzing mechanisms of resistance (both intrinsic and acquired), and exploring the potential for combining DDR-targeted therapies with chemotherapy, radiotherapy, and immunotherapy. This article provides an overview of the latest advancements in targeted anti-tumor therapies based on DDR and their implications for future cancer treatment strategies.

KEYWORDS

genomic instability, DNA damage response, vulnerability, synthetic lethality, resistance

Abbreviations: DCR, disease control rate; DDR, DNA damage response; DSBs, double-strand breaks; HR, homologous recombination; MMR, mismatch repair; mOS, median overall survival; mPFS, median progression-free survival; NER, nucleotide excision repair; NHEJ, non-homologous end joining; ORR, overall response rate; OS, overall survival; PFS, progression-free survival; PIKKs, PI3K-related kinases; rPFS, radiographic progression-free survival; SCLC, small cell lung cancer; SSBs, single-strand breaks; SCLC, small cell lung cancer.

1 Introduction

DNA damage response (DDR) is crucial for maintaining genome stability (Brandsma et al., 2017). Research shows that cells are constantly exposed to DNA damage from various sources, including UV radiation, ionizing radiation, chemical exposure, replication errors, cellular metabolism, and oxidative stress. These factors can cause either DNA single-strand breaks (SSBs) or DNA double-strand breaks (DSBs) (Malaquin et al., 2015; O'Connor, 2015). Cells utilize sophisticated DDR mechanisms to ensure cellular viability and genome integrity, such as non-homologous end joining (NHEJ), homologous recombination (HR), mismatch repair (MMR), nucleotide excision repair (NER), base excision repair (BER) (Figure 1). These systems are essential for DNA damage recognition, cell cycle arrest, DNA damage repair, and apoptosis initiation in cells with irreparable damage (Basu et al., 2012; Nickoloff et al., 2017).

Cancer cells often exhibit elevated levels of DNA damage repair proteins, allowing them to survive and proliferate despite DNA damage induced by chemotherapy or radiotherapy. Essential proteins frequently overexpressed in cancer cells include PARP, DNA-PKcs, BRCA1/2, ATM, ATR, and Chk1/2 (Kim et al., 2020; Okabe et al., 2023; Yang et al., 2020; Jin et al., 2022; Savva et al., 2019; Obata et al., 2023; Dilmac and Ozpolat, 2023; Tang et al., 2024; Gralewska et al., 2020). This overexpression facilitates DNA damage repair and contributes to treatment resistance. To counter this, scientists have developed inhibitors targeting these proteins to disrupt DNA repair processes in cancer cells (Figure 2). This approach effectively enhances the impact of therapy-induced DNA damage, thereby increasing the likelihood of inducing apoptosis in cancer cells and potentially improving treatment outcomes.

Conversely, defects in DDR pathways can lead to mutations and increased genomic instability, driving cancer initiation and progression. Cancer cells often have rapid division rates and are more vulnerable to specific DDR inhibitors like ATR and DNA-PK inhibitors. Exploiting this vulnerability allows targeted therapy to differentiate between normal cells with intact DDR and cancer cells with DDR defects (Pilié et al., 2019; Basourakos et al., 2017; McPherson and Korzhnev, 2021). Based on synthetic lethality, this innovative approach selectively eliminates cancer cells while sparing normal cells (Minchom et al., 2018), exemplified by the efficacy of ATR inhibitors in ATM-deficient cancers and Wee1 inhibitors in p53-mutant cancers (O'Neil et al., 2017). Synthetic lethality occurs when cell death is induced by simultaneous defects in two or more related genes, whereas a single defect alone might not compromise cell survival (Huang et al., 2020; Mullard, 2017). Advances in gene editing technologies such as RNAi and CRISPR have enabled large-scale screening of synthetic lethal targets, leading to new therapeutic discoveries.

PARP inhibitors are a notable application of synthetic lethality, effectively targeting tumors with DDR defects like BRCA1/2 gene mutations (Bryant et al., 2005; Farmer et al., 2005). Several PARP

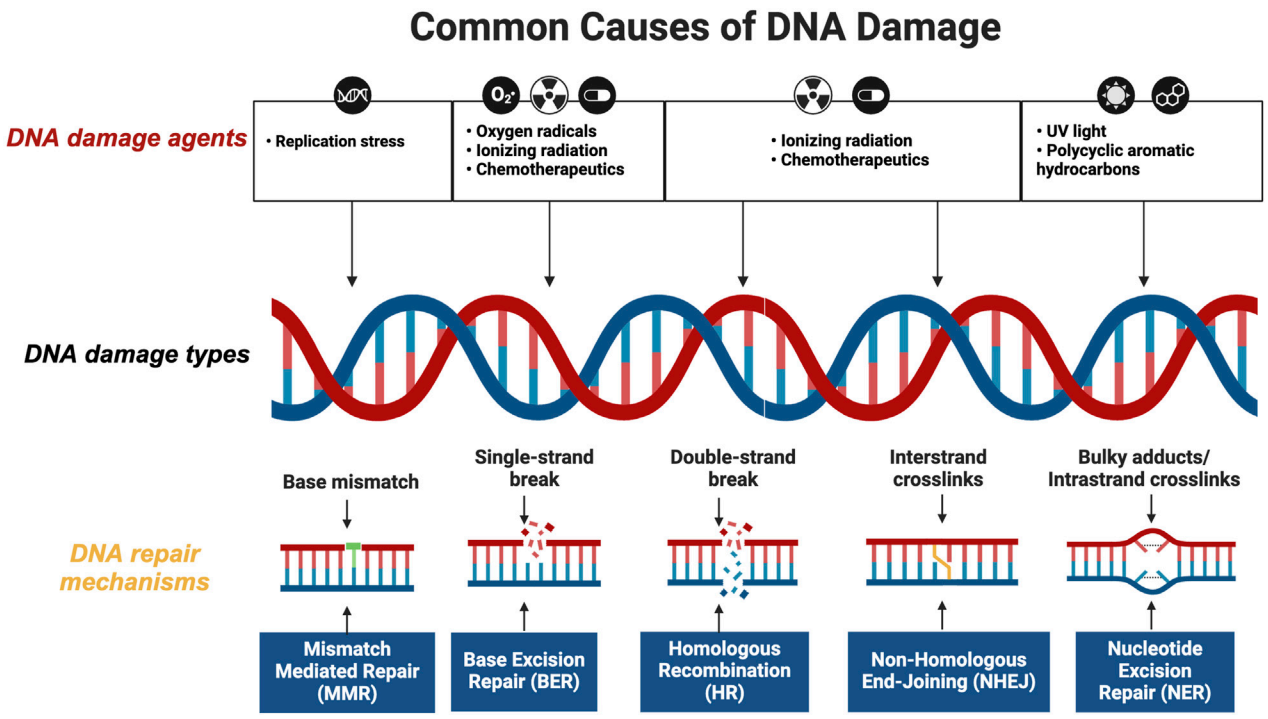

FIGURE 1
Overview of DNA Damage Response (DDR) Mechanisms Ensuring Cellular Viability and Genome Integrity. This figure illustrates the sophisticated network of DDR mechanisms that cells employ to maintain genome integrity. Central to the DDR are five key pathways: Non-Homologous End Joining (NHEJ), Homologous Recombination (HR), Mismatch Repair (MMR), Nucleotide Excision Repair (NER), and Base Excision Repair (BER). Each pathway is depicted with its specific role and interaction within the cellular environment to repair various types of DNA damage (created with BioRender.com, accessed on 25 August 2024).

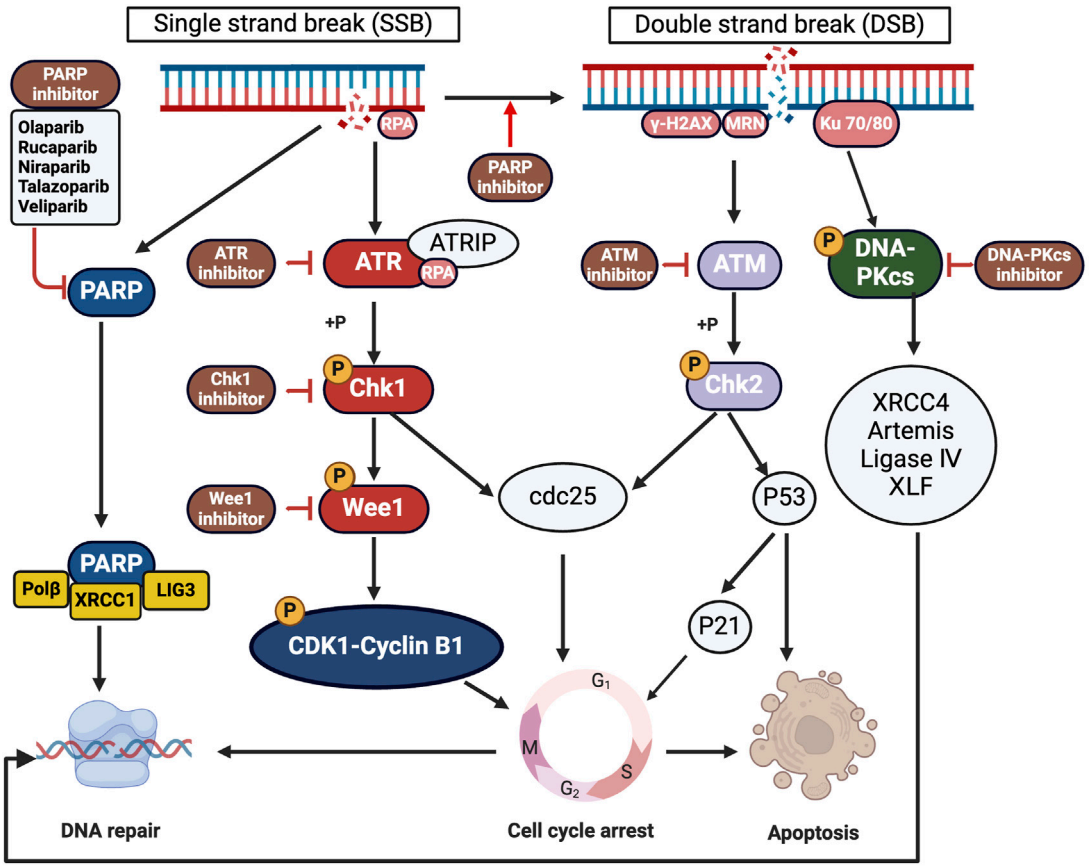

FIGURE 2
Targeting Overexpressed DNA Repair Proteins in Cancer Therapy. This figure details the critical proteins in cancer cells central to DNA repair mechanisms, contributing to treatment resistance. Highlighted proteins include PARP, DNA-PKcs, ATM, ATR, Wee1 and Chk1/2, which enhance DNA repair and contribute to treatment resistance. The diagram also shows inhibitors developed to disrupt these pathways, depicting how each inhibitor interacts with its target protein to increase cancer cell sensitivity to treatments and potentially overcome resistance (created with BioRender.com, accessed on 25 August 2024).

inhibitors have received FDA approval for cancer treatment, including Talazoparib, Rucaparib, Niraparib, and Olaparib (Min and Im, 2020; Pascal, 2018; Slade, 2020). Synthetic lethality-based strategies offer several advantages, such as overcoming resistance to traditional therapies and producing synergistic anticancer effects when combined with radiotherapy or chemotherapy (Lord and Ashworth, 2017; Hu and Guo, 2020; Tang et al., 2020). The discovery of numerous therapeutically relevant molecules has spurred increased interest in synthetic lethality-based therapies (Hengel et al., 2017). Many novel DDR-targeting molecules are undergoing clinical trials with promising results (Table 1) (Fok et al., 2019; Ricciuti et al., 2020; Sheng et al., 2020; Wengner et al., 2020). This paper summarizes the biological characteristics and limitations of various DDR inhibitors and reviews recent advancements in clinical research.

2 Historical development of DDR-targeted therapies in cancer

In the 1970s and 1980s, groundbreaking research on DNA repair mechanisms laid the foundation for understanding how cells detect and repair DNA damage. During this time, key pathways like NER, BER, and MMR were identified and characterized. These discoveries paved the way for significant advancements in the late 1980s–1990s, such as the discovery of the ATM gene and its crucial role in the DNA damage response. Additionally, the discovery of BRCA1 and BRCA2 genes highlighted their roles in HR, linking mutations in these genes to increased risks of breast and ovarian cancers (Sancar, 1995). By the early 2000s, the focus of research shifted to targeting specific DDR proteins, leading to the development of synthetic lethality strategies. This approach was particularly effective in BRCA-deficient cancers, exemplified using PARP inhibitors (Farmer et al., 2005; Fong et al., 2009). During this period, substantial advancements were achieved, particularly with the introduction of Olaparib, the first PARP inhibitor, into clinical trials. Olaparib exhibited efficacy in targeting cancers linked to BRCA gene mutations, representing a pivotal development in the field of oncology (Ledermann et al., 2012). The 2010s marked a pivotal era with the FDA approval of Olaparib in 2014 for ovarian cancer treatment. This milestone was soon followed by the approval of other PARP inhibitors, including Rucaparib, Niraparib, and Talazoparib (Swisher et al., 2017; Mirza et al., 2016; Litton et al., 2018). In recent years, the scope of DDR inhibitors has expanded,

TABLE 1 DDR inhibitors in clinical trial.

Pathway	Target	Compound	Stage	Disease	Clinical trial dentifier and status
NHEJ					
	DNA-PKcs	AZD7648	Phase I/II	Advanced malignancy Adult soft tissue sarcoma	NCT03907969 (COMPLETED) NCT05116254 (RECRUITING)
		M9831	Phase I	Advanced solid tumor	NCT02644278 (COMPLETED)
		M3814	Phase I	Glioblastoma Gliosarcoma Ovarian Cancer	NCT04555577 (RECRUITING) NCT04092270 (RECRUITING)
		CC-115	Phase I	Prostate cancer Advanced malignancy	NCT02833883 (PMID: 37980367) NCT01353625 (PMID: 31853198)
			Phase II	Glioblastoma	NCT02977780 (PMID: 37722087)
BER					
	PARP	E7016	Phase II	Melanoma	NCT01605162 (TERMINATED)
		Niraparib	Phase III	Ovarian cancer Breast cancer	NCT01847274 (PMID: 36970052) NCT01905592 (TERMINATED)
		Olaparib	Phase I	Lung cancer Carcinoma of the oesophagus Head and neck cancer Breast carcinoma	NCT02511795 (COMPLETED) NCT01460888 (UNKNOWN STATUS) NCT01562210 (PMID: 31500595) NCT01758731 (COMPLETED) NCT02308072 (ACTIVE, NOT RECRUITING) NCT02227082 (COMPLETED) NCT02229656 (PMID: 31500595)
			Phase III	Ovarian cancer Fallopian tube cancer Breast cancer Gastric cancer Pancreatic cancer Primary peritoneal cancer	NCT01844986 (PMID: 36082969) NCT01874353 (PMID: 35772665) NCT01924533 (PMID: 29103871) NCT02000622 (PMID: 32472001) NCT02032823 (PMID: 38301187) NCT02184195 (PMID: 38687918) NCT02282020 (PMID: 32073956) NCT02392676 (WITHDRAWN) NCT02446600 (PMID: 35290101) NCT02477644 (PMID: 31851799) NCT02502266 (ACTIVE, NOT RECRUITING)
			Phase IV	Ovarian cancer	NCT02476968 (PMID: 37030280)
		Rucaparib	Phase II	Prostate cancer	NCT03413995 (PMID: 38885246)
			Phase III	Ovarian carcinoma	NCT01968213 (PMID: 37262961)
		Talazoparib	Phase III	Prostate cancer Breast cancer	NCT03395197 (PMID: 37285865) NCT01945775 (PMID: 38886516)
		Veliparib	Phase I/II	Advanced solid malignancy with peritoneal carcinomatosis Epithelial ovarian cancer Fallopian cancer Primary peritoneal cancer Breast cancer Pancreatic cancer Non-small cell lung cancer Diffuse pontine gliomas	NCT01264432 (COMPLETED) NCT01477489 (PMID: 29558281) NCT01514201 (PMID: 32009149) NCT01618357 (COMPLETED) NCT01908478 (COMPLETED) NCT02412371 (TERMINATED)
			Phase III	Breast cancer Non-Small cell lung cancer Glioblastoma Gliosarcoma Ovarian cancer	NCT02032277 (PMID: 33599688) NCT02106546 (PMID: 34436928) NCT02152982 (PMID: 26615020) NCT02163694 (PMID: 32861273) NCT02264990 (PMID: 35331641) NCT02470585 (PMID: 34930617)
HR					
	ATR	AZD6738	Phase I	Refractory cancer	NCT02630199 (COMPLETED)

(Continued on following page)

TABLE 1 (*Continued*) DDR inhibitors in clinical trial.

Pathway	Target	Compound	Stage	Disease	Clinical trial dentifier and status
			Phase II	Gastric adenocarcinoma Malignant melanoma	NCT03780608 (UNKNOWN STATUS)
		M6620	Phase I	Oesophageal adenocarcinoma Solid tumor Squamous cell carcinoma	NCT03641547 (PMID: 38129525) NCT02487095 (PMID: 29252124)
		BAY-1895344	Phase I	Solid tumor Ovarian cancer Non-Hodgkin's lymphoma	NCT04267939 (TERMINATED) NCT03188965 (COMPLETED)
		M4344	Phase I	Ovarian cancer Solid tumor	NCT04149145 (WITHDRAWN) NCT02278250 (COMPLETED)
			Phase I/II	Advanced solid tumor Breast cancer	NCT04655183 (WITHDRAWN)
		M1774	Phase I	Endometrial carcinoma Ovarian carcinoma Solid tumor	NCT06308263 (RECRUITING) NCT05950464 (RECRUITING) NCT05396833 (RECRUITING) NCT05687136 (RECRUITING)
			Phase II	Merkel cell carcinoma Refractory prostate carcinoma	NCT05947500 (RECRUITING) NCT05828082 (RECRUITING)
			Phase I/II	Advanced microsatellite stable colorectal carcinoma Hematopoietic and lymphatic system neoplasm Non-small cell lung cancer	NCT05691491 (RECRUITING) NCT05882734 (RECRUITING)
	ATM	AZD1390	Phase I	Brain cancer Glioblastoma Glioblastoma multiforme Glioma Adult soft tissue sarcoma Non small cell lung cancer Healthy volunteer male subjects Solid tumor	NCT03423628 (RECRUITING) NCT05182905 (RECRUITING) NCT05116254 (RECRUITING) NCT05678010 (RECRUITING) NCT04550104 (RECRUITING) NCT03215381 (COMPLETED)
		AZD0156	Phase I	Solid tumor	NCT02588105 (COMPLETED)
Cell Cycle Checkpoint					
	Chk1	GDC-0575	Phase I	Lymphoma Solid tumor	NCT01564251 (PMID: 29788155)
		LY-2606368	Phase II	Ovarian cancer	NCT03414047 (PMID: 36192237)
		SRA737	Phase I/II	Solid tumor Non-Hodgkin's lymphoma	NCT02797964 (PMID: 37120671)
		MK-8776	Phase I	Hodgkin disease Non-Hodgkin's lymphoma Leukemia Adavance solid tumor	NCT00779584 (PMID: 25605849) NCT00907517 (TERMINATED) NCT01521299 (WITHDRAWN)
			Phase II	Leukemia	NCT01870596 (PMID: 28957699)
	Wee1	Debio 0123	Phase I	Solid tumor	NCT03968653 (RECRUITING)
		SY-4835	Phase I	Advanced Solid tumor	NCT05291182 (RECRUITING)
		IMP7068	Phase I	Advanced Solid tumor	NCT04768868 (RECRUITING)
		AZD1775	Phase I	Solid tumors Ovarian cancer	NCT02610075 (WITHDRAWN)
			Phase II	Ovarian cancer Fallopian tube cancer Peritoneal cancer Pancreatic cancer Acute myeloid leukemia	NCT02272790 (PMID: 34645648) NCT01357161 (PMID: 32611648) NCT02037230 (PMID: 31398082) NCT02791919 (WITHDRAWN)
		ZN-c3	Phase I	Fallopian tube carcinoma Ovarian carcinoma	NCT05368506 (WITHDRAWN) NCT05431582 (WITHDRAWN)

(Continued on following page)

TABLE 1 (*Continued*) DDR inhibitors in clinical trial.

Pathway	Target	Compound	Stage	Disease	Clinical trial dentifier and status
				Peritoneal carcinoma Breast cancer Lung cancer Pancreatic cancer Solid tumor	NCT04158336 (RECRUITING) NCT04516447 (RECRUITING)
			Phase II	Pancreatic cancer	NCT06015659 (RECRUITING)
			Phase I/II	Acute myeloid leukemia Metastatic colorectal cancer Breast cancer Uterine serous carcinoma Osteosarcoma	NCT05682170 (RECRUITING) NCT05743036 (RECRUITING) NCT06351332 (RECRUITING) NCT04814108 (ACTIVE, NOT RECRUITING) NCT04833582 (ACTIVE, NOT RECRUITING)

integrating these therapies with chemotherapy and immune checkpoint inhibitors to overcome resistance and enhance therapeutic outcomes. Ongoing research continues to explore their potential beyond traditional BRCA-mutant cancers, aiming to broaden their application in cancer therapy.

3 Molecular determinants of efficacy in DDR inhibitors

DDR inhibitors are designed to target crucial proteins involved in DNA repair pathways, making them powerful tools for cancer therapy, particularly for cancers heavily reliant on these pathways (Kelley et al., 2014; Teo et al., 2017). Most DDR inhibitors operate on the principle of synthetic lethality, whereby inhibiting a DDR pathway is fetal to cells already deficient in a complementary DNA repair mechanism (e.g., PARP inhibitors in BRCA-mutated cancers) (Yang et al., 2012). These inhibitors capitalize on the genetic instabilities and repair deficiencies common in cancer cells, aiming to block DNA repair and thereby induce cancer cell death (Kelley et al., 2014). The efficacy of DDR inhibitors, such as DNA-PKcs, PARP, ATR, ATM, Chk1/2, and Wee1 inhibitors, depends substantially on their specific molecular targets within the DDR pathways. The activation of these targets is influenced by the types of DNA damage and the genetic context of the cancer cells being treated. Each category of inhibitor interacts differently with its target, highlighting the importance of understanding the underlying molecular and genetic mechanisms to optimize therapeutic outcomes. Below is a closer examination of why some DDR inhibitors are more effective than others, grounded in the underlying molecular biology.

DNA-PKcs Inhibitors: DNA-PKcs is a key component of the NHEJ pathway, responsible for repairing DSBs. DNA-PKcs inhibitors impede the ability of cancer cells to repair these breaks, which is particularly important in rapidly dividing cells. These inhibitors are most effective in tumors with high rates of DSBs and deficient in other repair pathways like HR (Shrivastav et al., 2009).

ATM Inhibitors: ATM is activated by DSBs and plays a role in repair through HR. ATM inhibitors block this process, leading to cell death in tumors that rely on ATM for survival (Durocher and Jackson, 2001). However, developing ATM inhibitors has been challenging due to ATM's essential role in normal cell DNA repair (Pilié et al., 2019), and their effectiveness is limited in cancers where alternative pathways, like ATR, can compensate for the loss of ATM function.

PARP Inhibitors: PARP inhibitors, such as Olaparib, target PARP1 and PARP2 enzymes involved in the BER pathway, essential for repairing SSBs. In cells deficient in HR, such as those with BRCA1/2 mutations, inhibiting PARP leads to the accumulation of DNA damage and subsequent cell death, a phenomenon known as synthetic lethality (Lord and Ashworth, 2017). The effectiveness of PARP inhibitors highly depends on the presence of HR deficiencies. Some PARP inhibitors, like Talazoparib, exhibit a strong ability to "trap" PARP on DNA, which can lead to greater cytotoxicity but also increased side effects (Murai et al., 2012).

ATR Inhibitors: ATR kinase is activated in response to replication stress and helps stabilize replication forks, preventing their collapse and the formation of DSBs (Lecona and Fernandez-Capetillo, 2018; Karnitz and Zou, 2015). ATR inhibitors are particularly effective in cancers with high levels of replication stress or when used in combination with agents that induce replication stress. However, the effectiveness of these inhibitors can be limited in tumors with intact DDR pathways or in cases where alternative repair mechanisms compensate for ATR inhibition.

Chk1 and Chk2 Inhibitors: Chk1 and Chk2 are checkpoint kinases that regulate cell cycle progression in response to DNA damage (Bartek and Lukas, 2003). Chk1 is particularly critical during the S and G2 phases of the cell cycle, making its inhibition potentially lethal to rapidly dividing cancer cells. Chk1 inhibitors tend to be more effective in cancers where the G1/S checkpoint (controlled by p53) is dysfunctional, forcing the cells to rely heavily on the S/G2 checkpoint for survival (Merry et al., 2010). In contrast, Chk2 has more redundancy and is less commonly targeted alone (Antoni et al., 2007).

Wee1 Inhibitors: Wee1 kinase is a critical regulator of the G2/M checkpoint; inhibition of this kinase propels cells harboring DNA damage into premature mitosis. This premature entry into mitosis leads to mitotic catastrophe, ultimately resulting in cell death (Do et al., 2013; Geenen and Schellens, 2017). Wee1 inhibitors are particularly effective in cancers that depend heavily on the G2/M checkpoint, such as those with p53-deficient. However, their

effectiveness can be limited in tumors that can employ alternative mechanisms to regulate the cell cycle or handle mitotic stress.

In summary, the functionality of DDR inhibitors is intricately associated with the specific molecular pathways they target, as well as the genetic and cellular context of the tumors. The efficacy of DDR inhibitors is proportionally related to the extent to which cancer depends on the specific pathway targeted by the treatment. Conversely, tumors equipped with compensatory pathways or those lacking specific vulnerabilities may exhibit reduced responsiveness. This highlights the importance of precision medicine in selecting the most appropriate DDR inhibitor based on the molecular and genetic profile.

4 Advances in the applicaiton of treatment based on DDR

4.1 Advances in the application of DNA-PKcs inhibitors

DNA-PK is pivotal in NHEJ, a key DNA repair mechanism (Goodwin and Knudsen, 2014; Lieber, 2010). The Ku70/Ku80 complex recognizes and binds to broken DNA ends, recruiting monomeric DNA-PKcs to form an active DNA-PK complex. This complex serves as a scaffold that bridges the DNA ends, facilitating the recruitment and phosphorylation of repair proteins such as Ku70, Ku80, Artemis, XRCC4, XLF, and DNA Ligase IV, which are critical for completing the repair process. Research has shown that tumor cells often upregulated DNA-PKcs expression following radiotherapy or chemotherapy to repair damaged DNA and evade cell death, leading to acquired resistance against these therapies (Goodwin and Knudsen, 2014; Damia, 2020; Hu et al., 2021; Pospisilova et al., 2017). Thus, DNA-PKcs emerges as a promising target for anticancer therapy. Effectively suppressing DNA-PKcs with inhibitors, when used alongside radiotherapy or chemotherapy, can help overcome tumor cell resistance and enhance therapeutic outcomes.

Four DNA-PKcs inhibitors are currently in Phase I/II clinical trials: AZD7648, M9831, M3814, and CC-115. AZD7648 stands out for its high selectivity, showing over 100-fold specificity for DNA-PKcs compared to related kinases such as ATM, ATR, PI3Kα, PI3Kβ, and PI3Kδ (Goldberg et al., 2020). It is currently under evaluation in the Phase I trial for adult soft tissue sarcoma therapy (NCT05116254). Another completed study, NCT03907969, explored AZD7648 as a single agent and combined it with other anticancer therapies for advanced cancers, underscoring its potential for wider oncological use. M9831 is a DNA-PKcs inhibitor known for effectively suppressing NHEJ, thereby impeding the repair of DSBs induced by chemotherapy or radiotherapy (Timme et al., 2018). A clinical trial (NCT02644278) has also been completed investigating M9831 as a monotherapy or combined with PEGylated liposomal doxorubicin. M3814 is a potent DNA-PKcs inhibitor that sensitizes various cancer cell lines to agents inducing DSBs and ionizing radiation (Zenke et al., 2020). Several clinical trials assessing M3814 as a monotherapy or combined with radiotherapy and chemotherapy are ongoing (NCT04555577, NCT04092270). CC-115, a novel dual inhibitor targeting mTOR and DNA-PKcs, demonstrated promise as a well-tolerated and potentially groundbreaking anticancer therapy in a Phase I trial (NCT01353625) (Munster et al., 2019). A subsequent Phase I trial (NCT02833883) combining CC-115 with enzalutamide demonstrated good tolerability in treating metastatic castration-resistant prostate cancer (Zhao et al., 2024). Additionally, preliminary outcomes from a Phase II trial (NCT02977780) focused on innovative glioblastoma therapy revealed that although CC-115 was associated with significant treatment-related toxicity (≥ grade 3) in 58% of patients, it regrettably failed to deliver benefits in terms of progression-free survival (PFS) or overall survival (OS) (Rahman et al., 2023).

Despite significant clinical advancements with DNA-PKcs inhibitors, several challenges remain: 1) Limited Selectivity: Achieving optimal selectivity for DNA-PKcs over closely related kinases, such as PI3K (PI3Kα, β, δ, γ) and other PI3K-related kinases (PIKKs) like ATM and ATR, is challenging due to the high degree of sequence homology. To clarify, while DNA-PK inhibitors have the general trend of limited selectivity in the broader context, AZD7648 is still highlighted as a notable exception, which sets AZD7648 apart from many other inhibitors in this class, exhibiting broader kinase activity profiles and associated off-target effects. 2) Structural Limitations: The considerable molecular weight of DNA-PKcs presents technical difficulties in obtaining its crystal structure. Only the crystal structure of complexes formed by PI3Kγ and DNA-PKcs inhibitors has been elucidated.31 The lack of structural information limits the precise and rational design of highly selective DNA-PKcs inhibitors using computational simulations. 3) Potential Side Effects: Inhibiting DNA-PKcs can adversely affect normal tissues due to its critical role in DDR and repair mechanisms. The impairment of DNA repair in normal tissues can cause toxicity in rapidly dividing tissues, such as the bone marrow and gastrointestinal tract, leading to side effects like myelosuppression and gastrointestinal disturbances. Therefore, the therapeutic window for DNA-PKcs inhibitors must be carefully managed to optimize the anticancer efficacy while minimizing adverse effects on normal tissues. Despite demonstrating excellent anticancer efficacy in animal models (Fok et al., 2019; Gordhandas et al., 2022), standalone DNA-PKcs inhibitors have shown limited clinical efficacy. Future development strategies will likely involve combination therapies to enhance their anticancer effects. Additionally, researchers will focus on developing more selective, efficacious, and less toxic DNA-PKcs inhibitors to further improve therapeutic outcomes.

4.2 Advances in the application of PARP inhibitors

BRCA-deficient tumor cells heavily rely on PARP-mediated single-strand DNA repair pathway due to defects in double-strand DNA repair, making PARP a widely utilized anticancer target (Dziadkowiec et al., 2016). PARP inhibitors can function as sensitizers in chemotherapy and radiotherapy by inducing synthetic lethality in DNA damage, thereby augmenting the therapeutic efficacy of these treatments (Kamel et al., 2018). Mechanistically, upon oxidative stress or alkylation damage to DNA, PARP1 activation leads to the recruitment of nucleases such as MRE1 and Exo1 to assist in DNA repair, thereby

preserving genome stability. Inhibition of PARP1 disrupts the DNA damage repair pathway, resulting in aberrant apoptosis or cell death.

To date, four PARP1 selective inhibitors have been approved by US FDA for treating malignant tumors. Among these, Talazoparib, a next-generation PARP inhibitor, received approval in 2018 for patients with metastatic or locally advanced breast cancer carrying BRCA mutations based on EMBRACA (NCT01945775) (Hoy, 2018). Another Phase III trial evaluating the combination of Talazoparib and Enzalutamide in men with first-line metastatic castration-resistant prostate cancer has demonstrated a clinically and statistically significant improvement in radiographic progression-free survival (rPFS) compared to treatment with enzalutamide alone. Final OS data and extended safety follow-up are underway, which will provide further insight into the long-term clinical benefits of this treatment regimen (Agarwal et al., 2023). In 2016, US FDA approved Rucaparib as a third-line treatment for female ovarian cancer patients (Shirley, 2019). Additionally, Rucaparib was evaluated in a phase II trial (NCT03413995) as a monotherapy for patients with metastatic hormone-sensitive prostate cancer who have germline mutations in HR repair genes. However, this trial was terminated early due to failing to meet its pre-specified efficacy threshold, leading to discontinuation of enrollment (Markowski et al., 2024). Niraparib received US FDA approval in 2017 for the treatment of primary peritoneal cancer, fallopian tube cancer, or recurrent epithelial ovarian cancer that is resistant to first-line platinum-based chemotherapy (Heo and Duggan, 2018). A Phase III trial (NCT01905592) comparing Niraparib to a physician's choice of treatment in HER2-negative, germline BRCA mutation-positive breast cancer patients was also terminated early due to insufficient efficacy. Olaparib first obtained FDA approval in 2014 for treating germline BRCA-mutated advanced ovarian cancer after three or more prior lines of chemotherapy (Bochum et al., 2018). In 2017, it was approved for the maintenance treatment of adults with recurrent epithelial ovarian, fallopian tube, or primary peritoneal cancer in a complete or partial response to platinum-based chemotherapy (FDA, 2017). Furthermore, in 2018, Olaparib became the first PARP inhibitor to receive FDA approval for treating germline BRCA-mutated HER2-negative metastatic breast cancer after three or more prior lines of chemotherapy (FDA, 2018). Veliparib remains under investigation and has not yet received FDA approval. It has shown potential in enhancing the effects of several chemotherapeutics and has been included in numerous clinical trials of combination therapies (Table 1).

Combining PARP inhibitors with anti-angiogenic therapy has emerged as a recent research focus. Multi-kinase inhibitors targeting VEGFR, PDGFR, and FGFR can induce hypoxic environments and HR deficiency by inhibiting angiogenesis, thereby augmenting the sensitivity of tumor cells to PARP1/2 inhibitors (Ahn and Bekaii-Saab, 2020; Ivy et al., 2016). Furthermore, combining PARP inhibitors with alkylating agents such as Temozolomide and platinum-based drugs can enhance the "synthetic lethality" effect, leading to more effective tumor cell eradication (Lok et al., 2017). Currently, clinical studies are underway investigating the combination of Olaparib/Talazoparib with Temozolomide for the treatment of gliomas, small cell lung cancer (SCLC), and uterine smooth muscle tumors (Hanna et al., 2020). Additionally, combining PARP inhibitors with PD-1/PD-L1 inhibitors has demonstrated a higher overall response rate (ORR) of 71% in patients with platinum-sensitive recurrent ovarian cancer harboring BRCA mutations (Lampert et al., 2020). Niraparib combined with Pembrolizumab has achieved an ORR of 24% and a disease control rate (DCR) of 67% in treating platinum-resistant recurrent ovarian cancer patients (Konstantinopoulos et al., 2019). In conclusion, PARP inhibitors have exhibited significant therapeutic potential across a diverse range of cancers, both as standalone treatments and in combination with other therapies.

4.3 Advances in the application of ATR/ATM inhibitors

ATR and ATM are essential partners in synthetic lethality and cancer therapy. Numerous interactions between ATR and ATM signaling pathways ensure genome stability and cell survival (Burma et al., 2001; Matsuoka et al., 2007; Yang et al., 2004). Upon activation by RPA-coated single-stranded DNA, ATRIP binds directly to RPA, localizing ATR to DNA damage sites. This action triggers the ATR-Chk1 signaling cascade, leading to cell cycle arrest at the G2-M phase, thus providing a temporal window for DNA damage repair. Conversely, ATM responds to DSBs by interacting with MRN complex (MRE11-RAD50-NBS1), generatingγ-H2AX and subsequently phosphorylating and activating Chk2. This activation triggers G1-S checkpoints and delays entry to the S phase, facilitating DNA damage repair.

The synergistic effect of inhibiting both ATR and ATM is based on the critical interdependence of their pathways in managing DNA damage, particularly under conditions of oncogenic replication stress and therapeutic interventions such as radiation or chemotherapy. Inhibition of ATR leads to the accumulation of ssDNA regions due to replication stress, which can cause replication forks to collapse and the formation of DSBs. Normally, ATM would be activated by these DSBs to initiate repair. However, when ATM is also inhibited, the repair of these breaks is severely compromised, leading to a buildup of unrepairable DNA damage. This dual inhibition overwhelms the cancer cell repair mechanisms, significantly enhancing cell death. This strategy provides a strong rationale for the combined use of ATR and ATM inhibitors, particularly in tumors that heavily depend on these pathways due to existing DNA repair deficiencies.

Several ATR/ATM inhibitors have entered clinical trials for cancer treatment. AZD6738 is an effective oral bioavailable ATR inhibitor (Min et al., 2017). In a Phase I trial (NCT02630199), AZD6738 was administered at 240 mg twice daily in combination with paclitaxel, achieving a promising ORR of 22.6%, which increased to 33.3% in the melanoma subgroup. The median progression-free survival (mPFS) was 3.6 months, and the median overall survival (mOS) was 7.4 months, with the most common adverse reactions being neutropenia (68%), anemia (44%), and thrombocytopenia (37%) (Kim et al., 2021). M6620, another specific ATR inhibitor, significantly inhibits pancreatic tumor growth without notable toxicity to normal cells or tissues (Thomas et al., 2018). A Phase I trial (NCT03641547) demonstrated that combining M6620 with radiation therapy is feasible and well-tolerated in esophageal cancer patients. Its use with cisplatin and capecitabine also showed tolerability in advanced cancer cases

(Javed et al., 2024). Another Phase I study (NCT02487095) demonstrated that combining M6620 with Topotecan is especially effective in treating platinum-refractory small-cell lung cancer. This condition does not respond well to Topotecan alone.59 BAY-1895344 is a potent, highly selective, orally available ATR inhibitor, demonstrating significant efficacy as a monotherapy in cancer xenograft models with specific DNA damage repair deficiencies (Lücking et al., 2020). A Phase I clinical study (NCT03188965) investigating BAY-1895344 for treating patients with advanced solid tumors and lymphomas has completed recruitment. Initial results from this study, involving 22 patients, indicated that four achieved partial responses. Furthermore, patients exhibiting ATM mutations or loss had a median survival time of 315.5 days. Overall, BAY-1895344 is well-tolerated and shows antitumor activity in cancers with certain DDR defects, including ATM loss (Yap et al., 2021). However, another Phase I clinical study (NCT04267939), testing BAY-1895344 in combination with Niraparib, was terminated as the experimental combination did not provide the anticipated benefits over existing standard therapies. M4344, a potent ATR kinase inhibitor that effectively suppresses Chk1 phosphorylation (Gorecki et al., 2020), encountered challenges in its development. A Phase I study (NCT02278250) revealed that while M4344 was well-tolerated at lower doses, unexpected liver toxicity at higher doses could limit its therapeutic efficacy (Burris et al., 2024). Two additional trials of M4344 (NCT04149145/NCT04655183) were withdrawn for undisclosed reasons. M1774 is a potent ATR inhibitor currently in the recruitment phase for several clinical trials targeting various types of cancer (Table 1).

AZD0156 is an oral ATM inhibitor that efficiently blocks ATM kinase activity, induces apoptosis in malignant tumors, and leads to tumor cell death (Pike et al., 2018). The pharmacokinetics, tolerability, safety, and efficacy of AZD0156 are being evaluated in a Phase I clinical trial, which has completed recruitment (NCT02588105). AZD1390 is an orally active, CNS-penetrating ATM inhibitor distinguished by its exceptional selectivity for ATM, demonstrating potency more than 10,000 times greater than other enzymes in the PIKK family. It is also in the recruitment phase for multiple clinical trials aimed at treating various types of cancer (Table 1). These developments highlight the ongoing efforts to harness the therapeutic potential of ATR/ATM inhibitors in oncology.

Despite these developments, no ATM/ATR inhibitors have been approved for clinical use. The potential for tumors to bypass inhibited ATR/ATM pathways via alternative mechanisms underscores the importance of combining ATM or ATR inhibitors with PARP inhibitors. Cancers with ATM mutations often rely more heavily on ATR for survival and DNA repair (Armstrong et al., 2019; Cheng et al., 2022). This dependency makes ATR an appealing target because inhibiting ATR in these contexts can specifically sensitize cancer cells to treatment without similarly affecting healthy cells. This combination could provide a synergistic effect, enhancing antitumor outcomes through synthetic lethality. ATR is one of the most promising synthetic lethality targets, holding significant potential for treating cancers with ATM mutations or loss. These efforts continue to demonstrate the significant potential of ATR/ATM inhibitors in oncology.

4.4 Advances in the application of Chk1/Wee1 inhibitors

Overexpression of Chk1 and Wee1 has been observed in various cancers, including ovarian and breast cancer (Cleary et al., 2020; Ghelli Luserna Di Rorà et al., 2019). Inhibiting Wee1 or Chk1 causes tumor cells with DNA damage to enter mitosis prematurely, leading to apoptosis or cell death. Mechanistically, single-stranded DNA damage activates ATR, which phosphorylates and activates Chk1. This activation subsequently phosphorylates cdc25C and Wee1, leading to the activation of Wee1 and inhibition of cdc25C. Wee1 further phosphorylates the CDK1-Cyclin B complex, rendering it inactive and causing G2 arrest to allow for DNA repair (Du et al., 2020; Matheson et al., 2016). As a critical protein kinase, Wee1 effectively inhibits CDK2 and CDK1 to activate the G2/M checkpoint, inducing G2/M arrest to allow for DNA repair. Inhibiting Wee1 prevents the G2 checkpoint initiation, allowing cells to enter mitosis with incorrect DNA content, leading to a loss of genomic integrity and cell death. Cancer cells with dysregulated G1/S cell cycle checkpoints heavily rely on the G2/M checkpoint to prevent excessive DNA damage accumulation. Therefore, based on synthetic lethality, inhibiting Wee1 can block the G2/M checkpoint to treat p53-deficient tumor cells, as p53 plays a critical role in the G1 checkpoint. Current research primarily focuses on combining Wee1 inhibitors with other therapeutic agents that induce DNA damage, including PARP inhibitors, chemotherapy, or radiotherapy for patients carrying TP53 mutations. Chk1 is a highly conserved serine/threonine kinase that is involved in multiple signal transduction pathways activated by DNA damage events (Dent, 2019; Zhang and Hunter, 2014). Inhibiting Chk1 can disrupt the G2 checkpoint initiation, impair DNA repair and promote tumor cell apoptosis (Carrassa and Damia, 2011; Rundle et al., 2017).

LY-2606368 is a potent Chk1 kinase inhibitor with an IC50 of less than 1 nM for Chk1 and less than 8 nM for Chk2 (Heidler et al., 2020). It has shown promise in a Phase II clinical trial (NCT03414047), demonstrating durability as a single agent in certain patients with recurrent ovarian cancer (Konstantinopoulos et al., 2022). Another study comparing the activity and off-target effects of CHK1 inhibitors MK-8776, SRA737, and LY2606368 demonstrates that LY2606368 is the most selective CHK1 inhibitor (Ditano and Eastman, 2021). This finding supports the potential for further clinical development of LY2606368. Another Chk1 kinase inhibitor, GDC-0575, is known to enhance the sensitivity of cancer cells to chemotherapy-induced DNA damage (Li et al., 2021). Although GDC-0575 can be safely administered alone or in combination with gemcitabine, its antitumor efficacy was limited, achieving only a 15% PR rate among 102 patients treated with the combination in a Phase I study (NCT01564251) (Italiano et al., 2018). SRA737, a different orally active Chk1 inhibitor, was well-tolerated in Phase I/II trials (NCT02797964) focusing on solid tumors. However, it lacked sufficient efficacy as a monotherapy. Future studies should explore its use in combination therapies (Kristeleit et al., 2023). MK-8776 also exhibited strong and selective inhibition of Chk1 and was well-tolerated either alone or in combination with gemcitabine in a Phase I trial with advanced solid tumors (Daud et al., 2015). However, a randomized Phase II trial exploring the efficacy of

cytosine arabinoside with and without MK-8776 in relapsed and refractory acute myeloid leukemia found that while MK-8776 significantly increased DNA damage in leukemia cells, as indicated by elevated γ-H2AX levels, it did not lead to notable improvements in treatment responses or survival outcomes compared to the control group (Webster et al., 2017).

AZD1775, the pioneering Wee1 inhibitor to enter Phase I trial (NCT02610075), has demonstrated tolerability and efficacy in reducing tumor size in patients with advanced solid tumors. The inhibitor specifically targets the G2/M checkpoint, increasing the vulnerability of p53-deficient tumors to DNA damage induced by radiotherapy or chemotherapy. Zn-C3, another orally active, potent, and selective Wee1 inhibitor, is currently being evaluated in multiple clinical trials for a range of cancers, including ovarian cancer, fallopian tube cancer, uterine carcinoma, peritoneal cancer, acute myeloid leukemia, colorectal cancer, breast cancer, osteosarcoma and other solid tumors (Table 1). Additional novel Wee1 inhibitors such as Debio 0123, SY-4835, and IMP7068 are now entering Phase I clinical trials (NCT03968653, NCT05291182, NCT04768868), with hopes for positive outcomes.

5 Lessons from unsuccessful DDR inhibitor trials in oncology

The failure of clinical trials involving DDR inhibitors, such as those targeting PARP, ATR, and other key proteins, has provided critical insights for the future of tumor drug development. Several common factors contributing to these failures offer valuable lessons: 1) Biological Complexity and Tumor Heterogeneity: DDR pathways are inherently complex and often exhibit significant redundancy. Tumors can adapt by activating alternative survival pathways, which reduces the efficacy of DDR inhibitors. To overcome this challenge, a deeper understanding of tumor biology and heterogeneity is essential. Conducting biomarker-driven trials and developing companion diagnostics are crucial for identifying patients who are most likely to benefit from specific DDR inhibitors. Additionally, refining drug designs to boost specificity and minimize off-target effects could significantly improve the therapeutic potential of these inhibitors. 2) Inadequate Preclinical Models: Promising results from preclinical models often fail to translate into clinical success, largely because these models inadequately represent human tumors. To improve the predictive accuracy of preclinical studies, it is essential to adopt more representative models, such as patient-derived xenografts and organoids, which more closely mimic the biological complexities of human tumors. 3) Toxicity and Side Effects: DDR inhibitors can cause significant toxicity, particularly when combined with other treatments, such as chemotherapy or radiation. Optimal patient selection, precise dosing strategies, and comprehensive phase I studies to delineate toxicity profiles are critical steps in mitigating these risks. It is also important to base combination therapies on strong biological evidence supported by preclinical data to manage and prevent potential toxicities and interactions. 4) Drug Resistance: Resistance to DDR inhibitors can arise through various mechanisms, including mutations in the target enzymes or alterations in drug metabolism. Combination therapies that target multiple pathways simultaneously may help overcome resistance. Continuous monitoring of resistance mechanisms during clinical trials can provide essential feedback for adjusting treatment protocols. In summary, analyzing failed DDR inhibitor trials is crucial for gaining strategic insights that can improve trial designs, refine patient selection criteria, and optimize therapeutic strategies. These lessons are vital for increasing the probability of success in future oncological drug development endeavors.

6 Challenges and prospects

Recent advancements in DDR inhibitors for cancer therapy have ushered in a landscape filled with both significant challenges and immense prospects. Key challenges include managing severe side effects such as leukopenia and myelotoxicity, especially when these inhibitors are used alongside chemotherapy. There is also a critical need to enhance the selectivity and specificity of these therapies to minimize their impact on healthy cells, expand their therapeutic windows, and identify more genetic biomarkers that can accurately predict patient responses to treatments. On the promising side, ongoing research dedicated to refining molecular designs is leading to the development of more effective and less toxic drugs. These innovative inhibitors are precisely engineered to target specific DDR deficiencies, potentially expanding the range of treatable cancers. Furthermore, optimizing combination therapies aims to reduce the required dosages and overall cumulative toxicity, thereby transforming treatment outcomes. Looking forward, the trajectory of DDR inhibitors involves surmounting these existing limitations through groundbreaking drug design and advanced clinical strategies, potentially enabling their widespread implementation in cancer therapy protocols and significantly improving survival rates. These developments are poised to convert non-responders into responders and elevate existing responders to “super-responder” status, revolutionizing the cancer treatment landscape with more personalized, effective, and safer therapeutic options.

7 Conclusion

Significant advancements in targeted DNA repair inhibition for cancer therapy have been made, marked by the development of highly selective and efficacious DDR inhibitors. These therapies leverage synthetic lethality to tailor treatment for cancer patients with specific DDR deficiencies, achieving precision and personalized treatment outcomes. By inhibiting DDR, these therapies enhance the effectiveness of related drugs and overcome treatment resistance by preventing cancer cells from repairing DNA damage. However, the potential of DDR inhibitors comes with challenges, particularly when combined with chemotherapy, which can lead to side effects such as leukopenia, gastrointestinal toxicity, and myelotoxicity. Future research on DDR inhibitors will focus on improving their selectivity and specificity to reduce toxicity and minimize the dosage required for combination therapy. Another challenge is broadening their therapeutic windows and identifying additional genetic biomarkers sensitive to DDR inhibition. PARP inhibitors are the only FDA-approved DDR inhibitor due to their wide therapeutic windows. Further efforts will aim to discover more

biomarkers with therapeutic relevance, potentially expanding the patient population that benefits from DDR inhibitors.

Author contributions

JQ: Writing–review and editing, Writing–original draft, Visualization, Validation, Software, Resources, Project administration, Methodology, Investigation, Funding acquisition, Formal Analysis, Data curation, Conceptualization. GL: Writing–original draft, Visualization, Validation, Software, Resources, Methodology, Investigation, Formal Analysis, Data curation. MC: Writing–original draft, Software, Investigation. R-WP: Writing–review and editing. XY: Writing–review and editing, Investigation, Formal Analysis, Data curation. JD: Writing–review and editing, Software, Investigation. RH: Writing–review and editing, Software, Methodology. MP: Writing–review and editing, Methodology. YL: Writing–review and editing, Visualization. XG: Writing–review and editing, Visualization. GX: Writing–review and editing, Methodology. BZ: Writing–review and editing, Supervision, Project administration, Conceptualization. CC: Writing–review and editing, Supervision, Project administration, Conceptualization. ZY: Writing–review and editing, Supervision, Project administration, Conceptualization.

Funding

The author(s) declare that financial support was received for the research, authorship, and/or publication of this article. Sponsored by the Key Laboratory of Cardio-Thoracic Surgery (Fujian Medical University), Fujian Province University (Grant No. 2019–67); Sponsored by the Fujian Institute of Cardiothoracic Surgery. This research was funded by a grant from the Talent Fund Project of Fujian Medical University Union Hospital (2021XH029).

Acknowledgments

We thank our researchers for their hard work and the reviewers for their helpful feedback.

Conflict of interest

The authors declare that the research was conducted in the absence of any commercial or financial relationships that could be construed as a potential conflict of interest.

The author(s) declared that they were an editorial board member of Frontiers, at the time of submission. This had no impact on the peer review process and the final decision.

Publisher's note

References

Agarwal, N., Azad, A. A., Carles, J., Fay, A. P., Matsubara, N., Heinrich, D., et al. (2023). Talazoparib plus enzalutamide in men with first-line metastatic castration-resistant prostate cancer (TALAPRO-2): a randomised, placebo-controlled, phase 3 trial. *Lancet* 402 (10398), 291–303. doi:10.1016/S0140-6736(23)01055-3

Ahn, D. H., and Bekaii-Saab, T. (2020). Biliary tract cancer and genomic alterations in homologous recombinant deficiency: exploiting synthetic lethality with PARP inhibitors. *Chin. Clin. Oncol.* 9 (1), 6. doi:10.21037/cco.2020.02.02

Antoni, L., Sodha, N., Collins, I., and Garrett, M. D. (2007). CHK2 kinase: cancer susceptibility and cancer therapy - two sides of the same coin? *Nat. Rev. Cancer* 7 (12), 925–936. doi:10.1038/nrc2251

Armstrong, S. A., Schultz, C. W., Azimi-Sadjadi, A., Brody, J. R., and Pishvaian, M. J. (2019). ATM dysfunction in pancreatic adenocarcinoma and associated therapeutic implications. *Mol. cancer Ther.* 18 (11), 1899–1908. doi:10.1158/1535-7163.MCT-19-0208

Bartek, J., and Lukas, J. (2003). Chk1 and Chk2 kinases in checkpoint control and cancer. *Cancer Cell* 3 (5), 421–429. doi:10.1016/s1535-6108(03)00110-7

Basourakos, S. P., Li, L., Aparicio, A. M., Corn, P. G., Kim, J., and Thompson, T. C. (2017). Combination platinum-based and DNA damage response-targeting cancer therapy: evolution and future directions. *Curr. Med. Chem.* 24 (15), 1586–1606. doi:10.2174/0929867323666161214114948

Basu, B., Yap, T. A., Molife, L. R., and de Bono, J. S. (2012). Targeting the DNA damage response in oncology: past, present and future perspectives. *Curr. Opin. Oncol.* 24 (3), 316–324. doi:10.1097/CCO.0b013e32835280c6

Bochum, S., Berger, S., and Martens, U. M. (2018). Olaparib. *Recent results cancer Res.* 211, 217–233. doi:10.1007/978-3-319-91442-8_15

Brandsma, I., Fleuren, E. D. G., Williamson, C. T., and Lord, C. J. (2017). Directing the use of DDR kinase inhibitors in cancer treatment. *Expert Opin. investigational drugs* 26 (12), 1341–1355. doi:10.1080/13543784.2017.1389895

Bryant, H. E., Schultz, N., Thomas, H. D., Parker, K. M., Flower, D., Lopez, E., et al. (2005). Specific killing of BRCA2-deficient tumours with inhibitors of poly(ADP-ribose) polymerase. *Nature* 434 (7035), 913–917. doi:10.1038/nature03443

Burma, S., Chen, B. P., Murphy, M., Kurimasa, A., and Chen, D. J. (2001). ATM phosphorylates histone H2AX in response to DNA double-strand breaks. *J. Biol. Chem.* 276 (45), 42462–42467. doi:10.1074/jbc.C100466200

Burris, H. A., Berlin, J., Arkenau, T., Cote, G. M., Lolkema, M. P., Ferrer-Playan, J., et al. (2024). A phase I study of ATR inhibitor gartisertib (M4344) as a single agent and in combination with carboplatin in patients with advanced solid tumours. *Br. J. cancer* 130 (7), 1131–1140. doi:10.1038/s41416-023-02436-2

Carrassa, L., and Damia, G. (2011). Unleashing Chk1 in cancer therapy. *Cell Cycle* 10 (13), 2121–2128. doi:10.4161/cc.10.13.16398

Cheng, B., Pan, W., Xing, Y., Xiao, Y., Chen, J., and Xu, Z. (2022). Recent advances in DDR (DNA damage response) inhibitors for cancer therapy. *Eur. J. Med. Chem.* 230, 114109. doi:10.1016/j.ejmech.2022.114109

Cleary, J. M., Aguirre, A. J., Shapiro, G. I., and D'Andrea, A. D. (2020). Biomarker-guided development of DNA repair inhibitors. *Mol. Cell* 78 (6), 1070–1085. doi:10.1016/j.molcel.2020.04.035

Damia, G. (2020). Targeting DNA-PK in cancer. *Mutat. Res.* 821, 111692. doi:10.1016/j.mrfmmm.2020.111692

Daud, A. I., Ashworth, M. T., Strosberg, J., Goldman, J. W., Mendelson, D., Springett, G., et al. (2015). Phase I dose-escalation trial of checkpoint kinase 1 inhibitor MK-8776 as monotherapy and in combination with gemcitabine in patients with advanced solid tumors. *J. Clin. Oncol.* 33 (9), 1060–1066. doi:10.1200/JCO.2014.57.5027

Dent, P. (2019). Investigational CHK1 inhibitors in early phase clinical trials for the treatment of cancer. *Expert Opin. investigational drugs* 28 (12), 1095–1100. doi:10.1080/13543784.2019.1694661

Dilmac, S., and Ozpolat, B. (2023). Mechanisms of PARP-inhibitor-resistance in BRCA-mutated breast cancer and new therapeutic approaches. *Cancers* 15 (14), 3642. doi:10.3390/cancers15143642

Ditano, J. P., and Eastman, A. (2021). Comparative activity and off-target effects in cells of the CHK1 inhibitors MK-8776, SRA737, and LY2606368. *ACS Pharmacol. and Transl. Sci.* 4 (2), 730–743. doi:10.1021/acsptsci.0c00201

Do, K., Doroshow, J. H., and Kummar, S. (2013). Wee1 kinase as a target for cancer therapy. *Cell Cycle* 12 (19), 3159–3164. doi:10.4161/cc.26062

Du, X., Li, J., Luo, X., Li, R., Li, F., Zhang, Y., et al. (2020). Structure-activity relationships of Wee1 inhibitors: a review. *Eur. J. Med. Chem.* 203, 112524. doi:10.1016/j.ejmech.2020.112524

Durocher, D., and Jackson, S. P. (2001). DNA-PK, ATM, and ATR as sensors of DNA damage: variations on a theme? *Curr. Opin. Cell Biol.* 13 (2), 225–231. doi:10.1016/s0955-0674(00)00201-5

Dziadkowiec, K. N., Gąsiorowska, E., Nowak-Markwitz, E., and Jankowska, A. (2016). PARP inhibitors: review of mechanisms of action and BRCA1/2 mutation targeting. *Prz. Menopauzalny.* 15 (4), 215–219. doi:10.5114/pm.2016.65667

Farmer, H., McCabe, N., Lord, C. J., Tutt, A. N., Johnson, D. A., Richardson, T. B., et al. (2005). Targeting the DNA repair defect in BRCA mutant cells as a therapeutic strategy. *Nature* 434 (7035), 917–921. doi:10.1038/nature03445

FDA (2017). *FDA approves Olaparib tablets for maintenance treatment in ovarian cancer*. Silver Spring, MD: U.S. Food and Drug Administration.

FDA (2018). *FDA approves Olaparib for germline BRCA-mutated metastatic breast cancer*. Silver Spring, MD: U.S. Food and Drug Administration.

Fok, J. H. L., Ramos-Montoya, A., Vazquez-Chantada, M., Wijnhoven, P. W. G., Follia, V., James, N., et al. (2019). AZD7648 is a potent and selective DNA-PK inhibitor that enhances radiation, chemotherapy and olaparib activity. *Nat. Commun.* 10 (1), 5065. doi:10.1038/s41467-019-12836-9

Fong, P. C., Boss, D. S., Yap, T. A., Tutt, A., Wu, P., Mergui-Roelvink, M., et al. (2009). Inhibition of poly (ADP-ribose) polymerase in tumors from BRCA mutation carriers. *N. Engl. J. Med.* 361 (2), 123–134. doi:10.1056/NEJMoa0900212

Geenen, J. J. J., and Schellens, J. H. M. (2017). Molecular pathways: targeting the protein kinase Wee1 in cancer. *Clin. cancer Res.* 23 (16), 4540–4544. doi:10.1158/1078-0432.CCR-17-0520

Ghelli Luserna Di Rorà, A., Bocconcelli, M., Ferrari, A., Terragna, C., Bruno, S., Imbrogno, E., et al. (2019). Synergism through WEE1 and CHK1 inhibition in acute lymphoblastic leukemia. *Cancers* 11 (11), 1654. doi:10.3390/cancers11111654

Goldberg, F. W., Finlay, M. R. V., Ting, A. K. T., Beattie, D., Lamont, G. M., Fallan, C., et al. (2020). The discovery of 7-Methyl-2-[(7-methyl[1,2,4]triazolo[1,5-a]pyridin-6-yl) amino]-9-(tetrahydro-2H-pyran-4-yl)-7,9-dihydro-8H-purin-8-one (AZD7648), a potent and selective DNA-dependent protein kinase (DNA-PK) inhibitor. *J. Med. Chem.* 63 (7), 3461–3471. doi:10.1021/acs.jmedchem.9b01684

Goodwin, J. F., and Knudsen, K. E. (2014). Beyond DNA repair: DNA-PK function in cancer. *Cancer Discov.* 4 (10), 1126–1139. doi:10.1158/2159-8290.CD-14-0358

Gordhandas, S. B., Manning-Geist, B., Henson, C., Iyer, G., Gardner, G. J., Sonoda, Y., et al. (2022). Pre-clinical activity of the oral DNA-PK inhibitor, peposertib (M3814), combined with radiation in xenograft models of cervical cancer. *Sci. Rep.* 12 (1), 974. doi:10.1038/s41598-021-04618-5

Gorecki, L., Andrs, M., Rezacova, M., and Korabecny, J. (2020). Discovery of ATR kinase inhibitor berzosertib (VX-970, M6620): clinical candidate for cancer therapy. *Pharmacol. and Ther.* 210, 107518. doi:10.1016/j.pharmthera.2020.107518

Gralewska, P., Gajek, A., Marczak, A., and Rogalska, A. (2020). Participation of the ATR/CHK1 pathway in replicative stress targeted therapy of high-grade ovarian cancer. *J. Hematol. and Oncol.* 13 (1), 39. doi:10.1186/s13045-020-00874-6

Hanna, C., Kurian, K. M., Williams, K., Watts, C., Jackson, A., Carruthers, R., et al. (2020). Pharmacokinetics, safety, and tolerability of olaparib and temozolomide for recurrent glioblastoma: results of the phase I OPARATIC trial. *Neuro-oncology* 22 (12), 1840–1850. doi:10.1093/neuonc/noaa104

Heidler, C. L., Roth, E. K., Thiemann, M., Blattmann, C., Perez, R. L., Huber, P. E., et al. (2020). Prexasertib (LY2606368) reduces clonogenic survival by inducing apoptosis in primary patient-derived osteosarcoma cells and synergizes with cisplatin and talazoparib. *Int. J. cancer* 147 (4), 1059–1070. doi:10.1002/ijc.32814

Hengel, S. R., Spies, M. A., and Spies, M. (2017). Small-Molecule inhibitors targeting DNA repair and DNA repair deficiency in research and cancer therapy. *Cell Chem. Biol.* 24 (9), 1101–1119. doi:10.1016/j.chembiol.2017.08.027

Heo, Y. A., and Duggan, S. T. (2018). Niraparib: a review in ovarian cancer. *Target. Oncol.* 13 (4), 533–539. doi:10.1007/s11523-018-0582-1

Hoy, S. M. (2018). Talazoparib: first global approval. *Drugs* 78 (18), 1939–1946. doi:10.1007/s40265-018-1026-z

Hu, S., Hui, Z., Lirussi, F., Garrido, C., Ye, X. Y., and Xie, T. (2021). Small molecule DNA-PK inhibitors as potential cancer therapy: a patent review (2010-present). *Expert Opin. Ther. Pat.* 31 (5), 435–452. doi:10.1080/13543776.2021.1866540

Hu, Y., and Guo, M. (2020). Synthetic lethality strategies: beyond BRCA1/2 mutations in pancreatic cancer. *Cancer Sci.* 111 (9), 3111–3121. doi:10.1111/cas.14565

Huang, A., Garraway, L. A., Ashworth, A., and Weber, B. (2020). Synthetic lethality as an engine for cancer drug target discovery. *Nat. Rev. Drug Discov.* 19 (1), 23–38. doi:10.1038/s41573-019-0046-z

Italiano, A., Infante, J. R., Shapiro, G. I., Moore, K. N., LoRusso, P. M., Hamilton, E., et al. (2018). Phase I study of the checkpoint kinase 1 inhibitor GDC-0575 in combination with gemcitabine in patients with refractory solid tumors. *Ann. Oncol.* 29 (5), 1304–1311. doi:10.1093/annonc/mdy076

Ivy, S. P., Liu, J. F., Lee, J. M., Matulonis, U. A., and Kohn, E. C. (2016). Cediranib, a pan-VEGFR inhibitor, and olaparib, a PARP inhibitor, in combination therapy for high grade serous ovarian cancer. *Expert Opin. investigational drugs* 25 (5), 597–611. doi:10.1517/13543784.2016.1156857

Javed, S. R., Lord, S., El Badri, S., Harman, R., Holmes, J., Kamzi, F., et al. (2024). CHARIOT: a phase I study of berzosertib with chemoradiotherapy in oesophageal and other solid cancers using time to event continual reassessment method. *Br. J. cancer* 130 (3), 467–475. doi:10.1038/s41416-023-02542-1

Jin, T. Y., Park, K. S., Nam, S. E., Yoo, Y. B., Park, W. S., and Yun, I. J. (2022). *BRCA1/2* serves as a biomarker for poor prognosis in breast carcinoma. *Int. J. Mol. Sci.* 23 (7), 3754. doi:10.3390/ijms23073754

Kamel, D., Gray, C., Walia, J. S., and Kumar, V. (2018). PARP inhibitor drugs in the treatment of breast, ovarian, prostate and pancreatic cancers: an update of clinical trials. *Curr. drug targets* 19 (1), 21–37. doi:10.2174/1389450118666170711151518

Karnitz, L. M., and Zou, L. (2015). Molecular pathways: targeting ATR in cancer therapy. *Clin. cancer Res.* 21 (21), 4780–4785. doi:10.1158/1078-0432.CCR-15-0479

Kelley, M. R., Logsdon, D., and Fishel, M. L. (2014). Targeting DNA repair pathways for cancer treatment: what's new? *Future Oncol. Lond. Engl.* 10 (7), 1215–1237. doi:10.2217/fon.14.60

Kim, H., Xu, H., George, E., Hallberg, D., Kumar, S., Jagannathan, V., et al. (2020). Combining PARP with ATR inhibition overcomes PARP inhibitor and platinum resistance in ovarian cancer models. *Nat. Commun.* 11 (1), 3726. doi:10.1038/s41467-020-17127-2

Kim, S. T., Smith, S. A., Mortimer, P., Loembé, A. B., Cho, H., Kim, K. M., et al. (2021). Phase I study of ceralasertib (AZD6738), a novel DNA damage repair agent, in combination with weekly paclitaxel in refractory cancer. *Clin. cancer Res.* 27 (17), 4700–4709. doi:10.1158/1078-0432.CCR-21-0251

Konstantinopoulos, P. A., Lee, J. M., Gao, B., Miller, R., Lee, J. Y., Colombo, N., et al. (2022). A Phase 2 study of prexasertib (LY2606368) in platinum resistant or refractory recurrent ovarian cancer. *Gynecol. Oncol.* 167 (2), 213–225. doi:10.1016/j.ygyno.2022.09.019

Konstantinopoulos, P. A., Waggoner, S., Vidal, G. A., Mita, M., Moroney, J. W., Holloway, R., et al. (2019). Single-arm phases 1 and 2 trial of Niraparib in combination with Pembrolizumab in patients with recurrent platinum-resistant ovarian carcinoma. *JAMA Oncol.* 5 (8), 1141–1149. doi:10.1001/jamaoncol.2019.1048

Kristeleit, R., Plummer, R., Jones, R., Carter, L., Blagden, S., Sarker, D., et al. (2023). A Phase 1/2 trial of SRA737 (a Chk1 inhibitor) administered orally in patients with advanced cancer. *Br. J. cancer* 129 (1), 38–45. doi:10.1038/s41416-023-02279-x

Lampert, E. J., Zimmer, A., Padget, M., Cimino-Mathews, A., Nair, J. R., Liu, Y., et al. (2020). Combination of PARP inhibitor olaparib, and PD-L1 inhibitor durvalumab, in recurrent ovarian cancer: a proof-of-concept phase II study. *Clin. cancer Res.* 26 (16), 4268–4279. doi:10.1158/1078-0432.CCR-20-0056

Lecona, E., and Fernandez-Capetillo, O. (2018). Targeting ATR in cancer. *Nat. Rev. Cancer* 18 (9), 586–595. doi:10.1038/s41568-018-0034-3

Ledermann, J., Harter, P., Gourley, C., Friedlander, M., Vergote, I., Rustin, G., et al. (2012). Olaparib maintenance therapy in platinum-sensitive relapsed ovarian cancer. *N. Engl. J. Med.* 366 (15), 1382–1392. doi:10.1056/NEJMoa1105535

Li, M., Huang, T., Li, X., Shi, Z., Sheng, Y., Hu, M., et al. (2021). GDC-0575, a CHK1 inhibitor, impairs the development of colitis and colitis-associated cancer by inhibiting CCR2+ macrophage infiltration in mice. *OncoTargets Ther.* 14, 2661–2672. doi:10.2147/OTT.S297132

Lieber, M. R. (2010). The mechanism of double-strand DNA break repair by the nonhomologous DNA end-joining pathway. *Annu. Rev. Biochem.* 79, 181–211. doi:10.1146/annurev.biochem.052308.093131

Litton, J. K., Rugo, H. S., Ettl, J., Hurvitz, S. A., Gonçalves, A., Lee, K. H., et al. (2018). Talazoparib in patients with advanced breast cancer and a germline BRCA mutation. *N. Engl. J. Med.* 379 (8), 753–763. doi:10.1056/NEJMoa1802905

Lok, B. H., Gardner, E. E., Schneeberger, V. E., Ni, A., Desmeules, P., Rekhtman, N., et al. (2017). PARP inhibitor activity correlates with SLFN11 expression and demonstrates synergy with temozolomide in small cell lung cancer. *Clin. cancer Res.* 23 (2), 523–535. doi:10.1158/1078-0432.CCR-16-1040

Lord, C. J., and Ashworth, A. (2017). PARP inhibitors: synthetic lethality in the clinic. *Sci. (New York, N.Y.)* 355 (6330), 1152–1158. doi:10.1126/science.aam7344

Lücking, U., Wortmann, L., Wengner, A. M., Lefranc, J., Lienau, P., Briem, H., et al. (2020). Damage incorporated: discovery of the potent, highly selective, orally available ATR inhibitor BAY 1895344 with favorable pharmacokinetic properties and promising efficacy in monotherapy and in combination treatments in preclinical tumor models. *J. Med. Chem.* 63 (13), 7293–7325. doi:10.1021/acs.jmedchem.0c00369

Malaquin, N., Carrier-Leclerc, A., Dessureault, M., and Rodier, F. (2015). DDR-mediated crosstalk between DNA-damaged cells and their microenvironment. *Front. Genet.* 6, 94. doi:10.3389/fgene.2015.00094

Markowski, M. C., Sternberg, C. N., Wang, H., Wang, T., Linville, L., Marshall, C. H., et al. (2024). TRIUMPH: phase II trial of rucaparib monotherapy in patients with

metastatic hormone-sensitive prostate cancer harboring germline homologous recombination repair gene mutations. *Oncol.* 29, 794–800. doi:10.1093/oncolo/oyae120

Matheson, C. J., Backos, D. S., and Reigan, P. (2016). Targeting WEE1 kinase in cancer. *Trends Pharmacol. Sci.* 37 (10), 872–881. doi:10.1016/j.tips.2016.06.006

Matsuoka, S., Ballif, B. A., Smogorzewska, A., McDonald, E. R., 3rd, Hurov, K. E., Luo, J., et al. (2007). ATM and ATR substrate analysis reveals extensive protein networks responsive to DNA damage. *Sci. (New York, N.Y.)* 316 (5828), 1160–1166. doi:10.1126/science.1140321

McPherson, K. S., and Korzhnev, D. M. (2021). Targeting protein-protein interactions in the DNA damage response pathways for cancer chemotherapy. *RSC Chem. Biol.* 2 (4), 1167–1195. doi:10.1039/d1cb00101a

Merry, C., Fu, K., Wang, J., Yeh, I. J., and Zhang, Y. (2010). Targeting the checkpoint kinase Chk1 in cancer therapy. *Cell Cycle* 9 (2), 279–283. doi:10.4161/cc.9.2.10445

Min, A., and Im, S. A. (2020). PARP inhibitors as therapeutics: beyond modulation of PARylation. *Cancers* 12 (2), 394. doi:10.3390/cancers12020394

Min, A., Im, S. A., Jang, H., Kim, S., Lee, M., Kim, D. K., et al. (2017). AZD6738, A novel oral inhibitor of ATR, induces synthetic lethality with ATM deficiency in gastric cancer cells. *Mol. cancer Ther.* 16 (4), 566–577. doi:10.1158/1535-7163.MCT-16-0378

Minchom, A., Aversa, C., and Lopez, J. (2018). Dancing with the DNA damage response: next-generation anti-cancer therapeutic strategies. *Ther. Adv. Med. Oncol.* 10, 1758835918786658. doi:10.1177/1758835918786658

Mirza, M. R., Monk, B. J., Herrstedt, J., Oza, A. M., Mahner, S., Redondo, A., et al. (2016). Niraparib maintenance therapy in platinum-sensitive, recurrent ovarian cancer. *N. Engl. J. Med.* 375 (22), 2154–2164. doi:10.1056/NEJMoa1611310

Mullard, A. (2017). Synthetic lethality screens point the way to new cancer drug targets. *Nat. Rev. Drug Discov.* 16 (9), 589–591. doi:10.1038/nrd.2017.165

Munster, P., Mita, M., Mahipal, A., Nemunaitis, J., Massard, C., Mikkelsen, T., et al. (2019). First-in-human phase I study of A dual mTOR kinase and DNA-PK inhibitor (CC-115) in advanced malignancy. *Cancer Manag. Res.* 11, 10463–10476. doi:10.2147/CMAR.S208720

Murai, J., Huang, S. Y., Das, B. B., Renaud, A., Zhang, Y., Doroshow, J. H., et al. (2012). Trapping of PARP1 and PARP2 by clinical PARP inhibitors. *Cancer Res.* 72 (21), 5588–5599. doi:10.1158/0008-5472.CAN-12-2753

Nickoloff, J. A., Boss, M. K., Allen, C. P., and LaRue, S. M. (2017). Translational research in radiation-induced DNA damage signaling and repair. *Transl. cancer Res.* 6 (Suppl. 5), S875–S891. doi:10.21037/tcr.2017.06.02

Obata, H., Ogawa, M., and Zalutsky, M. R. (2023). DNA repair inhibitors: potential targets and partners for targeted radionuclide therapy. *Pharmaceutics* 15 (7), 1926. doi:10.3390/pharmaceutics15071926

O'Connor, M. J. (2015). Targeting the DNA damage response in cancer. *Mol. Cell* 60 (4), 547–560. doi:10.1016/j.molcel.2015.10.040

Okabe, S., Tanaka, Y., Moriyama, M., and Gotoh, A. (2023). WEE1 and PARP-1 play critical roles in myelodysplastic syndrome and acute myeloid leukemia treatment. *Cancer Cell Int.* 23 (1), 128. doi:10.1186/s12935-023-02961-3

O'Neil, N. J., Bailey, M. L., and Hieter, P. (2017). Synthetic lethality and cancer. *Nat. Rev. Genet.* 18 (10), 613–623. doi:10.1038/nrg.2017.47

Pascal, J. M. (2018). The comings and goings of PARP-1 in response to DNA damage. *DNA repair* 71, 177–182. doi:10.1016/j.dnarep.2018.08.022

Pike, K. G., Barlaam, B., Cadogan, E., Campbell, A., Chen, Y., Colclough, N., et al. (2018). The identification of potent, selective, and orally available inhibitors of ataxia telangiectasia mutated (ATM) kinase: the discovery of AZD0156 (8-{6-[3-(Dimethylamino)propoxy]pyridin-3-yl}-3-methyl-1-(tetrahydro-2 H-pyran-4-yl)-1,3-dihydro-2 H-imidazo[4,5- c]quinolin-2-one). *J. Med. Chem.* 61 (9), 3823–3841. doi:10.1021/acs.jmedchem.7b01896

Pilié, P. G., Tang, C., Mills, G. B., and Yap, T. A. (2019). State-of-the-art strategies for targeting the DNA damage response in cancer. *Nat. Rev. Clin. Oncol.* 16 (2), 81–104. doi:10.1038/s41571-018-0114-z

Pospisilova, M., Seifrtova, M., and Rezacova, M. (2017). Small molecule inhibitors of DNA-PK for tumor sensitization to anticancer therapy. *J. physiology Pharmacol.* 68 (3), 337–344.

Rahman, R., Trippa, L., Lee, E. Q., Arrillaga-Romany, I., Fell, G., Touat, M., et al. (2023). Inaugural results of the individualized screening trial of innovative glioblastoma therapy: a phase II platform trial for newly diagnosed glioblastoma using bayesian adaptive randomization. *J. Clin. Oncol.* 41 (36), 5524–5535. doi:10.1200/JCO.23.00493

Ricciuti, B., Recondo, G., Spurr, L. F., Li, Y. Y., Lamberti, G., Venkatraman, D., et al. (2020). Impact of DNA damage response and repair (DDR) gene mutations on efficacy of PD-(L)1 immune checkpoint inhibition in non-small cell lung cancer. *Clin. cancer Res.* 26 (15), 4135–4142. doi:10.1158/1078-0432.CCR-19-3529

Rundle, S., Bradbury, A., Drew, Y., and Curtin, N. J. (2017). Targeting the ATR-CHK1 Axis in cancer therapy. *Cancers* 9 (5), 41. doi:10.3390/cancers9050041

Sancar, A. (1995). DNA repair in humans. *Annu. Rev. Genet.* 29 (1), 69–105. doi:10.1146/annurev.ge.29.120195.000441

Savva, C., De Souza, K., Ali, R., Rakha, E. A., Green, A. R., and Madhusudan, S. (2019). Clinicopathological significance of ataxia telangiectasia-mutated (ATM) kinase and ataxia telangiectasia-mutated and Rad3-related (ATR) kinase in MYC overexpressed breast cancers. *Breast cancer Res. Treat.* 175 (1), 105–115. doi:10.1007/s10549-018-05113-8

Sheng, H., Huang, Y., Xiao, Y., Zhu, Z., Shen, M., Zhou, P., et al. (2020). ATR inhibitor AZD6738 enhances the antitumor activity of radiotherapy and immune checkpoint inhibitors by potentiating the tumor immune microenvironment in hepatocellular carcinoma. *J. Immunother. cancer* 8 (1), e000340. doi:10.1136/jitc-2019-000340

Shirley, M. (2019). Rucaparib: a review in ovarian cancer. *Target. Oncol.* 14 (2), 237–246. doi:10.1007/s11523-019-00629-5

Shrivastav, M., Miller, C. A., De Haro, L. P., Durant, S. T., Chen, B. P., Chen, D. J., et al. (2009). DNA-PKcs and ATM co-regulate DNA double-strand break repair. *DNA repair* 8 (8), 920–929. doi:10.1016/j.dnarep.2009.05.006

Slade, D. (2020). PARP and PARG inhibitors in cancer treatment. *Genes and Dev.* 34 (5-6), 360–394. doi:10.1101/gad.334516.119

Swisher, E. M., Lin, K. K., Oza, A. M., Scott, C. L., Giordano, H., Sun, J., et al. (2017). Rucaparib in relapsed, platinum-sensitive high-grade ovarian carcinoma (ARIEL2 Part 1): an international, multicentre, open-label, phase 2 trial. *Lancet. Oncol.* 18 (1), 75–87. doi:10.1016/S1470-2045(16)30559-9

Tang, L., Chen, R., and Xu, X. (2020). Synthetic lethality: a promising therapeutic strategy for hepatocellular carcinoma. *Cancer Lett.* 476, 120–128. doi:10.1016/j.canlet.2020.02.016

Tang, Q., Wang, X., Wang, H., Zhong, L., and Zou, D. (2024). Advances in ATM, ATR, WEE1, and CHK1/2 inhibitors in the treatment of PARP inhibitor-resistant ovarian cancer. *Cancer Biol. and Med.* 20 (12), 915–921. doi:10.20892/j.issn.2095-3941.2023.0260

Teo, M. Y., Bambury, R. M., Zabor, E. C., Jordan, E., Al-Ahmadie, H., Boyd, M. E., et al. (2017). DNA damage response and repair gene alterations are associated with improved survival in patients with platinum-treated advanced urothelial carcinoma. *Clin. cancer Res.* 23 (14), 3610–3618. doi:10.1158/1078-0432.CCR-16-2520

Thomas, A., Redon, C. E., Sciuto, L., Padiernos, E., Ji, J., Lee, M. J., et al. (2018). Phase I study of ATR inhibitor M6620 in combination with topotecan in patients with advanced solid tumors. *J. Clin. Oncol.* 36 (16), 1594–1602. doi:10.1200/JCO.2017.76.6915

Timme, C. R., Rath, B. H., O'Neill, J. W., Camphausen, K., and Tofilon, P. J. (2018). The DNA-PK inhibitor VX-984 enhances the radiosensitivity of glioblastoma cells grown *in vitro* and as orthotopic xenografts. *Mol. cancer Ther.* 17 (6), 1207–1216. doi:10.1158/1535-7163.MCT-17-1267

Webster, J. A., Tibes, R., Morris, L., Blackford, A. L., Litzow, M., Patnaik, M., et al. (2017). Randomized phase II trial of cytosine arabinoside with and without the CHK1 inhibitor MK-8776 in relapsed and refractory acute myeloid leukemia. *Leukemia Res.* 61, 108–116. doi:10.1016/j.leukres.2017.09.005

Wengner, A. M., Siemeister, G., Lücking, U., Lefranc, J., Wortmann, L., Lienau, P., et al. (2020). The novel ATR inhibitor BAY 1895344 is efficacious as monotherapy and combined with DNA damage-inducing or repair-compromising therapies in preclinical cancer models. *Mol. cancer Ther.* 19 (1), 26–38. doi:10.1158/1535-7163.MCT-19-0019

Yang, H., Yao, F., Marti, T. M., Schmid, R. A., and Peng, R. W. (2020). Beyond DNA repair: DNA-PKcs in tumor metastasis, metabolism and immunity. *Cancers* 12 (11), 3389. doi:10.3390/cancers12113389

Yang, J., Xu, Z. P., Huang, Y., Hamrick, H. E., Duerksen-Hughes, P. J., and Yu, Y. N. (2004). ATM and ATR: sensing DNA damage. *World J. gastroenterology* 10 (2), 155–160. doi:10.3748/wjg.v10.i2.155

Yang, Y., Shaffer, A. L., 3rd, Emre, N. C., Ceribelli, M., Zhang, M., Wright, G., et al. (2012). Exploiting synthetic lethality for the therapy of ABC diffuse large B cell lymphoma. *Cancer Cell* 21 (6), 723–737. doi:10.1016/j.ccr.2012.05.024

Yap, T. A., Tan, D. S. P., Terbuch, A., Caldwell, R., Guo, C., Goh, B. C., et al. (2021). First-in-Human trial of the oral ataxia telangiectasia and RAD3-related (ATR) inhibitor BAY 1895344 in patients with advanced solid tumors. *Cancer Discov.* 11 (1), 80–91. doi:10.1158/2159-8290.CD-20-0868

Zenke, F. T., Zimmermann, A., Sirrenberg, C., Dahmen, H., Kirkin, V., Pehl, U., et al. (2020). Pharmacologic inhibitor of DNA-PK, M3814, potentiates radiotherapy and regresses human tumors in mouse models. *Mol. cancer Ther.* 19 (5), 1091–1101. doi:10.1158/1535-7163.MCT-19-0734

Zhang, Y., and Hunter, T. (2014). Roles of Chk1 in cell biology and cancer therapy. *Int. J. cancer* 134 (5), 1013–1023. doi:10.1002/ijc.28226

Zhao, J. L., Antonarakis, E. S., Cheng, H. H., George, D. J., Aggarwal, R., Riedel, E., et al. (2024). Phase 1b study of enzalutamide plus CC-115, a dual mTORC1/2 and DNA-PK inhibitor, in men with metastatic castration-resistant prostate cancer (mCRPC). *Br. J. cancer* 130 (1), 53–62. doi:10.1038/s41416-023-02487-5

frontiers | Frontiers in Pharmacology

TYPE Original Research
PUBLISHED 11 November 2024
DOI 10.3389/fphar.2024.1487940

OPEN ACCESS

EDITED BY
Milica Pešić,
University of Belgrade, Serbia

REVIEWED BY
Shushu Zhao,
Wistar Institute, United States
Aleksandra Jaukovic,
University of Belgrade, Serbia

*CORRESPONDENCE
Ting Wang,
wangtingyaoli@foxmail.com
Xingang Guan,
guanxg@tzc.edu.cn
Hongxia Feng,
fenghongxia0472@163.com

†These authors have contributed equally to this work

RECEIVED 29 August 2024
ACCEPTED 30 October 2024
PUBLISHED 11 November 2024

CITATION
Liu Y, Yang F, Li Z, Wang T, Mu Y, Fan Y, Xue H, Hu X, Guan X and Feng H (2024) Concurrent immune checkpoint blockade for enhanced cancer immunotherapy utilizing engineered hybrid nanovesicles.
Front. Pharmacol. 15:1487940.
doi: 10.3389/fphar.2024.1487940

Concurrent immune checkpoint blockade for enhanced cancer immunotherapy utilizing engineered hybrid nanovesicles

Yuxuan Liu[1,2†], Fuxu Yang[2†], Zhimin Li[2†], Ting Wang[3*], Yeteng Mu[2], Yuxin Fan[2], Han Xue[2], Xiuli Hu[4], Xingang Guan[3*] and Hongxia Feng[1*]

[1]Department of Dermatology, The Affiliated Wenling Hospital of Taizhou University, Taizhou, China, [2]College of Medical Technology, Beihua University, Jilin, China, [3]Medical School, Taizhou University, Taizhou, China, [4]Institute of Polymer Science and Engineering, School of Chemical Engineering, Hebei University of Technology, Tianjin, China

Immune checkpoint inhibitors (ICIs) have revolutionized cancer treatment, demonstrating unprecedented efficacy against advanced cancers. However, their clinical applications are significantly hampered by low overall response rates. Dual blockade of two immune checkpoints represents a promising strategy to enhance immunotherapeutic efficacy. In this study, we developed hybrid cell membrane nanovesicles adorned with PD-1 and SIRPα receptors for combination immunotherapy in melanoma. Our hybrid nanovesicles (PD-1/SIRPα NVs) demonstrated high specificity to PD-L1 and CD47 ligands, facilitating the phagocytosis of melanoma cells by macrophages. In a melanoma mouse model, PD-1/SIRPα NVs significantly suppressed 77% of tumor growth and elicited a robust antitumor immune response for immunotherapy. In conclusion, our findings highlight the promising potential of PD-1/SIRPα NVs as novel and effective ICIs for cancer immunotherapy.

KEYWORDS

PD-1, SIRPα, cell membrane nanovesicle, immune checkpoint blockade, cancer immunotherapy

1 Introduction

Immune checkpoint inhibitors (ICIs), aimed to revive the exhausted immune cells for systemic antitumor immune response, have revolutionized cancer treatment with unprecedented efficacy in treating many advanced cancers (Johnson et al., 2022; Bagchi et al., 2021). Despite their great clinical success, only a few patients benefit from ICIs as a single treatment. Low response, immune-related adverse events (irAEs), and tumor resistance significantly limit the further application of ICIs (Bagchi et al., 2021; de Miguel and Calvo, 2020). Hence, there is an urgent need to develop novel drugs with enhanced efficacy for cancer immunotherapy (Fang W. et al., 2023; Chen et al., 2023).

Combining ICIs targeting two (or more) immune checkpoint receptors represents an effective strategy for improved cancer treatment (Willsmore et al., 2021; Burton and Tawbi, 2021). For example, combination therapy with anti-CTLA-4 plus anti-PD-1/PD-L1 has shown an outperformed therapeutic effect over single ICIs treatment in melanoma and non-small cell lung cancer (NSCLC) (Chae et al., 2018). The FDA recently approved a combination of PD-1 inhibitor (nivolumab) with LAG-3 inhibitor (relatlimab-rmbw) to

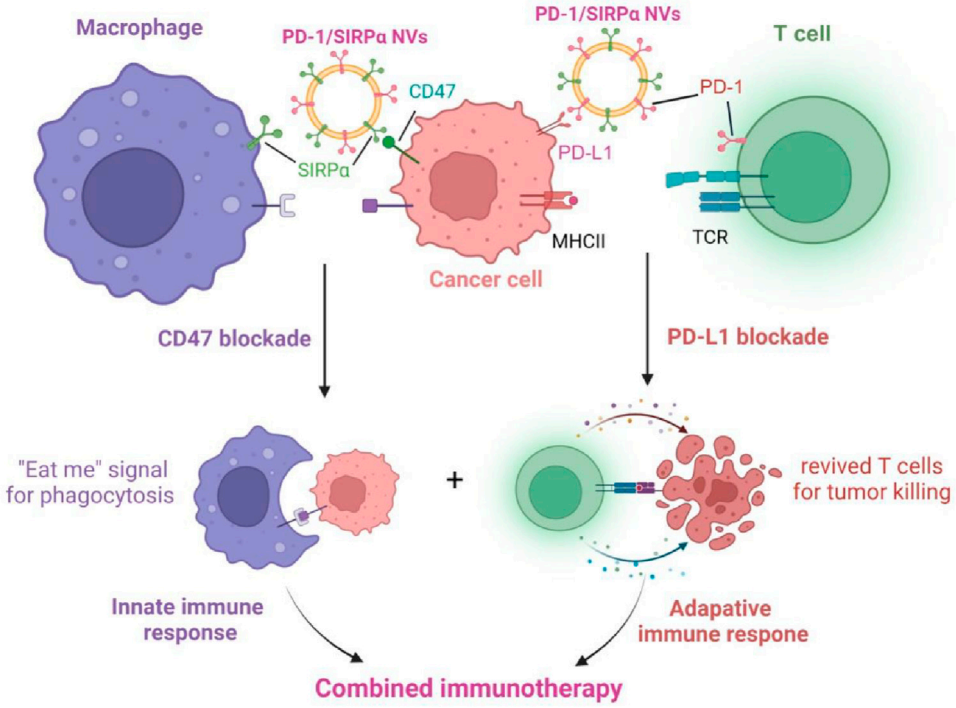

SCHEME 1
Schematic illustration of the mechanism of PD-1/SIRPα nanovesicles disrupting PD-L1/PD-1 and CD47/SIRPα axes for enhanced cancer immunotherapy.

treat advanced melanoma. PD-1/LAG-3 co-blockade showed prolonged progression-free survival and enhanced objective response rates in cancer patients compared to PD-1 blockade monotherapy (Abi-Aad et al., 2023). Given the superior efficacy of dual immune checkpoint inhibitor blockade, developing smart formulations (et. bispecific antibody, nanoparticle, fusion protein) for killing two birds with one stone holds advantageous potential for potentiated cancer immunotherapy (Wang R. et al., 2023; Gao et al., 2023; Meng et al., 2021).

The significant advance in nanotechnology has opened a new avenue for effective cancer therapy (Fan et al., 2023; Ren et al., 2021). Cell membrane nanovesicles (CMN) have emerged as a promising delivery platform in tumor diagnosis and cancer treatment (Le et al., 2021; Yang et al., 2022; Zhao et al., 2024). Due to the natural cell-derived biomaterial, cell membranes have inherently good biocompatibility and reduced immunogenicity for therapeutic use (Cheng et al., 2023). When transformed into nanovesicles, CMN exhibits good stability and prolonged circulation *in vivo* compared with synthetic nanocarriers (Mu et al., 2023). More importantly, CMN can be engineered to display a variety of functional proteins on the outer surface, conferring nanovesicles targeting delivery, therapeutic potential, or immunomodulatory properties for treating diseases (Fang T. et al., 2023; Yu et al., 2022; Zhang et al., 2023). Furthermore, by incorporating various therapeutic agents into its inner cavity, CMN could be developed into a versatile platform for combination cancer therapy (Hu et al., 2024; Wang M. et al., 2023). Notably, due to the inherent fusion ability of cell membranes, hybrid CMN could be prepared using two or more types of cell membranes for multifunctional application (Rao et al., 2020; Sun et al., 2023; Guo et al., 2024; Peng et al., 2024).

Herein, we fabricated a hybrid cell membrane nanovesicle with PD-1 and SIRPα co-decoration for combination immunotherapy in melanoma. Given the vital roles of PD-1/PD-L1 and SIRPα/CD47 axes in releasing 'do not find me' and 'do not eat me' signals (Xiao et al., 2023; Luo J. Q. et al., 2023), we aim to simultaneously disrupt these signals for inducing innate and adaptive immunity using an engineered nanovesicle (Scheme 1). *In vitro* cellular uptake, tumor-selective binding, and *in vivo* antitumor efficacy of PD-1/SIRPα NVs were investigated in detail.

2 Materials and methods

2.1 Materials

The lentiviral plasmids carrying PD-1-GFP or SIRPα-GFP were purchased from Origen. CellTracker Green and Red were purchased from Thermo Fisher. Antibodies targeting PD-1, SIRPα, and Na^+K^+ ATPase for Western blot analysis were purchased from Abcam. All antibodies used for blocking and flow cytometry in this study were obtained from BioLegend. 4′,6-diamidino-2-phenylindole (DAPI), perchlorate (DiO), perchlorate (DiI), and Cell Counting Kit-8 were purchased from Beyotime. Serum tumor necrosis factor-alpha (TNF-α) and interferon-γ (IFN-γ) ELISA kits were purchased from Keygen Biotech.

2.2 Cell culture

Murine melanoma cell B16F10, dendritic cells DC2.4, and HEK293T cells were cultured in Dulbecco's Modified Eagle's Medium (DMEM) containing 10% Fetal Bovine Serum (FBS) in a cell incubator at 37°C and 5% CO_2.

2.3 Preparation of PD-1 or SIRPα stable cells

Stable cells expressing mouse PD-1 or SIRPα receptors were prepared by transfecting lentiviral vectors carrying PD-1-GFP or SIRPα-GFP into HEK293T cells. Briefly, HEK293T cells were seeded in a six-well plate at a density of 1×10^6 per well. On the second day, Opti-MEM medium containing 6 μL Lipofectamine 3,000 reagent or 4 μg lentiviral plasmids was mixed at room temperature for 15 min and added into cells. After 2 days of transfection, the transfected cells were cultured under the puromycin selection (5 μg/mL). Stable cell lines with PD-1 or SIRPα expression were obtained from single-cell colonies through limited dilution.

2.4 Synthesis and characterization of PD-1/SIRPα NVs

HEK293T cells stably expressing SIRPα-GFP and PD-1-GFP were cultured in a DMEM medium containing 10% FBS. The Cells were washed at least three times with cold PBS by centrifuging at 1,000 rpm. Then, the cells were disrupted in a homogenization medium (HM) containing 0.25 M sucrose, 1 mM EDTA, 20 mM Hepes-NaOH, pH 7.4, and a proteinase inhibitor mixture by a Dounce homogenizer for at least 50 times on ice. The supernatant obtained after low-speed centrifugation of entire solutions was ultracentrifuged at 35,000 rpm for 2 h. The pellets were collected and washed with HM buffer containing proteinase inhibitor three times and then resuspended with suitable PBS. After sonicating for 5 min, the cell membranes in PBS finally passed stepwise through 1.0 and 0.4 μm nanopore polycarbonate membranes on an extruder at least 20 times. PD-1 NVs and SIRPα NVs were obtained. As for the hybrid nanovesicle preparation, the PD-1 cell membrane and SIRPα cell membrane were mixed (protein weight ratio of 1:1) and then extruded through 0.4 μm pores on the mini extruder. The obtained nanovesicle was named PD-1/SIRPα NVs. The quantification of nanovesicles was determined by measuring the total protein content within the nanovesicles using a BCA assay. The hydrodynamic diameter and zeta potential of cell membrane nanovesicles were monitored by dynamic light scatter (DLS). The morphologies of NVs were also observed by using transmission electron microscopy (TEM).

2.5 Biocompatibility analysis

Five thousand DC2.4 cells were seeded into each well in a 96-well plate and cultured for 12 h. Different concentrations of PD-1/SIRPα NVs were added to the cell medium for 48 h incubation. CCK-8 solution was added to each well for 4 h at 37°C. The absorbance of the solution in each well was determined at 450 nm wavelength using a microplate reader (TECAN M200).

2.6 *In vitro* blockade analysis

In vitro blockade analysis was performed by assessing the inhibitory binding effect of aPD-L1 on the interaction between nanovesicles and melanoma cells. Dil-labeled PD-1/SIRPα NVs were utilized to track the binding ability. B16F10 cells were seeded in a 12-well plate containing at a density of 2×10^5 cells per well for 12 h. On the second day, the melanoma cells were treated with CD47 antibody solution (50 μg/mL in DMEM), PD-L1 antibody solution (50 μg/mL in DMEM), or CD47 antibody plus PD-L1 antibody solution for 4 h at 37°C. PBS solution was used as a control. The cells were treated with Dil-labeled PD-1/SIRPα NVs for 2 h. After washing with PBS, the melanoma cells were subjected to flow cytometry analysis (gated at PE channel).

2.7 Nanovesicles binding assay

B16F10 cells were seeded in a six-well plate and cultured for 12 h. On the second day, mouse red blood cells (RBC) were added to the well. Dil-labeled PD-1/SIRPα NVs (100 μg/mL) were added to the wells containing mixed cells and incubated for 4 h. After that, RBCs were isolated from the supernatant, while B16F10 cells were digested with trypsin and collected. The nanovesicle binding was analyzed by flow cytometry.

2.8 *In vitro* phagocytosis assay

Bone marrow-derived macrophages (BMDMs) were isolated from C57BL/6 mice according to the literature. The femur and tibia were taken from mice to acquire bone marrow cells. After spinning at 1,000 rpm for 5 min, the bone marrow cells were mixed with red blood cell lysis buffer at room temperature for 3 min to clear away red blood cells. The marrow cells were washed and placed in DMEM with monocyte colony-stimulating factor (50 ng/mL) for 7 days. Fresh DMEM with M-CSF was changed every 2 days. At the 7-day mark, the sticking cells were colored with CD11b and F4/80 antibodies from Biolegend. The colored cells were confirmed to be BMDMs for later use.

We explored the phagocytosis of tumor cells using BMDMs isolated from C57BL/6 mice. The isolated BMDMs were cultured in DMEM supplemented with 20 ng/mL monocyte colony-stimulating factor (M-CSF) for 7 days to promote differentiation into macrophages. BMDMs were labeled with CellTracker Green, while B16F10 melanoma cells were stained with CellTracker Red. BMDMs were seeded at a density of 2×10^5 cells per well in a six-well plate and cultured overnight. Cells were then exposed to aCD47 or PD-1/SIRPα NVs in a serum-free medium for 2 h. Subsequently, CellTracker Red-stained B16F10 melanoma cells were added, and the mixture was incubated at 37°C for 4 h. After three washes, the uptake of B16F10 cells (labeled red) by BMDMs (labeled green) was visualized using fluorescent microscopy.

2.9 *In vivo* antitumor assay

All animal experiments were conducted following the National Institutes of Health Guidelines for the Care and Use of Laboratory Animals, and the guidelines were approved by the Animal Protection and Utilization Committee of Taizhou University (Taizhou, Zhejiang). Five million B16F10 cells were implanted into the right flanks of female C57BL/6 mice to obtain subcutaneous melanoma xenograft. When the tumor size reached 50–80 mm^3, mice were randomly divided into five groups (n = 5): PBS, Blank NVs (prepared by HEK293T cell membrane without immune checkpoint receptors), PD-1 NVs, SIRPα NVs, and PD-1/SIRPα NVs. The mice were treated with PBS, Blank NVs (25 mg/kg, protein weight), PD-1 NVs (25 mg/kg, protein weight), SIRPα NVs (25 mg/kg, protein weight), and PD-1/SIRPα NVs (25 mg/kg, protein weight) for five times every 3 days via tail vein injection. Tumors volume (V) was calculated to be $V = d^2 \times D/2$, where d is the shortest, and D is the longest diameter of the tumor, respectively. Animals were euthanized when exhibiting signs of impaired health or when the tumor volume exceeded 2 cm^3.

2.10 Flow cytometry

Immune cells infiltrated in tumor tissues were isolated for flow cytometry. The cell suspension was filtered with a 200 mesh filter and centrifuged at 1,000 rpm for 5 min. The collected cells were treated with the Zombie Violet dye Fixable Viability Kit and blocked with the FC blocking antibody CD16/32 (clone 93). Antibodies targeting CD45 (PerCP-Cyanine5.5; clone 30-F11), CD3 (APC; clone 17A2), CD8a (PE; clone 53–6.7), CD4 (FITC; clone GK1.5), CD80 (PECyanine7; clone 16-10A1), CD86 (APC; clone GL-1), CD206 (APC; clone C068C2) (Biolegend) were used to stain the relative protein. After washing with PBS, the cell suspensions were subjected to a CytoFLEX flow cytometer (Beckman) with CytoExpert software (Beckman Coulter).

2.11 Tissue section staining and cytokine detection

Mouse tumors and main organs, including heart, liver, spleen, lung, and kidney, were collected and subjected to hematoxylin and eosin (H&E) staining. Serum samples were isolated from mice treated with different formulations on day 15th after injection. According to the manufacturer's protocols, the IFN-γ and TNF-α in serum were determined by ELISA (KeyGen).

2.12 Statistical analysis

All results are expressed as the mean ± standard deviation. Statistical analysis was performed using SPSS software. One-way or two-way analysis of variance (ANOVA) and Tukey *post hoc* tests were used when more than two groups were compared (multiple comparisons) as indicated. All statistical analyses were carried out using the IBM SPSS statistics 19. The threshold for statistical significance was $P < 0.05$.

3 Results

3.1 Preparation and characterization of PD-1/SIRPα NVs

To achieve hybrid nanovesicles presenting PD-1 and SIRPα receptors, we generated stable cell lines expressing PD-1-GFP or SIRPα-GFP in HEK293T cells, chosen for their high membrane receptor expression. The stable cell lines were created via transfection with lentiviral plasmids carrying PD-1-GFP or SIRPα-GFP and selection with puromycin using a limited dilution method. Confocal laser scanning microscopy (CLSM) demonstrated the co-localization of PD-1 or SIRPα proteins with the cell membrane probe (Dil), indicating successful membrane expression of the two immune checkpoint receptors (Figure 1A). PD-1 or SIRPα-decorated cell membranes were then isolated via ultracentrifugation and transformed into PD-1 nanovesicles (PD-1 NVs) or SIRPα nanovesicles (SIRPα NVs) by extruding them through 1.0, 0.4, and 0.2 μm pore-sized polycarbonate membrane filters. Finally, PD-1/SIRPα NVs were prepared by extruding mixed cell membranes (protein ratio 1:1) through the mentioned filters. Dynamic light scattering (DLS) analysis revealed that PD-1/SIRPα NVs have a mean diameter of 190.6 nm (Figure 1B). The zeta potential of the hybrid NVs was determined to be −11.5 mV. Morphological analysis via transmission electron microscopy (TEM) indicated that the hybrid nanovesicles possessed a hollow sphere nanostructure (Figure 1C). Additionally, Western blotting analysis confirmed the presence of PD-1 and SIRPα proteins in the hybrid nanovesicles (Figure 1D).

3.2 Bioactivity analysis of PD-1/SIRPα NVs

We conducted stability assessments of PD-1/SIRPα NVs in a PBS solution (pH 7.4) over 15 days, revealing no significant changes in size, indicating robust colloidal stability (Figure 2A). Additionally, we evaluated the biocompatibility of PD-1/SIRPα NVs in DC2.4 cells through a CCK8 assay, demonstrating good compatibility across all tested concentrations (Figure 2B). Furthermore, the internalization of PD-1/SIRPα NVs was examined in B16F10 melanoma cells using CLSM analysis. Dil-labeled hybrid nanovesicles were incubated with melanoma cells for 4 hours at 37°C, revealing red fluorescent spots distributed within the cytoplasm, indicating efficient cellular uptake of our nanovesicles in melanoma cells (Figure 2C).

We examined whether our hybrid nanovesicles could block PD-L1 and CD47 ligands on cancer cells simultaneously, given their co-expression of PD-1 and SIRPα receptors. B16F10 melanoma cells, known for PD-L1 and CD47 overexpression, were used for checkpoint block assay. The cancer cells were pre-treated with aPD-L1 and aCD47 antibodies for 4 hours, followed by a two-hour incubation with Dil-labeled PD-1/SIRPα NVs. The resulting cancer cells with fluorescent nanovesicle binding were analyzed using flow cytometry. Our findings showed that aPD-L1 or aCD47 treatments significantly reduced nanovesicle binding compared to PBS treatment. aPD-L1 plus aCD47 treatment resulted in the depletion of approximately half of the tumor-bound nanovesicles (Figures 2D,E). These outcomes underscore the promising potential of PD-1/SIRPα NVs for concurrent immune checkpoint blockade.

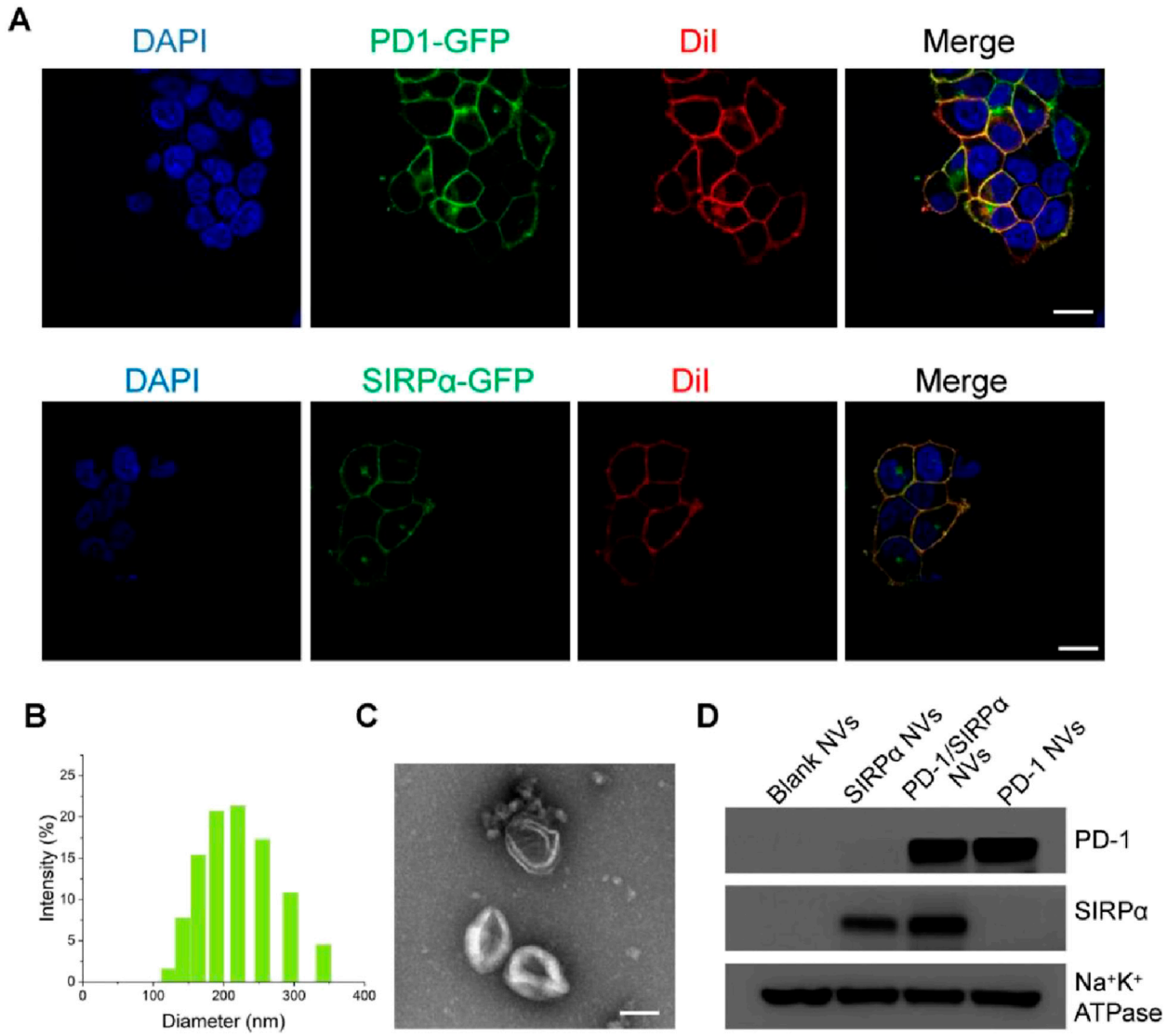

FIGURE 1
Preparation and characterization of PD-1/SIRPα NVs. **(A)** Confocal microscopy images of PD-1 and SIRPα stable cell lines. Stable cell lines were obtained by transfecting lentiviral vectors carrying PD-1-GFP or SIRPα-GFP through limited dilution. The cell membranes were stained with the membrane dye DiI (red). Scale bar: 10 μm. **(B)** Size distribution of PD-1/SIRPα NVs in PBS solution determined by dynamic light scattering (DLS). **(C)** Morphology analysis of PD-1/SIRPα NVs by TEM. Scale bar: 100 nm. **(D)** Western blot analysis of PD-1 and SIRPα protein expression in hybrid nanovisicles. Na^+K^+ ATPase was used as a positive control for membrane protein retained in cell membrane nanovesicles.

3.3 PD-1/SIRPα NVs promoted the phagocytosis of melanoma cells by BMDMs

The CD47/SIRPα interaction between cancer cells and macrophages serves as a crucial "don't eat me" signal, preventing cancer cells from phagocytosis by macrophages (Wang et al., 2022; Zhou et al., 2024). Targeting CD47 blockade can enhance macrophage-mediated phagocytosis of cancer cells, presenting a promising avenue for cancer immunotherapy (Luo J. Q. et al., 2023). In our study, we assessed the pro-phagocytic capacity of PD-1/SIRPα nanovesicles (NVs) *in vitro* due to the presence of the SIRPα receptor. Mouse bone marrow-derived macrophages were cultured and co-incubated with B16F10 cells. Interestingly, in the PBS control group, no phagocytic B16F10 cells (labeled in red) were observed within the BMDMs (labeled in green). In contrast, the treatment with SIRPα NVs or PD-1/SIRPα NVs resulted in the formation of multiple merged yellow spots (indicated by arrows) within the BMDMs (green) (Figure 3A). These findings suggest that SIRPα NVs and PD-1/SIRPα NVs effectively disrupt the CD47/SIRPα axis, significantly enhancing the phagocytosis of B16F10 cells by BMDMs.

The clinical findings indicated that some cancer patients treated with anti-CD47 experienced anemia symptoms (Chen et al., 2022), due to the CD47 expression in red blood cells (RBCs). To explore the tumor-binding property of PD-1/SIRPα NVs, we added DiI-labeled nanovesicles to a dish containing the B16F10 cells and RBCs. After 4 hours of incubation, the suspended RBC and adherent melanoma cells were collected

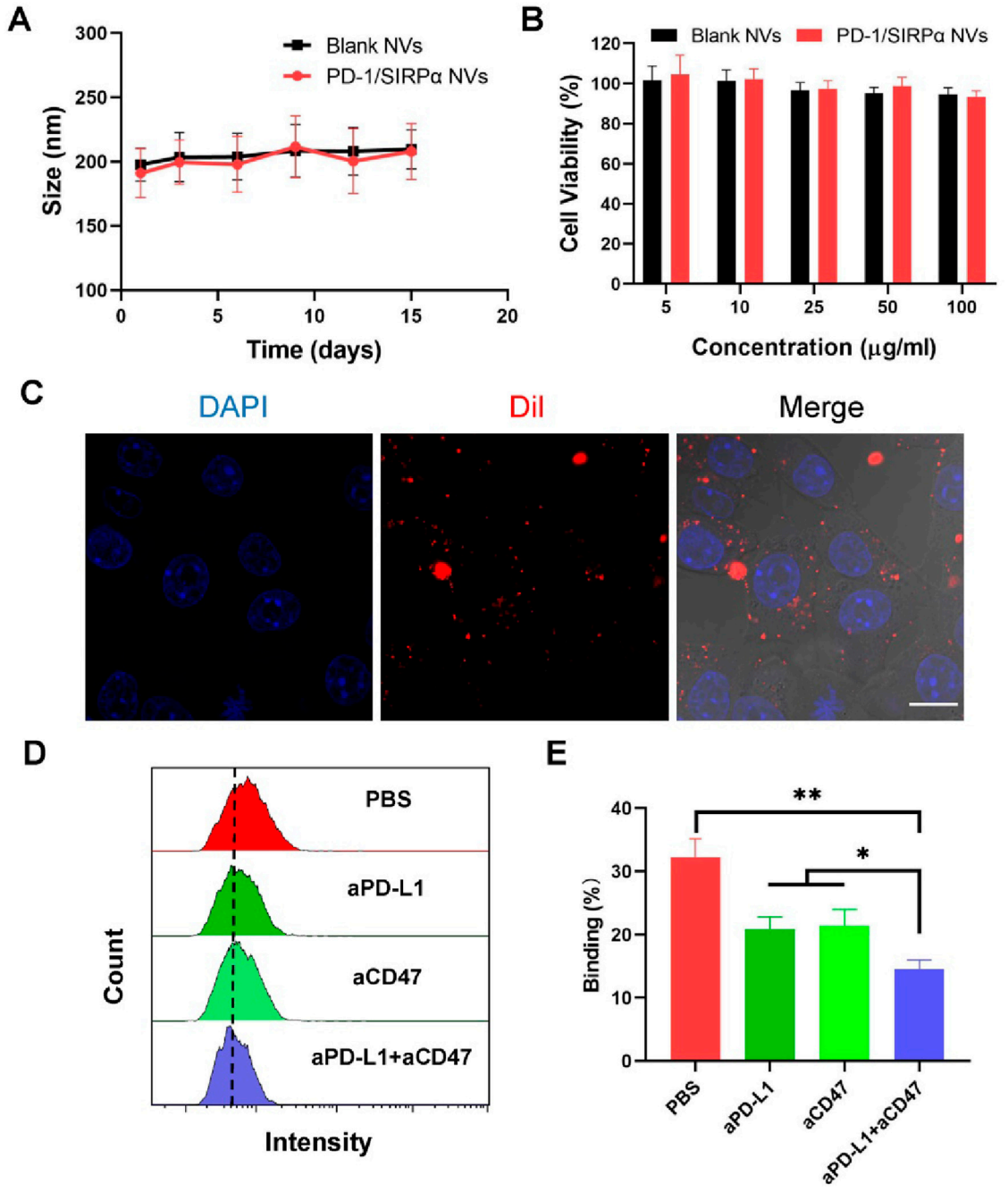

FIGURE 2
In vitro bioactivity analysis of PD-1/SIRPα NVs. **(A)** Stability analysis of PD-1/SIRPα NVs in PBS solution after different days of incubation. The nanovesicles were incubated in PBS with constant shaking at 100 rpm at 37°C. **(B)** Biocompatibility analysis of hybrid nanovesicles on DC2.4 cells by measuring the cell viability of treated cells. DC2.4 cells were treated with Blank NVs or PD-1/SIRPα NVs for 48 h at 37°C. The cell viability of treated cells was analyzed via CCK8 assay. **(C)** Cellular uptake of PD-1/SIRPα NVs in melanoma cells. B16F10 cells were incubated with Dil-labeled PD-1/SIRPα NVs for 2 hours at 37°C. Scale bar: 10 μm. **(D, E)** Flow cytometry curves and quantitative analysis of the blockade property of PD-1/SIRPα NVs. Melanoma cells were pretreated with PBS, anti-PD-L1 antibodies (aPD-L1), anti-CD47 antibodies (aCD47), or a combination of aPD-L1 and aCD47 for 4 hours at 37°C. After washing with PBS, Dil-labeled PD-1/SIRPα NVs were added to each well for a 2-hour incubation. Treated cells were digested and subjected to flow cytometry analysis (gated on PE).

and subjected to flow cytometry analysis (Figure 3B). The results revealed that PD-1 NVs exhibited selective binding with melanoma cells, possibly due to the high expression of PD-L1 on B16F10 cells. Conversely, SIRPα NVs showed no preference in binding between B16F10 cells and RBCs, likely because of CD47 expression on both cell types (Figure 3C). Remarkably, PD-1/SIRPα NVs maintained their tumor-binding preference even in the presence of RBCs. These findings highlight the potential of our hybrid nanovesicles with selective tumor-binding in minimizing side effects such as anemia.

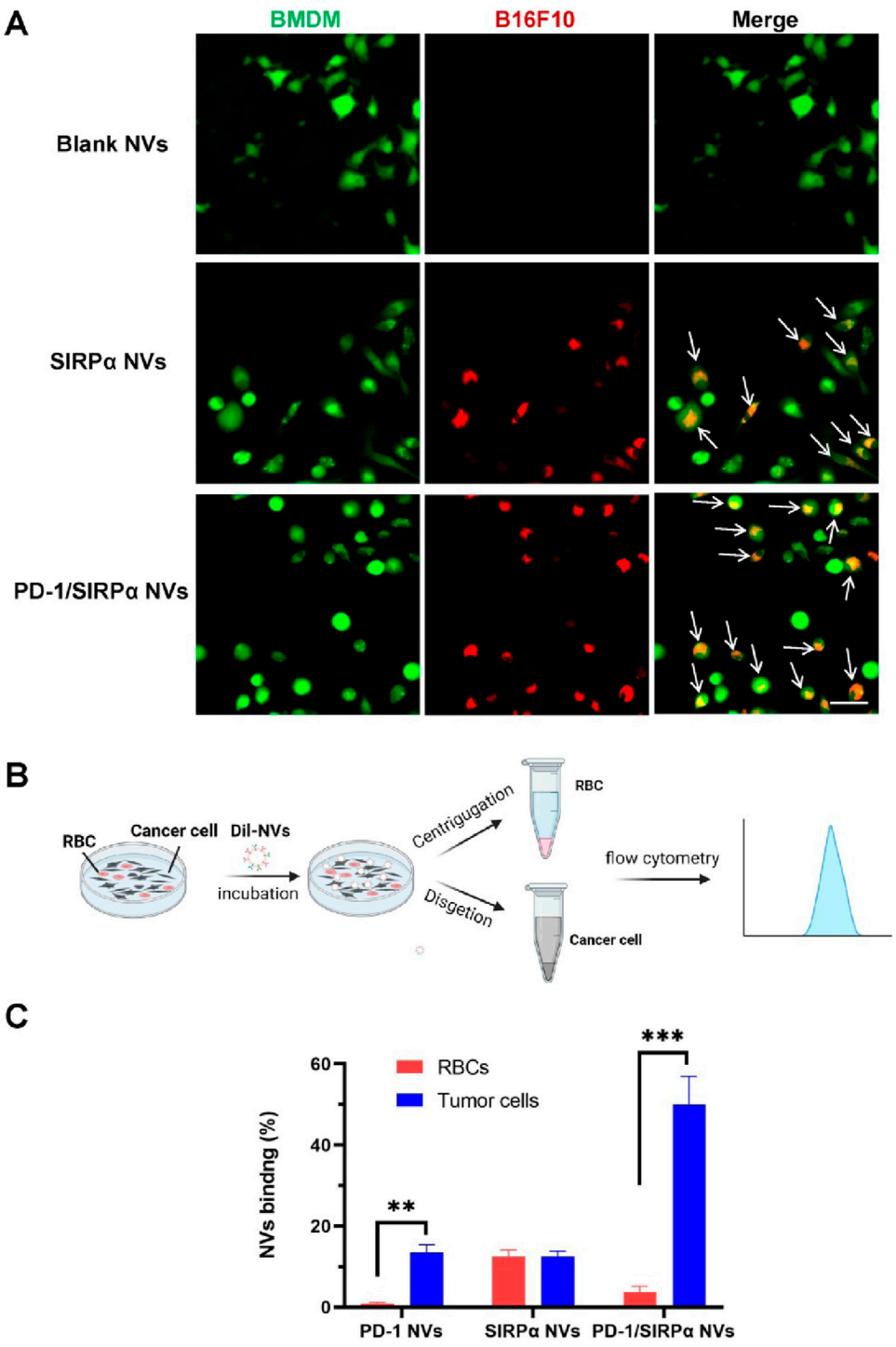

FIGURE 3
Pro-phagocytosis analysis and selective binding property of PD-1/SIRPα NVs *in vitro*. **(A)** PD-1/SIRPα NVs promoted the phagocytosis of melanoma cells by BMDMs *in vitro*. BMDMs were labeled with CellTracker Green, while B16F10 melanoma cells were stained with CellTracker Red. The phagocytosed cancer cells by macrophages were indicated as yellow (arrow). Scale bar: 20 μm. **(B)** Schematic illustration of selective binding of PD-1/SIRPα NVs with melanoma cells by flow cytometry analysis. **(C)** Quantitive analysis of nanovesicle binding with melanoma cells and red blood cells (RBC) in flow cytometry analysis.

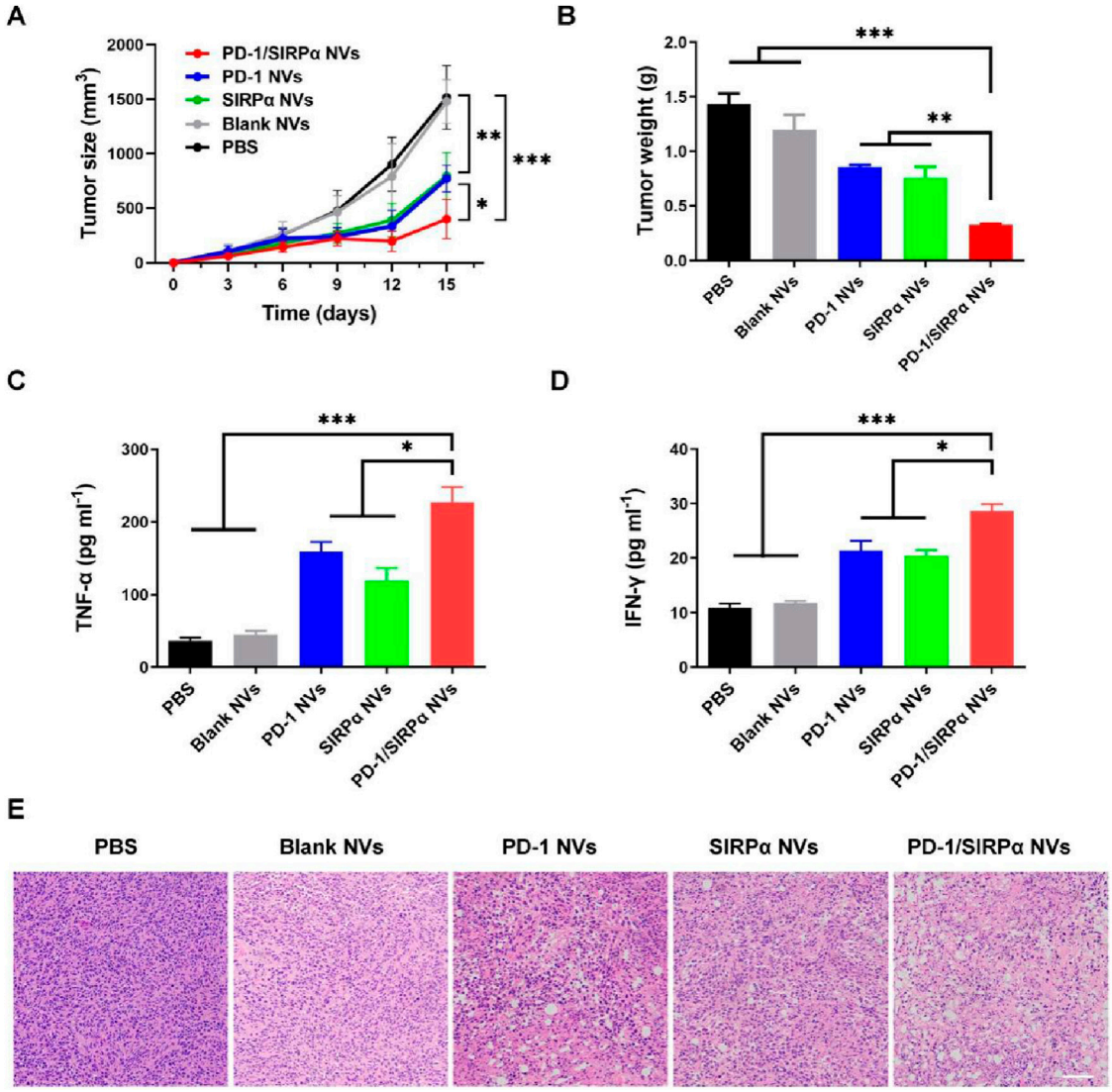

FIGURE 4
In vivo antitumor analysis of PD-1/SIRPα NVs in mice bearing melanoma xenograft **(A)** Tumor growth curves (n = 5). The mice were treated with PBS, Blank NVs, PD-1 NVs, SIRPα NVs, and PD-1/SIRPα NVs five times every 3 days via tail vein injection. **(B)** Tumor weight analysis in different groups. **(C, D)** Serum TNF-α and IFN-γ analysis in mice treated with different formulations. Mouse serum samples were isolated on day 15th after drug injection. **(E)** H&E staining of tumor tissues in different groups. Scale bar: 100 μm. Data were shown as mean ± SD. P values are from one-way ANOVA followed by Tukey's post-test. *$p < 0.05$, **$p < 0.01$, ***$p < 0.001$.

3.4 PD-1/SIRPα NVs suppressed tumor growth in mice bearing B16F10 melanoma xenograft

We further assessed the antitumor efficacy of PD-1/SIRPα NVs *in vivo*. Mice bearing B16F10 melanoma xenografts were established and subjected to treatment with PBS, Blank NVs, PD-1 NVs, SIRPα NVs, and PD-1/SIRPα NVs for five administrations. Notably, PD-1 NVs, SIRPα NVs, and PD-1/SIRPα NVs significantly inhibited tumor growth by day 15, with hybrid nanovesicles exhibiting the most robust tumor suppression effect (Figure 4A). Treatment with PD-1/SIRPα NVs led to a significant 77.2% reduction in tumor weight compared to the PBS group (Figure 4B). Furthermore, we assessed the levels of pro-inflammatory factors in mouse serum and observed a substantial increase in TNFα (Figure 4C) and IFN-γ (Figure 4D) upon treatment with our hybrid nanovesicles, indicative of an induced immune response. Histological examination of tumor tissues through H&E staining revealed evident tumor cell death in mice treated with PD-1/SIRPα NVs (Figure 4E), underscoring a potent therapeutic effect.

3.5 PD-1/SIRPα NVs elicited a robust antitumor immune response for effective immunotherapy

Given the notable tumor growth suppression effect, we evaluated the tumor-infiltrating immune cells to assess the immunotherapy efficacy. As illustrated in Figure 5A, treatment with PD-1/SIRPα NVs led to a 3.2-fold increase in $CD8^+$ T cell

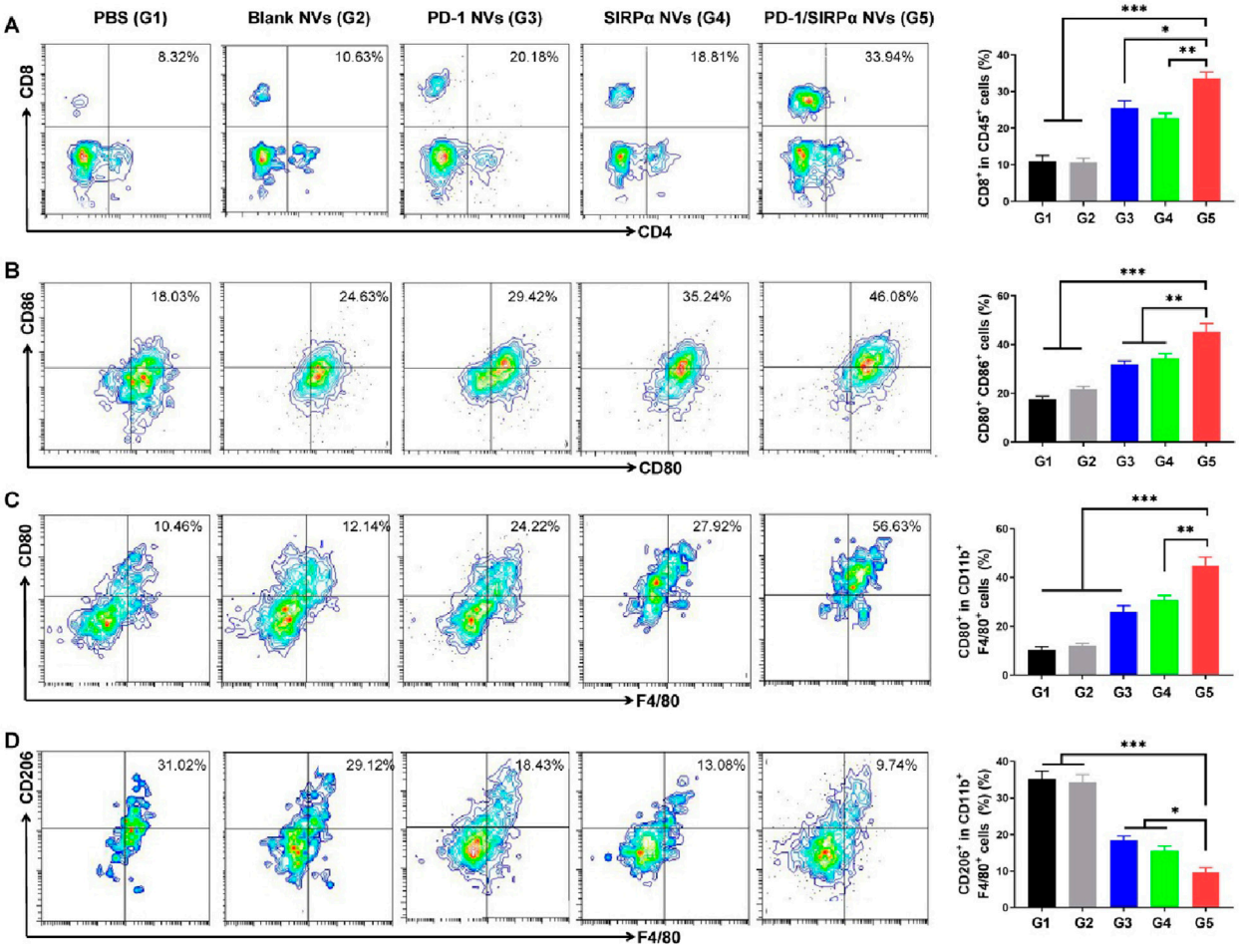

FIGURE 5
PD-1/SIRPα NVs elicited a solid antitumor immune response in mice bearing melanoma xenografts. **(A)** Flow cytometry analysis and percentage of $CD8^+$ T cell infiltration in tumors (gated on $CD45^+CD8^+$ cells). **(B)** Flow cytometry analysis and percentage of mature dendritic cells (gated on $CD80^+CD86^+$ cells). **(C)** Flow cytometry analysis and percentage of M1-type TAM cells (gated on $F4/80^+CD80^+$ cells). **(D)** Flow cytometry analysis and percentage of M2-type TAM cells (gated on $F4/80^+CD206^+$ cells). P values are from one-way ANOVA followed by Tukey's post-test. $^*p < 0.05$, $^{**}p < 0.01$, $^{***}p < 0.001$.

infiltration compared to the PBS group. Flow cytometry analysis indicated that our hybrid nanovesicles substantially facilitated the maturation of dendritic cells (Figure 5B). Furthermore, we examined the macrophage polarization induced by PD-L1 and CD47 blockade. Noteworthy is that the results demonstrated a significant enhancement in the percentage of $CD80^+$ M1 macrophages (Figure 5C) and a reduction in $CD206^+$ M2 macrophages (Figure 5D) upon treatment with PD-1/SIRPα NVs, indicating a polarization towards M1 macrophages. Collectively, these findings underscore the ability of our hybrid nanovesicle to evoke a robust antitumor immune response, showcasing its potential for effective immunotherapy.

We finally determined the biosafety of our hybrid nanovesicles via pathology examination. At the end of treatment, heart, liver, spleen, lung, and kidney tissues were excised and transformed into frozen slices. Hematoxylin and eosin (H&E) staining was performed to evaluate the side effects of PD-1/SIRPα NVs on normal tissues. The results demonstrated no obvious tissue damage during the treatment (Figure 6), suggesting good biosafety *in vivo*.

4 Discussion

ICIs can disrupt the inhibitory signals released by immune checkpoint receptors and restore the immune attack against cancer cells. Given the different roles of immune checkpoints (CTLA-4, PD-1, TIM-3, LAG-3, TIGIT) in immune regulation (de Miguel and Calvo, 2020), concurrent blockade of two immune checkpoints can elicit a high level of antitumor immune response, eventually improving clinical benefit over monotherapy. To this end, some fusion proteins or bispecific antibodies were developed for treating advanced solid tumors (Burton and Tawbi, 2021; Gao et al., 2023). Liu B developed a CD47/PD-L1 fusion protein to trigger innate and adaptive immune responses. Dual blockade of CD47 and PD-L1 by fusion protein induced synergistic antitumor immune response and exhibited potent antitumor activity in the MC38 mouse model (Liu et al., 2018). Wang R designed a CD47/PD-L1 bispecific antibody (6MW3211) for enhanced immunotherapy. 6MW3211 efficiently disrupted PD-1/DP-

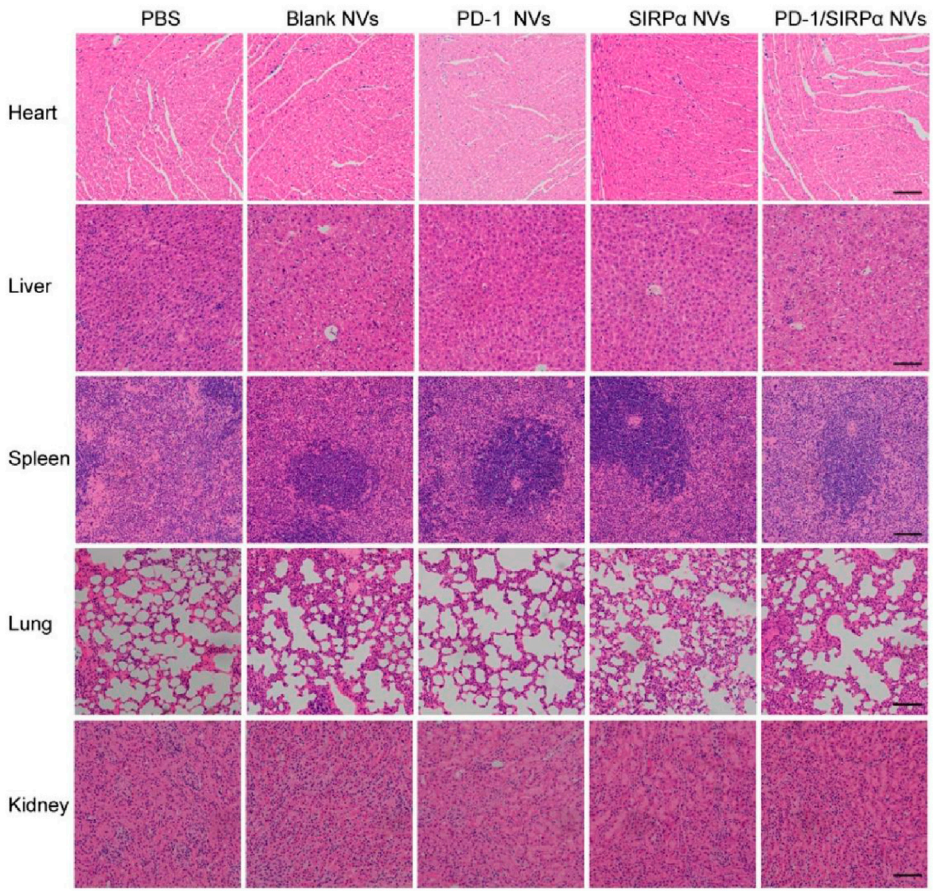

FIGURE 6
Biosafety analysis of PD-1/SIRPα NVs *in vivo*. H&E staining of main organs including heart, liver, spleen, lung, and kidney from the mice treated with PBS, Blank NVs, PD-1 NVs, SIRPα NVs, and PD-1/SIRPα NVs. Scale bar: 200 μm.

L1 and CD47/SIRPα signaling and demonstrated potent therapeutic effects in three tumor models (Le et al., 2021). Ma L et al. fabricated a PD-L1/TIGIT bispecific nanobody to disrupt PD-1/PD-L1 and TIGIT/CD155 interaction. The bispecific nanobody synergistically enhanced T cell function (Ma et al., 2020).

Cell membrane nanovesicles, derived from natural cell membranes, offer numerous advantages as a drug delivery platform for cancer therapy, including reduced clearance by the reticuloendothelial system and prolonged circulation time. Notably, engineered cell membrane nanovesicles can display membrane receptors on their surface, allowing them to perform the intrinsic functions of these receptors. In this study, we decorated cell membrane nanovesicles with PD-1 and SIRPα receptors to enhance immunotherapy efficacy in melanoma. The resulting hybrid nanovesicles demonstrated high specificity with PD-L1 and CD47 ligands expressed on melanoma cells. Notably, our hybrid nanovesicles exhibited mild binding with red blood cells (RBCs) compared to their strong interaction with melanoma cells. This difference in binding affinity can be attributed to the presence of only CD47 on RBCs *versus* the co-expression of PD-L1 and CD47 on melanoma cells. This suggests that PD-1/SIRPα nanovesicles may pose a low risk of blood-related side effects, such as anemia. However, the long-term safety profile and potential off-target effects of PD-1/SIRPα nanovesicles need to be investigated in future research.

The blockade of CD47 by our nanovesicles significantly enhanced the phagocytosis of melanoma cells by macrophages, facilitating the release and presentation of tumor-associated antigens and thereby promoting the maturation of dendritic cells. Additionally, disrupting the PD-L1/PD-1 axis with our nanovesicles reinvigorated exhausted cytotoxic T cells, eliciting a robust immune response against tumor cells. Consequently, in mice bearing melanoma xenografts, PD-1/SIRPα nanovesicles substantially promoted the infiltration of $CD8^+$ T cells and the polarization of M1-type tumor-associated macrophages (TAMs), collectively enhancing therapeutic outcomes. These findings suggest that cell membrane nanovesicles decorated with two or more checkpoint receptors hold promising potential for treating cancers and immune-related diseases. To fulfill the therapeutic potential of PD-1/SIRPα nanovesicles, future studies should be performed to optimize the hybrid nanovesicles. Several factors, including suitable cells for gene transfection, the optimal size of nanovesicles, receptor protein concentration, and the molar ratio of the two receptors, will determine the therapeutic outcomes of nanovesicles.

5 Conclusion

In summary, we developed a hybrid cell membrane nanovesicle for concurrent immune checkpoint blockade in melanoma. Our hybrid nanovesicles can promote the efficient phagocytosis of melanoma cells by macrophages. PD-1/SIRPα NVs significantly suppressed tumor growth and elicited a robust antitumor immune response with enhanced immunotherapy efficacy. In conclusion, our findings highlight the promising potential of PD-1/SIRPα NVs as novel therapeutic agents for cancer immunotherapy.

Data availability statement

The original contributions presented in the study are included in the article/supplementary material, further inquiries can be directed to the corresponding author/s.

Ethics statement

The animal study was approved by Animal Protection and Utilization Committee of Taizhou University. The study was conducted in accordance with the local legislation and institutional requirements.

Author contributions

YL: Investigation, Writing–original draft. FY: Investigation, Writing–original draft. ZL: Investigation, Writing–original draft. TW: Investigation, Writing–original draft. YM: Investigation, Writing–original draft. YF: Investigation, Writing–original draft. HX: Investigation, Writing–original draft. XH: Investigation, Writing–review and editing. XG: Conceptualization, Funding acquisition, Writing–original draft, Writing–review and editing. HF: Funding acquisition, Supervision, Writing–review and editing.

Funding

The author(s) declare that financial support was received for the research, authorship, and/or publication of this article. This study was supported by Zhejiang Provincial Natural Science Foundation of China (LY23C100001), Natural Science Foundation of Hebei Province (B2022202029), Zhejiang Provincial Medical and Health Program (2024KY550), Science and Technology Program of Taizhou City (22gya03).

Conflict of interest

The authors declare that the research was conducted in the absence of any commercial or financial relationships that could be construed as a potential conflict of interest.

Publisher's note

All claims expressed in this article are solely those of the authors and do not necessarily represent those of their affiliated organizations, or those of the publisher, the editors and the reviewers. Any product that may be evaluated in this article, or claim that may be made by its manufacturer, is not guaranteed or endorsed by the publisher.

References

Abi-Aad, S. J., Zouein, J., Chartouni, A., Naim, N., and Kourie, H. R. (2023). Simultaneous inhibition of PD-1 and LAG-3: the future of immunotherapy? *Immunotherapy* 15, 611–618. doi:10.2217/imt-2022-0185

Bagchi, S., Yuan, R., and Engleman, E. G. (2021). Immune checkpoint inhibitors for the treatment of cancer: clinical impact and mechanisms of response and resistance. *Annu. Rev. Pathology Mech. Dis.* 16, 223–249. doi:10.1146/annurev-pathol-042020-042741

Burton, E. M., and Tawbi, H. A. (2021). Bispecific antibodies to PD-1 and CTLA4: doubling down on T cells to decouple efficacy from toxicity. *Cancer Discov.* 11, 1008–1010. doi:10.1158/2159-8290.cd-21-0257

Chae, Y. K., Arya, A., Iams, W., Cruz, M. R., Chandra, S., Choi, J., et al. (2018). Current landscape and future of dual anti-CTLA4 and PD-1/PD-L1 blockade immunotherapy in cancer; lessons learned from clinical trials with melanoma and non-small cell lung cancer (NSCLC). *J. Immunother. Cancer* 6, 39. doi:10.1186/s40425-018-0349-3

Chen, B. Q., Zhao, Y., Zhang, Y., Pan, Y. J., Xia, H. Y., Kankala, R. K., et al. (2023). Immune-regulating camouflaged nanoplatforms: a promising strategy to improve cancer nano-immunotherapy. *Bioact. Mater* 21, 1–19. doi:10.1016/j.bioactmat.2022.07.023

Chen, Y.-C., Shi, W., Shi, J.-J., and Lu, J.-J. (2022). Progress of CD47 immune checkpoint blockade agents in anticancer therapy: a hematotoxic perspective. *J. Cancer Res. Clin.* 148, 1–14. doi:10.1007/s00432-021-03815-z

Cheng, Q., Kang, Y., Yao, B., Dong, J., Zhu, Y., He, Y., et al. (2023). Genetically engineered-cell-membrane nanovesicles for cancer immunotherapy. *Adv. Sci.* 10, 2302131. doi:10.1002/advs.202302131

de Miguel, M., and Calvo, E. (2020). Clinical challenges of immune checkpoint inhibitors. *Cancer Cell* 38, 326–333. doi:10.1016/j.ccell.2020.07.004

Fan, D., Cao, Y., Cao, M., Wang, Y., Cao, Y., and Gong, T. (2023). Nanomedicine in cancer therapy. *Signal Transduct. Target. Ther.* 8, 293. doi:10.1038/s41392-023-01536-y

Fang, T., Li, B., Li, M., Zhang, Y., Jing, Z., Li, Y., et al. (2023b). Engineered cell membrane vesicles expressing CD40 alleviate system lupus nephritis by intervening B cell activation. *Small Methods* 7, e2200925. doi:10.1002/smtd.202200925

Fang, W., Li, L., Lin, Z., Zhang, Y., Jing, Z., Li, Y., et al. (2023a). Engineered IL-15/IL-15Rα-expressing cellular vesicles promote T cell anti-tumor immunity. *Extracell. Vesicle* 2, 100021. doi:10.1016/j.vesic.2022.100021

Gao, X., Xu, N., Li, Z., Shen, L., Ji, K., Zheng, Z., et al. (2023). Safety and antitumour activity of cadonilimab, an anti-PD-1/CTLA-4 bispecific antibody, for patients with advanced solid tumours (COMPASSION-03): a multicentre, open-label, phase 1b/2 trial. *Lancet Oncol.* 24, 1134–1146. doi:10.1016/S1470-2045(23)00411-4

Guo, Y., Wu, J., Chen, L., Liu, L., Bi, T., Pan, Y., et al. (2024). Tea polyphenol-engineered hybrid cellular nanovesicles for cancer immunotherapy and androgen deprivation therapy. *J. nanobiotechnology* 22, 192. doi:10.1186/s12951-024-02458-9

Hu, N., Xue, H., Zhang, T., Fan, Y., Guo, F., Li, Z., et al. (2024). Harnessing PD-1 cell membrane-coated paclitaxel dimer nanoparticles for potentiated chemoimmunotherapy. *Biomed. Pharmacother.* 174, 116482. doi:10.1016/j.biopha.2024.116482

Johnson, D. B., Nebhan, C. A., Moslehi, J. J., and Balko, J. M. (2022). Immune-checkpoint inhibitors: long-term implications of toxicity. *Nat. Rev. Clin. Oncol.* 19, 254–267. doi:10.1038/s41571-022-00600-w

Le, Q.-V., Lee, J., Lee, H., Shim, G., and Oh, Y.-K. (2021). Cell membrane-derived vesicles for delivery of therapeutic agents. *Acta Pharm. Sin. B* 11, 2096–2113. doi:10.1016/j.apsb.2021.01.020

Liu, B., Guo, H., Xu, J., Qin, T., Guo, Q., Gu, N., et al. (2018). Elimination of tumor by CD47/PD-L1 dual-targeting fusion protein that engages innate and adaptive immune responses. *mAbs* 10, 315–324. doi:10.1080/19420862.2017.1409319

Luo, J. Q., Liu, R., Chen, F. M., Zhang, J. Y., Zheng, S. J., Shao, D., et al. (2023a). Nanoparticle-mediated CD47-sirpα blockade and calreticulin exposure for improved cancer chemo-immunotherapy. *ACS Nano* 17, 8966–8979. doi:10.1021/acsnano.2c08240

Luo, J.-Q., Liu, R., Chen, F.-M., Zhang, J.-Y., Zheng, S.-J., Shao, D., et al. (2023b). Nanoparticle-mediated CD47-SIRPα blockade and calreticulin exposure for improved cancer chemo-immunotherapy. *ACS Nano* 17, 8966–8979. doi:10.1021/acsnano.2c08240

Ma, L., Gai, J., Qiao, P., Li, Y., Li, X., Zhu, M., et al. (2020). A novel bispecific nanobody with PD-L1/TIGIT dual immune checkpoint blockade. *Biochem. Biophys. Res. Commun.* 531, 144–151. doi:10.1016/j.bbrc.2020.07.072

Meng, Q. F., Zhao, Y., Dong, C., Liu, L., Pan, Y., Lai, J., et al. (2021). Genetically programmable fusion cellular vesicles for cancer immunotherapy. *Angewandte Chemie Int. ed. Engl.* 60, 26320–26326. doi:10.1002/anie.202108342

Mu, Y., Fan, Y., He, L., Hu, N., Xue, H., Guan, X., et al. (2023). Enhanced cancer immunotherapy through synergistic ferroptosis and immune checkpoint blockade using cell membrane-coated nanoparticles. *Cancer Nanotechnol.* 14, 83. doi:10.1186/s12645-023-00234-2

Peng, X., Yang, L., Yuan, P., and Ding, X. (2024). Hybrid cell membrane-based nanoplatforms for enhanced immunotherapy against cancer and infectious diseases. *Adv. Healthc. Mater* 13, e2304477. doi:10.1002/adhm.202304477

Rao, L., Wu, L., Liu, Z., Tian, R., Yu, G., Zhou, Z., et al. (2020). Hybrid cellular membrane nanovesicles amplify macrophage immune responses against cancer recurrence and metastasis. *Nat. Commun.* 11, 4909. doi:10.1038/s41467-020-18626-y

Ren, E., Liu, C., Lv, P., Wang, J., and Liu, G. (2021). Genetically engineered cellular membrane vesicles as tailorable shells for therapeutics. *Adv. Sci.* 8, e2100460. doi:10.1002/advs.202100460

Sun, M., Yang, J., Fan, Y., Zhang, Y., Sun, J., Hu, M., et al. (2023). Beyond extracellular vesicles: hybrid membrane nanovesicles as emerging advanced tools for biomedical applications. *Adv. Sci.* 10, 2303617. doi:10.1002/advs.202303617

Wang, M., Wang, Y., Mu, Y., Yang, F., Yang, Z., Liu, Y., et al. (2023b). Engineering SIRPα cellular membrane-based nanovesicles for combination immunotherapy. *Nano Res.* 16, 7355–7363. doi:10.1007/s12274-023-5397-4

Wang, R., Zhang, C., Cao, Y., Wang, J., Jiao, S., Zhang, J., et al. (2023a). Blockade of dual immune checkpoint inhibitory signals with a CD47/PD-L1 bispecific antibody for cancer treatment. *Theranostics* 13, 148–160. doi:10.7150/thno.79367

Wang, Y., Zhao, C., Liu, Y., Wang, C., Jiang, H., Hu, Y., et al. (2022). Recent advances of tumor therapy based on the CD47-SIRPα axis. *Mol. Pharm.* 19, 1273–1293. doi:10.1021/acs.molpharmaceut.2c00073

Willsmore, Z. N., Coumbe, B. G. T., Crescioli, S., Reci, S., Gupta, A., Harris, R. J., et al. (2021). Combined anti-PD-1 and anti-CTLA-4 checkpoint blockade: treatment of melanoma and immune mechanisms of action. *Eur. J. Immunol.* 51, 544–556. doi:10.1002/eji.202048747

Xiao, Y., Zhu, T., Zeng, Q., Tan, Q., Jiang, G., and Huang, X. (2023). Functionalized biomimetic nanoparticles combining programmed death-1/programmed death-ligand 1 blockade with photothermal ablation for enhanced colorectal cancer immunotherapy. *Acta Biomater.* 157, 451–466. doi:10.1016/j.actbio.2022.11.043

Yang, F., Wang, M., and Guan, X. (2022). Exosomes and mimics as novel delivery platform for cancer therapy. *Front. Pharmacol.* 13, 1001417. doi:10.3389/fphar.2022.1001417

Yu, Y., Cheng, Q., Ji, X., Chen, H., Zeng, W., Zeng, X., et al. (2022). Engineered drug-loaded cellular membrane nanovesicles for efficient treatment of postsurgical cancer recurrence and metastasis. *Sci. Adv.* 8, eadd3599. doi:10.1126/sciadv.add3599

Zhang, E., Phan, P., and Zhao, Z. (2023). Cellular nanovesicles for therapeutic immunomodulation: a perspective on engineering strategies and new advances. *Acta Pharm. Sin. B* 13, 1789–1827. doi:10.1016/j.apsb.2022.08.020

Zhao, C., Pan, Y., Liu, L., Zhang, J., Wu, X., Liu, Y., et al. (2024). Hybrid cellular nanovesicles block PD-L1 signal and repolarize M2 macrophages for cancer immunotherapy. *Small* 20, e2311702. doi:10.1002/smll.202311702

Zhou, H., Wang, W., Xu, H., Liang, Y., Ding, J., Lv, M., et al. (2024). Metabolic reprograming mediated by tumor cell-intrinsic type I IFN signaling is required for CD47-SIRPα blockade efficacy. *Nat. Commun.* 15, 5759. doi:10.1038/s41467-024-50136-z

frontiers | Frontiers in Pharmacology

TYPE Systematic Review
PUBLISHED 06 December 2024
DOI 10.3389/fphar.2024.1495343

OPEN ACCESS

EDITED BY
Xinyu Wang,
Philadelphia College of Osteopathic Medicine (PCOM), United States

REVIEWED BY
Jian Chen,
Shanghai University of Traditional Chinese Medicine, China
Adila Aipire,
Xinjiang University, China

*CORRESPONDENCE
Dong-Liang Li,
dongliangli93@163.com

RECEIVED 12 September 2024
ACCEPTED 25 November 2024
PUBLISHED 06 December 2024

CITATION
Chen L, Zhu X-L, Lin J and Li D-L (2024) Efficacy and safety of TACE combined with traditional Chinese medicine versus TACE alone in hepatocellular carcinoma: bayesian network meta-analysis and pharmacological mechanisms study.
Front. Pharmacol. 15:1495343.
doi: 10.3389/fphar.2024.1495343

Efficacy and safety of TACE combined with traditional Chinese medicine versus TACE alone in hepatocellular carcinoma: bayesian network meta-analysis and pharmacological mechanisms study

Li Chen[1,2], Xiu-Ling Zhu[2], Jie Lin[3] and Dong-Liang Li[1,2]*

[1]Department of Hepatobiliary Disease, Fuzong Clinical Medical College of Fujian Medical University, Fuzhou, Fujian, China, [2]Department of Hepatobiliary Disease, 900 Hospital of the Joint Logistics Team of the Chinese PLA, Fuzhou, Fujian, China, [3]Department of Hepatobiliary and Pancreatic Surgery, Second Affiliated Hospital of Jilin University, Changchun, Jilin, China

Purpose: This study investigates the clinical benefits of integrating traditional Chinese medicine (TCM) with Transarterial Chemoembolization (TACE) in hepatocellular carcinoma (HCC) treatment via meta-analysis and an exploration of network pharmacology analysis (NPA).

Methods: A comprehensive search across different databases retrieved all randomized controlled trials (RCTs) evaluating TCM combined with TACE for HCC. Meta-analysis included 39 RCTs to assess the intervention effects. The bayesian network meta-analysis observed the relative efficacy and potential ranking of various interventions. Active compounds and target genes from frequently used TCM were sourced from the TCMSP database, while HCC disease targets were collected from five public disease databases. Regulatory networks connecting target genes with active components of key herbs were constructed. Following the identification of key genes, we conducted analyses of Gene Ontology (GO) and Kyoto Encyclopedia of Genes and Genomes (KEGG) to enrich our understanding of their functions. NPA and molecular docking methods were refined to reveal potential interactions between TCM components and their specific targets.

Results: The combination of TCM with TACE significantly enhances the efficacy and safety of HCC treatment, improving the overall response rate, disease control rate, and overall survival rate, while also reducing the incidence of adverse events. Among the TCM evaluated, Ganfu Formula proved to be the most effective in enhancing patient response rates. Analysis of all included medicinal herbs identified 10 pivotal TCMs and 17 core genes. GO analysis revealed their significance in protein interactions, whereas KEGG analysis highlighted their role in crucial oncological pathways. NPA and molecular docking techniques elucidate the underlying mechanisms of action of TCM components.

Conclusion: Adding TCM to TACE protocols significantly enhances treatment outcomes and safety in HCC patients by modulating tumor biology and systemic immune responses, highlighting its potential as an effective adjunct therapy. These findings support the inclusion of TCM in standard care regimens, offering potential for improved management of HCC.

Systematic Review Registration: https://www.crd.york.ac.uk/PROSPERO/, identifier CRD42024571280.

KEYWORDS

hepatocellular carcinoma, transarterial chemoembolization, traditional Chinese medicine, bayesian network meta-analysis, network pharmacology, molecular docking

1 Introduction

Hepatocellular carcinoma (HCC) ranks among the top three most common causes of cancer-associated mortality globally (Bray et al., 2024). Transarterial Chemoembolization (TACE) is a commonly employed therapeutic approach for HCC, especially in patients who are in the intermediate to advanced stages of the disease (Chang et al., 2020). However, TACE alone presents several limitations, including incomplete local treatment, absence of systemic effects and increased risks of tumor recurrence and metastasis (Kudo et al., 2020). Although TACE can deliver high concentrations of cytotoxic agents to tumor cells locally, it cannot effectively inhibit angiogenesis or disrupt the complex signaling networks within the tumor microenvironment, resulting in suboptimal therapeutic outcomes and diminished patient quality of life (Kudo, 2019).

Recently, the integration of traditional Chinese medicine (TCM) into therapeutic strategies for HCC has attracted heightened focus. TCM can effectively overcome the limitations of TACE through multi-targeted and multi-pathway mechanisms. Specific TCM components can inhibit angiogenesis, reducing the risks of tumor recurrence and metastasis (Li et al., 2022). Additionally, by modulating the complex signaling networks within the tumor microenvironment, TCM can enhance the systemic therapeutic effects of TACE, further improving overall efficacy and patient quality of life (Liao et al., 2020).

To rigorously assess the combined effectiveness of TCM and TACE in managing HCC, this study proposes to use meta- and network meta-analysis methods to integrate existing clinical trial data. Additionally, applying network pharmacology analysis (NPA) alongside molecular docking methods will help elucidate the underlying biological mechanisms of TCM. Bayesian network meta-analysis enables comparison of different treatment regimens' effects, and offers more comprehensive efficacy assessments through indirect comparisons (Ahn and Kang, 2021). Incorporating NPA with molecular docking techniques (Zhao et al., 2023) uncovers how TCM components interact with their biological targets, providing theoretical support for clinical applications. This research aims to generate solid clinical evidence supporting the concurrent application of TCM with TACE for treating HCC, serving as a foundation for future scientific exploration and pharmaceutical innovation.

2 Materials and methods

2.1 Meta-analysis method of TCM for HCC

This study employs a network meta-analysis method as stipulated by the PRISMA guidelines. Project details have been recorded and can be found on the PROSPERO database (Moher et al., 2015) under the identifier CRD42024571280.

2.2 Database search strategy

Searches were conducted across both English-language and Chinese-language databases including PubMed, Embase, Web of Science, Cochrane Library, Chinese National Knowledge Infrastructure (CNKI), Chinese Biomedical Literature Database (CBM), China Science and Technology Journal Database (VIP), and Wanfang Data to retrieve records available up to 5 July 2024, without imposing language restrictions. Key search terms included "Hepatocellular Carcinoma," "Traditional Chinese Medicine," "randomized controlled trials." Supplementary Table S1 includes the complete search methodologies.

2.3 Inclusion and exclusion criteria

Inclusion criteria: (1) All clinical randomized controlled trials (RCTs) assessing the effectiveness of combining TCM with TACE for treating HCC. (2) HCC diagnosis confirmed by pathological examination or established diagnostic criteria (Cannella, Zins, and Brancatelli, 2024). (3) Experimental group (EG) receiving TCM combined with TACE, control group (CG) receiving TACE treatment alone. (4) Defined outcome measures. Exclusion criteria: (1) Non-RCTs. (2) Studies unrelated to HCC. (3) Animal studies. (4) Reviews, meta-analyses, conference proceedings, letters.

2.4 Data extraction and quality assessment

LC and X-LZ meticulously screened and synthesized data, adhering strictly to predefined inclusion and exclusion criteria, in line with the Cochrane Collaboration's assessment framework (Cumpston et al., 2019). Extracted information included the primary author's name, sample size, the year of publication,

participant demographics, details of the interventions, gender composition, age and outcome indicators including overall survival (OS), overall response rate (ORR), disease control rate (DCR) and adverse events (AEs). Any discrepancies were resolved by verifying the original texts or through third-party adjudication.

2.5 Statistical analysis

The data analysis utilized Review Manager 5.2 alongside STATA 12, focusing on odds ratios (OR) to measure effect sizes for binary outcomes. When both $p \geq 0.1$ and $I^2 \leq 50\%$ suggested minimal heterogeneity, a fixed-effects model was employed. Conversely, significant heterogeneity prompted an exploration of underlying causes and the employment of a random-effects model. Sensitivity analysis assessed the heterogeneity sources and result robustness. Egger's and Begg's tests were utilized to assess the potential existence of publication bias. Network meta-analysis was conducted using Bayesian methods with the GeMTC package in R 4.1.0. Model convergence was assessed using residual plots. This analytical framework helped to compare the impacts across study groups, enhancing our understanding of different interventions' effectiveness.

2.6 Exploration and targeting of TCM

The top 10 most frequently used TCM prescriptions extracted from the meta-analysis studies were selected as the main subjects for study. The bioactive components and corresponding drug targets of these herbs were acquired from the Traditional Chinese Medicine Systems Pharmacology Database and Analysis Platform (TCMSP, https://tcmspw.com/index.php) (Ru et al., 2014). The selection criteria were set with an oral bioavailability threshold of 30% or higher and a drug-likeness index of at least 0.18. Subsequent gene annotation of these component targets was conducted using human gene information downloaded from The Universal Protein Database (UniProt, https://legacy.uniprot.org/) (Bairoch et al., 2005). To compile HCC-specific disease targets, we accessed several databases: GeneCards (https://www.genecards.org/), Therapeutic Target Database (TTD, http://db.idrblab.net/ttd/), DisGeNet (https://www.disgenet.org/), Online Mendelian Inheritance in Man (OMIM, http://omim.org/), and Comparative Toxicogenomics Database (CTD, https://ctdbase.org/). Gene intersections between TCM and HCC were identified using the 'VennDiagram' tool. The intersecting genes were then submitted to the STRING database (https://stringdb.org/), specifying humans as the target species, with a confidence score threshold set at > 0.4 to ensure interaction reliability. Independent proteins were excluded from the network to focus on biologically meaningful interactions. The resulting data were then imported into Cytoscape 3.8.2 (Doncheva et al., 2019) to generate a molecular network diagram of TCM components and intersecting genes. Central genes were identified using the Cytoscape software plugin cytoHubba, employing algorithms including Maximal Clique Centrality (MCC), Maximum Neighborhood Component (MNC), Degree, Closeness, Radiality, Stress, and Edge Percolated Component (EPC), which facilitated the selection of pivotal genes.

2.7 Network pharmacology analysis grounded in TCM hubs

Functional enrichment analysis, incorporating Gene Ontology (GO) and Kyoto Encyclopedia of Genes and Genomes (KEGG) pathway evaluations, was conducted to elucidate interaction pathways between TCM components and HCC-related genes. Essential genes were analyzed using packages like clusterProfiler and enrichplot, with p-value and q-value thresholds set at < 0.05. The UniProt database was used to retrieve the protein IDs for hub targets, and the corresponding 3D structures of each target protein were downloaded from the PDB database (https://www.rcsb.org/) (Shin and Cho, 2005). To minimize interference from non-essential molecules in subsequent molecular docking, water molecules, cofactors, and heteroatoms were removed using PyMOL software (Seeliger and de Groot, 2010), retaining only the core protein structure. Hydrogen atoms were then added to the protein, and energy minimization was conducted with AutoDockTools (Goodsell et al., 2021) to optimize the structure by removing geometric conflicts and relieving conformational strain, ensuring stability. Small molecule ligands' 2D chemical structures from PubChem (Wang et al., 2012) (https://pubchem.ncbi.nlm.nih.gov/) were converted into 3D models by the application of ChemBio3D Ultra 14.0, with subsequent calculations performed to optimize the structures. Potential binding sites on the proteins were identified using AutoDockTools, and docking simulations were carried out with AutoDock Vina to determine the optimal binding configurations, visualized through PyMOL.

2.8 *In vitro* validation of differential gene expression

To verify core gene expression in HCC, we obtained the TCGA-LIHC dataset from the Genomic Data Commons (GDC, https://gdc.cancer.gov/). Then we acquired the HCC cell line HepG2 (CL-0103) and the human liver epithelial cell line THLE-2 (CL-0833) from Punose Biotechnology Co., Ltd. (Wuhan, China). Both cell lines were cultured in DMEM basal medium (Meilunbio, MA0212), supplemented with 10% fetal bovine serum (Opcel, BS-1105) and 1% penicillin/streptomycin (Meilunbio, MA0110). At 70%–90% confluence, total RNA was extracted using the TransZol Up Plus RNA Kit (Transgene Biotech, ER501-01-V2, China). Genomic DNA was removed with gDNA Purge (Novoprotein, E047-01A, China) according to the manufacturer's instructions, and cDNA was synthesized. Quantitative reverse transcription PCR (qRT-PCR) was then performed using NovoStart® SYBR qPCR SuperMix Plus (Novoprotein, E09601B, China) on an Applied Biosystems 7,300 Real-Time PCR system (Applied Biosystems, United States) to assess mRNA expression levels of core genes identified as stable binding targets in molecular docking analyses. qRT-PCR primers were synthesized by SunYa (Fuzhou, China), with primer sequences

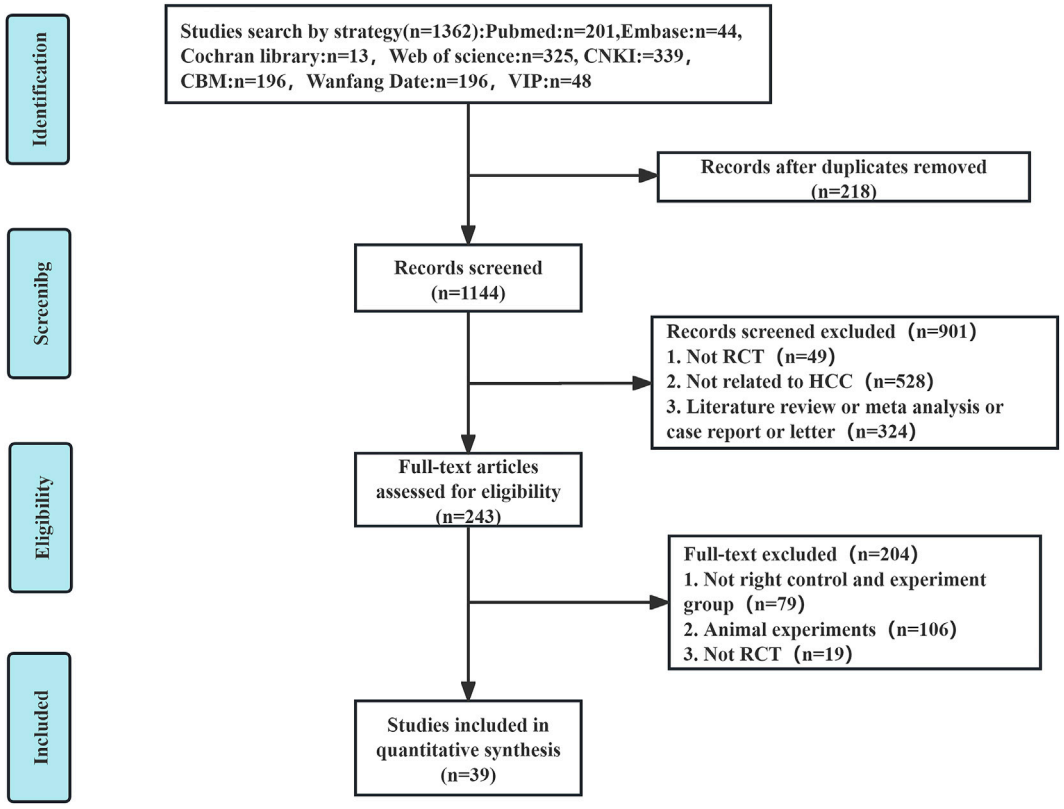

FIGURE 1
The flowchart for screening literature.

provided in the Supplementary Table S2. qRT-PCR cycling conditions were 95°C for 30 s for pre-denaturation, followed by 40 cycles at 95°C for 5 s and 60°C for 15 s for annealing. qRT-PCR data were analyzed using the $2^{-\Delta\Delta CT}$ method.

3 Results

3.1 Literature retrieval and screening

An extensive database search identified 1,362 relevant articles from sources including PubMed, Embase, Cochrane Library, Web of Science, CNKI, CBM, Wanfang Data, and VIP. Following the removal of 218 duplicate entries, an additional 901 articles were excluded after preliminary assessments. Of the 243 remaining articles, detailed evaluations excluded 79 for non-compliance with group criteria, 106 for being animal studies, and 19 for lacking randomization, resulting in 39 (Zhou et al., 2002; Shao et al., 2001; Ren and Cheng, 2004; Cao et al., 2005; Zhang C. Q. et al., 2005; Zhang Y. M. et al., 2005; Lin and Guo, 2005; Yuan et al., 2005; Ou et al., 2006; Wen and Peng, 2006; Yu et al., 2006; Liu et al., 2007; Wang and Chen, 2007; Zhang et al., 2007; Zhong et al., 2007; Wu et al., 2010; Zhou et al., 2010; Han et al., 2013; Liu et al., 2013; Song et al., 2013; Zhao et al., 2013; Yin et al., 2013; Li et al., 2014; Zheng, 2014; Li et al., 2015; Tang, 2017; Ding, 2018; Wan, 2018; Yang, 2018; Huang, 2019; Li et al., 2019; Qiao J., 2019; Tian et al., 2019; Qiao X. et al., 2019; Hong et al., 2020; Wang et al., 2020; Meng et al., 2021; Yan et al., 2021; Tong et al., 2022) eligible RCTs (Figure 1).

3.2 Basic characteristics of selected literature

The study included 3,939 HCC patients, with 2,027 assigned to the EG and 1,912 to the CG, the latter receiving only TACE therapy. The EG was administered a treatment regimen that combined TCM with TACE. The studies were divided based on TCM formulations into three categories: Liver-soothing (Shugan) herbs, Supporting vital qi (Fuzheng) herbs, and resolving blood stasis (Huayu) herbs, comprising 8 (Zhang C. Q. et al., 2005; Zhang Y. M. et al., 2005; Ou et al., 2006; Liu et al., 2013; Yang, 2018; Tian et al., 2019; Meng et al., 2021; Yan et al., 2021), 20 (Zhou et al., 2002; Ren and Cheng, 2004; Cao et al., 2005; Lin and Guo, 2005; Yuan et al., 2005; Wen and Peng, 2006; Wang and Chen, 2007; Han et al., 2013; Song et al., 2013; Zhao et al., 2013; Yin et al., 2013; Zheng, 2014; Li et al., 2015; Tang, 2017; Ding, 2018; Wan, 2018; Qiao J., 2019; Hong et al., 2020; Wang et al., 2020; Tong et al., 2022), and 11 (Shao et al., 2001; Yu et al., 2006; Liu et al., 2007; Zhong et al., 2007; Zhang et al., 2007; Wu et al., 2010; Zhou et al., 2010; Li et al., 2014; Huang, 2019; Li et al., 2019; Qiao X. et al., 2019) studies, respectively (Supplementary Table S3).

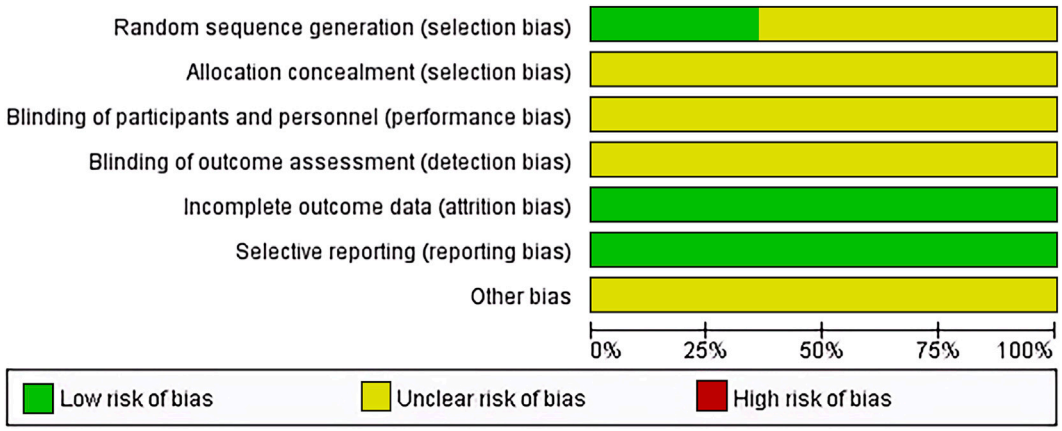

FIGURE 2
Risk assessment for the included studies.

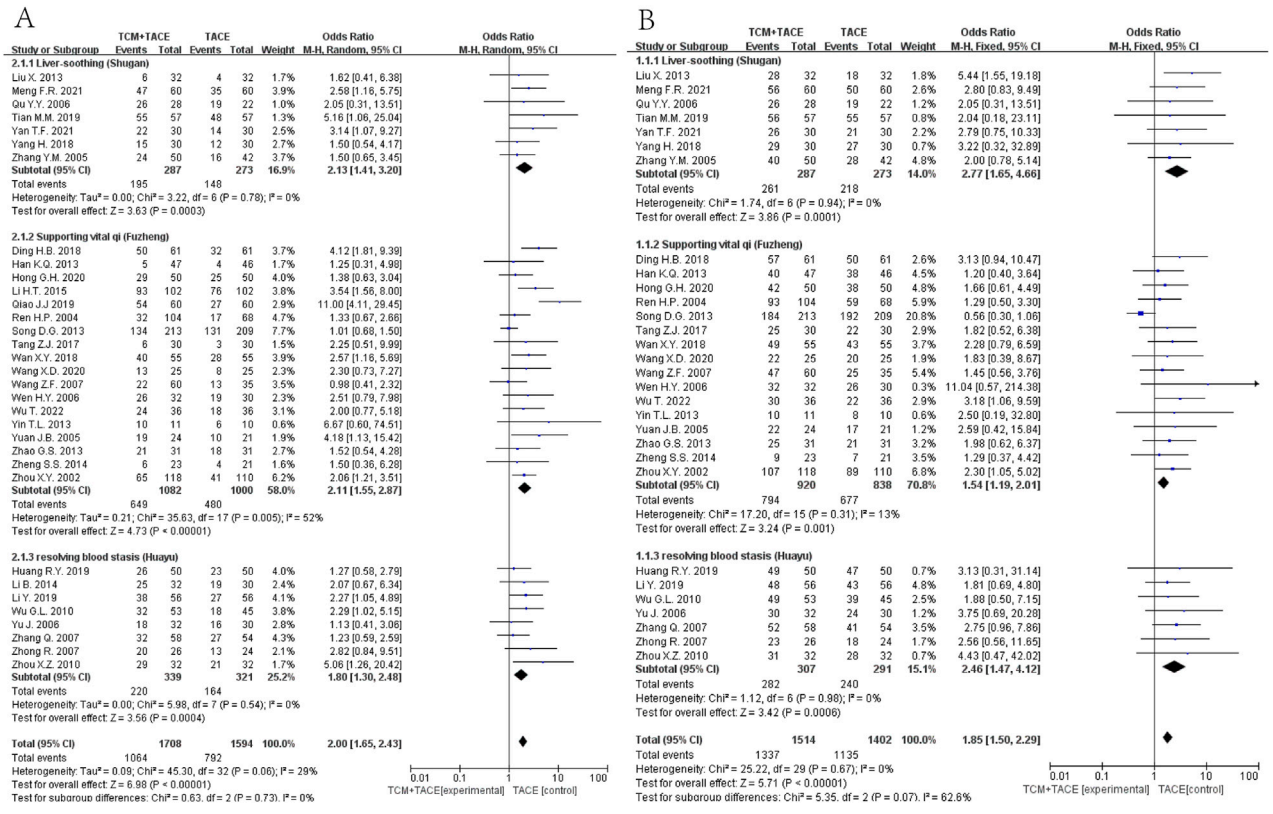

FIGURE 3
(A) ORR between EG and CG. **(B)** DCR between EG and CG.

3.3 Quality assessment of included literature

14 articles (Shao et al., 2001; Ren and Cheng, 2004; Lin and Guo, 2005; Zhang et al., 2007; Wu et al., 2010; Zhao et al., 2013; Tang, 2017; Wan, 2018; Yang, 2018; Li et al., 2019; Qiao J., 2019; Tian et al., 2019; Yan et al., 2021; Tong et al., 2022) used random number generation methods and were considered low risk; the rest employed random grouping methods. Allocation concealment and blinding were not reported in any of the articles, reflecting the practical challenges of implementing these in non-drug therapies like TACE. All studies completed data collection and reporting, thus considered low risk. Unreported potential biases were noted as presenting an unclear risk of bias (Figure 2).

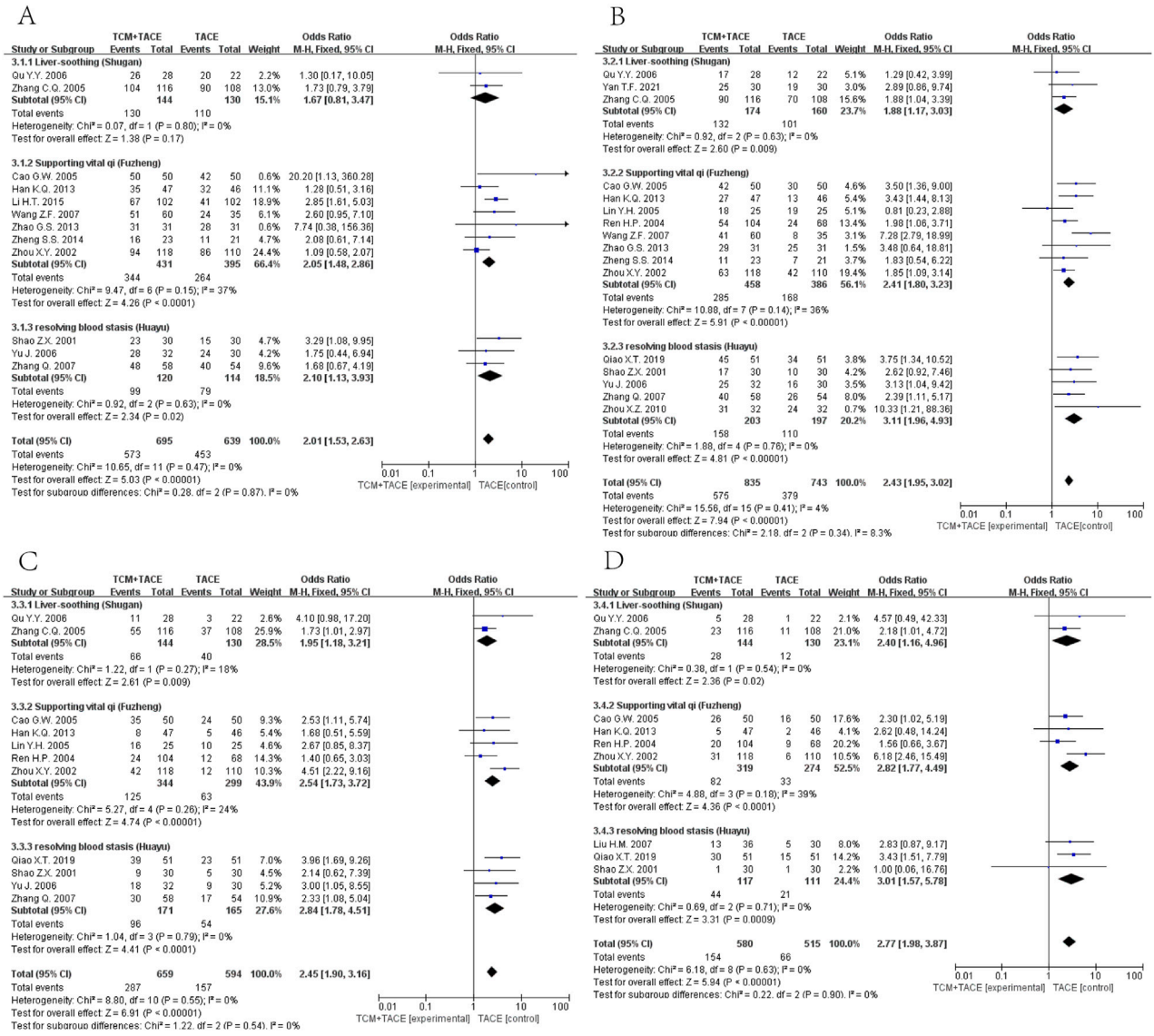

FIGURE 4
Forest plot and subgroup analysis. **(A)** half-year OS. **(B)** one-year OS. **(C)** two-year OS. **(D)** three-year OS.

3.4 Clinical outcomes

3.4.1 ORR and DCR

Data from 33 (Zhang Y. M. et al., 2005; Ou et al., 2006; Liu et al., 2013; Yang, 2018; Tian et al., 2019; Meng et al., 2021; Yan et al., 2021; Zhou et al., 2002; Ren and Cheng, 2004; Yuan et al., 2005; Wen and Peng, 2006; Wang and Chen, 2007; Han et al., 2013; Song et al., 2013; Zhao et al., 2013; Yin et al., 2013; Zheng, 2014; Li et al., 2015; Tang, 2017; Ding, 2018; Wan, 2018; Qiao J., 2019; Hong et al., 2020; Wang et al., 2020; Tong et al., 2022; Yu et al., 2006; Zhong et al., 2007; Zhang et al., 2007; Wu et al., 2010; Zhou et al., 2010; Li et al., 2014; Huang, 2019; Li et al., 2019) and 30 studies (Zhang Y. M. et al., 2005; Ou et al., 2006; Liu et al., 2013; Yang, 2018; Tian et al., 2019; Meng et al., 2021; Yan et al., 2021; Zhou et al., 2002; Ren and Cheng, 2004; Yuan et al., 2005; Wen and Peng, 2006; Wang and Chen, 2007; Han et al., 2013; Song et al., 2013; Zhao et al., 2013; Yin et al., 2013; Zheng, 2014; Tang, 2017; Ding, 2018; Wan, 2018; Hong et al., 2020; Wang et al., 2020; Tong et al., 2022; Yu et al., 2006; Zhong et al., 2007; Zhang et al., 2007; Wu et al., 2010; Zhou et al., 2010; Huang, 2019; Li et al., 2019), respectively, indicated significant improvements in ORR and DCR when combining TCM with TACE versus TACE alone (OR = 2.00, 95% CI [1.65, 2.43], $p < 0.00001$; OR = 1.85, 95% CI [1.50, 2.29], $p < 0.00001$). Subgroup analyses also demonstrated that Liver-soothing (Shugan), Supporting vital qi (Fuzheng) herbs, and resolving blood stasis (Huayu) herbs each notably enhanced ORR and DCR in HCC patients (all p-values < 0.05) (Figure 3).

3.4.2 OS

Data on half-year, 1-year, 2-year, and 3-year OS were reported in 12 (Zhang C. Q. et al., 2005; Ou et al., 2006; Zhou et al., 2002; Cao et al., 2005; Wang and Chen, 2007; Han et al., 2013; Zhao et al., 2013; Zheng, 2014; Li et al., 2015; Shao et al., 2001; Yu et al., 2006; Zhang et al., 2007), 16 (Zhang C. Q. et al., 2005; Ou et al., 2006; Yan et al.,

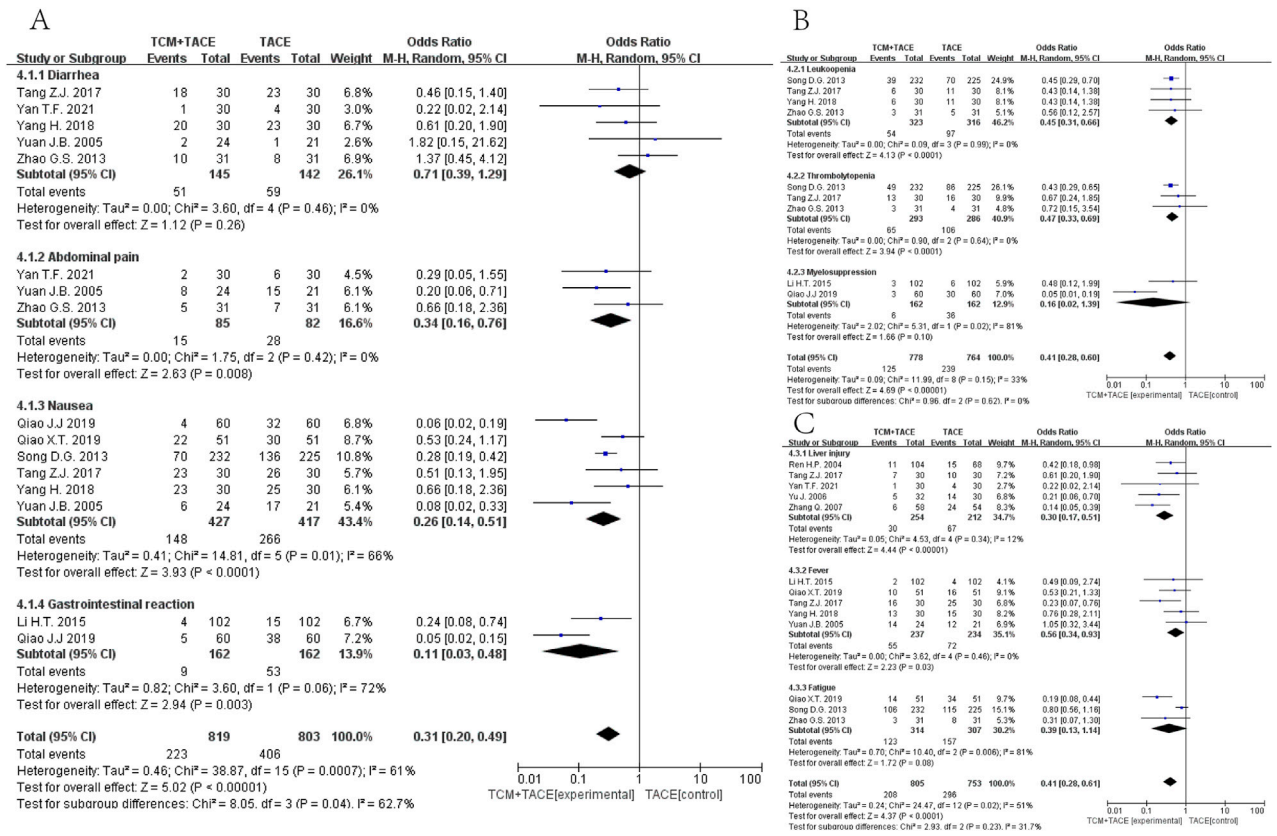

FIGURE 5
Forest plot and subgroup analysis. **(A)** Digestive system complications. **(B)** Hematologic system complications. **(C)** Other complications.

2021; Zhou et al., 2002; Ren and Cheng, 2004; Cao et al., 2005; Lin and Guo, 2005; Wang and Chen, 2007; Han et al., 2013; Zhao et al., 2013; Zheng, 2014; Shao et al., 2001; Yu et al., 2006; Zhang et al., 2007; Zhou et al., 2010; Qiao X. et al., 2019), 11 (Zhang C. Q. et al., 2005; Ou et al., 2006; Zhou et al., 2002; Ren and Cheng, 2004; Cao et al., 2005; Lin and Guo, 2005; Han et al., 2013; Shao et al., 2001; Yu et al., 2006; Zhang et al., 2007; Qiao X. et al., 2019) and 9 (Zhang C. Q. et al., 2005; Ou et al., 2006; Zhou et al., 2002; Ren and Cheng, 2004; Cao et al., 2005; Lin and Guo, 2005; Han et al., 2013; Shao et al., 2001; Yu et al., 2006; Zhang et al., 2007; Qiao X. et al., 2019) articles respectively. The meta-analysis revealed that the integration of TCM with TACE remarkably enhanced OS at all time points mentioned [OR = 2.01, 95% CI (1.53, 2.63), $p < 0.00001$; OR = 2.43, 95% CI (1.95, 3.02), $p < 0.00001$; OR = 2.45, 95% CI (1.90, 3.16), $p < 0.00001$; OR = 2.77, 95% CI (1.98, 3.87), $p < 0.00001$] (Figure 4).

3.4.3 AEs

Nine articles (Yuan et al., 2005; Zhao et al., 2013; Tang, 2017; Yang, 2018; Yan et al., 2021; Song et al., 2013; Qiao J., 2019; Qiao X. et al., 2019; Li et al., 2015) (Figure 5A) reported on digestive system complications, showing that the EG had reduced incidences of abdominal pain [OR = 0.34, 95% CI (0.16, 0.76), $p = 0.008$], nausea [OR = 0.26, 95% CI (0.14, 0.51), $p < 0.0001$], and gastrointestinal reactions [OR = 0.11, 95% CI (0.03, 0.48), $p = 0.003$], with no obvious effect on diarrhea rates [OR = 0.71, 95% CI (0.39, 1.29), $p = 0.26$]. Six articles (Song et al., 2013; Zhao et al., 2013; Tang, 2017; Yang, 2018; Li et al., 2015; Qiao J., 2019) (Figure 5B) reported hematologic complications, where combined TCM treatment reduced occurrences of leukopenia [OR = 0.45, 95% CI (0.31, 0.66), $p < 0.0001$] and thrombocytopenia [OR = 0.47, 95% CI (0.33, 0.69), $p < 0.0001$], but did not significantly impact rates of myelosuppression [OR = 0.16, 95% CI (0.02, 1.39), $p = 0.10$]. For the remaining AEs, nine articles (Ren and Cheng, 2004; Yu et al., 2006; Zhang et al., 2007; Tang, 2017; Yan et al., 2021; Yuan et al., 2005; Li et al., 2015; Yang, 2018; Qiao X. et al., 2019; Song et al., 2013; Zhao et al., 2013) (Figure 5C) summarized that the EG improved occurrences of liver injury [OR = 0.30, 95% CI (0.17, 0.51), $p < 0.00001$] and fever [OR = 0.56, 95% CI (0.34, 0.93), $p = 0.03$] in HCC patients.

3.4.4 Sensitivity analysis and publication bias

The sensitivity analysis demonstrated revealed that excluding any individual study did not alter the overall trend of the results, suggesting good stability of the study outcomes. Begg's and Egger's tests indicated the presence of publication bias for ORR ($p = 0.049$, $p = 0.006$). Further use of the trim-and-fill method, employing an iterative technique, estimated that 12 studies were missing; including these missing studies, the combined effect size estimate was 0.407 ($p < 0.001$), not substantially different from the original effect value of 0.372 ($p < 0.001$), suggesting minimal impact of publication bias and robust results. Detailed results are depicted in Supplementary Figures S1, S2.

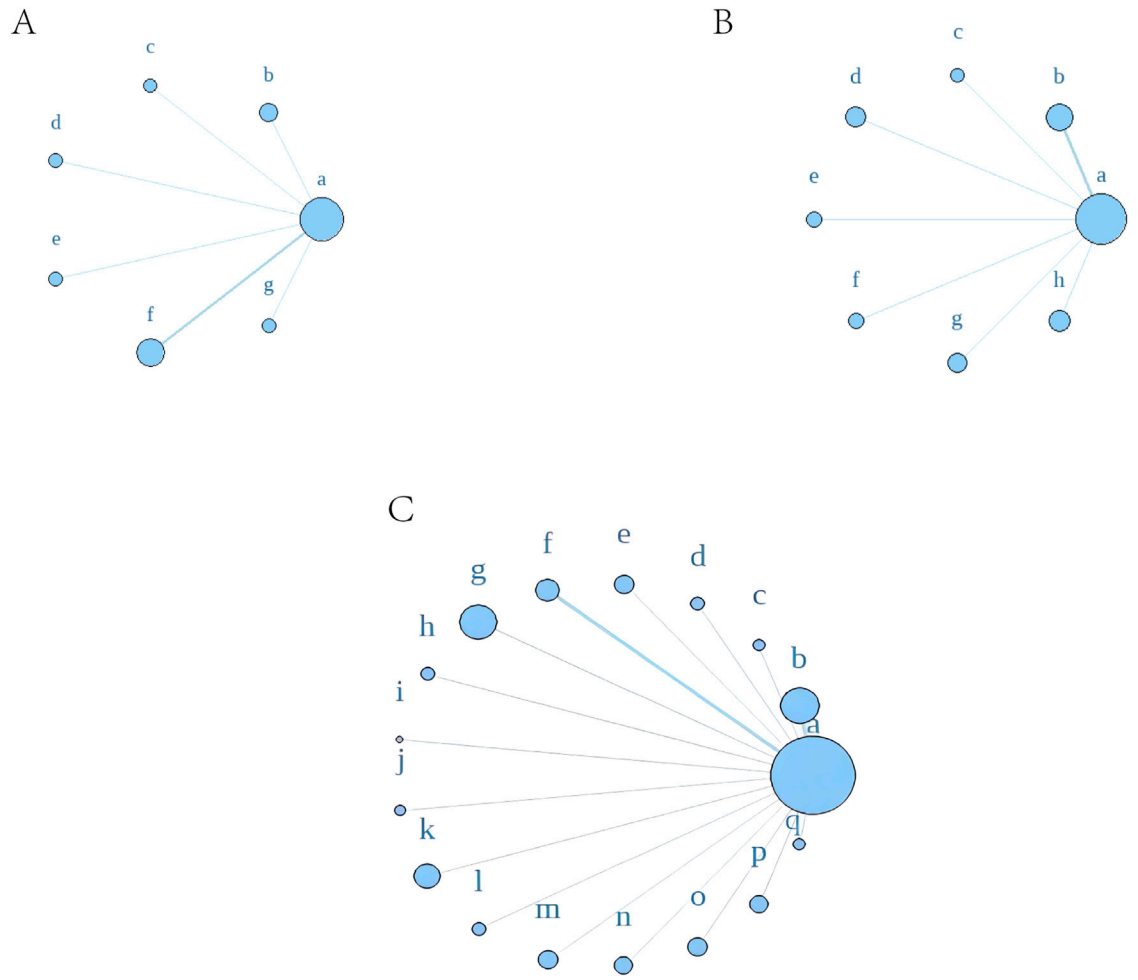

FIGURE 6
A network meta-analysis on ORR. **(A)** Liver-soothing (Shugan) herbs. **(B)** Resolving blood stasis (Huayu) herbs. **(C)** Supporting vital qi (Fuzheng) herbs. Notes: in **(A)** a: TACE, b: Shanxian Granule + TACE, c: E Tao Soup + TACE, d: Weitiao Formula II + TACE, e: Xiaoyao Powder + TACE, f: Xiao Chaihu Soup + TACE, g: Chaihu Shugan Powder + TACE. in **(B)** a: TACE, b: Guben Yiliu Formula II + TACE, c: Yiqi Huoxue Soup + TACE, d: Jinlong Capsule + TACE, e: Anti-cancer Formula + TACE, f: Jianpi Xiaotan Sanjie Formula + TACE, g: Ge Xia Zhu Yu Soup + TACE, h: Huangqin Soup + TACE. in **(C)** a: TACE, b: Jianpi Liqi Principle + TACE, c: Xiao Zheng Fuzheng Soup + TACE, d: Fuzheng Anti-cancer Formula + TACE, e: Fuzheng Pinggan Xiaoliu Soup + TACE, f: Fuzheng Jiedu Formula + TACE, g: Yangzheng Xiaoji Capsule + TACE, h: Huai Er Granule + TACE, i: Anti-cancer Formula + TACE, j: Songyou Drink + TACE, k: Jianpi Huayu Formula + TACE, l: Weitiao Formula II + TACE, m: Compound Hongdoushan Capsule + TACE, n: Zhengan Huazheng Formula + TACE, o: Ganfu Formula + TACE, p: Compound Banmao Capsule + TACE, q: Fuzheng Quxie Anti-cancer Formula + TACE.

3.4.5 Network meta-analysis of drugs

Using a Bayesian network, the effects of liver-soothing (Shugan), resolving blood stasis (Huayu), and supporting vital qi (Fuzheng) herbs on ORR in EG and CG were compared (Figure 6). The leverage plot (Supplementary Figure S3) shows that the studies are distributed within the curve, indicating good convergence of the Bayesian model. The surface under the cumulative ranking curve (SUCRA) values, suggesting intervention effectiveness, favored treatments with higher scores for better ORR outcomes. For liver-soothing (Shugan) herbs, the top three ORR rankings were Xiao Chaihu Soup (73.59%), Chaihu Shugan Powder (70.03%), E Tao Soup (55.70%) (Figure 7A); for resolving blood stasis (Huayu) herbs, the top three were Anti-cancer Formula (83.16%), Yiqi Huoxue Soup (65.48%), Jinlong Capsule (58.28%) (Figure 7B); and for supporting vital qi (Fuzheng) herbs, the top three were Ganfu Formula (89.19%), Anti-Cancer Formula (79.52%), Compound Hongdoushan Capsule (70.04%) (Figure 7C).

Additionally, we calculated the probabilities associated with each treatment plan's ranking. Chaihu Shugan Powder in the liver-soothing (Shugan) group, Anti-Cancer Formula in the blood stasis-resolving (Huayu) group, and Ganfu Formula in the supporting vital qi (Fuzheng) group were most likely to be the most effective TCMs in their respective categories (Figure 8). The ranking table (Figure 9) shows that compared to TACE alone, all types of combined TCM and TACE treatment improved patients' ORR, with vitality-supporting Ganfu Formula combined with TACE significantly improving ORR [OR = 11.75, 95% CI (1.58, 92.91)].

3.4.6 Hub TCM mining

Analysis of TCM formulations identified the 10 most frequently used herbs in this study: "Baizhu," "Huangqi," "Fuling," "Dangshen," "Gancao," "Ezhu," "Chaihu," "Baihuasheshecao," "Baishao," and "Chenpi" (Table 1). A novel formula combining these herbs was developed for subsequent NPA.

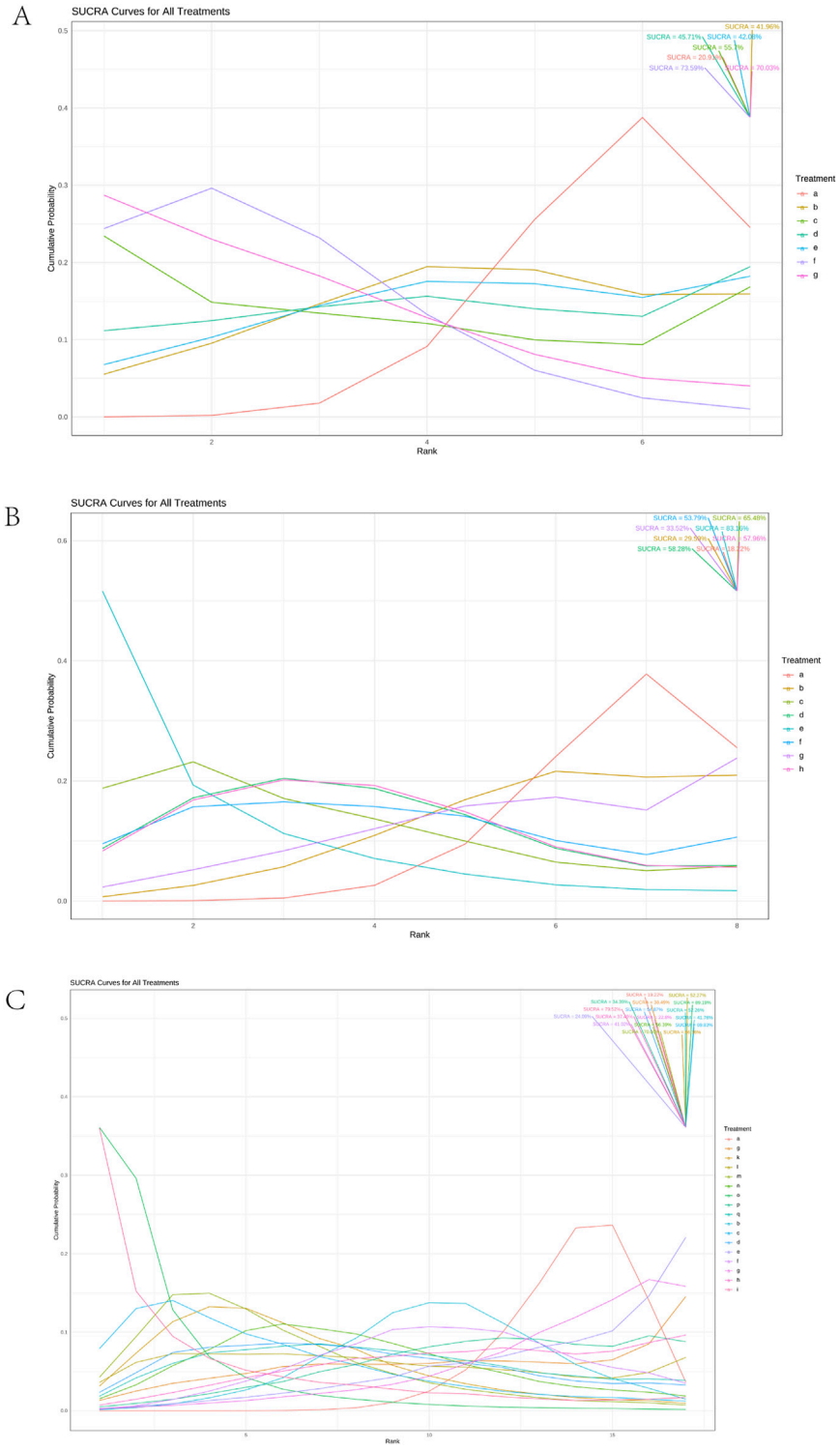

FIGURE 7
Results of SUCRA. **(A)** Liver-soothing (Shugan) herbs. **(B)** Resolving blood stasis (Huayu) herbs. **(C)** Supporting vital qi (Fuzheng) herbs. Notes: in **(A)** a: TACE, b: Shanxian Granule + TACE, c: E Tao Soup + TACE, d: Weitiao Formula II + TACE, e: Xiaoyao Powder + TACE, f: Xiao Chaihu Soup + TACE, g: Chaihu Shugan Powder + TACE. in **(B)** a: TACE, b: Guben Yiliu Formula II + TACE, c: Yiqi Huoxue Soup + TACE, d: Jinlong Capsule + TACE, e: Anti-cancer Formula + TACE, f: Jianpi Xiaotan Sanjie Formula + TACE, g: Ge Xia Zhu Yu Soup + TACE, h: Huangqin Soup + TACE. in **(C)** a: TACE, b: Jianpi Liqi Principle + TACE, c: Xiao Zheng Fuzheng Soup + TACE, d: Fuzheng Anti-cancer Formula + TACE, e: Fuzheng Pinggan Xiaoliu Soup + TACE, f: Fuzheng Jiedu Formula + TACE, g: Yangzheng Xiaoji Capsule + TACE, h: Huai Er Granule + TACE, i: Anti-cancer Formula + TACE, j: Songyou Drink + TACE, k: Jianpi Huayu Formula + TACE, l: Weitiao Formula II + TACE, m: Compound Hongdoushan Capsule + TACE, n: Zhengan Huazheng Formula + TACE, o: Ganfu Formula + TACE, p: Compound Banmao Capsule + TACE, q: Fuzheng Quxie Anti-cancer Formula + TACE.

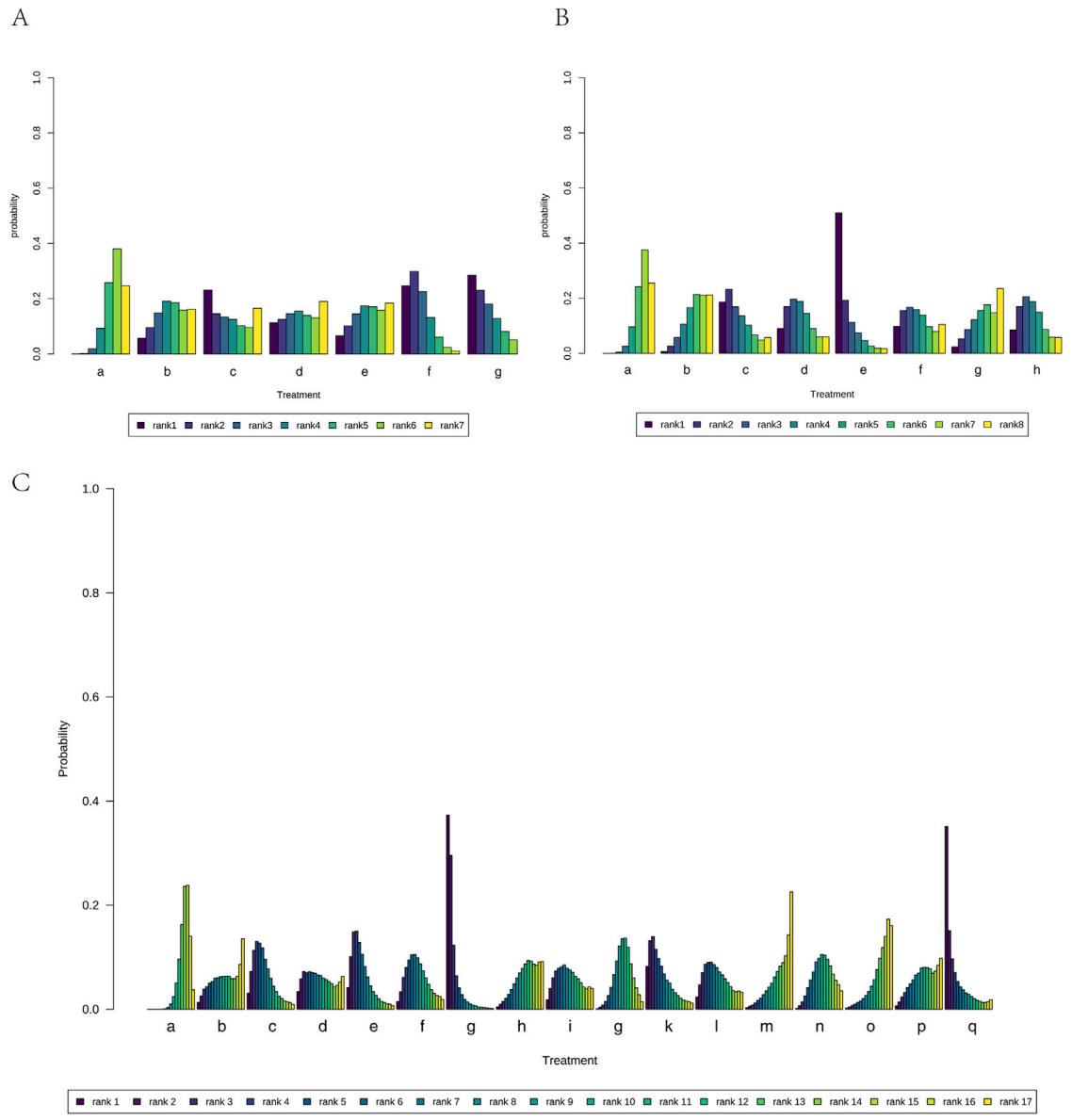

FIGURE 8
Ranking probability results for all treatment groups under different possible rankings. **(A)** Liver-soothing (Shugan) herbs. **(B)** Resolving blood stasis (Huayu) herbs. **(C)** Supporting vital qi (Fuzheng) herbs. Notes: in **(A)** a: TACE, b: Shanxian Granule + TACE, c: E Tao Soup + TACE, d: Weitiao Formula II + TACE, e: Xiaoyao Powder + TACE, f: Xiao Chaihu Soup + TACE, g: Chaihu Shugan Powder + TACE. in **(B)** a: TACE, b: Guben Yiliu Formula II + TACE, c: Yiqi Huoxue Soup + TACE, d: Jinlong Capsule + TACE, e: Anti-cancer Formula + TACE, f: Jianpi Xiaotan Sanjie Formula + TACE, g: Ge Xia Zhu Yu Soup + TACE, h: Huangqin Soup + TACE. in **(C)** a: TACE, b: Jianpi Liqi Principle + TACE, c: Xiao Zheng Fuzheng Soup + TACE, d: Fuzheng Anti-cancer Formula + TACE, e: Fuzheng Pinggan Xiaoliu Soup + TACE, f: Fuzheng Jiedu Formula + TACE, g: Yangzheng Xiaoji Capsule + TACE, h: Huai Er Granule + TACE, i: Anti-cancer Formula + TACE, j: Songyou Drink + TACE, k: Jianpi Huayu Formula + TACE, l: Weitiao Formula II + TACE, m: Compound Hongdoushan Capsule + TACE, n: Zhengan Huazheng Formula + TACE, o: Ganfu Formula + TACE, p: Compound Banmao Capsule + TACE, q: Fuzheng Quxie Anti-cancer Formula + TACE.

3.4.7 Drug-HCC gene screening and drug-component-target construction

Target genes were identified for components from the 10 prominent TCMs, containing 139 compounds and 241 target genes, illustrated in a Venn diagram (Figure 10A). We retrieved 6,434 HCC-associated genes from five databases for analysis (Figure 10B). After intersecting the drug and disease genes, 197 intersection genes were obtained (Figure 10C). These were used alongside drug components to construct a network in Cytoscape, visualizing the interactions between drug compounds and target genes (Figure 10D).

3.4.8 Core gene selection and functional enrichment analysis

A total of 197 intersecting genes were submitted to STRING for analysis (Figure 11A). Using seven algorithms in the cytoHubba plugin, we ranked genes according to score, with higher scores corresponding to higher ranks, and selected the top 30 genes for each algorithm

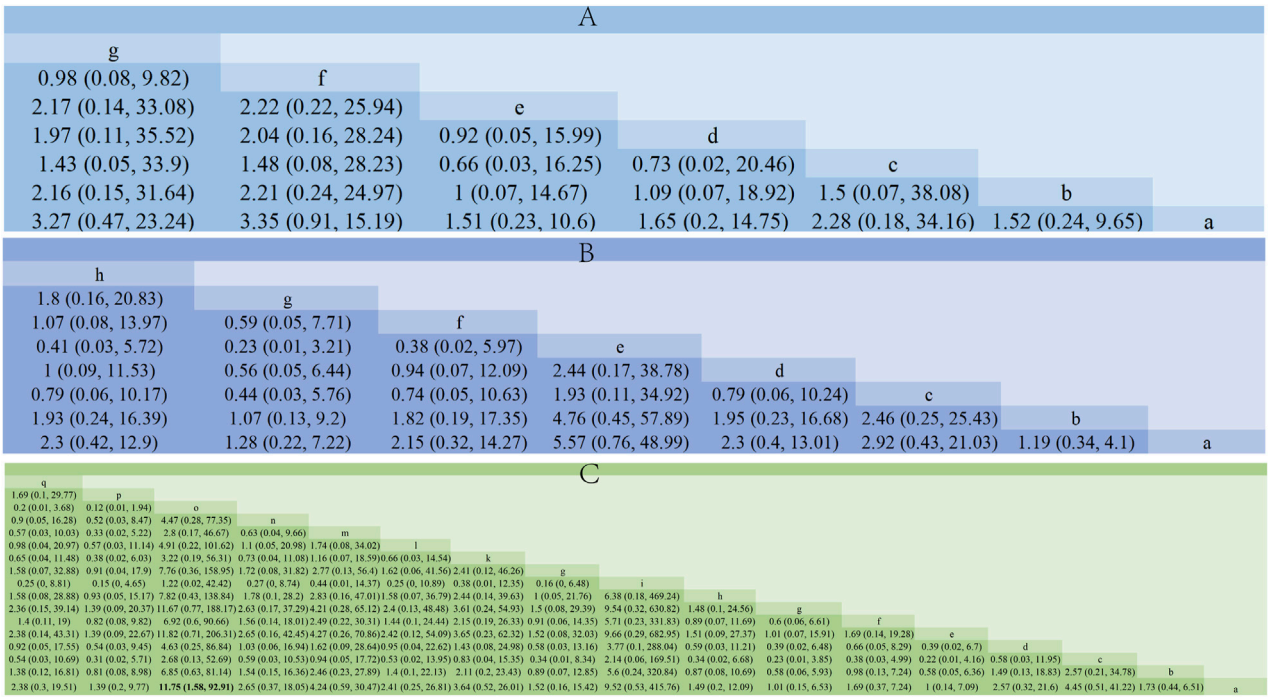

FIGURE 9
Comparison of network meta-analysis results. **(A)** Liver-soothing (Shugan) herbs. **(B)** Resolving blood stasis (Huayu) herbs. **(C)** Supporting vital qi (Fuzheng) herbs. Notes: in **(A)** a: TACE, b: Shanxian Granule + TACE, c: E Tao Soup + TACE, d: Weitiao Formula II + TACE, e: Xiaoyao Powder + TACE, f: Xiao Chaihu Soup + TACE, g: Chaihu Shugan Powder + TACE. in **(B)** a: TACE, b: Guben Yiliu Formula II + TACE, c: Yiqi Huoxue Soup + TACE, d: Jinlong Capsule + TACE, e: Anti-cancer Formula + TACE, f: Jianpi Xiaotan Sanjie Formula + TACE, g: Ge Xia Zhu Yu Soup + TACE, h: Huangqin Soup + TACE. in **(C)** a: TACE, b: Jianpi Liqi Principle + TACE, c: Xiao Zheng Fuzheng Soup + TACE, d: Fuzheng Anti-cancer Formula + TACE, e: Fuzheng Pinggan Xiaoliu Soup + TACE, f: Fuzheng Jiedu Formula + TACE, g: Yangzheng Xiaoji Capsule + TACE, h: Huai Er Granule + TACE, i: Anti-cancer Formula + TACE, j: Songyou Drink + TACE, k: Jianpi Huayu Formula + TACE, l: Weitiao Formula II + TACE, m: Compound Hongdoushan Capsule + TACE, n: Zhengan Huazheng Formula + TACE, o: Ganfu Formula + TACE, p: Compound Banmao Capsule + TACE, q: Fuzheng Quxie Anti-cancer Formula + TACE.

TABLE 1 Characteristics of ranking top 10 TCMs.

Pharmaceutical name	Chinese name	Counts	Frequency 1 (counts/total herb counts)	Frequency 2 (counts/study numbers)
Atractylodes Macrocephala Koidz	Baizhu	23	6.12%	58.97%
Hedysarum Multijugum Maxim	Huangqi	22	5.85%	56.41%
Poria Cocos (Schw.) Wolf	Fuling	18	4.79%	46.15%
Codonopsis Radix	Dangshen	16	4.26%	41.03%
licorice	Gancao	14	3.72%	35.90%
Curcumae Rhizoma	Ezhu	14	3.72%	35.90%
Radix Bupleuri	Chaihu	12	3.19%	30.77%
Hedyotis Diffusae Herba	Baihuasheshecao	11	2.93%	28.21%
Paeoniae Radix Alba	Baishao	10	2.66%	25.64%
Citrus Reticulata	Chenpi	9	2.39%	23.08%
Curcumae Radix	Yujin	8	2.13%	20.51%
Angelicae Sinensis Radix	Danggui	8	2.13%	20.51%
Scutellariae Barbatae Herba	Banzhilian	8	2.13%	20.51%

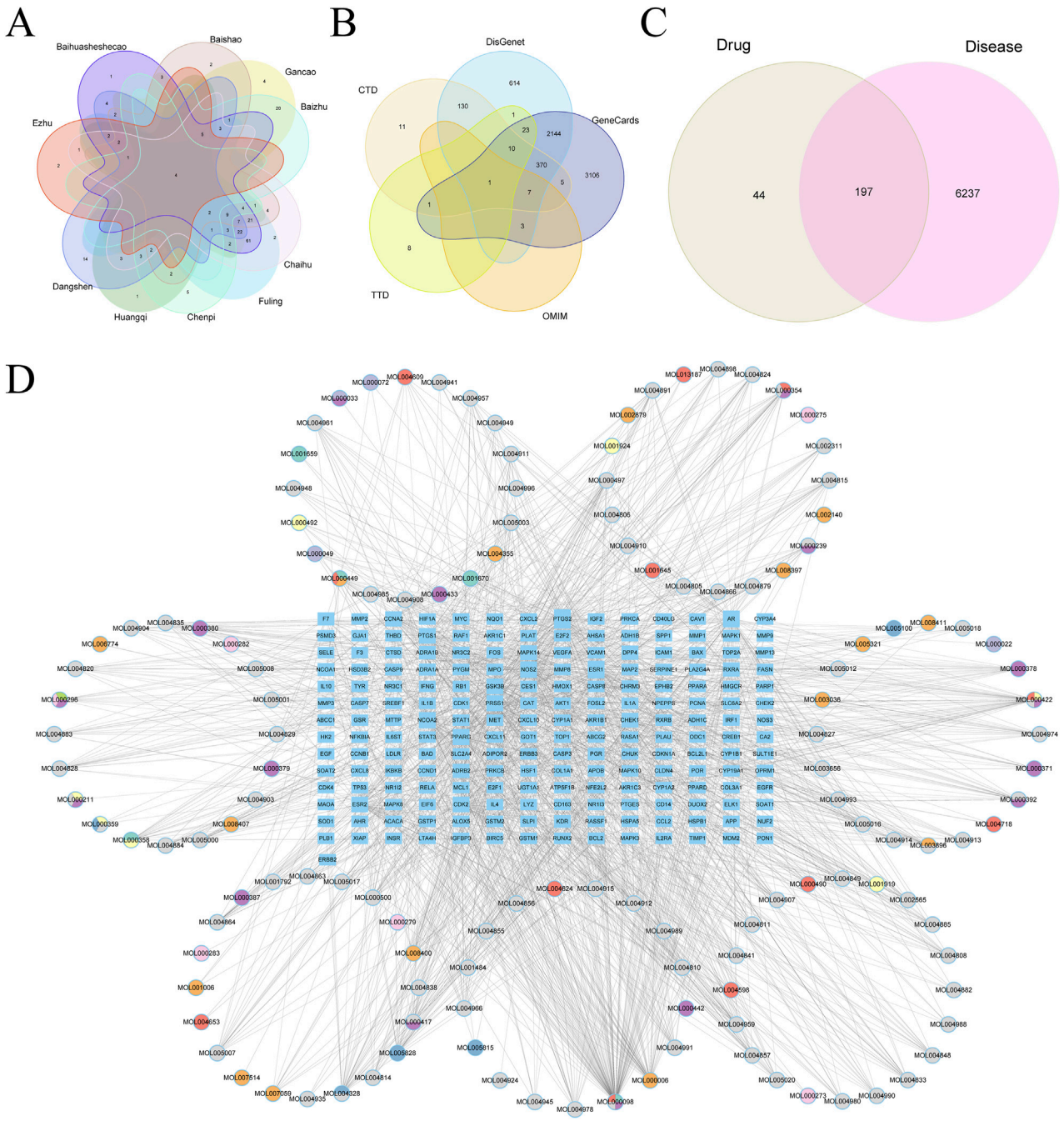

FIGURE 10
(A) Vene diagram of gene targets of ranking top 10 TCMs. **(B)** Vene diagram of multiple databases of disease targets for HCC. **(C)** Vene graph of TCM targets and HCC targets. **(D)** Ingredient-target-disease relationship network and PPI network diagram.

(Supplementary Table S4). After examining the Venn diagram intersection, we identified 17 core genes that satisfied all seven algorithms, including AKT1, TP53, IL1β, STAT3, EGFR, PTGS2, CASP3, ESR1, HIF1A, MMP9, BCL2, MYC, PPARG, MAPK3, FOS, ERBB2, and IL10 (Figure 11B). GO enrichment analysis (Figure 11C) showed that in biological processes (BP), genes primarily regulate cellular response to chemical stress and response to oxidative stress; in cellular components (CC), the RNA polymerase II transcription regulator complex exhibited the highest enrichment. In the molecular function (MF) category, genes were predominantly associated with DNA-binding transcription factor binding. KEGG analysis indicated significant enrichment of proteoglycans in cancer, lipid and atherosclerosis in positively regulated pathways, and toxoplasmosis in negatively regulated pathways (Figure 11D).

3.4.9 Molecular docking results

Molecular docking experiments were performed for each of the 17 selected core genes and their corresponding small-molecule ligands. Binding energies below −5 kJ/mol were considered indicative of binding stability, whereas energies below −7 kJ/mol

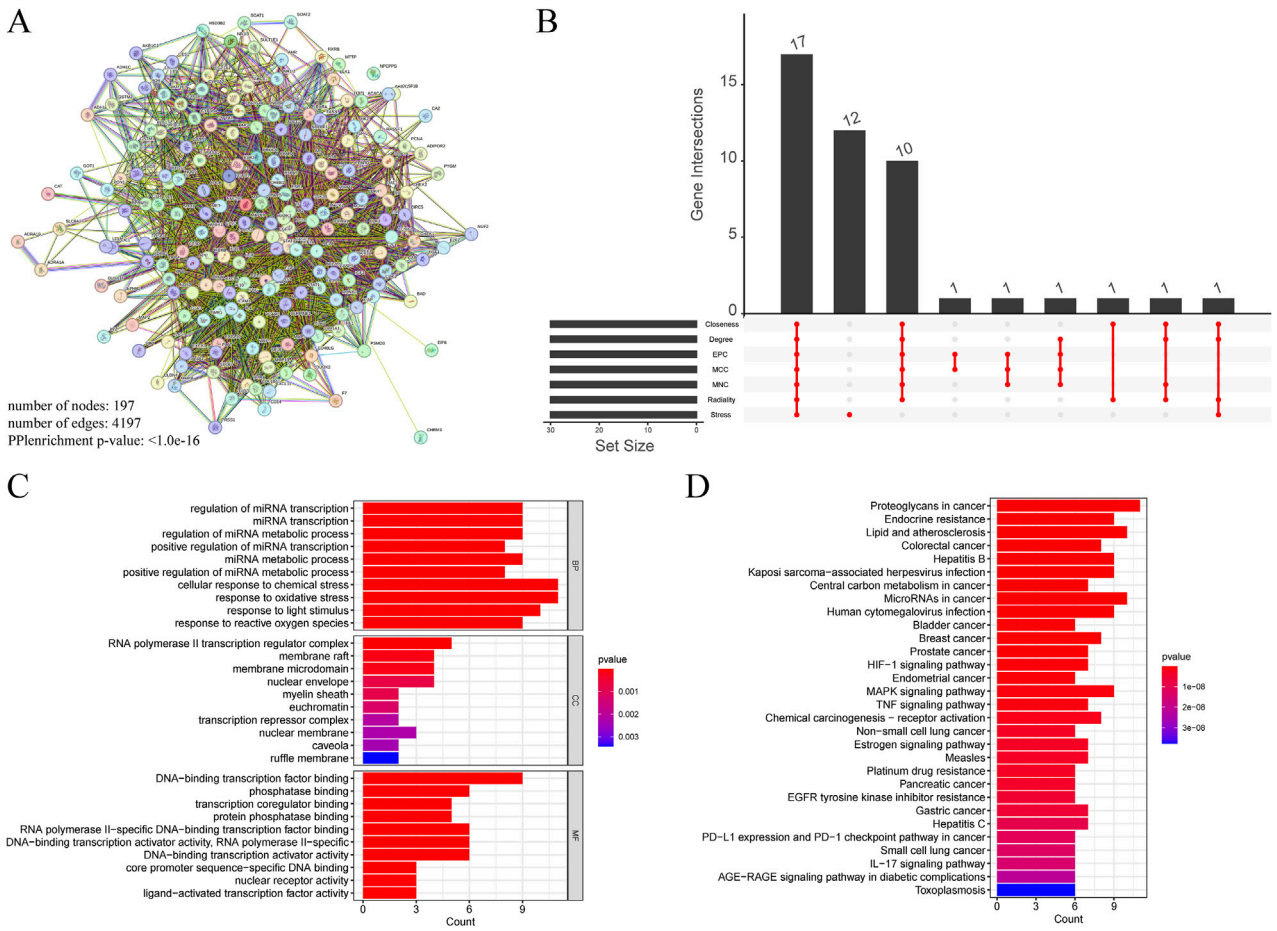

FIGURE 11
(A) PPI networks of cross genes between TCM targets and HCC targets. **(B)** The Venn diagram shows 17 core genes identified by seven algorithms. **(C)** GO analysis of core genes. **(D)** KEGG analysis of core genes.

TABLE 2 Lowest binding energy between active ingredient and key protein targets.

Name of Chinese medicine	Number	Active ingredient	Protein name	Lowest binding energy (kJ/mol)
BaiHuaSheSheCao, Chaihu, Gancao, Huangqi	MOL000098	quercetin	EGFR	−8.88
BaiHuaSheSheCao, Chaihu, Gancao, Huangqi	MOL000098	quercetin	PTGS2	−10.80
BaiHuaSheSheCao, Baishao	MOL000358	beta-sitosterol	PTGS2	−11.96
BaiHuaSheSheCao, Chaihu, Dangshen	MOL000449	Stigmasterol	PTGS2	−12.56
BaiHuaSheSheCao, Chaihu, Gancao, Huangqi	MOL000098	quercetin	ERBB2	−6.47
Dangshen	MOL000006	luteolin	ERBB2	−6.38
BaiHuaSheSheCao, Chaihu, Gancao, Huangqi	MOL000098	quercetin	IL10	−5.98
Dangshen	MOL000006	luteolin	IL10	−6.40
ChenPi, Gancao	MOL004328	naringenin	PPARG	−6.25

suggested strong binding stability (Kitchen et al., 2004). Results indicated that ERBB2, IL10, and PPARG exhibited measurable binding abilities with their corresponding ligands, while EGFR and PTGS2 displayed stable ligand binding (Table 2). Protein identifiers were retrieved from the UniProt database for the genes: EGFR (P00533), PTGS2 (P35354), ERBB2 (P04626), IL10 (P22301), and PPARG (P37231). Quercetin formed hydrogen bonds with EGFR at ASN-747, VAL-750, LEU-753, and ALA-743 (Figure 12A). For PTGS2, quercetin formed hydrogen bonds at GLN-192, ILE-517, PHE-518, MET-522, VAL-349, and HIS-90

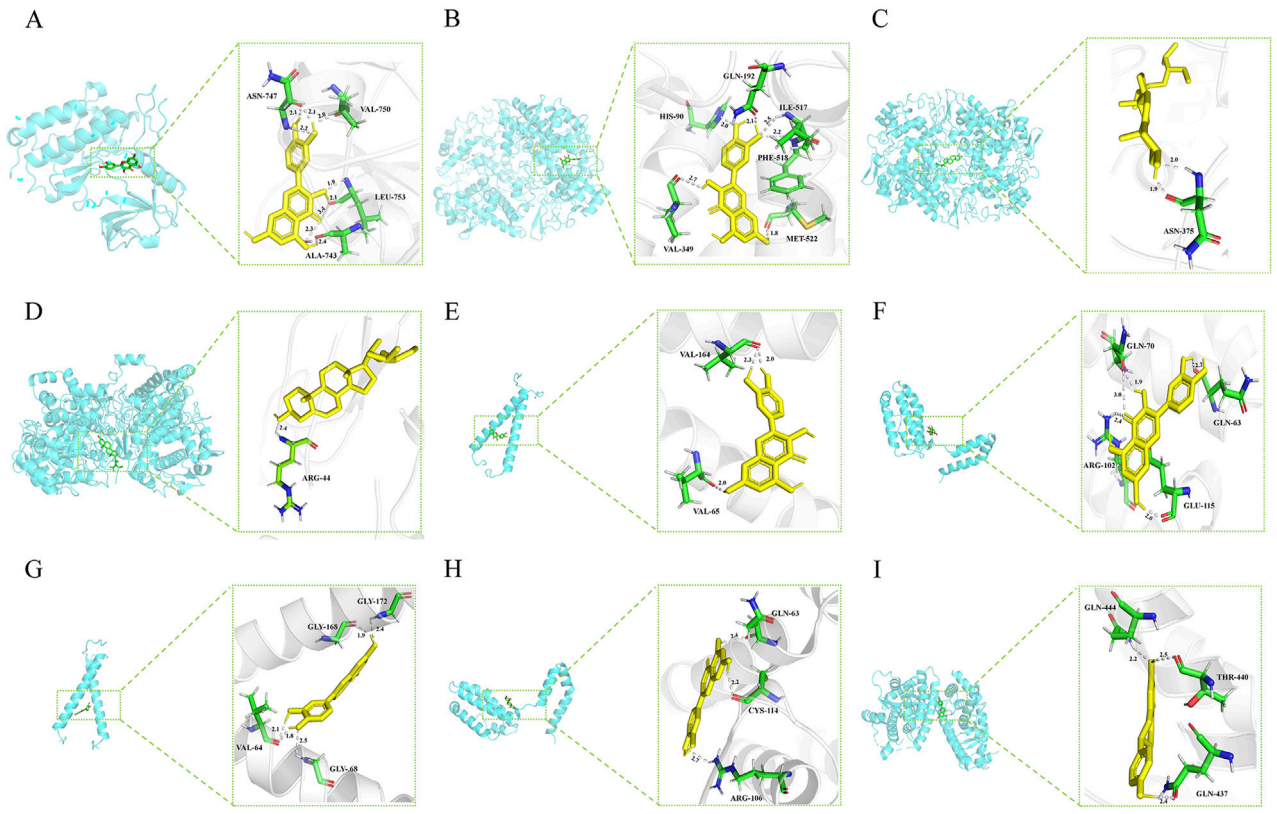

FIGURE 12
(A) EGFR (P00533) and quercetin. **(B)** PTGS2(P35354) and quercetin. **(C)** PTGS2 (P35354) and beta-sitosterol. **(D)** PTGS2 (P35354) and stigmasterol. **(E)** ERBB2 (P04626) and quercetin. **(F)** IL10 (P22301) and quercetin. **(G)** ERBB2 (P04626) and Luteolin. **(H)** IL10 (P22301) and Luteolin. **(I)** PPARG (P37231) and naringenin.

(Figure 12B), while beta-sitosterol and stigmasterol formed hydrogen bonds at ASN-375 and ARG-44, respectively (Figures 12C, D). Quercetin formed hydrogen bonds with ERBB2 at VAL-164 and VAL-65, and with IL10 at GLN-70, GLN-63, ARG-102, and GLU-115 (Figures 12E, F). Luteolin formed hydrogen bonds with ERBB2 at GLY-172, GLY-168, VAL-64, and GLY-68, and with IL-10 at GLN-63, CYS-114, and ARG-106 (Figures 12G, H). PPARG formed hydrogen bonds with naringenin at GLN-444, THR-440, and GLN-437 (Figure 12I).

3.4.10 Additional validation sets and *in vitro* experiments

In further analysis, we selected core genes with higher binding stability and validated their expression using the TCGA-LIHC dataset and qRT-PCR experiments. Results from both methods were consistent, showing that in HCC, the expression levels of EGFR, PTGS2, and IL10 were significantly downregulated (Figures 13A–F), whereas PPARG expression was notably upregulated (Figures 13G, H). However, no significant difference was detected in ERBB2 gene expression (Figures 13I, J).

4 Discussion

This study demonstrates that TCM combined with TACE treatment for HCC has significant clinical effects, providing strong evidence supporting this integrated treatment approach. Traditional Chinese Medicine attributes HCC pathogenesis to factors such as Qi stagnation, blood stasis, and accumulation of toxins, which purportedly weaken Zheng Qi and trap pathogenic Qi internally (Wang et al., 2015). TCM treatment for HCC emphasizes holistic adjustment, focusing on regulating liver Qi, strengthening the body's foundation, and promoting blood circulation, tailored to patients through differential diagnosis (Liao et al., 2020). Our meta-analysis results reveal that TCM, when used alongside TACE, significantly enhances ORR, DCR, and OS, and reduces the incidence of AEs compared to TACE alone. These findings indicate that TCM may be effectively utilized as an effective adjunct to conventional cancer treatments. Notably, the Bayesian network meta-analysis particularly highlights the significant effects of supporting vital qi (Fuzheng) herbs like Ganfu Formula combined with TACE in improving ORR. Ganfu Formula contains ingredients like Hedyotis Diffusae Herba and Scutellariae Barbatae Herba, which are extensively utilized to suppress cancer cell proliferation and promote tumor cell apoptosis, demonstrating notable anti-tumor effects in various experimental models (Yang et al., 2021; Hou et al., 2024). Hedysarum Multijugum Maxim. and Codonopsis Radix enhance immune function and liver health, with Hedysarum Multijugum Maxim. also exhibiting antioxidant and anti-inflammatory effects, thereby reducing liver damage (Sheik et al., 2021). Curcumae Radix and Radix Bupleuri significantly alleviate liver Qi stagnation and blood stasis, helping reduce pain and anxiety

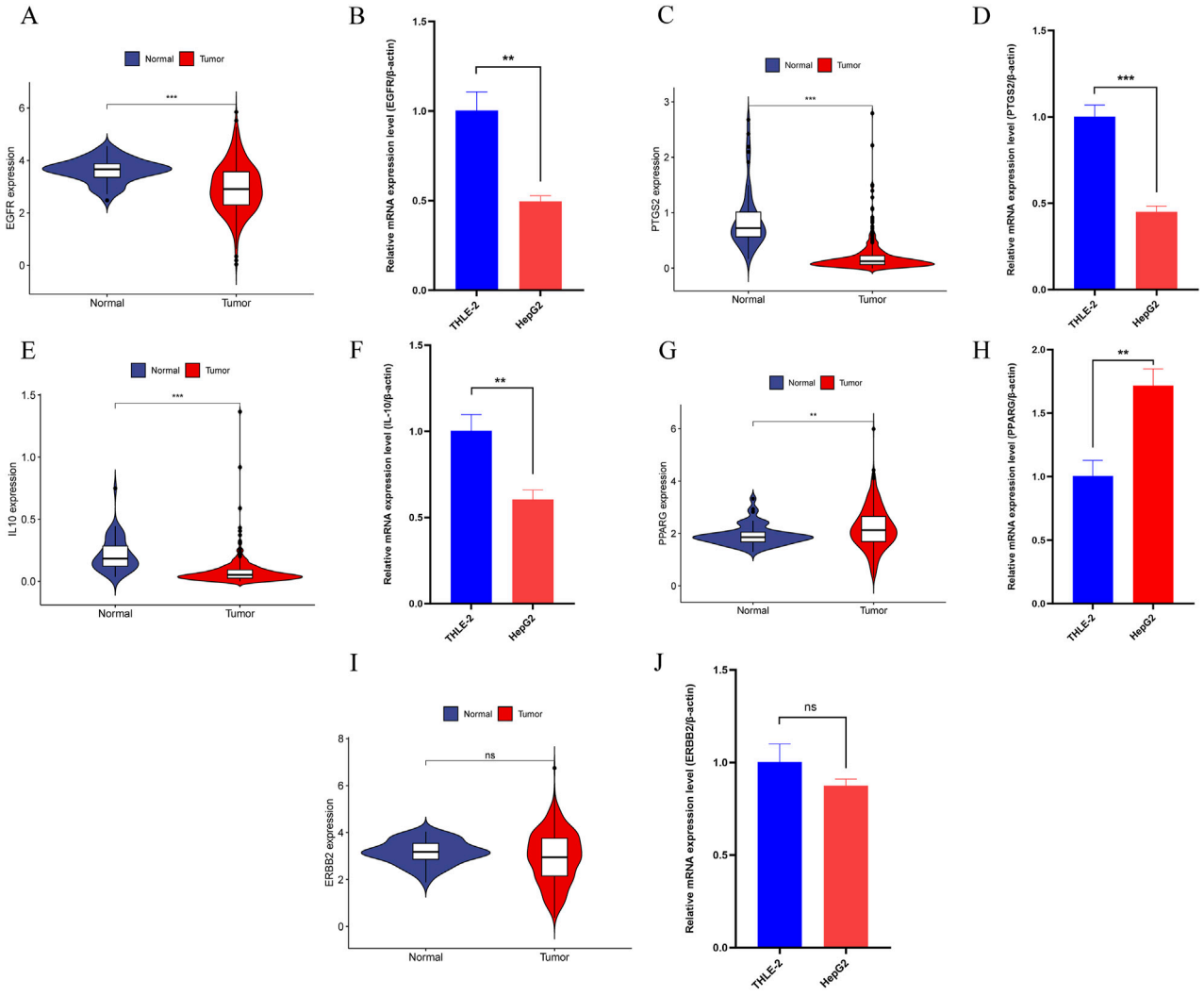

FIGURE 13
(A) The expression of EGFR in the TCGA-LIHC dataset. **(B)** qRT-PCR Results of EGFR in HCC cell lines. **(C)** The expression of PTGS2 in the TCGA-LIHC dataset. **(D)** qRT-PCR Results of PTGS2 in HCC cell lines. **(E)** The expression of IL10 in the TCGA-LIHC dataset. **(F)** qRT-PCR Results of IL10 in HCC cell lines. **(G)** The expression of PPARG in the TCGA-LIHC dataset. **(H)** qRT-PCR Results of PPARG in HCC cell lines. **(I)** The expression of ERBB2 in the TCGA-LIHC dataset. **(J)** qRT-PCR Results of ERBB2 in HCC cell lines. Note: "*", "**", and "***" indicate $p < 0.05$, $p < 0.01$, and $p < 0.001$, respectively. "ns" indicates $p > 0.05$.

in HCC patients and decrease tumor growth (Liu et al., 2022; Li et al., 2021). Pinellia and Licorice have expectorant, anti-inflammatory, and detoxifying effects, helping reduce AEs in HCC treatment (Bai et al., 2022; Aipire et al., 2017). These results provide additional evidence for the potential of TCM to modulate the tumor microenvironment, enhance immune responses, and mitigate TACE-related toxicity. However, due to the specific nature of TACE treatment, this study has limitations, including the absence of double-blinding and allocation concealment, leading to poor methodological quality. Additionally, the lack of sufficient literature prevents the evaluation of the impact of different categories of TCM on AEs in patients. Future high-quality RCTs should update meta-analysis conclusions to refine the data on AEs associated with TCM combined with TACE treatment for HCC. Additionally, this study does not investigate the *in vivo* metabolites of TCM or their specific biological activities, which limits a comprehensive understanding of TCM mechanisms, particularly regarding its potential effects on tumor microenvironment modulation and immune response enhancement. As TCM metabolites may exhibit pharmacological activities distinct from the original compounds, future studies will apply advanced analytical techniques, such as high-performance liquid chromatography-mass spectrometry, to systematically analyze these metabolites and their bioactivities. This will help elucidate the precise role of these metabolites in cancer treatment and provide a theoretical basis for optimizing the combined TCM and TACE strategy for HCC treatment.

NPA identified several key targets, including EGFR, PTGS2, ERBB2, IL10, PPARG, etc., that are intimately linked to the initiation and progression of HCC (Lin et al., 2024). BP analysis revealed that these genes primarily regulate cellular responses to chemical and oxidative stress. Consistent with existing literature, this suggests a

strong link between HCC development and the body's response to internal and external stimuli (Marra et al., 2011). TCM may boost the body's stress resistance and inhibit tumor growth by modulating these genes' expression. Interactions between RNA polymerase II and transcription factors regulate the expression of many tumor-related genes, crucial for the growth and differentiation of tumor cells (Martin, Hébert, and Tanny, 2020). CC analysis indicated significant enrichment of the RNA polymerase II transcription regulator complex, underscoring its role in HCC cell proliferation and metastasis. KEGG pathway analysis revealed that TCM may exert its anti-tumor effects by regulating various cancer-related signaling pathways, especially those involving proteoglycans and lipid metabolism. Proteoglycans are crucial in regulating cell proliferation, differentiation, and migration in HCC. Additionally, they influence the tumor microenvironment by modulating the extracellular matrix and cell signaling pathways (Wei et al., 2020). Additionally, lipid metabolism is closely linked to HCC development (Pope et al., 2019), with abnormal lipid metabolism promoting HCC cell growth via activation of the AKT/mTOR/SREBP1 pathway (Yin et al., 2017).

Quercetin suppresses cancer cell growth and triggers apoptosis by blocking EGFR-induced phosphorylation and downstream signaling pathways (Sharmila et al., 2014). Our docking analysis also indicates that quercetin forms hydrogen bonds at critical sites on the EGFR protein, suggesting that quercetin may regulate the proliferation and apoptosis of HCC cells by affecting EGFR signaling pathways. Additionally, studies show that quercetin and beta-sitosterol reduce cancer-related inflammation and tumor growth by inhibiting the expression and activity of PTGS2 (Manukyan, 2020; Salamatullah et al., 2021), supporting the relevance of our docking results where quercetin binds to PTGS2. Stigmasterol mitigates inflammation through the suppression of the NF-κB signaling pathway (Ahmad Khan et al., 2020) and impedes cancer cell proliferation and survival by targeting the Akt/mTOR and JAK/STAT pathways (Bakrim et al., 2022). Although existing studies have not directly proven that stigmasterol inhibits PTGS2 activity by binding to it, our molecular docking studies observed that stigmasterol can form stable hydrogen bonds with PTGS2, potentially reducing its activity and thereby inhibiting inflammation-related enzymatic reactions associated with PTGS2. The TCGA-LIHC and qRT-PCR results both indicate that EGFR and PTGS2 expression is significantly downregulated in HCC, providing preliminary support for the reliability of the molecular docking results in this study. Although these findings offer strong initial evidence and new insights for drug design and development, further experimental validation is required in the future.

5 Conclusion

In summary, TCM combined with TACE treatment shows more significant clinical efficacy and safety compared to TACE alone. NPA and molecular docking have uncovered multiple potential targets and their interactions pertinent to HCC treatment, offering insights into the disease mechanisms and references for further basic research and new drug development.

Data availability statement

The original contributions presented in the study are included in the article/Supplementary Material, further inquiries can be directed to the corresponding author.

Author contributions

LC: Data curation, Formal Analysis, Software, Visualization, Writing–original draft. X-LZ: Data curation, Formal Analysis, Investigation, Writing–original draft. JL: Data curation, Formal Analysis, Investigation, Writing–original draft. D-LL: Funding acquisition, Methodology, Supervision, Writing–review and editing.

Funding

The author(s) declare that financial support was received for the research, authorship, and/or publication of this article. This research was financially supported by the Clinical Application Research Special Project at the 900TH Hospital of the Joint Logistics Support Force (Grant numbers: 2021Y0062, 2021ZD04, 2021M22, and 2023XKXH06).

Conflict of interest

The authors declare that the research was conducted in the absence of any commercial or financial relationships that could be construed as a potential conflict of interest.

Publisher's note

Supplementary material

The Supplementary Material for this article can be found online at: https://www.frontiersin.org/articles/10.3389/fphar.2024.1495343/full#supplementary-material

References

Ahmad Khan, M., Sarwar, A., Rahat, R., Ahmed, R. S., and Umar, S. (2020). Stigmasterol protects rats from collagen induced arthritis by inhibiting proinflammatory cytokines. *Rev. Int Immunopharmacol* 85, 106642. doi:10.1016/j.intimp.2020.106642

Ahn, E., and Kang, H. (2021). Concepts and emerging issues of network meta-analysis. *Rev. Korean J Anesth.* 74 (5), 371–382. doi:10.4097/kja.21358

Aipire, A., Li, J., Yuan, P., He, J., Hu, Y., Liu, L., et al. (2017). Glycyrrhiza uralensis water extract enhances dendritic cell maturation and antitumor efficacy of HPV dendritic cell-based vaccine. *Rev. Sci Rep* 7, 43796. doi:10.1038/srep43796

Bai, J., Qi, J., Yang, L., Wang, Z., Wang, R., and Shi, Y. (2022). A comprehensive review on ethnopharmacological, phytochemical, pharmacological and toxicological evaluation, and quality control of Pinellia ternata (Thunb.) Breit. *Rev. J Ethnopharmacol* 298, 115650. doi:10.1016/j.jep.2022.115650

Bairoch, A., Apweiler, R., Wu, C. H., Barker, W. C., Boeckmann, B., Ferro, S., et al. (2005). The universal protein resource (UniProt). *Rev. Nucleic Acids Res* 33, D154–D159. doi:10.1093/nar/gki070

Bakrim, S., Benkhaira, N., Bourais, I., Benali, T., Lee, L. H., El Omari, N., et al. (2022). Health benefits and pharmacological properties of stigmasterol. *Rev. Antioxidants (Basel)* 11 (10), 1912. doi:10.3390/antiox11101912

Bray, F., Laversanne, M., Sung, H., Ferlay, J., Siegel, R. L., Soerjomataram, I., et al. (2024). Global cancer statistics 2022: GLOBOCAN estimates of incidence and mortality worldwide for 36 cancers in 185 countries. *Rev. CA Cancer J Clin* 74 (3), 229–263. doi:10.3322/caac.21834

Cannella, R., Zins, M., and Brancatelli, G. (2024). ESR Essentials: diagnosis of hepatocellular carcinoma-practice recommendations by ESGAR. *Rev. Eur Radiol* 34 (4), 2127–2139. doi:10.1007/s00330-024-10606-w

Cao, G. W., Wang, X. C., Zhang, F. L., Ning, H. F., Sun, Y. Q., and Yan, L. F. (2005). Clinical observation of the adjuvant treatment of HCC with self-made Ganfu Kang capsules (in Chinese). *Rev. Shandong Med. J.* 45 (2), 13–14. doi:10.3969/j.issn.1002-266X.2005.02.005

Chang, Y., Jeong, S. W., Young Jang, J., and Jae Kim, Y. (2020). Recent updates of transarterial chemoembololilzation in hepatocellular carcinoma. *Rev. Int J Mol Sci* 21 (21), 8165. doi:10.3390/ijms21218165

Cumpston, M., Li, T., Page, M. J., Chandler, J., Welch, V. A., Higgins, J. P., et al. (2019). Updated guidance for trusted systematic reviews: a new edition of the cochrane handbook for systematic reviews of interventions. *Cochrane Database Syst. Rev.* 10 (10), Ed000142. doi:10.1002/14651858.Ed000142

Ding, H. B. (2018). Effect of traditional Chinese medicine combined with TACE for primary liver cancer and its effect on liver function. *Rev. Pract. J. Cancer* 33 (05), 787–789. doi:10.3969/j.issn.1001-5930.2018.05.027

Doncheva, N. T., Morris, J. H., Gorodkin, J., and Jensen, L. J. (2019). Cytoscape StringApp: network analysis and visualization of proteomics data. *Rev. J Proteome Res* 18 (2), 623–632. doi:10.1021/acs.jproteome.8b00702

Goodsell, D. S., Sanner, M. F., Olson, A. J., and Forli, S. (2021). The AutoDock suite at 30. *Rev. Protein Sci* 30 (1), 31–43. doi:10.1002/pro.3934

Han, K. Q., Xie, G. Q., Chen, J., He, T. L., Qian, Z. P., Gu, W., et al. (2013). Clinical study on the efficacy of transcatheter arterial chemoembolization with Fuzhengjiedu prescription of traditional Chinese medicine on hepatocellular carcinoma in advanced stage. *Rev. Chin. J. Integr. Traditional West. Med. Dig.* 2, 57–60. CNKI:SUN:ZXPW.0.2013-02-000.

Hong, G. H., Chen, S. H., and Huang, S. (2020). Effect of compound cantharidin capsules on clinical efficacy and immune function in patients with primary liver cancer (in Chinese). *Rev. World J. Integr. Traditional West. Med.* 15 (02), 365–368+373. CNKI:SUN:SJZX.0.2020-02-037.

Hou, C., Wen, X., Yan, S., Gu, X., Jiang, Y., Chen, F., et al. (2024). Network-based pharmacology-based research on the effect and mechanism of the Hedyotis diffusa-Scutellaria Barbata pair in the treatment of hepatocellular carcinoma. *Rev. Sci Rep* 14 (1), 963. doi:10.1038/s41598-023-50696-y

Huang, R. Y. (2019). Clinical effect of Gexia Zhuyu decoction combined with precise hepatic arterial chemoembolization in the treatment of middle and advanced primary liver cancer. *Rev. China Mod. Dr.* 57 (19), 36–38+42. CNKI:SUN:ZDYS.0.2019-19-009.

Kitchen, D. B., Decornez, H., Furr, J. R., and Bajorath, J. (2004). Docking and scoring in virtual screening for drug discovery: methods and applications. *Rev. Nat Rev Drug Discov* 3 (11), 935–949. doi:10.1038/nrd1549

Kudo, M. (2019). A new treatment option for intermediate-stage hepatocellular carcinoma with high tumor burden: initial lenvatinib therapy with subsequent selective TACE. *Rev. Liver Cancer* 8 (5), 299–311. doi:10.1159/000502905

Kudo, M., Han, K. H., Ye, S. L., Zhou, J., Huang, Y. H., Lin, S. M., et al. (2020). A changing paradigm for the treatment of intermediate-stage hepatocellular carcinoma: asia-pacific primary liver cancer expert consensus statements. *Rev. Liver Cancer* 9 (3), 245–260. doi:10.1159/000507370

Li, B., Wang, Y., and Zhang, X. (2014). Clinical observation of spleen-strengthening, phlegm-resolving, and mass-dissipating formula for treating middle to late stage primary liver cancer (in Chinese). *Rev. Liaoning J. Traditional Chin. Med.* 41 (01), 108–110. CNKI:SUN:LNZY.0.2014-01-051.

Li, H. T., Chen, C., Zhang, H. Y., and Wang, Y. P. (2015). Observation of the effect of Jianpi Huayu formula combined with transcatheter arterial chemoembolization in the treatment of liver cancer (in Chinese). *Rev. Chin. J. Clin. Ration. Drug Use* 8 (25), 32–33. doi:10.15887/j.cnki.13-1389/r.2015.25.019

Li, K., Xiao, K., Zhu, S., Wang, Y., and Wang, W. (2022). Chinese herbal medicine for primary liver cancer therapy: perspectives and challenges. *Rev. Front Pharmacol* 13, 889799. doi:10.3389/fphar.2022.889799

Li, X., Qin, X. M., Tian, J. S., Gao, X. X., Du, G. H., and Zhou, Y. Z. (2021). Integrated network pharmacology and metabolomics to dissect the combination mechanisms of Bupleurum chinense DC-Paeonia lactiflora Pall herb pair for treating depression. *Rev. J Ethnopharmacol* 264, 113281. doi:10.1016/j.jep.2020.113281

Li, Y., Guo, P., and Tian, Y. (2019). Effects of Huangqin Decoction combined with sequential hepatic arterial chemoembolization on the expression of NF-κB and HIF-1α in patients with primary liver cancer. *Rev. China J Tradit Chin Med Pharma* 34 (8), 3870–3873. CNKI:SUN:BXYY.0.2019-08-146.

Liao, X., Bu, Y., and Jia, Q. (2020). Traditional Chinese medicine as supportive care for the management of liver cancer: past, present, and future. *Rev. Genes Dis* 7 (3), 370–379. doi:10.1016/j.gendis.2019.10.016

Lin, J., Guo, H., Qin, H., Zhang, X., and Sheng, J. (2024). Integration of meta-analysis and network pharmacology analysis to investigate the pharmacological mechanisms of traditional Chinese medicine in the treatment of hepatocellular carcinoma. *Rev. Front Pharmacol* 15, 1374988. doi:10.3389/fphar.2024.1374988

Lin, J., and Guo, W. (2005). Clinical observation on Jianpi Liqi recipe for treatment of 25 cases of distal metastasis of liver cancer. *Rev. J. Traditional Chin. Med.* 46 (1), 26–28. doi:10.3321/j.issn:1001-1668.2005.01.015

Liu, F., Liang, Y., Sun, R., Yang, W., Liang, Z., Gu, J., et al. (2022). Astragalus mongholicus Bunge and Curcuma aromatica Salisb. inhibits liver metastasis of colon cancer by regulating EMT via the CXCL8/CXCR2 axis and PI3K/AKT/mTOR signaling pathway. *Rev. Chin Med* 17 (1), 91. doi:10.1186/s13020-022-00641-4

Liu, H., Wang, H., and Hu, H. (2007). Integrated traditional Chinese and western medicine in the treatment of 66 cases of primary liver cancer (in Chinese). *Rev. Guangming J. Chin. Med.* 22 (5), 68–69. doi:10.3969/j.issn.1003-8914.2007.05.042

Liu, X., You, J., and Zhang, B. (2013). Modified formula II combined with interventional therapy for primary liver cancer: a study of 32 cases (in Chinese). *Rev. Shaanxi J. Traditional Chin. Med.* (5), 518–520. doi:10.3969/j.issn.1000-7369.2013.05.002

Manukyan, A. E. (2020). "Evaluation of the Quercetin semisynthetic derivatives interaction with ABCG2 and Cyclooxygenase-2," in Proceedings of ICNBME-2019 Paper presented at the 4th International Conference on Nanotechnologies and Biomedical Engineering, Chisinau, Moldova, September 18-21, 2019, 549–552. doi:10.1007/978-3-030-31866-6_98

Marra, M., Sordelli, I. M., Lombardi, A., Lamberti, M., Tarantino, L., Giudice, A., et al. (2011). Molecular targets and oxidative stress biomarkers in hepatocellular carcinoma: an overview. *Rev. J Transl Med* 9, 171. doi:10.1186/1479-5876-9-171

Martin, R. D., Hébert, T. E., and Tanny, J. C. (2020). Therapeutic targeting of the general RNA polymerase II transcription machinery. *Rev. Int J Mol Sci* 21 (9), 3354. doi:10.3390/ijms21093354

Meng, F., Sun, J., and Lun, J. (2021). Clinical efficacy of modified xiaochaihu decoction combined with hepatic arterial chemoembolization for the treatment of primary liver cancer (in Chinese). *Rev. Strait Pharm. J.* 33, 170–172. doi:10.3969/j.issn.1006-3765.2021.03.066

Moher, D., Shamseer, L., Clarke, M., Ghersi, D., Liberati, A., Petticrew, M., et al. (2015). Preferred reporting items for systematic review and meta-analysis protocols (PRISMA-P) 2015 statement. *Rev. Syst Rev* 4 (1), 1. doi:10.1186/2046-4053-4-1

Ou, Y., Yu, Q., Li, G., Liang, J., and Zeng, W. (2006). Clinical observation of primary liver cancer treated with hepatic arterial chemoembolization and integrated traditional Chinese and western medicine (in Chinese). *Rev. Guangzhou Med. J.* 37 (4), 69–70. CNKI:SUN:GZYY.0.2006-04-038.

Pope, E. D., 3rd, Kimbrough, E. O., Vemireddy, L. P., Surapaneni, P. K., Copland, J. A., 3rd, and Mody, K. (2019). Aberrant lipid metabolism as a therapeutic target in liver cancer. *Rev. Expert Opin Ther Targets* 23 (6), 473–483. doi:10.1080/14728222.2019.1615883

Qiao, X., Wang, H., and Yang, L. (2019). Fuyuan Huoxue decoction plus Huaji pills and hepatic artery embolization in the treatment of primary liver cancer. *Rev. Shaanxi J. Traditional Chin. Med.* 40 (08), 998–1000. doi:10.3969/j.issn.1000-7369.2019.08.004

Qiao J., J. (2019). Clinical observation of transcatheter arterial chemoembolization combined with Chinese medicine Ganfu method for the treatment of primary liver cancer with liver depression and spleen deficiency syndrome (in Chinese). *Rev. China"s Naturopathy* 27 (15), 66–68. doi:10.19621/j.cnki.11-3555/r.2019.1533

Ren, H., and Cheng, L. (2004). Clinical observation on the treatment of middle-late stage liver carcinoma by combined therapy of hepato-arterial chemo-embolising and

Chinese drugs for strengthening pi and regulating qi. *Rev. Zhongguo Zhong Xi Yi Jie He Za Zhi* 24 (9), 838–840. doi:10.7661/CJIM.2004.9.838

Ru, J., Li, P., Wang, J., Zhou, W., Li, B., Huang, C., et al. (2014). TCMSP: a database of systems pharmacology for drug discovery from herbal medicines. *Rev. J Cheminform* 6, 13. doi:10.1186/1758-2946-6-13

Salamatullah, A. M., Subash-Babu, P., Nassrallah, A., Alshatwi, A. A., and Alkaltham, M. S. (2021). Cyclotrisiloxan and β-Sitosterol rich *Cassia alata* (L.) flower inhibit HT-115 human colon cancer cell growth via mitochondrial dependent apoptotic stimulation. *Rev. Saudi J Biol Sci* 28 (10), 6009–6016. doi:10.1016/j.sjbs.2021.06.065

Seeliger, D., and de Groot, B. L. (2010). Ligand docking and binding site analysis with PyMOL and Autodock/Vina. *Rev. J Comput. Aided Mol Des* 24 (5), 417–422. doi:10.1007/s10822-010-9352-6

Shao, Z. X., Cheng, Z. G., and Yin, X. (2001). Clinical study on treatment of middle-advanced stage liver cancer by combined treatment of hepatic artery chemoembolization with gan'ai no. I and no. II. *Rev. Zhongguo Zhong Xi Yi Jie He Za Zhi* 21 (3), 168–170.

Sharmila, G., Bhat, F. A., Arunkumar, R., Elumalai, P., Raja Singh, P., Senthilkumar, K., et al. (2014). Chemopreventive effect of quercetin, a natural dietary flavonoid on prostate cancer in *in vivo* model. *Rev. Clin Nutr* 33 (4), 718–726. doi:10.1016/j.clnu.2013.08.011

Sheik, A., Kim, K., Varaprasad, G. L., Lee, H., Kim, S., Kim, E., et al. (2021). The anti-cancerous activity of adaptogenic herb Astragalus membranaceus. *Rev. Phytomedicine* 91, 153698. doi:10.1016/j.phymed.2021.153698

Shin, J. M., and Cho, D. H. (2005). PDB-Ligand: a ligand database based on PDB for the automated and customized classification of ligand-binding structures. *Rev. Nucleic Acids Res* 33, D238–D241. doi:10.1093/nar/gki059

Song, D. G., Tan, P., and Shi, H. (2013). Efficacy observation of yangzhengxiaoji capsule combined with hepatic artery chemotherapy embolism in improving liver function in patients with primary hepayic carcinoma. *Rev. World Chin. Med.*, 973–975. doi:10.3969/j.issn.1673-7202.2013.08.042

Tang, Z. Y. (2017). *Clinical study on the treatment of primary liver cancer with WeiDiao No. 2 (WD-2) combined with transcatheter arterial chemoembolization (TACE)*. Master's Thesis. Nanjing University of Chinese Medicine.

Tian, Y., Tian, B., Li, G., and Wang, C. (2019). Clinical observation of xiaochaihu decoction combined with transcatheter arterial chemoembolization for the treatment of primary liver cancer (in Chinese). *Rev. China"s Naturopathy* 27 (12), 63–64. doi:10.19621/j.cnki.11-3555/r.2019.1235

Tong, W. U., Yu, Z., Yu, Y., Yu, J., Ma, P., Li, H., et al. (2022). Effect of decoction of Fuzheng Jiedu Xiaoji formula plus chemoembolization on primary liver cancer in patients. *Rev. J Tradit Chin Med* 42 (3), 446–450. doi:10.19852/j.cnki.jtcm.2022.03.011

Wan, X. Y. (2018). Clinical study of Zhenggan recipe combined with TACE in treatment of patients with primary liver cancer. *Rev. Chin. J. Integr. Traditional West. Med. Dig.* 26 (03), 256–260. CNKI:SUN:ZXPW.0.2018-03-008.

Wang, X., Wang, N., Cheung, F., Lao, L., Li, C., and Feng, Y. (2015). Chinese medicines for prevention and treatment of human hepatocellular carcinoma: current progress on pharmacological actions and mechanisms. *Rev. J Integr Med* 13 (3), 142–164. doi:10.1016/s2095-4964(15)60171-6

Wang, X. D., Li, B., Cai, L. J., Huang, S. Q., and Wei, M. (2020). Short-term clinical observation of Fuzheng QuXie yiai recipe combined with TACE in the treatment of patients with advanced primary liver cancer (in Chinese). *Rev. Asia-Pacific Traditional Med.* (9), 151–155. doi:10.11954/ytctyy.202009050

Wang, Y., Xiao, J., Suzek, T. O., Zhang, J., Wang, J., Zhou, Z., et al. (2012). PubChem's BioAssay database. *Nucleic Acids Res.* 40, D400–D412. doi:10.1093/nar/gkr1132

Wang, Z., and Chen, W. (2007). Clinical observation of interventional therapy combined with Fuzheng pinggan Xiaoliu decoction for advanced liver cancer (in Chinese). *Rev. China Mod. Dr.* 45 (12X), 67–68. doi:10.3969/j.issn.1673-9701.2007.24.044

Wei, J., Hu, M., Huang, K., Lin, S., and Du, H. (2020). Roles of proteoglycans and glycosaminoglycans in cancer development and progression. *Rev. Int J Mol Sci* 21 (17), 5983. doi:10.3390/ijms21175983

Wen, H., and Peng, Y. (2006). Treatment of 32 cases of advanced liver cancer with integrated traditional Chinese and western medicine (in Chinese). *Rev. Shaanxi J. Traditional Chin. Med.* 27 (1), 26–28. doi:10.3969/j.issn.1000-7369.2006.01.014

Wu, G. L., Zhang, L., Li, T. Y., Chen, J., Yu, G. Y., and Li, J. P. (2010). Short-term effect of combined therapy with Jinlong Capsule and transcatheter arterial chemoembolization on patients with primary hepatic carcinoma and its influence on serum osteopontin expression. *Rev. Chin J Integr Med* 16 (2), 109–113. doi:10.1007/s11655-010-0109-9

Yan, T. F., Cao, Z. Q., Yao, S. S., and Xu, H. J. (2021). Clinical observation of Chaihu shugan powder combined with transcatheter arterial chemoembolization in the treatment of primary liver cancer (in Chinese). *Rev. World J. Integr. Traditional West. Med.* 16 (07), 1357–1361. doi:10.13935/j.cnki.sjzx.210737

Yang, H. (2018). *Clinical observation of xiaoyaosan jiawei combined with TACE in the treatment of primary liver cancer (liver stagnation and spleen deficiency type)*. Master's Thesis. Guangxi University of Chinese Medicine.

Yang, P. W., Chen, T. T., Zhao, W. X., Liu, G. W., Feng, X. J., Wang, S. M., et al. (2021). Scutellaria barbata D.Don and Oldenlandia diffusa (Willd.) Roxb crude extracts inhibit hepatitis-B-virus-associated hepatocellular carcinoma growth through regulating circRNA expression. *Rev. J Ethnopharmacol* 275, 114110. doi:10.1016/j.jep.2021.114110

Yin, F., Sharen, G., Yuan, F., Peng, Y., Chen, R., Zhou, X., et al. (2017). TIP30 regulates lipid metabolism in hepatocellular carcinoma by regulating SREBP1 through the Akt/mTOR signaling pathway. *Rev. Oncog.* 6 (6), e347. doi:10.1038/oncsis.2017.49

Yin, T. L., Zhang, Y. F., Zhou, X. F., and Luan, S. C. (2013). Clinical observation of anticancer medicine combined with transhepatic arterial chemotherapy and embolization in treatment of primary hepatocellular carcinoma. *Rev. China Mod. Med.* 20 (35), 110–111. CNKI:SUN:ZGUD.0.2013-35-059.

Yu, J., Zhang, Q., and Wang, X. M. (2006). Treatment of primary liver cancer with Gubenyiliu Formula II combined with artery perfusion of chemical drugs. *Rev. J. Bjing Univ. Traditional Chin.* 13 (3), 9–11. doi:10.3969/j.issn.1672-2205.2006.03.004

Yuan, J. B., Su, C. Z., Wang, W. Z., Xu, P., Xu, Z. F., Xu, J. G., et al. (2005). Observation of the efficacy of interventional therapy combined with xiaozheng Fuzheng decoction in treating 24 cases of liver cancer (in Chinese). *Rev. New Chin. Med.* 37 (3), 63–65. doi:10.3969/j.issn.0256-7415.2005.03.030

Zhang, C. Q., Liang, T. J., and Yuan, M. J. (2005). Clinical studies of the combination therapy with Jin Long capsule and chemical therapy and embolization by hepatic artery catheterization on primary hepatic carcinoma. *Rev. Beijing Yi Xue* 27 (6), 357–359. doi:10.3969/j.issn.0253-9713.2005.06.013

Zhang, Q., Chi, H. C., Yu, J., Wang, X. M., and Zhao, W. S. (2007). Clinical study of Gu Ben Yi Liu II combined with chemicals arterial perfusion for advanced hepatoma of 58 cases. *Rev. Zhong Yi Za Zhi* 48 (3), 235–236. doi:10.3321/j.issn:1001-1668.2007.03.015

Zhang, Y. M., Peng, Y. X., and Guan, H. Z. (2005). Observation on the treatment of liver cancer with shanshen granules combined with interventional therapy (in Chinese). *Rev. J. Shaanxi Univ. Chin. Med.* 28 (3), 31–32. doi:10.3969/j.issn.1002-168X.2005.03.019

Zhao, G. S., Liu, Y., Zhang, Y. W., Li, C., Tang, S. X., Zhou, J., et al. (2013). Huaier granules combined with intraarterial chemoembolization for the treatment of hepatocellular carcinoma. *Rev. Chin. J. General Surg.*, 440–443. doi:10.3760/cma.j.issn.1007-631X.2013.06.011

Zhao, L., Zhang, H., Li, N., Chen, J., Xu, H., Wang, Y., et al. (2023). Network pharmacology, a promising approach to reveal the pharmacology mechanism of Chinese medicine formula. *Rev. J Ethnopharmacol* 309, 116306. doi:10.1016/j.jep.2023.116306

Zheng, S. S. (2014). *Clinical research and molecular mechanism exploration of Songyou Drink combined with TACE in the treatment of unresectable liver cancer*. Master's Thesis. Fudan University.

Zhong, R., Su, C., and Yuan, J. (2007). Yi qi huo xue decoction combined with interventional therapy for primary liver cancer: observation of 26 cases (in Chinese). *Rev. Shaanxi J. Traditional Chin. Med.* 28 (9), 1117–1119. doi:10.3969/j.issn.1000-7369.2007.09.008

Zhou, X. Y., Wu, X. D., Zuo, X., Ge, R., and Xue, Y. B. (2002). Clinical research of TACE combined with Chinese medicine in the treatment of 118 cases of mid-and late-stage hepatocellular carcinoma. *Rev. Jiangsu Zhong Yi Yao* 23 (11), 15–17. doi:10.3969/j.issn.1672-397X.2002.11.008

Zhou, X. Z., Sun, X. F., Ma, W. F., Huang, Q. G., Xu, W. J., Zhan, B. L., et al. (2010). Clinical observation on anti-cancer decoction combined with TACE for HCC in Qi-deficiency and blood stasis. *Rev. J. Traditional Chin. Med. Univ. Hunan* 30 (11), 55–57. doi:10.3969/j.issn.1674-070X.2010.11.018.055.03

frontiers | Frontiers in Pharmacology

TYPE Mini Review
PUBLISHED 21 February 2025
DOI 10.3389/fphar.2025.1556245

OPEN ACCESS

EDITED BY
Xinyu Wang,
Philadelphia College of Osteopathic Medicine (PCOM), United States

REVIEWED BY
Yuancheng Li,
Emory University, United States

*CORRESPONDENCE
Jianbao Gong,
giianbao2020@sina.com
Baoxin Shang,
912848865@qq.com
Xuwen Li,
lcyblxw@163.com

RECEIVED 06 January 2025
ACCEPTED 04 February 2025
PUBLISHED 21 February 2025

CITATION
Shi X, Tang K, Zhang Q, Han Q, Quan L, Li Y, Cui J, Feng N, Gong J, Shang B and Li X (2025) Antibody-drug conjugate combinations in cancer treatment: clinical efficacy and clinical study perspectives.
Front. Pharmacol. 16:1556245.
doi: 10.3389/fphar.2025.1556245

Antibody-drug conjugate combinations in cancer treatment: clinical efficacy and clinical study perspectives

Xianglong Shi[1], Kai Tang[2], Quanbin Zhang[3], Qingkun Han[4], Lin Quan[1], Yijing Li[1], Jianqiao Cui[1], Nuan Feng[5], Jianbao Gong[6]*, Baoxin Shang[1]* and Xuwen Li[1,7]*

[1]The Affffliated Hospital of Qingdao University, Qingdao University, Qingdao, China, [2]Department of Urology, Zibo Central Hospital, Zibo, China, [3]Department of Trauma Orthopedics, Zibo Central Hospital, Zibo, China, [4]Hematology Department, Zibo Central Hospital, Zibo, China, [5]Qingdao Women and Children's Hospital, Qingdao University, Qingdao, China, [6]Qingdao Hospital, University of Health and Rehabilitation Sciences, Qingdao Municipal Hospital, Qingdao, China, [7]Traumatology Department, Affiliated Hospital of Qingdao University, Qingdao, China

Antibody-drug conjugates have emerged as a promising cancer treatment, combining targeted delivery of cytotoxic agents with the specificity of monoclonal antibodies. Despite their potential, ADCs face limitations such as resistance and off-target effects. To enhance their efficacy, ADCs are increasingly being combined with other therapeutic strategies, including immune checkpoint inhibitors, chemotherapy, small-molecule inhibitors, anti-angiogenic agents, and CAR-T cell therapies. These combination therapies aim to overcome resistance mechanisms, improve tumor targeting, and boost immune responses. Clinical studies have shown that such combinations can significantly improve response rates and progression-free survival across various cancers. This review explores the mechanisms, clinical efficacy, key studies, challenges, and future perspectives of Antibody-drug conjugates combinations in cancer therapy.

KEYWORDS

antibody-drug conjugates (ADC), cancer therapy, combination strategies, clinical studies, tumor microenvironment

1 Introduction

Cancer remains one of the leading causes of death worldwide, with millions of new diagnoses each year. Despite significant advances in cancer treatment, the prognosis for patients with advanced and metastatic cancers remains poor, particularly for malignancies that are resistant to conventional therapies such as chemotherapy and radiation (Goswami et al., 2024; Zhang and Wu, 2023; Misawa et al., 2025; Xu W. et al., 2024; Zhang et al., 2023). In recent years, ADCs have emerged as a promising therapeutic strategy, offering targeted drug delivery to cancer cells while minimizing off-target toxicity (Dumontet et al., 2023; Liu et al., 2023). ADCs consist of a monoclonal antibody linked to a potent cytotoxic drug, allowing for precise targeting of tumor cells based on specific surface antigens, such as HER2, CD20, and Trop-2 (Shih et al., 2024; Belluomini et al., 2023a).

While ADCs have demonstrated significant efficacy in certain cancers, their full potential is often limited by factors such as resistance mechanisms, side effects, and the complexity of tumor biology (Díaz-Rodríguez et al., 2022; Tsuchikama et al., 2024; Zhao

et al., 2023). To overcome these limitations, researchers have increasingly explored the potential of combining ADCs with other therapeutic modalities, including immune checkpoint inhibitors, small-molecule targeted therapies, and traditional chemotherapies (Wei et al., 2024; Nicolò et al., 2022). The rationale behind these combination therapies is to enhance the overall therapeutic effect by attacking tumors through multiple mechanisms, thereby overcoming resistance and improving clinical outcomes (Lu et al., 2023; Yu et al., 2024; Jiang et al., 2024).

Combination therapies leveraging ADCs have shown promise across a variety of cancers, including breast cancer, lung cancer, urothelial carcinoma, and lymphoma (Wei et al., 2024). In these settings, ADCs work synergistically with immune modulators and chemotherapy agents to not only target and destroy tumor cells but also to stimulate the immune system, enhance tumor-specific responses, and promote long-term remission. This combination approach represents a new Frontier in cancer therapy, with the potential to significantly improve patient outcomes, reduce side effects, and ultimately change the treatment paradigm for several difficult-to-treat cancers (Wang et al., 2022).

2 Mechanisms of action of ADCs and their combinations

ADCs are designed to deliver potent cytotoxic drugs directly to cancer cells while sparing normal tissues. The core mechanism of ADCs relies on the specificity of monoclonal antibodies (mAbs) that target tumor-associated antigens, such as HER2, CD20, and Trop-2 (Filis et al., 2023). However, the effectiveness of ADCs is often constrained by several factors, including antigen heterogeneity, resistance mechanisms, and off-target toxicity (Parakh et al., 2021). Antigen heterogeneity, such as varying levels of HER2 expression in breast cancer, can result in suboptimal binding and reduced drug delivery, while changes in antigen expression during disease progression further diminish ADC efficacy (Schettini and Prat, 2021; Li et al., 2024). Resistance mechanisms include antigen downregulation, as seen in Trop-2-targeting ADCs like Sacituzumab govitecan, overexpression of multidrug resistance transporters like P-glycoprotein that expel cytotoxic payloads, and impaired lysosomal function that hinders payload release (Abelman et al., 2023; Chen et al., 2023). Additionally, off-target toxicity remains a challenge, with unintended binding and payload leakage contributing to adverse effects. For instance, Enfortumab vedotin, targeting Nectin-4, has been linked to peripheral neuropathy, and unstable linkers in earlier ADCs have caused systemic toxicity. Addressing these limitations is crucial for improving ADC therapeutic outcomes (Aoyama et al., 2022; Sardinha et al., 2023).

To overcome these challenges, ADCs are increasingly being combined with other therapeutic strategies to enhance their efficacy. One such combination is with immune checkpoint inhibitors, like anti-PD-1 or anti-CTLA-4 antibodies. These inhibitors work by reactivating the immune system to recognize and destroy cancer cells. When combined with ADCs, immune checkpoint inhibitors can help eliminate tumors that evade immune detection, thereby enhancing both the immune response and the cytotoxic effects of ADCs (Wang et al., 2023).

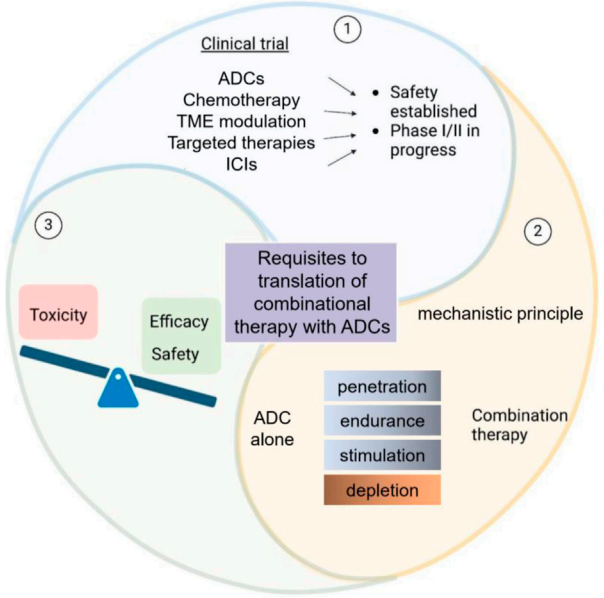

FIGURE 1
Schematic overview of ADCs in clinical trials and combinational therapy requirements. This diagram depicts the considerations in ADC-based clinical trials. It balances toxicity, efficacy, and safety for ADCs alone. Additionally, it outlines the prerequisites for translating ADC - based combinational therapy, featuring mechanistic principles and therapy components such as penetration and depletion.

In addition, ADCs are being combined with targeted therapies, such as small-molecule inhibitors of tyrosine kinases, which can disrupt key signaling pathways in tumor cells. These combinations can prevent the activation of compensatory survival mechanisms, increasing the likelihood that the ADC will successfully kill the tumor cell (Abuhelwa et al., 2022). Chemotherapy can also be combined with ADCs to enhance cytotoxicity through synergistic effects (Wei et al., 2024). By attacking the tumor from multiple angles, these combination therapies hold the potential to overcome resistance and improve patient outcomes in cancers that are difficult to treat with monotherapy (Figure 1).

3 Current ADC options in clinical practice

ADCs are complex molecules composed of three key components: (Goswami et al., 2024): a monoclonal antibody that specifically binds to a tumor-associated antigen, (Zhang and Wu, 2023), a cytotoxic payload that kills cancer cells, and (Misawa et al., 2025) a chemical linker that connects the antibody to the payload. The antibody ensures targeted delivery of the payload to cancer cells, while the linker controls the release of the payload, minimizing off-target toxicity (Katrini et al., 2024). Several ADCs have been approved for clinical use, each with unique structural and functional characteristics. For example, Trastuzumab emtansine (T-DM1) consists of the HER2-targeting antibody trastuzumab linked to the maytansinoid derivative DM1 via a non-cleavable thioether linker. Upon internalization, DM1 is released and disrupts

microtubule assembly, leading to cell cycle arrest and apoptosis in HER2-positive breast cancer cells (Barok et al., 2014). Similarly, Enfortumab vedotin combines an anti-Nectin-4 antibody with the microtubule-disrupting agent monomethyl auristatin E (MMAE) through a cleavable protease-sensitive linker. This ADC is approved for advanced urothelial carcinoma and demonstrates potent tumor-killing activity (Challita-Eid et al., 2016). Another example, Sacituzumab govitecan, targets Trop-2 using a humanized antibody linked to SN-38, a topoisomerase I inhibitor, via a hydrolyzable linker. This ADC has shown significant efficacy in triple-negative breast cancer (TNBC) by inducing DNA damage and cell death (Bardia et al., 2021). These ADCs exemplify the potential of targeted drug delivery, but challenges such as resistance mechanisms and off-target effects persist, underscoring the need for innovative combination strategies to further enhance their therapeutic impact.

4 Clinical efficacy and advances in ADC combinations

ADCs have revolutionized targeted cancer therapies by combining the specificity of monoclonal antibodies with the potent cytotoxic effects of chemotherapeutics. However, the clinical success of ADCs often requires rationally designed combination therapies to overcome limitations such as resistance, antigen heterogeneity, and tumor microenvironment barriers (Wei et al., 2024). This section explores the efficacy of ADC combinations, key clinical trials, and their implications for future therapeutic strategies. For clarity, the discussion is divided into two parts: Section 4.1 focuses on the clinical outcomes of ADC combinations, while Section 4.2 highlights pivotal trials and ongoing studies that have advanced this field.

4.1 Clinical efficacy of ADC combinations

The combination of ADCs with other therapeutic modalities has shown immense promise in improving the efficacy of cancer treatments. ADCs, designed to deliver cytotoxic agents directly to tumor cells via targeted antibodies, can be further optimized by combining them with chemotherapy, immunotherapy, and other targeted agents. These combinations have demonstrated substantial improvements in clinical outcomes, including overall survival (OS), progression-free survival (PFS), and overall response rates (ORR), and are a key focus in cancer therapeutics (Kang et al., 2024).

4.1.1 ADCs and chemotherapy

In clinical trials, resistance to ADCs has been reported as a significant barrier to durable responses (Belluomini et al., 2023b). For instance, in HER2-positive breast cancer, resistance to T-DM1 has been associated with HER2 downregulation and upregulation of compensatory signaling pathways such as PI3K/AKT (Dey et al., 2024). Similarly, resistance to Trop-2-targeted Sacituecan in TNBC has been linked to increased drug efflux activity mediated by MDR transporters. Combining ADCs with traditional chemotherapeutic agents aims to exploit their synergistic effects, overcoming tumor resistance mechanisms and enhancing treatment efficacy.

4.1.1.1 Combination of ADCs and taxanes

Taxanes, such as Docetaxel and Paclitaxel, are widely used in various cancers, including breast cancer, lung cancer, and ovarian cancer (Sun et al., 2022; Mosca et al., 2021). These drugs work by stabilizing microtubules, preventing cell division, and ultimately leading to cell death. The combination of taxanes with ADCs, particularly in HER2-positive breast cancer, has shown promising results.

For instance, the combination of T-DM1 with Paclitaxel has been explored in HER2-positive breast cancer (Ruddy et al., 2021). Clinical trials have demonstrated that this combination leads to enhanced tumor regression, improved PFS, and a reduction in the incidence of disease progression compared to monotherapy with either agent alone. This combination benefits from the synergistic effects of Paclitaxel, which may enhance ADC internalization and drug delivery (Krop et al., 2016).

4.1.1.2 Combination of ADCs and platinum-based chemotherapies

Platinum-based agents like Cisplatin and Carboplatin are frequently used in solid tumors such as ovarian, non-small cell lung cancer (NSCLC), and head and neck cancers (Zhang et al., 2022). ADCs targeting tumor-specific antigens, such as Enfortumab vedotin (anti-Nectin-4) and Sacituzumab govitecan (anti-Trop-2), are being combined with platinum-based chemotherapies to enhance their cytotoxic effect (Belluomini et al., 2023a; Wong and Rosenberg, 2021). This approach may reduce the development of resistance and improve the distribution of ADCs within the tumor by inducing DNA damage and enhancing tumor cell death.

For example, Sacituzumab govitecan combined with Cisplatin in TNBC has shown to significantly improve ORR and PFS in clinical trials, providing a promising strategy for patients with metastatic or resistant TNBC (Tagawa et al., 2024).

4.1.2 ADCs and immune checkpoint inhibitors

Immunotherapy, particularly immune checkpoint inhibitors (ICIs) targeting PD-1/PD-L1 or CTLA-4, has significantly improved cancer treatment outcomes (Wang et al., 2024). Combining ADCs with ICIs aims to harness the power of the immune system to eradicate cancer cells while maintaining the targeted cytotoxic action of ADCs.

4.1.2.1 Combination of ADCs and PD-1/PD-L1 inhibitors

The combination of ADCs with PD-1/PD-L1 inhibitors is an active area of clinical investigation. Atezolizumab (anti-PD-L1) and Pembrolizumab (anti-PD-1) have been combined with ADCs such as Enfortumab vedotin (anti-Nectin-4) in urothelial carcinoma (Nucera et al., 2024). In clinical trials, these combinations have resulted in significantly improved ORR, OS, and PFS compared to monotherapy. The rationale behind these combinations is that PD-1/PD-L1 blockade enhances T-cell activation and immune responses, allowing the immune system to more effectively recognize and eliminate tumor cells, including those targeted by ADCs (Pessino et al., 2024).

In HER2-positive breast cancer, T-DM1 combined with Pembrolizumab has shown encouraging early-phase clinical results (Waks et al., 2022). The addition of the immune

checkpoint inhibitor boosts the immune response against residual tumor cells, which is particularly important in metastatic settings where immune evasion is a major challenge (Waks et al., 2024).

4.1.2.2 Combination of ADCs and CTLA-4 inhibitors

The combination of T-DM1 with Ipilimumab (anti-CTLA-4) is being explored in clinical trials for HER2-positive and other solid tumors (Müller et al., 2015). CTLA-4 inhibitors stimulate T-cell activation and can help overcome immune suppression within the TME. Combining Ipilimumab with ADCs may synergize by improving immune-mediated destruction of cancer cells while the ADC delivers targeted cytotoxicity directly to tumor cells. Early results suggest that this combination may improve survival rates and reduce disease progression in patients with metastatic cancer.

4.1.3 ADCs and targeted therapies

Targeted therapies that block specific molecular pathways involved in cancer growth can be combined with ADCs to provide a multi-pronged approach to cancer treatment (Pérez-Herrero and Fernández-Medarde, 2015; Gujarathi et al., 2024). These combinations aim to target both the tumor and its supporting environment, leading to enhanced tumor regression and reduced relapse rates.

4.1.3.1 Combination of ADCs and tyrosine kinase inhibitors (TKIs)

TKIs, such as Lapatinib (targeting HER2 and EGFR) and Osimertinib (targeting EGFR), are used in cancers with specific mutations. Combining these inhibitors with ADCs like T-DM1 has been studied in HER2-positive breast cancer (Scheck et al., 2024; Aggarwal et al., 2023). Lapatinib enhances the therapeutic effects of T-DM1 by blocking signaling pathways that promote tumor cell survival, thus improving ADC efficacy. The combination has shown promising results in metastatic breast cancer, particularly in patients who have developed resistance to single-agent therapies.

4.1.3.2 Combination of ADCs and anti-angiogenesis agents

Bevacizumab, an anti-VEGF monoclonal antibody, is used to block angiogenesis, thereby limiting the tumor's ability to grow new blood vessels. When combined with ADCs such as T-DM1, Bevacizumab helps improve ADC penetration into solid tumors by reducing the dense extracellular matrix and normalizing the blood vessel structure within tumors. In clinical studies, this combination has shown increased tumor shrinkage and improved clinical outcomes in patients with HER2-positive breast cancer (Pondé et al., 2020).

4.1.4 ADCs and tumor microenvironment modulation

The tumor microenvironment (TME), characterized by fibrosis, hypoxia, and immunosuppressive factors, can create barriers to effective drug delivery and reduce treatment efficacy. Combining ADCs with therapies that modulate the TME is a promising strategy for improving treatment outcomes. The dense stromal components of the TME can impede the penetration of ADCs into tumors. Interleukin-2 (IL-2) and other immune modulators can be combined with ADCs to promote T-cell activation and overcome immunosuppressive barriers in the TME. For instance, T-DM1 combined with IL-2 or GM-CSF (Granulocyte-Macrophage Colony-Stimulating Factor) is being explored to enhance immune responses, leading to better control of residual disease and prolonged survival (Xu M. et al., 2024).

In summary, the clinical efficacy of ADC combinations in cancer therapy has made significant strides, providing a multi-faceted approach to overcoming resistance and improving therapeutic outcomes. Combining ADCs with chemotherapy, immunotherapy, targeted therapies, and tumor microenvironment modulators not only enhances tumor-specific drug delivery but also works synergistically to improve overall treatment responses. These combinations have shown promise in multiple cancers, including breast cancer, urothelial carcinoma, leukemia, and solid tumors like pancreatic cancer. While the combination of therapies continues to evolve, the next-generation of ADC combinations is likely to further define cancer treatment paradigms, offering more personalized and effective treatment options for patients. With ongoing clinical trials and refinement of treatment regimens, ADC-based combination therapies are poised to play a critical role in advancing cancer treatment.

4.2 Key clinical studies and ongoing trials

The development of ADCs in combination therapies has shown significant promise in a variety of cancer types, highlighting their potential to improve patient outcomes. Numerous clinical studies and ongoing trials have been pivotal in advancing our understanding of the clinical efficacy and safety of ADC combinations. These trials span multiple malignancies, including breast cancer, urothelial carcinoma, lymphoma, and others, and have underscored the advantages of combining ADCs with other therapeutic modalities, such as immune checkpoint inhibitors, targeted therapies, and traditional chemotherapy.

4.2.1 Trastuzumab emtansine (T-DM1) and Pembrolizumab in HER2-Positive breast cancer

One of the key studies in HER2-positive metastatic breast cancer (MBC) is the Phase II trial combining Trastuzumab emtansine (T-DM1), an ADC targeting HER2, with Pembrolizumab, an anti-PD-1 immune checkpoint inhibitor (Janjigian et al., 2023). This study aimed to investigate whether the combination could enhance immune responses while also leveraging the cytotoxic properties of T-DM1. Early results from this trial indicated improved progression-free survival (PFS) and overall survival (OS) in patients who had previously been heavily treated. The synergy between these two agents appears to work by enhancing the immune system's ability to recognize and attack tumor cells, while T-DM1 directly delivers its chemotherapeutic payload to the cancer cells. Notably, the combination was well tolerated, with manageable side effects, mainly related to Pembrolizumab, such as fatigue and immune-related adverse events. These findings suggest that ADCs can work synergistically with immune checkpoint inhibitors, potentially offering a novel treatment strategy for HER2-positive breast cancer (Waks et al., 2022; Smyth and Sundar, 2023).

TABLE 1 Summary of combination therapies involving ADCs in cancer treatment.

Combination therapy	Therapeutic agents	Mechanism of action	Targeted cancer types	Key findings
ADCs + Immune Checkpoint Inhibitors	- PD-1 inhibitors (e.g., Pembrolizumab)	- ADCs deliver cytotoxic drugs to tumor cells; immune checkpoint inhibitors reactivate immune response against cancer cells	HER2-positive breast cancer, triple-negative breast cancer, urothelial carcinoma	- ADCs enhance immune responses by reactivating immune surveillance - Combined therapy increases progression-free survival. - Can improve tumor-specific responses
	- PD-L1 inhibitors (e.g., Atezolizumab)	- Block PD-1/PD-L1 interactions to enhance T-cell activity against cancer cells		- Synergistic effects observed in improving overall response rates in various cancers - Immune-related adverse events like fatigue and rash are manageable
ADCs + Chemotherapy	- Traditional chemotherapies (e.g., paclitaxel, carboplatin)	- Chemotherapy enhances ADC efficacy by directly killing proliferating tumor cells while ADCs target specific antigens	Non-small cell lung cancer, breast cancer, lymphoma	- Increased tumor response when ADCs and chemotherapy are used together - Synergistic cytotoxic effects - Risk of overlapping toxicities like neutropenia and GI symptoms
	- Taxanes (e.g., Docetaxel)	- ADCs kill tumor cells while chemotherapy accelerates tumor cell death and inhibits growth		- Enhanced tumor control, particularly in chemotherapy-resistant cancers - Potential for reduced drug resistance when used in combination
ADCs + Targeted Small-Molecule Inhibitors	- Tyrosine kinase inhibitors (e.g., Erlotinib, Lapatinib)	- ADCs target cancer-specific antigens, while TKIs inhibit downstream signaling pathways critical for cancer cell survival	Lung cancer, breast cancer, other solid tumors	- ADCs combined with TKIs enhance anti-cancer effects and block compensatory signaling - Can improve outcomes in cancers with resistance to monotherapy
	- AKT inhibitors (e.g., Ipatasertib)	- ADCs deliver cytotoxic agents, while AKT inhibitors block cell survival pathways triggered by PI3K/AKT/mTOR signaling		- Synergistic cytotoxicity observed, especially in breast cancer and other solid tumors - Potential to overcome resistance by blocking adaptive survival pathways
ADCs + Anti-Angiogenic Agents	- VEGF inhibitors (e.g., Bevacizumab)	- ADCs target tumor cells, while anti-angiogenics inhibit vascular growth, improving drug delivery and reducing tumor hypoxia	HER2-positive breast cancer, ovarian cancer	- Anti-angiogenic agents increase ADC penetration in tumors by normalizing the vasculature - Improved progression-free survival and enhanced response rates in clinical trials
	- VEGFR inhibitors (e.g., Axitinib)	- Disrupts blood vessel formation within tumors, increasing ADC delivery		- Tumor vascular normalization improves ADC efficacy - Decreased drug resistance due to better tumor perfusion
ADCs + CAR-T Cell Therapy	- Chimeric Antigen Receptor T-cell (CAR-T) therapy	- ADCs deliver targeted cytotoxic agents, while CAR-T cells kill cancer cells through engineered immune responses	Hematological malignancies, solid tumors	- Synergistic effect observed in hematologic cancers like leukemia and lymphoma - CAR-T cells help further target antigen-positive tumor cells after ADC delivery
	- CAR-T (e.g., Kymriah, Yescarta)	- Combining CAR-T's targeting capabilities with ADC's cytotoxic payload enhances tumor cell		- Early-phase studies show promising results - Challenges remain in optimizing dosing and

(Continued on following page)

TABLE 1 (*Continued*) Summary of combination therapies involving ADCs in cancer treatment.

Combination therapy	Therapeutic agents	Mechanism of action	Targeted cancer types	Key findings
		targeting and immune destruction		reducing CAR-T related toxicity
ADCs + Immune Modulators	- TLR agonists (e.g., CpG oligodeoxynucleotides)	- ADCs deliver targeted toxins while TLR agonists activate innate immune responses to boost adaptive immunity	Melanoma, breast cancer, ovarian cancer	- TLR agonists enhance the immune response induced by ADCs - Increases tumor-specific immunity and reduces tumor growth
	- STING agonists (e.g., ADU-S100)	- Activates the STING pathway to induce tumor cell death and promote immune response, complementing ADC cytotoxicity	Various cancers (e.g., melanoma, breast cancer)	- Synergistic tumor destruction through enhanced immune activation - Significant increase in tumor regression in preclinical models
ADCs + Other Immunotherapies	- CTLA-4 inhibitors (e.g., Ipilimumab)	- ADCs deliver cytotoxic drugs to tumor cells while CTLA-4 inhibitors enhance T-cell-mediated immune responses	Melanoma, non-small cell lung cancer, head and neck cancers	- Combining ADCs with CTLA-4 inhibitors increases T-cell activation and tumor rejection - Promising results in early-phase trials for advanced cancers
	- OX40 agonists (e.g., MedImmune's MEDI-575)	- ADCs and OX40 agonists work together to enhance anti-tumor T-cell responses and cytotoxic activity	Solid tumors, including melanoma and breast cancer	- Synergistic T-cell activation and increased anti-tumor activity - Tumor-specific immunity improves while reducing immune evasion

4.2.2 Sacituzumab govitecan and Pembrolizumab in triple-negative breast cancer (TNBC)

In a Phase I/II clinical trial exploring Sacituzumab govitecan, an ADC targeting Trop-2, in combination with Pembrolizumab, an anti-PD-1 antibody, the combination therapy has shown promising results for patients with metastatic triple-negative breast cancer (TNBC) (Grivas et al., 2024). TNBC is notoriously difficult to treat due to the lack of targeted therapies, and patients often face poor prognosis. This trial demonstrated that combining Sacituzumab govitecan with Pembrolizumab resulted in a significantly higher overall response rate (ORR) compared to monotherapies. Patients in this study also exhibited durable responses, with some experiencing long-term remission. The safety profile was manageable, with adverse effects such as diarrhea and neutropenia primarily linked to Sacituzumab govitecan. The success of this combination suggests that combining ADCs with immunotherapy could provide a potent treatment for TNBC, which remains a major unmet clinical need (Tolaney et al., 2024).

4.2.3 Enfortumab vedotin and Pembrolizumab in urothelial carcinoma

The combination of Enfortumab vedotin, an ADC targeting Nectin-4, with Pembrolizumab is currently being evaluated in patients with metastatic urothelial carcinoma (UC) (Niegisch, 2024; Powles et al., 2024). UC, particularly in its advanced stages, is a difficult-to-treat cancer with few effective therapies. A Phase II study demonstrated that this combination resulted in substantial improvements in both progression-free survival (PFS) and overall response rates (ORR) in patients who had previously failed platinum-based chemotherapy. The combination works by targeting the cancer cells with the cytotoxic payload of Enfortumab vedotin while also stimulating the immune system through Pembrolizumab. Early results indicate a favorable safety profile, with manageable side effects including rash, fatigue, and peripheral neuropathy. This study underscores the potential for ADC-immunotherapy combinations to offer a new therapeutic approach for patients with advanced urothelial carcinoma (Hoimes et al., 2022; Bantounou et al., 2023; O'Donnell et al., 2023).

4.2.4 Ongoing trials and future directions

Beyond the completed and ongoing studies mentioned above, many other clinical trials are investigating the potential of ADC combinations in various cancer types. These trials are exploring combinations with other targeted therapies, small molecule inhibitors, and chemotherapy agents to further enhance ADC efficacy. For example, combinations of ADCs with TKIs are being tested in lung cancer, while others are evaluating ADCs combined with anti-angiogenic agents to target the tumor vasculature.

In the hematological malignancies space, several trials are investigating the combination of ADCs with immunotherapies or other targeted therapies. One example is the combination of Polatuzumab vedotin, an anti-CD79 b ADC, with Rituximab (a CD20-targeting monoclonal antibody) in patients with relapsed or refractory non-Hodgkin lymphoma (NHL). Early results have shown promising efficacy, with many patients achieving complete responses. These ongoing studies are crucial in determining the full

potential of ADC combinations in treating hematological cancers (Vodicka et al., 2022; Morschhauser et al., 2019; Terui et al., 2021).

Moreover, ongoing trials are exploring combinations with other immune checkpoint inhibitors, such as CTLA-4 inhibitors, to further enhance the anti-tumor immune response and overcome resistance mechanisms in tumors that evade immune detection. By combining ADCs with agents that modulate immune checkpoints or other immunological pathways, these trials aim to improve the overall efficacy of cancer therapies, especially in tumors with complex immune evasion mechanisms (Müller et al., 2015).

In summary, these key clinical studies demonstrate the promise of ADC combinations in improving clinical outcomes across a variety of cancer types (Table 1). As these studies progress into later stages of development, the combination of ADCs with immunotherapy, targeted therapies, and chemotherapy is expected to become an increasingly important strategy in cancer treatment. The results so far have been encouraging, and these therapies hold the potential to significantly enhance the treatment landscape for patients with cancers that are difficult to treat with conventional therapies alone.

5 Concluding insights: overcoming challenges and shaping the future of ADC combinations

The clinical development of ADCs in combination with other therapeutic modalities has demonstrated substantial promise in advancing cancer treatment. Combining ADCs with immune checkpoint inhibitors, targeted therapies, and chemotherapy has yielded encouraging clinical results across a range of cancers, including HER2-positive breast cancer, triple-negative breast cancer, urothelial carcinoma, and lymphoma. The synergy between ADCs and other therapies enhances therapeutic efficacy by leveraging multiple mechanisms of action, including direct cytotoxicity, immune modulation, and targeted tumor destruction. These combination strategies not only improve treatment outcomes but also offer hope for patients with cancers that have limited therapeutic options.

However, despite these promising developments, several challenges remain. One significant hurdle is the management of adverse effects, which can become more pronounced when combining ADCs with other treatment regimens. While ADCs typically have more targeted effects, the combination with chemotherapy or immune checkpoint inhibitors can lead to overlapping toxicities, such as neutropenia, diarrhea, fatigue, and immune-related adverse events. Careful dose optimization and monitoring are essential to minimize these toxicities and improve the overall safety profile of combination therapies. Moreover, the development of resistance to ADCs and other therapeutic agents remains a persistent issue. Tumors may evolve mechanisms to evade the effects of ADCs, such as altering drug target expression or activating compensatory signaling pathways. Overcoming these resistance mechanisms will require more in-depth understanding of tumor biology and the molecular factors that drive treatment failure.

In the realm of immuno-oncology, combining ADCs with next-generation immune checkpoint inhibitors, such as those targeting LAG-3, TIM-3, and TIGIT, holds the potential to further enhance immune responses and overcome immune evasion. Additionally, the combination of ADCs with cellular therapies, such as CAR-T cells, represents an exciting avenue for exploration. These strategies could potentially provide a multi-pronged approach to fighting cancer by utilizing both direct cytotoxicity and immune-based tumor destruction. In conclusion, while ADC combinations have already shown substantial promise in clinical settings, there are still many challenges to overcome, particularly in terms of safety, resistance mechanisms, and patient stratification. Continued research and clinical trials will be essential in addressing these issues and unlocking the full potential of ADC combination therapies. With ongoing advancements in technology, biomarker discovery, and molecular engineering, ADCs are poised to play a central role in the future of cancer therapy, offering more personalized, effective, and less toxic treatment options for patients worldwide.

Overcoming these limitations through rationally designed combination therapies is critical. For example, combining ADCs with immune checkpoint inhibitors can counteract antigen heterogeneity by amplifying immune-mediated destruction of tumor cells regardless of antigen expression levels. Similarly, incorporating MDR inhibitors in combination regimens can suppress efflux pump activity, restoring the efficacy of cytotoxic payloads. Advances in linker stability and targeting strategies also offer promising approaches to minimize off-target toxicity and improve therapeutic outcomes.

Author contributions

XS: Writing–original draft, Writing–review and editing. KT: Writing–original draft. QZ: Writing–review and editing. QH: Data curation, Writing–review and editing. LQ: Data curation, Writing–review and editing. YL: Data curation, Writing–review and editing. JC: Data curation, Writing–review and editing. NF: Data curation, Writing–review and editing. JG: Writing–review and editing. BS: Writing–original draft, Writing–review and editing. XL: Writing–original draft, Writing–review and editing.

Funding

The author(s) declare that no financial support was received for the research, authorship, and/or publication of this article.

Conflict of interest

The authors declare that the research was conducted in the absence of any commercial or financial relationships that could be construed as a potential conflict of interest.

Generative AI statement

The authors declare that no Generative AI was used in the creation of this manuscript.

Publisher's note

References

Abelman, R. O., Wu, B., Spring, L. M., Ellisen, L. W., and Bardia, A. (2023). Mechanisms of resistance to antibody–drug conjugates. *Cancers* 15, 1278. doi:10.3390/cancers15041278

Abuhelwa, Z., Alloghbi, A., and Nagasaka, M. (2022). A comprehensive review on antibody-drug conjugates (ADCs) in the treatment landscape of non-small cell lung cancer (NSCLC). *Cancer Treat. Rev.* 106, 102393. doi:10.1016/j.ctrv.2022.102393

Aggarwal, C., Azzoli, C. G., Spira, A. I., Solomon, B. J., Le, X., Rolfo, C., et al. (2023). EGRET: a first-in-human study of the novel antibody-drug conjugate (ADC) AZD9592 as monotherapy or combined with other anticancer agents in patients (pts) with advanced solid tumors. *J. Clin. Oncol.* 41 (16_Suppl. l), TPS3156. doi:10.1200/JCO.2023.41.16_suppl.TPS3156

Aoyama, M., Tada, M., Yokoo, H., Demizu, Y., and Ishii-Watabe, A. (2022). Fcγ receptor-dependent internalization and off-target cytotoxicity of antibody-drug conjugate aggregates. *Pharm. Res.* 39 (1), 89–103. doi:10.1007/s11095-021-03158-x

Bantounou, M. A., Plascevic, J., MacDonald, L., Wong, M. C., O'Connell, N., and Galley, H. F. (2023). Enfortumab vedotin and pembrolizumab as monotherapies and combination treatment in locally advanced or metastatic urothelial carcinoma: a narrative review. *Curr. Urol.* 17 (4), 271–279. doi:10.1097/cu9.0000000000000204

Bardia, A., Hurvitz Sara, A., Tolaney Sara, M., Loirat, D., Punie, K., Oliveira, M., et al. (2021). Sacituzumab govitecan in metastatic triple-negative breast cancer. *N. Engl. J. Med.* 384 (16), 1529–1541. doi:10.1056/NEJMoa2028485

Barok, M., Joensuu, H., and Isola, J. (2014). Trastuzumab emtansine: mechanisms of action and drug resistance. *Breast Cancer Res.* 16 (2), 209. doi:10.1186/bcr3621

Belluomini, L., Avancini, A., Sposito, M., Milella, M., Rossi, A., and Pilotto, S. (2023a). Antibody-drug conjugates (ADCs) targeting TROP-2 in lung cancer. *Expert Opin. Biol. Ther.* 23 (11), 1077–1087. doi:10.1080/14712598.2023.2198087

Belluomini, L., Sposito, M., Avancini, A., Insolda, J., Milella, M., Rossi, A., et al. (2023b). Unlocking new horizons in small-cell lung cancer treatment: the onset of antibody–drug conjugates. *Cancers* 15, 5368. doi:10.3390/cancers15225368

Challita-Eid, P. M., Satpayev, D., Yang, P., An, Z., Morrison, K., Shostak, Y., et al. (2016). Enfortumab vedotin antibody–drug conjugate targeting nectin-4 is a highly potent therapeutic agent in multiple preclinical cancer models. *Cancer Res.* 76 (10), 3003–3013. doi:10.1158/0008-5472.CAN-15-1313

Chen, Y.-F., Xu, Y.-y., Shao, Z.-M., and Yu, K.-D. (2023). Resistance to antibody-drug conjugates in breast cancer: mechanisms and solutions. *Cancer Commun.* 43 (3), 297–337. doi:10.1002/cac2.12387

Dey, N., Sun, Y., Carlson, J. H., Wu, H., Lin, X., Leyland-Jones, B., et al. (2024). *Anti-tumor efficacy of BEZ235 is complemented by its anti-angiogenic effects via downregulation of PI3K-mTOR-HIF1alpha signaling in HER2-defined breast cancers*. 2156–6976. (Print).

Díaz-Rodríguez, E., Gandullo-Sánchez, L., Ocaña, A., and Pandiella, A. (2022). Novel ADCs and strategies to overcome resistance to anti-HER2 ADCs. *Cancers*. doi:10.3390/cancers14010154

Dumontet, C., Reichert, J. M., Senter, P. D., Lambert, J. M., and Beck, A. (2023). Antibody–drug conjugates come of age in oncology. *Nat. Rev. Drug Discov.* 22 (8), 641–661. doi:10.1038/s41573-023-00709-2

Filis, P., Zerdes, I., Soumala, T., Matikas, A., and Foukakis, T. (2023). The ever-expanding landscape of antibody-drug conjugates (ADCs) in solid tumors: a systematic review. *Crit. Rev. Oncology/Hematology* 192, 104189. doi:10.1016/j.critrevonc.2023.104189

Goswami, S., Pauken, K. E., Wang, L., and Sharma, P. (2024). Next-generation combination approaches for immune checkpoint therapy. *Nat. Immunol.* 25 (12), 2186–2199. doi:10.1038/s41590-024-02015-4

Grivas, P., Pouessel, D., Park, C. H., Barthelemy, P., Bupathi, M., Petrylak, D. P., et al. (2024). Sacituzumab govitecan in combination with pembrolizumab for patients with metastatic urothelial cancer that progressed after platinum-based chemotherapy: TROPHY-U-01 cohort 3. *J. Clin. Oncol.* 42 (12), 1415–1425. doi:10.1200/JCO.22.02835

Gujarathi, R., Franses, J. W., Pillai, A., and Liao, C.-Y. (2024). Targeted therapies in hepatocellular carcinoma: past, present, and future. *Front. Oncol.* 14, 1432423. doi:10.3389/fonc.2024.1432423

Hoimes, C. J., Flaig, T. W., Milowsky, M. I., Friedlander, T. W., Bilen, M. A., Gupta, S., et al. (2022). Enfortumab vedotin plus pembrolizumab in previously untreated advanced urothelial cancer. *J. Clin. Oncol.* 41 (1), 22–31. doi:10.1200/JCO.22.01643

Janjigian, Y. Y., Kawazoe, A., Bai, Y., Xu, J., Lonardi, S., Metges, J. P., et al. (2023). Pembrolizumab plus trastuzumab and chemotherapy for HER2-positive gastric or gastro-oesophageal junction adenocarcinoma: interim analyses from the phase 3 KEYNOTE-811 randomised placebo-controlled trial. *Lancet* 402 (10418), 2197–2208. doi:10.1016/S0140-6736(23)02033-0

Jiang, H., Gong, Q., Zhang, R., and Yuan, H. (2024). Tetrazine-based metal-organic frameworks. *Coord. Chem. Rev.* 499, 215501. doi:10.1016/j.ccr.2023.215501

Kang, Z., Jin, Y., Yu, H., Li, S., and Qi, Y. (2024). Relative efficacy of antibody-drug conjugates and other anti-HER2 treatments on survival in HER2-positive advanced breast cancer: a systematic review and meta-analysis. *BMC Cancer* 24 (1), 708. doi:10.1186/s12885-024-12478-1

Katrini, J., Boldrini, L., Santoro, C., Valenza, C., Trapani, D., and Curigliano, G. (2024). Biomarkers for antibody–drug conjugates in solid tumors. *Mol. Cancer Ther.* 23 (4), 436–446. doi:10.1158/1535-7163.MCT-23-0482

Krop, I. E., Modi, S., LoRusso, P. M., Pegram, M., Guardino, E., Althaus, B., et al. (2016). Phase 1b/2a study of trastuzumab emtansine (T-DM1), paclitaxel, and pertuzumab in HER2-positive metastatic breast cancer. *Breast Cancer Res.* 18 (1), 34. doi:10.1186/s13058-016-0691-7

Li, M., Zhao, X., Yu, C., and Wang, L. (2024). Antibody-drug conjugate overview: a state-of-the-art manufacturing process and control strategy. *Pharm. Res.* 41 (3), 419–440. doi:10.1007/s11095-023-03649-z

Liu, X., Deng, J., Zhang, R., Xing, J., Wu, Y., Chen, W., et al. (2023). The clinical development of antibody-drug conjugates for non-small cell lung cancer therapy. *Front. Immunol.* 14, 1335252. doi:10.3389/fimmu.2023.1335252

Lu, L., Niu, Z., Chao, Z., Fu, C., Chen, K., and Shi, Y. (2023). Exploring the therapeutic potential of ADC combination for triple-negative breast cancer. *Cell. Mol. Life Sci.* 80 (12), 350. doi:10.1007/s00018-023-04946-x

Misawa, K., Bhat, H., Adusumilli, P. S., and Hou, Z. (2025). Combinational CAR T-cell therapy for solid tumors: requisites, rationales, and trials. *Pharmacol. and Ther.* 266, 108763. doi:10.1016/j.pharmthera.2024.108763

Morschhauser, F., Flinn, I. W., Advani, R., Sehn, L. H., Diefenbach, C., Kolibaba, K., et al. (2019). Polatuzumab vedotin or pinatuzumab vedotin plus rituximab in patients with relapsed or refractory non-Hodgkin lymphoma: final results from a phase 2 randomised study (ROMULUS). *Lancet Haematol.* 6 (5), e254–e265. doi:10.1016/S2352-3026(19)30026-2

Mosca, L., Ilari, A., Fazi, F., Assaraf, Y. G., and Colotti, G. (2021). Taxanes in cancer treatment: activity, chemoresistance and its overcoming. *Drug Resist. Updat.* 54, 100742. doi:10.1016/j.drup.2020.100742

Müller, P., Kreuzaler, M., Khan, T., Thommen, D. S., Martin, K., Glatz, K., et al. (2015). Trastuzumab emtansine (T-DM1) renders HER2+ breast cancer highly susceptible to CTLA-4/PD-1 blockade. *Sci. Transl. Med.* 7 (315), 315ra188. doi:10.1126/scitranslmed.aac4925

Nicolò, E., Giugliano, F., Ascione, L., Tarantino, P., Corti, C., Tolaney, S. M., et al. (2022). Combining antibody-drug conjugates with immunotherapy in solid tumors: current landscape and future perspectives. *Cancer Treat. Rev.* 106, 102395. doi:10.1016/j.ctrv.2022.102395

Niegisch, G. (2024). Enfortumab vedotin and pembrolizumab — a new perspective on urothelial cancer. *N. Engl. J. Med.* 390 (10), 944–946. doi:10.1056/NEJMe2400311

Nucera, S., Conti, C., Martorana, F., Wilson, B., and Genta, S. (2024). Antibody-drug conjugates to promote immune surveillance: lessons learned from breast cancer. *Biomedicines* 12, 1491. doi:10.3390/biomedicines12071491

O'Donnell, P. H., Milowsky, M. I., Petrylak, D. P., Hoimes, C. J., Flaig, T. W., Mar, N., et al. (2023). Enfortumab vedotin with or without pembrolizumab in cisplatin-ineligible patients with previously untreated locally advanced or metastatic urothelial cancer. *J. Clin. Oncol.* 41 (25), 4107–4117. doi:10.1200/JCO.22.02887

Parakh, S., Nicolazzo, J., Scott, A. M., and Gan, H. K. (2021). Antibody drug conjugates in glioblastoma – is there a future for them? *Front. Oncol.* 11, 718590. doi:10.3389/fonc.2021.718590

Pérez-Herrero, E., and Fernández-Medarde, A. (2015). Advanced targeted therapies in cancer: drug nanocarriers, the future of chemotherapy. *Eur. J. Pharm. Biopharm.* 93, 52–79. doi:10.1016/j.ejpb.2015.03.018

Pessino, G., Scotti, C., Maggi, M., and Immuno, H. U. B. C. (2024). Hepatocellular carcinoma: old and emerging therapeutic targets. *Cancers* 16, 901. doi:10.3390/cancers16050901

Pondé, N., Wildiers, H., Awada, A., de Azambuja, E., Deliens, C., and Lago, L. D. (2020). Targeted therapy for breast cancer in older patients. *J. Geriatric Oncol.* 11 (3), 380–388. doi:10.1016/j.jgo.2019.05.012

Powles, T., Valderrama Begoña, P., Gupta, S., Bedke, J., Kikuchi, E., Hoffman-Censits, J., et al. (2024). Enfortumab vedotin and pembrolizumab in untreated advanced urothelial cancer. *N. Engl. J. Med.* 390 (10), 875–888. doi:10.1056/NEJMoa2312117

Ruddy, K. J., Zheng, Y., Tayob, N., Hu, J., Dang, C. T., Yardley, D. A., et al. (2021). Chemotherapy-related amenorrhea (CRA) after adjuvant ado-trastuzumab emtansine (T-DM1) compared to paclitaxel in combination with trastuzumab (TH) (TBCRC033: ATEMPT Trial). *Breast Cancer Res. Treat.* 189 (1), 103–110. doi:10.1007/s10549-021-06267-8

Sardinha, M., Palma dos Reis, A. F., Barreira, J. V., Fontes Sousa, M., Pacey, S., and Luz, R. (2023). Antibody-drug conjugates in prostate cancer: a systematic review. *Cureus* 15 (2), e34490. doi:10.7759/cureus.34490

Scheck, M. K., Hofheinz, R. D., and Lorenzen, S. (2024). HER2-Positive gastric cancer and antibody treatment: state of the art and future developments. *Cancers* 16, 1336. doi:10.3390/cancers16071336

Schettini, F., and Prat, A. (2021). Dissecting the biological heterogeneity of HER2-positive breast cancer. *Breast* 59, 339–350. doi:10.1016/j.breast.2021.07.019

Shih, C.-H., Lin, Y.-H., Luo, H.-L., and Sung, W.-W. (2024). Antibody-drug conjugates targeting HER2 for the treatment of urothelial carcinoma: potential therapies for HER2-positive urothelial carcinoma. *Front. Pharmacol.* 15, 1326296. doi:10.3389/fphar.2024.1326296

Smyth, E. C., and Sundar, R. (2023). Combining chemotherapy, trastuzumab, and immune-checkpoint inhibitors in HER2-positive gastro-oesophageal cancer. *Lancet* 402 (10418), 2168–2170. doi:10.1016/S0140-6736(23)02296-1

Sun, L., Zhao, P., Chen, M., Leng, J., Luan, Y., Du, B., et al. (2022). Taxanes prodrug-based nanomedicines for cancer therapy. *J. Control. Release* 348, 672–691. doi:10.1016/j.jconrel.2022.06.004

Tagawa, S. T., Grivas, P., Petrylak, D. P., Sternberg, C. N., Swami, U., Bhatia, A., et al. (2024). TROPHY-U-01 cohort 4: sacituzumab govitecan (SG) in combination with cisplatin (Cis) in platinum (PLT)-naïve patients (pts) with metastatic urothelial cancer (mUC). *J. Clin. Oncol.* 40 (6_Suppl. l), TPS581. doi:10.1200/JCO.2022.40.6_suppl.TPS581

Terui, Y., Rai, S., Izutsu, K., Yamaguchi, M., Takizawa, J., Kuroda, J., et al. (2021). A phase 2 study of polatuzumab vedotin + bendamustine + rituximab in relapsed/refractory diffuse large B-cell lymphoma. *Cancer Sci.* 112 (7), 2845–2854. doi:10.1111/cas.14937

Tolaney, S. M., DeMichele, A., Takano, T., Rugo, H. S., Perou, C., Lynce, F., et al. (2024). OptimICE-RD: sacituzumab govitecan + pembrolizumab vs pembrolizumab (±capecitabine) for residual triple-negative breast cancer. *Future Oncol.* 20 (31), 2343–2355. doi:10.1080/14796694.2024.2357534

Tsuchikama, K., Anami, Y., Ha, S. Y. Y., and Yamazaki, C. M. (2024). Exploring the next generation of antibody–drug conjugates. *Nat. Rev. Clin. Oncol.* 21 (3), 203–223. doi:10.1038/s41571-023-00850-2

Vodicka, P., Benesova, K., Janikova, A., Prochazka, V., Belada, D., Mocikova, H., et al. (2022). Polatuzumab vedotin plus bendamustine and rituximab in patients with relapsed/refractory diffuse large B-cell lymphoma in the real world. *Eur. J. Haematol.* 109 (2), 162–165. doi:10.1111/ejh.13784

Waks, A. G., Keenan, T., Li, T., Tayob, N., Wulf, G. M., Richardson, E. T., et al. (2024). A phase Ib study of pembrolizumab (pembro) plus trastuzumab emtansine (T-DM1) for metastatic HER2+ breast cancer (MBC). *J. Clin. Oncol.* 38 (15_Suppl. l), 1046. doi:10.1200/JCO.2020.38.15_suppl.1046

Waks, A. G., Keenan, T. E., Li, T., Tayob, N., Wulf, G. M., Richardson, E. T., et al. (2022). Phase Ib study of pembrolizumab in combination with trastuzumab emtansine for metastatic HER2-positive breast cancer. *J. Immunother. Cancer* 10 (10), e005119. doi:10.1136/jitc-2022-005119

Wang, A.-J., Gao, Y., Shi, Y.-Y., Dai, M.-Y., and Cai, H.-B. (2022). A review of recent advances on single use of antibody-drug conjugates or combination with tumor immunology therapy for gynecologic cancer. *Front. Pharmacol.* 13, 1093666. doi:10.3389/fphar.2022.1093666

Wang, B., Yu, W., Jiang, H., Meng, X., Tang, D., and Liu, D. (2024). Clinical applications of STING agonists in cancer immunotherapy: current progress and future prospects. *Front. Immunol.* 15, 1485546. doi:10.3389/fimmu.2024.1485546

Wang, Z., Li, H., Gou, L., Li, W., and Wang, Y. (2023). Antibody–drug conjugates: recent advances in payloads. *Acta Pharm. Sin. B* 13 (10), 4025–4059. doi:10.1016/j.apsb.2023.06.015

Wei, Q., Li, P., Yang, T., Zhu, J., Sun, L., Zhang, Z., et al. (2024). The promise and challenges of combination therapies with antibody-drug conjugates in solid tumors. *J. Hematol. and Oncol.* 17 (1), 1. doi:10.1186/s13045-023-01509-2

Wong, J. L., and Rosenberg, J. E. (2021). Targeting nectin-4 by antibody-drug conjugates for the treatment of urothelial carcinoma. *Expert Opin. Biol. Ther.* 21, 863–873. doi:10.1080/14712598.2021.1929168

Xu, M., Kong, Y., Xing, P., Chen, R., Ma, Y., Shan, C., et al. (2024b). An open-label, multicenter, phase II study of RC48-ADC combined with radiotherapy, PD-1/PD-L1 inhibitor sequential GM-CSF and IL-2 for salvage therapy in patients with HER2-expressing advanced solid tumors(PRaG3.0). *J. Clin. Oncol.* 40 (16_Suppl. l), e14565. doi:10.1200/JCO.2022.40.16_suppl.e14565

Xu, W., Jia, A., Lei, Z., Wang, J., Jiang, H., Wang, S., et al. (2024a). Stimuli-responsive prodrugs with self-immolative linker for improved cancer therapy. *Eur. J. Med. Chem.* 279, 116928. doi:10.1016/j.ejmech.2024.116928

Yu, P., Zhu, C., You, X., Gu, W., Wang, X., Wang, Y., et al. (2024). The combination of immune checkpoint inhibitors and antibody-drug conjugates in the treatment of urogenital tumors: a review insights from phase 2 and 3 studies. *Cell Death and Dis.* 15 (6), 433. doi:10.1038/s41419-024-06837-w

Zhang, C., Xu, C., Gao, X., and Yao, Q. (2022). Platinum-based drugs for cancer therapy and anti-tumor strategies. *Theranostics* 12 (5), 2115–2132. doi:10.7150/thno.69424

Zhang, Q., and Wu, S. (2023). Tertiary lymphoid structures are critical for cancer prognosis and therapeutic response. *Front. Immunol.* 13, 1063711. doi:10.3389/fimmu.2022.1063711

Zhang, R., Zhao, X., Jia, A., Wang, C., and Jiang, H. (2023). Hyaluronic acid-based prodrug nanomedicines for enhanced tumor targeting and therapy: a review. *Int. J. Biol. Macromol.* 249, 125993. doi:10.1016/j.ijbiomac.2023.125993

Zhao, H., Yu, J., Zhang, R., Chen, P., Jiang, H., and Yu, W. (2023). Doxorubicin prodrug-based nanomedicines for the treatment of cancer. *Eur. J. Med. Chem.* 258, 115612. doi:10.1016/j.ejmech.2023.115612

frontiers | Frontiers in Pharmacology

TYPE Review
PUBLISHED 10 March 2025
DOI 10.3389/fphar.2025.1493346

OPEN ACCESS

EDITED BY
Ana Podolski-Renic,
Institute for Biological Research "Siniša Stanković" – National Institute of Republic of Serbia, Serbia

REVIEWED BY
Jung-Mao Hsu,
China Medical University, Taiwan
Yifan Zhang,
Shenzhen University, China
Asmat Ullah,
Zhejiang Provincial People's Hospital, China

*CORRESPONDENCE
Guangxian Xu,
xuguangxian@gdmu.edu.cn

†These authors have contributed equally to this work

RECEIVED 09 September 2024
ACCEPTED 20 February 2025
PUBLISHED 10 March 2025

CITATION
He W, Cui K, Farooq MA, Huang N, Zhu S, Jiang D, Zhang X, Chen J, Liu Y and Xu G (2025) TCR-T cell therapy for solid tumors: challenges and emerging solutions.
Front. Pharmacol. 16:1493346.
doi: 10.3389/fphar.2025.1493346

TCR-T cell therapy for solid tumors: challenges and emerging solutions

Wanjun He[1,2†], Kai Cui[1,2†], Muhammad Asad Farooq[1], Na Huang[1,2], Songshan Zhu[1,2], Dan Jiang[1,2], Xiqian Zhang[1,2,3], Jian Chen[3], Yinxia Liu[1] and Guangxian Xu[1,2*]

[1]Guangdong Provincial Key Laboratory of Medical Immunology and Molecular Diagnostics, The First Dongguan Affiliated Hospital, School of Medical Technology, Guangdong Medical University, Dongguan, China, [2]Dongguan Key Laboratory of Molecular Immunology and Cell Therapy, Guangdong Medical University, Dongguan, China, [3]Yinchuan Guolong Orthopedic Hospital, Yinchuan, China

With the use of T cell receptor T cells (TCR-T cells) and chimeric antigen receptor T cells (CAR-T cells), T-cell immunotherapy for cancer has advanced significantly in recent years. CAR-T cell therapy has demonstrated extraordinary success when used to treat hematologic malignancies. Nevertheless, there are several barriers that prevent this achievement from being applied to solid tumors, such as challenges with tumor targeting and inadequate transit and adaption of genetically modified T-cells, especially in unfavorable tumor microenvironments The deficiencies of CAR-T cell therapy in the treatment of solid tumors are compensated for by TCR-T cells, which have a stronger homing ability to initiate intracellular commands, 90% of the proteins can be used as developmental targets, and they can recognize target antigens more broadly. As a result, TCR-T cells may be more effective in treating solid tumors. In this review, we discussed the structure of TCR-T and have outlined the drawbacks of TCR-T in cancer therapy, and suggested potential remedies. This review is crucial in understanding the current state and future potential of TCR-T cell therapy. We emphasize how important it is to use combinatorial approaches, combining new combinations of various emerging strategies with over-the-counter therapies designed for TCR-T, to increase the anti-tumor efficacy of TCR-T inside the TME and maximize treatment safety, especially when it comes to solid tumor immunotherapies.

KEYWORDS

adoptive cell therapy, immunotherapy, solid tumor, TCR, TCR-T cell

1 Introduction

Cancer treatment is still a major global concern, and standard approaches, including surgery, radiation, and chemotherapy, are frequently associated with metastasis and recurrence. Therefore, it is essential to develop new anti-cancer therapies. By genetically altering human immune cells to accurately detect and eliminate malignant cells, immune cell therapy has completely changed traditional methods while minimizing collateral damage to healthy organs. As such, it now forms the fourth essential cornerstone of cancer treatment, following radiation, surgery, and targeted therapy. T-cell therapy has made significant strides in recent years (Mo et al., 2017), establishing it as a key treatment strategy for cancer patients.

TABLE 1 Current clinical targets of TCR-T cell therapy for solid tumors (ClinicalTrials.gov).

Antigen target	Type of antigen	Clinical trial number	Start	Complete	Phase	Country	HLA[a]	Status	Conditions
HPV[b]	TSA[j]	NCT05357027 NCT05686226 NCT05639972 NCT04015336 NCT04411134 NCT05973487	2022.08 2023.03 2024.06 2020.07 2020.05 2024.02	2024.08 2025.01 2026.10 2020.07 2020.07 2026.12	III II III II I I	China United States United States United States United States United States	HLA-A2 HLA-A*02:01 HLA-A*02:01 HLA-A*02:01 HLA-A*02:01 HLA-C*07:02, HLA-A*02:01 and HLA-C*07:02 plus HLA-A*02:01	Recruiting Recruiting Not yet recruiting Terminated Withdrawn Recruiting	Cervical Carcinoma Cervical Cancer Throat Cancer Oropharynx Cancer
HBV[c]	TSA	NCT05905731 NCT04745403	2023.06 2022.05	2026.06 2028.07	I I	China Singapore	— HLA-A*02:01/24:02	Active, not recruiting Recruiting	Chronic Hepatitis B Hepatocellular Carcinoma
EBV[d]	TSA	NCT06135922 NCT04156217 NCT06119256 NCT05587543 NCT04509726	2023.08 2020.02 2023.08 2022.12 2023.03	2026.12 2021.10 2026.12 2030.10 2023.08	I I I I III	China China China China China		Recruiting Completed Recruiting Recruiting Recruiting	EBV-associated Hemophagocytic Lymphohistiocytosis EBV Infection EBV Emia and EBV Positive PTLD After Allogenic HSCT
CMV[e]	TSA	NCT05140187 NCT05089838	2021.10 2021.01	2024.12 2023.10	I I	China China	HLA-A*11:01/02:01/24:02	Recruiting Unknown status	CMV Infection After Allogenic HSCT Allogeneic Hematopoietic Stem Cell Transplantation CMV Infection
KRAS[f]	TSA	NCT05438667 NCT04146298 NCT05933668 NCT06043713 NCT06218914 NCT06253520 NCT06105021	2022.06 2021.10 2023.07 2023.12 2024.02 2024.03 2024.02	2026.05 2025.03 2026.07 2025.12 2040.01 2033.06 2029.12	I III I I I I III	China China China United States United States United States United States	HLA-A*11:01 HLA-A*11:01 HLA-A*11:01 HLA-A*11:01 HLA-C*08:02 — HLA-A*11:01	Recruiting Recruiting Not yet recruiting Recruiting Recruiting Recruiting Recruiting	Pancreatic Cancer Pancreatic Neoplasms Pancreatic Ductal Adenocarcinoma
MAGE[g]	CGA[k]	NCT04729543	2020.10	2027.10	III	Netherlands	HLA-A2*0,201	Recruiting	Melanoma Melanoma, Uveal Head and Neck Cancer
NY-ESO-1	CGA	NCT05881525 NCT05989828	2023.06 2024.04	2025.03 2027.04	I I	China United States	HLA-A2 (excluding HLA-A*0,203) HLA-A2	Recruiting Not yet recruiting	Triple Negative Breast Cancer
TRAIL[h]	TAA[l]	NCT05357027	2022.08	2024.08	III	China	HLA-A2	Recruiting	Cervical Carcinoma
PRAME[i]	TAA	NCT05973487	2024.02	2026.12	I	United States	HLA-A*02:01	Recruiting	Head and Neck Cancer Cervical Cancer Non-small Cell Carcinoma

[a]Human leukocyte antigen.
[b]HumanPapillomavirus.
[c]Hepatitis B virus.
[d]Epstein-Barr virus.
[e]Cytomegalovirus.
[f]Kirsten rats arcomaviral oncogene homolog.
[g]Melanoma-associated antigen.
[h]TNF-related apoptosis inducing ligand.
[i]Preferentially expressed antigen melanoma.
[j]Tumor-specific antigen.
[k]Cancer germline antigen.
[l]Tumor associated antigen.

CAR-T cell therapy, at the forefront of therapeutic innovation, has numerous authorized medications that target different hematological cancers, such as lymphoma and myeloma (Wang et al., 2021; Hu et al., 2021). CAR-T cell therapy in hematological malignancies has brought new life hope to many patients who were previously difficult to treat. However, the application of this therapy in the treatment of solid tumors faces many challenges, including the complex microenvironment of solid tumors, high antigenic heterogeneity, and the difficulty of effective penetration of CAR T cells into the tumor (Zhao and Cao, 2019). Pancreatic carcinoma (PC) is one of the most common malignancies. In an investigation, 4.1R can suppress the anti-tumor activity of T cell responses. And overcome the problem of tumor-specific targets. The absence of 4.1R in natural killer group 2D (NKG2D) -CAR T cells enables to overcome the problem of tumor-specific targets and have stronger proliferation and killing function, providing a potential therapeutic strategy for the clinical treatment of PC (Gao et al., 2021). In one study, a CAR T cell co-expressing CXCR5 and IL-7 (C5/IL7-CAR-T) was designed to enhance the survival of CAR T cells and reduce cell depletion and apoptosis through the pSTAT5 signaling pathway, showing significant efficacy in the treatment of osteosarcoma (Hui et al., 2024). Another study delineates a new type of CAR T cell therapy based on stem cell-like T cells (T_{STEM}), which has a greater ability to expand compared to traditional T cell-based CAR T cells. Five days after a single infusion in the best patient of the same batch, an MRI scan showed almost complete regression of the solid tumor (Choi et al., 2024). This is an exciting milestone on the road to cancer treatment, given that blood tumors have been largely conquered by cell therapy and solid tumors have been left in the dark. This research results not only validate the feasibility of CAR-T cell therapy in the treatment of solid tumors. More importantly, it shows us the great potential of this therapy to rapidly and significantly reduce the size of tumors.

With research endeavors in solid tumor treatment progressively surging year by year (Table 1), TCR-T cell therapy is the optimal alternative to the CAR-T cell therapy regimen, amalgamating numerous advantages into one comprehensive approach. Given the ability of major histocompatibility complex (MHC) molecules to present peptide chains derived from both cell surface and intracellular proteins, TCR-T cell therapy enjoys an inherent advantage over CAR-T cell therapy by targeting a broader spectrum of antigens. In 1988, Blüthmann et al. ushered in a new era of TCR gene therapy by introducing a novel TCR gene into conventional T cells, thereby endowing the modified T cells with identical antigenic specificity (Blüthmann et al., 1988). In both hematological and solid tumor treatments, TCR-T cell therapy has exhibited a favorable safety and efficacy profile (Garber, 2018; Chapuis et al., 2019). Thus far, the emphasis of TCR-T cell therapy has primarily centered on solid tumors, and more and more new targets have been discovered (Ma et al., 2024; Ullah et al., 2024a). This includes the recognition of tumor-specific intracellular proteins, thereby enhancing the capacity of the targeted antigen pool to encompass tumor self-proteins (Tran et al., 2017; Vormehr et al., 2016; Schumacher and Schreiber, 2015), neoantigens resulting from tumor-specific random mutations, and cancer testicular antigens. With the added benefit that genital tissues lack MHC molecules, these antigens are typically only expressed in specific tumors and genital tissues. As a result, TCR-T cell therapy has a broader range of applications in solid tumors, which improves treatment effectiveness. Moreover, researchers find it easier to identify tumor antigens with high specificity, rendering the process of TCR-T cell therapy safer and associated with a reduced incidence of therapeutic side effects, such as neurotoxicity. This presents an opportunity to position TCR-T as a viable alternative to CAR-T cell therapy in treating solid tumors (Garber, 2018). The cancer/testis antigen New York esophageal squamous cell carcinoma 1 (NY-ESO-1), renowned for its high immunogenicity and widespread expression, stands out as an exemplary target antigen for TCR-T cell therapy. TCR-T cell therapy specifically targeting NY-ESO-1 can treat multiple myeloma (Rapoport et al., 2015), metastatic melanoma, metastatic synovial sarcoma (Robbins et al., 2011; Robbins et al., 2015; D'Angelo et al., 2018), provided antigen-specific and multifunctional activity, durable antitumor responses, and showed promising results. Nevertheless, inadequate *in vivo* persistence of infused T cells during early clinical trials resulted in the inability to demonstrate clinical efficacy in certain patients with solid tumors (Michalek et al., 2007; Fraietta et al., 2018). For patients experiencing advanced relapse, TCR-T cell therapy exhibits diminished efficacy in infiltrating due to the heightened immunosuppressive nature of the TME (Hafezi et al., 2021). While TCR-T cells targeting tumor antigens hold promise for treating solid tumors, numerous potential obstacles persist, underscoring the imperative for ongoing enhancements in TCR-T cell therapy.

Here, we discuss the structure and function of TCR-T cell therapies and suggest possible solutions by outlining the challenges of TCR-T for solid tumors and new strategies for innovative coupling of TCR-T with today's popular therapeutic approaches. This will bring hope that subsequent TCR-T can be effective in defeating solid tumors.

2 The structure and function of TCR-T cells

The TCR molecule is a heterodimer made up of two transmembrane polypeptide chains joined by different disulfide linkages found on T cells' surface. It enhances immunological responses and performs the specialized function of antigen recognition. The four peptide chains that make TCRs are α, β, γ, and δ. Most mature T cells have TCR molecules made up of α and β chains, but some also have TCR molecules made up of γ and δ chains. Less than 5% of all T cells in the circulation are γδ T cells (Pang et al., 2023; Zhang and Wang, 2019). TCR αβ cells recognize antigenic peptides presented on the surface of antigen-presenting cells (APCs) by class I or II MHC molecules in a selective manner. After being recognized, they grow and differentiate into effector cells, which produce cytokines or carry out cytotoxic actions. This process helps the body defend against pathogenic invasion and tumor growth by stimulating B cells or innate immune cells (Muro et al., 2019). On the other hand, TCR γδ cells are considered innate immune cells since they do not require sophisticated activation processes and are not restricted to the MHC (Hayday, 2019). During the immune response, γδ T cells may play a role in initiating, coordinating, and complementing αβ T cell functions (Park et al., 2022). T cells bearing αβ-type TCRs hold a pivotal role in adaptive immunity. Immunological surveillance by T cells stems from the

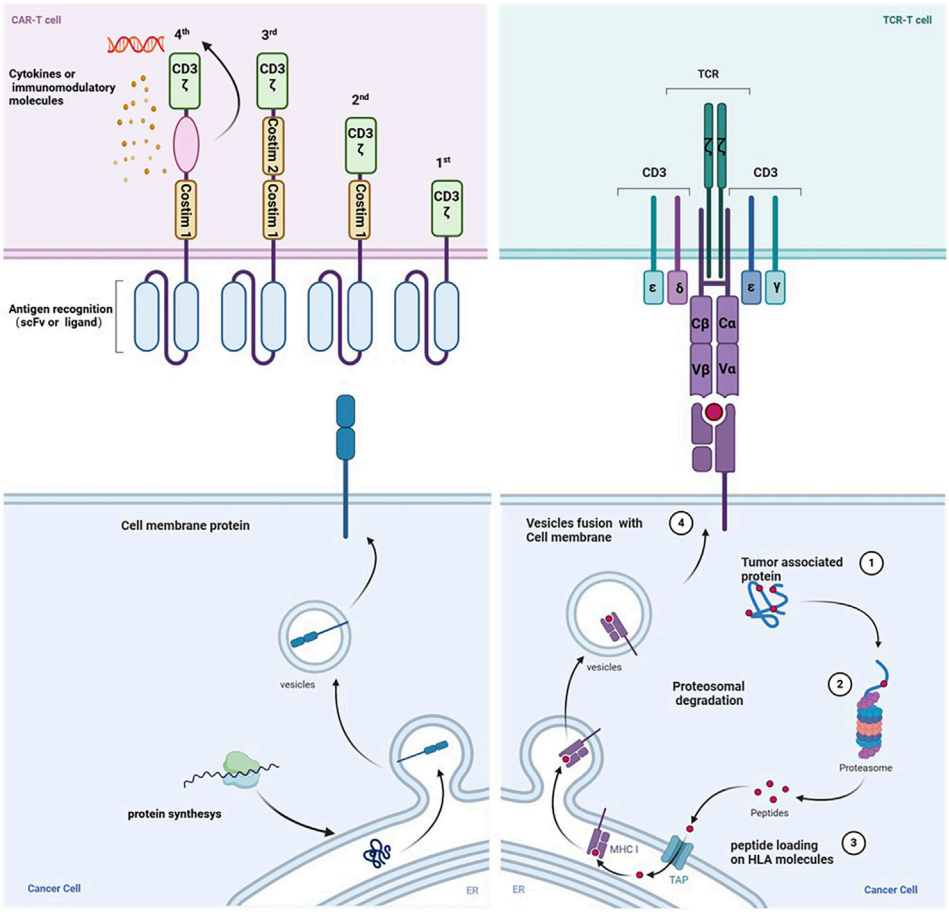

FIGURE 1
The mechanism of action differs between CAR-T cells and TCR-T cells. The generations of chimeric antigen receptors (CARs) and their structural distinctions are illustrated. CARs typically identify surface proteins using antibody-derived scFv recognition structural domains. Conversely, TCR T-cells operate on the principle of modifying T-cells' natural receptors to improve cancer cell recognition. The structure of the endogenous or genetically engineered T-cell receptor (TCR)-CD3 complex can recognize peptides presented by HLA molecules originating from various cellular compartments. Created with BioRender.com.

process wherein peptide fragments of degraded intracellular proteins are transported into the endoplasmic reticulum, where they bind to self-recognized proteins. A recent study has unveiled the high-resolution cryo-electron microscopy structure of a human TCR-CD3 complex containing eight subunits, offering a comprehensive molecular insight into the complex (Dong et al., 2019). Consistent with earlier biochemical data, the TCR-CD3 complex consists of an antigen-recognition module of disulfide-bonded TCRα/β heterodimers and three CD3 dimers, including CD3γε and CD3δε heterodimers, and a CD3ζζ homodimer, with a stoichiometry of 1:1:1:1 (Call et al., 2004).

An immunoreceptor tyrosine (ITAM) activation motif and an extracellular immunoglobulin (Ig) superfamily structural domain are present in each CD3γ/δ/ε subunit. On the other hand, CD3ζ has three ITAMs and a brief extracellular structural domain (ECD). As a result, a complete TCR-CD3 complex with 10 ITAMs has 20 tyrosine phosphorylation sites, which allows for reactions to various antigenic stimuli (Courtney et al., 2018). To activate T cells (Signal 1) and produce co-stimulatory molecules (Signal 2), which work in concert to increase the activity of activated cells, the TCR-CD3 complex initiates a signaling cascade. This mechanism helps cytotoxic T lymphocytes recognize and destroy sick or cancerous cells (Banchereau and Steinman, 1998; Chen and Flies, 2013). A secondary activation signal for T cells necessitates the involvement of co-stimulatory receptors. For instance, CD28 triggers T cell activation, and upon binding to its ligands B7 (CD80 and CD86) on the surface of APCs (Chen and Flies, 2013), it enhances TCR-driven tyrosine phosphorylation. This activation process recruits phosphatidylinositol 3-kinase (PI3K) to collaborate with growth factor receptor-bound protein 2 (Grb2) (Rudd et al., 2009). In the absence of CD28 engagement, TCR activation often results in an anergic state, characterized by functional inactivation of T cells upon antigen encounter, albeit they persist for a period in a hyporesponsive state (Linsley and Ledbetter, 1993). The collective impact of these signals dictates T-cell expansion, memory formation, and functional persistence (Rath and Arber, 2020).

TCR signaling strength is usually correlated with peptide-MHC (pMHC) binding affinity (Sibener et al., 2018), and T cell signaling constraints dictate a consensus TCR-pMHC docking topology that is highly conserved, enabling canonical TCR-pMHC I docking to localize CD8/Lck to CD3 complexes optimally (Zareie et al., 2021). However, this process can be constrained by the reversal of TCR-

TABLE 2 Comparison of car-t and tcr-t.

	Factors	CAR-T	TCR-T
Common ground	Genetic modification	Difficult, expensive	Difficult, expensive
	Procedure of treatment	Reinfusion after *in vitro* modification	Reinfusion after *in vitro* modification
	Specificity	High	High
	Immune suppression	Overcoming efficiently	Overcoming efficiently
	Flexibility	Less	Less
Distinction	Structure	An engineered receptor composed of intracellular and extracellular domains	Native or minimally designed TCR
	Core advantage	Cell surface antigen (no MHC restriction)	Intracellular antigen (pMHC restriction)
	Number of ITAMs	Three	Ten
	Adverse effect	Cytokine release syndrome; neurotoxicity	Cytokine release syndrome; neurotoxicity
	Tumor applications	CAR-T therapy has taken a leading position in the field of hematologic malignancies	TCR-T therapy places greater emphasis on research and development within the field of solid tumors

pMHC polarity, a phenomenon intricately involved in immune responses (Gras et al., 2016). TCR binding affinity to pMHC ranges from 500 μM to 1 μM (Huppa and Davis, 2003). Mechanical force initiates dynamic mechano-chemical coupling, leading to sequential alterations in agonist pMHC conformation. In this process, the TCR establishes a capture bond with agonist pMHC while forming a slip bond with non-agonist pMHC ligands (Sibener et al., 2018; Wu et al., 2019). Different tumor tissues form with different stiffnesses, especially solid tumors, generating mechanical forces that may directly affect the TCR-pMHC capture bond dynamic structural model. Cancer-associated somatic mutations or subtle polymorphic changes in HLA class I inhibit TCR-pMHC capture bond formation and reduce T cell recognition of cancer cells (Sibener et al., 2018).

TCR and CAR-engineered T cells are manipulated *ex vivo* using peripheral blood from either patients or healthy donors. Following expansion in culture to attain adequate cell numbers, these engineered T cells are reintroduced into patients to target and eliminate cancer cells (Figure 1). However, they exhibit distinct mechanisms for antigen recognition (Table 2). In contrast to CARs, TCRs display greater sensitivity in antigen recognition. The TCR-pMHC interaction process demonstrates remarkable specificity, heightened sensitivity, and rapid biochemical reaction kinetics. Under physiological conditions, tumor cells carry abundant self-antigens and hidden tumor antigens to achieve antigen escape. TCR-T accurately differentiates between abnormal and low concentrations of pMHC ligands and triggers an adaptive immune response in the presence of most autoantigenic interferences (Feinerman et al., 2008). If pMHC is in tandem with multiple TCR molecules, a more significant stimulus signal can be generated (Valitutti, 2012). TCR-T cells release fewer cytokines compared to CAR-T cells. While CAR T cells have demonstrated effectiveness as effector cells targeting the same malignancy, they exhibit transiently elevated cytokine levels, increasing the risk of cytokine storms. Conversely, TCR-T cells exhibit superior expansion capabilities under heightened antigen exposure to CAR-T cells. They also pose a reduced risk of cytokine storm, exhibit diminished expression of co-inhibitory molecules, better navigate the immunosuppressive microenvironment of solid tumors, and sustain T-cell activity to efficiently eradicate tumors (Wachsmann et al., 2022).

3 Limitations of TCR-T therapy for solid tumor treatment

The current TCR-T for solid tumors dilemma can be divided into four segments: TCR mismatch and multiple limitations of targets, potential toxicity, cytokinetic storm, and tumor microenvironment (Figure 2). Overcoming these challenges will be key to constructing TCR-T cells capable of recognizing reliable targets with sufficient affinity and function to eliminate existing tumors and prevent recurrence.

3.1 TCR mismatch

The mismatch between exogenous and endogenous TCR chains has been a non-negligible problem for engineered TCR-T cell therapy. Exogenous TCR chains can have a competitive relationship with endogenous TCR chains, and exogenous TCR chains introduced after screening have a high affinity to dominate (Heemskerk et al., 2007). The introduction of exogenous TCRs into T cells has several effects, including the formation of mixed TCR dimers. However, the properties of different mixed TCR dimers are unpredictable and may affect the subsequent biological activity of T cells. These dimers might prevent transferring TCR-T cell therapy to clinical applications. It has been shown that TCR transfer leads to the generation of hybrid TCR dimers of unknown specificity, which may cause these T cells to cannibalize each other and exhibit novel deleterious reactivity, such as graft-versus-host response (GVHD) (van Loenen et al., 2010). Mixed TCR dimers may compete with

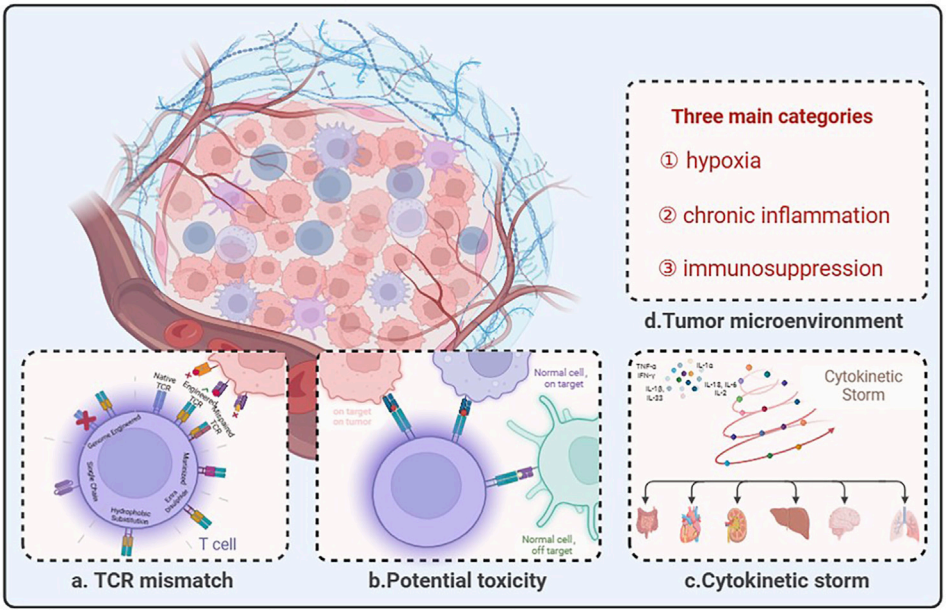

FIGURE 2
The predicament of TCR-T therapy in solid tumors lies in its limited efficacy due to several challenges. **(A)** Description of pairing errors between endogenous and engineered TCRs and potential strategies. **(B)** TCR-modified T cells are designed to redirect antigenic responses and maintain specificity, but at the same time TCR-engineered T cells have the potential to: "On target, on tumor": appropriate antigen recognition leading to tumor eradication; "Normal cell, on target": TCR-T recognizes low-level antigens on normal tissues; "Normal cell, off-target": TCR-T recognizes relevant or irrelevant antigens on target or non-targeted tissues. **(C)** Cytokine storm is an immune dysregulation disorder encompassing several conditions characterized by systemic symptoms, systemic inflammation, and multiorgan dysfunction, which may lead to multiorgan failure if not properly treated. **(D)** The tumor microenvironment comprises three main categories: hypoxia, chronic inflammation, and immunosuppression. Created with BioRender.com.

engineered TCR heterodimers for binding of restricted CD3 components, resulting in off-target presentation of new antigenic peptides to the surface and triggering off-target effects. In the absence of the ability to eliminate mixed dimers, cysteines were used to design TCR constant regions of the exogenous chain, increasing the total surface expression of the introduced TCR chain, reducing the extent of mismatch, and decreasing the risk of developing graft-versus-host disease (Kuball et al., 2007). Enhanced TCR chain expression using hybridized human TCR chains containing mouse constant structural domains does not bind to endogenous TCR chains containing human constant structural domains (Chen et al., 2017). However, immunogenicity can limit T-cell viability to some extent (Cohen et al., 2006). In contrast to phage display methods, since the binding affinity of TCRs or mutants expressed on yeast cells can be directly assessed, yeast surface display technology screens for high-affinity TCRs and reduces the chance of TCR mismatch (Smith et al., 2015; Shafer et al., 2022). By introducing an additional stable disulfide bond between residue 48 of the TCR constant region α and residue 57 of the TCR constant region β through cysteine substitution, the inter stream binding affinity of the engineered TCR α/β chains is enhanced while simultaneously reducing their binding affinity to the endogenous TCR α/β chains (Krshnan et al., 2016). The stability of the engineered TCR α chain can be enhanced through the selection of hydrophobic substitutions in the transmembrane region (Haga-Friedman et al., 2012). Single-chain TCR (scTCR) entails the incorporation of TCR antigen recognition and signaling domains into a singular chain, thereby minimizing mismatches through spatial site-blocking (Knies et al., 2016).

3.2 Multiple limitations of targets

For a considerable time, tumor-specific antigens, or TSAs, have been considered ideal targets for cellular immunotherapy. Nonetheless, the existing repertory of TSAs against solid tumors is still restricted, which reduces the effectiveness of traditional CAR-T cell therapy. On the other hand, the advantage of TCR-T treatment is that it targets both intracellular and cell surface antigens, greatly expanding the pool of potential targets. Notwithstanding this promise, very few peptide antigen targets have been shown to be both safe and efficacious for TCR-T immunotherapy. Research to detect immunogenic neoantigens in tumor cells may provide a significant discovery. Tumor cell-produced neoantigens need to be unique to tumor cells, not expressed in normal cells, and have high expression levels so that MHC molecules can recognize them (Wang and Cao, 2020). Not all people produce neoantigens in the same way, and even individuals with the same type of solid tumor have diverse tumor cells that express different antigens. Individual differences in neoantigens need the creation of customized TCR-T cell therapy regimens, which are closely related to the financial and schedule aspects of TCR-T cell therapy (Li et al., 2023a). Clear studies on the stability of neoantigens are lacking, posing challenges to mitigating the risk of

neoantigen loss. Downregulation or loss of MHC class I molecules on tumor cells diminishes the sensitivity of TCR-T therapy and serves as a prominent pathway for tumor evasion (Dutta et al., 2006; Singh and Banerjee, 2020; Xu et al., 2022). The targets of TCR-T cell therapies are further constrained by MHC type. HLA genes encoded MHC molecules exhibit extensive diversity within the population, with over 20,000 HLA I human alleles identified to date (Gonzalez-Galarza et al., 2020). At present, the research field of TCR-T therapy is constantly exploring new targets to improve the therapeutic effect and expand the therapeutic scope. The research and development of novel targets mainly include tumor-specific neoantigens (Xie et al., 2023), virus-associated antigens and cancer-testis antigens (Gordeeva, 2018) (Table 1).

3.3 Potential toxicity

Regarding the dynamics of therapy, TCR-T therapy is more sensitive than CAR-T therapy, making it more vulnerable to non-tumor-targeted toxicity (on-target off-tumor) and cross-reactivity (off-target off-tumor). The former is related to the expression of target antigen in normal tissues, especially in the case of TAA. The latter refers to the fact that the TCR recognizes different antigens on normal cells, especially when the affinity of the TCR sequence is enhanced. This vulnerability may cause damage to normal human tissues that have comparable antigenic epitopes. An illustrative instance involves the treatment of myeloma and melanoma patients with engineered T cells targeting the affinity-enhancing TCR of MAGE-A3, resulting in unforeseen occurrences of cardiogenic shock and mortality. In these cases of myocardial injury, histopathological analysis revealed the infiltration of T cells but no expression of MAGE-A3 was detected in cardiac autopsy tissue. Because TCR-T cells recognize an unrelated peptide from the rhabdomyosarcoma-specific protein titin, it is thought to be due to cross-reactivity (Linette et al., 2013). In a clinical investigation, highly reactive transferred TCR-T cells transported to melanoma tumors in patients and destroyed melanoma in their bodies, but patients showed damage to normal melanocytes in the skin, eyes, and ears (Johnson et al., 2009). Another study delineates instances of severe acute colitis induced in patients with metastatic colorectal cancer who were treated with TCR-T cells targeting carcinoembryonic antigen (CEA). This outcome arose from the expression of the target antigen on normal intestinal tissue as well (Parkhurst et al., 2011). The concept of TCR affinity embodies a paradox. It is widely acknowledged that robust affinity is imperative for sustaining T-cell expansion and facilitating the regression of human cancers. Excessive affinity, however, can cause cross-reactivity with self-antigens by targeting healthy cells across the body that carry homologous antigens and prematurely exhausting T cells.

3.4 Cytokinetic storm

Cytokine storm represents a spectrum of clinical disorders marked by significant health risks arising from the excessive production of inflammatory factors by cell therapy. This phenomenon encompasses manifestations such as fever, tachycardia, hypotension, rash, and respiratory distress, emerging as the predominant adverse reaction to T-cell immunotherapy. Key cytokines implicated in a cytokine storm, including Interferon-gamma, IL-1, IL-6, TNF, and IL-18, exhibit consistently elevated levels and are believed to orchestrate the central pathological mechanisms underlying cytokine release syndrome (CRS). Since TCR-T can recognize peptide epitopes derived from proteins in any subcellular (e.g., membrane, cytoplasmic, and nuclear) compartment (Chandran and Klebanoff, 2019), has a broader range of antigen selection, and the TCR chain has intrinsic signaling and regulates T cells, resulting in a lower rate of CRS as compared to CAR-T cells, T cell receptor (TCR)-T cells are also considered promising immunotherapy. Low incidence is not the same as complete avoidance. Mikiya Ishihara et al. utilized retroviral vectors to engineer precise silencing of endogenous TCRs and induce the forced expression of the affinity-enhancing NY-ESO-1-specific TCR in T cells. The system expresses small interfering RNAs (siRNAs) that are specific to endogenous TCR genes to enhance the expression of transduced tumor-specific TCR while minimizing potential TCR mispairing. In patients with tumors that highly express NY - ESO - 1, the infusion of TCR - T cells led to a significant tumor response as well as early-onset CRS (Ishihara et al., 2022). Similarly, a patient with fallopian tube cancer, unresponsive to adjuvant chemotherapy, participated in a clinical trial of MAGE-A4-targeted T-cell receptor T-cell therapy. Following T-cell infusion, the patient experienced CRS and pseudogouty arthritis accompanied by immune effector cell-associated neurotoxicity syndrome (ICANS) within 7 days. Notably, the drug tocilizumab was ultimately utilized to eliminate CRS and ICANS successfully (Kim et al., 2021). Hence, to enhance the safety and efficacy of TCR-T cell immunotherapy, it is imperative to prudently evaluate the significance of cytokine storm risk for patient prognosis.

3.5 Tumor microenvironment

The first obstacle genetically modified T cells must overcome while fighting solid tumors is to infiltrate the tumor's hostile environment successfully. Solid tumors reinforce their conquered area by creating complex and formidable ecosystems. Cancer cells are remarkably adaptive as tumors progress, repurposing various non-tumor cell types to create an environment that supports their growth and survival (Heindl et al., 2015; Wang S. et al., 2020). The tumor microenvironment comprises three main categories: hypoxia, chronic inflammation, and immunosuppression (Policastro et al., 2013). Within the relatively constrained confines of solid tumors, hypoxia emerges as a pervasive condition, significantly impacting the rapid proliferation and metabolic activity of T cells. While $CD8^+$ T cells serve as the cornerstone of tumor elimination, their vigor wanes, and exhaustion sets in when confronted with hypoxic conditions. Recent discoveries have unveiled a paradox: as this fundamental component becomes terminally exhausted, it transforms, upregulating CD39 expression to foster an immunosuppressive milieu that undermines the robust anti-tumor capabilities of other T cells (Vignali et al., 2023; Canale et al., 2018). Tumor-associated macrophages (TAMs) constitute pivotal constituents of the tumor microenvironment. Studies in hepatocellular carcinoma therapeutics have unveiled a robust correlation between downregulation of xanthine oxidoreductase

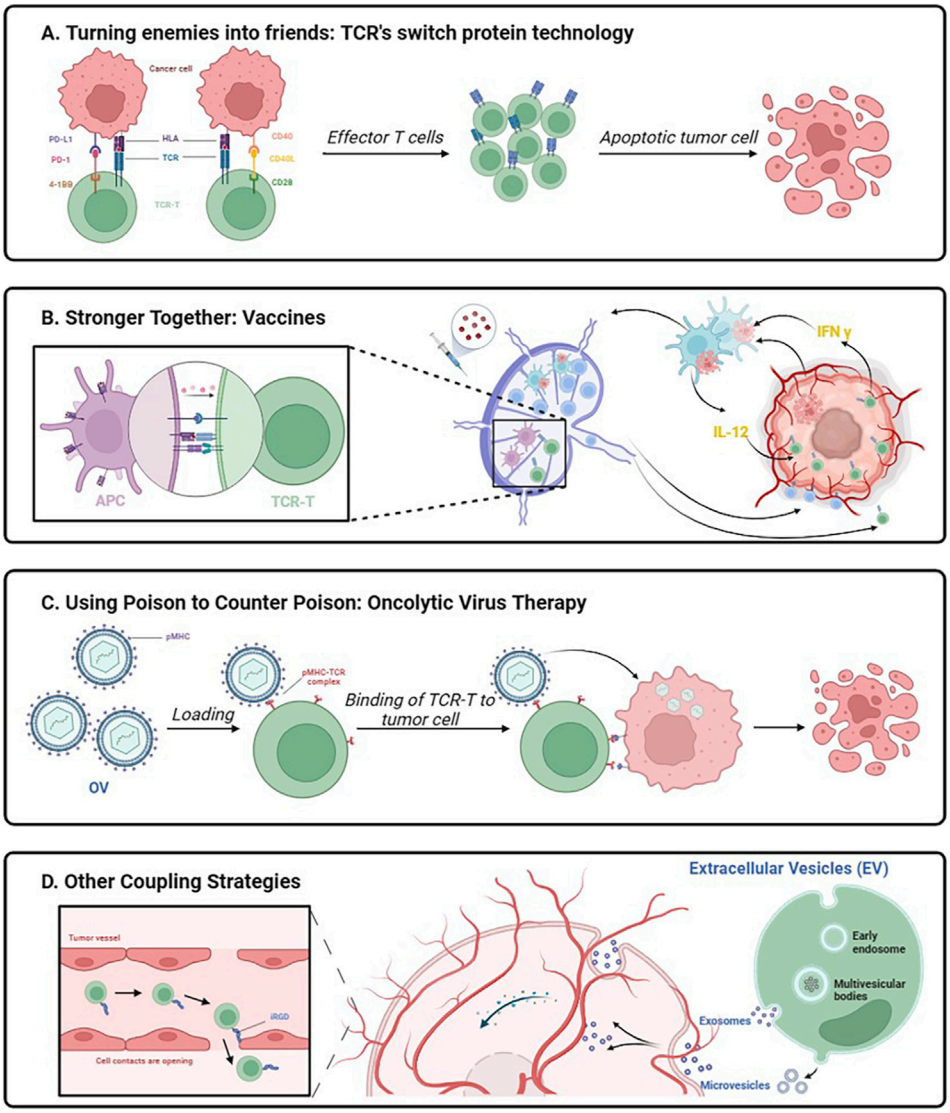

FIGURE 3
Schematic diagram of innovative association working mechanism. Created with BioRender.com.

(XOR) expression and specific tumor microenvironment traits, particularly hypoxia (Ullah et al., 2024b; Ullah et al., 2024c). Deletion or dysfunction of XOR in monocyte-derived macrophages fosters CD8+ T cell depletion by inducing the upregulation of immunosuppressive metabolites (Lu et al., 2023). Most tumor stromal cells within the TME exhibit numerous immunosuppressive signaling proteins, including programmed death ligand-1 (PD-L1). The interaction between PD-L1 and programmed cell death protein-1 (PD-1) (Noman et al., 2014) expressed in T cells can result in immune cell dysfunction and apoptosis (Dermani et al., 2019). Hypoxia induces elevated potassium levels and an acidic milieu, disrupting potassium homeostasis in tumor-infiltrating lymphocytes (TILs) within necrotic tumor microenvironment regions (Conforti, 2017). This severely suppresses T-cell effector function, impacting cytokine secretion capacity and activity (Eil et al., 2016).

4 Innovative association

TCR-T therapy needs to improve T cell expansion and persistence *in vivo* to avoid rapid loss of effector function. Because TCR-T alone may not be sufficient to generate an effective antitumor response, innovative combination strategies may improve response rates in patients with high tumor loads and reduce the need for large numbers of TCR-T cells as a potential approach to improving clinical outcomes (Figure 3).

4.1 Turning enemies into friends: TCR's switch protein technology

The PD-1/PD-L1 inhibitory axis represents an immune checkpoint mechanism evolved by the body to regulate the magnitude and duration of immune responses, thereby preventing

excessive inflammatory reactions and autoimmune diseases that may harm healthy tissues (Dai et al., 2014; Dyble et al., 2015). In the endeavor to corral tumor cells, the PD-1/PD-L1 inhibitory axis is a vulnerability. Tumor cells accomplish immune evasion by elevating PD-L1 ligand expression and inhibiting T cell function through PD-1 engagement. PD-L1, functioning as a natural ligand for PD-1 (Ji et al., 2019), assumes the role of a guardian for tumor cells, endowed with the capability to convey anti-apoptotic signals and foster tumor proliferation (Dong et al., 2018).

When this route is unchecked, T cells' ability to fight cancer is compromised. To prevent the PD-1/PD-L1 pathway, scientists have developed a variety of PD-1/PD-L1 immune checkpoint inhibitors. These inhibitors have been successfully used to treat a variety of malignancies, including classical Hodgkin's lymphoma, melanoma, non-small cell lung cancer, and squamous cell carcinoma of the head and neck. Moon EK et al. reported that the combination of TCR-T cell therapy with PD-1 antibody reduced hypofunctionality in tumor-infiltrating lymphocytes (TILs) and augmented the efficacy of overt metastatic T cells under conditions of chronic antigenic stimulation (Moon et al., 2016). At present, cellular immunotherapies engineered to produce autocrine PD-1 antibodies or to suppress PD-1 expression are available for treating solid tumors (Hamilton et al., 2023; Wu et al., 2023; Zhang et al., 2022). PD-1/PD-L1 immune checkpoint inhibitors provide advantages but also significant hazards. Studies reveal significant effects on the heart, resulting in serious illnesses such as myocarditis, stress cardiomyopathy, pericardial disease, and an increased risk of complications associated to the heart's immune system (Varricchi et al., 2017; Costa et al., 2017; Khunger et al., 2020).

If playing hardball proves ineffective, why not transform adversaries into allies? The EtoE platform introduces an inherent 2-in-1 combination therapy (Schendel, 2023). The pivotal element of this therapy lies in the utilization of the PD1-41BB co-stimulatory switch protein (CPS) incorporated into TCR-T cells, enabling these cells to concurrently express recombinant TCR and PD1-41BB switch receptors (Sailer et al., 2022). The ingenuity of the concept resides in substituting the inhibitory signaling structural domain of PD-1 with the activating signaling structural domain of 4-1BB while retaining the external structural domain of PD-1 responsible for binding to PD-L1 on tumor cells. The intracellular signaling domain of the 4-1BB protein offers a comprehensively characterized pathway for co-stimulation, augmenting T-cell responses, and activating various immune cells (Vinay and Kwon, 2014). Therefore, by not impeding PD-1 binding to PD-L1, PD1-41BB-modified TCR-T cells exhibit enhanced tumor cell killing even in the presence of PD-L1-overexpressing tumor cells. This scenario converts potent inhibitory signals into secondary activating signals, prompting T-cell proliferation, cytokine expression, and bolstering T-cell effector function (Schlenker et al., 2017). The PD1-41BB CPS efficiently regulates the self-defense mechanism of tumor cells.

Another co-stimulatory switch protein targets the CD40L/CD40 pathway and the CD28 co-stimulatory signal. The CD40 receptor and its ligand, CD40L, constitute one of the most crucial molecular pairs of stimulatory immune checkpoints. CD40 binds to its ligand, CD40L, which is transiently expressed in T cells and other non-immune cells under inflammatory conditions (Elgueta et al., 2009). Initially characterized on B cells (Sacco et al., 2023), CD40 is expressed on professional antigen-presenting cells as well as non-immune cells and tumors (van Kooten and Banchereau, 1997). The CD40L-CD28 CPS is composed of an extracellular CD40L structural domain combined with an intracellular signaling structural domain of the CD28 co-stimulatory receptor (Olguín-Contreras et al., 2021). The principles related to the chimeric design of this CPS are not yet clear, and it is still unknown whether it can successfully achieve biological effects (Oda et al., 2017). CD40L-CD28 co-stimulatory switching protein-modified TCR-T cells provide a variety of new attributes that can contribute to the enhancement of cellular immune responses. As multiple cells in the tumor microenvironment express CD40, CD40L-CD28 engineers enhanced T-cell infiltration, and CD40L activates CD40-expressing immune cells to amplify anti-tumor responses. The presence of the CD28 signaling structural domain in the CSP provides further stimulation of TCR-T cells, improving cytokine secretion and antigen-specific cytotoxicity. This intrinsic combination enhances the function of TCR-T cells, alters the strong inhibitory nature of the tumor microenvironment against T cells, and mobilizes immune cells in the tumor microenvironment to participate in the battle against solid tumors (Schendel, 2023).

4.2 Stronger together: vaccines

Although TCR-T cell therapy has great promise in treating solid tumors, it still confronts several obstacles and frequently produces unsatisfactory clinical results. TCR-T therapy faces significant challenges in efficiently treating solid tumors due to factors such low T-cell infiltration capacity, hostile tumor milieu for T-cell activation, and limited *in vivo* durability of infused TCR-T cells. Permissive T cells can be genetically engineered to express different pro-inflammatory molecules, such as IL-12 (Liu et al., 2019; Pegram et al., 2012), IL-15 (Nguyen et al., 2023), IL-18 (Avanzi et al., 2018), CD40L (Kuhn et al., 2019), or DC growth factor FLT3 (Zhu et al., 2024; Lai et al., 2020). These modified T cells have the ability to self-supply pro-inflammatory chemicals, promote epitope dissemination, and enhance T cells' anti-tumor activity *in vivo*. These tactics are supported by the fact that transformed T cells are viable and abundant *in vivo* and that T-cell death reduces the release of pro-inflammatory chemicals. However, because the *in vitro* production method takes time, there is a chance that genetically altered T cells will not be easily accessible for subsequent infusion. In contrast, the simplicity of tumor vaccine preparation and the ability to control the infusion timing outweigh these strategies. Consequently, the combination of vaccines with TCR-T cell therapy holds promise in overcoming the lackluster outcomes associated with TCR-T cell therapy in the treatment of solid tumors.

While co-stimulatory signaling plays a crucial role in T cell activation, the downregulation of co-stimulatory ligand expression within the tumor microenvironment presents a challenge by restricting T cell activation. Attempts to enhance TCR-T efficacy through combined vaccination in early TCR-T trials did not yield the anticipated results in providing both TCR stimulation and co-stimulation *in vivo* (Nowicki et al., 2019; Kageyama et al., 2015). Significantly, the integration of vaccines with overt cellular therapies effectively triggers the activation of the endogenous immune system, facilitating the generation of host T cells targeting additional tumor antigens, thus preventing antigen-negative tumor escapes (Author anonymous, 2023; Mateus-Tique and Brown, 2023; Corbière et al., 2011). The phenomenon, termed "Antigen Spreading" (AS), has the

potential to enhance the efficacy of TCR-T cell therapy for solid tumors. Recent studies conducted by Elicio Therapeutics have demonstrated that the combination of amphiphilic (AMP) vaccination, which selectively targets homologous peptides and adjuvants to lymph nodes, induces dendritic cell activation. This activation not only enhances T-cell activation through endogenous co-stimulation and cytokine-supported delivery of TCR-stimulants but also has the potential to trigger the collaboration of newly generated tumor-specific T cells with TCR-T cells, thus collectively combating tumors (Drakes et al., 2024).

In order to facilitate the targeted growth of T cells *in vivo*, customized vaccinations can also be made to target certain antigens of interest called neoantigens (Hellmann and Snyder, 2017). Personalized vaccinations can undoubtedly enhance antigen-specific T cells *in vivo*, as evidenced by research done on human HLA transgenic mice and cancer vaccine trial subjects (Sahin et al., 2017; Kunert et al., 2016). However, the combination of TCR-T cell treatments and cancer vaccines has only been studied in a small number of clinical trials, thus more study is needed to determine their therapeutic efficacy and develop a thorough and well-defined rationale.

4.3 Using poison to counter poison: oncolytic virus therapy

Immunotherapy against the oncolytic virus (OV) is a new and exciting treatment approach. Oncolytic viruses, whether natural or recombinant, have the ability to preferentially infect tumor cells, multiply within the tumor cells, and lyse tumor cells directly while sparing healthy cells. T-cell treatment with an oncolytic virus combination shows a synergistic impact. Targeting by lyssaviruses can compensate for the deficiency in T-cell trafficking (Kaufman et al., 2015), converting the "cold" tumor microenvironment into a "hot" one (Bommareddy et al., 2018). Moreover, it inhibits tumor immune evasion mechanisms and angiogenesis (Streby et al., 2017), achieving multifaceted tumor eradication. In addition to eliciting classical apoptosis and pyroptosis by targeting tumor antigens, it can induce autosis, a previously undocumented form of cancer cell demise. A study report delineates the synergy between an oncolytic virus and adoptive cellular therapies (CAR-T, TCR-T), effectively directing its attack toward drug-resistant cancer cells, ushering in new optimism for combating treatment-resistant cancers (Zheng et al., 2022).

4.4 Other coupling strategies

Tumor-homing cell-penetrating peptides (CPPs) constitute small amino acid sequences, typically short peptides (comprising less than 30 residues) (Ye et al., 2016), capable of traversing cell membranes. These peptides serve as effective vehicles for intracellular delivery, both *in vitro* and *in vivo*, facilitating the transportation of diverse biologically active cargoes, ranging from nucleic acids to large proteins and other compounds, with molecular weights extending up to 120 kDa. CPP enhances the penetration of small molecule drugs and nanoparticles into tumor tissues (Silva et al., 2019). Naiqing Ding et al. achieved enhanced infiltration of tumor-specific T cells through the rapid modification of T cells with the tumor-penetrating peptide iRGD using a lipid insertion approach (Ding et al., 2019). This method circumvents the need for intricate gene editing procedures. A novel bifunctional drug, iRGD-anti-CD3, tightly bridges internalizing RGD (Arg-Gly-Asp) peptide (iRGD) and T cells by binding to CD3. iRGD-anti-CD3-modified T cells not only alleviate the challenging infiltration of T cells in the tumor microenvironment but also induce T-cell activation and cytotoxicity against cancer cells (Zhou et al., 2021). Using CPP in conjunction with TCR-T cell treatment is a novel approach that has the potential to eventually improve the therapeutic efficacy of off-the-shelf cell therapy.

A common and serious side effect of cell treatment is called CRS, which is caused by immune cells releasing cytokines out of control. Cytokine storm is characterized by its intensity and presents serious dangers, including organ failure and death. Researchers have started looking into the use of genetically altered exosomes made from altered cells in cancer treatment as a way to lessen this difficulty. Exosomes provide a significant benefit over using genetically changed post-modified cells directly because of their nanoscale size and innate ability to cross biological barriers, especially when it comes to solid tumor therapy. Exosomes have been shown in numerous studies to be able to be tailored for target specificity, which allows them to act as nanocarriers for anti-tumor medicines and antigen-specific anti-tumor immune responses (Roma-Rodrigues et al., 2014; Cheng and Hill, 2022). Therefore, exosome-based treatments show great therapeutic promise for cancer patients. Several examples of these therapies have been reported in preclinical models or clinical trials, including dendritic cell exosomes (DC-Exos) (Li et al., 2023b) and natural killer exosomes (NK-Exos) (Sun et al., 2020; Sun et al., 2019). Exosomes have advantages over cell-based therapies, including higher yield, increased safety, easier storage, and lower costs (Nag et al., 2023; Xu et al., 2020; Wang et al., 2016). Vδ2-T cells are known for their potential in anti-tumor and anti-infective capabilities, and they play a crucial role in recognizing and attacking both tumor and infected cells. Additionally, they are essential in controlling inflammatory pathways and immunological responses. A method of treating EBV-associated tumors with Vδ2-T-Exos, which possesses the cytotoxic and immunostimulatory characteristics of Vδ2-T cells, was suggested by Xiwei Wang et al. This strategy effectively controls EBV-associated tumors by combining the benefits of merging NK-Exos and DC-Exos (Wang X. et al., 2020). Exosomes produced from TCR-T cell culture can be used as a unique and potentially very effective cancer therapy approach. By acting as direct attackers and taking the place of TCR-T cells *in vivo*, they improve the safety and controllability of treatment.

5 Future perspective

TCR-T therapy holds significant promise for the treatment of solid tumors, yet various challenges must be addressed to fully realize its potential. There are related strategies to reduce TCR mismatch by interfering with endogenous TCRs. Tumor cells genetically engineered to express antigens from genetically modified T cells exhibit enhanced cytotoxic activity by specifically silencing endogenous TCRs and introducing tumor-specific TCR vectors (Ochi et al., 2011; Okamoto et al., 2009). Knockdown of its own TCR by gene editing (Georgiadis et al., 2018; Eyquem et al., 2017) or the use of the TCR γδ structural domain in TCRαβ to improve TCR pairwise binding (Hiasa et al., 2009;

Parlar et al., 2019; Ishihara et al., 2023; Wang et al., 2023) to increase the level of functional exogenous TCRs on the surface of the T cells, which also avoids the risk of generating attacking self-antigens. The high cost of development and production of personalized TCR-T drugs has led to high market prices. How to reduce costs and achieve large-scale production will be the key to future commercialization. In a stride toward advancing scientific research, TCR-T cell therapies are transitioning towards the allogeneic generalization of this concept, departing from the customized design of individual antigens. The challenge of insufficient targets for TCR-T cell therapy has been addressed by a ground-breaking study that suggests using membrane-fused nanoparticles (NPs) as targets for specific recognition by TCR-T cells, regardless of the original HLA type, thereby modifying peptide-HLA (pHLA) onto the surface of tumor cells and allowing for the selective identification and elimination of tumor cells (Xu et al., 2023). Lower affinity T cells that have been developed might be a more secure option, but they frequently do not have the required antitumor effect. A potential solution to this conundrum is to introduce a suicide gene into TCR-T cells. This strategy prevents nonspecific damage to other tissues by maintaining effective tumor killing while inducing death in T cells at certain nodes. Another solution is to screen for TSA that is more tumor-specific than TAA, or to reduce the risk of toxicity and improve anti-tumor efficacy through affinity optimization and sequence modification. To counteract the diverse adverse conditions within the tumor microenvironment, engineered cytokines resistant to hypoxic and acidic environments commonly found in tumors are directed toward weakening the physical barriers of the extracellular matrix within the TME. This strategy aims to enhance T-cell infiltration capacity and augment the efficacy of adoptive T-cell therapies (Gaggero et al., 2022). Targeting TCR-T cells with immunosuppressive factors or enhancing the signaling function of intracellular signaling structural domains can reduce T cell depletion to counteract the immunosuppressive effects of tumors and become effective potential strategies. TCR-T therapy has the potential to become a transformative treatment for solid tumors.

6 Conclusion

Genetically engineered T cells represent a groundbreaking therapy for refractory tumors, capable of selectively eliminating cancer cells while sparing normal ones. TCR-T cell therapy and CAR-T cell therapy stand out among the various over-the-counter T cell therapies. However, CAR-T therapy often falls short in treating solid tumors, highlighting the superior potential of TCR-T cells. TCR-T cells offer unmatched advantages, as they can recognize epitopes from both surface and intracellular proteins, enabling the detection of a broader range of targets, including tumor-associated antigens (TAAs), cancer germline antigens, viral oncoproteins, and tumor neoantigens, compared to CAR-T cells. Furthermore, TCR-T cells require a broader range of affinities to activate T cells effectively compared to CAR-T cells. Thus, TCR-T cell therapy holds promising prospects for solid tumor treatment, with numerous studies progressing to the clinical stage.

Despite its potential, TCR-T cell therapy faces significant obstacles, including TCR mismatch, potential toxicity, cytokine storms, the tumor microenvironment, and target limitations. Various novel technologies and strategies are being applied to enhance the efficacy and safety of TCR-T therapy. These efforts primarily focus on reducing TCR mispairing to enhance TCR expression and function, augmenting the persistence and anti-tumor activity of engineered T cells, improving the homing and infiltration of engineered T cells into solid tumors, overcoming the immunosuppressive tumor microenvironment, and targeting neoantigens to enhance tumor-specific killing.

The innovative combination approach has sparked a research frenzy, with TCR-T cell therapy and other immunotherapies striving to identify the optimal "golden pair" through rational combinations, aiming for synergistic anti-tumor efficacy. However, developing innovative combinations poses significant challenges, with high barriers in the research and development process. While early studies provide valuable insights, a long road is still ahead before mature product development can be achieved. Additionally, TCR-T therapy requires further refinement and optimization of its production process to emerge as a potent tool in the fight against cancer and substantial tumors, ultimately revolutionizing cancer immunotherapy.

Author contributions

WH: Conceptualization, Software, Writing–original draft, Writing–review and editing, Data curation. KC: Conceptualization, Software, Writing–original draft, Writing–review and editing. MF: Software, Writing–original draft, Writing–review and editing, Conceptualization. NH: Data curation, Writing–review and editing. SZ: Data curation, Writing–review and editing. DJ: Data curation, Writing–review and editing. XZ: Data curation, Writing–review and editing. JC: Data curation, Writing–review and editing. YL: Data curation, Writing–review and editing. GX: Conceptualization, Funding acquisition, Resources, Supervision, Writing–review and editing.

Funding

The author(s) declare financial support was received for the research, authorship, and/or publication of this article. This research was funded by the Guangdong Basic and Applied Basic Research Foundation (2023A1515140148); Ningxia Key R&D Program (2022CMG02041); Dongguan Science and Technology of Social Development Program (20221800905062); the High-level Talent Research Funding Program of the First Dongguan Affiliated Hospital of Guangdong Medical University (GCC2023004).

Acknowledgments

To enhance clarity and ensure grammatical accuracy, we utilized advanced language models, specifically ChatGPT version 3.5, Grammarly.

Conflict of interest

The authors declare that the research was conducted in the absence of any commercial or financial relationships that could be construed as a potential conflict of interest.

Publisher's note

References

Author anonymous, (2023). Vaccine-Boosted CAR T-cell therapy elicits antigen spreading. *Cancer Discov.* 13(9):doi:10.1158/2159-8290

Avanzi, M. P., Yeku, O., Li, X., Wijewarnasuriya, D. P., van Leeuwen, D. G., Cheung, K., et al. (2018). Engineered tumor-targeted T cells mediate enhanced anti-tumor efficacy both directly and through activation of the endogenous immune system. *Cell Rep.* 23 (7), 2130–2141. doi:10.1016/j.celrep.2018.04.051

Banchereau, J., and Steinman, R. M. (1998). Dendritic cells and the control of immunity. *Nature* 392 (6673), 245–252. doi:10.1038/32588

Blüthmann, H., Kisielow, P., Uematsu, Y., Malissen, M., Krimpenfort, P., Berns, A., et al. (1988). T-cell-specific deletion of T-cell receptor transgenes allows functional rearrangement of endogenous alpha- and beta-genes. *Nature* 334 (6178), 156–159. doi:10.1038/334156a0

Bommareddy, P. K., Shettigar, M., and Kaufman, H. L. (2018). Integrating oncolytic viruses in combination cancer immunotherapy. *Nat. Rev. Immunol.* 18 (8), 498–513. doi:10.1038/s41577-018-0014-6

Call, M. E., Pyrdol, J., and Wucherpfennig, K. W. (2004). Stoichiometry of the T-cell receptor-CD3 complex and key intermediates assembled in the endoplasmic reticulum. *Embo J.* 23 (12), 2348–2357. doi:10.1038/sj.emboj.7600245

Canale, F. P., Ramello, M. C., Núñez, N., Araujo Furlan, C. L., Bossio, S. N., Gorosito Serrán, M., et al. (2018). CD39 expression defines cell exhaustion in tumor-infiltrating CD8(+) T cells. *Cancer Res.* 78 (1), 115–128. doi:10.1158/0008-5472.CAN-16-2684

Chandran, S. S., and Klebanoff, C. A. (2019). T cell receptor-based cancer immunotherapy: emerging efficacy and pathways of resistance. *Immunol. Rev.* 290 (1), 127–147. doi:10.1111/imr.12772

Chapuis, A. G., Egan, D. N., Bar, M., Schmitt, T. M., McAfee, M. S., Paulson, K. G., et al. (2019). T cell receptor gene therapy targeting WT1 prevents acute myeloid leukemia relapse post-transplant. *Nat. Med.* 25 (7), 1064–1072. doi:10.1038/s41591-019-0472-9

Chen, L., and Flies, D. B. (2013). Molecular mechanisms of T cell co-stimulation and co-inhibition. *Nat. Rev. Immunol.* 13 (4), 227–242. doi:10.1038/nri3405

Chen, X., Poncette, L., and Blankenstein, T. (2017). Human TCR-MHC coevolution after divergence from mice includes increased nontemplate-encoded CDR3 diversity. *J. Exp. Med.* 214 (11), 3417–3433. doi:10.1084/jem.20161784

Cheng, L., and Hill, A. F. (2022). Therapeutically harnessing extracellular vesicles. *Nat. Rev. Drug Discov.* 21 (5), 379–399. doi:10.1038/s41573-022-00410-w

Choi, B. D., Gerstner, E. R., Frigault, M. J., Leick, M. B., Mount, C. W., Balaj, L., et al. (2024). Intraventricular CARv3-TEAM-E T cells in recurrent glioblastoma. *N. Engl. J. Med.* 390 (14), 1290–1298. doi:10.1056/NEJMoa2314390

Cohen, C. J., Zhao, Y., Zheng, Z., Rosenberg, S. A., and Morgan, R. A. (2006). Enhanced antitumor activity of murine-human hybrid T-cell receptor (TCR) in human lymphocytes is associated with improved pairing and TCR/CD3 stability. *Cancer Res.* 66 (17), 8878–8886. doi:10.1158/0008-5472.CAN-06-1450

Conforti, L. (2017). Potassium channels of T lymphocytes take center stage in the fight against cancer. *J. Immunother. Cancer* 5, 2. doi:10.1186/s40425-016-0202-5

Corbière, V., Chapiro, J., Stroobant, V., Ma, W., Lurquin, C., Lethé, B., et al. (2011). Antigen spreading contributes to MAGE vaccination-induced regression of melanoma metastases. *Cancer Res.* 71 (4), 1253–1262. doi:10.1158/0008-5472.CAN-10-2693

Costa, R., Carneiro, B. A., Agulnik, M., Rademaker, A. W., Pai, S. G., Villaflor, V. M., et al. (2017). Toxicity profile of approved anti-PD-1 monoclonal antibodies in solid tumors: a systematic review and meta-analysis of randomized clinical trials. *Oncotarget* 8 (5), 8910–8920. doi:10.18632/oncotarget.13315

Courtney, A. H., Lo, W. L., and Weiss, A. (2018). TCR signaling: mechanisms of initiation and propagation. *Trends Biochem. Sci.* 43 (2), 108–123. doi:10.1016/j.tibs.2017.11.008

Dai, S., Jia, R., Zhang, X., Fang, Q., and Huang, L. (2014). The PD-1/PD-Ls pathway and autoimmune diseases. *Cell Immunol.* 290 (1), 72–79. doi:10.1016/j.cellimm.2014.05.006

D'Angelo, S. P., Melchiori, L., Merchant, M. S., Bernstein, D., Glod, J., Kaplan, R., et al. (2018). Antitumor activity associated with prolonged persistence of adoptively transferred NY-ESO-1 (c259)T cells in synovial sarcoma. *Cancer Discov.* 8 (8), 944–957. doi:10.1158/2159-8290.CD-17-1417

Dermani, F. K., Samadi, P., Rahmani, G., Kohlan, A. K., and Najafi, R. (2019). PD-1/PD-L1 immune checkpoint: potential target for cancer therapy. *J. Cell Physiol.* 234 (2), 1313–1325. doi:10.1002/jcp.27172

Ding, N., Zou, Z., Sha, H., Su, S., Qian, H., Meng, F., et al. (2019). iRGD synergizes with PD-1 knockout immunotherapy by enhancing lymphocyte infiltration in gastric cancer. *Nat. Commun.* 10 (1), 1336. doi:10.1038/s41467-019-09296-6

Dong, P., Xiong, Y., Yue, J., Hanley, S. J. B., and Watari, H. (2018). Tumor-intrinsic PD-L1 signaling in cancer initiation, development and treatment: beyond immune evasion. *Front. Oncol.* 8, 386. doi:10.3389/fonc.2018.00386

Dong, D., Zheng, L., Lin, J., Zhang, B., Zhu, Y., Li, N., et al. (2019). Structural basis of assembly of the human T cell receptor-CD3 complex. *Nature* 573 (7775), 546–552. doi:10.1038/s41586-019-1537-0

Drakes, D. J., Abbas, A. M., Shields, J., Steinbuck, M. P., Jakubowski, A., Seenappa, L. M., et al. (2024). Lymph node-targeted vaccine boosting of TCR T-cell therapy enhances antitumor function and eradicates solid tumors. *Cancer Immunol. Res.* 12 (2), 214–231. doi:10.1158/2326-6066.CIR-22-0978

Dutta, N., Gupta, A., Mazumder, D. N., and Banerjee, S. (2006). Down-regulation of locus-specific human lymphocyte antigen class I expression in Epstein-Barr virus-associated gastric cancer: implication for viral-induced immune evasion. *Cancer* 106 (8), 1685–1693. doi:10.1002/cncr.21784

Dyble, M., Salali, G. D., Chaudhary, N., Page, A., Smith, D., Thompson, J., et al. (2015). Human behavior. Sex equality can explain the unique social structure of hunter-gatherer bands. *Science* 348 (6236), 796–798. doi:10.1126/science.aaa5139

Eil, R., Vodnala, S. K., Clever, D., Klebanoff, C. A., Sukumar, M., Pan, J. H., et al. (2016). Ionic immune suppression within the tumour microenvironment limits T cell effector function. *Nature* 537 (7621), 539–543. doi:10.1038/nature19364

Elgueta, R., Benson, M. J., de Vries, V. C., Wasiuk, A., Guo, Y., and Noelle, R. J. (2009). Molecular mechanism and function of CD40/CD40L engagement in the immune system. *Immunol. Rev.* 229 (1), 152–172. doi:10.1111/j.1600-065X.2009.00782.x

Eyquem, J., Mansilla-Soto, J., Giavridis, T., van der Stegen, S. J., Hamieh, M., Cunanan, K. M., et al. (2017). Targeting a CAR to the TRAC locus with CRISPR/Cas9 enhances tumour rejection. *Nature* 543 (7643), 113–117. doi:10.1038/nature21405

Feinerman, O., Germain, R. N., and Altan-Bonnet, G. (2008). Quantitative challenges in understanding ligand discrimination by alphabeta T cells. *Mol. Immunol.* 45 (3), 619–631. doi:10.1016/j.molimm.2007.03.028

Fraietta, J. A., Lacey, S. F., Orlando, E. J., Pruteanu-Malinici, I., Gohil, M., Lundh, S., et al. (2018). Determinants of response and resistance to CD19 chimeric antigen receptor (CAR) T cell therapy of chronic lymphocytic leukemia. *Nat. Med.* 24 (5), 563–571. doi:10.1038/s41591-018-0010-1

Gaggero, S., Martinez-Fabregas, J., Cozzani, A., Fyfe, P. K., Leprohon, M., Yang, J., et al. (2022). IL-2 is inactivated by the acidic pH environment of tumors enabling engineering of a pH-selective mutein. *Sci. Immunol.* 7 (78), eade5686. doi:10.1126/sciimmunol.ade5686

Gao, Y., Lin, H., Guo, D., Cheng, S., Zhou, Y., Zhang, L., et al. (2021). Suppression of 4.1R enhances the potency of NKG2D-CAR T cells against pancreatic carcinoma via activating ERK signaling pathway. *Oncogenesis* 10 (9), 62. doi:10.1038/s41389-021-00353-8

Garber, K. (2018). Driving T-cell immunotherapy to solid tumors. *Nat. Biotechnol.* 36 (3), 215–219. doi:10.1038/nbt.4090

Georgiadis, C., Preece, R., Nickolay, L., Etuk, A., Petrova, A., Ladon, D., et al. (2018). Long terminal repeat CRISPR-CAR-coupled "universal" T cells mediate potent anti-leukemic effects. *Mol. Ther.* 26 (5), 1215–1227. doi:10.1016/j.ymthe.2018.02.025

Gonzalez-Galarza, F. F., McCabe, A., Santos, E., Jones, J., Takeshita, L., Ortega-Rivera, N. D., et al. (2020). Allele frequency net database (AFND) 2020 update: gold-standard data classification, open access genotype data and new query tools. *Nucleic Acids Res.* 48 (D1), D783-D788–d8. doi:10.1093/nar/gkz1029

Gordeeva, O. (2018). Cancer-testis antigens: unique cancer stem cell biomarkers and targets for cancer therapy. *Semin. Cancer Biol.* 53, 75–89. doi:10.1016/j.semcancer.2018.08.006

Gras, S., Chadderton, J., Del Campo, C. M., Farenc, C., Wiede, F., Josephs, T. M., et al. (2016). Reversed T cell receptor docking on a major histocompatibility class I complex limits involvement in the immune response. *Immunity* 45 (4), 749–760. doi:10.1016/j.immuni.2016.09.007

Hafezi, M., Lin, M., Chia, A., Chua, A., Ho, Z. Z., Fam, R., et al. (2021). Immunosuppressive drug-resistant armored T-cell receptor T cells for immune therapy of HCC in liver transplant patients. *Hepatology* 74 (1), 200–213. doi:10.1002/hep.31662

Haga-Friedman, A., Horovitz-Fried, M., and Cohen, C. J. (2012). Incorporation of transmembrane hydrophobic mutations in the TCR enhance its surface expression and T cell functional avidity. *J. Immunol.* 188 (11), 5538–5546. doi:10.4049/jimmunol.1103020

Hamilton, A. G., Swingle, K. L., Joseph, R. A., Mai, D., Gong, N., Billingsley, M. M., et al. (2023). Ionizable lipid nanoparticles with integrated immune checkpoint inhibition for mRNA CAR T cell engineering. *Adv. Healthc. Mater* 12 (30), e2301515. doi:10.1002/adhm.202301515

Hayday, A. C. (2019). Γδ T cell update: adaptate orchestrators of immune surveillance. *J. Immunol.* 203 (2), 311–320. doi:10.4049/jimmunol.1800934

Heemskerk, M. H., Hagedoorn, R. S., van der Hoorn, M. A., van der Veken, L. T., Hoogeboom, M., Kester, M. G., et al. (2007). Efficiency of T-cell receptor expression in dual-specific T cells is controlled by the intrinsic qualities of the TCR chains within the TCR-CD3 complex. *Blood* 109 (1), 235–243. doi:10.1182/blood-2006-03-013318

Heindl, A., Nawaz, S., and Yuan, Y. (2015). Mapping spatial heterogeneity in the tumor microenvironment: a new era for digital pathology. *Lab. Invest.* 95 (4), 377–384. doi:10.1038/labinvest.2014.155

Hellmann, M. D., and Snyder, A. (2017). Making it personal: neoantigen vaccines in metastatic melanoma. *Immunity* 47 (2), 221–223. doi:10.1016/j.immuni.2017.08.001

Hiasa, A., Nishikawa, H., Hirayama, M., Kitano, S., Okamoto, S., Chono, H., et al. (2009). Rapid alphabeta TCR-mediated responses in gammadelta T cells transduced with cancer-specific TCR genes. *Gene Ther.* 16 (5), 620–628. doi:10.1038/gt.2009.6

Hu, Y., Zhou, Y., Zhang, M., Ge, W., Li, Y., Yang, L., et al. (2021). CRISPR/Cas9-Engineered universal CD19/CD22 dual-targeted CAR-T cell therapy for relapsed/refractory B-cell acute lymphoblastic leukemia. *Clin. Cancer Res.* 27 (10), 2764–2772. doi:10.1158/1078-0432.CCR-20-3863

Hui, X., Farooq, M. A., Chen, Y., Ajmal, I., Ren, Y., Xue, M., et al. (2024). A novel strategy of co-expressing CXCR5 and IL-7 enhances CAR-T cell effectiveness in osteosarcoma. *Front. Immunol.* 15, 1462076. doi:10.3389/fimmu.2024.1462076

Huppa, J. B., and Davis, M. M. (2003). T-cell-antigen recognition and the immunological synapse. *Nat. Rev. Immunol.* 3 (12), 973–983. doi:10.1038/nri1245

Ishihara, M., Kitano, S., Kageyama, S., Miyahara, Y., Yamamoto, N., Kato, H., et al. (2022). NY-ESO-1-specific redirected T cells with endogenous TCR knockdown mediate tumor response and cytokine release syndrome. *J. Immunother. Cancer* 10 (6), e003811. doi:10.1136/jitc-2021-003811

Ishihara, M., Miwa, H., Fujiwara, H., Akahori, Y., Kato, T., Tanaka, Y., et al. (2023). αβ-T cell receptor transduction gives superior mitochondrial function to γδ-T cells with promising persistence. *iScience* 26 (10), 107802. doi:10.1016/j.isci.2023.107802

Ji, C., Roy, M. D., Golas, J., Vitsky, A., Ram, S., Kumpf, S. W., et al. (2019). Myocarditis in cynomolgus monkeys following treatment with immune checkpoint inhibitors. *Clin. Cancer Res.* 25 (15), 4735–4748. doi:10.1158/1078-0432.CCR-18-4083

Johnson, L. A., Morgan, R. A., Dudley, M. E., Cassard, L., Yang, J. C., Hughes, M. S., et al. (2009). Gene therapy with human and mouse T-cell receptors mediates cancer regression and targets normal tissues expressing cognate antigen. *Blood* 114 (3), 535–546. doi:10.1182/blood-2009-03-211714

Kageyama, S., Ikeda, H., Miyahara, Y., Imai, N., Ishihara, M., Saito, K., et al. (2015). Adoptive transfer of MAGE-A4 T-cell receptor gene-transduced lymphocytes in patients with recurrent esophageal cancer. *Clin. Cancer Res.* 21 (10), 2268–2277. doi:10.1158/1078-0432.CCR-14-1559

Kaufman, H. L., Kohlhapp, F. J., and Zloza, A. (2015). Oncolytic viruses: a new class of immunotherapy drugs. *Nat. Rev. Drug Discov.* 14 (9), 642–662. doi:10.1038/nrd4663

Khunger, A., Battel, L., Wadhawan, A., More, A., Kapoor, A., and Agrawal, N. (2020). New insights into mechanisms of immune checkpoint inhibitor-induced cardiovascular toxicity. *Curr. Oncol. Rep.* 22 (7), 65. doi:10.1007/s11912-020-00925-8

Kim, S. T., Tayar, J., Fu, S., Ke, D., Norry, E., Sun, A., et al. (2021). Newly developed pseudogout arthritis after therapy with MAGE-A4 directed TCR T cells responded to treatment with tocilizumab. *J. Immunother. Cancer* 9 (7), e002716. doi:10.1136/jitc-2021-002716

Knies, D., Klobuch, S., Xue, S. A., Birtel, M., Echchannaoui, H., Yildiz, O., et al. (2016). An optimized single chain TCR scaffold relying on the assembly with the native CD3-complex prevents residual mispairing with endogenous TCRs in human T-cells. *Oncotarget* 7 (16), 21199–21221. doi:10.18632/oncotarget.8385

Krshnan, L., Park, S., Im, W., Call, M. J., and Call, M. E. (2016). A conserved αβ transmembrane interface forms the core of a compact T-cell receptor-CD3 structure within the membrane. *Proc. Natl. Acad. Sci. U. S. A.* 113 (43), E6649-E6658–e58. doi:10.1073/pnas.1611445113

Kuball, J., Dossett, M. L., Wolfl, M., Ho, W. Y., Voss, R. H., Fowler, C., et al. (2007). Facilitating matched pairing and expression of TCR chains introduced into human T cells. *Blood* 109 (6), 2331–2338. doi:10.1182/blood-2006-05-023069

Kuhn, N. F., Purdon, T. J., van Leeuwen, D. G., Lopez, A. V., Curran, K. J., Daniyan, A. F., et al. (2019). CD40 ligand-modified chimeric antigen receptor T cells enhance antitumor function by eliciting an endogenous antitumor response. *Cancer Cell* 35 (3), 473–488. doi:10.1016/j.ccell.2019.02.006

Kunert, A., van Brakel, M., van Steenbergen-Langeveld, S., da Silva, M., Coulie, P. G., Lamers, C., et al. (2016). MAGE-C2-Specific TCRs combined with epigenetic drug-enhanced antigenicity yield robust and tumor-selective T cell responses. *J. Immunol.* 197 (6), 2541–2552. doi:10.4049/jimmunol.1502024

Lai, J., Mardiana, S., House, I. G., Sek, K., Henderson, M. A., Giuffrida, L., et al. (2020). Adoptive cellular therapy with T cells expressing the dendritic cell growth factor Flt3L drives epitope spreading and antitumor immunity. *Nat. Immunol.* 21 (8), 914–926. doi:10.1038/s41590-020-0676-7

Li, J., Xiao, Z., Wang, D., Jia, L., Nie, S., Zeng, X., et al. (2023a). The screening, identification, design and clinical application of tumor-specific neoantigens for TCR-T cells. *Mol. Cancer* 22 (1), 141. doi:10.1186/s12943-023-01844-5

Li, J., Li, J., Peng, Y., Du, Y., Yang, Z., and Qi, X. (2023b). Dendritic cell derived exosomes loaded neoantigens for personalized cancer immunotherapies. *J. Control Release* 353, 423–433. doi:10.1016/j.jconrel.2022.11.053

Linette, G. P., Stadtmauer, E. A., Maus, M. V., Rapoport, A. P., Levine, B. L., Emery, L., et al. (2013). Cardiovascular toxicity and titin cross-reactivity of affinity-enhanced T cells in myeloma and melanoma. *Blood* 122 (6), 863–871. doi:10.1182/blood-2013-03-490565

Linsley, P. S., and Ledbetter, J. A. (1993). The role of the CD28 receptor during T cell responses to antigen. *Annu. Rev. Immunol.* 11, 191–212. doi:10.1146/annurev.iy.11.040193.001203

Liu, Y., Di, S., Shi, B., Zhang, H., Wang, Y., Wu, X., et al. (2019). Armored inducible expression of IL-12 enhances antitumor activity of glypican-3-targeted chimeric antigen receptor-engineered T cells in hepatocellular carcinoma. *J. Immunol.* 203 (1), 198–207. doi:10.4049/jimmunol.1800033

Lu, Y., Sun, Q., Guan, Q., Zhang, Z., He, Q., He, J., et al. (2023). The XOR-IDH3α axis controls macrophage polarization in hepatocellular carcinoma. *J. Hepatol.* 79 (5), 1172–1184. doi:10.1016/j.jhep.2023.06.022

Ma, S., Ong, L.-T., Jiang, Z., Lee, W. C., Lee, P. L., Yusuf, M., et al. (2024). Targeting P4HA1 promotes CD8+ T cell progenitor expansion toward immune memory and systemic anti-tumor immunity. *Cancer Cell* 43, 213–231.e9. doi:10.1016/j.ccell.2024.12.001

Mateus-Tique, J., and Brown, B. (2023). Tumour antigen spreading mediated by vaccine-boosted CAR T cells. *Nat. Rev. Immunol.* 23 (1), 7. doi:10.1038/s41577-022-00811-3

Michalek, J., Kocak, I., Fait, V., Zaloudik, J., and Hajek, R. (2007). Detection and long-term *in vivo* monitoring of individual tumor-specific T cell clones in patients with metastatic melanoma. *J. Immunol.* 178 (11), 6789–6795. doi:10.4049/jimmunol.178.11.6789

Mo, Z., Du, P., Wang, G., and Wang, Y. (2017). The multi-purpose tool of tumor immunotherapy: gene-engineered T cells. *J. Cancer* 8 (9), 1690–1703. doi:10.7150/jca.18681

Moon, E. K., Ranganathan, R., Eruslanov, E., Kim, S., Newick, K., O'Brien, S., et al. (2016). Blockade of programmed death 1 augments the ability of human T cells engineered to target NY-ESO-1 to control tumor growth after adoptive transfer. *Clin. Cancer Res.* 22 (2), 436–447. doi:10.1158/1078-0432.CCR-15-1070

Muro, R., Takayanagi, H., and Nitta, T. (2019). T cell receptor signaling for γδT cell development. *Inflamm. Regen.* 39, 6. doi:10.1186/s41232-019-0095-z

Nag, S., Bhattacharya, B., Dutta, S., Mandal, D., Mukherjee, S., Anand, K., et al. (2023). Clinical theranostics trademark of exosome in glioblastoma metastasis. *ACS Biomater. Sci. Eng.* 9 (9), 5205–5221. doi:10.1021/acsbiomaterials.3c00212

Nguyen, R., Doubrovina, E., Mousset, C. M., Jin, B. Y., Okada, R., Zhang, X., et al. (2023). Cooperative armoring of CAR and TCR T-cells by T cell-restricted IL-15 and IL-21 universally enhances solid tumor efficacy. *Clin. Cancer Res.* 30, 1555–1566. doi:10.1158/1078-0432.ccr-23-1872

Noman, M. Z., Desantis, G., Janji, B., Hasmim, M., Karray, S., Dessen, P., et al. (2014). PD-L1 is a novel direct target of HIF-1α, and its blockade under hypoxia enhanced MDSC-mediated T cell activation. *J. Exp. Med.* 211 (5), 781–790. doi:10.1084/jem.20131916

Nowicki, T. S., Berent-Maoz, B., Cheung-Lau, G., Huang, R. R., Wang, X., Tsoi, J., et al. (2019). A pilot trial of the combination of transgenic NY-ESO-1-reactive adoptive cellular therapy with dendritic cell vaccination with or without ipilimumab. *Clin. Cancer Res.* 25 (7), 2096–2108. doi:10.1158/1078-0432.CCR-18-3496

Ochi, T., Fujiwara, H., Okamoto, S., An, J., Nagai, K., Shirakata, T., et al. (2011). Novel adoptive T-cell immunotherapy using a WT1-specific TCR vector encoding silencers for endogenous TCRs shows marked antileukemia reactivity and safety. *Blood* 118 (6), 1495–1503. doi:10.1182/blood-2011-02-337089

Oda, S. K., Daman, A. W., Garcia, N. M., Wagener, F., Schmitt, T. M., Tan, X., et al. (2017). A CD200R-CD28 fusion protein appropriates an inhibitory signal to enhance T-cell function and therapy of murine leukemia. *Blood* 130 (22), 2410–2419. doi:10.1182/blood-2017-04-777052

Okamoto, S., Mineno, J., Ikeda, H., Fujiwara, H., Yasukawa, M., Shiku, H., et al. (2009). Improved expression and reactivity of transduced tumor-specific TCRs in human lymphocytes by specific silencing of endogenous TCR. *Cancer Res.* 69 (23), 9003–9011. doi:10.1158/0008-5472.CAN-09-1450

Olguín-Contreras, L. F., Mendler, A. N., Popowicz, G., Hu, B., and Noessner, E. (2021). Double strike approach for tumor attack: engineering T cells using a cd40l:

CD28 chimeric Co-stimulatory switch protein for enhanced tumor targeting in adoptive cell therapy. *Front. Immunol.* 12, 750478. doi:10.3389/fimmu.2021.750478

Pang, Z., Lu, M. M., Zhang, Y., Gao, Y., Bai, J. J., Gu, J. Y., et al. (2023). Neoantigen-targeted TCR-engineered T cell immunotherapy: current advances and challenges. *Biomark. Res.* 11 (1), 104. doi:10.1186/s40364-023-00534-0

Park, J. H., Kang, I., and Lee, H. K. (2022). Γδ T cells in brain homeostasis and diseases. *Front. Immunol.* 13, 886397. doi:10.3389/fimmu.2022.886397

Parkhurst, M. R., Yang, J. C., Langan, R. C., Dudley, M. E., Nathan, D. A., Feldman, S. A., et al. (2011). T cells targeting carcinoembryonic antigen can mediate regression of metastatic colorectal cancer but induce severe transient colitis. *Mol. Ther.* 19 (3), 620–626. doi:10.1038/mt.2010.272

Parlar, A., Sayitoglu, E. C., Ozkazanc, D., Georgoudaki, A. M., Pamukcu, C., Aras, M., et al. (2019). Engineering antigen-specific NK cell lines against the melanoma-associated antigen tyrosinase via TCR gene transfer. *Eur. J. Immunol.* 49 (8), 1278–1290. doi:10.1002/eji.201948140

Pegram, H. J., Lee, J. C., Hayman, E. G., Imperato, G. H., Tedder, T. F., Sadelain, M., et al. (2012). Tumor-targeted T cells modified to secrete IL-12 eradicate systemic tumors without need for prior conditioning. *Blood* 119 (18), 4133–4141. doi:10.1182/blood-2011-12-400044

Policastro, L. L., Ibañez, I. L., Notcovich, C., Duran, H. A., and Podhajcer, O. L. (2013). The tumor microenvironment: characterization, redox considerations, and novel approaches for reactive oxygen species-targeted gene therapy. *Antioxid. Redox Signal* 19 (8), 854–895. doi:10.1089/ars.2011.4367

Rapoport, A. P., Stadtmauer, E. A., Binder-Scholl, G. K., Goloubeva, O., Vogl, D. T., Lacey, S. F., et al. (2015). NY-ESO-1-specific TCR-engineered T cells mediate sustained antigen-specific antitumor effects in myeloma. *Nat. Med.* 21 (8), 914–921. doi:10.1038/nm.3910

Rath, J. A., and Arber, C. (2020). Engineering strategies to enhance TCR-based adoptive T cell therapy. *Cells* 9 (6), 1485. doi:10.3390/cells9061485

Robbins, P. F., Morgan, R. A., Feldman, S. A., Yang, J. C., Sherry, R. M., Dudley, M. E., et al. (2011). Tumor regression in patients with metastatic synovial cell sarcoma and melanoma using genetically engineered lymphocytes reactive with NY-ESO-1. *J. Clin. Oncol.* 29 (7), 917–924. doi:10.1200/JCO.2010.32.2537

Robbins, P. F., Kassim, S. H., Tran, T. L., Crystal, J. S., Morgan, R. A., Feldman, S. A., et al. (2015). A pilot trial using lymphocytes genetically engineered with an NY-ESO-1-reactive T-cell receptor: long-term follow-up and correlates with response. *Clin. Cancer Res.* 21 (5), 1019–1027. doi:10.1158/1078-0432.CCR-14-2708

Roma-Rodrigues, C., Fernandes, A. R., and Baptista, P. V. (2014). Exosome in tumour microenvironment: overview of the crosstalk between normal and cancer cells. *Biomed. Res. Int.* 2014, 179486. doi:10.1155/2014/179486

Rudd, C. E., Taylor, A., and Schneider, H. (2009). CD28 and CTLA-4 coreceptor expression and signal transduction. *Immunol. Rev.* 229 (1), 12–26. doi:10.1111/j.1600-065X.2009.00770.x

Sacco, A., Desantis, V., Celay, J., Giustini, V., Rigali, F., Savino, F. D., et al. (2023). Targeting the immune microenvironment in Waldenström macroglobulinemia via halting the CD40/CD40-ligand axis. *Blood* 141 (21), 2615–2628. doi:10.1182/blood.2022019240

Sahin, U., Derhovanessian, E., Miller, M., Kloke, B. P., Simon, P., Löwer, M., et al. (2017). Personalized RNA mutanome vaccines mobilize poly-specific therapeutic immunity against cancer. *Nature* 547 (7662), 222–226. doi:10.1038/nature23003

Sailer, N., Fetzer, I., Salvermoser, M., Braun, M., Brechtefeld, D., Krendl, C., et al. (2022). T-cells expressing a highly potent PRAME-specific T-cell receptor in combination with a chimeric PD1-41BB Co-stimulatory receptor show a favorable preclinical safety profile and strong anti-tumor reactivity. *Cancers (Basel)* 14 (8), 1998. doi:10.3390/cancers14081998

Schendel, D. J. (2023). Evolution by innovation as a driving force to improve TCR-T therapies. *Front. Oncol.* 13, 1216829. doi:10.3389/fonc.2023.1216829

Schlenker, R., Olguín-Contreras, L. F., Leisegang, M., Schnappinger, J., Disovic, A., Rühland, S., et al. (2017). Chimeric PD-1:28 receptor upgrades low-avidity T cells and restores effector function of tumor-infiltrating lymphocytes for adoptive cell therapy. *Cancer Res.* 77 (13), 3577–3590. doi:10.1158/0008-5472.CAN-16-1922

Schumacher, T. N., and Schreiber, R. D. (2015). Neoantigens in cancer immunotherapy. *Science.* 348 (6230), 69–74. doi:10.1126/science.aaa4971

Shafer, P., Kelly, L. M., and Hoyos, V. (2022). Cancer therapy with TCR-engineered T cells: current strategies, challenges, and prospects. *Front. Immunol.* 13, 835762. doi:10.3389/fimmu.2022.835762

Sibener, L. V., Fernandes, R. A., Kolawole, E. M., Carbone, C. B., Liu, F., McAffee, D., et al. (2018). Isolation of a structural mechanism for uncoupling T cell receptor signaling from peptide-MHC binding. *Cell* 174 (3), 672–687. doi:10.1016/j.cell.2018.06.017

Silva, S., Almeida, A. J., and Vale, N. (2019). Combination of cell-penetrating peptides with nanoparticles for therapeutic application: a review. *Biomolecules* 9 (1), 22. doi:10.3390/biom9010022

Singh, S., and Banerjee, S. (2020). Downregulation of HLA-ABC expression through promoter hypermethylation and downmodulation of MIC-A/B surface expression in LMP2A-positive epithelial carcinoma cell lines. *Sci. Rep.* 10 (1), 5415. doi:10.1038/s41598-020-62081-0

Smith, S. N., Harris, D. T., and Kranz, D. M. (2015). T cell receptor engineering and analysis using the yeast display platform. *Methods Mol. Biol.* 1319, 95–141. doi:10.1007/978-1-4939-2748-7_6

Streby, K. A., Geller, J. I., Currier, M. A., Warren, P. S., Racadio, J. M., Towbin, A. J., et al. (2017). Intratumoral injection of HSV1716, an oncolytic herpes virus, is safe and shows evidence of immune response and viral replication in young cancer patients. *Clin. Cancer Res.* 23 (14), 3566–3574. doi:10.1158/1078-0432.CCR-16-2900

Sun, H., Shi, K., Qi, K., Kong, H., Zhang, J., Dai, S., et al. (2019). Natural killer cell-derived exosomal miR-3607-3p inhibits pancreatic cancer progression by targeting IL-26. *Front. Immunol.* 10, 2819. doi:10.3389/fimmu.2019.02819

Sun, H., Shi, K., Qi, K., Kong, H., Zhang, J., Dai, S., et al. (2020). Corrigendum: natural killer cell-derived exosomal miR-3607-3p inhibits pancreatic cancer progression by targeting IL-26. *Front. Immunol.* 11, 277. doi:10.3389/fimmu.2020.00277

Tran, E., Robbins, P. F., and Rosenberg, S. A. (2017). Final common pathway' of human cancer immunotherapy: targeting random somatic mutations. *Nat. Immunol.* 18 (3), 255–262. doi:10.1038/ni.3682

Ullah, A., Razzaq, A., Zhou, C., Ullah, N., Shehzadi, S., Aziz, T., et al. (2024a). Biological significance of EphB4 expression in cancer. *Curr. Protein Pept. Sci.* 25 (3), 244–255. doi:10.2174/0113892037269589231017055642

Ullah, A., Shehzadi, S., Ullah, N., Nawaz, T., Iqbal, H., and Aziz, T. (2024b). Hypoxia A typical target in human lung cancer therapy. *Curr. Protein Pept. Sci.* 25 (5), 376–385. doi:10.2174/0113892037252820231114045234

Ullah, A., Razzaq, A., Alfaifi, M. Y., Elbehairi, S. E. I., Menaa, F., Ullah, N., et al. (2024c). Sanguinarine attenuates lung cancer progression via oxidative stress-induced cell apoptosis. *Curr. Mol. Pharmacol.* 17, e18761429269383. doi:10.2174/0118761429269383231119062233

Valitutti, S. (2012). The serial engagement model 17 Years after: from TCR triggering to immunotherapy. *Front. Immunol.* 3, 272. doi:10.3389/fimmu.2012.00272

van Kooten, C., and Banchereau, J. (1997). Functions of CD40 on B cells, dendritic cells and other cells. *Curr. Opin. Immunol.* 9 (3), 330–337. doi:10.1016/s0952-7915(97)80078-7

van Loenen, M. M., de Boer, R., Amir, A. L., Hagedoorn, R. S., Volbeda, G. L., Willemze, R., et al. (2010). Mixed T cell receptor dimers harbor potentially harmful neoreactivity. *Proc. Natl. Acad. Sci. U. S. A.* 107 (24), 10972–10977. doi:10.1073/pnas.1005802107

Varricchi, G., Galdiero, M. R., Marone, G., Criscuolo, G., Triassi, M., Bonaduce, D., et al. (2017). Cardiotoxicity of immune checkpoint inhibitors. *ESMO Open* 2 (4), e000247. doi:10.1136/esmoopen-2017-000247

Vignali, P. D. A., DePeaux, K., Watson, M. J., Ye, C., Ford, B. R., Lontos, K., et al. (2023). Hypoxia drives CD39-dependent suppressor function in exhausted T cells to limit antitumor immunity. *Nat. Immunol.* 24 (2), 267–279. doi:10.1038/s41590-022-01379-9

Vinay, D. S., and Kwon, B. S. (2014). 4-1BB (CD137), an inducible costimulatory receptor, as a specific target for cancer therapy. *BMB Rep.* 47 (3), 122–129. doi:10.5483/bmbrep.2014.47.3.283

Vormehr, M., Diken, M., Boegel, S., Kreiter, S., Türeci, Ö., and Sahin, U. (2016). Mutanome directed cancer immunotherapy. *Curr. Opin. Immunol.* 39, 14–22. doi:10.1016/j.coi.2015.12.001

Wachsmann, T. L. A., Wouters, A. K., Remst, D. F. G., Hagedoorn, R. S., Meeuwsen, M. H., van Diest, E., et al. (2022). Comparing CAR and TCR engineered T cell performance as a function of tumor cell exposure. *Oncoimmunology* 11 (1), 2033528. doi:10.1080/2162402X.2022.2033528

Wang, Z., and Cao, Y. J. (2020). Adoptive cell therapy targeting neoantigens: a frontier for cancer research. *Front. Immunol.* 11, 176. doi:10.3389/fimmu.2020.00176

Wang, J., Zheng, Y., and Zhao, M. (2016). Exosome-based cancer therapy: implication for targeting cancer stem cells. *Front. Pharmacol.* 7, 533. doi:10.3389/fphar.2016.00533

Wang, S., Rong, R., Yang, D. M., Fujimoto, J., Yan, S., Cai, L., et al. (2020a). Computational staining of pathology images to study the tumor microenvironment in lung cancer. *Cancer Res.* 80 (10), 2056–2066. doi:10.1158/0008-5472.CAN-19-1629

Wang, X., Xiang, Z., Liu, Y., Huang, C., Pei, Y., Wang, X., et al. (2020b). Exosomes derived from Vδ2-T cells control Epstein-Barr virus-associated tumors and induce T cell antitumor immunity. *Sci. Transl. Med.* 12 (563), eaaz3426. doi:10.1126/scitranslmed.aaz3426

Wang, H., Wang, L., Li, Y., Li, G., Zhang, X., Jiang, D., et al. (2021). Nanobody-armed T cells endow CAR-T cells with cytotoxicity against lymphoma cells. *Cancer Cell Int.* 21 (1), 450. doi:10.1186/s12935-021-02151-z

Wang, C. Q., Lim, P. Y., and Tan, A. H. (2023). Gamma/delta T cells as cellular vehicles for anti-tumor immunity. *Front. Immunol.* 14, 1282758. doi:10.3389/fimmu.2023.1282758

Wu, P., Zhang, T., Liu, B., Fei, P., Cui, L., Qin, R., et al. (2019). Mechano-regulation of peptide-MHC class I conformations determines TCR antigen recognition. *Mol. Cell* 73 (5), 1015–1027. doi:10.1016/j.molcel.2018.12.018

Wu, J. Y., Xu, B., Zhu, X. J., Ming, X., Luo, H., Mao, X., et al. (2023). PD-1 inhibitor in chronic active Epstein-Barr virus infection: a report of six cases and literature review. *Zhonghua Xue Ye Xue Za Zhi* 44 (2), 165–168. doi:10.3760/cma.j.issn.0253-2727.2023.02.016

Xie, N., Shen, G., Gao, W., Huang, Z., Huang, C., and Fu, L. (2023). Neoantigens: promising targets for cancer therapy. *Signal Transduct. Target Ther.* 8 (1), 9. doi:10.1038/s41392-022-01270-x

Xu, Z., Zeng, S., Gong, Z., and Yan, Y. (2020). Exosome-based immunotherapy: a promising approach for cancer treatment. *Mol. Cancer* 19 (1), 160. doi:10.1186/s12943-020-01278-3

Xu, R., Du, S., Zhu, J., Meng, F., and Liu, B. (2022). Neoantigen-targeted TCR-T cell therapy for solid tumors: how far from clinical application. *Cancer Lett.* 546, 215840. doi:10.1016/j.canlet.2022.215840

Xu, R., Wang, Q., Zhu, J., Bei, Y., Chu, Y., Sun, Z., et al. (2023). Membrane fusogenic nanoparticle-based HLA-peptide-addressing universal T cell receptor-engineered T (HAUL TCR-T) cell therapy in solid tumor. *Bioeng. Transl. Med.* 8 (6), e10585. doi:10.1002/btm2.10585

Ye, J., Liu, E., Yu, Z., Pei, X., Chen, S., Zhang, P., et al. (2016). CPP-assisted intracellular drug delivery, what is next? *Int. J. Mol. Sci.* 17 (11), 1892. doi:10.3390/ijms17111892

Zareie, P., Szeto, C., Farenc, C., Gunasinghe, S. D., Kolawole, E. M., Nguyen, A., et al. (2021). Canonical T cell receptor docking on peptide-MHC is essential for T cell signaling. *Science* 372 (6546), eabe9124. doi:10.1126/science.abe9124

Zhang, J., and Wang, L. (2019). The emerging world of TCR-T cell trials against cancer: a systematic review. *Technol. Cancer Res. Treat.* 18, 1533033819831068. doi:10.1177/1533033819831068

Zhang, Y., Yang, S., Jiang, D., Li, Y., Ma, S., Wang, L., et al. (2022). Screening and identification of an anti-PD-1 nanobody with antitumor activity. *Biosci. Rep.* 43 (1). doi:10.1042/BSR20221546

Zhao, L., and Cao, Y. J. (2019). Engineered T cell therapy for cancer in the clinic. *Front. Immunol.* 10, 2250. doi:10.3389/fimmu.2019.02250

Zheng, N., Fang, J., Xue, G., Wang, Z., Li, X., Zhou, M., et al. (2022). Induction of tumor cell autosis by myxoma virus-infected CAR-T and TCR-T cells to overcome primary and acquired resistance. *Cancer Cell* 40 (9), 973–985.e7. doi:10.1016/j.ccell.2022.08.001

Zhou, S., Meng, F., Du, S., Qian, H., Ding, N., Sha, H., et al. (2021). Bifunctional iRGD-anti-CD3 enhances antitumor potency of T cells by facilitating tumor infiltration and T-cell activation. *J. Immunother. Cancer* 9 (5), e001925. doi:10.1136/jitc-2020-001925

Zhu, C., Wu, Q., Sheng, T., Shi, J., Shen, X., Yu, J., et al. (2024). Rationally designed approaches to augment CAR-T therapy for solid tumor treatment. *Bioact. Mater* 33, 377–395. doi:10.1016/j.bioactmat.2023.11.002

frontiers | Frontiers in Pharmacology

TYPE Original Research
PUBLISHED 24 March 2025
DOI 10.3389/fphar.2025.1535444

OPEN ACCESS

EDITED BY
Ana Podolski-Renic,
Institute for Biological Research "Siniša Stanković" – National Institute of Republic of Serbia, Serbia

REVIEWED BY
Tongyi Huang,
The First Affiliated Hospital of Sun Yat-sen University, China
Chenguang Su,
Second Hospital of Hebei Medical University, China

*CORRESPONDENCE
Fei Zhou,
dr_zhoufei@163.com

RECEIVED 27 November 2024
ACCEPTED 04 March 2025
PUBLISHED 24 March 2025

CITATION
Tang P and Zhou F (2025) Efficacy and safety of PD-1/PD-L1 inhibitors combined with tyrosine kinase inhibitors as first-line treatment for hepatocellular carcinoma: a meta-analysis and trial sequential analysis of randomized controlled trials .
Front. Pharmacol. 16:1535444.
doi: 10.3389/fphar.2025.1535444

Efficacy and safety of PD-1/PD-L1 inhibitors combined with tyrosine kinase inhibitors as first-line treatment for hepatocellular carcinoma: a meta-analysis and trial sequential analysis of randomized controlled trials

Peng Tang[1] and Fei Zhou[2]*

[1]Department of Gastroenterology, Sichuan Provincial People's Hospital, University of Electronic Science and Technology of China, Chengdu, China, [2]Department of Obstetrics and Gynaecology, Sichuan Provincial People's Hospital, University of Electronic Science and Technology of China, Chengdu, China

Background: The use of immune checkpoint inhibitors (ICIs) in treating hepatocellular carcinoma (HCC) has grown significantly. However, the therapeutic benefits of ICIs alone are notably modest. This meta-analysis assesses the efficacy and safety of using PD-1/PD-L1 inhibitors in conjunction with tyrosine kinase inhibitors (TKIs) for patients with advanced or unresectable HCC.

Methods: An extensive search of the literature was performed using databases such as PubMed, Web of Science, Embase, and the Cochrane Library, capturing randomized controlled trials (RCTs) until 16 October 2024. Efficacy was measured by progression-free survival (PFS), overall survival (OS), objective response rate (ORR), and disease control rate (DCR). Safety was gauged through the occurrence of treatment-related adverse events (TRAEs). Hazard ratios (HRs) for PFS and OS, along with risk ratios (RRs) for ORR, DCR, and TRAEs, were calculated, each with 95% confidence intervals (CIs). Heterogeneity among studies was quantified using Cochran's Q test, I^2 statistics, and 95% prediction intervals (PIs).

Results: This analysis incorporated 4 studies with a total of 2,174 patients. Treatment regimens combining PD-1/PD-L1 inhibitors with TKIs significantly improved PFS (HR = 0.694, 95% CI: 0.527–0.914; 95% PI: 0.228–2.114) and ORR (RR = 2.303, 95% CI: 1.360–3.902; 95% PI: 0.408–12.991) compared with first-line monotherapy or TKI monotherapy in the overall population. Subgroup analysis indicated that the improvements in PFS and OS were particularly significant among patients of Asian descent or those with hepatitis B virus (HBV) infection (all $p < 0.05$). While the occurrence of any grade TRAEs did not differ significantly between the two groups (RR = 1.016, 95% CI: 0.996–1.036; 95% PI: 0.941–1.097), the incidence of serious (RR = 2.068, 95% CI: 1.328–3.222;

95% PI: 0.487–8.776) and grade ≥3 TRAEs (RR = 1.287, 95% CI: 1.020–1.624; 95% PI: 0.574–2.883) increased in patients treated with the combination of PD-1/PD-L1 inhibitors and TKIs.

Conclusion: This study revealed that combining PD-1/PD-L1 inhibitors with TKIs in the treatment of advanced or unresectable HCC leads to superior clinical outcomes compared to first-line monotherapy or TKIs alone, particularly in patients with HBV infection and those of Asian descent. Clinicians are advised to be vigilant regarding the potential for TRAEs in clinical settings.

KEYWORDS

PD-1 inhibitor, PD-L1 inhibitor, tyrosine kinase inhibitor, combination therapy, hepatocellular carcinoma

1 Introduction

Globally, primary liver cancer poses a significant public health challenge, being the sixth most common and the third deadliest cancer type (Sung et al., 2021). Hepatocellular carcinoma (HCC) accounts for approximately 75%–85% of all primary liver cancer instances (Singal et al., 2020), with a substantial 72% of these cases diagnosed in Asia, where hepatitis B virus (HBV) infection is the predominant risk factor (Singal et al., 2020). Individuals diagnosed with HCC typically present at advanced stages; nevertheless, the introduction of targeted and immune therapies has extended their life expectancy (Llovet et al., 2021; Villanueva, 2019). The first-line systemic treatments for advanced HCC include monotherapy with the oral multitargeted tyrosine kinase inhibitors (TKIs) sorafenib and lenvatinib (Kudo et al., 2018; Llovet et al., 2008). Nonetheless, these targeted therapies have only yielded modest improvements in survival (Choi et al., 2022; De Matteis et al., 2021; Zhang et al., 2021). Moreover, it has been observed that sorafenib is less effective in patients with HBV-associated HCC compared to those without such infections (Choi et al., 2022; De Matteis et al., 2021).

In the last 5 years, immune checkpoint inhibitors (ICIs) that target the PD-1/PD-L1 pathway have been introduced as novel therapeutic options for advanced HCC (Finn et al., 2020c; Qin et al., 2020; Yau et al., 2022; Zhu et al., 2018). However, the response to ICI monotherapy remains limited to a small fraction of HCC patients (Finn et al., 2020c; Qin et al., 2020; Yau et al., 2022; Zhu et al., 2018), and it has not demonstrated a survival advantage over sorafenib in the first-line treatment context. Consequently, the integration of TKIs with PD-1 and PD-L1 ICIs has been pursued to enhance therapeutic outcomes. In the phase 1 b 116-KEYNOTE-524 study, the combination of lenvatinib and the PD-1 ICI pembrolizumab exhibited promising antitumor effects, achieving an objective response rate (ORR) of 36.0% and a median response duration of 12.6 months in patients with unresectable HCC. Additionally, these patients saw a median overall survival (OS) of 22.0 months and a median progression-free survival (PFS) of 8.6 months, alongside a manageable safety profile (Finn et al., 2020a). The phase three COSMIC-312 trial assessed the efficacy of the PD-L1 inhibitor atezolizumab combined with the multikinase inhibitor cabozantinib versus sorafenib in previously untreated patients with advanced HCC. The results indicated no significant improvement in OS for the combination therapy compared to sorafenib alone (Kelley et al., 2022). In another phase three trial, CARES-310, the efficacy of the PD-1 inhibitor camrelizumab combined with the TKI rivoceranib was evaluated as a first-line treatment. This combination significantly improved both median OS and median PFS, recording values of 22.1 months and 5.6 months, respectively, with an ORR of 25.4%, surpassing the performance of the sorafenib control group (Qin et al., 2023).

In recent times, the approach to systemic treatment of HCC has transitioned from multikinase inhibitors to regimens centered on immunotherapy that employ combination strategies (Abou-Alfa et al., 2022; Finn et al., 2020b; Finn et al., 2020c; Yau et al., 2020). Yet, when comparing the combination therapy of PD-1/PD-L1 inhibitors and TKIs with first-line monotherapy or TKI monotherapy, the outcomes have been inconsistent. In addition, previous systematic reviews and meta-analyses have primarily focused on the efficacy and safety of PD-1/PD-L1 inhibitors combined with anti-angiogenic agents for the treatment of HCC (Cao et al., 2024; Huang et al., 2023; Zhu et al., 2024). Although the pooled analysis has reported the benefits of PD-1/PD-L1 inhibitors combined with TKIs in improving OS, ORR, and disease control rate (DCR) (Liu et al., 2023), the supporting evidence is predominantly derived from prospective cohort studies, with a notable lack of evidence from randomized controlled trials (RCTs). Therefore, we undertook a meta-analysis of RCTs to comprehensively evaluate the efficacy and safety of integrating PD-1/PD-L1 inhibitors with TKIs in treating advanced or unresectable HCC. Additionally, we also examined whether specific subgroups demonstrated superior PFS and OS, aiming to identify populations that derive greater benefit from this therapeutic approach.

2 Materials and methods

2.1 Study design

Following the PRISMA guidelines, pertinent studies were screened and analyzed systematically (Page et al., 2021). Additionally, this research has been registered at the International Prospective Register of Systematic Reviews (PROSPERO) with the registration number CRD42024605243.

2.2 Literature retrieval

We conducted a thorough search for RCTs in several databases, including PubMed, Web of Science, Embase, and Cochrane Library,

covering all publications up to 16 October 2024. The search strategy focused on two main categories: therapy-related terms such as "PD-1 inhibitors", "PD-L1 inhibitors", "immune checkpoint inhibitors", "tyrosine kinase inhibitors", "TKIs", "pembrolizumab", "atezolizumab", "camrelizumab", "nivolumab", "sorafenib", "lenvatinib", and "cabozantinib"; and disease-specific terms including "hepatocellular carcinoma", "liver cancer", "liver neoplasms", "hepatocarcinoma", "HCC", and "liver cell carcinoma". No language constraints were imposed on the search. A comprehensive search strategy for each database is detailed in Supplementary Files S1. Further, we examined the references of all pertinent articles to find additional relevant studies.

2.3 Inclusion and exclusion criteria

Eligibility for inclusion in the study was determined by the following criteria: (1) RCTs; (2) Participants suffering from advanced or unresectable HCC; (3) Intervention involving a combination of PD-1/PD-L1 inhibitors and TKIs; (4) Control group treated with first-line monotherapies such as sorafenib or lenvatinib, or other TKIs administered alone or in conjunction with a placebo; (5) Reporting of outcomes including PFS, OS, ORR, DCR, any grade treatment-related adverse events (TRAEs), grade ≥3 TRAEs, or serious TRAEs. Studies were excluded if they were: (1) single-arm, non-randomized, or observational; (2) utilized monotherapy or combinations not involving PD-1/PD-L1 inhibitors with TKIs; (3) characterized by insufficient or duplicate data; (4) case reports, conference abstracts, systematic reviews, animal studies, or correspondences.

2.4 Data extraction and quality assessment

Two independent professionals extracted the data, gathering details such as the first author's name, year of publication, name of the trial, phase of the study, geographical area, patient population, number of participants, ages of participants, treatment protocols for the experimental and control groups, and the duration of follow-up. The primary endpoints analyzed in the meta-analysis were PFS and OS, with secondary outcomes including ORR, DCR, any grade TRAEs, grade ≥3 TRAEs, and serious TRAEs. In cases where direct data on PFS or OS were unavailable, we used Engauge Digitizer Version 10.8 and the approach by Tierney et al. (2007) to derive these metrics from Kaplan-Meier curves (Xie et al., 2022). Quality assessment of the RCTs was independently performed by two investigators using the modified Jadad scale (Jadad et al., 1996), which evaluates RCTs on five parameters and assigns a score ranging from 0 to 7 based on aspects of randomization, allocation concealment, blinding, and the rate of dropouts/withdrawals. Trials scoring between 0 and 3 were categorized as low quality, whereas scores of 4 or above indicated high quality.

2.5 Statistical analysis

Statistical analyses were conducted using R software 4.3.2 and STATA Version 12.0. We calculated pooled hazard ratios (HRs) and 95% confidence intervals (CIs) for PFS and OS, in addition to pooled risk ratios RRs and 95% CIs for ORR, DCR, any grade TRAEs, grade ≥3 TRAEs, and serious TRAEs. We assessed heterogeneity using the I^2 statistic, Cochran's Q test, and 95% prediction intervals (PIs) (Bowden et al., 2011; IntHout et al., 2016). In the presence of significant heterogeneity ($p < 0.1$ and $I^2 > 50\%$), analysis proceeded under a random-effects model; otherwise, a fixed-effects model was applied (Higgins and Thompson, 2002). Subgroup analyses were performed, focusing on the stratified results for PFS and OS from the included RCTs. Sensitivity analyses were performed by sequentially excluding individual studies to assess the impact on the pooled HRs or RRs. To detect publication bias, Begg's and Egger's tests were utilized, indicating no significant bias with p-values over 0.05 (Begg and Mazumdar, 1994; Egger et al., 1997). Statistical significance was established at a two-sided p-value of less than 0.05.

2.6 Trial sequential analysis

In this meta-analysis, trial sequential analysis (TSA) was implemented to reduce the likelihood of type I and type II errors (Wetterslev et al., 2017). We conducted TSA on the PFS and OS data using STATA Version 12.0 and R software 4.3.2, employing the *a priori* information size (APIS) methodology. For binary outcomes, TSA was executed using TSA software v0.9.5.10 Beta to ascertain the required information size (RIS). When the cumulative Z-curve crossed the RIS (or APIS) boundary or the trial sequential monitoring boundary, it indicated that sufficient evidence to conclude the analysis without the need for further studies. The determination of the RIS and APIS utilized settings including a two-sided α of 0.05, a power (1-β) of 0.80, and a 15% reduction in RR.

3 Results

3.1 Study selection

Figure 1 outlines the process of literature selection used in our study. An initial search across four databases identified 6,774 potentially relevant studies. We eliminated 2,887 duplicates, then assessed the titles and abstracts of the remaining 3,887 studies. A vast majority, 3,855, were excluded for failing to meet the relevance criteria, which left 32 articles for detailed full-text evaluation to assess their suitability for inclusion. Of these, 28 studies were further excluded for various reasons: 5 were disqualified due to their single-arm trial design; 11 did not report the necessary outcome data; and 12 were rejected because their intervention group treatment regimens did not satisfy the inclusion standards. Ultimately, 4 studies qualified for inclusion in the meta-analysis (Kelley et al., 2022; Llovet et al., 2023; Qin et al., 2023; Yau et al., 2024a).

3.2 Characteristics and quality assessment of selected studies

Table 1 summarizes the general information, baseline patient characteristics, and therapeutic protocols. This meta-analysis

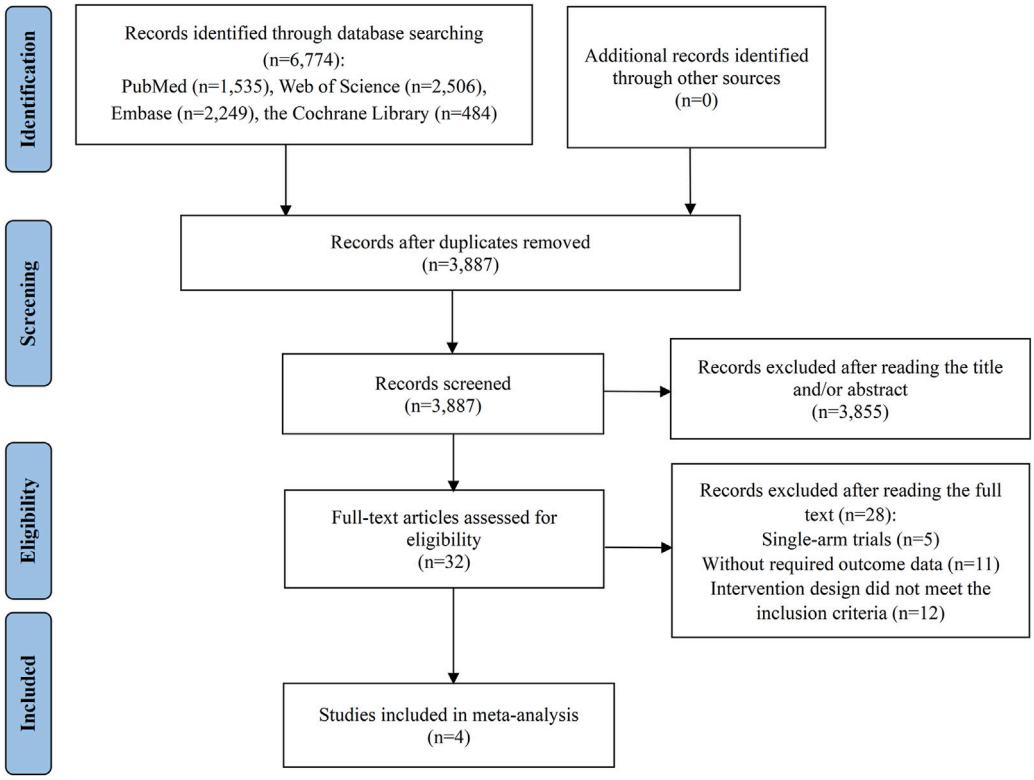

FIGURE 1
Flow diagram of the process of study selection.

covered 4 studies, including 3 Phase 3 RCTs. Notably, the COSMIC-312 trial featured two distinct control arms: one receiving sorafenib and the other cabozantinib. Yau et al. (2024b) and Kelley et al. (2022) provided differing outcomes from the COSMIC-312 trial at various follow-up intervals. We focused on extracting data from the longer follow-up periods. Additionally, outcome data not reported by Yau et al. were supplemented by findings from Kelley et al. In total, 1,099 patients with HCC were treated with a combination of PD-1/PD-L1 inhibitors and TKIs, compared to 1,075 patients who received only TKIs or TKIs plus placebo. The administered PD-1/PD-L1 inhibitors were camrelizumab, pembrolizumab, and atezolizumab, while the TKIs included sorafenib, rivoceranib, lenvatinib, and cabozantinib. These 4 studies were considered high-quality due to their stringent design (with scores ranging from 5 to 7 on the modified Jadad scale) and publication in high-impact journals. A methodological limitation noted was the lack of double-blinding in the trial design (Supplementary Files S2).

3.3 Survival outcomes

Each of the 4 studies assessed PFS outcome in HCC patients. Results indicated that those treated with PD-1/PD-L1 inhibitors in conjunction with TKIs showed a significantly better PFS rate than the controls (HR = 0.694, 95% CI: 0.527–0.914; 95% PI: 0.228–2.114, I^2 = 80.4%) (Table 2; Figure 2A). Subgroup analysis revealed that combining PD-1/PD-L1 inhibitors with TKIs significantly improved PFS in HCC patients over those receiving first-line sorafenib (HR = 0.624, 95% CI: 0.459–0.849; 95% PI: 0.029–13.563, I^2 = 68.6%) or TKIs with placebo (HR = 0.830, 95% CI: 0.707–0.975) (Table 2; Supplementary Figure S1). Additionally, we obtained stratified analysis outcomes for PFS from the included studies based on factors including age, sex, region, race, Eastern Cooperative Oncology Group (ECOG) performance status, Barcelona Clinic Liver Cancer (BCLC) stage, baseline alpha-fetoprotein, disease aetiology, macrovascular invasion. These stratified findings were consolidated to form detailed subgroup analyses of PFS, as outlined in Table 2 and Supplementary Figures S2-S10. Significantly, the therapeutic regimen combining PD-1/PD-L1 inhibitors with TKIs was particularly effective in enhancing PFS among male patients, those from Asian regions, of Asian ethnicity, with an ECOG performance status of 0, diagnosed with BCLC stage C, and those whose disease etiology was related to hepatitis B or C virus, as well as those presenting with macrovascular invasion (all $p < 0.05$). In contrast, among females, individuals from regions other than Asia, Caucasians, patients with an ECOG performance status of 1, BCLC stage B, non-viral disease etiology, and without macrovascular invasion, the improvement in PFS was not significant when compared to controls (all $p > 0.05$).

4 studies investigated the effects of combining PD-1/PD-L1 inhibitors with TKIs on OS in HCC patients. The combined data indicated that the addition of PD-1/PD-L1 inhibitors to

TABLE 1 Summary of the characteristics of included RCTs.

First author (Year)	Trial name	Study phase	Region	Patient population	Sample size (M/F)	Age (I/C, median [IQR], year)	Experimental arm	Control arm	Follow-up duration (month, median [IQR])
Qin et al. (2023)	CARES-310	Phase 3	95 study centres across 13 countries and regions	Patients (aged 18 years or older) with histopathologically or cytologically confirmed HCC; BCLC stage B or C; Not amenable to or had progressed after surgical or locoregional therapy; ECOG PS of 0 or 1	I: 227/45; C: 230/41	58 (48–66)/56 (47–64)	Camrelizumab 200 mg intravenously every 2 weeks + Rivoceranib 250 mg orally once daily (28-day cycles)	Sorafenib 400 mg orally twice daily (28-day cycles)	14.5 (9.1–18.7)
Llovet et al. (2023)	LEAP-002	Phase 3	172 global sites	Patients (aged 18 years or older) had histologically, cytologically, or radiographically confirmed HCC; ECOG PS of 0 or 1	I: 317/78; C: 327/72	66.0 (57.0–72.0)/ 66.0 (57.0–73.0)	Pembrolizumab 200 mg intravenously once every 3 weeks + Lenvatinib 8 mg (or 12 mg) orally once daily (up to 35 cycles)	Placebo 200 mg intravenously once every 3 weeks + Lenvatinib 8 mg (or 12 mg) orally once daily (up to 35 cycles)	32.1 (29.4–35.3)
Yau et al. (2024a)	COSMIC-312	Phase 3	178 centres in 32 countries	Patients (aged 18 years or older) had a pathological diagnosis of HCC or a radiological diagnosis of HCC in patients with cirrhosis; BCLC stage B or C; ECOG PS of 0 or 1	I: 360/72; C: 186/ 31(Sorafenib); 158/30 (Cabozantinib)	64 (58–70)/64 (57–71) (Sorafenib); 64 (58–71) (Cabozantinib)	Atezolizumab 1,200 mg intravenously every 3 weeks + Cabozantinib tablets 40 mg orally once daily	Sorafenib 400 mg orally twice daily Cabozantinib tablets 60 mg orally once daily	22.1 (19.3–24.8)
Kelley et al. (2022)	COSMIC-312	Phase 3	178 centres in 32 countries	Patients (aged 18 years or older) had a pathological diagnosis of HCC or a radiological diagnosis of HCC in patients with cirrhosis; BCLC stage B or C; ECOG PS of 0 or 1	I: 360/72; C: 186/ 31(Sorafenib); 158/30 (Cabozantinib)	64 (58–70)/64 (57–71) (Sorafenib); 64 (58–71) (Cabozantinib)	Atezolizumab 1,200 mg intravenously every 3 weeks + Cabozantinib tablets 40 mg orally once daily	Sorafenib 400 mg orally twice daily Cabozantinib tablets 60 mg orally once daily	13.3 (10.5–16.0)

M, male; F, female; I, intervention group; C, control group; IQR, interquartile range; HCC, hepatocellular carcinoma; BCLC, barcelona clinic liver cancer; ECOG, eastern cooperative oncology group; PS, performance status.

TKI regimens did not significantly enhance OS relative to the control group (HR = 0.804, 95% CI: 0.634–1.019; 95% PI: 0.318–2.032, I^2 = 72.7%) (Table 2; Figure 2B). Subgroup analyses were performed according to the specific TKIs used in the control groups. These analyses demonstrated that the co-administration of PD-1/PD-L1 inhibitors with TKIs did not yield an OS benefit over the use of sorafenib alone (HR = 0.781, 95% CI: 0.499–1.223; 95% PI: 0.007–94.385, I^2 = 85.9%). However, a notable improvement in OS was observed with the combination of PD-1/PD-L1 inhibitors and TKIs compared to TKIs plus placebo, though this result was based on a single study (HR = 0.840, 95% CI: 0.708–0.997) (Table 2; Supplementary Figure S11). Detailed results of the OS subgroup analysis, stratified by the data from the included studies, are provided in Table 2 and Supplementary Figures S12-S22.

3.4 Tumor responses

Figure 3 illustrates tumor responses, including ORR and DCR, as forest plots. These metrics were each evaluated in 4 studies. The comprehensive assessment revealed that the ORR for the combination of PD-1/PD-L1 inhibitors with TKIs in treating HCC was significantly superior to that observed in the

TABLE 2 Pooled effect and subgroup analysis of the primary outcomes of PD-1/PD-L1 inhibitors combined with tyrosine kinase inhibitors as first-line treatment for hepatocellular carcinoma.

Outcomes and subgroups	Number of studies	Meta-analysis				Heterogeneity	
		HR	95% CI	*p* value	95% PI	I^2, tau^2	*p* value
PFS							
Overall	3	0.694	0.527–0.914	0.009	0.228–2.114	80.4%, 0.0472	0.006
Subgrouped by control groups							
PD-1/PD-L1 inhibitors + TKIs vs Sorafenib alone	2	0.624	0.459–0.849	0.003	0.029–13.563	68.6%, 0.0341	0.074
PD-1/PD-L1 inhibitors + TKIs vs TKIs + Placebo	1	0.830	0.707–0.975	0.023			
Age							
<65 years	2	0.696	0.527–0.918	0.010	0.050–9.594	56.4%, 0.0227	0.130
≥65 years	3	0.651	0.508–0.834	0.001	0.237–1.816	36.4%, 0.0294	0.208
Sex							
Male	2	0.634	0.543–0.741	<0.001	0.090–4.471	47.8%, 0.0115	0.166
Female	2	0.817	0.400–1.666	0.577	0.001–1,058.553	70.2%, 0.1858	0.067
Region							
Asia	2	0.562	0.466–0.679	<0.001	0.166–1.907	0%, 0	0.808
Other	2	0.750	0.483–1.162	0.198	0.010–54.510	59.4%, 0.0637	0.117
Race							
Asian	2	0.567	0.469–0.687	<0.001	0.165–1.957	0%, 0	0.936
White	2	0.763	0.489–1.189	0.232	0.011–53.509	55.3%, 0.0605	0.135
ECOG performance status							
0	2	0.697	0.573–0.847	<0.001	0.197–2.467	0%, 0	0.472
1	2	0.663	0.418–1.052	0.081	0.006–79.414	77.3%, 0.0863	0.036
BCLC stage							
Stage B	2	0.934	0.687–1.270	0.663	0.127–6.862	0%, 0	0.323
Stage C	2	0.590	0.501–0.694	<0.001	0.118–2.969	30.4%, 0.0061	0.231
Baseline alpha-fetoprotein (ng/mL)							
<400	2	0.749	0.625–0.897	0.002	0.080–7.022	46.9%, 0.0150	0.170
≥400	2	0.464	0.362–0.594	<0.001	0.042–5.114	29.2%, 0.0132	0.235
Disease aetiology							
Hepatitis B virus	2	0.554	0.456–0.674	<0.001	0.156–1.970	0%, 0	0.672
Hepatitis C virus	2	0.709	0.503–0.998	0.049	0.015–31.177	26.2%, 0.0365	0.245
Non-viral	2	0.764	0.431–1.353	0.356	0.002–252.109	71.3%, 0.1231	0.062
Macrovascular invasion							
Yes	2	0.536	0.400–0.718	<0.001	0.081–3.569	0%, 0	0.643
No	2	0.714	0.457–1.118	0.141	0.006–85.298	85.8%, 0.0895	0.008
OS							
Overall	3	0.804	0.634–1.019	0.071	0.318–2.032	72.7%, 0.0318	0.026
Subgrouped by control groups							
PD-1/PD-L1 inhibitors + TKIs vs Sorafenib alone	2	0.781	0.499–1.223	0.280	0.007–94.385	85.9%, 0.0900	0.008
PD-1/PD-L1 inhibitors + TKIs vs TKIs + Placebo	1	0.840	0.708–0.997	0.046			
Age							
<65 years	3	0.866	0.638–1.175	0.356	0.264–2.846	71.7%, 0.0522	0.029
≥65 years	4	0.797	0.670–0.947	0.010	0.602–1.054	0%, 0	0.445

(Continued on following page)

TABLE 2 (*Continued*) Pooled effect and subgroup analysis of the primary outcomes of PD-1/PD-L1 inhibitors combined with tyrosine kinase inhibitors as first-line treatment for hepatocellular carcinoma.

Outcomes and subgroups	Number of studies	Meta-analysis				Heterogeneity	
		HR	95% CI	*p* value	95% PI	I^2, tau^2	*p* value
Sex							
Male	3	0.787	0.606–1.023	0.073	0.280–2.214	74.8%, 0.0399	0.019
Female	3	1.049	0.785–1.403	0.746	0.554–1.986	0%, 0	0.773
Region							
Asia	2	0.688	0.550–0.860	0.001	0.162–2.924	0%, 0	0.548
Other	2	0.834	0.420–1.657	0.604	0.001–1,053.612	76.4%, 0.1931	0.040
Race							
Asian	2	0.666	0.533–0.834	<0.001	0.156–2.849	0%, 0	0.903
White	2	0.901	0.375–2.162	0.815	-	84.3%, 0.3398	0.012
ECOG performance status							
0	3	0.882	0.666–1.167	0.378	0.307–2.528	65.3%, 0.0395	0.056
1	3	0.741	0.619–0.887	0.001	0.470–1.169	7.7%, 0.0021	0.339
BCLC stage							
Stage B	3	0.999	0.770–1.297	0.995	0.428–2.298	19.2%, 0.0145	0.290
Stage C	3	0.778	0.633–0.956	0.017	0.369–1.640	57.4%, 0.0190	0.096
Child-Pugh classification							
A5	2	0.910	0.781–1.060	0.227	0.232–3.615	22.2%, 0.0037	0.257
A6	2	0.814	0.594–1.115	0.199	0.106–6.266	0%, 0	0.782
Baseline alpha-fetoprotein (ng/mL)							
<400	3	0.917	0.665–1.264	0.596	0.257–3.273	75.9%, 0.0606	0.016
≥400	3	0.636	0.527–0.768	<0.001	0.421–0.961	0%, 0	0.887
Disease aetiology							
Hepatitis B virus	3	0.693	0.584–0.822	<0.001	0.476–1.009	0%, 0	0.708
Hepatitis C virus	3	0.930	0.725–1.193	0.569	0.263–3.015	44.2%, 0.0454	0.167
Non-viral	3	0.962	0.785–1.179	0.709	0.321–2.885	49.9%, 0.0388	0.136
Extrahepatic metastasis							
Yes	2	0.673	0.488–0.930	0.016	0.027–16.911	67.9%, 0.0373	0.078
No	2	0.930	0.732–1.180	0.549	0.198–4.374	0%, 0	0.590
Macrovascular invasion							
Yes	3	0.726	0.570–0.925	0.010	0.427–1.235	0%, 0	0.607
No	3	0.864	0.673–1.110	0.253	0.332–2.253	68.5%, 0.0333	0.042

PFS, progression-free survival; TKIs, tyrosine kinase inhibitors; ECOG, eastern cooperative oncology group; BCLC, barcelona clinic liver cancer; OS, overall survival.

control group (RR = 2.303, 95% CI: 1.360–3.902; 95% PI: 0.408–12.991, I^2 = 79.4%). Subgroup analyses further indicated that this combination therapy achieved a higher ORR compared to either sorafenib alone or TKIs alone (or combined with placebo) (all $p < 0.05$). Nonetheless, analyses showed no significant differences in DCR between patients receiving the combination therapy and those in the control groups (RR = 1.134, 95% CI: 0.955–1.347; 95% PI: 0.619–2.076, I^2 = 92.7%). Further subgroup analysis suggested an improved DCR with the PD-1/PD-L1 inhibitors and TKIs combination compared to sorafenib alone (RR = 1.319, 95% CI: 1.106–1.573; 95% PI: 0.214–8.143, I^2 = 77.1%), but not when compared to TKIs alone (or with placebo) (RR = 0.986, 95% CI: 0.891–1.091; 95% PI: 0.352–2.759, I^2 = 72.3%) (Table 3; Supplementary Figures S23, S24).

3.5 Treatment-related adverse events

4 studies evaluated the occurrence of any grade TRAEs within experimental and control groups. The overall analysis indicated that there was no significant difference in the incidence of any grade TRAEs between the cohort treated with PD-1/PD-L1 inhibitors combined with TKIs and the control group (RR = 1.016, 95% CI:

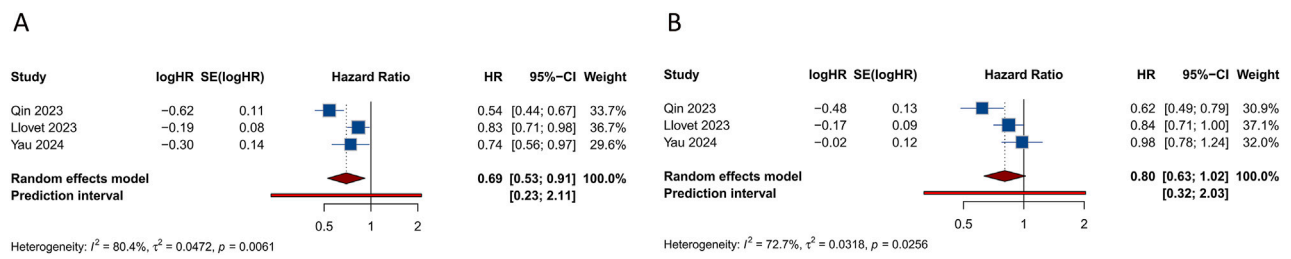

FIGURE 2
Forest plots of the survival outcomes after PD-1/PD-L1 inhibitors combined with tyrosine kinase inhibitors for hepatocellular carcinoma. **(A)** Progression-free survival **(B)** Overall survival.

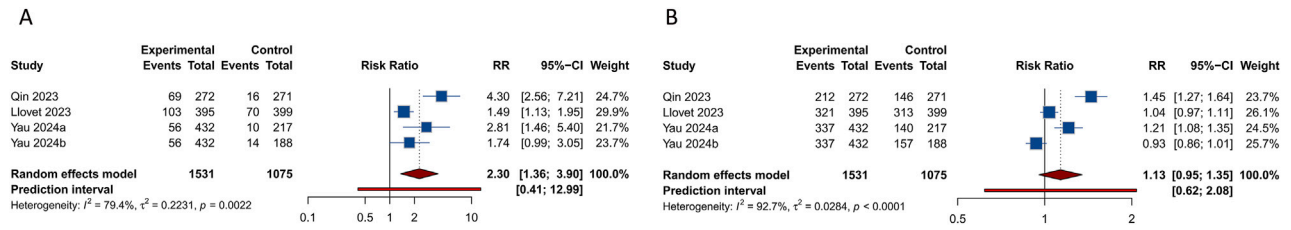

FIGURE 3
Forest plots of tumor responses after PD-1/PD-L1 inhibitors combined with tyrosine kinase inhibitors for hepatocellular carcinoma. **(A)** Objective response rate **(B)** Disease control rate.

0.996–1.036; 95% PI: 0.941–1.097, I^2 = 49.6%) (Figure 4A). Nevertheless, subgroup analyses demonstrated that this combination therapy led to a higher risk of any grade TRAEs compared to treatment with sorafenib alone (RR = 1.038, 95% CI: 1.006–1.072; 95% PI: 0.853–1.273, I^2 = 0%). Specifically, the combination therapy was associated with significantly higher incidences of increased aspartate aminotransferase (AST), increased alanine aminotransferase (ALT), decreased platelet count, increased blood bilirubin, hypothyroidism, and increased lipase compared with the control (all $p < 0.05$). Conversely, there were no notable differences in the incidence of hypertension, proteinuria, palmar-plantar erythrodysesthesia syndrome, diarrhea, fatigue, rash, reduced appetite, weight loss, asthenia, and nausea between the experimental and control groups (all $p > 0.05$) (Table 3; Supplementary Figures S25-S28).

Analysis from 4 studies revealed a significantly elevated occurrence of grade ≥3 TRAEs in patients receiving a combination of PD-1/PD-L1 inhibitors and TKIs compared to those in the control group (RR = 1.287, 95% CI: 1.020–1.624; 95% PI: 0.574–2.883, I^2 = 90.4%) (Figure 4B). Subsequent subgroup analyses further confirmed that this combination therapy increased the risk of grade ≥3 TRAEs relative to sorafenib monotherapy (RR = 1.590, 95% CI: 1.419–1.780; 95% PI: 0.779–3.181, I^2 = 0%). In particular, treatment with the combination therapy significantly increased the occurrences of elevated AST, proteinuria, elevated ALT, and increased blood bilirubin, while simultaneously reducing the incidence of decreased appetite and nausea relative to the control group (all $p < 0.05$). However, no significant differences were observed in the rates of grade ≥3 hypertension, reduced platelet count, palmar-plantar erythrodysesthesia syndrome, diarrhea, fatigue, rash, weight loss, asthenia, and increased lipase between the experimental and control cohorts (all $p > 0.05$) (Table 3; Supplementary Figures S29-S32).

4 investigations evaluated the incidence of serious TRAEs. The comprehensive analysis indicated that the regimen combining PD-1/PD-L1 inhibitors with TKIs was associated with an increased occurrence of serious TRAEs compared to the control group (RR = 2.068, 95% CI: 1.328–3.222; 95% PI: 0.487–8.776, I^2 = 77.4%) (Figure 4C). Moreover, this increase in risk was also observed when the combination therapy was compared to either sorafenib monotherapy or TKIs alone (or in conjunction with placebo) (all $p < 0.05$) (Table 3; Supplementary Figure S33).

3.6 Sensitivity analysis and publication bias

In this study, a leave-one-out sensitivity analysis was carried out to assess the influence of each individual study on the overall pooled HRs and RRs. Given the limited number of studies included, the sensitivity analysis revealed that the exclusion of individual study could potentially affect the overall results (Supplementary Figure S34). To further evaluate publication bias, we applied both funnel plots and Begg's and Egger's tests. These methods collectively found no indication of publication bias in the outcomes related to efficacy and safety (all $p > 0.05$). The associated funnel plots can be found in Supplementary Figure S35.

3.7 Trial sequential analysis results

In the TSA for PFS and OS, we calculated an APIS of 1,990. It was observed that the cumulative Z-curves for PFS, ORR, and

TABLE 3 Pooled effect of the secondary outcomes of PD-1/PD-L1 inhibitors combined with tyrosine kinase inhibitors as first-line treatment for hepatocellular carcinoma.

Outcomes	Number of studies	Meta-analysis				Heterogeneity	
		RR	95% CI	*p* value	95% PI	I^2, tau^2	*p* value
ORR							
Overall	4	2.303	1.360–3.902	0.002	0.408–12.991	79.4%, 0.2231	0.002
PD-1/PD-L1 inhibitors + TKIs vs Sorafenib alone	2	3.624	2.421–5.424	<0.001	0.264–50.526	0%, 0	0.319
PD-1/PD-L1 inhibitors + TKIs vs TKIs alone (or plus placebo)	2	1.542	1.208–1.969	0.001	0.317–7.405	0%, 0	0.616
DCR							
Overall	4	1.134	0.955–1.347	0.152	0.619–2.076	92.7%, 0.0284	<0.001
PD-1/PD-L1 inhibitors + TKIs vs Sorafenib alone	2	1.319	1.106–1.573	0.002	0.214–8.143	77.1%, 0.0125	0.037
PD-1/PD-L1 inhibitors + TKIs vs TKIs alone (or plus placebo)	2	0.986	0.891–1.091	0.782	0.352–2.759	72.3%, 0.0039	0.058
Any grade TRAEs							
Overall	4	1.016	0.996–1.036	0.114	0.941–1.097	49.6%, 0.0004	0.114
PD-1/PD-L1 inhibitors + TKIs vs Sorafenib alone	2	1.038	1.006–1.072	0.021	0.853–1.273	0%, 0	0.384
PD-1/PD-L1 inhibitors + TKIs vs TKIs alone (or plus placebo)	2	0.998	0.974–1.022	0.857	0.856–1.168	0.9%, <0.0001	0.315
Hypertension	4	1.102	0.767–1.584	0.599	0.316–3.845	90.8%, 0.1199	<0.001
Aspartate aminotransferase increased	4	1.501	1.114–2.022	0.008	0.580–3.882	74.2%, 0.0660	0.009
Proteinuria	4	1.210	0.756–1.935	0.427	0.255–5.732	86.9%, 0.1815	<0.001
Alanine aminotransferase increased	4	1.623	1.097–2.402	0.015	0.443–5.947	82.5%, 0.1265	0.001
Platelet count decreased	4	1.250	1.070–1.460	0.005	0.692–2.278	41.9%, 0.0216	0.160
Blood bilirubin increased	4	1.269	1.071–1.504	0.006	0.695–2.221	34.8%, 0.0193	0.204
Palmar-plantar erythrodysaesthesia syndrome	4	0.886	0.690–1.137	0.341	0.379–2.072	85.2%, 0.0551	<0.001
Diarrhoea	4	0.976	0.825–1.153	0.772	0.582–1.635	65.7%, 0.0190	0.033
Hypothyroidism	4	2.282	1.105–4.709	0.026	0.189–27.547	92.2%, 0.4760	<0.001
Fatigue	4	1.328	0.854–2.065	0.208	0.298–5.927	85.4%, 0.1702	<0.001
Rash	4	0.997	0.668–1.487	0.987	0.274–3.631	74.2%, 0.1233	0.009
Decreased appetite	4	1.080	0.772–1.511	0.653	0.359–3.254	78.8%, 0.0907	0.003
Weight decreased	4	0.914	0.591–1.413	0.686	0.218–3.833	78.2%, 0.1535	0.003
Asthenia	4	1.148	0.930–1.418	0.199	0.548–2.488	42.0%, 0.0353	0.160
Nausea	4	1.153	0.789–1.684	0.463	0.357–3.721	67.2%, 0.0982	0.027
Lipase increased	4	1.950	1.407–2.702	<0.001	1.138–3.272	0%, 0	0.936
Grade ≥ 3 TRAEs							
Overall	4	1.287	1.020–1.624	0.033	0.574–2.883	90.4%, 0.0502	<0.001
PD-1/PD-L1 inhibitors + TKIs vs Sorafenib alone	2	1.590	1.419–1.780	<0.001	0.779–3.181	0%, 0	0.543
PD-1/PD-L1 inhibitors + TKIs vs TKIs alone (or plus placebo)	2	1.057	0.965–1.158	0.233	0.587–1.908	0%, 0	0.431
Hypertension	4	1.179	0.639–2.176	0.599	0.145–9.604	88.5%, 0.3367	<0.001
Aspartate aminotransferase increased	4	2.177	1.564–3.030	<0.001	0.798–5.661	29.9%, 0.0517	0.233
Proteinuria	4	1.854	1.175–2.926	0.008	0.209–25.115	47.0%, 0.3555	0.129
Alanine aminotransferase increased	4	2.198	1.154–4.187	0.017	0.309–15.639	63.8%, 0.2721	0.041
Platelet count decreased	4	1.890	0.632–5.649	0.255	0.054–65.684	77.0%, 0.9310	0.005
Blood bilirubin increased	4	2.706	1.556–4.705	<0.001	0.335–21.454	34.7%, 0.2461	0.204
Palmar-plantar erythrodysaesthesia syndrome	4	0.952	0.730–1.241	0.717	0.613–1.455	0%, 0	0.541
Diarrhoea	4	1.075	0.474–2.434	0.863	0.083–13.959	71.3%, 0.4752	0.015
Fatigue	4	1.334	0.620–2.868	0.461	0.158–11.295	50.9%, 0.2980	0.106
Rash	4	1.943	0.800–4.717	0.142	0.411–7.936	0%, 0	0.774
Decreased appetite	4	0.565	0.321–0.992	0.047	0.219–1.438	0%, 0	0.446
Weight decreased	4	0.788	0.466–1.333	0.374	0.307–1.920	1.8%, 0.0056	0.383
Asthenia	4	1.496	0.891–2.511	0.128	0.592–3.315	0%, 0	0.408
Nausea	4	0.334	0.113–0.986	0.047	0.004–26.811	21.9%, 0.4533	0.278
Lipase increased	4	1.519	0.919–2.510	0.103	0.655–3.414	0%, 0	0.671

(Continued on following page)

TABLE 3 (*Continued*) Pooled effect of the secondary outcomes of PD-1/PD-L1 inhibitors combined with tyrosine kinase inhibitors as first-line treatment for hepatocellular carcinoma.

Outcomes	Number of studies	Meta-analysis				Heterogeneity	
		RR	95% CI	*p* value	95% PI	I^2, tau^2	*p* value
Serious TRAEs							
Overall	4	2.068	1.328–3.222	0.001	0.487–8.776	77.4%, 0.1551	0.004
PD-1/PD-L1 inhibitors + TKIs vs Sorafenib alone	2	3.092	1.803–5.303	<0.001	0.020–483.941	54.3%, 0.0824	0.139
PD-1/PD-L1 inhibitors + TKIs vs TKIs alone (or plus placebo)	2	1.490	1.179–1.883	0.001	0.328–6.791	0%, 0	0.796

ORR, objective response rate; TKIs, tyrosine kinase inhibitors; DCR, disease control rate; TRAEs, treatment-related adverse events.

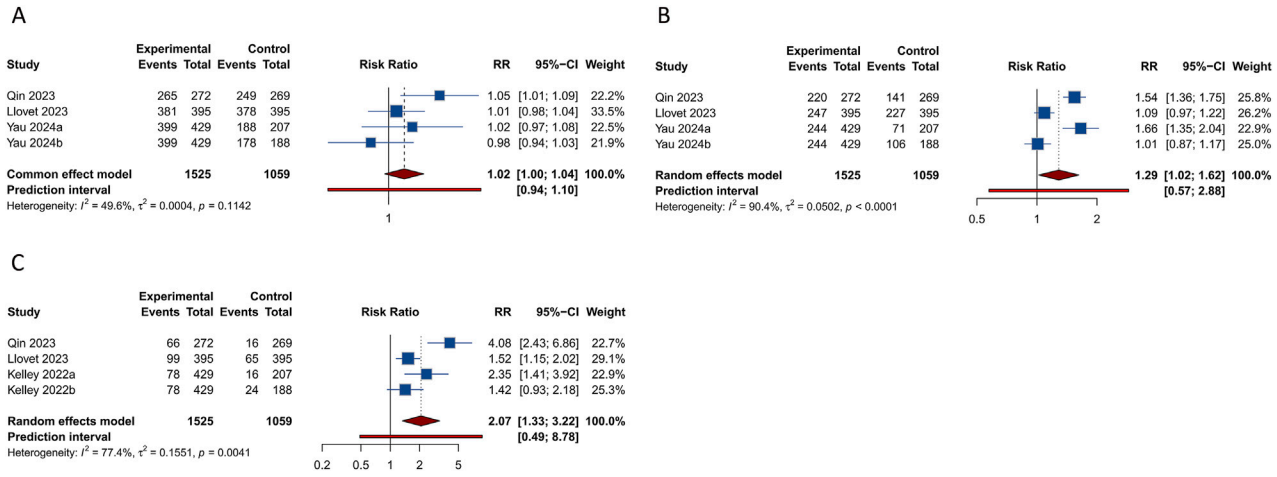

FIGURE 4
Forest plots of the safety outcomes after PD-1/PD-L1 inhibitors combined with tyrosine kinase inhibitors for hepatocellular carcinoma. **(A)** Any grade treatment-related adverse events (TRAEs) **(B)** Grade ≥3 TRAEs **(C)** Serious TRAEs.

serious TRAEs crossed the trial sequential monitoring boundary, though they did not exceed the RIS boundary. This suggests the potential for drawing robust conclusions from these parameters. However, the cumulative Z-curves for OS, DCR, any grade TRAEs, and grade ≥3 TRAEs did not breach either the RIS threshold or the trial sequential monitoring boundary, indicating that these findings remain inconclusive and potentially subject to false positives (Figures 5, 6).

4 Discussion

In the treatment of advanced HCC, single-agent ICIs have demonstrated ORRs of 15%–20%, generally without notable improvements in OS. Additionally, intrinsic resistance to ICIs occurs in approximately 30% of HCC cases (Rimassa et al., 2023). With no predictive biomarkers available to determine which patients would most benefit from immunotherapy, researchers have shifted focus to evaluate combination therapies that might be effective in a wider range of patients. Among these, the combination of PD-1/PD-L1 inhibitors with TKIs has emerged as a particularly promising strategy for advanced HCC. Our meta-analysis, which pooled data from RCTs, found that this combination therapy significantly improved PFS and ORR when compared to either first-line monotherapy or TKI monotherapy. However, it also raised the incidence of grade ≥3 and serious TRAEs. Additionally, the combined regimen of PD-1/PD-L1 inhibitors and TKIs did not significantly impact OS, DCR, or the occurrence of any grade TRAEs.

The reasons for the discrepancy between PFS and OS in our analysis remain uncertain. Numerous oncology studies have demonstrated a weak association between PFS and OS, with one proposed explanation being that OS may be adversely impacted by reduced treatment duration due to toxicity (Merino et al., 2023). Furthermore, the combination of PD-1/PD-L1 inhibitors with TKIs is associated with an increased incidence of immune-related AEs, which may necessitate dose reductions, interruptions, or discontinuation of therapy (Yau et al., 2024b), thereby potentially diminishing overall therapeutic efficacy and affecting OS. Additionally, the impact of subsequent therapies after disease progression also plays a crucial role in influencing OS. Patients who experience disease progression following first-line treatment with PD-1/PD-L1 inhibitors and TKIs may undergo second-line therapies that affect their OS outcomes. Variability in post-progression treatments among the included studies could have contributed to the observed lack of OS improvement. Moreover,

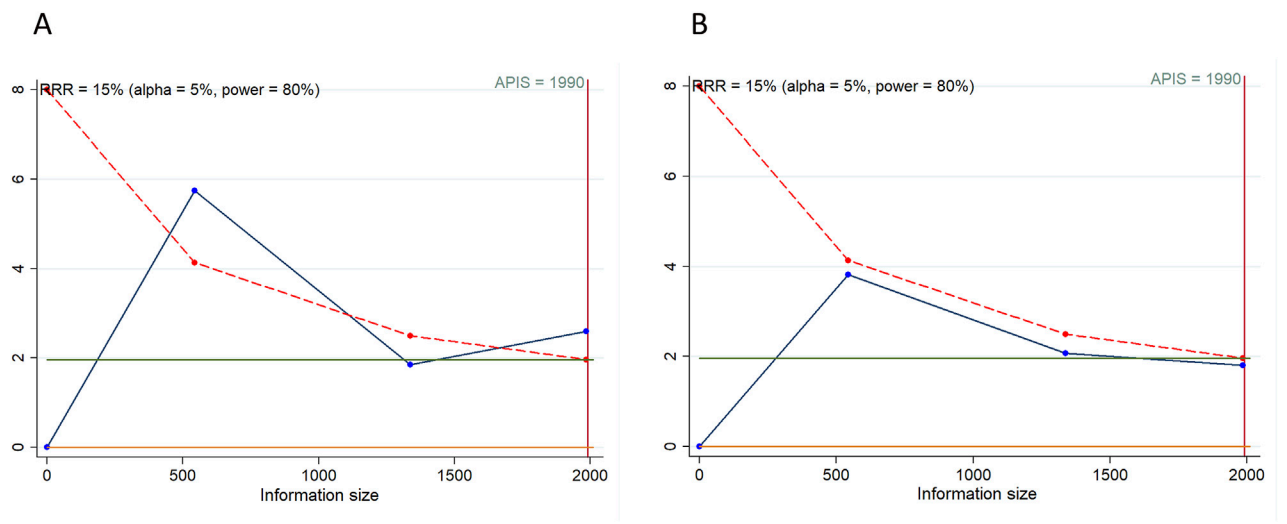

FIGURE 5
Trial sequential analysis of PD-1/PD-L1 inhibitors combined with tyrosine kinase inhibitors for hepatocellular carcinoma. **(A)** Progression-free survival **(B)** Overall survival. Red inward-sloping line to the left represents trial sequential monitoring boundary. Blue line represents evolution of cumulative Z-score. Horizontal green lines represent the conventional boundaries for statistical significance. Heterogeneity-adjusted required information size to demonstrate or reject 15% relative risk (*a priori* estimate) of mortality risk (with alpha of 5% and beta of 20%) is 1,990 patients for PFS and OS (vertical red line). Cumulative Z-curve crossing the trial sequential monitoring boundary or the APIS boundary provides firm evidence of effect.

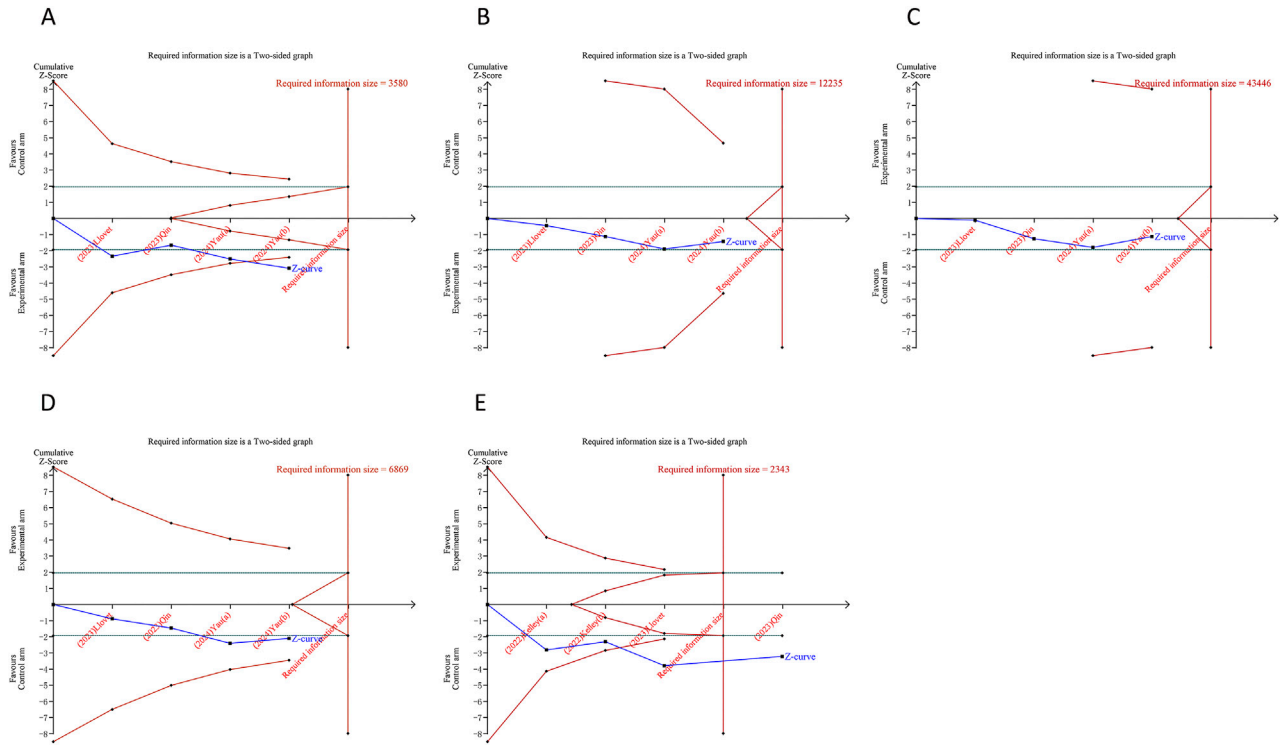

FIGURE 6
Trial sequential analysis of PD-1/PD-L1 inhibitors combined with tyrosine kinase inhibitors for hepatocellular carcinoma. **(A)** Objective response rate **(B)** Disease control rate **(C)** Any grade treatment-related adverse events (TRAEs) **(D)** Grade ≥3 TRAEs **(E)** Serious TRAEs. Uppermost and lowermost red curves represent trial sequential monitoring boundary lines for benefit and harm, respectively. Inner red lines represent the futility boundary. Blue line represents evolution of cumulative Z-score. Horizontal green lines represent the conventional boundaries for statistical significance. Cumulative Z-curve crossing the trial sequential monitoring boundary or the RIS boundary provides firm evidence of effect.

the time needed for PD-1/PD-L1 inhibitors to generate a significant anti-tumor response may exceed the follow-up durations of some included studies. Extended follow-up periods might be required to fully capture the OS benefits.

The progression of cancer is intricately linked to its ability to circumvent immune surveillance. Checkpoint proteins play a crucial role in modulating the immune system's response to both pathogens and tumor cells. Specifically, PD-1 impedes T-cell receptor signaling, curbing T-cell proliferation and the release of cytotoxic substances; sustained activation of PD-1 results in T-cell fatigue (Sen et al., 2016). Agents such as atezolizumab, camrelizumab, pembrolizumab, nivolumab, durvalumab, and tislelizumab, which inhibit PD-1 and PD-L1, have been shown to elicit objective tumor responses in approximately 15% of patients in phase 2 and 3 prospective trials (Sangro et al., 2021). The immunologic implications of TKIs have begun to be explored and remain incompletely elucidated. TKIs commonly target receptors for vascular endothelial growth factor (VEGF) and platelet-derived growth factor (PDGF), which are pivotal in their anti-angiogenic effects (Sampat and O'Neil, 2013). The inhibition of VEGF might also provoke immune-stimulating responses. TKIs can alter the immunological landscape of tumors, turning "cold" tumors "hot" and thereby broadening the cohort of patients who respond to checkpoint inhibitors due to unique immunomodulatory effects (Llovet et al., 2022). Experimental research has highlighted such transformations in the tumor microenvironment with the combination of pembrolizumab and lenvatinib in HCC, notably increasing the CD8 T-cell count while reducing regulatory T-cell numbers (Torrens et al., 2021). The combination of PD-1/PD-L1 inhibitors and multi-targeted TKIs is a VEGF-based method to enhance therapeutic efficacy. Beyond targeting the VEGF receptor, TKIs also interact with various other kinases, potentially influencing the effectiveness of PD-1/PD-L1 inhibitors (Rimassa et al., 2023). This synergistic interaction likely underpins the observed improvements in PFS and ORR with the combination therapy in our study. While no enhancements in OS or DCR were noted, more RCTs are necessary to further validate these findings.

Notably, our subgroup analysis revealed that combination therapy substantially enhanced OS in patients aged 65 years or older, of Asian descent, with an ECOG performance status of 1, BCLC stage C, baseline alpha-fetoprotein levels exceeding 400 ng/mL, and presenting with extrahepatic metastasis, macrovascular invasion, or HBV infection. Similarly, this therapeutic approach notably improved PFS in patients of male, Asian descent, with an ECOG performance status of 0, BCLC stage C, infected with HBV or hepatitis C virus (HCV), or exhibiting macrovascular invasion. These findings indicate that tailoring combination therapy to these specific demographics may enhance clinical outcomes. It is understood that chronic HBV infection leads to virus-specific T cell exhaustion, with the PD-1/PD-L1 pathway playing a critical role in inhibiting the activity of HBV-specific $CD8^+$ T cells (Ye et al., 2015). Blocking PD-1/PD-L1 can, therefore, rejuvenate HBV-specific T-cell responses to viral antigens, potentially increasing the effectiveness of ICIs (Raziorrouh et al., 2010; Zhao et al., 2022). Conversely, non-viral HCC, including cases with hepatic steatosis, appears less responsive to immunotherapy compared to other HCC etiologies (Pfister et al., 2021). This pattern of response has been corroborated by studies like CheckMate 459 (Yau et al., 2022), KEYNOTE-240 (Finn et al., 2020c) and IMbrave150 (Finn et al., 2020b), where immunotherapy appeared less effective in patients with non-viral causes of HCC (Pfister et al., 2021). Furthermore, in subgroups with alpha-fetoprotein levels at or above 400 ng/mL, combination therapy also demonstrated a preference over the subgroups with alpha-fetoprotein less than 400 ng/mL in terms of both PFS and OS. The angiogenic nature of HCC and the association between high alpha-fetoprotein levels, increased VEGF expression, and immunosuppression might explain these outcomes (Galle et al., 2019). However, the scarcity of studies addressing these specific subgroup factors necessitates further investigation to elucidate the impact of immune-combination therapy on HCC treatment. Additionally, we established two subgroups based on the type of TKIs used in control treatments. Compared with first-line sorafenib monotherapy, the combination therapy of PD-1/PD-L1 inhibitors and TKIs significantly improved PFS, ORR, and DCR, but had no significant effect on OS. Similarly, compared to other TKI monotherapy (or plus placebo), adding PD-1/PD-L1 inhibitors to TKI monotherapy markedly improved PFS and OS, and increased ORR, but did not significantly influence DCR. Given the limited number of studies within these comparisons, further research is needed to refine and validate these findings.

The superior effectiveness of PD-1/PD-L1 inhibitors combined with TKIs in HBV-infected HCC patients can be linked to the distinct immune microenvironment shaped by chronic HBV infection. Chronic HBV is known to upregulate PD-L1 expression within the tumor microenvironment (Raziorrouh et al., 2014), potentially increasing the susceptibility of these tumors to PD-1/PD-L1 blockade. Furthermore, antiviral treatment in HBV-positive individuals may complement immunotherapy by lowering viral loads and mitigating inflammation, thereby restoring immune activity (Zheng et al., 2022). TKIs, through their antiangiogenic properties, may further augment the impact of ICIs by remodeling tumor vasculature and facilitating immune cell infiltration (Xing et al., 2021). Additionally, the enhanced outcomes of combination therapy observed in Asian populations can be attributed to several factors. First, HBV infection, the leading cause of HCC in Asian patients, is associated with elevated PD-L1 levels and a more immunogenic tumor milieu (Xuan Hoan et al., 2022). Second, genetic and pharmacokinetic variations in this population, including differences in drug-metabolizing enzymes and immune-related gene polymorphisms, may boost responsiveness to PD-1/PD-L1 inhibitors and TKIs. Moreover, the prevalent use of antiviral therapies and early detection strategies in Asian regions likely contributes to more favorable responses to combination treatments. These findings highlight the importance of understanding the underlying mechanisms driving enhanced efficacy in HBV-infected and Asian patients. A deeper understanding of these biological and clinical factors could inform patient stratification and optimize treatment strategies for advanced HCC. Future studies should explore the genetic, immunological, and pharmacological factors that contribute to these observed differences, with the goal of developing personalized treatment approaches.

Besides therapeutic efficacy, TRAEs warrant close scrutiny (Zeng et al., 2023). In our research, a majority of participants from both the experimental and control arms reported experiencing TRAEs. The use of PD-1/PD-L1 inhibitors

combined with TKIs led to a higher incidence of serious and grade ≥3 TRAEs compared to the control regimen. Across the included 4 studies, prevalent TRAEs observed in combination and control therapies included hypertension, elevated AST, proteinuria, increased ALT, reduced platelet counts, increased blood bilirubin, palmar-plantar erythrodysaesthesia syndrome, diarrhea, fatigue, rash, reduced appetite, weight decreased, asthenia, nausea, and increased lipase levels. Notably, the combination therapy group showed a significant uptick in cases of elevated AST, ALT, and blood bilirubin compared to controls. Although the majority of TRAEs were classified as grade 1–2, suggesting manageability, the elevated risk of AEs highlights the imperative for rigorous monitoring and proactive management of these toxicities. The engagement of multidisciplinary care teams, encompassing hepatologists, oncologists, and supportive care professionals, is vital for enhancing patient outcomes and sustaining quality of life (QoL) throughout the treatment process (Xu and Sun, 2022).

This study has several limitations. First, this meta-analysis did not incorporate individual patient data, leading to an inherent selection bias. Second, our analysis only encompassed 4 studies that compared the efficacy and safety of PD-1/PD-L1 inhibitors combined with TKIs against first-line monotherapy or TKI monotherapy in patients with advanced or unresectable HCC. More comprehensive clinical trials are needed to generate robust data that could be included in subsequent analyses. Third, the RCTs included in this meta-analysis featured a variety of therapeutic agents and had diverse patient baseline characteristics, such as age, sex, region, race, ECOG performance status, BCLC stage, baseline alpha-fetoprotein levels, disease etiology, macrovascular invasion, Child-Pugh classification, and extrahepatic metastasis. These factors could potentially introduce significant heterogeneity in the analysis of clinical outcomes and TRAEs. Thus, subgroup analyses were performed to categorize data based on baseline characteristics, aiming to reduce the effects of heterogeneity. Future research could more comprehensively explore the efficacy and safety of the combination therapy through further subgroup analyses, such as PD-L1 expression levels and Albumin-Bilirubin (ALBI) grade, or by employing network meta-analysis. Fourth, the RCTs analyzed in this study did not report QoL outcomes, despite QoL being a critical factor in the management of advanced HCC. The lack of QoL information hinders a comprehensive evaluation of the benefit-risk profile of combination therapies when compared to TKI monotherapy or other established first-line options. Future RCTs should prioritize the collection and reporting of QoL outcomes using standardized and validated instruments to provide a more holistic evaluation of treatment efficacy and safety.

5 Conclusion

In conclusion, the combination of PD-1/PD-L1 inhibitors with TKIs emerges as a promising therapeutic option for advanced or unresectable HCC. This meta-analysis has demonstrated the efficacy of this combination therapy in enhancing PFS and ORR, and for the first time, identified better survival benefits among patients with HBV infection and within the Asian demographic. Nonetheless, the associated increase in serious and grade ≥3 TRAEs demands rigorous patient selection and management strategies. Future studies should concentrate on optimizing treatment protocols and investigate new therapeutic combinations.

Data availability statement

The original contributions presented in the study are included in the article/Supplementary Material. Further inquiries can be directed to the corresponding author.

Author contributions

PT: Conceptualization, Data curation, Formal Analysis, Investigation, Methodology, Software, Funding acquisition, Writing–original draft. FZ: Methodology, Supervision, Validation, Visualization, Writing–review and editing.

Funding

The author(s) declare that financial support was received for the research and/or publication of this article. This work was supported by the Key Research Project of Science and Technology Department of Sichuan Province (2022YFS0176) and Sichuan Provincial Medical Youth Innovation Research Project (Q21078).

Conflict of interest

The authors declare that the research was conducted in the absence of any commercial or financial relationships that could be construed as a potential conflict of interest.

Generative AI statement

The authors declare that no Generative AI was used in the creation of this manuscript.

Publisher's note

Supplementary material

The Supplementary Material for this article can be found online at: https://www.frontiersin.org/articles/10.3389/fphar.2025.1535444/full#supplementary-material

References

Abou-Alfa, G. K., Lau, G., Kudo, M., Chan, S. L., Kelley, R. K., Furuse, J., et al. (2022). Tremelimumab plus durvalumab in unresectable hepatocellular carcinoma. *NEJM Evid.* 1 (8), EVIDoa2100070. doi:10.1056/EVIDoa2100070

Begg, C. B., and Mazumdar, M. (1994). Operating characteristics of a rank correlation test for publication bias. *Biometrics* 50 (4), 1088–1101. doi:10.2307/2533446

Bowden, J., Tierney, J. F., Copas, A. J., and Burdett, S. (2011). Quantifying, displaying and accounting for heterogeneity in the meta-analysis of RCTs using standard and generalised Q statistics. *BMC Med. Res. Methodol.* 11, 41. doi:10.1186/1471-2288-11-41

Cao, Y. Z., Zheng, G. L., Zhang, T. Q., Shao, H. Y., Pan, J. Y., Huang, Z. L., et al. (2024). Hepatic arterial infusion chemotherapy with anti-angiogenesis agents and immune checkpoint inhibitors for unresectable hepatocellular carcinoma and meta-analysis. *World J. Gastroenterol.* 30 (4), 318–331. doi:10.3748/wjg.v30.i4.318

Choi, N. R., Kim, J. Y., Hong, J. H., Hur, M. H., Cho, H., Park, M. K., et al. (2022). Comparison of the outcomes between sorafenib and lenvatinib as the first-line systemic treatment for HBV-associated hepatocellular carcinoma: a propensity score matching analysis. *BMC Gastroenterol.* 22 (1), 135. doi:10.1186/s12876-022-02210-3

De Matteis, S., Ghetti, M., Gramantieri, L., Marisi, G., and Casadei-Gardini, A. (2021). Sorafenib in the treatment of virus-related HCC: differences between HCV and HBV. *Onco Targets Ther.* 14, 4305–4308. doi:10.2147/ott.S312748

Egger, M., Davey Smith, G., Schneider, M., and Minder, C. (1997). Bias in meta-analysis detected by a simple, graphical test. *Bmj* 315 (7109), 629–634. doi:10.1136/bmj.315.7109.629

Finn, R. S., Ikeda, M., Zhu, A. X., Sung, M. W., Baron, A. D., Kudo, M., et al. (2020a). Phase ib study of lenvatinib plus pembrolizumab in patients with unresectable hepatocellular carcinoma. *J. Clin. Oncol.* 38 (26), 2960–2970. doi:10.1200/jco.20.00808

Finn, R. S., Qin, S., Ikeda, M., Galle, P. R., Ducreux, M., Kim, T. Y., et al. (2020b). Atezolizumab plus bevacizumab in unresectable hepatocellular carcinoma. *N. Engl. J. Med.* 382 (20), 1894–1905. doi:10.1056/NEJMoa1915745

Finn, R. S., Ryoo, B. Y., Merle, P., Kudo, M., Bouattour, M., Lim, H. Y., et al. (2020c). Pembrolizumab as second-line therapy in patients with advanced hepatocellular carcinoma in KEYNOTE-240: a randomized, double-blind, phase III trial. *J. Clin. Oncol.* 38 (3), 193–202. doi:10.1200/jco.19.01307

Galle, P. R., Foerster, F., Kudo, M., Chan, S. L., Llovet, J. M., Qin, S., et al. (2019). Biology and significance of alpha-fetoprotein in hepatocellular carcinoma. *Liver Int.* 39 (12), 2214–2229. doi:10.1111/liv.14223

Higgins, J. P., and Thompson, S. G. (2002). Quantifying heterogeneity in a meta-analysis. *Stat. Med.* 21 (11), 1539–1558. doi:10.1002/sim.1186

Huang, D., Ke, L., Cui, H., and Li, S. (2023). Efficacy and safety of PD-1/PD-L1 inhibitors combined with anti-angiogenic therapy for the unresectable hepatocellular carcinoma and the benefit for hepatitis B virus etiology subgroup: a systematic review and meta-analysis of randomized controlled trials. *BMC Cancer* 23 (1), 474. doi:10.1186/s12885-023-10960-w

IntHout, J., Ioannidis, J. P., Rovers, M. M., and Goeman, J. J. (2016). Plea for routinely presenting prediction intervals in meta-analysis. *BMJ Open* 6 (7), e010247. doi:10.1136/bmjopen-2015-010247

Jadad, A. R., Moore, R. A., Carroll, D., Jenkinson, C., Reynolds, D. J., Gavaghan, D. J., et al. (1996). Assessing the quality of reports of randomized clinical trials: is blinding necessary? *Control Clin. Trials* 17 (1), 1–12. doi:10.1016/0197-2456(95)00134-4

Kelley, R. K., Rimassa, L., Cheng, A. L., Kaseb, A., Qin, S., Zhu, A. X., et al. (2022). Cabozantinib plus atezolizumab versus sorafenib for advanced hepatocellular carcinoma (COSMIC-312): a multicentre, open-label, randomised, phase 3 trial. *Lancet Oncol.* 23 (8), 995–1008. doi:10.1016/s1470-2045(22)00326-6

Kudo, M., Finn, R. S., Qin, S., Han, K. H., Ikeda, K., Piscaglia, F., et al. (2018). Lenvatinib versus sorafenib in first-line treatment of patients with unresectable hepatocellular carcinoma: a randomised phase 3 non-inferiority trial. *Lancet* 391 (10126), 1163–1173. doi:10.1016/s0140-6736(18)30207-1

Liu, Y., Pan, J., Gao, F., Xu, W., Li, H., and Qi, X. (2023). Efficacy and safety of PD-1/PD-L1 inhibitors in advanced hepatocellular carcinoma: a systematic review and meta-analysis. *Adv. Ther.* 40 (2), 521–549. doi:10.1007/s12325-022-02371-3

Llovet, J. M., Castet, F., Heikenwalder, M., Maini, M. K., Mazzaferro, V., Pinato, D. J., et al. (2022). Immunotherapies for hepatocellular carcinoma. *Nat. Rev. Clin. Oncol.* 19 (3), 151–172. doi:10.1038/s41571-021-00573-2

Llovet, J. M., Kelley, R. K., Villanueva, A., Singal, A. G., Pikarsky, E., Roayaie, S., et al. (2021). Hepatocellular carcinoma. *Nat. Rev. Dis. Prim.* 7 (1), 6. doi:10.1038/s41572-020-00240-3

Llovet, J. M., Kudo, M., Merle, P., Meyer, T., Qin, S., Ikeda, M., et al. (2023). Lenvatinib plus pembrolizumab versus lenvatinib plus placebo for advanced hepatocellular carcinoma (LEAP-002): a randomised, double-blind, phase 3 trial. *Lancet Oncol.* 24 (12), 1399–1410. doi:10.1016/s1470-2045(23)00469-2

Llovet, J. M., Ricci, S., Mazzaferro, V., Hilgard, P., Gane, E., Blanc, J. F., et al. (2008). Sorafenib in advanced hepatocellular carcinoma. *N. Engl. J. Med.* 359 (4), 378–390. doi:10.1056/NEJMoa0708857

Merino, M., Kasamon, Y., Theoret, M., Pazdur, R., Kluetz, P., and Gormley, N. (2023). Irreconcilable differences: the divorce between response rates, progression-free survival, and overall survival. *J. Clin. Oncol.* 41 (15), 2706–2712. doi:10.1200/jco.23.00225

Page, M. J., McKenzie, J. E., Bossuyt, P. M., Boutron, I., Hoffmann, T. C., Mulrow, C. D., et al. (2021). The PRISMA 2020 statement: an updated guideline for reporting systematic reviews. *Bmj* 372, n71. doi:10.1136/bmj.n71

Pfister, D., Núñez, N. G., Pinyol, R., Govaere, O., Pinter, M., Szydlowska, M., et al. (2021). NASH limits anti-tumour surveillance in immunotherapy-treated HCC. *Nature* 592 (7854), 450–456. doi:10.1038/s41586-021-03362-0

Qin, S., Chan, S. L., Gu, S., Bai, Y., Ren, Z., Lin, X., et al. (2023). Camrelizumab plus rivoceranib versus sorafenib as first-line therapy for unresectable hepatocellular carcinoma (CARES-310): a randomised, open-label, international phase 3 study. *Lancet* 402 (10408), 1133–1146. doi:10.1016/s0140-6736(23)00961-3

Qin, S., Ren, Z., Meng, Z., Chen, Z., Chai, X., Xiong, J., et al. (2020). Camrelizumab in patients with previously treated advanced hepatocellular carcinoma: a multicentre, open-label, parallel-group, randomised, phase 2 trial. *Lancet Oncol.* 21 (4), 571–580. doi:10.1016/s1470-2045(20)30011-5

Raziorrouh, B., Heeg, M., Kurktschiev, P., Schraut, W., Zachoval, R., Wendtner, C., et al. (2014). Inhibitory phenotype of HBV-specific CD4+ T-cells is characterized by high PD-1 expression but absent coregulation of multiple inhibitory molecules. *PLoS One* 9 (8), e105703. doi:10.1371/journal.pone.0105703

Raziorrouh, B., Schraut, W., Gerlach, T., Nowack, D., Grüner, N. H., Ulsenheimer, A., et al. (2010). The immunoregulatory role of CD244 in chronic hepatitis B infection and its inhibitory potential on virus-specific CD8+ T-cell function. *Hepatology* 52 (6), 1934–1947. doi:10.1002/hep.23936

Rimassa, L., Finn, R. S., and Sangro, B. (2023). Combination immunotherapy for hepatocellular carcinoma. *J. Hepatol.* 79 (2), 506–515. doi:10.1016/j.jhep.2023.03.003

Sampat, K. R., and O'Neil, B. (2013). Antiangiogenic therapies for advanced hepatocellular carcinoma. *Oncologist* 18 (4), 430–438. doi:10.1634/theoncologist.2012-0388

Sangro, B., Sarobe, P., Hervás-Stubbs, S., and Melero, I. (2021). Advances in immunotherapy for hepatocellular carcinoma. *Nat. Rev. Gastroenterol. Hepatol.* 18 (8), 525–543. doi:10.1038/s41575-021-00438-0

Sen, D. R., Kaminski, J., Barnitz, R. A., Kurachi, M., Gerdemann, U., Yates, K. B., et al. (2016). The epigenetic landscape of T cell exhaustion. *Science* 354 (6316), 1165–1169. doi:10.1126/science.aae0491

Singal, A. G., Lampertico, P., and Nahon, P. (2020). Epidemiology and surveillance for hepatocellular carcinoma: new trends. *J. Hepatol.* 72 (2), 250–261. doi:10.1016/j.jhep.2019.08.025

Sung, H., Ferlay, J., Siegel, R. L., Laversanne, M., Soerjomataram, I., Jemal, A., et al. (2021). Global cancer statistics 2020: GLOBOCAN estimates of incidence and mortality worldwide for 36 cancers in 185 countries. *CA Cancer J. Clin.* 71 (3), 209–249. doi:10.3322/caac.21660

Tierney, J. F., Stewart, L. A., Ghersi, D., Burdett, S., and Sydes, M. R. (2007). Practical methods for incorporating summary time-to-event data into meta-analysis. *Trials* 8, 16. doi:10.1186/1745-6215-8-16

Torrens, L., Montironi, C., Puigvehí, M., Mesropian, A., Leslie, J., Haber, P. K., et al. (2021). Immunomodulatory effects of lenvatinib plus anti-programmed cell death protein 1 in mice and rationale for patient enrichment in hepatocellular carcinoma. *Hepatology* 74 (5), 2652–2669. doi:10.1002/hep.32023

Villanueva, A. (2019). Hepatocellular carcinoma. *N. Engl. J. Med.* 380 (15), 1450–1462. doi:10.1056/NEJMra1713263

Wetterslev, J., Jakobsen, J. C., and Gluud, C. (2017). Trial Sequential Analysis in systematic reviews with meta-analysis. *BMC Med. Res. Methodol.* 17 (1), 39. doi:10.1186/s12874-017-0315-7

Xie, M., Zhong, Y., Yang, Y., Shen, F., and Nie, Y. (2022). Extended adjuvant endocrine therapy for women with hormone receptor-positive early breast cancer: a meta-analysis with trial sequential analysis of randomized controlled trials. *Front. Oncol.* 12, 1039320. doi:10.3389/fonc.2022.1039320

Xing, R., Gao, J., Cui, Q., and Wang, Q. (2021). Strategies to improve the antitumor effect of immunotherapy for hepatocellular carcinoma. *Front. Immunol.* 12, 783236. doi:10.3389/fimmu.2021.783236

Xu, B., and Sun, H. C. (2022). Camrelizumab: an investigational agent for hepatocellular carcinoma. *Expert Opin. Investig. Drugs* 31 (4), 337–346. doi:10.1080/13543784.2022.2022121

Xuan Hoan, N., Thi Minh Huyen, P., Dinh Tung, B., Phuong Giang, D., Tat Trung, N., Tien Sy, B., et al. (2022). Association of PD-L1 gene polymorphisms and circulating sPD-L1 levels with HBV infection susceptibility and related liver disease progression. *Gene* 806, 145935. doi:10.1016/j.gene.2021.145935

Yau, T., Kang, Y. K., Kim, T. Y., El-Khoueiry, A. B., Santoro, A., Sangro, B., et al. (2020). Efficacy and safety of nivolumab plus ipilimumab in patients with advanced hepatocellular carcinoma previously treated with sorafenib: the CheckMate

040 randomized clinical trial. *JAMA Oncol.* 6 (11), e204564. doi:10.1001/jamaoncol.2020.4564

Yau, T., Kaseb, A., Cheng, A. L., Qin, S., Zhu, A. X., Chan, S. L., et al. (2024a). Cabozantinib plus atezolizumab versus sorafenib for advanced hepatocellular carcinoma (COSMIC-312): final results of a randomised phase 3 study. *Lancet Gastroenterol. Hepatol.* 9 (4), 310–322. doi:10.1016/s2468-1253(23)00454-5

Yau, T., Kaseb, A., Cheng, A. L., Qin, S., Zhu, A. X., Chan, S. L., et al. (2024b). Cabozantinib plus atezolizumab versus sorafenib for advanced hepatocellular carcinoma (COSMIC-312): final results of a randomised phase 3 study. *Lancet Gastroenterol. Hepatol.* 9 (4), 310–322. doi:10.1016/s2468-1253(23)00454-5

Yau, T., Park, J. W., Finn, R. S., Cheng, A. L., Mathurin, P., Edeline, J., et al. (2022). Nivolumab versus sorafenib in advanced hepatocellular carcinoma (CheckMate 459): a randomised, multicentre, open-label, phase 3 trial. *Lancet Oncol.* 23 (1), 77–90. doi:10.1016/s1470-2045(21)00604-5

Ye, B., Liu, X., Li, X., Kong, H., Tian, L., and Chen, Y. (2015). T-cell exhaustion in chronic hepatitis B infection: current knowledge and clinical significance. *Cell Death Dis.* 6 (3), e1694. doi:10.1038/cddis.2015.42

Zeng, H., Xu, Q., Wang, J., Xu, X., Luo, J., Zhang, L., et al. (2023). The effect of anti-PD-1/PD-L1 antibodies combined with VEGF receptor tyrosine kinase inhibitors versus bevacizumab in unresectable hepatocellular carcinoma. *Front. Immunol.* 14, 1073133. doi:10.3389/fimmu.2023.1073133

Zhang, X., Wang, F., Gu, G., and Wu, Q. (2021). High HBV load weakens predictive effect of serum miR-122 on response to sorafenib in hepatocellular carcinoma patients. *J. Oncol.* 2021, 9938207. doi:10.1155/2021/9938207

Zhao, J., Zhang, Y., Qin, S., Zou, B., and Wang, Y. (2022). Hepatitis B virus reactivation in cancer patients undergoing immune checkpoint inhibitors therapy: a systematic review. *J. Cancer* 13 (14), 3539–3553. doi:10.7150/jca.77247

Zheng, J. R., Wang, Z. L., and Feng, B. (2022). Hepatitis B functional cure and immune response. *Front. Immunol.* 13, 1075916. doi:10.3389/fimmu.2022.1075916

Zhu, A. X., Finn, R. S., Edeline, J., Cattan, S., Ogasawara, S., Palmer, D., et al. (2018). Pembrolizumab in patients with advanced hepatocellular carcinoma previously treated with sorafenib (KEYNOTE-224): a non-randomised, open-label phase 2 trial. *Lancet Oncol.* 19 (7), 940–952. doi:10.1016/s1470-2045(18)30351-6

Zhu, H., Zhao, W., Chen, H., Zhu, X., You, J., and Jin, C. (2024). Evaluation of the effectiveness and safety of combining PD-1/PD-L1 inhibitors with anti-angiogenic agents in unresectable hepatocellular carcinoma: a systematic review and meta-analysis. *Front. Immunol.* 15, 1468440. doi:10.3389/fimmu.2024.1468440

frontiers | Frontiers in Pharmacology

TYPE Original Research
PUBLISHED 25 March 2025
DOI 10.3389/fphar.2025.1557925

OPEN ACCESS

EDITED BY
Milica Pešić,
University of Belgrade, Serbia

REVIEWED BY
Ivana Z. Matic,
Institute of Oncology and Radiology of Serbia, Serbia
Mario Durán-Prado,
University of Castilla-La Mancha, Spain
Marija Grozdanic,
University of Belgrade, Serbia

*CORRESPONDENCE
Bo Zhang,
zhangbo@hospital.westlake.edu.cn
Nengming Lin,
lnm1013@zju.edu.cn

†These authors have contributed equally to this work

RECEIVED 09 January 2025
ACCEPTED 17 March 2025
PUBLISHED 25 March 2025

CITATION
Ma J, Wu S, Yang X, Shen S, Zhu Y, Wang R, Xu W, Li Y, Zhu H, Yan Y, Lin N and Zhang B (2025) Milciclib-mediated CDK2 inhibition to boost radiotherapy sensitivity in colorectal cancer. *Front. Pharmacol.* 16:1557925. doi: 10.3389/fphar.2025.1557925

Milciclib-mediated CDK2 inhibition to boost radiotherapy sensitivity in colorectal cancer

Junjie Ma[1,2†], Shanshan Wu[1,2†], Xinxin Yang[1,2†], Shuying Shen[1,2†], Yiqian Zhu[1,2], Ruoqi Wang[1,2], Wei Xu[1,2], Yue Li[1,2], Haixin Zhu[1,2], Youyou Yan[2,3], Nengming Lin[1,2,3]* and Bo Zhang[1,2,3]*

[1]School of Pharmaceutical Sciences, Hangzhou First People's Hospital, Zhejiang Chinese Medical University, Hangzhou, Zhejiang, China, [2]Key Laboratory of Clinical Cancer Pharmacology and Toxicology Research of Zhejiang Province, Affiliated Hangzhou First People's Hospital, Westlake University, Hangzhou, Zhejiang, China, [3]Westlake Laboratory of Life Sciences and Biomedicine of Zhejiang Province, Hangzhou, Zhejiang, China

Background: Colorectal cancer (CRC) ranks as the third most common cancer globally. Neoadjuvant radiotherapy is the standard treatment for locally advanced rectal cancer; however, primary or acquired resistance often leads to treatment failure. Identifying new targets to overcome radiotherapy resistance in CRC is crucial for improving patient outcomes.

Methods: To evaluate the antitumor effects of Milciclib in CRC cells, we conducted assays measuring cell viability, cell cycle progression, and apoptosis in HCT116 and RKO cell lines following Milciclib treatment. Additionally, CRC cells were treated with a combination of Milciclib and irradiation to determine whether Milciclib could enhance their radiosensitivity. The efficacy of Milciclib was also assessed in radiation-resistant CRC cells.

Results: The results of cytotoxicity and proliferation assays indicated that the IC50 values of Milciclib for human colorectal cancer cell lines HCT-116 and RKO, based on cell viability measurements, were 0.275 μM and 0.403 μM, respectively. Milciclib induced a dose-dependent reduction in the proportion of CRC cells in the G2/M phase and promoted apoptosis. When combined with irradiation, Milciclib led to a 20% increase in the proportion of cells in the G1 phase and a 10% decrease in the G2 phase, suggesting an alteration in cell cycle distribution. Additionally, Milciclib impaired DNA damage repair by inhibiting Rad51, thereby enhancing radiation sensitivity. In radiation-resistant CRC cells, the combination of Milciclib and irradiation demonstrated increased efficacy, with a sensitizer enhancement ratio (SER) above 1, indicating a potential radiosensitizing effect.

Conclusion: Milciclib exhibits antitumor activity in CRC cells as a monotherapy and enhances the effectiveness of radiotherapy when used in combination. It disrupts the G2/M checkpoint and impairs DNA repair mechanisms. These findings suggest that Milciclib has the potential to be an effective therapeutic agent for CRC.

KEYWORDS

Milciclib, CDK2 inhibitor, colorectal cancer, radiotherapy resistance, DNA repair

Introduction

Colorectal cancer (CRC) is the third most common cancer worldwide and the second leading cause of cancer-related deaths. In 2020, there were approximately 1.9 million new cases of CRC globally, resulting in 935,000 deaths. By 2035, the number of CRC cases is expected to rise to 2.5 million (Sung et al., 2021; Dekker et al., 2019). Advanced CRC is characterized by a high recurrence and distant metastasis rate, with limited treatment options in chemotherapy and targeted therapies (e.g., anti-angiogenic agent bevacizumab and epidermal growth factor receptor (EGFR) inhibitor cetuximab), leading to a 5-year survival rate of only 14% (Modest et al., 2019).The currently available conventional therapies for CRC are surgical techniques, radiation, and chemotherapy treatment (Wahab et al., 2021). However, after neoadjuvant chemoradiotherapy, only 50%–60% of patients achieve partial remission, with just 15%–20% attaining a pathological complete response (pCR) (Shao et al., 2023). Some patients, particularly those with poor responses to preoperative radiotherapy, do not benefit from neoadjuvant chemoradiotherapy, leading to disease progression and delayed surgery. While it is well known that the effectiveness of radiotherapy increases with higher radiation doses, the risk of severe side effects, such as radiation-induced enteritis, limits the radiation dose in clinical practice (Van Cutsem et al., 2016). Therefore, an alternative strategy to improve clinical outcomes is to enhance tumor sensitivity to radiation. Developing effective methods to overcome radioresistance is urgently needed to achieve this goal.

CDK2, a member of the cyclin-dependent kinase family that regulates the cell cycle, plays a critical role in cell proliferation by controlling progression from the late G1 phase through the S phase (Faber et al., 2020; Zardavas et al., 2017). It is involved in various biological processes such as signal transduction, DNA damage repair, protein degradation and metabolism, and is functionally linked to the excessive proliferation and drug resistance of various cancer cells (Fagundes and Teixeira, 2021; Liu et al., 2020; Tadesse et al., 2020). Increasing evidence suggests that CDK2 contributes to radioresistance in cancer cells by enhancing DNA damage repair. CDK2 promotes homologous recombination and non-homologous end joining, facilitating the efficient repair of radiation-induced DNA damage. This enhanced repair capacity allows cancer cells to survive and proliferate despite radiotherapy, highlighting CDK2 as a potential therapeutic target for overcoming radioresistance. (Tadesse et al., 2020; Morgan and Lawrence, 2015; Deans et al., 2006; Ceccaldi et al., 2016). Additionally, CDK2 inhibitors are currently under clinical investigation for their potential to treat various cancers by inhibiting cell cycle progression (Jin et al., 2020; Satriyo et al., 2021; Wang et al., 2016). However, their clinical application faces significant challenges, including limited selectivity, toxicity, and the development of drug resistance, which necessitate further research to optimize their efficacy and safety. Milciclib is an orally bioavailable CDK inhibitor with potential antitumor activity. It effectively targets and inhibits CDK2, which may lead to cell cycle arrest and apoptosis in CDK2-expressing tumor cells (Shi et al., 2015; Lim et al., 2014). However, the effect of Milciclib on colorectal cancer (CRC), whether as a monotherapy or in combination with radiotherapy, remains unclear and requires further research.

This study aims to investigate the expression and prognostic significance of CDK2 in CRC and explore the therapeutic potential of CDK2 inhibition. Specifically, we examine the effects of Milciclib, a CDK2 inhibitor, on CRC cell cycle progression, apoptosis, and response to radiotherapy. By elucidating the underlying mechanisms, we seek to determine whether Milciclib could serve as a promising therapeutic agent for CRC, either alone or in combination with radiotherapy.

Materials and methods

Cell culture and drugs

Human CRC cells (Colorectal carcinoma cell lines: HCT116, RKO; Colorectal adenocarcinoma cell lines: DLD-1, HT-29) and human normal intestinal epithelial cells (NCM460) were cultured at 37°C with 5% CO_2. The cells were maintained in 90% DMEM (HyClone, United States) or RPMI1640 medium (HyClone, United States), supplemented with 10% fetal bovine serum (HyClone, United States) and 1% penicillin-streptomycin (Life Technologies, Grand Island, NY). The stable radioresistant HCT-116RR and DLD-1RR cell lines were established from their parental HCT-116 and DLD-1 cell lines through repeated exposure to 2 Gy X-ray per day for a total of 25 fractions (typically 5 fractions per week), accumulating a total radiation dose of 50 Gy. All cell lines were purchased from the Chinese Academy of Sciences (Shanghai, China). Milciclib (HY-10424) was purchased from MedChemExpress (MCE, USA), dissolved in dimethyl sulfoxide (DMSO) (Sigma) at a concentration of 10 mM, and added to the culture medium at a final concentration not exceeding 0.1% DMSO. 3-Methyladenine (HY-19312), Z-VAD-FMK (HY-16658B), Belnacasan (HY-13205), Necrostatin-1 (HY-15760) and Ferrostatin-1 (HY-100579) were purchased from MedChemExpress (MCE, United States).

Cell viability assay

Each of the tested cell lines was seeded into 96-well plates at a density of 3000 cells per well and incubated overnight in a complete medium. Following a 72-h drug treatment, cell viability was measured using the Cell Counting Kit-8 (CCK8) (MCE, United States) according to the protocol and assessed with a microplate reader (BioRad, United States) at an absorbance of 450 nm. The method of action of programmed cell death inhibitors: The two groups of colon cancer cells were seeded in 96-well plates at a density of 3000 cells per well. After 24 h, various programmed cell death inhibitors were added to each column (each column had 6 replicate wells), including the autophagy inhibitor 3-Methyladenine (1 μM), the apoptosis inhibitor Z-VAD-FMK (20 μM), the necroptosis inhibitor Necrostatin-1 (2 μM), the ferroptosis inhibitor Ferrostatin-1 (1 μM), and the pyroptosis inhibitor Belnacasan (1 μM), and pretreated for 6 h. Then, 400 nM Milciclib was added to each column, and the cells were treated for an additional 72 h. Cell proliferation activity was assessed using the CCK-8 assay. Assays were performed on three independent experiments.

Colony formation assay

The effect of varying concentrations of Milciclib on tumor cells was evaluated using a colony formation assay. Briefly, 1×10^3 cells were cultured in 6-well plates and treated with different concentrations of Milciclib (200, 400, 800 nM). After 72 h, the media was replaced with fresh drug-free medium and then the plate was incubated at 37°C, until visible colonies formed. The cells were then fixed with 4% paraformaldehyde (PFA, Solarbio, Beijing, China) for 15 min, followed by staining with 0.1% crystal violet at room temperature for 30 min. After washing with phosphate buffered saline (PBS, Bio-Channel, Jiangsu, China), colonies were observed under a microscope (ECLIPSE TS100, Nikon, JAPAN). Colonies containing more than 50 cells were counted using ImageJ software 1.53a version. Assays were performed on three independent experiments.

Clonogenic survival assay

The parental HCT116 and DLD-1 cells, along with their radiation-resistant counterparts, HCT116-R and DLD-1-R, were cultured in six-well plates and subjected to a single-dose irradiation of 0, 2, 4, or 8 Gy. The initial seeding densities were adjusted according to the radiation dose, with 2000 cells for 0 Gy, 3000 cells for 2 Gy, 4000 cells for 4 Gy, and 6000 cells for 8 Gy. Cells were irradiated using a Precision X-RAD 225 machine operating at 225 kV and 13.3 mA with a 2-mm Al filter (source-to-skin distance (SSD)): 36 cm; dose rate: 1.3 Gy/min). The medium was changed 2 days after irradiation. 2 weeks post-irradiation, the plates were fixed with 4% PFA for 15 min, stained with 0.1% crystal violet for 30 min, and then washed with PBS. The linear quadratic (LQ) model ($SF = \exp(-aD-bD^2)$) was used to fit the survival curves. Each experiment included three duplicate wells and was performed thrice.

Cell cycle assay

After exposure to Milciclib (with or without radiotherapy) for 24 h, the adherent cells were harvested and washed three times with PBS. It is important to note that floating dead cells in the supernatant were not collected, which may result in an underestimation of the sub-G1 population and represents a limitation of this study. The harvested cells were then fixed in 75% pre-cooled ethanol and incubated overnight at −20°C. Following three additional washes with PBS, the cells were stained with propidium iodide (PI)/RNase solutions using a commercial cell cycle detection kit (BD Biosciences) at room temperature for 15 min in the dark. The stained cells were analyzed using the BD FACS Canto II (BD Biosciences) within 1 h. Data analysis was performed using ModFit LT version 5.0 software (Verity Software House, Topsham, ME). Assays were performed on three independent experiments.

Cell apoptosis assay

Cells were cultured in 6-well plates and treated with Milciclib, radiotherapy, or a combination of both for 72 h. Following treatment, all cells were collected and washed with PBS. They were then double-stained using the Annexin V-Phycoerythrin (PE) kit and the FITC apoptosis detection kit (BD Biosciences, Erembodegem, Belgium) for 30 min. Apoptotic cells, including both early (Annexin V+/PI−) and late apoptosis (Annexin V+/PI+), were detected by flow cytometry (BD Biosciences) within 1 h. The total apoptotic rate was calculated as the sum of early and late apoptotic cells. Data analysis was performed using FlowJo version 10.8.1 software (FlowJo, Oregon). Assays were conducted in three independent experiments.

Western blot analysis

Cells were seeded in 6-well plates at a density of 2×10^5 cells per well and lysed using Radio Immunoprecipitation Assay Lysis buffer (RIPA buffer, Beyotime, China) supplemented with 1 x protease inhibitor (Solarbio, China) and phosphatase inhibitor (Solarbio, China). The proteins were denatured by boiling in a 1.5 × SDS loading buffer. Equal amounts of proteins were separated by SDS-PAGE and transferred to NC membranes. The membranes were blocked at room temperature with 5% non-fat milk and then incubated overnight at 4°C with primary antibodies. After washing with Tris-buffered saline containing Tween 20 (TBST), the membranes were incubated with secondary antibodies at room temperature for 1 h. Following another wash, an ECL reagent was applied, and the membranes were analyzed using the Bio-Rad Molecular Imager ChemiDoc XRS + system (BioRad, United States). We have normalized the Western blot results by comparing the grayscale values of the target protein to those of the housekeeping protein in the same sample to ensure consistency. Regarding the concentration of Milciclib, we determined it based on the IC50 values in 2 cell lines, selecting three concentrations on either side of the IC50 (200, 400, and 800 nM) for treatment. To investigate the time-dependent effects of Milciclib on colon cancer cells, we first conducted cell cycle and apoptosis experiments on RKO cells, choosing time points of 24, 48, and 72 h (sub 1D,E). The results showed that Milciclib significantly inhibited the cell cycle in RKO cells at 24 h, so we selected 24 h as the time point for detecting cell cycle-related proteins. In the apoptosis experiment, colon cancer cells showed significant apoptosis at 72 h, so we selected 72 h as the time point for detecting apoptosis-related proteins.

The primary antibodies against CDK2 (#2546T), phosphor-CDK2 (THr160, #2561S), phospho-H2AX (S139, #9718T), CyclinE (#20808T), β-Actin (#4970T), PARP (#9532S), Cleaved PARP (#5625S), Bcl-2 (#3498S), Bax (#5023T), Rad51 (#8875T), Rad50 (#3427T) and GAPDH (#2118T) were purchased from Cell Signaling Technology (Danvers, MA), The secondary antibodies against, anti-rabbit (A0208) and anti-mouse (A0216) were purchased from Beyotime (Shanghai, China).

Statistical analysis

The data were analyzed and visualized using GraphPad Prism 8.0, Modfit 5, FlowJo, and SPSS 26.0 software. All experiments were performed in triplicate, and the results are presented as mean ± SD.

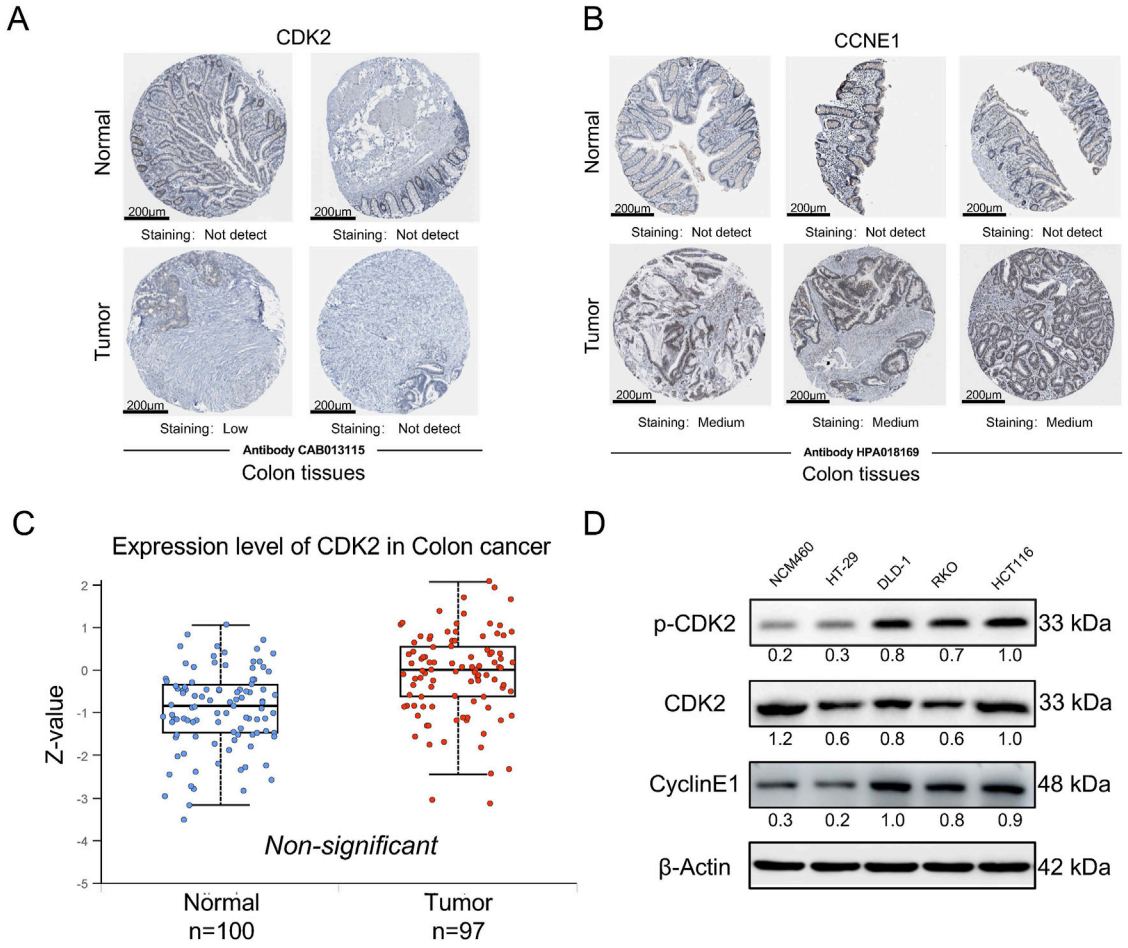

FIGURE 1
p-CDK2 and CCNE1 expression in CRCs tissues at protein levels **(A, B)**. Immunohistochemical tissue chip images of CDK2 and CCNE1 proteins obtained from the HPA database. **(C)** The expression of total CDK2 protein in normal and cancer tissues was obtained from the HPA website CPTAC database **(D)**. Western blot analysis of p-CDK2 and CyclinE1 expression in NCM460, HCT116, RKO, HT-29, and DLD-1 cells.

Statistical analysis was conducted using the t-test, with a p-value of less than 0.05 considered statistically significant. The significance levels are indicated as follows: $*p < 0.05$, $**p < 0.01$, $***p < 0.001$, $****p < 0.0001$.

Results

Phosphorylated CDK2 expression is upregulated in colorectal cancer cells

We initially assessed the expression of CDK2 and CCNE1 (the gene encoding the G1/S phase-specific cell cycle protein Cyclin E1) in human cancers using public databases. The results presented here are based, in whole or in part, on data generated by the UALCAN platform (https://ualcan.path.uab.edu). In colorectal cancer (CRC), both CDK2 and CCNE1 were significantly upregulated (sub 1A,B). Compared to normal tissues, the expression levels of these genes were markedly higher in cancerous tissues (sub 1C). Additionally, we examined the protein expression levels of CDK2 and CCNE1 in normal and cancerous intestinal tissues using the HPA database (https://www.proteinatlas.org). The immunohistochemistry results showed no difference in total CDK2 protein levels between normal and tumor tissues, while CCNE1 protein expression exhibited significant differences in the tumor group (Figures 1A, B). Subsequently, we re-evaluated the expression differences of total CDK2 protein levels between normal and tumor groups using the CPTAC database on the HPA website. The results showed that there was no significant difference in total CDK2 protein expression between the two groups (Figure 1C). This discrepancy suggests that RNA and protein expression may be regulated by different mechanisms, particularly post-transcriptional modifications. Although CDK2 RNA expression was elevated in cancerous tissues, its protein levels may be influenced by post-translational modifications, such as phosphorylation. Given that CDK2 function is contingent on its phosphorylation status, we hypothesized that alterations in CDK2 phosphorylation might underlie these observations. To investigate this further, we analyzed the expression of phosphorylated CDK2 and total CDK2 in normal intestinal epithelial cells and colorectal cancer cells. The results demonstrated a significant upregulation of phosphorylated CDK2 in colorectal cancer cells (Figure 1D).

10.3389/fphar.2025.1557925

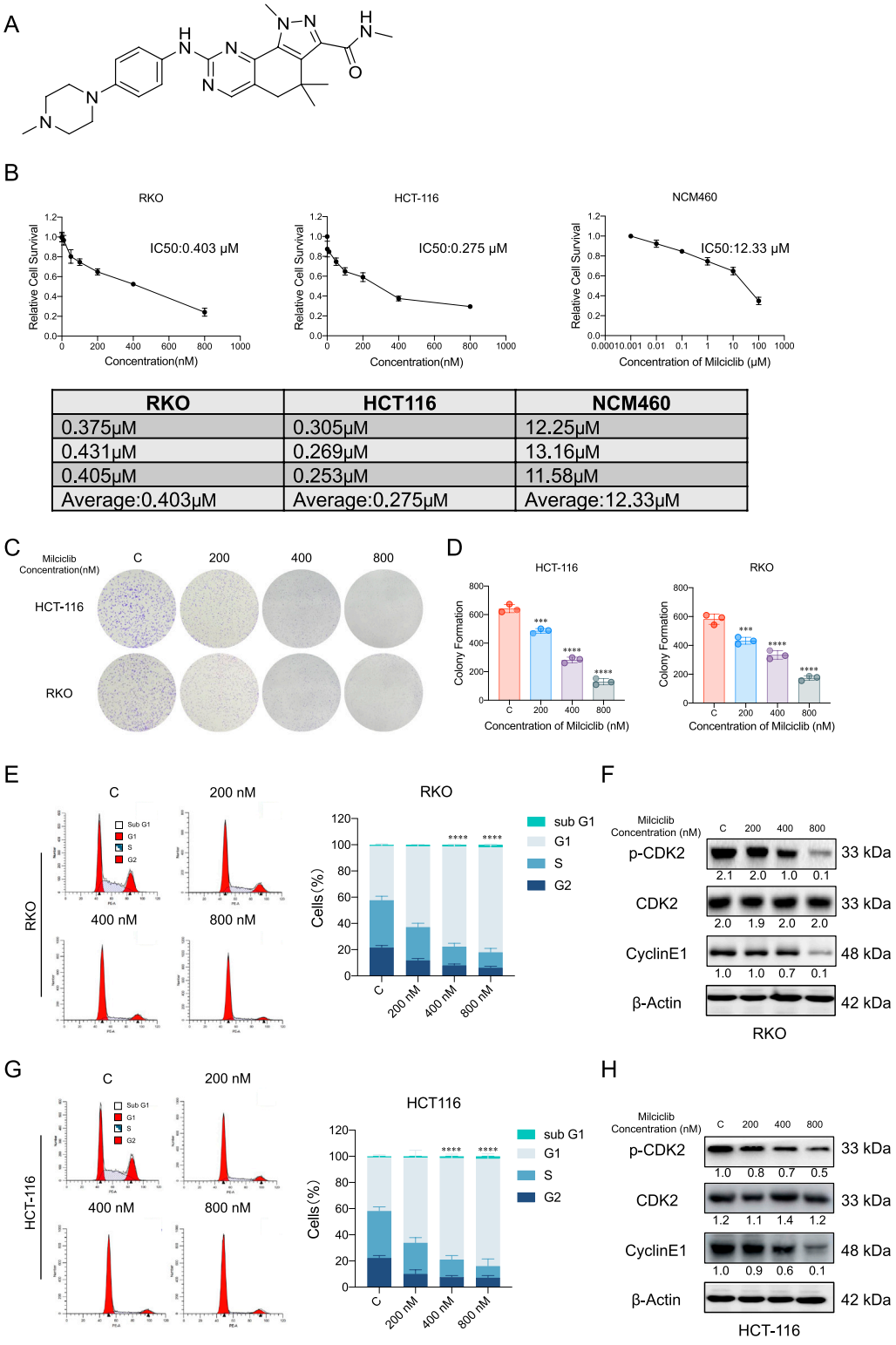

RKO	HCT116	NCM460
0.375μM	0.305μM	12.25μM
0.431μM	0.269μM	13.16μM
0.405μM	0.253μM	11.58μM
Average:0.403μM	Average:0.275μM	Average:12.33μM

FIGURE 2
Milciclib blocks G1/S phase of the cell cycle in a dose-dependent manner **(A)**. Chemical structure of Milciclib **(B)**. The IC50 of Milciclib in RKO, HCT116 and NCM460 cells **(C, D)**. Colony formation assay of CRC cells treated with varying concentrations (0 nM, 200 nM, 400 nM, and 800 nM) of Milciclib **(E, G)**. Flow cytometry analysis indicates Milciclib-induced G1 phase arrest in CRC cells **(F, H)**. Western blot analysis shows the inhibition of cell cycle-related proteins in CRC cells mediated by Milciclib. The statistical significance shown in the figure is compared to the control group. *P < 0.05, **P < 0.01, ***P < 0.001, ****p < 0.0001.

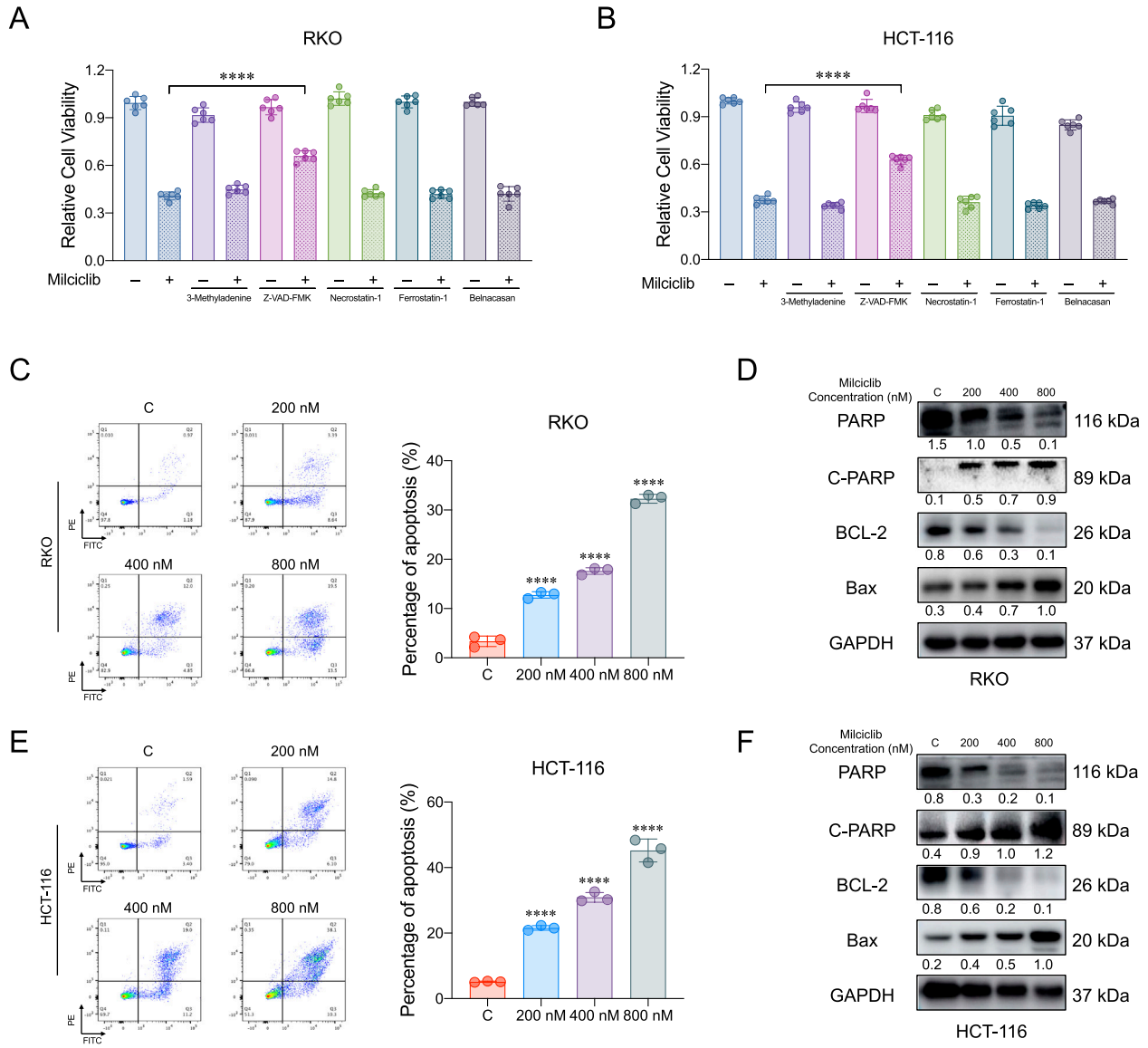

FIGURE 3
Milciclib induce apoptosis in a dose-dependent manner **(A, B)**. Cells were pretreated with various cell death inhibitors for 6 h, followed by co-incubation with Milciclib for 72 h, and cell proliferation was subsequently assessed using the CCK-8 assay **(C, E)**. Milciclib induced apoptosis in CRC cells in a concentration-dependent manner (The statistical significance shown in the figure is compared to the control group) **(D, F)**. Changes in the expression of apoptosis-related proteins were induced by Milciclib. *P < 0.05, **P < 0.01, ***P < 0.001, ****p < 0.0001.

The CDK2 inhibitor Milciclib induces cell cycle arrest by inhibiting activated CDK2 in colorectal cancer

To evaluate the anti-tumor effects of Milciclib in CRC cells, we assessed cell viability at various concentrations of Milciclib (Figure 2A). The results showed that the IC50 values of Milciclib in two CRC cell lines were 0.275 μM for HCT116 and 0.403 μM for RKO, which were lower than those in NCM460 cells (Figure 2B). This difference may be related to the elevated expression of p-CDK2 and CCNE1 in CRC cells. A dose-escalation colony formation assay conducted with Milciclib in HCT116 and RKO cells revealed a decrease in the number of cell colonies as the dose of Milciclib increased (Figures 2C, D). Since CDK2 is a critical kinase in the G1/S phase of the cell cycle, we further explored the mechanism of action of Milciclib in CRC cells by treating HCT116 and RKO cells with different concentrations of the drug (200, 400, and 800 nM). After 24 h of treatment, cells were collected for flow cytometry to analyze cell cycle distribution. The results indicated that Milciclib induced G1 phase arrest in a concentration-dependent manner, as evidenced by an increasing percentage of cells in the G1 phase. This was accompanied by a corresponding decrease in the percentage of cells in the S and G2/M phases. Additionally, after 24 h of treatment with 800 nM Milciclib, the percentage of cells in the sub-G1 phase remained low, with RKO cells at 1.9% and HCT116 cells at 1.85%. (Figures 2E–G). Additionally, protein samples were collected for Western blot analysis to detect the expression levels of cell cycle-related markers, and the results were consistent with those from the flow cytometry analysis (Figures 2F–H).

Milciclib induces apoptosis in CRC cells

To further investigate the mechanism by which Milciclib affects CRC cells, we pretreated HCT116 and RKO cells with various inhibitors for 6 h: autophagy inhibitor 3-Methyladenine (1 μM), apoptosis inhibitor Z-VAD-FMK (20 μM), necroptosis inhibitor Necrostatin-1 (2 μM), ferroptosis inhibitor Ferrostatin-1 (1 μM), and pyroptosis inhibitor Belnacasan (1 μM). After pretreatment, the cells were incubated with 400 nM Milciclib for 72 h, and their proliferative activity was measured using the CCK-8 assay. The results showed that the apoptosis inhibitor partially reversed the proliferation inhibition of HCT116 and RKO cells induced by 400 nM Milciclib, while the autophagy, necroptosis, ferroptosis, and pyroptosis inhibitors had no such effect (Figures 3A,B). To confirm that Milciclib induces apoptosis in CRC cells, we performed apoptosis assays on HCT116 and RKO cells. Annexin V staining demonstrated that the proportion of apoptotic cells significantly increased in a dose-dependent manner after 72 h of Milciclib treatment at different concentrations (Figures 3C–E). This finding was further supported by dose-dependent alterations in apoptosis-related proteins. As the Milciclib concentration increased, there was a marked upregulation of the pro-apoptotic protein Bax and cleaved PARP, accompanied by a downregulation of both PARP and Bcl-2 proteins. (Figures 3D–F).

The combination of Milciclib and radiotherapy may enhance the anti-tumor effect

Currently, the first-line clinical treatment for CRC involves a combination of chemotherapy and radiotherapy. To evaluate the effect of combining Milciclib with radiotherapy, HCT116, and RKO cells were cultured in six-well plates and Milciclib was added 24 h before irradiation. 24 h post-irradiation, cells were collected for flow cytometry and Western blot analysis. Flow cytometry results showed that Milciclib induced G1 arrest in CRC cells, with a significant reduction in the proportion of cells in the G2 phase (Figures 4A–C). Western blot analysis further confirmed these results, revealing a downregulation of key G1/S phase proteins, including CDK2, p-CDK2, and cyclin E1 in the combination treatment group (Figures 4B–D). The disruption of the cell cycle also triggered apoptosis, and the combination of Milciclib with irradiation exhibited an accumulative effect in CRC cells (Figures 4E, G). Western blot results were consistent with flow cytometry findings, showing a downregulation of Bcl2 and PARP expression, alongside an upregulation of cleaved PARP expression (Figures 4F, H).

Milciclib partially reversed the radioresistance of cells by inhibiting CDK2

We analyzed whole-genome sequencing data from the GEO gene expression database (https://www.ncbi.nlm.nih.gov/geo/), comparing 4 radiotherapy-tolerant patients to 4 radiotherapy-sensitive patients (Zhou et al., 2023). The analysis revealed that CDK2 and CCNE1 were more highly expressed in radiotherapy-tolerant patients than in those sensitive to radiotherapy (Figures 5A,B). To validate these findings, we established radiotherapy-resistant strains of HCT116 and DLD-1 cells (named HCT116-R and DLD-1-R). Using a colony formation assay, we confirmed their radioresistance (Figure 5D). We further examined the protein levels of CDK2 and CCNE1 in the radioresistant cells, which aligned with our initial analysis from the GEO database (Figure 5C). To assess Milciclib's effect on these radioresistant cells, HCT116, DLD-1, and their radioresistant strains were treated with varying concentrations of Milciclib 24 h before irradiation. After 72 h of gradient irradiation, cell proliferation activity was measured using the CCK-8 assay. In the HCT116 parental cell line, the Sensitization Enhancement Ratio (SER) for 100 nM Milciclib combined with 2Gy radiation compared to 2Gy radiation alone was 1.68. In the DLD-1 parental cell line, the SER for the same combination was 1.88. In the HCT116 radiation-resistant cell line, the SER for 100 nM Milciclib combined with 2Gy radiation compared to 2Gy radiation alone was 1.67, while in the DLD-1 radiation-resistant cell line, the SER was 1.78. These results suggest that Milciclib can enhance the sensitivity to radiotherapy, thereby improving the effectiveness of radiotherapy (Figure 5E).

Milciclib induces apoptosis in radiation-resistant colorectal cancer cells by inhibiting RAD51

To assess the impact of Milciclib on radiation-resistant colorectal cancer (CRC) cells, HCT116-R and DLD-1-R cells were seeded in six-well plates and treated with Milciclib 24 h before irradiation. After 24 h of irradiation, cells were collected for flow cytometry and Western blot analysis. Flow cytometry results revealed that the combination of Milciclib and radiation significantly altered the cell cycle distribution. While irradiation alone caused a prominent G2/M phase arrest, the addition of Milciclib further enhanced this arrest, with a notable reduction in the proportion of cells in the G2/M phase compared to irradiation alone (Figures 6A, B). This suggests that Milciclib may synergize with radiation by impairing the cells' ability to repair DNA damage, thereby amplifying the cytotoxic effects.

Furthermore, this disruption in cell cycle progression was closely associated with an increase in apoptosis. Both flow cytometry (Figures 6C, D) and Western blot analysis confirmed that the combination treatment induced a significantly higher apoptotic rate than either Milciclib or irradiation alone. Specifically, Western blotting showed a downregulation of anti-apoptotic proteins such as Bcl-2 and PARP, while cleaved PARP levels were upregulated, indicating a marked increase in apoptosis following the combination treatment (Figure 6E).

Given the critical role of DNA damage in radiation-induced cell death, we further investigated the effect of Milciclib on the DNA damage repair pathways in resistant cells. Western blot analysis demonstrated a significant upregulation of γ-H2AX (H2A histone family member X, a well-established marker of DNA double-strand breaks), in cells treated with the combination of Milciclib and

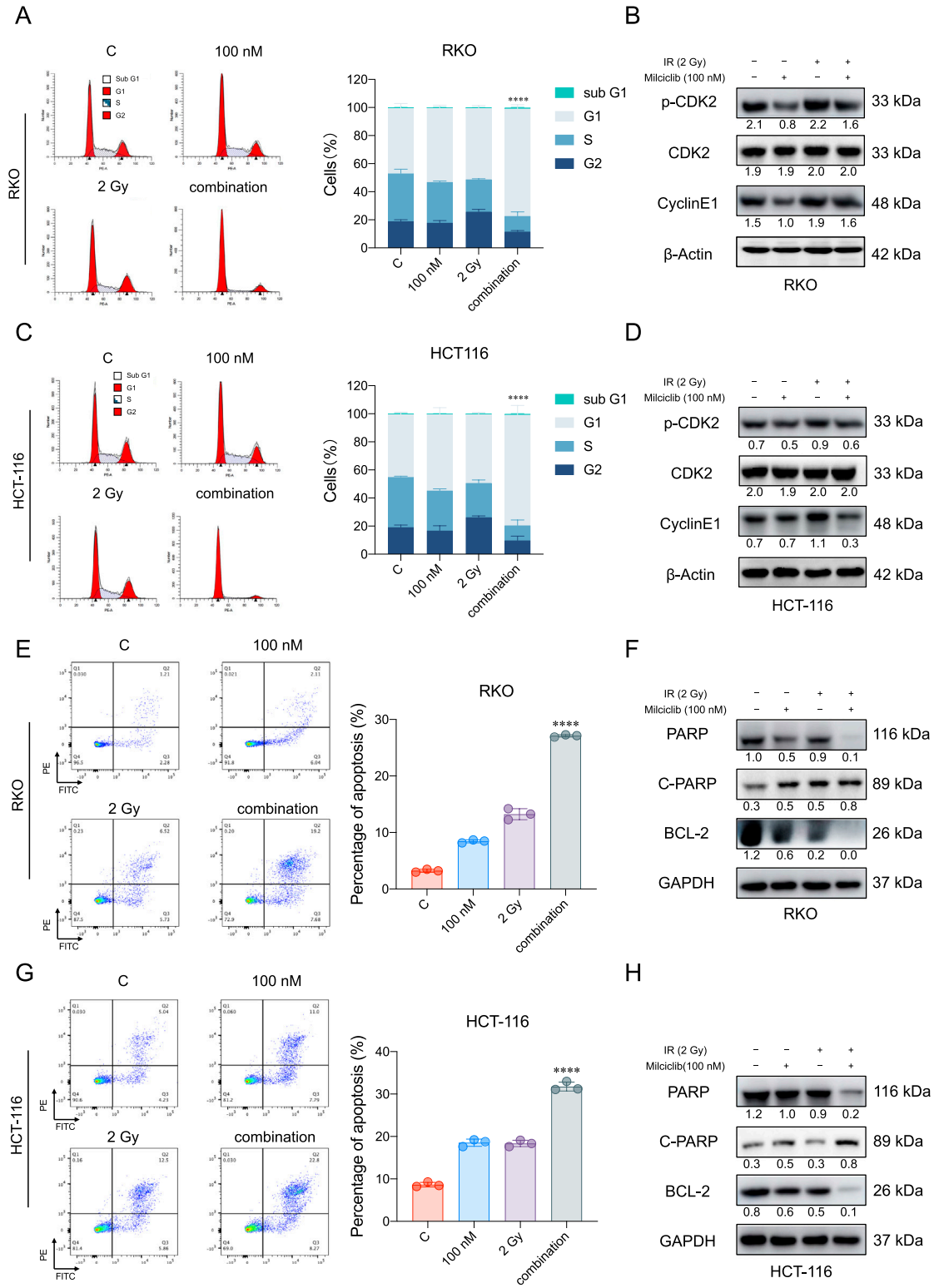

FIGURE 4
Combination therapy of Milciclib and radiotherapy enhances apoptosis in CRCs **(A, C)**. The combination of Milciclib and radiotherapy induces G1/S phase cell cycle arrest **(B, D)**. Changes in cell cycle-related proteins caused by the combination of Milciclib and radiotherapy **(E, G)**. The combination of Milciclib and radiotherapy increases the apoptosis rate in CRC tumor cells **(F, H)**. The combination of Milciclib and radiotherapy alters the levels of apoptosis-related proteins. The statistical significance shown in the figure represents comparisons between the combined radiotherapy and drug treatment group *versus* the radiotherapy-only and drug-only treatment groups, respectively. *P < 0.05, **P < 0.01, ***P < 0.001, ****p < 0.0001.

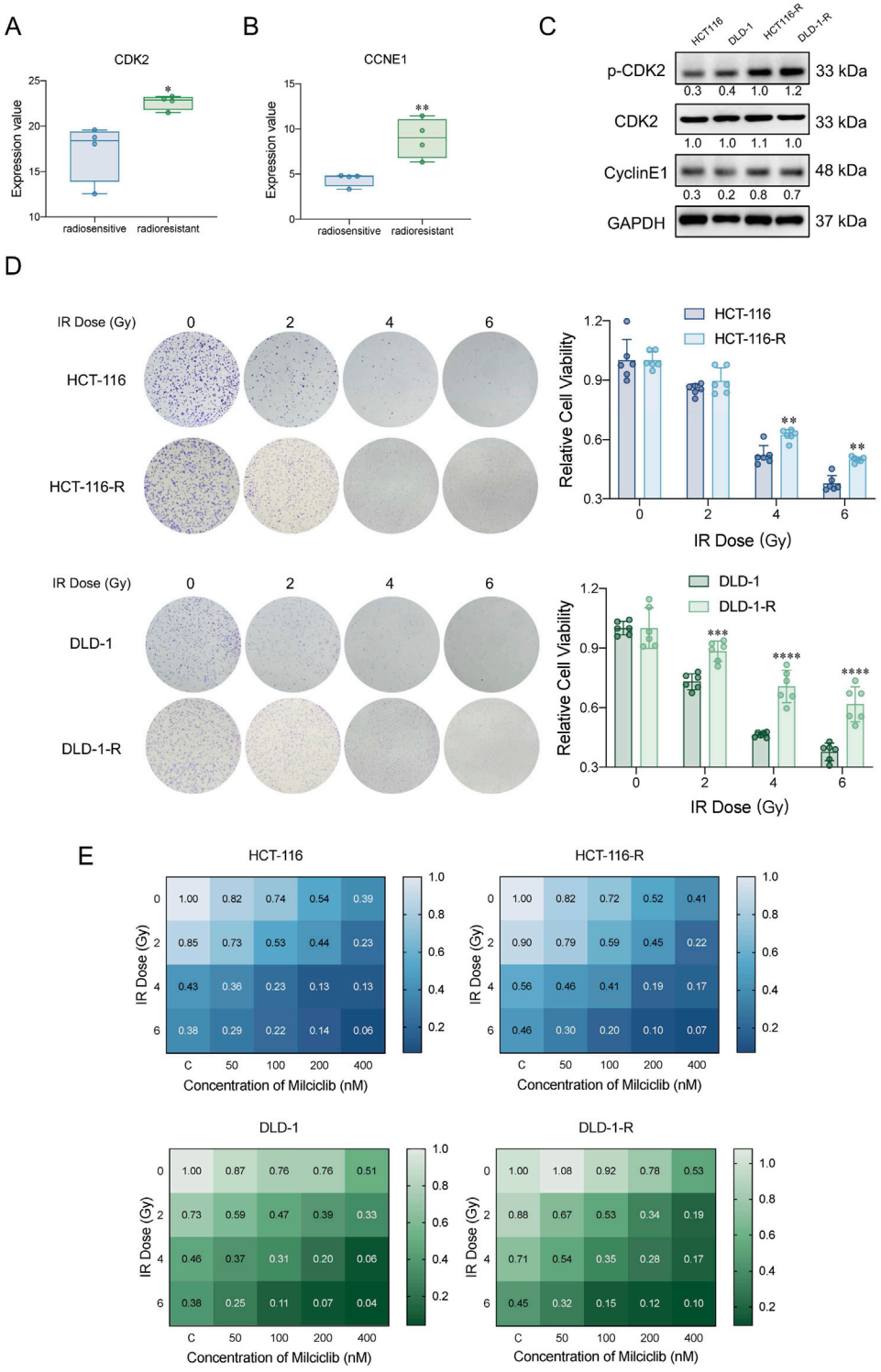

FIGURE 5
Milciclib mitigated cellular radioresistance by partially inhibiting CDK2 activity **(A, B)**. Expression differences of CDK2 and CCNE1 between radiotherapy-sensitive and -resistant patients in the GSE186940 dataset analyzed via RNASeq (n = 4). (The statistical significance shown in the figure represents the comparison between the radiotherapy-resistant group and the radiotherapy-sensitive group) **(C)**. Western blot analysis of CDK2 and CyclinE1 expression in HCT116-R and DLD-1-R cells **(D)**. Clonogenic survival assay of HCT116-R and DLD-1-R cells under different irradiation doses. (The statistical significance shown in the figure represents the comparison between the radiotherapy-resistant group and the parental group) **(E)**. Proliferative activity of CRC cells and radiotherapy-resistant cells treated with Milciclib in combination with radiotherapy, assessed using the CCK-8 assay. The Sensitization Enhancement Ratio (SER) is calculated by comparing the effect of a combination treatment (e.g., a drug plus radiation) to the effect of the treatment alone (e.g., radiation alone) on a specific biological endpoint, such as cell viability. In other words, it compares how much more effective the combination treatment is compared to the treatment used alone. SER >1 = Synergistic effect (combining Milciclib with radiotherapy enhances the effectiveness of radiotherapy).*p < 0.05, **p < 0.01, ***p < 0.001, ****p < 0.0001.

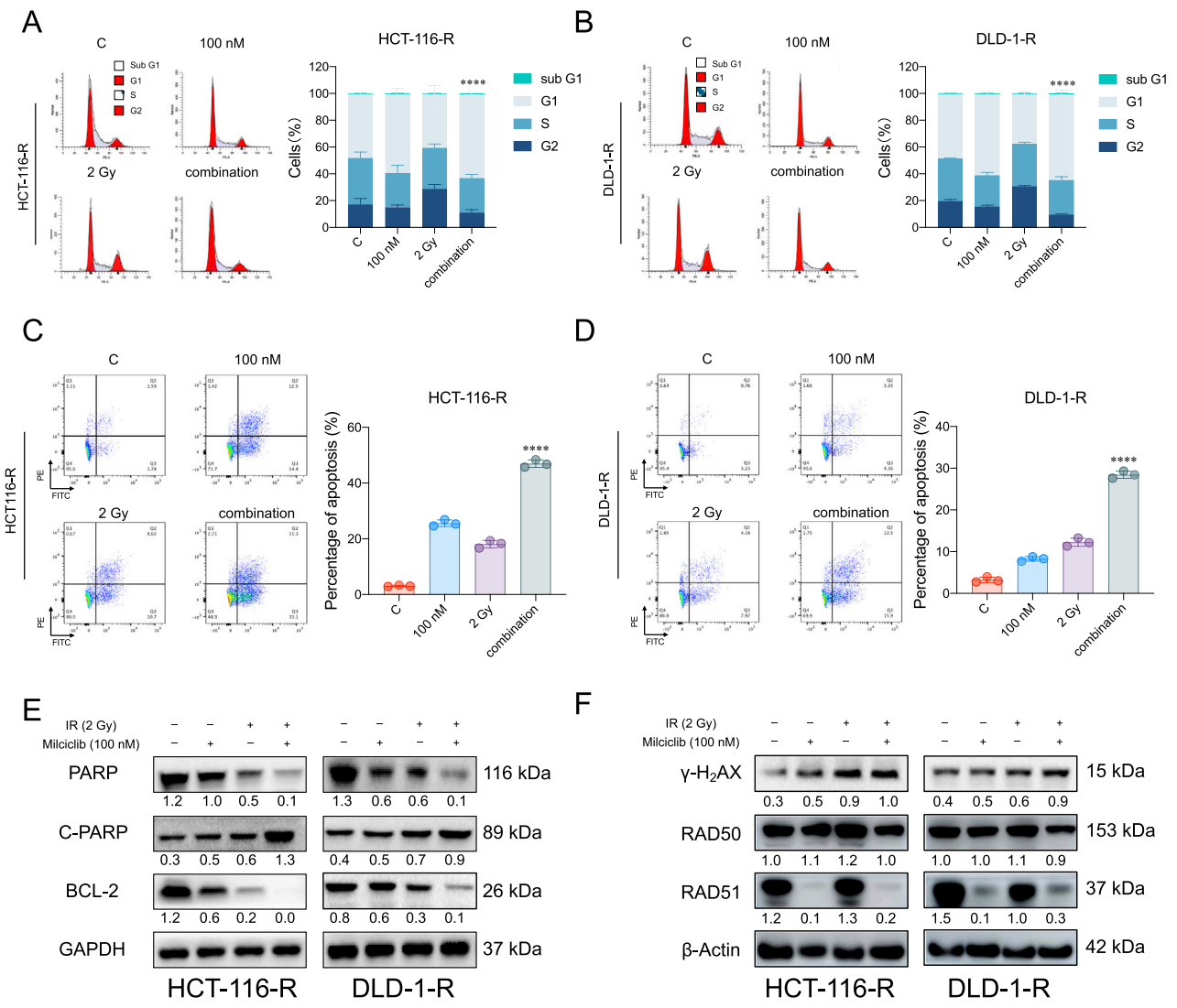

FIGURE 6
Milciclib promotes apoptosis in radiation-resistant colorectal cancer cells by suppressing RAD51 activity **(A, B)**. The combination of Milciclib and radiotherapy reduces the proportion of G2/M phase cells in radiotherapy-resistant cells **(C, D)**. The combination of Milciclib and radiotherapy increases the apoptosis rate in CRC radiotherapy-resistant cells **(E)**. The combination of Milciclib and radiotherapy alters the levels of apoptosis-related proteins **(F)**. The combination of Milciclib and radiotherapy inhibits the expression of proteins involved in damage repair. The statistical significance shown in the figure represents comparisons between the combined radiotherapy and drug treatment group *versus* the radiotherapy-only and drug-only treatment groups, respectively. *p < 0.05, **p < 0.01, ***p < 0.001, ****p < 0.0001.

irradiation. In contrast, RAD51, a key protein involved in homologous recombination repair of DNA breaks, was notably downregulated, suggesting that Milciclib may impair the DNA repair machinery, thereby enhancing the DNA damage caused by irradiation (Figure 6F). These results highlight the cooperative effects of Milciclib and irradiation in disrupting the cell cycle, promoting apoptosis, and inhibiting DNA repair pathways in radiation-resistant CRC cells.

Discussion

Colorectal cancer (CRC) is one of the leading causes of cancer-related mortality worldwide. Despite advancements in treatment modalities, the clinical prognosis of CRC patients remains poor. Radiotherapy, as one of the crucial treatment strategies, is often challenged by radioresistance. Tumor cells counteract radiation-induced DNA damage during radiotherapy by activating DNA repair mechanisms and cell cycle checkpoints, thereby enhancing their radioresistance (Morgan and Lawrence, 2015). Therefore, overcoming radioresistance and improving tumor sensitivity to radiation have become key issues in improving the prognosis of CRC patients.

Currently, chemotherapy combined with radiotherapy (chemoradiotherapy) is one of the most effective strategies for treating various human cancers, particularly CRC (Glynne-Jones et al., 2006; Wilson et al., 2006; Gerard et al., 2006). The combination of 5-fluorouracil (5-FU) and radiotherapy has

become the standard treatment regimen in CRC (Sauer et al., 2012). Studies have shown that the synergistic effect of 5-FU and radiation has been successfully applied in the clinical treatment of several cancers, including rectal cancer, pancreatic cancer, and cholangiocarcinoma (Ojima et al., 2006). 5-FU enhances the efficacy of radiotherapy by affecting multiple biological processes. For example, 5-FU increases radiosensitivity by inducing the degradation of SIRT7, thereby reducing the proportion of cells in the S phase (Kiran et al., 2015; Tang et al., 2017). In this study, we explored the potential of Milciclib, a CDK2 inhibitor, to enhance CRC cell sensitivity to radiotherapy. Our results demonstrated that Milciclib significantly inhibited CRC cell growth when used alone, with its mechanism involving the reduction of the G2/M phase cell proportion and induction of dose-dependent apoptosis. Importantly, when combined with radiotherapy, Milciclib significantly increased the radiosensitivity of both standard and radioresistant CRC cells, as evidenced by a sensitization enhancement ratio (SER) greater than 1. This suggests that, compared to existing chemoradiotherapy strategies, Milciclib not only enhances the radiotherapeutic effect but also reduces the side effects of radiotherapy by decreasing the required radiation dose. In contrast to conventional chemotherapy drugs such as 5-FU, which typically require higher sensitizing concentrations (around 10 μM) (Tang et al., 2017), our study shows that Milciclib can effectively enhance radiotherapy efficacy at concentrations as low as 0.1 μM. This marked difference highlights the superior potential of Milciclib in enhancing radiotherapy sensitivity.

Moreover, our study also reveals that Milciclib can effectively overcome radiotherapy resistance, a topic that has not been fully explored in current research. Radiotherapy resistance is a critical factor contributing to poor clinical outcomes and tumor recurrence in CRC patients (Yao et al., 2022). Only 15%–20% of patients with tumor volume reduction after radiotherapy exhibit complete responses, and their 5-year survival rate is less than 65% (Siegel et al., 2022). Milciclib, by inhibiting CDK2, significantly reverses radiotherapy resistance, reduces the DNA repair capacity of cancer cells, and enhances radiotherapy efficacy. Previous studies have indicated that CDK2 plays a key role in both homologous recombination (HR) and non-homologous end joining (NHEJ) DNA repair pathways, and the expression of Rad51 is an important marker of HR repair (Deans et al., 2006; Ceccaldi et al., 2016). We found that Milciclib could suppress Rad51 expression, reduce the DNA repair capability of radioresistant cells and significantly enhance their sensitivity to radiation. This is consistent with previous research findings.

In conclusion, our study demonstrates that Milciclib, by targeting and inhibiting CDK2, significantly enhances CRC cell sensitivity to radiotherapy and overcomes radiotherapy resistance by suppressing the G2/M checkpoint and DNA repair mechanisms. Compared to conventional chemotherapy drugs like 5-FU, Milciclib shows a stronger radiosensitizing effect at lower concentrations. Our findings provide important experimental evidence for the application of Milciclib as a radiosensitizer in CRC treatment and offer a novel therapeutic strategy to overcome radiotherapy resistance in clinical settings.

Data availability statement

The raw data supporting the conclusions of this article will be made available by the authors, without undue reservation.

Ethics statement

Ethical approval was not required for the studies on humans in accordance with the local legislation and institutional requirements because only commercially available established cell lines were used. Ethical approval was not required for the studies on animals in accordance with the local legislation and institutional requirements because only commercially available established cell lines were used.

Author contributions

JM: Conceptualization, Data curation, Formal Analysis, Investigation, Writing–original draft. SW: Data curation, Investigation, Methodology, Resources, Writing–original draft. XY: Investigation, Methodology, Writing–original draft. SS: Investigation, Methodology, Writing–original draft. YZ: Investigation, Writing–original draft. RW: Investigation, Writing–original draft. WX: Investigation, Writing–original draft. YL: Investigation, Writing–original draft. HZ: Investigation, Writing–original draft. YY: Supervision, Validation, Writing–original draft. NL: Conceptualization, Funding acquisition, Supervision, Validation, Writing–review and editing. BZ: Funding acquisition, Project administration, Supervision, Validation, Writing–review and editing.

Funding

The author(s) declare that financial support was received for the research, authorship, and/or publication of this article. This study was funded by National Natural Science Foundation of China (82073297), Key Project of Science and Technology Commission of Zhejiang Province (2022C03155 and 2023C03112), Zhejiang Provincial Program for the Cultivation of High-level Innovative Health Talents (ZWB-2020-18), Zhejiang Medical Key Discipline Foundation (ZWB-2018-02-03), Hangzhou Medical Key Discipline Foundation (HWF-2021-21-16).

Acknowledgments

We thank Dr. Jun Deng from the First Affiliated Hospital of Guangxi Medical University for their invaluable technical support in the selection of the research topic.

Conflict of interest

The authors declare that the research was conducted in the absence of any commercial or financial relationships that could be construed as a potential conflict of interest.

Generative AI statement

The author(s) declare that no Gen AI was used in the creation of this manuscript.

Publisher's note

All claims expressed in this article are solely those of the authors and do not necessarily represent those of their affiliated organizations, or those of the publisher, the editors and the reviewers. Any product that may be evaluated in this article, or claim that may be made by its manufacturer, is not guaranteed or endorsed by the publisher.

Supplementary material

The Supplementary Material for this article can be found online at: https://www.frontiersin.org/articles/10.3389/fphar.2025.1557925/full#supplementary-material

References

Ceccaldi, R., Rondinelli, B., and D'Andrea, A. D. (2016). Repair pathway choices and consequences at the double-strand break. *Trends Cell. Biol.* 26 (1), 52–64. doi:10.1016/j.tcb.2015.07.009

Deans, A. J., Khanna, K. K., McNees, C. J., Mercurio, C., Heierhorst, J., and McArthur, G. A. (2006). Cyclin-dependent kinase 2 functions in normal DNA repair and is a therapeutic target in BRCA1-deficient cancers. *Cancer Res.* 66 (16), 8219–8226. doi:10.1158/0008-5472.CAN-05-3945

Dekker, E., Tanis, P. J., Vleugels, J. L. A., Kasi, P. M., and Wallace, M. B. (2019). Colorectal cancer. *Colorectal cancer. Lancet.* 394 (10207), 1467–1480. doi:10.1016/S0140-6736(19)32319-0

Faber, E. B., Wang, N., and Georg, G. I. (2020). Review of rationale and progress toward targeting cyclin-dependent kinase 2 (CDK2) for male contraception†. *Biol. Reprod.* 103 (2), 357–367. doi:10.1093/biolre/ioaa107

Fagundes, R., and Teixeira, L. K. (2021). Cyclin E/CDK2: DNA replication, replication stress and genomic instability. *Front. Cell. Dev. Biol.* 9, 774845. doi:10.3389/fcell.2021.774845

Gerard, J. P., Conroy, T., Bonnetain, F., Bouche, O., Chapet, O., Closon-Dejardin, M. T., et al. (2006). Preoperative radiotherapy with or without concurrent fluorouracil and leucovorin in T3-4 rectal cancers: results of FFCD 9203. *J. Clin. Oncol.* 24 (28), 4620–4625. doi:10.1200/JCO.2006.06.7629

Glynne-Jones, R., Dunst, J., and Sebag-Montefiore, D. (2006). The integration of oral capecitabine into chemoradiation regimens for locally advanced rectal cancer: how successful have we been? *Ann. Oncol.* 17 (3), 361–371. doi:10.1093/annonc/mdj052

Jin, X., Ge, L. P., Li, D. Q., Shao, Z. M., Di, G. H., Xu, X. E., et al. (2020). LncRNA TROJAN promotes proliferation and resistance to CDK4/6 inhibitor via CDK2 transcriptional activation in ER+ breast cancer. *Mol. Cancer* 19 (1), 87. doi:10.1186/s12943-020-01210-9

Kiran, S., Oddi, V., and Ramakrishna, G. (2015). Sirtuin 7 promotes cellular survival following genomic stress by attenuation of DNA damage, SAPK activation and p53 response. *Exp. Cell. Res.* 331 (1), 123–141. doi:10.1016/j.yexcr.2014.11.001

Lim, T. G., Lee, S. Y., Huang, Z., Lim, D. Y., Chen, H., Jung, S. K., et al. (2014). Curcumin suppresses proliferation of colon cancer cells by targeting CDK2. *Cancer Prev. Res. (Phila)* 7 (4), 466–474. doi:10.1158/1940-6207.CAPR-13-0387

Liu, Q., Gao, J., Zhao, C., Guo, Y., Wang, S., Shen, F., et al. (2020). To control or to be controlled? Dual roles of CDK2 in DNA damage and DNA damage response. *DNA Repair (Amst)* 85, 102702. doi:10.1016/j.dnarep.2019.102702

Modest, D. P., Pant, S., and Sartore-Bianchi, A. (2019). Treatment sequencing in metastatic colorectal cancer. *Eur. J. Cancer* 109, 70–83. doi:10.1016/j.ejca.2018.12.019

Morgan, M. A., and Lawrence, T. S. (2015). Molecular pathways: overcoming radiation resistance by targeting DNA damage response pathways. *Clin. Cancer Res.* 21 (13), 2898–2904. doi:10.1158/1078-0432.CCR-13-3229

Ojima, E., Inoue, Y., Watanabe, H., Hiro, J., Toiyama, Y., Miki, C., et al. (2006). The optimal schedule for 5-fluorouracil radiosensitization in colon cancer cell lines. *Oncol. Rep.* 16, 1085–1091. doi:10.3892/or.16.5.1085

Satriyo, P. B., Su, C. M., Ong, J. R., Huang, W. C., Fong, I. H., Lin, C. C., et al. (2021). 4-Acetylantroquinonol B induced DNA damage response signaling and apoptosis via suppressing CDK2/CDK4 expression in triple negative breast cancer cells. *Toxicol. Appl. Pharmacol.* 422, 115493. doi:10.1016/j.taap.2021.115493

Sauer, R., Liersch, T., Merkel, S., Fietkau, R., Hohenberger, W., Hess, C., et al. (2012). Preoperative versus postoperative chemoradiotherapy for locally advanced rectal cancer: results of the German CAO/ARO/AIO-94 randomized phase III trial after a median follow-up of 11 years. *J. Clin. Oncol.* 30 (16), 1926–1933. doi:10.1200/JCO.2011.40.1836

Shao, Y., Liu, Z., Song, X., Sun, R., Zhou, Y., Zhang, D., et al. (2023). ALKBH5/YTHDF2-mediated m6A modification of circAFF2 enhances radiosensitivity of colorectal cancer by inhibiting Cullin neddylation. *Clin. Transl. Med.* 13 (7), e1318. doi:10.1002/ctm2.1318

Shi, X. N., Li, H., Yao, H., Liu, X., Li, L., Leung, K. S., et al. (2015). *In silico* identification and *in vitro* and *in vivo* validation of anti-psychotic drug fluspirilene as a potential CDK2 inhibitor and a candidate anti-cancer drug. *PLoS One* 10 (7), e0132072. doi:10.1371/journal.pone.0132072

Siegel, R. L., Miller, K. D., Fuchs, H. E., and Jemal, A. (2022). Cancer statistics, 2022. *CA Cancer J. Clin.* 72 (1), 7–33. doi:10.3322/caac.21708

Sung, H., Ferlay, J., Siegel, R. L., Laversanne, M., Soerjomataram, I., Jemal, A., et al. (2021). Global cancer statistics 2020: GLOBOCAN estimates of incidence and mortality worldwide for 36 cancers in 185 countries. *CA Cancer J. Clin.* 71 (3), 209–249. doi:10.3322/caac.21660

Tadesse, S., Anshabo, A. T., Portman, N., Lim, E., Tilley, W., Caldon, C. E., et al. (2020). Targeting CDK2 in cancer: challenges and opportunities for therapy. *Drug Discov. Today* 25 (2), 406–413. doi:10.1016/j.drudis.2019.12.001

Tang, M., Lu, X., Zhang, C., Du, C., Cao, L., Hou, T., et al. (2017). Downregulation of SIRT7 by 5-fluorouracil induces radiosensitivity in human colorectal cancer. *Theranostics* 7 (5), 1346–1359. doi:10.7150/thno.18804

Van Cutsem, E., Cervantes, A., Adam, R., Sobrero, A., Van Krieken, J. H., Aderka, D., et al. (2016). ESMO consensus guidelines for the management of patients with metastatic colorectal cancer. *Ann. Oncol.* 27 (8), 1386–1422. doi:10.1093/annonc/mdw235

Wahab, S., Alshahrani, M. Y., Ahmad, M. F., and Abbas, H. (2021). Current trends and future perspectives of nanomedicine for the management of colon cancer. *Eur. J. Pharmacol.* 910, 174464. doi:10.1016/j.ejphar.2021.174464

Wang, J., Yang, T., Xu, G., Liu, H., Ren, C., Xie, W., et al. (2016). Cyclin-dependent kinase 2 promotes tumor proliferation and induces Radio resistance in glioblastoma. *Transl. Oncol.* 9 (6), 548–556. doi:10.1016/j.tranon.2016.08.007

Wilson, G. D., Bentzen, S. M., and Harari, P. M. (2006). Biologic basis for combining drugs with radiation. *Semin. Radiat. Oncol.* 16 (1), 2–9. doi:10.1016/j.semradonc.2005.08.001

Yao, P. A., Wu, Y., Zhao, K., Li, Y., Cao, J., and Xing, C. (2022). The feedback loop of ANKHD1/lncRNA MALAT1/YAP1 strengthens the radioresistance of CRC by activating YAP1/AKT signaling. *Cell. Death Dis.* 13 (2), 103. doi:10.1038/s41419-022-04554-w

Zardavas, D., Ponde, N., and Tryfonidis, K. (2017). CDK4/6 blockade in breast cancer: current experience and future perspectives. *Expert Opin. Investig. Drugs* 26 (12), 1357–1372. doi:10.1080/13543784.2017.1389896

Zhou, Y., Shao, Y., Hu, W., Zhang, J., Shi, Y., Kong, X., et al. (2023). A novel long noncoding RNA SP100-AS1 induces radioresistance of colorectal cancer via sponging miR-622 and stabilizing ATG3. *Cell. Death Differ.* 30 (1), 111–124. doi:10.1038/s41418-022-01049-1

frontiers | Frontiers in Pharmacology

TYPE Original Research
PUBLISHED 27 March 2025
DOI 10.3389/fphar.2025.1529010

OPEN ACCESS

EDITED BY
Ana Podolski-Renic,
Institute for Biological Research "Siniša Stanković" – National Institute of Republic of Serbia, Serbia

REVIEWED BY
Zhirong Qi,
China-Japan Friendship Hospital, China
Zhizheng Zhao,
China Academy of Chinese Medical Sciences, China
Tong Zhang,
China Academy of Chinese Medical Sciences, China

*CORRESPONDENCE
Wenting He,
65030147@qq.com

RECEIVED 15 November 2024
ACCEPTED 27 February 2025
PUBLISHED 27 March 2025

CITATION
Li H, Zhang H and He W (2025) Enhancing survival outcomes in unresectable hepatocellular carcinoma: a prospective cohort study on the effects of Huaier granules with targeted therapy plus immunotherapy.
Front. Pharmacol. 16:1529010.
doi: 10.3389/fphar.2025.1529010

Enhancing survival outcomes in unresectable hepatocellular carcinoma: a prospective cohort study on the effects of Huaier granules with targeted therapy plus immunotherapy

Hui Li[1], Hongliang Zhang[2] and Wenting He[2]*

[1]Affiliated Tumor Hospital of Xinjiang Medical University, Urumqi, China, [2]Department of Oncology, Traditional Chinese Medicine Hospital of Xinjiang Uygur Autonomous Region, Urumqi, China

Objective: This study evaluated the clinical efficacy of Huaier granules combined with targeted therapy plus immunotherapy in patients with unresectable hepatocellular carcinoma (HCC) who had not undergone systemic treatment.

Methods: Patients with unresectable HCC and no prior treatments were recruited from the Hospital of Traditional Chinese Medicine of Xinjiang and the First Affiliated Hospital of Xinjiang Medical University between March 2022 and July 2023. Patients received targeted therapy and immunotherapy with (exposure group) or without Huaier Granules (non-exposure group). The primary endpoint was progression-free survival (PFS), with secondary endpoints including 6-month PFS rate, HCC Symptom Severity Quantitative Response, EORTC QLQ-HCC18 Score, and safety.

Results: The mPFS in the exposure group was 8.9 months compared to 5 months in the non-exposure group (P = 0.001; HR = 0.50). The 6-month PFS rates were 66.7% and 34.1% for the exposure and non-exposure groups, respectively (P = 0.001). The clinical efficacy rate of TCM symptom classification in HCC was higher in the exposure group (87.50% vs 59.09%; P = 0.001). The exposure group also showed improvement in fatigue (P = 0.023). Extrahepatic metastasis was an independent prognostic factor (HR = 1.77; P = 0.016), while Huaier granules reduced the risk of disease progression by 47% (HR = 0.53; P = 0.006). No significant differences were observed for adverse events. The most common adverse events were hypertension, proteinuria, abnormal liver function, and diarrhea.

Conclusion: Huaier granules significantly prolong PFS and improve the 6-month PFS rate, reducing disease progression risk in HCC patients. Subgroup analysis showed more pronounced benefits in patients with vascular invasion and alcohol consumption, with mPFS extending beyond 1 year.

KEYWORDS

hepatocellular carcinoma, Huaier granules, immune checkpoint inhibitors, targeted therapy, clinical efficacy

Introduction

HCC is the predominant pathological type of primary liver cancer, accounting for 75%–85% of cases (Petrick et al., 2020). According to statistics from 2022, the detection rate and mortality rate of HCC in China rank fourth and second among all malignant tumors, respectively, with new and fatal cases representing nearly half of the global total (Xia et al., 2022). The 5-year survival rate is merely 12.1%, reflecting a high incidence and poor prognosis that contribute to significant disease and economic burdens (Wang and Deng, 2023). The incidence continues to rise, and it is estimated that by 2040, there will be 1.4 million new cases globally, presenting a persistent challenge to global public health (Rumgay et al., 2022).

In China, since more than 70% of patients have no chance of receiving curative treatment at the time of initial diagnosis and require systemic therapy, the current guidelines recommend a combination of targeted therapy and immunotherapy as the first-line treatment for patients with unresectable HCC. Although this approach has improved overall survival, the PFS is around 4–6 months, highlighting an urgent need for new strategies to improve PFS. Huaier granules have been shown to reduce the postoperative recurrence rate of liver cancer by 33% and are an independent protective factor for 5-year survival ($P < 0.0001$) (Chen et al., 2018; Liu et al., 2019). The Chinese Society of Clinical Oncology (CSCO) Primary Liver Cancer Diagnosis and Treatment Guidelines 2022 Edition provides a grade II recommendation for its use in postoperative adjuvant therapy. The Chinese Integrative Therapy of Primary Liver Cancer Working Group has recommended that, following the eight principles of Zheng identification, liver cancer should be categorized according to eight basic Zheng types: qi stagnation, blood stasis, heat, (water) dampness, qi deficiency, blood deficiency, yin deficiency and yang deficiency, after retrieving, organizing and reviewing both classical and modern TCM literature, summarizing a large amount of clinical experience and examining epidemiological survey results (Ling et al., 2018). In this study, we enrolled patients who were diagnosed with Qi Deficiency and Blood Stasis Syndrome, a Traditional Chinese Medicine (TCM) classification.

It has been demonstrated that adjuvant Huaier therapy Huaier can significantly prolongs patients survival as well as improving the quality of life for patients (Shi et al., 2023). However, due to a lack of large-scale, high-level clinical studies, no explicit recommendation has been made in the guidelines. Huaier granules may have a synergistic effect with targeted therapies and immune checkpoint inhibitors (ICIs), but there is currently no evidence from clinical studies to support this. Therefore, we conducted a prospective cohort study to observe the clinical efficacy of combining Huaier granules with targeted therapy and ICIs in patients with unresectable HCC who had not received systemic treatment.

Material and methods

Study population

Patients with unresectable hepatocellular carcinoma (HCC) who had not received prior anti-tumor systemic treatment were enrolled between 1 March 2022, and 1 July 2023, at the Hospital of Traditional Chinese Medicine of Xinjiang Uygur Autonomous Region and the First Affiliated Hospital of Xinjiang Medical University. This study is registered with the Chinese Clinical Trial Registry, registration number ChiCTR2400079626, and has been approved by the Ethics Committee of the Hospital of Traditional Chinese Medicine of Xinjiang Uygur Autonomous Region (2023-GS012). Inclusion criteria: 1) Age ≥18 years; 2) unresectable locally advanced, or metastatic HCC at diagnosis, (BCLC C or unsuitable for curative surgery or local treatment at stage B); 3) Presence of measurable lesions as assessed by the Response Evaluation Criteria in Solid Tumors (RECIST) version 1.1; 4) Performance status (PS) score of 0–1 and Child-Pugh liver function score ≤7; 5) Expected survival time of more than 12 weeks; 6) received targeted therapy plus immunotherapy 7) diagnosed with Qi Deficiency and Blood Stasis Syndrome, a Traditional Chinese Medicine (TCM) classification. The TCM syndrome diagnostic criteria for Qi Deficiency and Blood Stasis Syndrome referred to the "Guiding Principles for Clinical Research of New Chinese Medicine (Trial)" (Zheng, 2002) and the "Study of a qualitative diagnostic criterion for basic syndromes of traditional Chinese medicine in patients with primary liver cancer" (Ling et al., 2005). Main Symptoms: ① Fatigue and weakness ② Lumps under the costal cartilage; Other Symptoms: ① Dull complexion or cyan and purple lips and nails ② Numbness or abdominal distension after eating ③ Pain fixed without moving; Tongue Manifestation: light and fat tongue, or purple tongue or ecchymosis; Pulse Manifestation: Weak or thin or astringent pulse. If both main symptoms ① and ② are present along with at least two or more other symptoms, a diagnosis of Qi Deficiency with Blood Stasis Syndrome can be made. This syndrome type is an indication for Huaier Granules. Exclusion criteria: 1) History of autoimmune diseases or liver transplantation; 2) Acute or chronic active hepatitis B virus (HBV) or hepatitis C virus (HCV) infection, with HBV DNA levels greater than 2,000 IU/mL or 1,054 copies/mL, HCV RNA levels greater than 10^3 copies/mL, or simultaneous positivity for hepatitis B surface antigen and anti-HCV antibodies (nucleotide antiviral therapy is permitted); 3) Central nervous system metastasis or presence of inferior vena cava tumor thrombus; 4) Interstitial lung disease or pulmonary fibrosis.

Treatments

The use of Huaier granules during treatment was considered as the exposure factor, dividing the patients into two groups: those receiving Huaier granules (exposure group) and those who did not (non-exposure group). For the exposure group: Initiation of HuaiEr Granules oral administration concurrently with ICIs and targeted therapy treatments, 20 g per granule, produced and supplied by Qidong Gaitianli Pharmaceutical Co., Ltd., at a dosage of 20 g per administration, three times daily. Exposure to Huaier granules must be maintained for at least 15 days, and targeted therapy must include a minimum of two treatment cycles. For the non-exposure group, the dosage of ICIs and targeted drugs is to be determined by the attending clinician. No other systemic anti-tumor treatments are allowed for the target lesions, but localized palliative radiotherapy for isolated lesions (non-liver lesions) and treatment for bone metastases are permitted to control symptoms.

The use of other Chinese patent medicines or herbal decoctions with confirmed anti-tumor effects is prohibited. Following enrollment, patients will undergo baseline abdominal CT or MRI scans, with follow-up scans conducted every 1.5–2 months. Traditional Chinese Medicine (TCM) symptom grading for HCC and HCC-related quality of life assessments will be conducted at baseline and 1 day prior to the third treatment cycle. Before each treatment cycle, alpha-fetoprotein (AFP) levels and safety parameters will be monitored, and adverse events, as well as concomitant medication use, will be recorded until disease progression, patient death, or the study's conclusion.

Endpoints and assessments

The primary endpoint of this study was PFS. PFS was defined as the time from the date of enrollment to the occurrence of either disease progression, death, or the end of the study. The key secondary endpoints included 6-month PFS rate, HCC Symptom Severity Quantitative Response, EORTC QLQ-HCC18 Score and safety. The formula of Six-month PFS Rate is: (Number of non-progressed patients/Total number of patients) × 100%. Improvement Rate of HCC-Related Quality of Life: Quality of life is assessed across eight dimensions, each with a maximum score of 100 points. Scores are recorded at baseline and 1 day before the third treatment cycle. For each dimension, the scores from these two time points are compared; a decrease in score compared to the baseline is considered an improvement, while unchanged or increased scores indicate no improvement. The improvement rate is calculated for each dimension.

Statistical analysis

The sample size for the cohort study was calculated using the formula:

$$n = \left(\frac{Z_\alpha \sqrt{2P\,(1-P)} + Z_\beta \sqrt{P_1\,(1-P1) + P_2\,(1-P2)}}{P_1 - P_2} \right)^2$$

Utilizing PASS 15.0 software, with a significance level (α) set at 0.05 and statistical power at 0.8 and based on literature and pre-exposure group results with P1 = 0.65 and P2 = 0.90, the calculation determined that n1 = n2 = 44. Accounting for a 10% loss to follow-up rate, the required sample size for each group was adjusted to 48, resulting in a total of 96 participants across the two groups.

The final follow-up date for this study is 30 October 2023. The PFS of the two groups was compared using SAS JMP (Pro 16.0) software for data processing. Continuous data with a normal distribution are presented as mean ± standard deviation, while data not following a normal distribution are expressed as median (interquartile range) [M (P25, P75)]. Baseline characteristics, including age, gender, alcohol consumption, BCLC stage, tumor number, presence of hepatitis, liver cirrhosis, intrahepatic metastasis, extrahepatic metastasis, vascular invasion, and AFP levels, were analyzed using the Chi-square test. For variables where the sample size did not meet the requirements of the Chi-square test, Fisher's exact test was applied.

PFS was assessed using Kaplan-Meier survival analysis to construct survival curves. Subsequently, a multivariate Cox proportional hazards analysis was employed to explore further and establish a nomogram prediction model. The receiver operating characteristic (ROC) curve was plotted, and the area under the curve (AUC) was calculated. The model's goodness-of-fit was evaluated using the Hosmer-Lemeshow test, with calibration curves constructed accordingly. Decision curve analysis (DCA) was also utilized to predict the risk of PFS events. The 6-month PFS rate was analyzed using the Chi-square test, with a significance level set at α = 0.05. A p-value of less than 0.05 was considered statistically significant.

Results

Baseline characteristics

A total of 98 participants were initially enrolled in the study. During the treatment phase, six participants were excluded: four due to the use of additional anti-tumor herbal decoctions and two who voluntarily withdrew (Figure 1). Consequently, 92 participants were included in the final efficacy analysis—48 in the exposure group and 44 in the non-exposure group. The study concluded with the final follow-up on 30 October 2023.

Baseline characteristics of the participants are summarized in Table 1. At enrollment, the two groups were balanced and comparable regarding baseline characteristics such as gender, history of alcohol consumption, history of hepatitis, AFP levels, lesion size, presence of cirrhosis, intrahepatic and extrahepatic metastasis, tumor number, vascular invasion, Child-Pugh score, and BCLC staging. The average age of the exposure group was significantly higher than that of the non-exposure group ($P = 0.009$), but this bias does not exaggerate the efficacy of the exposure group.

Survival outcomes

The exposure group had a significantly longer mPFS of 8.9 months compared to 5 months in the non-exposure group (HR = 0.50; 95% CI, 0.317–0.783; P = 0.001) as shown in Figure 2. The 6-month PFS rate was significantly higher in the exposure group compared to the non-exposure group, at 66.7% versus 34.1%, respectively, with a statistically significant difference ($P = 0.001$).

Subgroup analysis suggested that those with hepatitis, cirrhosis, vascular invasion, extrahepatic metastasis, tumor maximum diameter ≥5 cm, a history of alcohol consumption, no history of alcohol consumption or baseline AFP ≥400 ng/mL, had the prolonged mPFS in the exposure group compared to the non-exposure group, with all differences being statistically significant. Detailed results are presented in Table 2 and Supplementary Figure 1.

In patients with hepatitis, cirrhosis, vascular invasion, extrahepatic metastasis, tumor diameter ≥5 cm, the mPFS was significantly extended in the exposure group compared to the non-exposure group (9 months vs 5 months, 10 months vs 4 months, 13 months vs 3 months, 8.3 months vs 4 months, 9 months vs 4 months, and 9 months vs 5 months, respectively), all showing statistical significance ($P = 0.002$, $P = 0.003$, $P = 0.000$, $P = 0.014$, $P = 0.001$, and $P = 0.007$) (Supplementary Figure 1). In patients with a history of alcohol

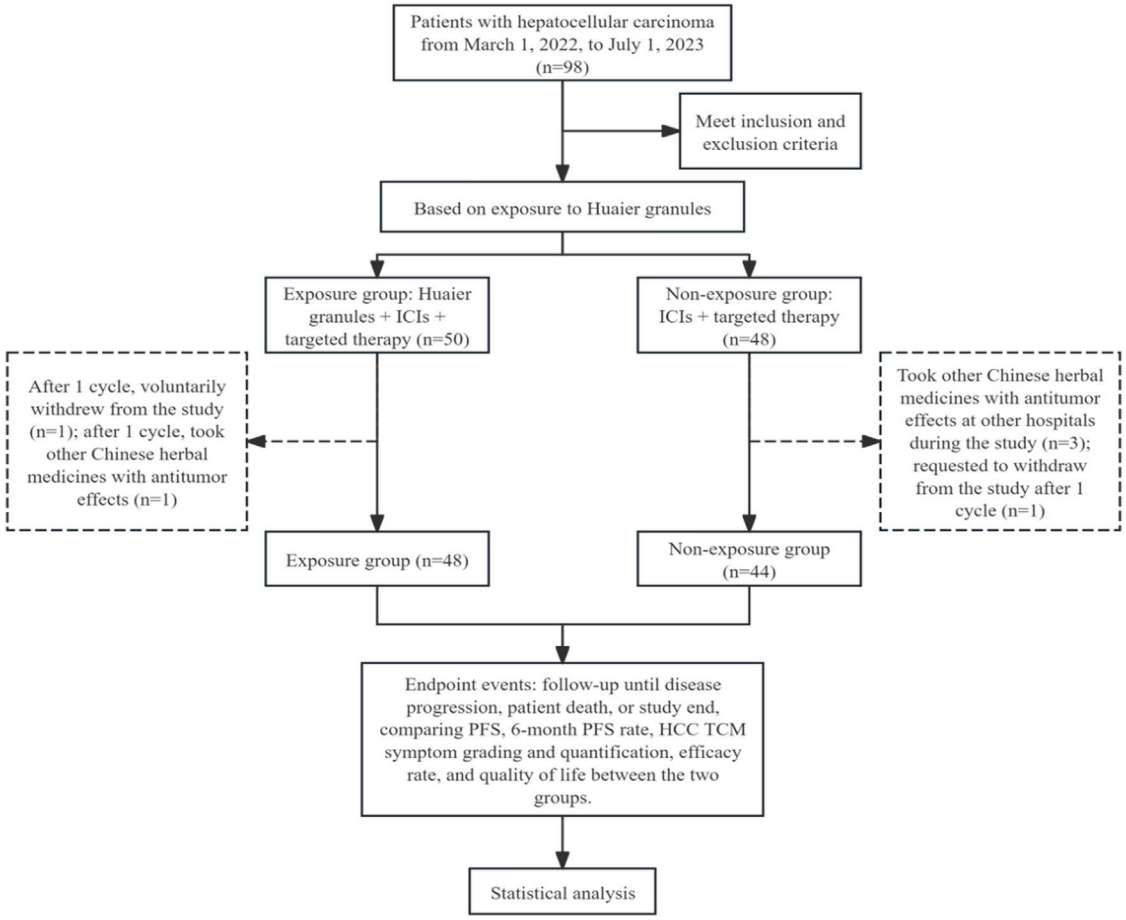

FIGURE 1
Flowchart of patient selection.

consumption, mPFS was extended by 9 months in the exposure group compared to the non-exposure group (14 months vs 5 months; P = 0.010), while in those without a history of alcohol consumption, mPFS was extended by 3.7 months (8.7 months vs 5 months; P = 0.022). For patients with baseline AFP ≥400 ng/mL, mPFS was extended by 6 months (9 months vs 3 months; P = 0.017), and for those with baseline AFP <400 ng/mL, mPFS was extended by 2.9 months (8.9 months vs 6 months; P = 0.024). All comparisons were statistically significant Supplementary Figure 1.

Safety results and liver cancer-related quality of life

The most common adverse events of any grade observed were primarily hypertension, proteinuria, abnormal liver function, diarrhea, and hypothyroidism (Table 3). All of them were of graded 1 or 2, indicating a favorable safety profile. No statistically significant difference was observed between the two groups.

This study utilized the EORTC QLQ-HCC18 scoring scale, which includes eight dimensions of quality of life related to liver cancer. Only the fatigue dimension showed a statistically significant improvement, with improvement rates of 68.75% in the exposure group versus 45.45% in the non-exposure group (P = 0.023).

COX regression model analysis

A multivariate COX proportional hazards regression model was used to explore factors influencing the prognosis of all HCC patients enrolled. PFS was used as the dependent variable, and independent variables included the presence of extrahepatic metastasis, vascular invasion, AFP ≥400 ng/mL, and treatments. Analysis indicated that extrahepatic metastasis was an independent prognostic factor, with the risk of disease progression being 1.807 times higher in patients with extrahepatic metastasis compared to those without (HR = 1.807; 95% CI, 1.138–2.867; P = 0.013). The use of Huaier Granule was identified as a protective factor (HR = 0.514; 95% CI, 0.326–0.810; P = 0.004) as shown in Table 4.

Construction of a nomogram prediction model

Based on the results of the multivariate Cox proportional hazards analysis, exposure to Huaier Granule and the presence of extrahepatic metastasis were identified as key factors for inclusion in the nomogram prediction model. The nomogram was developed (Figure 3A), with each variable assigned a specific score. By adding

TABLE 1 Baseline characteristics.

		Exposure group (n = 48)	Non-exposure Group (n = 44)	χ^2/Fisher's exact test	*P*
Gender	Male	40 (83.33%)	36 (81.82%)	0.037	0.848
	Female	8 (16.67%)	8 (18.18%)		
Drinking	Yes	15 (31.25%)	21 (47.73%)	2.626	0.105
	No	33 (68.75%)	23 (52.27%)		
History of Hepatitis	Yes	40 (83.33%)	41 (93.18%)	-	0.202#
	No	8 (16.67%)	3 (6.82%)		
AFP (ng/mL)	<400	34 (70.83%)	25 (56.82%)	1.965	0.161
	≥400	14 (29.17%)	19 (43.18%)		
Tumor	<5 cm	20 (41.67%)	15 (34.09%)	0.560	0.454
	≥5 cm	28 (58.33%)	29 (65.91%)		
Cirrhosis	Yes	23 (47.92%)	25 (56.82%)	0.730	0.392
	No	25 (52.08%)	19 (43.18%)		
Intrahepatic Metastasis	Yes	30 (62.50%)	25 (56.82%)	0.308	0.578
	No	18 (37.50%)	19 (43.18%)		
Extrahepatic Metastasis	Yes	15 (31.25%)	22 (50.00%)	3.373	0.066
	No	33 (68.75%)	22 (50.00%)		
Child-Pugh Score	A	38 (79.19%)	32 (72.73%)	0.523	0.569
	B	10 (20.83%)	12 (27.27%)		
Tumor Count	Single	8 (16.67%)	6 (13.64%)	0.164	0.685
	Multiple	40 (83.33%)	38 (86.36%)		
Vascular Invasion	Yes	19 (39.58%)	20 (45.45%)	0.324	0.569
	No	29 (60.42%)	24 (54.55%)		
BCLC Stage	B	3 (6.25%)	8 (18.18%)	-	0.074#
	C	45 (93.75%)	36 (81.82%)		
Age	-	48 (61.89 ± 1.38)	44 (56.52 ± 1.44)	9.339	0.009*

Note: * indicates that there is a statistically significant difference between the two groups with $P < 0.05$ as determined by the Chi-square test. # indicates that Fisher's exact test was used.

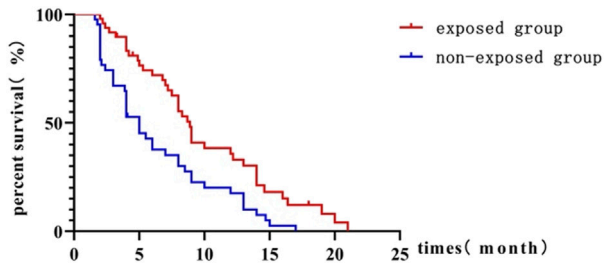

FIGURE 2
Kaplan-Meier curve comparing progression-free survival between exposed and non-exposed groups.

up these scores, the probability of PFS events for individual patients can be estimated, with a higher total score indicating a greater likelihood of PFS events.

Performance and clinical utility of the predictive model

The ROC curve was generated to evaluate the predictive accuracy of the nomogram. The area under the curve (AUC) for the 6-month follow-up prediction model was 0.713, while the AUC for the 12-month follow-up prediction model was 0.629 (Figure 3B). At the 6-month follow-up, the calibration curve of the nomogram demonstrated good concordance between predicted and observed outcomes (Figure 3C). The Hosmer-Lemeshow goodness-of-fit test indicated that the model fit was not statistically significant (P > 0.05), suggesting a good alignment with the observed data. The 12-month follow-up exhibited similar results, though the model's fit was superior at 6 months compared to 12 months. Decision curve analysis (DCA) was conducted using the nomogram prediction model to evaluate PFS events for the selected variables. The analysis showed that at the 6-month follow-up, the net benefit of predicting PFS event risk using the nomogram was higher for threshold probabilities

TABLE 2 Subgroup analysis of PFS between two groups.

Subgroup		PFS (95%CI)		Chi-square value (χ^2)	*P*
		Exposure group	Non-exposure group		
Hepatitis		9 (7.2.13)	5 (4.8)	9.3988	0.0022*
Cirrhosis		10 (5.14)	4 (3.6)	8.8167	0.0030*
Vascular invasion	Yes	13 (6.20)	3 (2.7)	12.8767	0.0003*
	No	8.3 (6.8.9)	6 (4.10)	0.9702	0.3246
Drinking	Yes	14 (7.19)	5 (2.9)	6.6855	0.0097*
	No	8.7 (5.3.9)	5 (3.8)	5.2260	0.0223*
Tumor size	≥5 cm	9 (6.14)	4 (2.1.6)	12.2333	0.0005*
	<5 cm	8 (4.2.12)	8 (4.13)	0.8193	0.3564
Sintilimab plus bevacizumab	Yes	6.8 (4.10)	5 (2.1.8)	2.0846	0.1488
	No	9 (7.5.14)	5 (3.9)	7.3017	0.0069*
Sintilimab	Yes	9 (7.5.13)	5 (3.10)	3.3245	0.0683
AFP level (ng/mL)	<400	8.9 (7.2.12.2)	6 (4.8.5)	5.0665	0.0244*
	≥400	9 (4.14.6)	3 (2.8)	5.7314	0.0167*
Extrahepatic metastasis	Yes	8.3 (4.12.2)	4 (2.5)	5.996	0.014*
	No	9 (6.8.14)	8 (3.9.10)	3.641	0.056

*Indicates a statistically significant difference between the two groups.

TABLE 3 Incidence of Adverse events.

	Exposure group (n = 48)	Non-exposure group (n = 44)	χ^2/Fisher's exact test	*P*
Hypertension	3 (6.25%)	7 (15.91%)	-	0.133#
Proteinuria	15 (31.25%)	8 (18.18%)	2.121	0.145*
Abnormal Liver Function (Baseline Normal, Post-Treatment Abnormal)	15 (31.25%)	7 (15.91%)	3.032	0.082
Diarrhea	13 (27.08%)	9 (20.45%)	0.557	0.455
Hypothyroidism	18 (37.5%)	19 (43.18%)	0.308	0.579

*Chi-square test, $P > 0.05$ indicates no statistical significance.
#Fisher's Exact Test.

TABLE 4 Multivariate cox analysis of factors influencing disease progression.

Factor	β	SE	Wald χ^2	*P*	HR	95%CI
Extrahepatic metastasis (Yes/No)	0.296	0.118	6.152	0.013	1.807	1.138–2.867
Huaier granule (Yes/No)	0.333	0.116	8.217	0.004	0.514	0.326–0.810

between 0 and 0.680. At the 12-month follow-up, the net benefit was higher for threshold probabilities between 0 and 0.830 (Figure 3D).

Discussion

In this prospective cohort study, we demonstrated that the inclusion of Huaier granules alongside standard targeted therapy and immunotherapy markedly improved progression-free survival in patients with unresectable hepatocellular carcinoma (HCC), extending median PFS from 5 months in the non-exposure group to 8.9 months in the exposure group (P = 0.001; HR = 0.50; 95% CI 0.32–0.78). This significant enhancement not only underscores the potential of Huaier granules as an effective adjunct in HCC treatment. Furthermore, our findings highlight a notable improvement in the quality of life, particularly in reducing fatigue, which is often one of the most debilitating symptoms for cancer patients, thereby supporting the integration of traditional Chinese

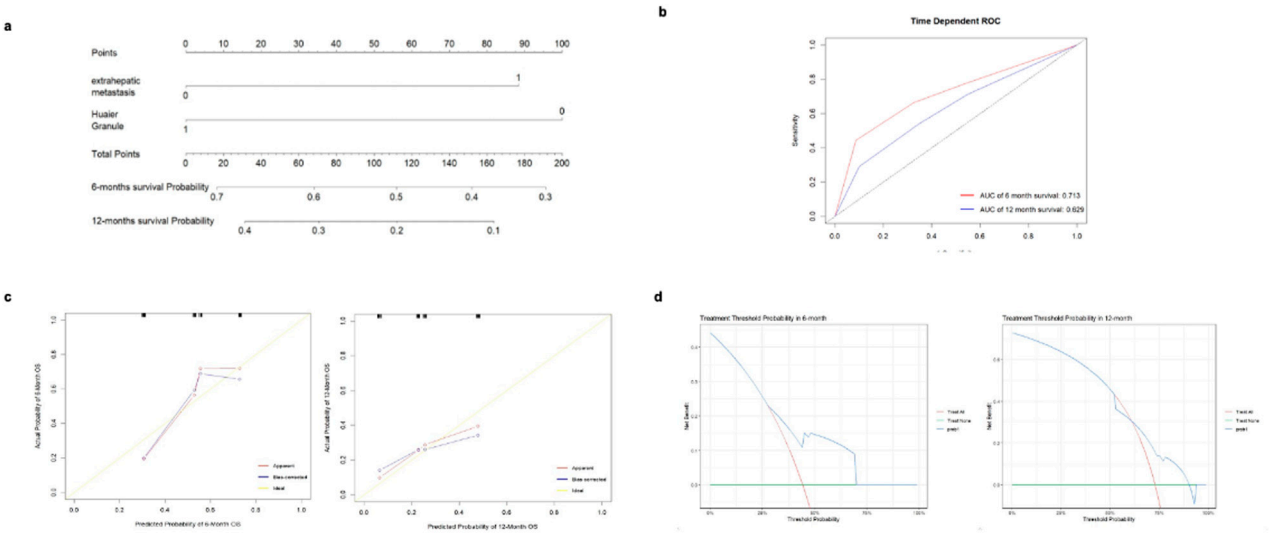

FIGURE 3
Analysis of predictive accuracy for 6 and 12-month survival probabilities. **(A)** nomogram for predicting the risk of PFS events. **(B)** ROC curve for predicting the risk of PFS events using the cox proportional hazards model. **(C)** Calibration curve of the nomogram for predicting the risk of PFS events. **(D)** Decision curve for the nomogram prediction model of PFS events.

medicine in modern oncologic care regimens. The primary bioactive constituents of Huaier consist of fungal-derived compounds, including polysaccharides, proteins, ketones, alkaloids, and minerals, which are part of the main essential nutrients required for the body to function and maintain overall health to avoid fatigue. From the TCM perspective, Huaier can also enhance Qi, invigorate blood, and resolve blood stasis, which make Qi and blood move through the body very well to help fight fatigue. Not only was quality of life improvement observed in our study as first-line treatment setting, but also it was shown the same as adjuvant therapy (Shi et al., 2023).

In vitro experiments and animal experiment data revealed the underlying anti-HCC mechanism of Huaier and further showed that Huaier had synergistic effect with targeted therapy of sorafenib. Li X. et al. (2024) observed that HP showed a weaker proliferation inhibitory effect on the mouse source and human HCC cells *in vitro* but exhibited stronger anti-HCC effects in animals. And nude mice models confirmed that macrophages play an important role in the anti-HCC effect of Huaier. Zhang et al. (2024) utilized 7-day-old goldfish embryos as hosts and successfully established an orthotopic xenograft model of HCC in goldfish livers. They evaluated the efficacy of the targeted therapy drug Sorafenib and Huaier granules, alone or in combination in the goldfish HCC orthotopic xenograft model and found that the combination therapy showed the best efficacy against HCC cells in terms of macrophage infiltration, polarization as well as tumor cells proliferation, metastasis and apoptosis.

In the subgroup analysis of patients with a history of alcohol consumption, the PFS of the exposure group was significantly extended to 14 months. This is related to the well-documented effect of moderate alcohol consumption in improving the tumor microenvironment, enhancing T-cell activation, and boosting immune responses (Bonavita et al., 2020). Huaier granules can upregulate PD-L1 expression in tumor tissues, positively modulating immune function (Li H. et al., 2024). Therefore, a history of alcohol consumption may enhance T-cell activation and improve immune responses, combined with the immunoregulatory effects of ICIs and Huaier granules, contributing to prolonged PFS. A similar trend was observed in the hepatitis subgroup, likely related to the role of inflammatory factors in improving the immune microenvironment. Vascular invasion is recognized as a critical marker of poor prognosis, representing greater invasiveness and metastatic potential, significantly shortening patient survival (Li et al., 2020). In this study, we found that in the subgroup with vascular invasion, patients treated with Huaier granules experienced a significant extension of PFS to 13 months. This effect may be related to Huaier granules' ability to inhibit tumor angiogenesis and suppress tumor metastasis (Li et al., 2020).

In China, most HCC cases occur against the background of viral hepatitis and cirrhosis. Statistics show that approximately 20% of hepatitis patients eventually develop cirrhosis, with nearly 80% potentially progressing to HCC (Rizzo et al., 2022). In our study, the subgroup analysis of cirrhosis patients demonstrated that combining Huaier granules extended PFS to 10 months. Huaier granules may exert their effects by enhancing Qi, invigorating blood, and resolving blood stasis. These actions can inhibit inflammatory factors and the epithelial-mesenchymal transition, thereby slowing the progression of cirrhosis (Luo et al., 2023). By delaying the progression of cirrhosis, liver function can be preserved, which in turn improves the tolerance of HCC patients to anti-tumor treatments, ultimately enhancing patient survival.

In this study, the treatment subgroup analysis included patients who received sintilimab combined with bevacizumab. The results indicate variable efficacy when sintilimab was part of the therapeutic regimen. For patients treated with sintilimab plus bevacizumab, the mPFS was 6.8 months, compared to 5 months in patients who did not receive this combination, although this difference did not reach statistical significance (P = 0.1488). In the subgroup receiving sintilimab alone, mPFS extended to 9 months, compared to 5 months for those not treated with sintilimab, suggesting a

more favorable outcome, although this result approached but did not reach statistical significance (P = 0.0683). These findings suggest a potential benefit of sintilimab in extending PFS among patients with unresectable hepatocellular carcinoma when used in combination with other treatments, although the benefits vary depending on the combination of therapies used. Further studies are warranted to clarify the specific impact of sintilimab, particularly in combination regimens, to better understand its role in the management of hepatocellular carcinoma.

AFP was initially identified as a specific tumor marker in serum, later confirmed to exist in tumor cell cytoplasm, functioning as an oncogene (Chen et al., 2020). As a tumor marker, AFP assists in diagnosing HCC and predicting prognosis, but as an oncogene, it resists apoptosis, promotes proliferation, migration, and invasion of tumor cells (Zhang et al., 2020; Li H. et al., 2021), inhibits immune function, and facilitates immune evasion (Munson et al., 2023). In HCC treatment, AFP is a key cytokine leading to resistance against anti-tumor therapies. Studies have found that silencing the AFP gene can enhance the efficacy of treatments like all-trans retinoic acid analogs for HCC (Li W. et al., 2021). Based on the aforementioned reasons, the poor prognosis associated with high serum AFP levels is primarily due to its function as an oncogene that promotes tumor initiation, progression, and metastasis. Studies have shown that the traditional Chinese medicine, Huaier granules, can reduce the expression of serum AFP (Shi et al., 2024). In our previous research, we found that Huaier granules can downregulate AFP expression, leading to more significant benefits in patients with high AFP expression by inhibiting tumor growth.

Results indicate that extrahepatic metastasis is an independent prognostic factor, with a disease progression risk 1.807 times higher in patients with extrahepatic metastasis than those without (*HR* = 1.807, 95% CI 1.138–2.867, *P* = 0.013). The combination with Huaier granules was identified as a protective factor (*HR* = 0.514, 95% CI 0.326–0.810, *P* = 0.004). Therefore, patients with extrahepatic metastasis and without exposure to Huaier granules are more likely to experience disease progression. From the perspective of traditional Chinese medicine, according to the Pharmacopoeia, Huaier has a bitter taste and is non-toxic, functioning to "treat wind, break blood, and enhance strength," promoting vital energy and blood circulation while eliminating tumors. It is thought that the core pathogenesis of liver cancer involves an underlying deficiency (Chang et al., 2023), with subsequent treatments like surgery, chemotherapy, radiotherapy, and targeted therapies further depleting vital energy. Vital energy deficiency persists throughout HCC, suggesting that herbal interventions should be integrated into liver cancer treatment, including post-surgery and in combination with localized or molecular-targeted therapies in intermediate and advanced stages. It has been confirmed that integrating Chinese herbal medicine can synergistically inhibit tumor growth and improve patients' quality of life (Wang et al., 2019). Basic research indicates that herbal medicine can upregulate immune responses, inhibit tumor growth and metastasis, and promote tumor cell apoptosis (Wang et al., 2020).

However, this study has several limitations that warrant careful consideration when interpreting its results. First, the follow-up period, concluding in October 2023, does not allow for a comprehensive assessment of long-term outcomes such as overall survival, suggesting a need for extended follow-up to more accurately evaluate the treatment's efficacy. An extension phase of survival follow up is ongoing by collecting patients' death events through phone call every 3 months. In addition, the lack of blinding for both patients and clinicians could introduce bias, particularly in subjective assessments such as quality of life. The use of diagnostic criteria based on Traditional Chinese Medicine, specifically Qi Deficiency and Blood Stasis Syndrome, may not resonate in non-TCM clinical settings. Future research will use blinding to mitigate and limit the occurrence of conscious and unconscious biases. Several relative points will be considered, including clinical supply planning, dispensing and inventory management, and disclosure of unplanned unblinding events. Lastly, despite efforts to balance baseline characteristics, the potential influence of unmeasured confounding factors, including lifestyle and genetic disparities, cannot be discounted.

In conclusion, the results of this study illustrate the significant clinical benefit of incorporating Huaier granules with standard targeted therapy and immunotherapy in the treatment of unresectable hepatocellular carcinoma. The use of Huaier granules led to a substantial extension of progression-free survival and was associated with notable improvements in the quality of life, specifically in managing fatigue. These findings suggest that Huaier granules can play a crucial role in enhancing the efficacy of existing cancer therapies while simultaneously managing symptoms, thereby providing a dual therapeutic benefit. Furthermore, the safety profile of this combination therapy proved to be favorable, encouraging its use in clinical practice. This study not only supports the incorporation of traditional Chinese medicine into contemporary treatment paradigms but also calls for further investigation into its mechanisms and potential benefits across different patient subgroups. Future research should focus on randomized, blinded, controlled trials to confirm these results and to explore the long-term outcomes and optimal integration of Huaier granules in the management of liver cancer.

Data availability statement

The raw data supporting the conclusions of this article will be made available by the authors, without undue reservation.

Ethics statement

The studies involving humans were approved by Ethics Committee of the Hospital of Traditional Chinese Medicine of Xinjiang Uygur Autonomous Region. The studies were conducted in accordance with the local legislation and institutional requirements. The participants provided their written informed consent to participate in this study.

Author contributions

HL: Investigation, Methodology, Software, Writing–original draft. HZ: Validation, Visualization, Writing–original draft. WH: Writing–review and editing.

Funding

The author(s) declare that no financial support was received for the research, authorship, and/or publication of this article.

Conflict of interest

The authors declare that the research was conducted in the absence of any commercial or financial relationships that could be construed as a potential conflict of interest.

Generative AI statement

The author(s) declare that no Generative AI was used in the creation of this manuscript.

Publisher's note

Supplementary material

The Supplementary Material for this article can be found online at: https://www.frontiersin.org/articles/10.3389/fphar.2025.1529010/full#supplementary-material

SUPPLEMENTARY FIGURE 1
Kaplan-Meier survival curves comparing clinical outcomes of exposed and non-exposed groups across various subgroups.

References

Bonavita, E., Bromley, C. P., Jonsson, G., Pelly, V. S., Sahoo, S., Walwyn-Brown, K., et al. (2020). Antagonistic inflammatory phenotypes dictate tumor fate and response to immune checkpoint blockade. *Immunity* 53 (6), 1215–1229. e8. doi:10.1016/j.immuni.2020.10.020

Chang, X., Chang, C., Chang, Q., and Zeng, Z. (2023). Discussing the pathogenesis and treatment of primary liver cancer from the perspective of 'life instinct. *Chin. J. Integr. Traditional West. Med. Liver Dis.* 33 (05), 444–446.

Chen, Q., Shu, C., Laurence, A. D., Chen, Y., Peng, B. G., Zhen, Z. J., et al. (2018). Effect of Huaier granule on recurrence after curative resection of HCC: a multicentre, randomised clinical trial. *Gut* 67 (11), 2006–2016. doi:10.1136/gutjnl-2018-315983

Chen, W., Peng, J., Ye, J., Dai, W., Li, G., and He, Y. (2020). Aberrant AFP expression characterizes a subset of hepatocellular carcinoma with distinct gene expression patterns and inferior prognosis. *J. Cancer* 11 (2), 403–413. doi:10.7150/jca.31435

Li, H., Liu, Y., Jiang, W., Xue, J., Cheng, Y., Wang, J., et al. (2021a). Icaritin promotes apoptosis and inhibits proliferation by down-regulating AFP gene expression in hepatocellular carcinoma. *BMC Cancer* 21, 318–412. doi:10.1186/s12885-021-08043-9

Li, H., You, J., Wei, Y., Zheng, L., Yang, J., Xu, J., et al. (2024b). Huaier improves the efficacy of anti-PD-L1 Ab in the treatment of hepatocellular carcinoma by regulating tumor immune microenvironment. *Phytomedicine* 123, 155189. doi:10.1016/j.phymed.2023.155189

Li, J., Hongzhi, Y., and Junli, M. (2020). Zhenqi Fuzheng granules inhibit angiogenesis in rats with hepatocellular carcinoma via the miR-200c/ZEB pathway. *Chin. J. Comp. Med.* 30 (6), 31–38.

Li, W., Liu, K., Chen, Y., Zhu, M., and Li, M. (2021b). Role of alpha-fetoprotein in hepatocellular carcinoma drug resistance. *Curr. Med. Chem.* 28 (6), 1126–1142. doi:10.2174/0929867327999200729151247

Li, X., Zhang, H., Deng, Y., Fang, Q., Zhang, X., Ding, S., et al. (2024a). Huaier polysaccharides inhibits hepatocellular carcinoma via gut microbiota mediated M2 macrophage polarization. *Int. J. Biol. Macromol.* 293, 139357. doi:10.1016/j.ijbiomac.2024.139357

Ling, C. Q., Fan, J., Lin, H. S., Shen, F., Xu, Z. Y., Lin, L. Z., et al. (2018). Clinical practice guidelines for the treatment of primary liver cancer with integrative traditional Chinese and Western medicine. *J. Integr. Med.* 16 (4), 236–248. doi:10.1016/j.joim.2018.05.002

Ling, C. Q., Liu, Q., Li, D. T., Yue, X. Q., Hou, F. G., Zhu, D. Z., et al. (2005). Study of a qualitative diagnostic criterion for basic syndromes of traditional Chinese medicine in patients with primary liver cancer. *Zhong Xi Yi Jie He Xue Bao* 3 (2), 95–98. doi:10.3736/jcim20050204

Liu, X., Li, M., Wang, X., Dang, Z., Yu, L., Wang, X., et al. (2019). Effects of adjuvant traditional Chinese medicine therapy on long-term survival in patients with hepatocellular carcinoma. *Phytomedicine* 62, 152930. doi:10.1016/j.phymed.2019.152930

Luo, K. F., Zhou, L. X., Wu, Z. W., Tian, Y., Jiang, J., and Wang, M. H. (2023). Molecular mechanisms and therapeutic applications of huaier in breast cancer treatment. *Front. Pharmacol.* 14, 1269096. doi:10.3389/fphar.2023.1269096

Munson, P. V., Adamik, J., Hartmann, F. J., Favaro, P. M. B., Ho, D., Bendall, S. C., et al. (2023). Polyunsaturated fatty acid–bound α-fetoprotein promotes immune suppression by altering human dendritic cell metabolism. *Cancer Res.* 83 (9), 1543–1557. doi:10.1158/0008-5472.CAN-22-3551

Petrick, J. L., Florio, A. A., Znaor, A., Ruggieri, D., Laversanne, M., Alvarez, C. S., et al. (2020). International trends in hepatocellular carcinoma incidence, 1978–2012. *Int. J. cancer* 147 (2), 317–330. doi:10.1002/ijc.32723

Rizzo, G. E. M., Cabibbo, G., and Craxì, A. (2022). Hepatitis B virus-associated hepatocellular carcinoma. *Viruses* 14 (5), 986. doi:10.3390/v14050986

Rumgay, H., Arnold, M., Ferlay, J., Lesi, O., Cabasag, C. J., Vignat, J., et al. (2022). Global burden of primary liver cancer in 2020 and predictions to 2040. *J. hepatology* 77 (6), 1598–1606. doi:10.1016/j.jhep.2022.08.021

Shi, K., Bi, Y., Zeng, X., and Wang, X. (2023). Effects of adjuvant huaier granule therapy on survival rate of patients with hepatocellular carcinoma. *Front. Pharmacol.* 14, 1163304. doi:10.3389/fphar.2023.1163304

Shi, X., and Lu, J. (2024). *Clinical Study on huaier granules Combined with western Medicine for Patients with advanced primary liver cancer undergoing transcatheter arterial chemoembolization*. *New Chin. Med.* 56 (01), 191–195.

Wang, D., Wu, C., Liu, D., Zhang, L., Long, G., Hu, G., et al. (2019). Ginsenoside Rg3 inhibits migration and invasion of nasopharyngeal carcinoma cells and suppresses epithelial mesenchymal transition. *BioMed Res. Int.* 2019 (1), 8407683. doi:10.1155/2019/8407683

Wang, Y., and Deng, B. (2023). Hepatocellular carcinoma: molecular mechanism, targeted therapy, and biomarkers. *Cancer Metastasis Rev.* 42 (3), 629–652. doi:10.1007/s10555-023-10084-4

Wang, Y., Zhang, Q., Chen, Y., Liang, C. L., Liu, H., Qiu, F., et al. (2020). Antitumor effects of immunity-enhancing traditional Chinese medicine. *Biomed. and Pharmacother.* 121, 109570. doi:10.1016/j.biopha.2019.109570

Xia, C., Dong, X., Li, H., Cao, M., Sun, D., He, S., et al. (2022). Cancer statistics in China and United States, 2022: profiles, trends, and determinants. *Chin. Med. J.* 135 (05), 584–590. doi:10.1097/CM9.0000000000002108

Zhang, C., Zhang, J., Wang, J., and Yan, Y. (2020). Alpha-fetoprotein accelerates the progression of hepatocellular carcinoma by promoting Bcl-2 gene expression through an RA-RAR signalling pathway. *J. Cell. Mol. Med.* 24 (23), 13804–13812. doi:10.1111/jcmm.15962

Zhang, F., Qu, Z., Zeng, J., Yu, L., Zeng, L., and Li, X. (2024). A novel goldfish orthotopic xenograft model of hepatocellular carcinoma developed to evaluate antitumor drug efficacy. *Fish. Shellfish Immunol.* 155, 109998. doi:10.1016/j.fsi.2024.109998

Zheng, X. Y. (2002). *Guiding principles of clinical research on new drugs of Chinese medicines*. Beijing: China Medical Science and Technology Press.

frontiers | Frontiers in Pharmacology

TYPE Original Research
PUBLISHED 17 April 2025
DOI 10.3389/fphar.2025.1571786

OPEN ACCESS

EDITED BY
Milica Pešić,
University of Belgrade, Serbia

REVIEWED BY
Aleksandra Jaukovic,
University of Belgrade, Serbia
Danyu Du,
Fourth Military Medical University, China
Zhu Xu,
First Affiliated Hospital of Anhui Medical University, China

*CORRESPONDENCE
Youcheng Zhang,
zhangyouchengphd@163.com
Shuping Wang,
wangsp16@126.com

†These authors have contributed equally to this work

RECEIVED 06 February 2025
ACCEPTED 31 March 2025
PUBLISHED 17 April 2025

CITATION
Li J, Yong T, Chen Y, Zeng T, Zhang K, Wang S and Zhang Y (2025) Targeting PCNA/PARP1 axis inhibits the malignant progression of hepatocellular carcinoma.
Front. Pharmacol. 16:1571786.
doi: 10.3389/fphar.2025.1571786

Targeting PCNA/PARP1 axis inhibits the malignant progression of hepatocellular carcinoma

Jipin Li[1,2†], Tao Yong[1,2†], Yali Chen[2], Tingyu Zeng[2], Kaifeng Zhang[2], Shuping Wang[2*] and Youcheng Zhang[1*]

[1]Department of General Surgery, The Second Hospital of Lanzhou University, Lanzhou, China, [2]Key Laboratory of Preclinical Study for New Drugs of Gansu Province, Institute of Biochemistry and Molecular Biology, School of Basic Medical Sciences, Lanzhou University, Lanzhou, China

Introduction: Proliferating cell nuclear antigen (PCNA) is associated with the proliferation and recurrence of various cancers, and its high expression is associated with poor prognosis in hepatocellular carcinoma (HCC) patients. However, the mechanistic role of PCNA in HCC progression remains poorly understood. This study aimed to investigate how PCNA regulates DNA damage repair and cell cycle progression in HCC, with a focus on its interaction with poly (ADP-ribose) polymerase 1 (PARP1) and therapeutic implications.

Methods: PCNA was targeted genetically and pharmacologically in HCC cells to assess its effects on DNA damage repair and cell cycle arrest. Protein-protein interactions between PCNA and PARP1 were validated through co-immunoprecipitation and functional assays. The sensitivity of HCC cells to the PARP1 inhibitor Olaparib was evaluated under PCNA inhibition. Synergistic effects of AOH1160 (a PCNA inhibitor) and Olaparib were tested in vitro and in vivo using proliferation assays, DNA damage quantification, and cell cycle analysis. Prognostic relevance of PCNA expression was analyzed using TCGA datasets.

Results: Targeting PCNA suppressed DNA damage repair and induced cell cycle arrest in HCC cells. Mechanistically, PARP1 was identified as a downstream target of PCNA and directly interacted with PCNA. Inhibiting the expression or activity of PCNA increased the sensitivity of HCC cells to the PARP1 inhibitor, Olaparib. In addition, AOH1160 and Olaparib synergistically inhibited the proliferation, DNA damage repair and cell cycle progression of HCC cells. Elevated PCNA levels correlated with unfavorable HCC prognosis, supporting its role as a therapeutic biomarker. In vivo experiments also confirmed that repression of the PCNA/PARP1 axis significantly reduced HCC tumor growth.

Discussion: This study elucidates the relationship between PCNA and PARP1 in regulating the malignant progression of HCC, and highlight the pivotal role of PCNA/PARP1 axis in DNA damage repair and cell cycle progression. The correlation between elevated PCNA levels and unfavorable prognosis underscores its potential as a therapeutic biomarker. Repression of PCNA/PARP1 axis significantly inhibits the malignant proliferation of HCC cells both in vitro and in vivo. Collectively, the study provides a mechanistic foundation for therapies targeting PCNA/PARP1 axis.

KEYWORDS

hepatocellular carcinoma, PCNA, PARP1, DNA damage repair, cell cycle progression

1 Introduction

Hepatocellular carcinoma (HCC) is a common malignancy and one of the leading causes of cancer-related death worldwide (Dopazo et al., 2024; Sankar et al., 2024). In particular, the incidence of HCC in China accounts for over 50% of the global total (Rumgay et al., 2022). Because the subtle early symptoms of HCC, many patients are diagnosed at an advanced stage. At this stage, HCC shows significant invasiveness and metastatic potential, resulting in an extremely high mortality rate, making it become one of the most difficult malignancies to treat (Dopazo et al., 2024; Sankar et al., 2024; Yang et al., 2024). Surgical resection is currently the most effective curative treatment for HCC patients with localized lesions, however, it is not available for more than 50% of HCC at advanced stage (Vogel et al., 2022; Brown et al., 2023). Systematic chemotherapy has become the main treatment for advanced HCC. Besides, there have been significant advances in the systemic treatment options for HCC over the past few decades, with several approvals of immune checkpoint inhibitors and tyrosine kinase inhibitors in patients with HCC (Rimassa et al., 2023; Sankar et al., 2024). Despite the emergence of new systemic therapies, survival for patients with advanced HCC remains poor, most patients with advanced HCC still suffer from therapeutic resistance and disease malignant progression (Brown et al., 2023; Lei et al., 2024). Meanwhile, the side effects of systemic chemotherapy seriously affect the life quality of patients. With the development of sequencing technology and bioinformatics, novel targets and pathways driving the malignant progression of HCC have been rapidly discovered (Yang et al., 2024; Suresh et al., 2023). Therefore, identification of novel targets and discovery of innovative targeted therapies have potential to improve survival and quality of life for patients with challenging HCC.

Proliferating cell nuclear antigen (PCNA) is a ring-shaped homotrimer protein, and it is evolutionarily well conserved found in all eukaryotic species from yeast to humans, reflecting its essential role in cellular processes (Cardano et al., 2020). The overall structure of PCNA resembles a sliding clamp around DNA, which is crucial for its role in DNA replication (Arbel et al., 2021; Shao et al., 2023). PCNA serves as a processivity factor for DNA polymerase and is regulated by cell cycle checkpoints to maintain genomic integrity and prevent the propagation of DNA errors (Cazzalini et al., 2003). PCNA is not only involved in DNA replication, but also in other vital cellular processes such as DNA damage repair, chromatin remodeling, and cell cycle progression (Boehm et al., 2016). Mechanistically, PCNA interacts with its binding partner PCNA clamp-associated factor (PCLAF/PAF15/KIAA0101) to stabilize the trimeric conformation of PCNA, thereby facilitating the recruitment of DNA polymerases to replication forks and ensuring efficient DNA synthesis (Xie et al., 2024). Beyond replication, the PCNA-PCLAF complex orchestrates DNA repair pathway selection and modulates cell cycle checkpoints, particularly under genotoxic stress (Kim B. et al., 2024). Notably, PCNA is frequently overexpressed in highly proliferating tumor cells, where it functions as both a biomarker of uncontrolled proliferation and a promising therapeutic target. Elevated PCNA levels are associated with poor prognosis in various cancers (Suresh et al., 2023). Emerging evidence indicates that PCNA drives the malignant progression of cancer through modulating various pathophysiological processes. For instance, phosphorylation of PCNA at tyrosine 211 (Y211) has been shown to promote metastatic dissemination and sustain cancer stemness, highlighting its role in tumor evolution (Wang et al., 2022). Meanwhile, PCNA on cell surface can enhance immune evasion by prevention of natural killer cells activation and degranulation through the inhibitory receptor NKp44 (Kundu et al., 2019; Knaneh et al., 2023). Furthermore, PCNA participates in the DNA damage repair of various tumors by regulating or interacting with other factors such as nuclear insulin-like growth factor 1 receptor (IGF1R) and a nuclease scaffold SLX4 (Waraky et al., 2017; Yang et al., 2020; Kim S. et al., 2024). This suggests that targeted inhibition of PCNA expression or activity may be an effective strategy to inhibit cancer cell proliferation (Kwan et al., 2024). Previous studies have shown that PCNA is overexpressed in HCC tissues compared to normal liver tissues, and is associated with aggressive tumor behavior, poor differentiation, and unfavorable clinical outcomes, suggesting that PCNA may be a potential target for the treatment of HCC (Cheng et al., 2020; Shen et al., 2022).

In recent years, targeted DNA damage response network strategies have achieved remarkable results in the treatment of cancer (Groelly et al., 2023). Indubitability, poly (ADP-ribose) polymerase (PARP) inhibitors represented by Olaparib are the most successful representatives and have been used in the clinical treatment of breast cancer, ovarian cancer, prostate cancer, colon cancer, pancreatic cancer, and other cancers (Morganti et al., 2024; Zeng et al., 2024). Similar to PCNA, PARP1 is another important DNA repair signaling molecule that is overexpressed in many cancers and associated with poor prognosis. PARP1 plays a crucial role in DNA single-strand breaks (SSBs) repair through the base excision repair (BER) pathway (Wei et al., 2024; Laspata et al., 2024). When the expression or enzymatic activity of PARP1 is inhibited, SSBs accumulate and eventually lead to double-strand breaks (DSBs) during DNA replication. If the homologous recombination (HR) repair pathway, the precise DNA DSBs repair pathway, is not activated at this time, it will lead to a large accumulation of DNA fragments, resulting in chromosome instability and cell death (Wei et al., 2024; Zhang and Zha, 2024; Laspata et al., 2023). Based on synthetic lethality, PARP inhibitors have been widely used in the treatment of cancers with HR deficiency. However, only a small portion of cancers exhibit HR deficiency, and the majority of cancer patients still do not benefit from PARP inhibitors (Li et al., 2020). Meanwhile, the issue of resistance to PARP inhibitors also limits its clinical application (Dilmac and Ozpolat, 2023). PCNA is the center of DNA replication and DNA damage repair and plays an important role in coordinating the function of protein factors such as polymerase δ (Cazzalini et al., 2003). Importantly, the repair of DNA damage is tightly regulated by cell cycle checkpoints, which act as surveillance mechanisms to ensure genomic stability. In response to DNA damage, key checkpoint kinases such as ATM (ataxia-telangiectasia mutated) and ATR (ataxia-telangiectasia and Rad3-related) activate downstream effectors, including CHK1 and CHK2, to halt cell cycle progression and facilitate repair (Smith et al., 2020). If damage is beyond repair, these pathways can induce apoptosis or senescence to prevent malignant transformation. Given that both PCNA and PARP1 are closely linked to DNA replication stress and repair, investigating the molecular mechanism of PCNA in

regulating DNA damage repair and the regulatory relationship between PCNA and PARP1 can not only provide a novel strategy for targeted therapy of HCC but also expand the clinical indication of PARP inhibitors.

Herein, we delineate the mechanistic interplay between PCNA and PARP1 in HCC progression and therapeutic resistance. We demonstrate that PCNA directly interacts with PARP1 to sustain DNA repair proficiency and cell cycle progression. Genetic or pharmacological PCNA inhibition sensitizes HCC cells to Olaparib by impairing compensatory DDR pathways. Furthermore, the PCNA inhibitor AOH1160 synergizes with Olaparib to suppress HCC growth *in vitro* and *in vivo*. Our findings establish the PCNA/PARP1 axis as a key regulator of HCC malignancy and provide theoretical support for combining PCNA inhibitors with PARP inhibitors in HCC treatment, as well as for the development of dual-target PCNA/PARP1 inhibitors.

2 Materials and methods

2.1 Reagents, primers, and antibodies

AOH1160, a PCNA inhibitor, which targets amino acids region L126-Y133 of PCNA (Gu et al., 2018), and Olaparib (AZD2281), a PARP inhibitor, were purchased from Targetmol (Wellesley Hills, MA, United States) and dissolved in dimethyl sulfoxide (DMSO) at 10 mM to produce stock solutions at −20°C. All other chemicals used were analytical grade without purification. The antibodies are listed in Supplementary Table 1.

2.2 Bioinformatics analysis

The differential expression of genes in the cancer genome atlas (TCGA) database was analyzed by Gene Expression Profiling Interactive Analysis (GEPIA) online website. The mRNA expression of genes in cancer samples were compared with that in normal adjacent from TCGA database, and the P value was obtained by one-way ANOVA. The significant values of P-value and folding change are 0.05 and 2.0 respectively. The correlation between gene and patient survival was evaluated using the Kaplan-Meier Plotter. Samples were divided into groups with high and low expression according to the median expression. The 95% confidence interval, log-rank risk ratio (HR), and P value of overall survival (OS) and disease-free survival (DFS) were analyzed. The relationship between gene expression and prognosis was analyzed using receiver operating characteristic (ROC) curves. The original clinical data source of 424 HCC RNA sequencing information was obtained from the TCGA database. The R package pROC analyzed the area under the curve (AUC) values, and the data were visualized as ggplot2. The AUC value greater than 0.9 indicates strong evidence of model success (Zhang et al., 2021). Statistical analysis and visualization were performed in R v4.0.3. The expression correlation of genes was performed using TCGA data in the GEPIA online tool. Immunohistochemical results for the differential expression of PCNA and PARP1 in HCC tissues and normal adjacent tissues were obtained from the Human Protein Atlas (HPA) online database (https://www.proteinatlas.org/). The protein-protein interaction (PPI) network of PCNA was constructed using the Search Tool for the Retrieval of Interacting Genes/Proteins (STRING) protein-protein interaction networks functional enrichment online platform (https://cn.string-db.org/).

2.3 Cell culture

The human HCC cell lines HepG2 and Hep3B cell lines were procured from Cell Resources Center of Shanghai Academy of Life Sciences (Shanghai, China). Huh7 cell lines were purchased from Procell Life Science & Technology Co., Ltd. (Wuhan, China). HepG2 cells, Hep3B cells, and Huh7 cells were cultured in DMEM (KGL1206, KeyGEN Biotech, Nanjing, Jiangsu, China) with 10% fetal bovine serum (FBS). All cells were incubated at 37°C in a 5% CO_2 atmosphere. The cells were not passaged more than six times from collection to use and were authenticated by STR profiling regularly every half year.

2.4 Lentivirus transfection

Lentiviral recombination vectors of human PCNA gene (pGV492-PCNA) and its scrambled control (pGV492-NC), Lentiviral recombination vectors of short-hairpin RNA against PCNA (pGV112-shPCNA), short-hairpin RNA against PARP1 (pGV248-shPARP1) and the scrambled control (pGV112-shNC) were constructed and purchased from Genechem Co. Ltd. (Shanghai, China). The pGV112-shPCNA vector and pGV248-shPARP1 vector were confirmed by sequencing. HepG2 cells and Huh7 cells were infected with oePCNA, shPCNA, shPARP1 and shNC Lentiviral vectors using HitransG A promoting reagent according to the manufacturer's instructions. Hep3B cells were infected with oePCNA and oeNC. After infection with lentiviral vector for 3 days, culture medium containing virus was removed. Transfected cells were allowed for growth for 3–5 days, and then treated with 2.0 μg/mL puromycin for 24 h to select positive infected cells. For the rescue experiment, cells were infected with one lentiviral vector for 3 days and the culture medium containing virus was removed. The cells were then infected with another vector for 3 days, and the culture medium containing virus was removed. Cells transfected with two vectors were allowed for growth for 3–5 days, and then treated with 2.0 μg/mL puromycin for 24 h to select positive infected cells. All transfected cells were validated by quantitative PCR and Western blots, and maintained in a medium containing 1.0 μg/mL puromycin. The target sequence of shPCNA is 5′-AAGCCACTCCACTCTCTTCAA-3′, target sequence of shPARP1 is 5′-CAACTCCAGGAAGGAAACCAA-3′, target sequence of shNC is 5′-TTCTCCGAACGTGTCACGT-3'.

2.5 RNA sequencing and data processing of DEGs

According to the manufacturer's manual, total RNA was extracted from the HepG2 cells transfected with shNC or shPCNA using TRIzol reagent (Vazyme, Nanjing, China). A total of 500 ng of RNA was used

to prepare libraries using the NEBNext Ultra RNA Library Prep Kit for Illumina. RNA quantity and quality were assessed on an Agilent 2,100 Bioanalyzer. RNA library sequencing was performed on an Illumina HiSeqTM 2,500/4,000 by Gene *Denovo* Biotechnology Co., Ltd. (Guangzhou, Guangdong, China). Differentially expressed genes (DEGs) in the shNC group vs. the shPCNA group were identified based on a $|\log2FC| > 1.0$ and an adjusted $P < 0.05$. DEGs with a $|\log2FC| < 1.0$ were considered downregulated genes, while DEGs with a $|\log2FC| > 1.0$ were considered upregulated genes (Wang et al., 2021).

2.6 GO, KEGG pathway, reactome and GSEA enrichment analysis

The biological attributes of the DEGs were identified using gene ontology (GO) enrichment and gene set enrichment analysis (GSEA) enrichment analysis. The functional attributes of the DEGs were identified using Kyoto Encyclopedia of Genes and Genomes (KEGG) pathway enrichment, Reactome enrichment and GSEA enrichment analysis. GO enrichment analysis, KEGG pathway enrichment analysis, Reactome enrichment, and GSEA enrichment analysis were performed using Omicsmart online platform (http://www.omicsmart.com) (Huang et al., 2022).

2.7 Colony formation assay

For colony formation analysis, single-cell suspensions were seeded at 1×10^3 cells/well into 24-well plates. After overnight incubation, the cells were treated with the designed drugs for 10–14 days, and the medium was replaced every 3 days. The colonies were fixed in formaldehyde and stained with 0.1% crystal violet (Solarbio Life Sciences, China), and imaged using a fully automated live cell imaging system (Thermo Fisher EVOS M7000, Waltham, MA, United States). The quantitative analysis on the results of the colony formation assay was performed by ImageJ software (Version 1.53K).

2.8 Cell viability assay and determination of drug synergy

The cells of interest (1.5×10^3–4×10^3 cells per well) were seeded into 96-well plates overnight in 100 μL of complete growth medium and then treated with AOH1160 and Olaparib at different combination ratios for 6 days in triplicate. Following treatments, MTT solution was added to each well, plates were incubated for 4 h at 37°C, medium was removed, and formazan crystals were dissolved in DMSO. Cell viability was evaluated by measuring the well absorbances at 490 nm using microplate reader (Synergy NEO2, BioTek). The combined effects of AOH1160 and Olaparib were assessed using Calcusyn software (Biosoft, Cambridge, UK). Combination indexes (CI), which were used to evaluate the effects of two-drug combinations, were calculated using the Chou-Talalay method. Drug synergism was defined as a CI value of <1, while antagonism was defined as a value of >1. Additivity was defined as a CI = 1 (Chou, 2006; Wu et al., 2022).

2.9 Analysis of apoptosis and cell cycle

Flow cytometry analysis was used to assess cell apoptosis and the cell cycle (Huang et al., 2022). The cells of interest were treated with the designed drugs for 6 days and digested with EDTA-free trypsin. For apoptosis evaluation, the cells were collected and stained using an Annexin V-FITC/PI apoptosis kit (AT101, MultiSciences, Hangzhou, China) or Annexin V-PE/7-AAD apoptosis kit (AT104, Multisciences, Hangzhou, China). The cell cycle was analyzed by a PI cell cycle detection kit (CCS012, MultiSciences, Hangzhou, China). The above cells were all identified and quantified by a flow cytometer (NovoCyte Quanteon, United States) according to the manufacturer's instructions, and the data were analyzed by FlowJo v10 software, and the cell cycle data were analyzed by ModFit LT5.

2.10 Alkaline comet assay

Alkaline comet assay was performed as previously reported (Wu et al., 2022; Walsh and Kato, 2023). Briefly speaking, HepG2 cells or Huh7 cells were treated with different concentrations of AOH1160, Olaparib and their combination for 6 days. After treatment, 1×10^4 cells were mixed with low melting point agarose at a ratio of 1:10 (v/v), layered onto the slide, lysed by the lysis buffer at 4°C for 2 h, and unwound by alkaline unwinding solution for 30 min at room temperature. The gel electrophoresis was conducted in the condition of 25V and 40 min. The DNA was finally stained with propidium iodide (PI) for 15 min at room temperature. Then the slides were observed and imaged under a fluorescence microscope (Nikon-ECLIPSE 80i, Tokyo, Japan). Subsequently, we employed the CASP software (Version 1.2.3) to quantify the percentage of tail DNA measured in the comet assay (Collins et al., 2023).

2.11 Immunoblotting (IB) and immunoprecipitation (IP) assays

The western blot protocol has been described in detail previously (Wang et al., 2021; Wu et al., 2022). In short, HepG2 cells were lysed in RIPA cell-lysis buffer (KGB5203-100, KeyGEN Biotech, Nanjing, China) containing protease and phosphatase inhibitors on ice for 30 min. The lysates were centrifuged at 12,000 rpm for 15 min, the supernatants were collected, and the protein concentrations were determined with a Bicinchoninic (BCA) Protein Assay Kit (Solarbio, PC0020). A total of 20–30 μg of protein was separated on 8%–15% SDS-PAGE gels and transferred to PVDF membranes (Millipore, United States, IPVH00010, ISEQ00010). Membranes with protein were blocked with 5% (w/v) skim milk, incubated with primary antibody overnight at 4°C, and then incubated with secondary antibodies (1:5,000) for detection. The primary and secondary antibodies are described in Supplementary Table 1. The immunoprecipitation (IP) assay was performed using Protein A/G Magnetic IP/Co-IP kit (ACE Biotechnology, Nanjing, China). Briefly, the cells were lysed in enhanced lysis buffer containing protease and phosphatase inhibitors. The supernatants were incubated with 1–4 μg of primary antibodies overnight at 4°C on a rotating platform, followed by immunoblotting analysis. ImageJ

was used to quantify the immunoblotting results by measuring the protein band densities.

2.12 RNA extraction and Q-PCR

Total RNA was extracted with TRIzol reagent (Vazyme, Nanjing, Jiangsu, China) according to the manufacturer's instructions. RNA was reverse transcribed into cDNA by using a HiScript II one-step RT-PCR kit (P612-01, Vazyme, Nanjing, China) with 1.0 μg of total RNA in a 20 μL reaction system. 1.0 μL of the resulting cDNA was used in per quantitative PCR (Q-PCR) in triplicate. Q-PCR was carried out using ChamQ SYBR Q-PCR master mix (Q311–02, Vazyme, Nanjing, China) on a QuantStudio three real-time PCR detection system (Life Tech, New York, United States). Relative expression levels were calculated as ratios normalized against the endogenous control (GAPDH). The relative fold changes of candidate genes were analyzed using the $2^{-\Delta\Delta CT}$ method. All primers were synthesized by Tsingke Biotech (Wu et al., 2022). The sequences of the primers are listed in Supplementary Table 2.

2.13 Immunofluorescence assay

After treatment, cells (5×10^4) were seeded on a confocal plate. After overnight incubation, cells were treated as described in the text. Cells were then collected and fixed with 4% formaldehyde, permeabilized with 0.1% (v/v) Triton X-100 in PBS, and blocked with 1% (w/v) BSA in PBS for 1.0 h. After blocking, cells were incubated with the phospho-Histone H2A.X (Ser139) rabbit antibody at 4°C overnight, washed twice with PBS, and incubated for 2.0 h at room temperature with appropriate secondary antibodies. Cells were counterstained with DAPI (4′,6-diamidine-2′-phenylindole dihydrochloride). Fluorescence signals were visualized using a Zeiss LSM 900 laser scanning confocal microscope (Jena, Germany) and photographs were taken at a magnification of ×40 (Wang et al., 2021; Wu et al., 2022). The γ-H2AX foci in each cell were captured and counted.

2.14 Mouse xenograft tumor model

All animal procedures were carried out following the institutional guidelines for the care and use of laboratory animals and approved by the Committee on the Ethics of Animal Experiments of Lanzhou University (Lzujcyxy20230314). Every effort was made to ensure the comfort and safety of the animals. Female BALB/c nude mice aged 6–8 weeks were randomly used to establish xenograft models. 5×10^6 HepG2 cells (wild-type, empty control vector-transfected, stably PCNA-knockdown vector transfected) were subcutaneously inoculated into the right axilla of the mice. After the average tumor volume (mm^3) reached to $50mm^3$, the tumor-bearing mice were treated using different strategies (n = 5/group). Olaparib (40 mg/kg), AOH1160 (20 mg/kg), the combined group of Olaparib (20 mg/kg) and AOH1160 (10 mg/kg), the sequential treatment (40 mg/kg Olaparib for 10 days, followed by 20 mg/kg AOH1160 for 10 days) were administered by intraperitoneal injection for 21 consecutive days. The sequential regimen was designed to model clinical scenarios where PARP inhibitor resistance emerges, thereby evaluating potential of AOH1160 to overcome acquired therapeutic resistance. Tumor volume was recorded every 2 days using a digital caliper. Tumor volume was calculated using the formula, $(ab^2)/2$, where a and b represent the length and width of the tumor (Wu et al., 2022). For ethical considerations, mice were euthanized via CO_2 inhalation after 28 days.

2.15 Histological staining

The xenografted tumor tissues for immunohistochemistry (IHC) staining and the lung, liver, heart, kidney and spleen tissue samples of HepG2 xenograft tumor model mice were fixed in 4% paraformaldehyde, embedded in paraffin and sectioned at 3-μm thickness. For IHC staining, the slides were incubated in primary antibody diluted in blocking solution overnight at 4 °C. After incubation peroxidase conjugated secondary antibody was used against the primary antibody. For chromogenic detection, 3,3′-diaminobenzidine tetrahydrochloride (DAB) (Sigma, United States) was used as the substrate for peroxidase. Slides were counterstained with hematoxylin. Cells with brown nuclei were considered as positively stained. For haematoxylin and eosin (H&E) staining, slides were stained with Mayer's haematoxylin and 0.1% sodium bicarbonate and counterstained with Eosin Y solution (Beyotime, Shanghai, China). Each group of samples was observed with Nikon-ECLIPSE 80i microscope with a Nikon DS-Ri2 Digital Camera (Tokyo, Japan).

2.16 Statistics

All data were representative of three independent experiments and illustrated as means ± standard error of the mean. Differences between groups were analyzed by one-way or repeated measures ANOVA using SPSS Version 20.0 software (SPSS Inc., Chicago, IL). $P < 0.05$ was considered statistically significant.

3 Results

3.1 PCNA promotes the malignant proliferation of HCC cells

We evaluated the differential expression of PCNA in HCC tissues and adjacent normal tissues from TCGA and HPA databases. As depicted in Figures 1A–C, the expression of PCNA was significantly higher in HCC tissues compared to normal liver tissues and its expression levels increased with the progression of tumor stages. The ROC curve analysis for PCNA revealed an AUC value of 0.949, indicating that PCNA expression was significantly associated with poor prognosis of HCC (Figure 1D). The log-rank test analysis revealed that patients with HCC with lower PCNA expression had significantly longer survival than those with higher PCNA (Figure 1E). PCNA expression was highly expressed in HepG2 cells and Huh7 cells among three HCC cell lines (Figures

10.3389/fphar.2025.1571786

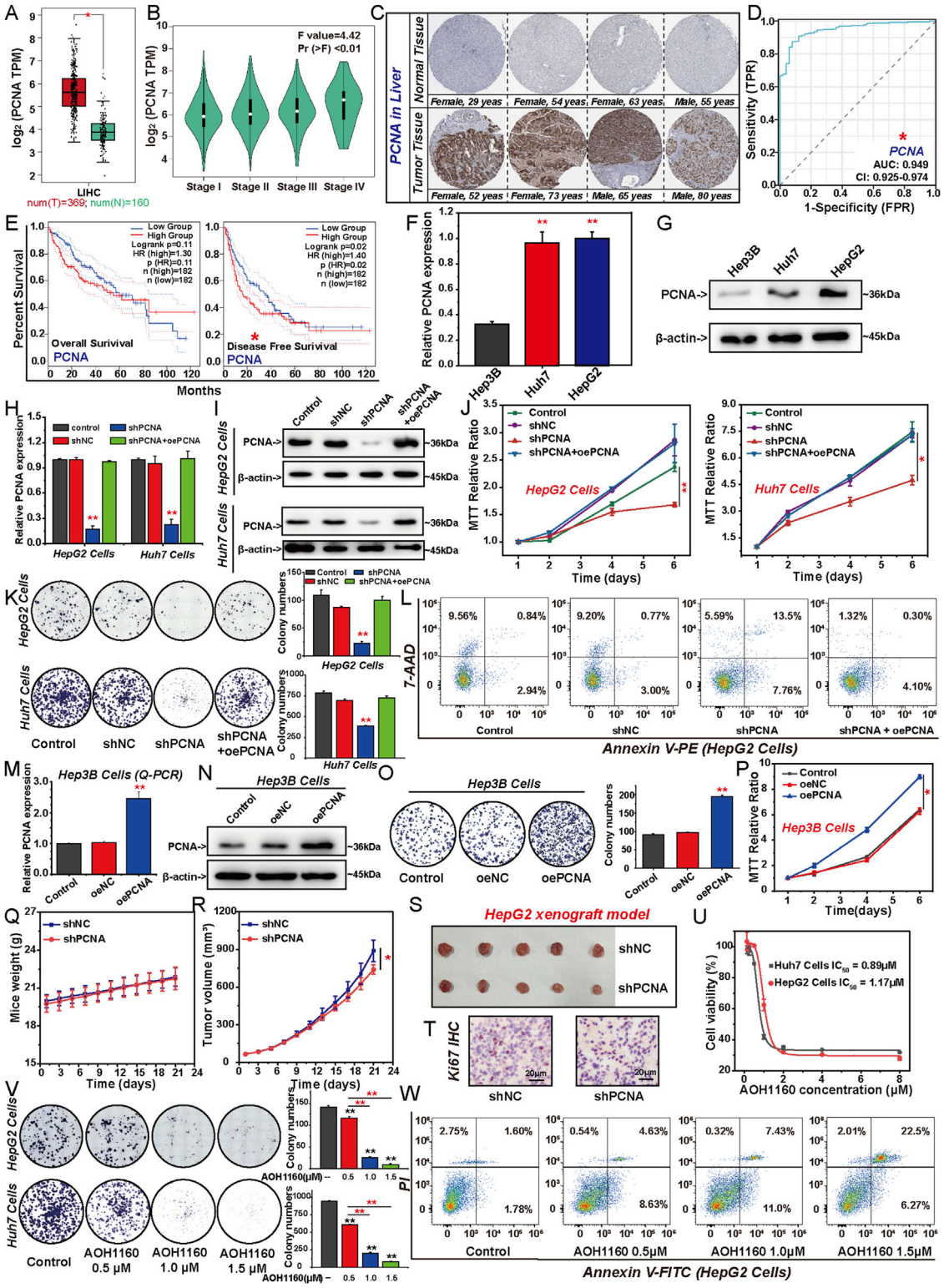

FIGURE 1
PCNA promotes the malignant proliferation of HCC cells. The differential expression of PCNA between HCC tissues and adjacent tissues obtained from TCGA dataset **(A, B)** and the HPA databases **(C)**. **(D)** Diagnostic ROC for PCNA in HCC and normal samples. **(E)** The impact of PCNA mRNA expression on patient survival was analyzed by Kaplan-Meier survival curve. The expression levels of PCNA in HCC cell lines were detected via Q-PCR **(F)** and Western blotting **(G)**. HepG2 cells and Huh7 cells were transfected by shNC, shPCNA, shPCNA and oePCNA, the transfected efficiency was verified by Q-PCR **(H)** and Western blotting **(I)**. The viability and colongenic growth of HepG2 cells and Huh7 cells with or without PCNA knockdown was analyzed using MTT assay **(J)** and colony formation assay, followed by quantification of colony numbers. **(K)**. **(L)** Apoptosis of HepG2 cells with or without PCNA knockdown was assessed via flow cytometry with 7-AAD and annexin V-PE double staining. Hep3B cells was transfected by oeNC and oePCNA, the transfected efficiency was verified by Q-PCR **(M)** and Western blotting **(N)**. The viability and colongenic growth of Hep3B cells with or without PCNA overexpression

(*Continued*)

FIGURE 1 (Continued)
was analyzed using colony formation assay, followed by quantification of colony numbers. **(O)** and MTT assay **(P)**. **(Q–S)** HepG2 cells were subcutaneously implanted into nude mice after shNC or shPCNA transfection. Mice weight **(Q)** and tumor volume **(R)** were measured. The picture shows the size of the tumor **(S)**. **(T)** Immunohistochemical staining of Ki67 in the isolated xenograft tumor. **(U)** The IC_{50} of AOH1160, PCNA inhibitor, in HepG2 and Huh7 cells. **(V)** Colony formation of HepG2 cells and Huh7 cells treated with different concentrations of AOH1160, followed by quantification of colony numbers. **(W)** Apoptosis of HepG2 cells treated with different concentrations of AOH1160. The results from three independent experiments were statistically analyzed using one-way ANOVA: *P < 0.05, **P < 0.01.

1F, G), so we selected them to investigate the effect of PCNA knockdown on the proliferation of HCC cells (Figures 1H, I). As shown in Figures 1J, K, PCNA knockdown inhibited proliferation and clonogenic growth, whereas overexpress of PCNA rescued these effects. PCNA silencing significantly promoted apoptosis in HepG2 cells (Figure 1L). To further explore the role of PCNA in HCC progression, we investigated its effect on Hep3B cells by inducing PCNA overexpression (Figures 1M, N). The result showed that PCNA overexpression enhanced Hep3B cells proliferation and clonogenic potential. Furthermore, we assessed the impact of PCNA knockdown on tumor growth in a HepG2 xenograft model using nude mice. Silencing PCNA significantly reduced tumor volume without affecting body weight and led to a notable decrease in Ki67 expression (Figure 1Q-T). AOH1160 is a small molecular inhibitor of PCNA identified through high-throughput screening, targeting a surface pocket partly delineated by the L126-Y133 region of PCNA (Gu et al., 2018). To evaluate its cytotoxic effects on HCC cells, HepG2 and Huh7 cells were treated with AOH1160. MTT assays revealed that AOH1160 exhibited potent anticancer effect in a dose-dependent manner on HCC cells (Figure 1U), with calculated half-maximal inhibitory concentration (IC_{50}) values of 1.17 μM for HepG2 and 0.89 μM for Huh7 cells. Based on these results, AOH1160 was used at concentrations of 0.5 μM, 1.0 μM, and 1.5 μM in the subsequent assays. Similar to the genetic inhibition of PCNA, AOH1160 treatment significantly reduced HepG2 and Huh7 colony formation while also increasing apoptosis in HepG2 cells (Figures 1V, W).

3.2 PCNA regulates genes involved in DNA repair and cell cycle progression

To elucidate the mechanism of PCNA in promoting the proliferation of HCC cells, we performed RNA sequencing (RNA-Seq) to analyze the effect of PCNA on the expression of total genes in HepG2 cells (Figures 2A–D). Knockdown of PCNA induced upregulation of 537 DEGs and downregulation of 156 DEGs in HepG2 cells. The results of GO functional enrichment, KEGG pathway enrichment and Reactome enrichment demonstrated that DEGs induced by knockdown of PCNA were mostly associated with DNA replication, DNA repair and cell cycle (Figure 2A). Supportively, the GSEA enrichment showed that high PCNA expression was positively correlated with the enrichment of gene sets related to DNA replication, DNA repair and cell cycle pathways (Figure 2B). Subsequently, we constructed the protein-protein interaction (PPI) network of PCNA, and analyzed the top 50 protein by the GO enrichment and KEGG pathway enrichment. The enrichment results showed that proteins in the PCNA PPI network were mainly involved in DNA replication, DNA repair, and the cell cycle (Figure 2C). And then, we selected the key genes-involved in DNA repair and cell cycle. Knockdown of PCNA led to significant downregulation of five genes-involved in DNA repair, exonuclease 1 (EXO1), PARP1, histone H2AX (H2AX), breast cancer susceptibility gene 1 (BRCA1), and recombinase Rad51 (RAD51), and four genes-involved in cell cycle progression, cyclin B1 (CCNB1), cyclin E2 (CCNE2), cyclin-dependent kinase 1 (CDK1), and cell-division cycle 25C (CDC25C) (Figure 2D). In addition, expression analysis of those key genes in HCC tissues compared to normal tissues demonstrated that EXO1, PARP1, H2AX, BRCA1, RAD51, CCNB1, CDK1, CDC25C, and CCNE2 were overexpressed in HCC tissues, further supporting the role of these genes in HCC progression (Figure 2E).

3.3 Repression of PCNA inhibits DNA repair in HCC cells

We next investigated the impact of PCNA depletion in the DNA damage repair of HCC cells. Damaged DNA has a tail in the comet assay that resembles a comet. Knockdown of PCNA significantly increased the number and extent of tailed DNA in HepG2 and Huh7 cells, indicating that repression of PCNA promoted DNA damage (Figure 3A). The accumulation of γH2AX foci also reflects the extent of DNA damage (Prabhu et al., 2024). Similarly, we found that the increased nuclear γH2AX foci was induced by PCNA silencing which was confirmed by confocal microscopy. However, overexpression of PCNA impaired the extent of DNA damage induced by knockdown of PCNA (Figures 3B, C). We then applied Q-PCR assays to assess the expression of genes-involved in DNA repair, including PARP1, EXO1, BRCA1, RAD51, X-ray repair cross complementing 1 (XRCC1), X-ray repair cross complementing 2 (XRCC2), breast cancer susceptibility gene 2 (BRCA2), partner and localizer of breast cancer 2 (PALB2), and DNA polymerase θ (POLQ), the mRNA levels of these genes were reduced in PCNA knockdown cells (Figure 3D; Supplementary Figure 1A). PCNA inhibitor AOH1160 also resulted in a dose-dependent increase in DNA damage in both HepG2 and Huh7 cells, as evidenced by the comet assay (Figure 3E). Correspondingly, Q-PCR analysis showed that AOH1160 significantly inhibited the expression of DNA repair genes in a dose-dependent manner (Figure 3F; Supplementary Figure 1B). Analysis of TCGA data demonstrated a significant positive correlation between PCNA expression and DNA damage repair-related gene expression in HCC (Figure 3F; Supplementary Figure 1C). These findings demonstrated that targeting PCNA genetically or pharmacologically inhibits DNA repair of HCC cells.

10.3389/fphar.2025.1571786

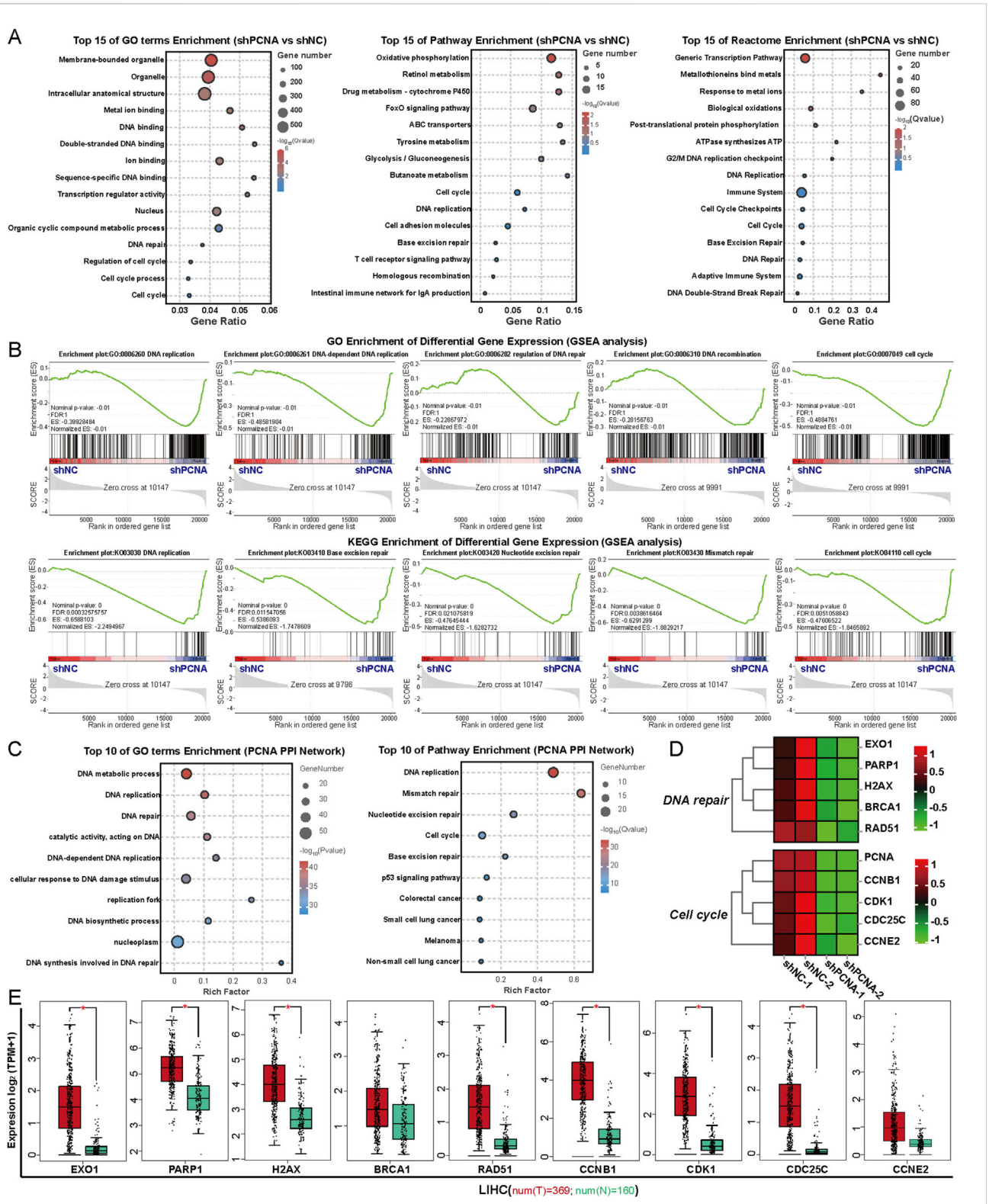

FIGURE 2
PCNA regulates genes involved in DNA repair and cell cycle progression. **(A)** Top 15 biological pathways of these downregulated genes after PCNA knockdown in HepG2 cells were analyzed by GO enrichment, KEGG pathway enrichment, and Reactome enrichment. **(B)** GSEA plots of the downregulated gene signature resulting from the knockdown of PCNA in HepG2 cells. **(C)** GO enrichment and KEGG pathway enrichment analysis of PCNA PPI network. **(D)** Heatmap plot of the key DEGs induced by PCNA knockdown. **(E)** The differential expression of the key DEGs in HCC of the TCGA project.

10.3389/fphar.2025.1571786

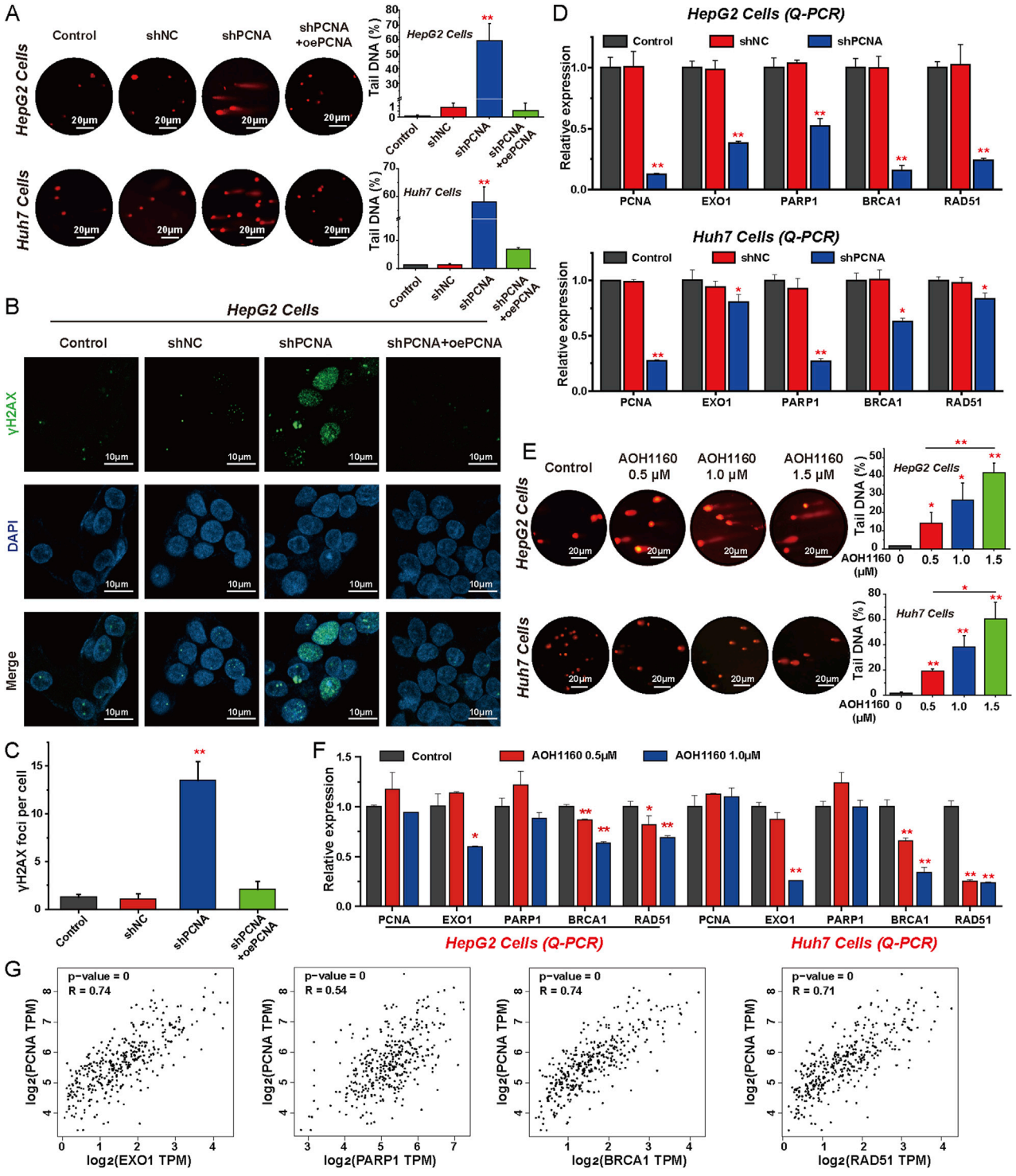

FIGURE 3
Repression of PCNA inhibits DNA repair in HCC cells. **(A)** The alkaline comet assay was performed to evaluate DNA damage in PCNA-knockdown HepG2 and Huh7 cells, with DNA damage levels quantified by measuring the percentage of tail DNA. **(B)** The foci of γH2AX were measured via immunofluorescence to evaluate the DNA double-strand break of HepG2 cells after PCNA knockdown. Magnification is ×100, scale bar = 10 μm. **(C)** Quantification of the number of γ-H2AX-positive foci in each cell based on immunofluorescence in HepG2 cells. **(D)** The Relative mRNA levels of indicated regulators of DNA repair following PCNA knockdown in HepG2 cells and Huh7 cells. **(E)** The effects of AOH1160 on DNA damage were assessed using the alkaline comet assay, with results quantified by measuring the percentage of tail DNA. **(F)** The effects of AOH1160 on the expression of DNA repair-related genes were analyzed by Q-PCR. **(G)** Expression correlation analysis of PCNA and key factors involved in DNA damage repair using the data from TCGA project. The results from three independent experiments were statistically analyzed using one-way ANOVA: *P < 0.05, **P < 0.01 compared with the control.

10.3389/fphar.2025.1571786

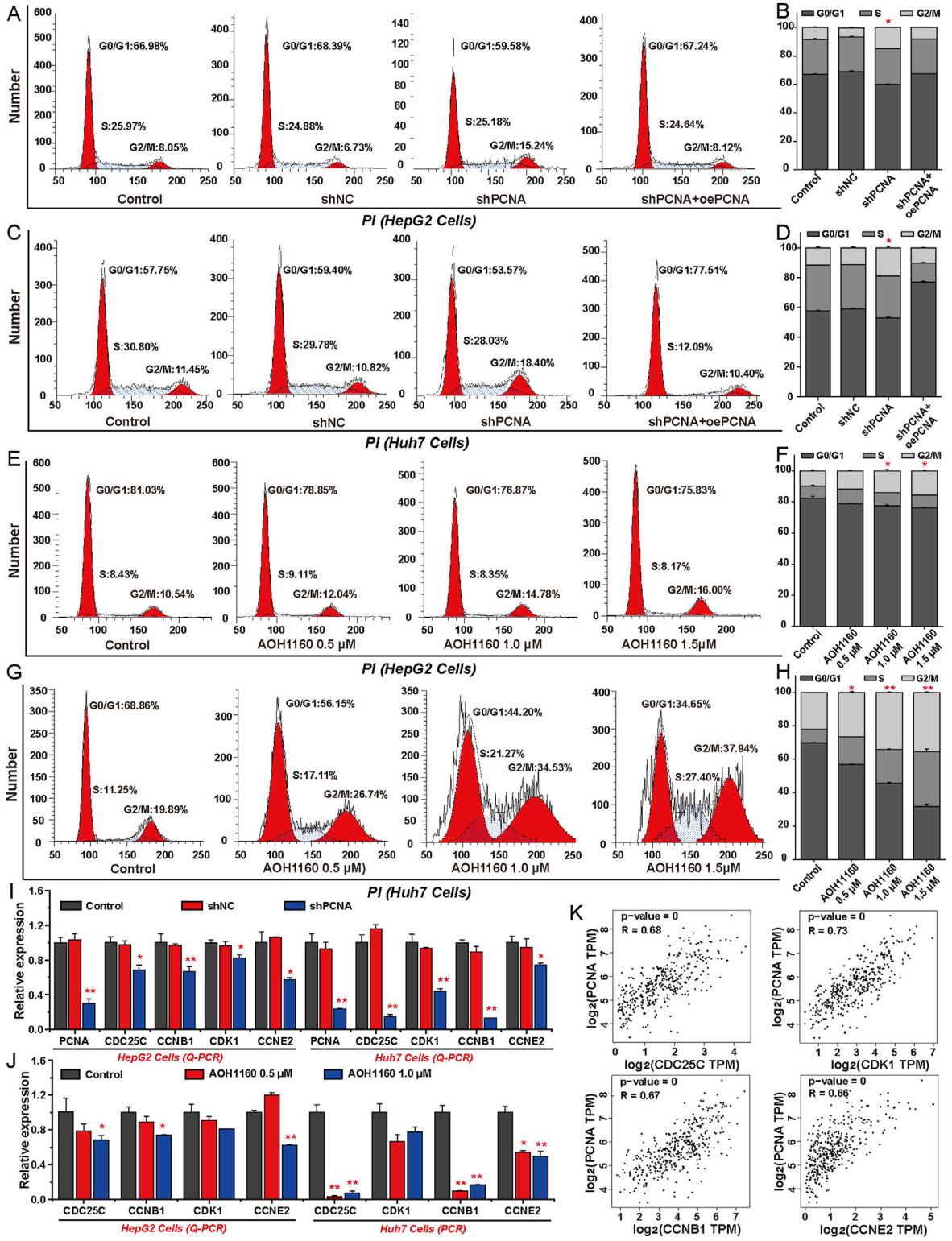

FIGURE 4
Inhibition of PCNA arrests cell cycle progression in HCC cells. **(A–D)** Cell cycle analysis was performed by flow cytometry in HepG2 cells and Huh7 cells with or without PCNA knockdown. **(E–H)** Cell cycle analysis was performed by flow cytometry in HepG2 cells and Huh7 cells treated with AOH1160. **(I)** Relative mRNA levels of indicated regulators of cell cycle progression following PCNA knockdown in HepG2 cells and Huh7 cells. **(J)** The effects of AOH1160 on the expression of genes involved in the cell cycle were analyzed by Q-PCR. **(K)** Expression correlation analysis of PCNA and the genes involved in cell cycle progression using the data from TCGA project. The results from three independent experiments were statistically analyzed using one-way ANOVA: *P < 0.05, **P < 0.01 compared with the control.

10.3389/fphar.2025.1571786

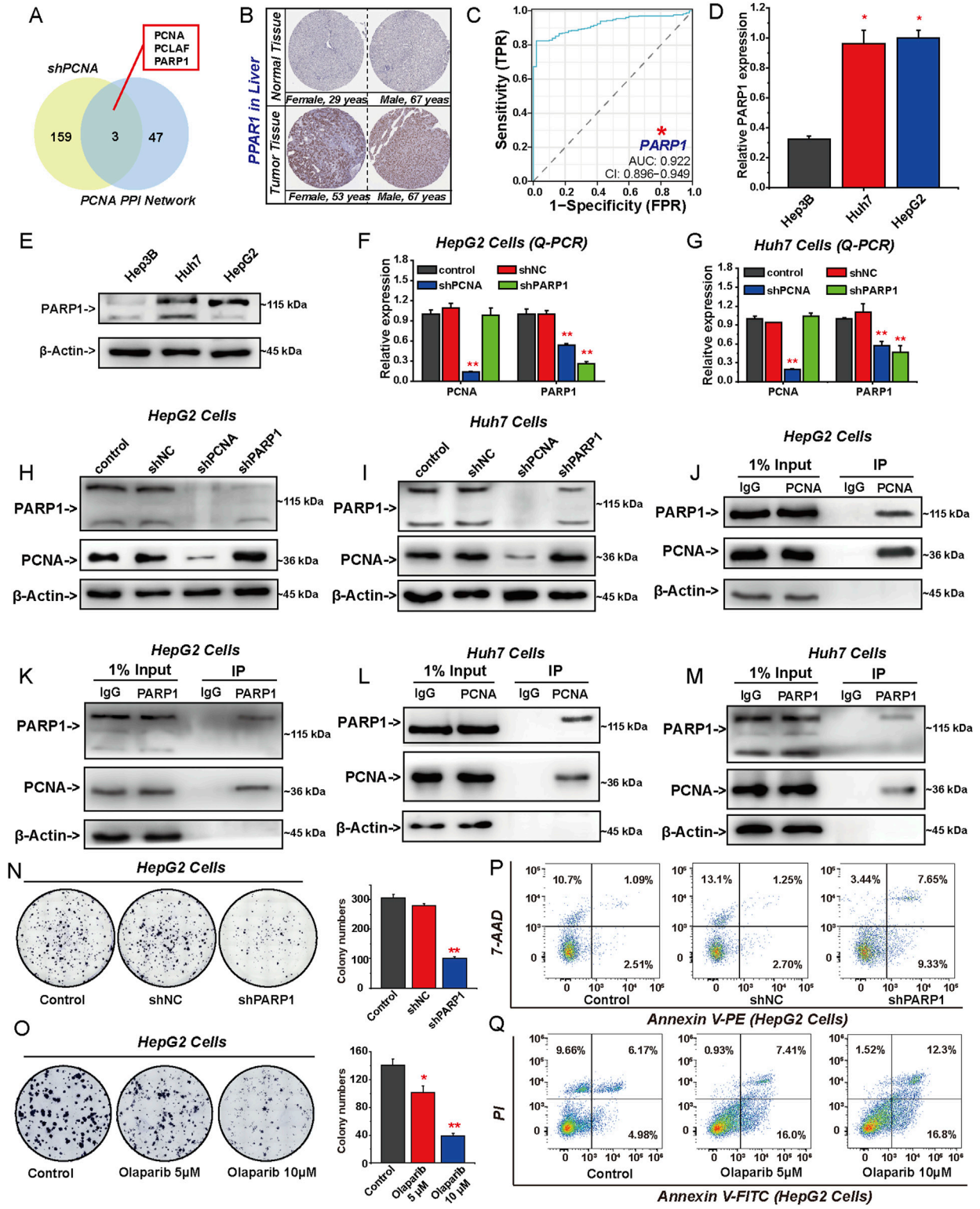

FIGURE 5
PCNA directly interacted with PARP1 to promote HCC proliferation. **(A)** Venn diagram for downregulated gene signature resulting from knockdown of PCNA and the PCNA PPI network. **(B)** Representative IHC staining intensity of PARP1 in HCC and normal tissues from the HPA databases. **(C)** ROC curves of PARP1 for HCC prediction in TCGA. The expression of PARP1 among different HCC cell lines was detected by Q-PCR **(D)** and Western blotting **(E)**. The expression of PCNA and PARP1 in HepG2 cells and Huh7 cells transduced with shPCNA or shPARP1 was analyzed by Q-PCR **(F, G)** and Western blotting **(H, I)**. **(J–M)** The relationship between PCNA and PARP1 was analyzed by Co-IP assay. Colony formation assays were performed to analyze proliferation in PARP1-knockdown **(N)** and Olaparib-treated **(O)** HepG2 cells, followed by quantification of colony numbers. Apoptosis of HepG2 cells with PARP1 knockdown **(P)** or Olaparib **(Q)** was assessed by flow cytometry. The results from three independent experiments were statistically analyzed using one-way ANOVA: *P < 0.05, **P < 0.01.

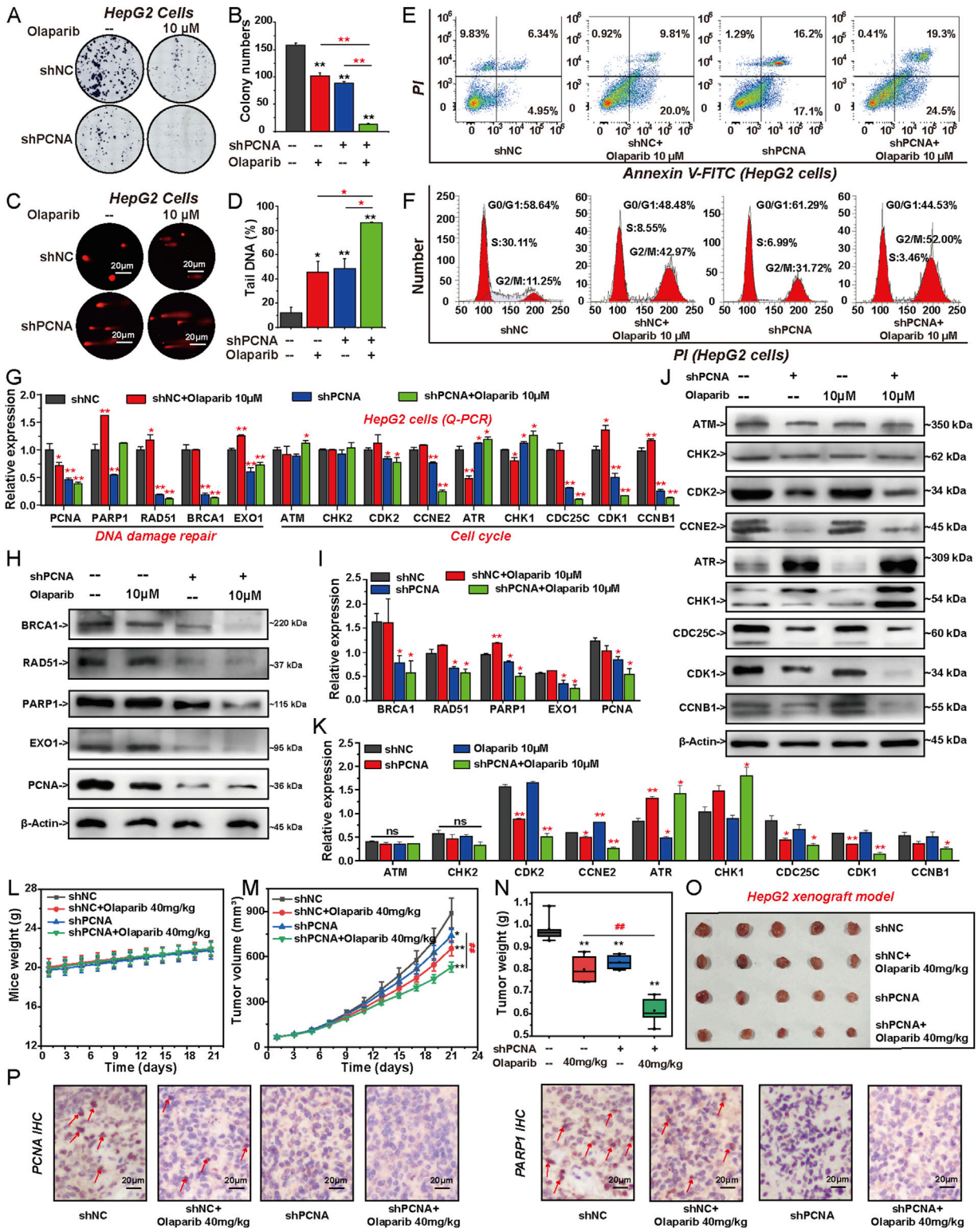

FIGURE 6
Knockdown of PCNA increases the sensitivity of HCC cells to PARP1 inhibitor Olaparib. HepG2 cells were transfected with shNC or shPCNA and followed by Olaparib (10 μM) treatment for 6 days. **(A, B)** Proliferation was detected by colony formation assay, followed by quantification of colony numbers. **(C, D)** DNA damage level was assessed by alkaline comet assay, followed by quantification of the percentage of tail DNA. **(E)** Apoptosis was assessed by flow cytometry with PI and annexin V-FITC double staining. **(F)** Cell cycle analyses were conducted by flow cytometry. **(G)** Relative expression of DNA repair-related genes and factors involved in cell cycle progression were analyzed by Q-PCR. **(H, I)** The protein expression levels of DNA repair-related factors following each individual treatment were analyzed via Western blotting. **(J, K)** The protein expression levels of factors involved in cell cycle progression were analyzed by Western blotting. The effects of shPCNA, Olaparib, and their combination on mice weight **(L)**, tumor

(*Continued*)

FIGURE 6 (Continued)
volume **(M)**, and tumor weight **(N)**. The photos of tumor nodules **(O)** in each group. **(P)** Immunohistochemical staining of PCNA and PARP1 in the isolated xenograft tumor. The results from three independent experiments were statistically analyzed using one-way ANOVA: *P < 0.05, **P < 0.01 compared with the shNC group; #P < 0.05, ##P < 0.01 compared with the shPCNA/Olaparib combined group (Olaparib: 40 mg/kg).

3.4 Inhibition of PCNA arrests cell cycle progression in HCC cells

To assess the effect of targeting PCNA on cell cycle progression, flow cytometry analysis was performed in HCC cells. The analysis revealed that PCNA silencing increased the proportion of HepG2 and Huh7 cells in the G2/M phase, which may further lead to the death of HCC cells. In contrast, overexpression of PCNA reduced the proportion of the G2/M phase to accelerate the rate of cell mitosis (Figures 4A–D). Furthermore, AOH1160 inhibited the G2/M transition and arrested the cell cycle at the G2/M phase (Figures 4E–H). To further clarify the potential mechanisms, we evaluated the expression of genes-involved in cell cycle regulation using Q-PCR. The results demonstrated that inhibition of the expression or activity of PCNA decreased the expression levels of CDC25C, CCNB1, CDK1, CCNE2, cell-division cycle 25A (CDC25A), and cyclin-dependent kinase 2 (CDK2) (Figures 4I, J; Supplementary Figure 2A). Based on the data from TCGA project, correlation analysis revealed that PCNA expression was positively associated with the expression of CDC25C (R = 0.68), CDK1 (R = 0.73), CCNB1 (R = 0.67), CCNE2 (R = 0.66), CDC25A (R = 0.62), and CDK2 (R = 0.75) in HCC tissues (Figure 4K; Supplementary Figure 2B). These data suggested that inhibition of PCNA induced cell cycle arrest at G2/M phase in HCC cells.

3.5 PCNA directly interacted with PARP1 to promote HCC proliferation

To delineate the molecular mechanism of PCNA in HCC tumorigenesis, we systematically identified key effector proteins downstream of PCNA. Through Venn diagram analysis integrating DEGs downregulated upon PCNA silencing with genes within the PCNA protein-protein interaction (PPI) network, we identified three overlapping candidates: PCNA, PCLAF, and PARP1. Structural and functional analyses confirmed that PCNA interacts with PCLAF to orchestrate its canonical roles in DNA replication and repair. Building on this foundation, we further discovered that PCNA mechanistically modulates PARP1 expression (Figure 5A). Based on these findings, we postulated that PARP1 may serve as the pivotal mechanistic target through which PCNA drives HCC pathogenesis. Subsequently, we explored that the expression of PARP1 is significantly higher in HCC tissues compared to normal adjacent tissues (Figure 5B). The ROC curve analysis indicates that the AUC value of PARP1 is 0.922, suggesting a high diagnostic value (Figure 5C). Correlation analysis also showed that PARP1 was associated with DNA repair-related genes and cell cycle regulation genes (Supplementary Figure 3). And we also that the differential expression of PARP1 among different HCC cell lines was similar to PCNA, which was highest in HepG2 cells (Figures 5D, E). Surprisingly, knockdown of PCNA inhibited the expression of PARP1 in mRNA and protein levels, however, knockdown of PARP1 had no effect on the expression of PCNA (Figures 5F–I). Indeed, Co-IP assay suggested that PCNA directly interacted with PARP1 (Figure 5J-M). Collectively, these results indicate that PARP1 is the downstream target of PCNA and directly interacts with PCNA. We further explored the effect of PARP1 on the proliferation of HepG2 cells. Inhibition expression or enzymatic activity of PARP1 significantly inhibited the formation of HepG2 clones (Figures 5N, O), and promoted the apoptosis of HepG2 cells (Figures 5P, Q). In summary, these results suggest that PARP1 is the key downstream target of PCNA-mediated HCC proliferation.

3.6 Knockdown of PCNA increases the sensitivity of HCC cells to PARP1 inhibitor olaparib

To investigate the effect of knocking down PCNA on the sensitivity of HCC to PARP1 inhibitor, HepG2 cells were treated with shPCNA or 10 μM Olaparib for 6 days separately or in combination. Both Olaparib and shPCNA inhibited the proliferation and DNA repair of HepG2 cells and promoted cell apoptosis (Figures 6A–E). Besides, Olaparib and shPCNA inhibited the cell cycle transition from G2 phase to M phase in HepG2 cells (Figure 6F). Compared with the shPCNA infected group and Olaparib treated group, the combination of shPCNA and Olaparib significantly inhibited the proliferation and DNA repair of HepG2 cells, promoted cancer cell apoptosis, and arrested the cell cycle at G2/M phase (Figures 6A–F). Q-PCR and Western blotting were used to investigate the mRNA and protein levels of factors-involved in DNA repair and cell cycle progression (Figures 6G–K). Knockdown of PCNA significantly inhibited the expression of PARP1, RAD51, BRCA1, and EXO1 in both mRNA and protein levels. Olaparib significantly promoted the expression of PARP1, RAD51 and EXO1 after 6 days of treatment. The combination of shPCNA and Olaparib induced a significant decrease of these DNA repair-related genes (Figures 6G–I). Subsequently, we investigated the effects of shPCNA, Olaparib, and their combination on cell cycle regulatory genes. Knockdown of PCNA significantly promoted the expression of ATR and CHK1, and inhibited the expression of CDC25C, CDK1, CCNB1, CDK2 and CCNE2, but did not affect the expression of ATM and CHK2. Olaparib promoted the expression of CDK1, CCNB1 and CCNE2. The combination group significantly promoted the expression of ATR and CHK1, and inhibited the expression of CDC25C, CDK1, CCNB1, CDK2, and CCNE2 in mRNA and protein levels (Figures 6G, J, K). We also investigated the effect of knocking down PCNA on the sensitivity to PARP1 inhibitor Olaparib *in vivo*. To construct the xenograft tumor mouse model, PCNA-knockdown stable HepG2 cell lines were subcutaneously injected into nude mice. Subsequently, Olaparib treatment was performed once a day at 40 mg/kg for 21 days, and the tumor growth curve was detected. As shown in Figure 6L-O, knockdown of PCNA or treatment with Olaparib significantly inhibited the growth

10.3389/fphar.2025.1571786

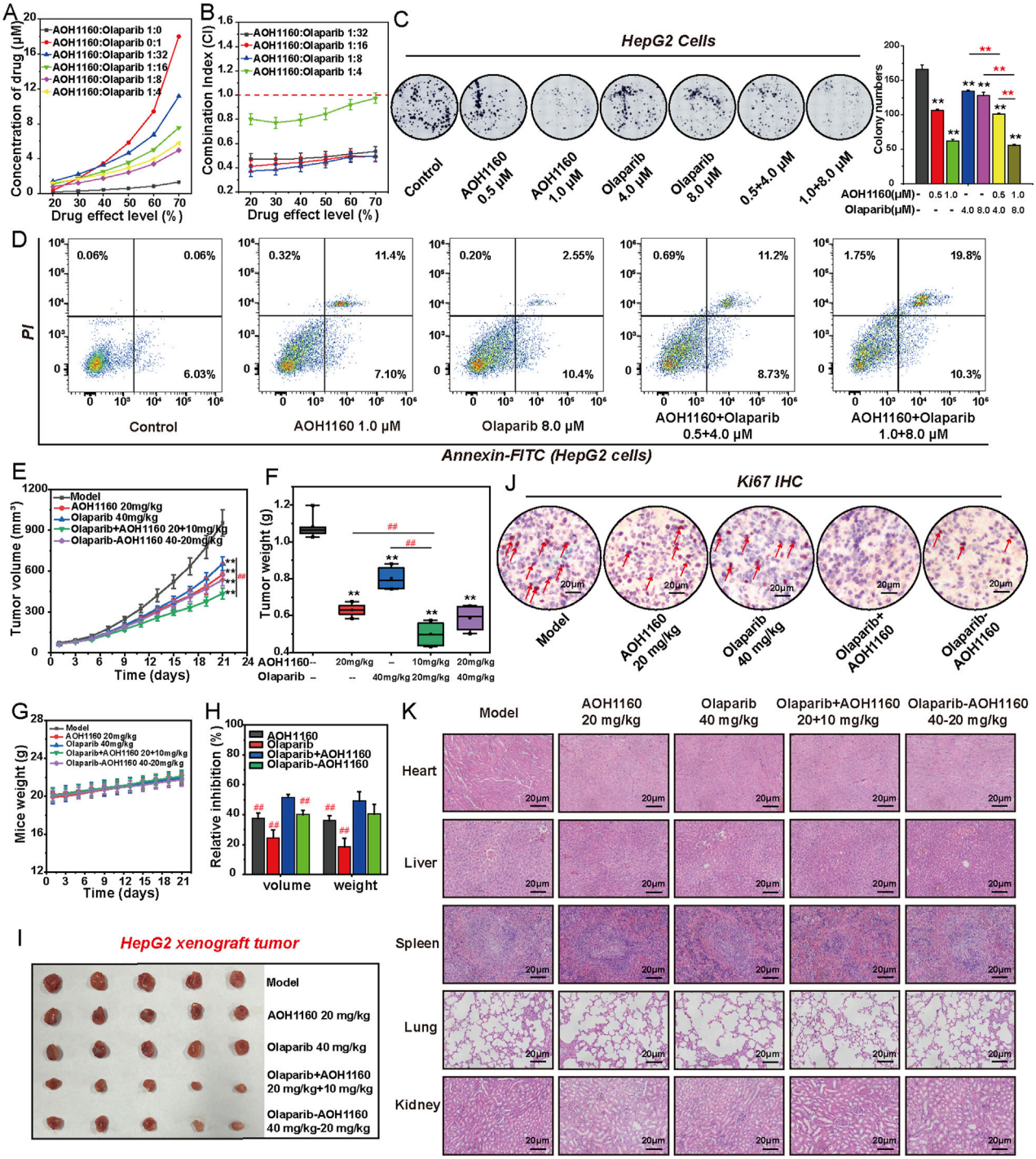

FIGURE 7
Combined inhibition of PCNA and PARP1 has a synergistic effect on HCC cells. **(A)** The effects of combining AOH1160 and Olaparib on the proliferation of HepG2 cells. **(B)** CI values for concurrent treatment with AOH1160 and Olaparib in HepG2 cells. **(C)** The effects of AOH1160 and/or Olaparib on the proliferation of HepG2 cells were measured by colony formation assay, followed by quantification of colony numbers. **(D)** The effects of AOH1160 and/or Olaparib on the apoptosis of HepG2 cells. **(E–I)** HepG2 cells were injected into nude mice and the mice were subsequently treated with AOH1160 and/or Olaparib at the indicated times. The tumor volume **(E)**, tumor weight **(F)**, mice weight **(G)**, relative volume and weight inhibition **(H)**, and tumor nodules **(I)** in each group. **(J)** Immunohistochemical staining of Ki67 in the isolated xenograft tumor. **(K)** Tissue damage was determined by H&E staining. The results from three independent experiments were statistically analyzed using one-way ANOVA: *P < 0.05, **P < 0.01 compared with the control; #P < 0.05, ##P < 0.01 compared with the AOH1160/Olaparib combined group (AOH1160/Olaparib: 10 + 20 mg/kg).

10.3389/fphar.2025.1571786

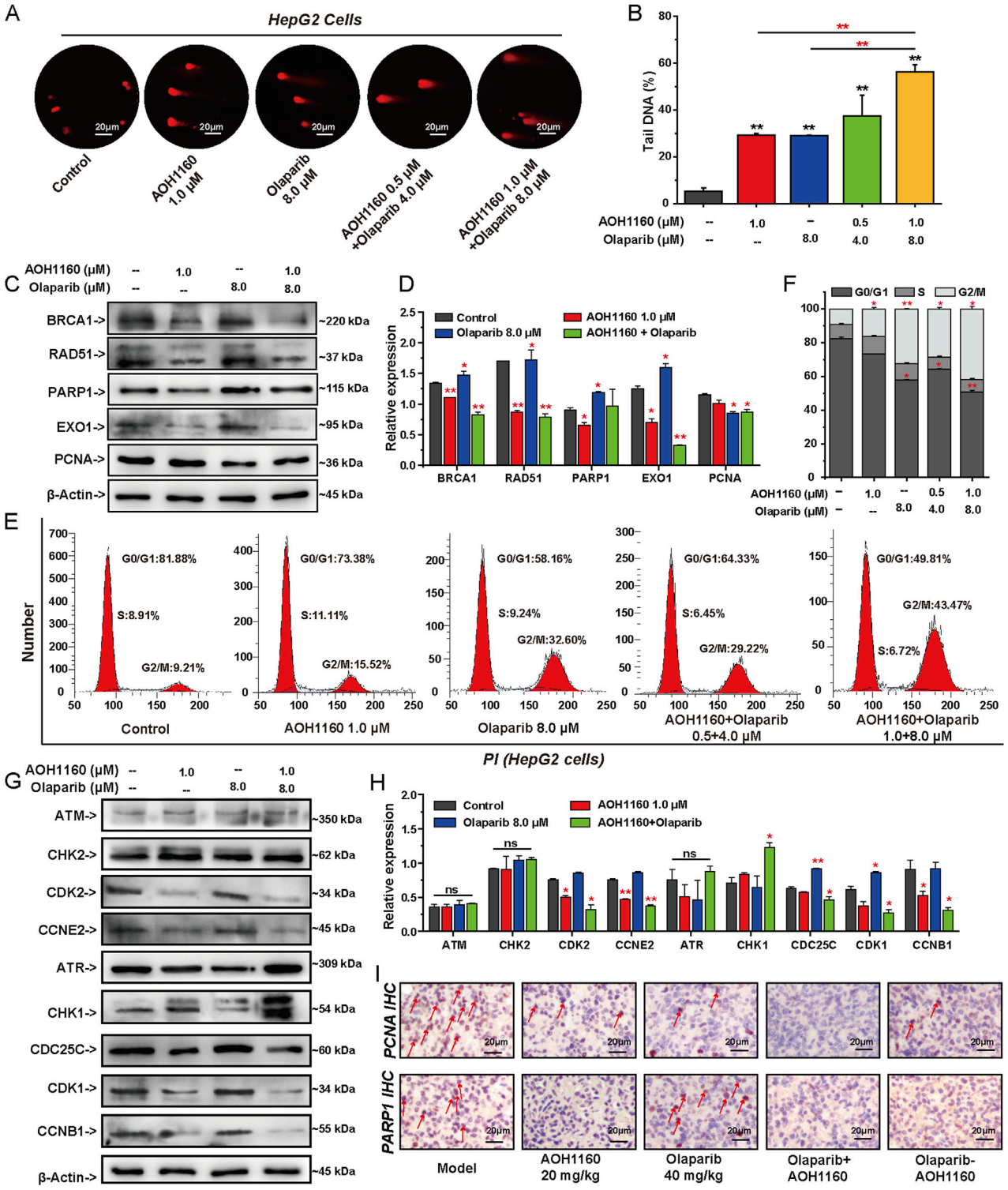

FIGURE 8
AOH1160 and Olaparib synergistically inhibit DNA damage repair and cell cycle progression. **(A)** The effects of AOH1160 and/or Olaparib on DNA damage detected by alkaline comet assay. **(B)** Quantified results by the percentage of tail DNA in the comet assay. **(C, D)** The effects of AOH1160 and/or Olaparib on the expression of DNA repair-related proteins were analyzed by Western blotting in HepG2 cells. **(E, F)** The effects of AOH1160 and/or Olaparib on cell cycle progression in HepG2 cells. **(G, H)** The effects of AOH1160 and/or Olaparib on the expression of proteins involved in cell cycle control were analyzed by Western blotting in HepG2 cells. **(I)** Effects of AOH1160 and/or Olaparib on the expression of PCNA and PARP1 *in vivo* analyzed by immunohistochemistry.

of HepG2 xenograft tumors. Compared with the shPCNA infection group and Olaparib treatment group, the combined treatment group had a more significant inhibition effect on HepG2 xenograft tumor growth. Further research showed that knockdown of PCNA significantly repressed the expression of PCNA and PARP1 in HepG2 xenograft tumor tissues. Olaparib decreased PCNA expression and increased PARP1 expression. Their combination significantly inhibited the expression of PCNA and PARP1 (Figure 6P). Collectively, these results suggest that knockdown of PCNA promotes the sensitivity of HCC cells to Olaparib *in vitro* and *in vivo*.

3.7 Combined inhibition of PCNA and PARP1 has a synergistic effect on HCC cells

To evaluate the therapeutic potentials of targeting PCNA and PAPR1, we treated HepG2 cells with AOH1160/Olaparib alone or in combination for 6 days to assess their anticancer efficiency. The effect of AOH1160 and Olaparib (1:32, 1:16, 1:8, 1:4) in combination were examined in HepG2 cells (Figure 7A). The drug combination indexes (CI) values were less than 1.0 for all concentration groups, suggesting a synergistic effect between AOH1160 and PARP1 at the indicated concentrations (Figure 7B). The dose ratio of 1:8 induced the most significant inhibition (CI < 0.5), therefore, we selected the dose ratio of 1:8 for further study. Compared with AOH1160 (1.0 μM) alone- and Olaparib (8.0 μM) alone-treated group, the combination of AOH1160 (0.5 μM) and Olaparib (4.0 μM) at lower concentrations could significantly inhibit the clonogenic growth of HepG2 cells (Figure 7C). Meanwhile, AOH1160 and Olaparib synergistically promoted the apoptosis of HepG2 cells after 6 days of treatment (Figure 7D). To further evaluate the anticancer effect of the combined inhibition of PCNA and PARP1 *in vivo*, BALB/c nude mice were subcutaneously injected with HepG2 cells. Approximately 1 week later, the mice were equally divided into five groups and intraperitoneally injected with 20 mg/kg AOH1160, 40 mg/kg Olaparib, a combination of both drugs (10 mg/kg AOH1160 plus 20 mg/kg Olaparib), a sequential treatment (40 mg/kg Olaparib for 10 days, followed by 20 mg/kg AOH1160 for 10 days), or an equal volume of saline as a control group. After 21 days of treatment, AOH1160 and Olaparib synergistically inhibited tumor size and tumor weight but did not affect the body weight of mice at our tested dosages, and it also reduced the expression of Ki67 (Figures 7E–J). After analysis of H&E-stained organs, we found that AOH1160, Olaparib, and their combination did not cause significant damage to the kidney, lung, spleen, liver, or heart (Figure 7K). Together, these results suggested that AOH1160 and Olaparib synergistically inhibited the malignant proliferation of HepG2 cells *in vitro* and *in vivo*.

3.8 AOH1160 and olaparib synergistically inhibit DNA damage repair and cell cycle progression

To evaluate the effect of AOH1160 and Olaparib in combination on DNA repair and cell cycle progression, we conducted a series of *in vitro* experiments (Figures 8A–H). Compared with single treatment, DNA damage was more pronounced in the AOH1160 and Olaparib combined group, as determined by the comet assay (Figures 8A, B). Western blots were used to analyze the expression of proteins involved in DNA repair, Olaparib significantly promoted the expression of PARP1, RAD51 and EXO1, AOH1160 significantly inhibited the expression of PARP1, BRCA1, EXO1, and RAD51, but did not affect the expression of PCNA. The combination of AOH1160 and Olaparib synergistically inhibited the expression of BRCA1, EXO1, XRCC1, XRCC2, and RAD51, but did not affect the expression of PARP1 and PCNA (Figures 8C, D). AOH1160 (1.0 μM) inhibited the G2/M transition and arrested the cell cycle at the G2/M phase. Olaparib (8.0 μM) promoted the G1/S transition and arrested the cell cycle at the G2/M phases. Combining AOH1160 (1.0 μM) with Olaparib (8.0 μM) arrested the cell cycle at the G2/M phase (Figures 8E,F). Western blots were used to analyze the expression of proteins involved in cell cycle progression (Figures 8G, H). Olaparib significantly promoted the expression of CDC25C, and CDK1 to accelerate mitosis. AOH1160 significantly inhibited the expression of CCNB1, CDK2 and CCNE2. The combination of AOH1160 and Olaparib promoted the expression of ATR and CHK1, and inhibited the expression of CDC25C, CDK1, CCNB1, CDK2 and CCNE2. AOH1160 impaired Olaparib-induced expression of these proteins in HepG2 cells. IHC staining for PCNA and PARP1 confirmed that Olaparib combined with AOH1160 could induce the down expression of PARP1 and PCNA respectively (Figure 8I). Overall, these findings indicated that PCNA and PARP1 depletion synergistically inhibit DNA repair and cell cycle progression.

4 Discussion

HCC is the leading causes of cancer-related death worldwide, due to mild symptoms at early stage and almost half of the patients are diagnosed at advanced stage (Sadagopan and He, 2024; Wang et al., 2024). With advances in sequencing technology and bioinformatics, innovative targeted therapies can potentially improve survival and quality of life for patients with challenging HCC (Wang et al., 2024; Becht et al., 2024). The success of antiangiogenic agents and tyrosine kinase inhibitors in treating HCC demonstrates that targeted therapy is another option and hope for the treatment of challenging HCC (Becht et al., 2024). However, existing targeted drugs have limitations such as drug resistance, significant side effects, narrow clinical indications, and high tendency for relapse (Lei et al., 2024). Therefore, novel targets and strategies are urgently required for the treatment of HCC. Previous studies have found that PCNA is highly expressed in various types of tumors and contributes to malignant progression and poor prognosis (Lv et al., 2016; Gu et al., 2023). Targeting PCNA in monotherapy or combination therapy may have a good therapeutic effect on HCC (Cheng et al., 2020). Herein, we investigated the mechanism of PCNA in regulating the malignant progression of HCC cells from the perspective of regulating DNA repair and cell cycle progression.

PCNA is the center of DNA replication and DNA damage repair that plays an important role in maintaining genomic integrity and preventing the propagation of DNA errors (González-Magaña and

Blanco, 2020). PCNA is highly expressed in many cancers and contributes to malignant proliferation and poor prognosis (Lv et al., 2016). Consistently, our research confirmed that PCNA is overexpressed in HCC cells and high expression of PCNA is associated with poor prognosis and short survival in HCC patients. Additionally, we found that suppression of PCNA with shPCNA or AOH1160 significantly inhibited the proliferation of HCC cells both *in vitro* and *in vivo*. AOH1160 is a PCNA inhibitor that can selectively kill many types of cancer cells at below micromolar concentrations through specifically targeting the L126-Y133 region of PCNA in cancer cells, without causing significant toxicity to a broad range of nonmalignant cells (Gu et al., 2018). To elucidate the specific mechanisms, we performed RNA sequencing to analyze the effect of PCNA on total mRNA expression in HepG2 cells. The result showed that PCNA promoted the malignant progression of HCC cells by regulating cell cycle progression and DNA damage repair. Further mechanism studies showed that knockdown of PCNA inhibited the expression of EXO1, BRCA1, RAD51, PARP1, and other genes-involved in DNA damage repair. The long-range end-resection factor EXO1 is a multipotent DNA exonerase that is mainly involved in HR repair and non-homologous end-link repair (Gioia et al., 2023; van de Kooij et al., 2024). BRCA1 and RAD51 are the essential factors involved in HR repair pathway that trigger the precise repair of DNA DSBs (Zhao et al., 2017). In cells lacking EXO1, BRCA1 and RAD51, the precise DSB repair pathway does not work properly (van de Kooij et al., 2024; Zhao et al., 2017). PARP1 is involved in DNA SSBs repair through the BER pathway. The effect of PCNA on the expression of these genes suggested that PCNA could repair both SSBs and DSBs of DNA through multiple pathways. Precise DNA damage repair occurs in the S and G2 phases of the cell cycle, especially in the HR repair pathway (Bournaka et al., 2024). Indeed, knockdown of PCNA blocked the cell cycle in the G2/M phase and inhibited the expression of CDC25C, CDK1, and CCNB1. CDC25C is a cell cycle regulatory protein that can activate CDK1 and CCNB1 to promote cell mitosis (Liu et al., 2020). The combination of CDK1 and CCNB1 can promote cells from G2 phase to M phase and ensure normal cell division and proliferation (Smith et al., 2020). Decreased expression of CDC25C, CDK1, and CCNB1 inhibited the transfer of cell cycle from G2 phase to M phase, resulting in the inhibition of cancer cell proliferation (Liu et al., 2020; Smith et al., 2020). When the cell cycle is blocked in the G2 phase, precise DNA repair is initiated. If DNA cannot be repaired in this phase, large amounts of DNA fragments accumulate, leading to chromosomal instability and cell death (Wang et al., 2021; Smith et al., 2020). The regulatory effects of PCNA on DNA repair and cell cycle progression suggest that PCNA is a key driving target for HCC progression and poor prognosis. Targeting PCNA has the potential to improve survival and quality of life for patients with advanced and metastasis HCC.

Subsequently, we identified PARP1 as the key target involved in the PCNA-mediated HCC proliferation. While previous studies have established that PCNA orchestrates DNA replication and repair via its functional interplay with PCLAF (De March et al., 2018), our work extends this paradigm by revealing the role of PCNA as a modulator of PARP1 expression. To dissect the cooperative mechanism underlying PCNA-PARP1 oncogenic activity, we employed Co-IP assays and confirmed their direct interaction. Our results position PARP1 as a downstream effector of PCNA and suggest its potential integration into a tripartite regulatory complex involving PCNA and PCLAF. This cooperative interaction likely fine-tunes DNA replication fidelity and repair pathway selection. Clinically, PARP inhibitors such as Olaparib have demonstrated synthetic lethality in homologous recombination (HR)-deficient cancers. Emerging strategies aim to overcome PARP inhibitors resistance and broaden their utility to HR-proficient malignancies, including HCC. Based on our findings, we propose that PCNA inhibition may sensitize HR-competent HCC to PARP inhibitors by destabilizing the PCNA/PARP1 axis, thereby exacerbating replication stress-induced genomic instability. This synergistic therapeutic vulnerability could expand PARP inhibitors applications in HCC treatment, particularly in tumors resistant to conventional therapies. Supporting this hypothesis, we used shPCNA or AOH1160 to inhibit the expression or activity of PCNA and investigated the regulatory effect of PCNA on the sensitivity of HepG2 cells to Olaparib *in vitro* and *in vivo*. Knockdown of PCNA promoted the inhibitory effect of Olaparib on the malignant proliferation of HepG2 cells *in vitro* and *in vivo*. Meanwhile, silencing PCNA expression enhanced the effect of Olaparib on cell apoptosis and DNA repair and cell cycle progression. Moreover, AOH1160 and Olaparib synergistically inhibited the proliferation of HepG2 cells and HepG2 xenograft tumors. Further mechanistic studies showed that knockdown of PCNA inhibited the expression of BRCA1, RAD51, XRCC1, and EXO1. AOH1160 also inhibited the expression of these DNA repair-related genes. The reduction of these genes would block HR-mediated repair, thereby increasing the sensitivity of HCC cells to Olaparib. Olaparib induced the upregulation of PARP1 and RAD51, a compensatory feedback mechanism activated in response to persistent DNA damage, which may drive the development of therapeutic resistance (Fu et al., 2024; Liu et al., 2024). Suppression of PCNA impaired Olaparib-induced overexpression of PARP1 and RAD51, thereby reversing the resistance of cancer cells to Olaparib. Meanwhile, we found that inhibition of PCNA with AOH1160 and inhibition of PARP1 with Olaparib could arrest the cell cycle at the G2/M phases. Olaparib significantly promoted the expression of CCNE2 to accelerate mitosis (Smith et al., 2020; Ditano et al., 2021). Olaparib-induced accelerating of cell cycle progression was beneficial for HR-mediated DNA repair (Wicks et al., 2022). AOH1160 repressed the expression of CDK1, CCNB1, CDK2 and CCNE2 to arrest the cell cycle at G2/M phase, thus blocking the promotion of cancer cell mitosis. The combination of Olaparib and AOH1160 promoted the expression of ATR and CHK1, inhibited the expression of CD25C, CDK1, CCNB1, CDK2 and CCNE2. DNA single-strand breaks activate ATR, which phosphorylates and activates CHK1. Activated CHK1 then phosphorylates CDC25C, resulting in its inactivation and maintaining CDK1 in an inactive phosphorylated state, thereby arrested the cell cycle at G2/M phase to inhibit the malignant proliferation of HCC cells (Smith et al., 2020). However, neither AOH1160 nor Olaparib affects the expression of ATM and CHK2, whether they influence the phosphorylation of these targets will be explored in our further studies.

In conclusion, we clarified the mechanism for the effect of PCNA on the proliferation of challenging HCC *in vitro* and *in vivo*. PCNA is overexpressed in HCC cells and closely correlated with the poor prognosis of HCC patients. PCNA promotes the proliferation and progression of HCC by regulating DNA repair and cell cycle progression. Mechanistically, PARP1 is the downstream

target of PCNA and directly interacts with PCNA. Targeting PCNA increase the sensitivity of HCC cells to Olaparib. Further AOH1160 and Olaparib synergistically inhibited the proliferation, DNA damage repair and cell cycle progression of HCC cells. The present findings support the premise coinhibition of PCNA and PAPR1 for the treatment of advanced HCC. Collectively, the study provides a mechanistic foundation for therapies targeting PCNA/PARP1 axis and the development of dual-target PCNA/PARP1 inhibitors.

Data availability statement

The original contributions presented in the study are publicly available. This data can be found here: https://www.ncbi.nlm.nih.gov/, accession number PRJNA1247785.

Ethics statement

The animal study was approved by the Committee on the Ethics of Animal Experiments of Lanzhou University. The study was conducted in accordance with the local legislation and institutional requirements.

Author contributions

JL: Conceptualization, Data curation, Investigation, Methodology, Writing – original draft. TY: Formal Analysis, Methodology, Validation, Writing – original draft. YC: Investigation, Writing – original draft. TZ: Investigation, Writing – original draft. KZ: Writing – original draft. SW: Conceptualization, Funding acquisition, Writing – review and editing. YZ: Conceptualization, Supervision, Writing – review and editing.

Funding

The author(s) declare that financial support was received for the research and/or publication of this article. This study was supported by the National Natural Science Foundation of China (Nos 82104206 and 82373890).

Acknowledgments

This work was supported by the NewMedical Innovation Platform of Lanzhou University and Key Lab of Preclinical Study for New Drugs of Gansu Province (Lanzhou, Gansu, China). We are grateful for the sequencing platform and bioinformaticanalysis of Gene Denovo Biotechnology Co., Ltd. (Guangzhou, Guangdong, China), and the support of animal experiments ofOG Pharmaceutical Technology Co., Ltd (Nanjing, Jiangsu, China).

Conflict of interest

The authors declare that the research was conducted in the absence of any commercial or financial relationships that could be construed as a potential conflict of interest.

Generative AI statement

The author(s) declare that no Generative AI was used in the creation of this manuscript.

Publisher's note

Supplementary material

The Supplementary Material for this article can be found online at: https://www.frontiersin.org/articles/10.3389/fphar.2025.1571786/full#supplementary-material

References

Arbel, M., Choudhary, K., Tfilin, O., and Kupiec, M. (2021). PCNA loaders and unloaders-one ring that rules them all. *Genes (Basel)* 12 (11), 1812. doi:10.3390/genes12111812

Becht, R., Kiełbowski, K., and Wasilewicz, M. P. (2024). New opportunities in the systemic treatment of hepatocellular carcinoma-today and tomorrow. *Int. J. Mol. Sci.* 25 (3), 1456. doi:10.3390/ijms25031456

Boehm, E. M., Gildenberg, M. S., and Washington, M. T. (2016). The many roles of PCNA in eukaryotic DNA replication. *Enzymes* 39, 231–254. doi:10.1016/bs.enz.2016.03.003

Bournaka, S., Badra-Fajardo, N., Arbi, M., Taraviras, S., and Lygerou, Z. (2024). The cell cycle revisited: DNA replication past S phase preserves genome integrity. *Semin. Cancer Biol.* 99, 45–55. doi:10.1016/j.semcancer.2024.02.002

Brown, Z. J., Tsilimigras, D. I., Ruff, S. M., Mohseni, A., Kamel, I. R., Cloyd, J. M., et al. (2023). Management of hepatocellular carcinoma: a review. *JAMA Surg.* 158 (4), 410–420. doi:10.1001/jamasurg.2022.7989

Cardano, M., Tribioli, C., and Prosperi, E. (2020). Targeting proliferating cell nuclear antigen (PCNA) as an effective strategy to inhibit tumor cell proliferation. *Curr. Cancer Drug Targets* 20 (4), 240–252. doi:10.2174/1568009620666200115162814

Cazzalini, O., Perucca, P., Riva, F., Stivala, L. A., Bianchi, L., Vannini, V., et al. (2003). p21CDKN1A does not interfere with loading of PCNA at DNA replication sites, but inhibits subsequent binding of DNA polymerase delta at the G1/S phase transition. *Cell Cycle* 2 (6), 596–603. doi:10.4161/cc.2.6.502

Cheng, H., Cao, X., Min, X., Zhang, X., Kong, Q., Mao, Q., et al. (2020). Heat-Shock protein A12A is a novel PCNA-binding protein and promotes hepatocellular carcinoma growth. *Febs J.* 287 (24), 5464–5477. doi:10.1111/febs.15276

Chou, T. C. (2006). Theoretical basis, experimental design, and computerized simulation of synergism and antagonism in drug combination studies. *Pharmacol. Rev.* 58 (3), 621–681. doi:10.1124/pr.58.3.10

Collins, A., Møller, P., Gajski, G., Vodenková, S., Abdulwahed, A., Anderson, D., et al. (2023). Measuring DNA modifications with the comet assay: a compendium of protocols. *Nat. Protoc.* 18 (3), 929–989. doi:10.1038/s41596-022-00754-y

De March, M., Barrera-Vilarmau, S., Crespan, E., Mentegari, E., Merino, N., Gonzalez-Magaña, A., et al. (2018). p15PAF binding to PCNA modulates the DNA sliding surface. *Nucleic Acids Res.* 46 (18), 9816–9828. doi:10.1093/nar/gky723

Dilmac, S., and Ozpolat, B. (2023). Mechanisms of PARP-inhibitor-resistance in BRCA-mutated breast cancer and new therapeutic approaches. *Cancers (Basel)* 15 (14), 3642. doi:10.3390/cancers15143642

Ditano, J. P., Sakurikar, N., and Eastman, A. (2021). Activation of CDC25A phosphatase is limited by CDK2/cyclin A-mediated feedback inhibition. *Cell Cycle* 20 (13), 1308–1319. doi:10.1080/15384101.2021.1938813

Dopazo, C., Søreide, K., Rangelova, E., Mieog, S., Carrion-Alvarez, L., Diaz-Nieto, R., et al. (2024). Hepatocellular carcinoma. *Eur. J. Surg. Oncol.* 50 (1), 107313. doi:10.1016/j.ejso.2023.107313

Fu, X., Li, P., Zhou, Q., He, R., Wang, G., Zhu, S., et al. (2024). Mechanism of PARP inhibitor resistance and potential overcoming strategies. *Genes Dis.* 11 (1), 306–320. doi:10.1016/j.gendis.2023.02.014

Gioia, M., Payero, L., Salim, S., Fajish, V. G., Farnaz, A. F., Pannafino, G., et al. (2023). Exo1 protects DNA nicks from ligation to promote crossover formation during meiosis. *PLoS Biol.* 21 (4), e3002085. doi:10.1371/journal.pbio.3002085

González-Magaña, A., and Blanco, F. J. (2020). Human PCNA structure, function and interactions. *Biomolecules* 10 (4), 570. doi:10.3390/biom10040570

Groelly, F. J., Fawkes, M., Dagg, R. A., Blackford, A. N., and Tarsounas, M. (2023). Targeting DNA damage response pathways in cancer. *Nat. Rev. Cancer* 23 (2), 78–94. doi:10.1038/s41568-022-00535-5

Gu, L., Hickey, R. J., and Malkas, L. H. (2023). Therapeutic targeting of DNA replication stress in cancer. *Genes (Basel)* 14 (7), 1346. doi:10.3390/genes14071346

Gu, L., Lingeman, R., Yakushijin, F., Sun, E., Cui, Q., Chao, J., et al. (2018). The anticancer activity of a first-in-class small-molecule targeting PCNA. *Clin. Cancer Res.* 24 (23), 6053–6065. doi:10.1158/1078-0432.Ccr-18-0592

Huang, S. H., Cao, R., Lin, Q. W., Wu, S. Q., Gao, L. L., Sun, Q., et al. (2022). Design, synthesis and mechanism studies of novel dual PARP1/BRD4 inhibitors against pancreatic cancer. *Eur. J. Med. Chem.* 230, 114116. doi:10.1016/j.ejmech.2022.114116

Kim, B., Huang, Y., Ko, K.-P., Zhang, S., Zou, G., Zhang, J., et al. (2024a). PCLAF-DREAM drives alveolar cell plasticity for lung regeneration. *Nat. Commun.* 15 (1), 9169. doi:10.1038/s41467-024-53330-1

Kim, S., Park, S. H., Kang, N., Ra, J. S., Myung, K., and Lee, K. Y. (2024b). Polyubiquitinated PCNA triggers SLX4-mediated break-induced replication in alternative lengthening of telomeres (ALT) cancer cells. *Nucleic Acids Res.* 52 (19), 11785–11805. doi:10.1093/nar/gkae785

Knaneh, J., Hodak, E., Fedida-Metula, S., Edri, A., Eren, R., Yoffe, Y., et al. (2023). mAb14, a monoclonal antibody against cell surface PCNA: a potential Tool for sezary syndrome diagnosis and targeted immunotherapy. *Cancers (Basel)* 15 (17), 4421. doi:10.3390/cancers15174421

Kundu, K., Ghosh, S., Sarkar, R., Edri, A., Brusilovsky, M., Gershoni-Yahalom, O., et al. (2019). Inhibition of the NKp44-PCNA immune checkpoint using a mAb to PCNA. *Cancer Immunol. Res.* 7 (7), 1120–1134. doi:10.1158/2326-6066.Cir-19-0023

Kwan, A., McDermott-Brown, I., and Muthana, M. (2024). Proliferating cell nuclear antigen in the era of oncolytic virotherapy. *Viruses* 16 (8), 1264. doi:10.3390/v16081264

Laspata, N., Kaur, P., Mersaoui, S. Y., Muoio, D., Liu, Z. S., Bannister, M. H., et al. (2023). PARP1 associates with R-loops to promote their resolution and genome stability. *Nucleic Acids Res.* 51 (5), 2215–2237. doi:10.1093/nar/gkad066

Laspata, N., Muoio, D., and Fouquerel, E. (2024). Multifaceted role of PARP1 in maintaining genome stability through its binding to alternative DNA structures. *J. Mol. Biol.* 436 (1), 168207. doi:10.1016/j.jmb.2023.168207

Lei, Y. R., He, X. L., Li, J., and Mo, C. F. (2024). Drug resistance in hepatocellular carcinoma: theoretical basis and therapeutic aspects. *Front. Biosci. Landmark Ed.* 29 (2), 52. doi:10.31083/j.fbl2902052

Li, H., Liu, Z. Y., Wu, N., Chen, Y. C., Cheng, Q., and Wang, J. (2020). PARP inhibitor resistance: the underlying mechanisms and clinical implications. *Mol. Cancer* 19 (1), 107. doi:10.1186/s12943-020-01227-0

Liu, C., Li, J., Xu, F., Chen, L., Ni, M., Wu, J., et al. (2024). PARP1-DOT1L transcription axis drives acquired resistance to PARP inhibitor in ovarian cancer. *Mol. Cancer* 23 (1), 111. doi:10.1186/s12943-024-02025-8

Liu, K., Zheng, M., Lu, R., Du, J., Zhao, Q., Li, Z., et al. (2020). The role of CDC25C in cell cycle regulation and clinical cancer therapy: a systematic review. *Cancer Cell Int.* 20, 213. doi:10.1186/s12935-020-01304-w

Lv, Q., Zhang, J., Yi, Y., Huang, Y., Wang, Y., Wang, Y., et al. (2016). Proliferating cell nuclear antigen has an association with prognosis and risks factors of cancer patients: a systematic review. *Mol. Neurobiol.* 53 (9), 6209–6217. doi:10.1007/s12035-015-9525-3

Morganti, S., Marra, A., De Angelis, C., Toss, A., Licata, L., Giugliano, F., et al. (2024). PARP inhibitors for breast cancer treatment: a review. *JAMA Oncol.* 10 (5), 658–670. doi:10.1001/jamaoncol.2023.7322

Prabhu, K. S., Kuttikrishnan, S., Ahmad, N., Habeeba, U., Mariyam, Z., Suleman, M., et al. (2024). H2AX: a key player in DNA damage response and a promising target for cancer therapy. *Biomed. Pharmacother.* 175, 116663. doi:10.1016/j.biopha.2024.116663

Rimassa, L., Finn, R. S., and Sangro, B. (2023). Combination immunotherapy for hepatocellular carcinoma. *J. Hepatol.* 79 (2), 506–515. doi:10.1016/j.jhep.2023.03.003

Rumgay, H., Arnold, M., Ferlay, J., Lesi, O., Cabasag, C. J., Vignat, J., et al. (2022). Global burden of primary liver cancer in 2020 and predictions to 2040. *J. Hepatol.* 77 (6), 1598–1606. doi:10.1016/j.jhep.2022.08.021

Sadagopan, N., and He, A. R. (2024). Recent progress in systemic therapy for advanced hepatocellular carcinoma. *Int. J. Mol. Sci.* 25 (2), 1259. doi:10.3390/ijms25021259

Sankar, K., Gong, J., Osipov, A., Miles, S. A., Kosari, K., Nissen, N. N., et al. (2024). Recent advances in the management of hepatocellular carcinoma. *Clin. Mol. Hepatol.* 30 (1), 1–15. doi:10.3350/cmh.2023.0125

Shao, Z., Yang, J., Gao, Y., Zhang, Y., Zhao, X., Shao, Q., et al. (2023). Structural and functional studies of PCNA from African swine fever virus. *J. Virol.* 97 (8), e0074823. doi:10.1128/jvi.00748-23

Shen, C., Li, J., Zhang, Q., Tao, Y., Li, R., Ma, Z., et al. (2022). LncRNA GASAL1 promotes hepatocellular carcinoma progression by up-regulating USP10-stabilized PCNA. *Exp. Cell Res.* 415 (1), 112973. doi:10.1016/j.yexcr.2021.112973

Smith, H. L., Southgate, H., Tweddle, D. A., and Curtin, N. J. (2020). DNA damage checkpoint kinases in cancer. *Expert Rev. Mol. Med.* 22, e2. doi:10.1017/erm.2020.3

Suresh, D., Srinivas, A. N., Prashant, A., Harikumar, K. B., and Kumar, D. P. (2023). Therapeutic options in hepatocellular carcinoma: a comprehensive review. *Clin. Exp. Med.* 23 (6), 1901–1916. doi:10.1007/s10238-023-01014-3

van de Kooij, B., Schreuder, A., Pavani, R., Garzero, V., Uruci, S., Wendel, T. J., et al. (2024). EXO1 protects BRCA1-deficient cells against toxic DNA lesions. *Mol. Cell* 84 (4), 659–674.e7. doi:10.1016/j.molcel.2023.12.039

Vogel, A., Meyer, T., Sapisochin, G., Salem, R., and Saborowski, A. (2022). Hepatocellular carcinoma. *Lancet* 400 (10360), 1345–1362. doi:10.1016/s0140-6736(22)01200-4

Walsh, K. D., and Kato, T. A. (2023). Alkaline comet assay to detect DNA damage. *Methods Mol. Biol.* 2519, 65–72. doi:10.1007/978-1-0716-2433-3_7

Wang, M. D., Xu, X. J., Wang, K. C., Diao, Y. K., Xu, J. H., Gu, L. H., et al. (2024). Conversion therapy for advanced hepatocellular carcinoma in the era of precision medicine: current status, challenges and opportunities. *Cancer Sci.* 115 (7), 2159–2169. doi:10.1111/cas.16194

Wang, S. P., Wu, S. Q., Huang, S. H., Tang, Y. X., Meng, L. Q., Liu, F., et al. (2021). FDI-6 inhibits the expression and function of FOXM1 to sensitize BRCA-proficient triple-negative breast cancer cells to Olaparib by regulating cell cycle progression and DNA damage repair. *Cell Death Dis.* 12 (12), 1138. doi:10.1038/s41419-021-04434-9

Wang, Y. L., Wu, W. R., Lin, P. L., Shen, Y. C., Lin, Y. Z., Li, H. W., et al. (2022). The functions of PCNA in tumor stemness and invasion. *Int. J. Mol. Sci.* 23 (10), 5679. doi:10.3390/ijms23105679

Waraky, A., Lin, Y., Warsito, D., Haglund, F., Aleem, E., and Larsson, O. (2017). Nuclear insulin-like growth factor 1 receptor phosphorylates proliferating cell nuclear antigen and rescues stalled replication forks after DNA damage. *J. Biol. Chem.* 292 (44), 18227–18239. doi:10.1074/jbc.M117.781492

Wei, X., Zhou, F., and Zhang, L. (2024). PARP1-DNA co-condensation: the driver of broken DNA repair. *Signal Transduct. Target Ther.* 9 (1), 135. doi:10.1038/s41392-024-01832-1

Wicks, A. J., Krastev, D. B., Pettitt, S. J., Tutt, A. N. J., and Lord, C. J. (2022). Opinion: PARP inhibitors in cancer-what do we still need to know? *Open Biol.* 12 (7), 220118. doi:10.1098/rsob.220118

Wu, S. Q., Huang, S. H., Lin, Q. W., Tang, Y. X., Huang, L., Xu, Y. G., et al. (2022). FDI-6 and olaparib synergistically inhibit the growth of pancreatic cancer by repressing BUB1, BRCA1 and CDC25A signaling pathways. *Pharmacol. Res.* 175, 106040. doi:10.1016/j.phrs.2021.106040

Xie, L., Cheng, Y., Hu, B., Chen, X., An, Y., Xia, Z., et al. (2024). PCLAF induces bone marrow adipocyte senescence and contributes to skeletal aging. *Bone Res.* 12 (1), 38. doi:10.1038/s41413-024-00337-5

Yang, C., Zhang, Y., Chen, Y., Ragaller, F., Liu, M., Corvigno, S., et al. (2020). Nuclear IGF1R interact with PCNA to preserve DNA replication after DNA-damage in a variety of human cancers. *PLoS One* 15 (7), e0236291. doi:10.1371/journal.pone.0236291

Yang, X., Yang, C., Zhang, S., Geng, H., Zhu, A. X., Bernards, R., et al. (2024). Precision treatment in advanced hepatocellular carcinoma. *Cancer Cell* 42 (2), 180–197. doi:10.1016/j.ccell.2024.01.007

Zeng, Y., Arisa, O., Peer, C. J., Fojo, A., and Figg, W. D. (2024). PARP inhibitors: a review of the pharmacology, pharmacokinetics, and pharmacogenetics. *Semin. Oncol.* 51 (1-2), 19–24. doi:10.1053/j.seminoncol.2023.09.005

Zhang, H., and Zha, S. (2024). The dynamics and regulation of PARP1 and PARP2 in response to DNA damage and during replication. *DNA Repair (Amst)* 140, 103690. doi:10.1016/j.dnarep.2024.103690

Zhang, Y., Han, X., and Shao, Y. (2021). The ROC of Cox proportional hazards cure models with application in cancer studies. *Lifetime Data Anal.* 27 (2), 195–215. doi:10.1007/s10985-021-09516-6

Zhao, W., Steinfeld, J. B., Liang, F., Chen, X., Maranon, D. G., Jian Ma, C., et al. (2017). BRCA1-BARD1 promotes RAD51-mediated homologous DNA pairing. *Nature* 550 (7676), 360–365. doi:10.1038/nature24060

frontiers | Frontiers in Pharmacology

TYPE Review
PUBLISHED 30 April 2025
DOI 10.3389/fphar.2025.1586948

OPEN ACCESS

EDITED BY
Xinyu Wang,
Philadelphia College of Osteopathic Medicine (PCOM), United States

REVIEWED BY
Shameer Pillarisetti,
University of Studies G. d'Annunzio Chieti and Pescara, Italy
Lin-Lin Bu,
Wuhan University, China
Guangtao Yu,
Southern Medical University, China

*CORRESPONDENCE
Jun-Jie Zhou,
zhoujunjie@whu.edu.cn

RECEIVED 03 March 2025
ACCEPTED 23 April 2025
PUBLISHED 30 April 2025

CITATION
Zhou J-J, Feng Y-C, Zhao M-L, Guo Q and Zhao X-B (2025) Nanotechnology-driven strategies in postoperative cancer treatment: innovations in drug delivery systems. *Front. Pharmacol.* 16:1586948. doi: 10.3389/fphar.2025.1586948

Nanotechnology-driven strategies in postoperative cancer treatment: innovations in drug delivery systems

Jun-Jie Zhou*, Yan-Chuan Feng, Min-Long Zhao, Qi Guo and Xi-Bo Zhao

The Stomatological Hospital, Anyang Sixth People's Hospital, Anyang, China

Cancer remains a global health challenge, and this challenge comes with a significant burden. Current treatment modalities, such as surgery, chemotherapy, and radiotherapy, have their limitations. The emergence of nanomedicines presents a new frontier in postoperative cancer treatment, offering potential to inhibit tumor recurrence and manage postoperative complications. This review deeply explores the application and potential of nanomedicines in the treatment of cancer after surgery. In particular, it focuses on local drug delivery systems (LDDS), which consist of *in situ* injection, implantation, and spraying. LDDS can provide targeted drug delivery and controlled release, which enhancing therapeutic efficacy. At the same time, it minimizes damage to healthy tissues and reduces systemic side effects. The nanostructures of these systems are unique. They facilitate the sustained release of drugs, prolong the effects of treatment, and decrease the frequency of dosing. This is especially beneficial in the postoperative period. Despite their potential, nanomedicines have limitations. These include high production costs, concerns regarding long-term toxicity, and complex regulatory approval processes. This paper aims to analyze several aspects. These include the advantages of nanomedicines, their drug delivery systems, how they combine with multiple treatment methods, and the associated challenges. Future research should focus on certain issues. These issues are stability, tumor specificity, and clinical translation. By addressing these, the delivery methods can be optimized and their therapeutic efficacy enhanced. With the advancements in materials science and biomedical engineering, the future design of LDDS is set to become more intelligent and personalized. It will cater to the diverse needs of clinical treatment and offer hope for better outcomes in cancer patients after surgery.

KEYWORDS

local drug delivery system, nanomedicines, postoperative treatment, anti-cancer, combination therapies

1 Introduction

Cancer, a disease that has been plaguing humanity, continues to represent a significant challenge to global health. (Cronin et al., 2022; Jassim et al., 2023; Mahalingam and Newsom-Davis, 2023; Bray et al., 2024). The International Agency for Research on Cancer (IARC), through its Global Cancer Observatory, provides a crucial view of the present global cancer situation. (Bray et al., 2024). The latest data in 2022 reveals a reality: t there are

almost 20 million new cancer cases emerging, and nearly 10 million lives are unfortunately lost to cancer. (Bray et al., 2024). These figures not only highlight the unyielding rise in the global cancer burden but also underscore the pressing need for comprehensive cancer control strategies (Dhas et al., 2024; Li Q. et al., 2024; Taranto et al., 2024). China, with its extensive population and evolving healthcare dynamics, bears a significant share of this burden. In collaboration with the IARC, the National Cancer Center (NCC) of China has reported that in 2022, the country faced approximately 4.82 million new cancer cases and 2.57 million cancer-related deaths (Bray et al., 2024). These statistics translate to a substantial proportion of the global cancer incidence and mortality rates, with lung, colorectal, thyroid, liver, and stomach cancers being the most frequently diagnosed, and lung, liver, stomach, colorectal, and esophageal cancers leading as the primary causes of cancer mortality (Cronin et al., 2022; Labrie et al., 2022; Bray et al., 2024; Budczies et al., 2024; Lasser et al., 2024).

Currently, the primary treatment modalities for cancer include surgery, chemotherapy, radiotherapy, and immunotherapy (Lim et al., 2018; Cramer et al., 2019; Chow and Longo, 2020). Surgical resection remains the predominant treatment strategy for most solid tumors in clinical practice (Schröder et al., 2021; Mi et al., 2023). Despite the remarkable progress in surgical techniques in recent years, however, minuscule tumor cells may still remain at the surgical margins, significantly increasing the risk of tumor recurrence and metastasis and being closely associated with a diminished overall survival rate (Cannon et al., 2017; Hiller et al., 2017; Tohme et al., 2017; Joshi and Badgwell, 2021).

As for chemotherapy and radiotherapy, which are often employed as adjuvant treatments after surgery, they bring about a host of side effects (Bu et al., 2019; Ji et al., 2020; McLaughlin et al., 2020). Immunosuppression renders patients more susceptible to infections and can delay the recovery process (Ji et al., 2020; McLaughlin et al., 2020).

In this context, the utilization of nanomedicines and controllable drug delivery systems implanted in the surgical region emerges as a highly promising strategy (Wang K-N. et al., 2024). Nanomedicines have the potential to inhibit local tumor recurrence and distant metastasis after surgery. Moreover, they can also deal with postoperative complications. (Shao et al., 2018; Chu et al., 2021; Yang X. et al., 2021; Cheng et al., 2022; Li et al., 2022; Wang et al., 2023; Wang R. et al., 2024; Wei et al., 2024). Nanomedicines provide multiple advantages. These advantages include enhanced targeting capabilities, which allow for a more accurate delivery of drugs to cancer cells and minimize the damage to healthy tissues. (Shi et al., 2016; Zhou et al., 2021; Li ZZ. et al., 2024; Pan et al., 2024). This can be particularly beneficial during the postoperative period. It enables a more sustained treatment approach over time. Moreover, nanomedicines have the potential to target and reduce inflammation at the surgical site. This helps to prevent wound infections and promote the healing process. (Siemer et al., 2019; Jiang et al., 2020; Huang et al., 2024; Zhen et al., 2024).

However, nanomedicines also have some limitations (Shi et al., 2016). The synthesis and formulation of nanomedicines are complex, and this complexity can result in high production costs. (Shi et al., 2016). Besides, there are concerns regarding their long-term toxicity and the potential for accumulation within the body. (Shi et al., 2016). Additionally, the regulatory approval process for nanomedicines tends to be long and filled with challenges.

This paper focuses on exploring the application and potential of nanomedicines in postoperative cancer treatment. It aims to analyze the advantages of nanomedicines, their drug delivery systems, multiple treatment methods, and the associated challenges. The goal is to provide new insights and strategies. These can enhance the effectiveness of cancer treatment, reduce the recurrence risk, minimize postoperative complications, and improve the quality of life of cancer patients.

In the field of cancer treatment, LDDS of nanomedicines have emerged. These methods are a highly promising approach for postoperative therapy. (Zhang et al., 2022; Mimansa et al., 2024). The LDDS has a host of unique advantages. These advantages are crucial for enhancing the effectiveness and safety of cancer treatment after surgery. (Zhang et al., 2022; Mimansa et al., 2024).

First and foremost, when compared with systemic drug delivery, local delivery significantly increases the drug dose in the surgical area (Wang et al., 2023; Lin et al., 2024). This targeted approach ensures a higher concentration of therapeutic agents directly at the site where these agents are most needed. As a result, this maximizes the potential for eliminating residual cancer cells. (Chao et al., 2023; Cao et al., 2024; Wei et al., 2024). For example, in the cases of solid tumors, a concentrated dose of nanomedicines in the surgical bed can be highly effective. This effectiveness is shown in contending with any tumor cells that might have remained after the main tumor is removed. (Erthal et al., 2023; Lin et al., 2024; Wang R. et al., 2024).

Secondly, LDDS can decrease the toxic and side effects of drugs on other organs and tissues. (Li et al., 2021; Liu et al., 2021; Dang et al., 2022). By restricting the drugs to the surgical area, the risk of systemic toxicity is minimized (Zhao et al., 2020). This is especially significant because traditional systemic chemotherapy and radiotherapy frequently lead to a wide variety of adverse effects, including nausea, hair loss, fatigue, and damage to the liver, kidneys, and immune system. (Lu et al., 2021; Guan et al., 2022; Wang et al., 2022). With local nanomedicine delivery, patients can experience fewer side effects and a better quality of life during the recovery period (Xu et al., 2020; Lu Q. et al., 2022).

Moreover, LDDS facilitate the continuous and controllable release of drugs (Wang et al., 2022; Wei et al., 2024). Nanoparticles can be engineered to release drugs at a predetermined rate, ensuring a sustained therapeutic effect over an extended period (Liu et al., 2022a; Wang et al., 2023; Lin et al., 2024). This not only decreases the dosing frequency but also offers a more stable and consistent drug concentration level in the target area. For instance, biodegradable nanoparticles are able to slowly degrade and release drugs over a period of time. This maintains an effective drug level and minimizes the risk of overdosage or underdosage simultaneously (Huang et al., 2021; Yang X. et al., 2021; Liu et al., 2022a; Lu Y. et al., 2022).

Finally, LDDS of nanomedicines can facilitate the growth of normal tissues and the healing of wounds in the surgical area. Some nanomedicines can be designed to release growth factors or other bioactive molecules that are capable of stimulating tissue regeneration and repair. This can not only speed up the healing

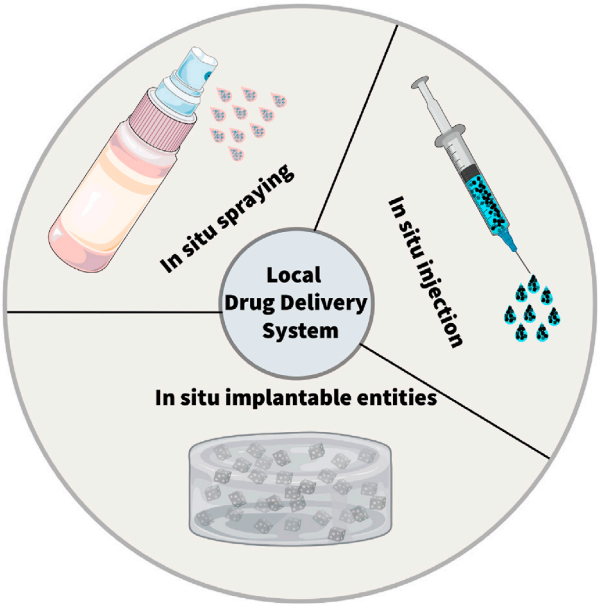

FIGURE 1
Schematic illustration of the local drug delivery systems (LDDSs). There are three typical strategies within LDDSs, including *in situ* injection, *in situ* implantation, *in situ* spraying.

process but also contribute to the restoration of the normal function of the affected area (Lu Y. et al., 2022; Luo et al., 2022).

In this section, we delve deeper into three main LDDS: *in situ* injection, *in situ* implantation, and *in situ* spraying. *In situ* injection involves directly injecting nanomedicines into the surgical site (Zhang H. et al., 2021; Xie et al., 2023; Zhang P. et al., 2024). This method is relatively straightforward. It can be carried out rapidly, enabling the immediate delivery of drugs to the target area. (Figure 1).

In situ implantation, in contrast, consists of placing an implant loaded with drugs into the surgical area (Hu et al., 2021; Mimansa et al., 2024). This approach can achieve long-term and sustained release of drugs. (Zhou et al., 2021). Biodegradable implants can degrade gradually over time, enabling the controlled release of drugs. *In situ* spraying means spraying a nanomedicine solution onto the surgical wound. (Chen et al., 2018; Shao et al., 2018; Chu et al., 2021). This method can cover the wound surface evenly and ensure a consistent distribution of drugs (Chen et al., 2018; Li et al., 2021). It is especially valuable for large wounds or surgical areas with irregular shapes. Meanwhile, these LDDS offer new hope to patients by cleverly combining multiple advanced treatment methods (Table 1). These methods include chemotherapy, radiotherapy, photothermal and photodynamic therapy, immunotherapy, chimeric antigen receptor T - cell (CAR - T) therapy, and magnetic hyperthermia (Figure 2) (Wu et al., 2018;

TABLE 1 Representative nanomaterials summarized in this review for administration strategies of postoperative cancer treatment.

Administration strategies	Materials	In vitro/vivo model	Therapeutics	Reference
In situ injection	$DOXC_{12}$-LNC^{CL}	GL261 tumor mice model	Chemotherapy	Wang et al. (2023)
	GlioGel	U-87 tumor mice model	Chemotherapy	Erthal et al. (2023)
	DTX-CTs/Gel	B16F10/4T1 tumor mice model	Chemotherapy	Liu et al. (2021)
	GPDF	A375 tumor mice model	Photothermal Therapy	Luo et al. (2022)
	PLCNP	patient-derived GICs tumor mice model	Photodynamic Therapy	Lin et al. (2024)
	Tel@PGE	B16F10/4T1 tumor mice model	Immunotherapy	Liu et al. (2022a)
	THINRTHINR-CXCL10	Luci + $GL261^{R132H}$ tumor mice model	Immunotherapy	Zhang et al. (2021c)
	CAR-T@Met/gel	HGC-27 tumor mice model	Immune cell therapy	Chao et al. (2023)
	GODM-gel	H22 tumor mice model	Immune cell therapy	Cheng et al. (2022)
	GM-CSF	Panc02 tumor mice model	Immune cell therapy	Lu et al. (2022b)
In situ implantation	PDA@DH/PLGA	bone tumor mice model	Chemotherapy	Lu et al. (2021)
	TB/αPD-1@AuNCs/OBC	SCC7 tumor mice model	Photothermal Therapy	Zhou et al. (2021)
	Gel-SA-CuO	H22 tumor mice model	Photothermal Therapy	Dang et al. (2022)
	BI(R848 + aOX40)	CT26 tumor mice model	Immunotherapy	Ji et al. (2020)
	3D-ENHANCE-NK cells	MDA-MB-231 tumor mice model	Immune cell therapy	Ahn et al. (2020)
In situ spraying	BP@PLEL	HeLa tumor mice model	Photothermal Therapy	Shao et al. (2018)
	GOx@MnCaP@fibrin	IDH1 (R132H) U87 tumor mice model	Starvation/Chemodynamic Therapy	Li et al. (2021)
	aCD47@CaCO3	B16F10 tumor mice model	Immunotherapy	Chen et al. (2018)

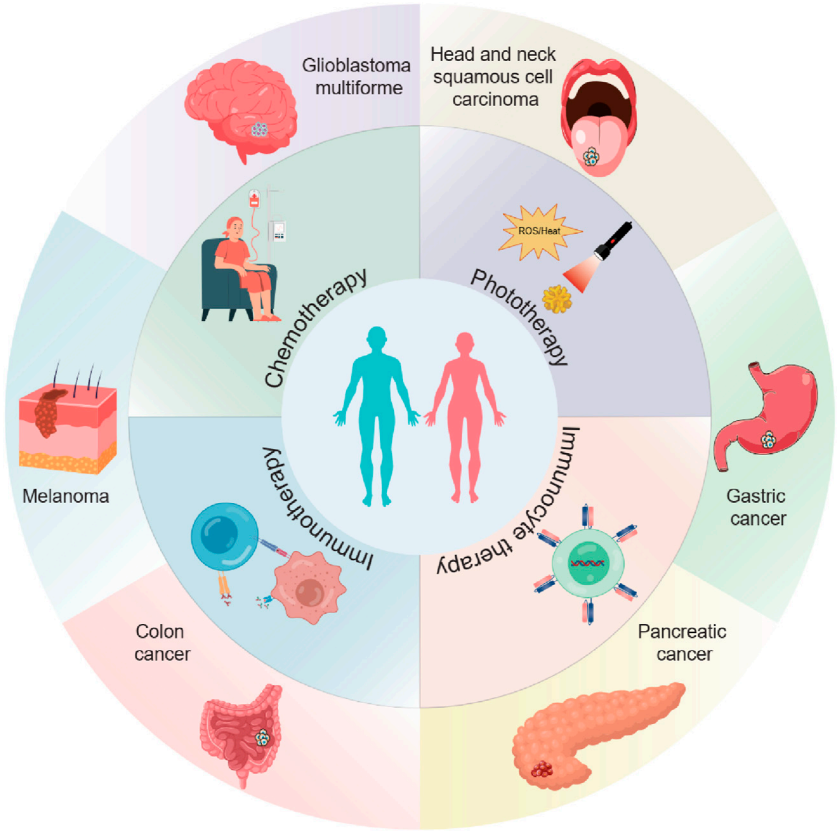

FIGURE 2
The scheme illustrates the application of local drug delivery systems (LDDSs) in the postoperative treatment of various tumors. The LDDSs are combined with chemotherapy, phototherapy, immunotherapy, and immunocyte therapy.

Zhang et al., 2018; Hu et al., 2021; Li et al., 2021; Wang et al., 2021; Guan et al., 2022; Chao et al., 2023).

In conclusion, LDDS of nanomedicines have significant advantages for postoperative cancer treatment. These systems can provide targeted drug delivery, reduce side effects, facilitate controlled release, and promote tissue healing. Therefore, these methods hold great promise in improving the outcomes of cancer patients after surgery. Furthermore, further research and development in this field are required to perfect these delivery methods and enhance their therapeutic efficacy.

2 *In situ* injection

In the field of treatment for tumor recurrence after surgery, the local *in situ* injection drug delivery system offers a brand-new ray of hope to patients deeply afflicted by illness through artfully integrating multiple advanced treatment modalities (Xiong et al., 2021; Zhang J. et al., 2021). Within this diversified treatment landscape, it covers a variety of highly promising means such as chemotherapy, radiotherapy, photothermal and photodynamic therapy, immunotherapy, CAR-T, and magnetic hyperthermia (Yang X. et al., 2021; Luo et al., 2022; Wang et al., 2022; Erthal et al., 2023; Xie et al., 2023; Wei et al., 2024).

2.1 Combination of chemotherapy

Local *in situ* injection can accurately deliver chemotherapeutic drugs to the site of tumor recurrence or the surgical area (Erthal et al., 2023; Wang et al., 2023; Wang R. et al., 2024). This targeted approach increases the local drug concentration, enhances the cytotoxic effect of chemotherapy, can more effectively kill residual tumor cells, reduce the risk of tumor recurrence, and simultaneously minimize systemic side effects (Liu et al., 2021; Wang R. et al., 2024).

Glioblastoma multiforme (GBM) is the most common brain tumor and one of the most aggressive cancers in humans (Fiorica et al., 2006; Zhao et al., 2019; Tan et al., 2020; Schaff and Mellinghoff, 2023). Currently, the main clinical treatment for GBM is still surgical resection supplemented by radiotherapy and chemotherapy (Reardon et al., 2006; Roca et al., 2023; Wu and Lim, 2023). However, due to the high permeability of GBM, after the above treatments, tiny tumor cells unavoidably remain in the operative region, ultimately leading to tumor recurrence and metastasis (Zhang W. et al., 2024). As a result, various forms of LDDS *in situ* injection have been used in the treatment of tumor recurrence after surgery.

Eduardo Ruiz-Hernandez 's research group designed an LDDS (GlioGel), which is composed of an injectable hydrogel carrying free temozolomide and stimulus-responsive paclitaxel-loaded MSN for

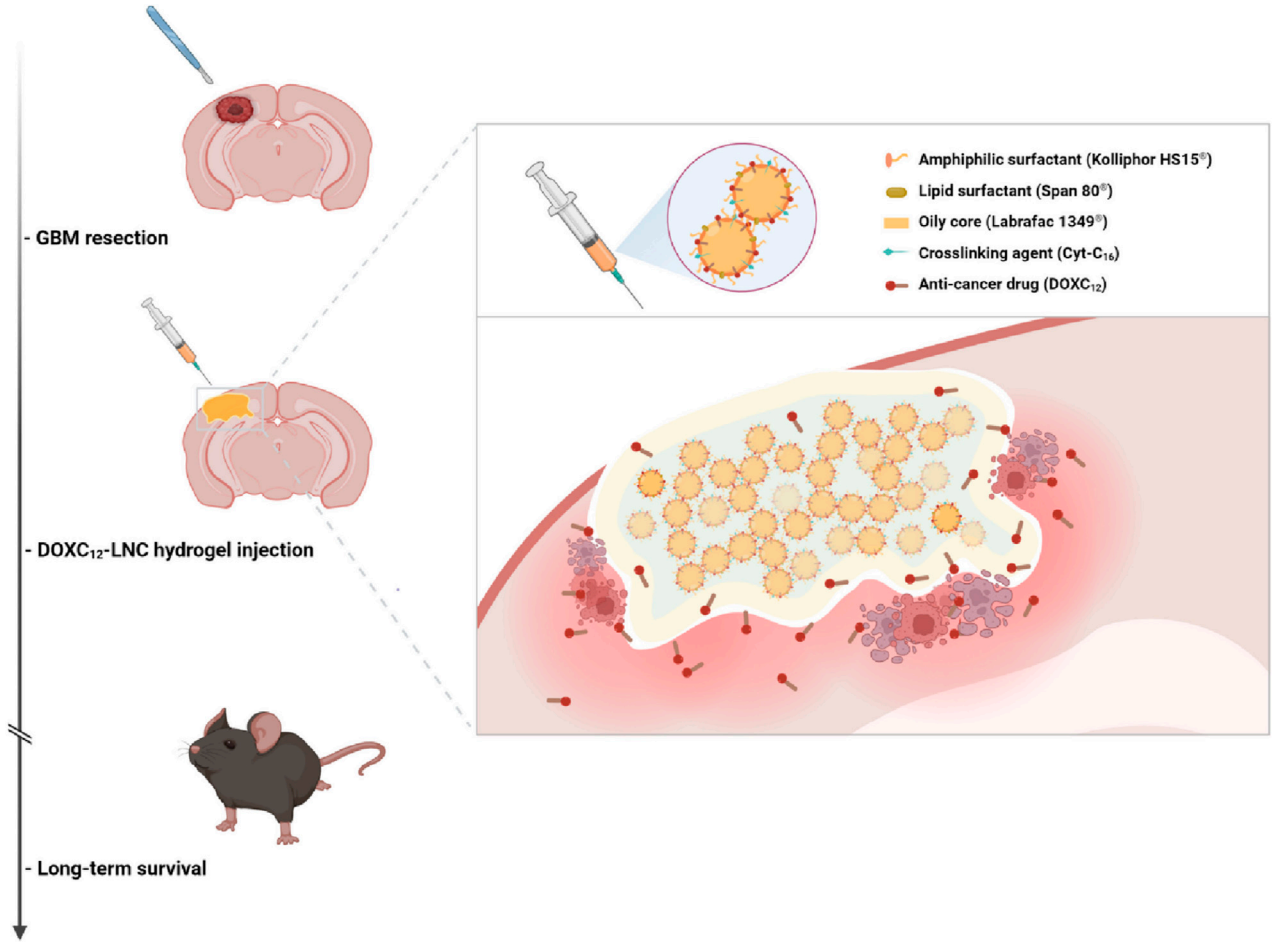

FIGURE 3
The scheme illustrates the application of $DOXC_{12}$-LNC^{CL} for postoperative local treatment of GBM. Reprinted with permission from Ref (Wang et al., 2023). Copyright 2024 Springer.

postoperative local treatment of GBM(Erthal et al., 2023). GlioGel demonstrated a greater ability to penetrate GBM spheroids. The new formulation demonstrated efficacy in decelerating tumor regrowth *in vivo*. It augmented the survival of mice bearing U-87 tumors and enhanced their wellbeing. Simultaneously, Mingchao Wang et al. constructed an injectable lipid nanocapsule (LNC)–based formulation loaded with lauroyl-doxorubicin prodrug ($DOXC_{12}$) ($DOXC_{12}$-LNC^{CL}) that integrates the advantages of nanomedicine and local drug delivery to target these infiltrating GBM cells (Figure 3) (Wang et al., 2023). *In vitro* experiments, $DOXC_{12}$-LNC^{CL} showed sustained drug release for more than 1 month, suggesting its potential as a long-term drug delivery system. Moreover, in an orthotopic GL261 GBM preclinical model, the injection of $DOXC_{12}$-LNC^{CL} into the tumor resection cavity resulted significantly inhibiting the recurrence of GBM and prolonging the survival period of mice.

In situ injection of LDDS combining chemotherapy are also used in the treatment of melanoma (Liu et al., 2021; Wang R. et al., 2024). Melanoma is a type of skin cancer that develops from the pigment-producing cells called melanocytes (Ajithkumar et al., 2015; Ossio et al., 2017; Centeno et al., 2023). It is often characterized by the uncontrolled growth of abnormal melanocytes, which can form tumors on the skin (Shain and Bastian, 2016; Luke et al., 2017; Carvajal et al., 2023). Melanoma has a risk of tumor recurrence after surgery, especially if it had spread before the operation, and metastasis to other parts of the body may also occur (Lian et al., 2022; Patel et al., 2023). Therefore, surgery plus adjuvant therapy remains the preferred clinical strategy for melanoma (Carvajal et al., 2023; Centeno et al., 2023; Patel et al., 2023). Tianyue Jiang et al. constructed a LDDS (DTX-CTs/Gel) that encapsulates DTX within cell-penetrating peptide-modified transfersomes, followed by embedding them in an oligopeptide hydrogel (Liu et al., 2021). DTX- CTs/Gel can precisely deliver the chemotherapeutic drug DTX to the tumor site, enabling LDDS and increasing the concentration of the drug in the tumor tissue. DTX-CTs has a high skin and tumor penetration efficiency, which can promote the chemotherapeutic drug to cross the skin and penetrate into the tumor tissue, enhancing the therapeutic effect. In mouse melanoma and breast tumor models, DTX-CTs/Gel can effectively slow down tumor recurrence, reduce tumor volume, and improve the therapeutic effect (Liu et al., 2021).

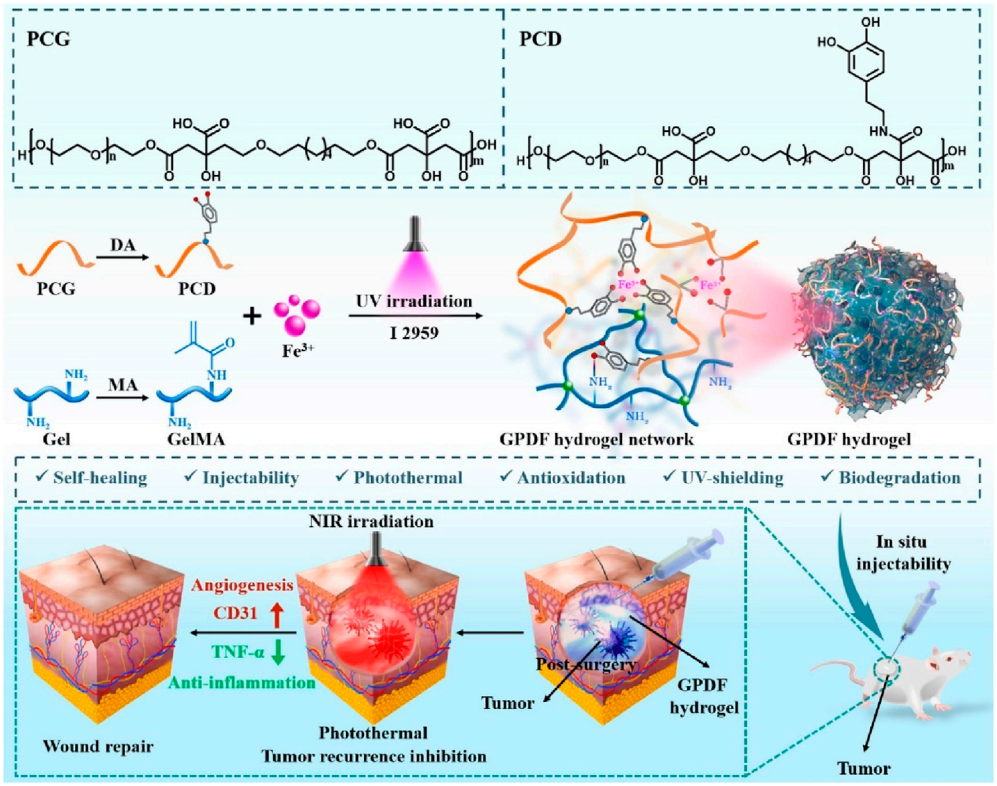

FIGURE 4
The scheme illustrates a multifunctional photothermal ferric citrate hydrogel scaffold (GPDF) for the treatment of postoperative melanoma. Reprinted with permission from Ref (Luo et al., 2022). Copyright 2022 Elsevier.

2.2 Combination of photothermal and photodynamic therapy

Photothermal therapy (PTT), as a minimally invasive treatment method, can convert light energy into heat energy and eliminate tumor tissue through thermal ablation (Li et al., 2020; Xiong et al., 2023; Zhao et al., 2023). Studies have shown that compared with radiotherapy and chemotherapy, PTT is less invasive in the treatment of cancer (Alamdari et al., 2022; Bian et al., 2024). Indocyanine green (ICG) is a near-infrared (NIR) absorbing material widely used in tumor diagnosis and treatment approved by the U.S. Food and Drug Administration (FDA) (Wang et al., 2018; Changalvaie et al., 2019). However, ICG shows limitations such as low light stability, potential toxicity, and poor water stability as a photothermal conversion material (Changalvaie et al., 2019). The new ICG (IR820) has good biocompatibility and stability (Della Pelle et al., 2021; Yang X. et al., 2021; Liu et al., 2024). Therefore, Jinfeng Liao et al. constructed a methylcellulose photothermal hydrogel (IR820/Mgel) for postoperative treatment of breast cancer (Yang X. et al., 2021). The IR820/Mgel hydrogel can quickly heat up under NIR irradiation and can achieve a significant inhibitory effect on tumor recurrence *in vivo* through PTT (Yang X. et al., 2021). At the same time, the IR820/Mgel hydrogel can also achieve breast augmentation by filling the residual cavity after breast surgery and promote breast reconstruction. PTT hydrogels can also be used for postoperative treatment of melanoma. Recently, Lei Bo's team designed a multifunctional bioactive therapeutic ferric citrate hydrogel scaffold (GPDF) for the treatment of postoperative melanoma (Figure 4) (Luo et al., 2022). The GPDF scaffold has the abilities of injectability, self-healing, antioxidation, enhanced photothermal effect and ultraviolet shielding, and can achieve the purposes of inhibiting tumor recurrence and accelerating wound repair at the same time. The polycitric acid-dopamine (PCD) and Fe^{3+} ions are prepared into a GPDF with a double network through the photo-crosslinking of the gel. Among them, PCD can chelate with Fe^{3+} ions to form dynamic coordination bonds, so that the hydrogel scaffold has injectable and self-healing properties. At the same time, PCD-Fe^{3+} shows excellent photothermal treatment effect and ultra-high efficiency (100%). In conclusion, the GPDF scaffold not only significantly inhibits tumor recurrence but also achieves effective wound repair treatment (Luo et al., 2022). Photodynamic therapy (PDT) indeed shows great promise as a non-invasive cancer treatment approach (Abbas et al., 2017; Yang et al., 2023; Zou et al., 2023). The role of the photosensitizer in PDT is crucial as it facilitates the production of singlet oxygen (Wan et al., 2021; Liu et al., 2022b; Zou et al., 2023). Through the energy transfer between its excited triplet state and the ground triplet state of molecular oxygen, reactive oxygen species (ROS) are generated. These ROS have the ability to selectively target and destroy cancer cells (Wan et al., 2021; Liu et al., 2022b; Zou et al., 2023). Gan Jiang's research group developed a self - disassembling and oxygen - generating porphyrin - lipoprotein nanoparticle (PLCNP) that can be used for fluorescence - guided surgery and enhanced postoperative PDT in GBM(Lin et al., 2024). The

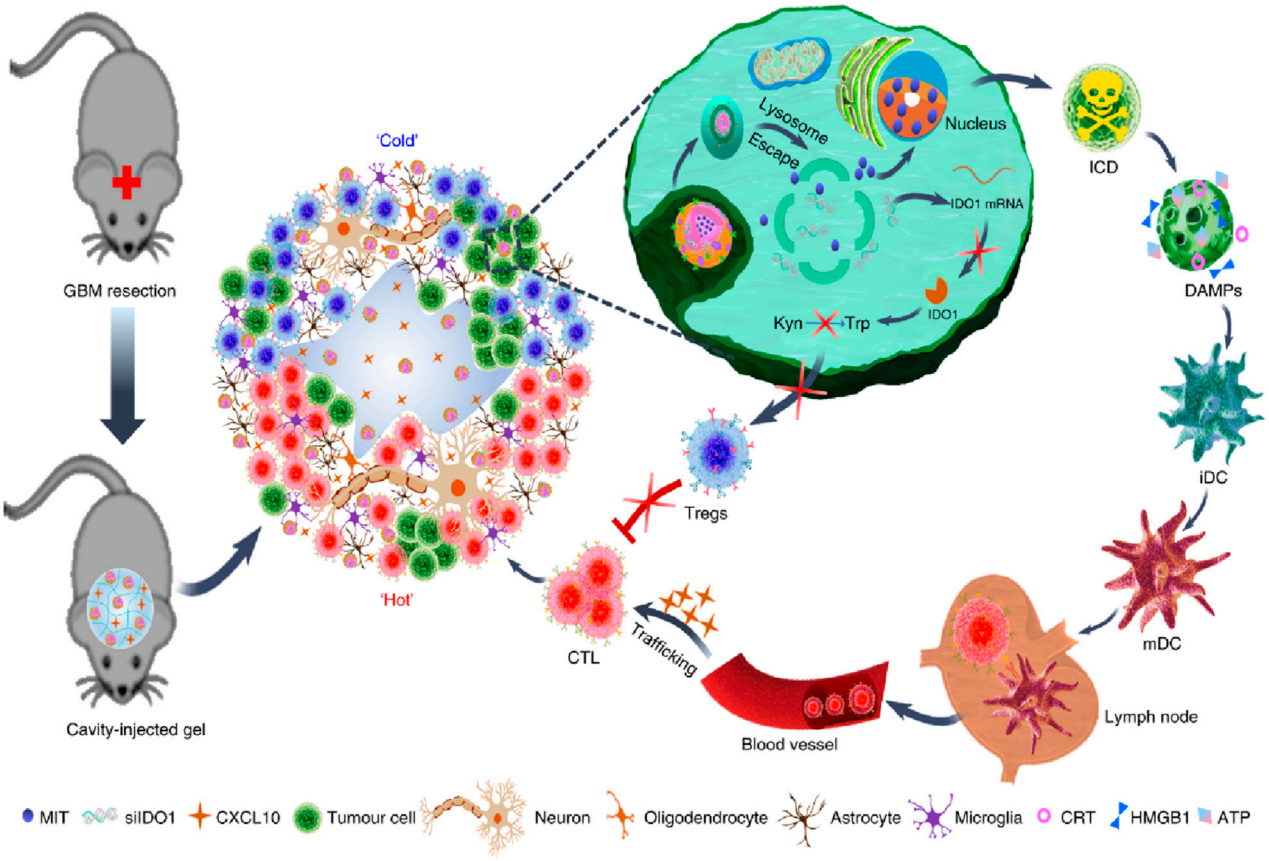

FIGURE 5
The scheme illustrates an *in situ* self-assembling hydrogel LDDS (THINRTHINR-CXCL10) based on oligopeptides for the treatment of a postoperative mouse model of GBM. Reprinted with permission from Ref (Zhang J. et al., 2021). Copyright 2021 Springer Nature.

porphyrin - lipoprotein shell enables targeted accumulation of PLCNP in GBM tissue, and the CaO2 core enhances the fluorescence intensity of the porphyrin photosensitizer, improves the imaging effect, and increases the oxygen level and PDT efficiency in GICs(Lin et al., 2024). This nanoplatform prolongs the survival of GICs - bearing mice and can be combined with clinical surgical practices, providing a new strategy for the precise elimination of GBM and future research (Lin et al., 2024).

2.3 Combination of immunotherapy

Immunotherapeutic agents can also be easily loaded into hydrogels (Yang A. et al., 2021). In recent years, immunotherapy has prevented tumor recurrence after surgery by activating T cells at the tumor site through immune checkpoint blockades (ICB) therapy (Hargadon et al., 2018). However, less than 20% of patients have a sustained clinical response to ICB treatment (Pérez-Ruiz et al., 2020; Schoenfeld and Hellmann, 2020). In addition, ICB is ineffective in tumors characterized by new antigens and somatic mutations. Therefore, it is extremely urgent to relieve the immunosuppressive environment in the tumor microenvironment (TME) (Byun et al., 2017; He and Xu, 2020). Recently, Jiang Xinyi's research group designed an *in situ* self-assembling hydrogel LDDS (THINRTHINR-CXCL10) based on oligopeptides for the treatment of a postoperative mouse model of GBM (Figure 5) (Zhang H. et al., 2021). The THINRTHINR-CXCL10 hydrogel has the characteristics of high biocompatibility and low viscosity. It is easy to flow during administration and can quickly form a gel network in the cavity of the surgical area. Subsequently, the THINRTHINR-CXCL10 hydrogel acts as a drug reservoir and synergistically releases CXCL10 and THINR in a sustained manner in the surgical area. THINR specifically targets residual tumor cells and is stimulated to decompose under the acidic environment of the TME. The released siIDO1 can relieve Treg-related immunosuppression and activate T cells. At the same time, the CXCL10 chemokine can activate the body's systemic immunity and enrich T cells to kill residual tumor cells, ultimately significantly inhibiting the recurrence of GBM and prolonging the survival period of mice (Zhang J. et al., 2021). Postoperative recurrence and metastasis of cancer are the main reasons for the high mortality rate. Some immunostimulants can reduce local recurrence and distant metastasis and increase the survival rate during the perioperative period, but excessive immune response is a key therapeutic challenge. Telratolimod (Tel), a TLR 7/8 agonist, has a lipid tail structure to improve hydrophobicity and lymphatic targeting ability, but an effective delivery system is still needed to reduce systemic exposure and inflammatory reactions (Liu et al., 2022a). Liu Hongzhuo developed an injectable delivery platform (Tel@PGE) to deliver Tel to the

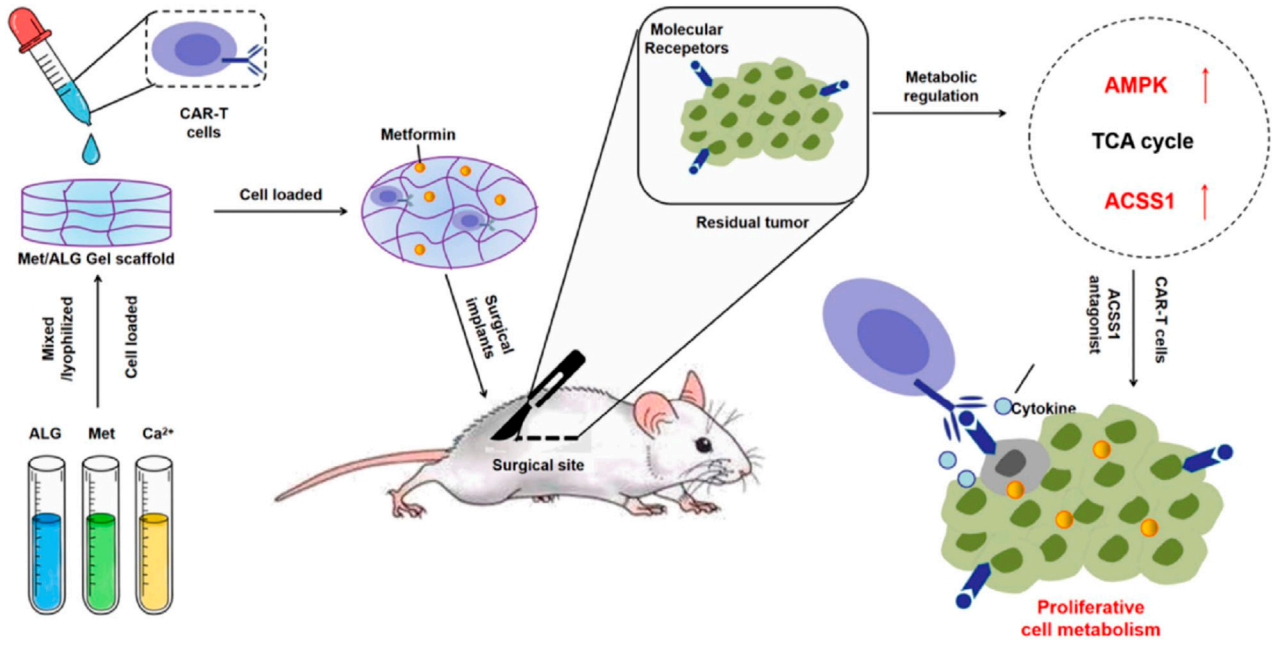

FIGURE 6
The scheme illustrates a hydrogel scaffold based on sodium alginate to load metformin and CAR-T cells (CAR-T@Met/gel) for the post-surgical tumor models of gastric and pancreatic cancers. Reprinted with permission from Ref (Chao et al., 2023). Copyright 2023 Elsevier.

tumor resection site, which can lead to more infiltration of CD8+T cells and DCs in the tumor tissue and draining lymph nodes, convert M2 macrophages to M1 macrophages, and make the tumor change from "cold" to "hot" and trigger a strong local and systemic immune response at the resection site, inhibit postoperative tumor recurrence and metastasis, improve the survival rate of B16F10 and 4T1 tumor models (Liu et al., 2022a).

2.4 Combination of immune cell therapy

Immunocyte therapy is an emerging approach for cancer treatment that utilizes the body's own immune system to combat tumors (Maxwell et al., 2024; Zeng et al., 2024). This therapy mainly includes cytotoxic T lymphocyte (CTL) therapy, CAR-T therapy, natural killer (NK) cell therapy, tumor-infiltrating lymphocyte (TIL) therapy, and dendritic cell (DC) vaccine therapy, etc., (Maxwell et al., 2024; Zeng et al., 2024). These therapies enhance the recognition and killing ability of immune cells against tumor cells through different means, such as *in vitro* expansion and activation of immune cells, genetic modification of immune cells, and loading of tumor antigens, thereby achieving the goal of treating cancer (Chan et al., 2021; López-Cantillo et al., 2022). Immunocyte therapy has achieved remarkable efficacy in the treatment of some tumors, but further research and development are still needed to improve its therapeutic effect and safety.

Studies have shown that *ex vivo* edited T cells are a source of tumor-specific T cells (López-Cantillo et al., 2022). It has been proven that T cells expressing chimeric antigen receptor are particularly effective in the treatment of some patients with malignant hematological tumors (Sterner and Sterner, 2021; López-Cantillo et al., 2022). In contrast, the application of CAR-T cell therapy in solid tumors is still challenging. This may be because the TME in solid tumors has a highly immunosuppressive effect and can induce CAR-T cell exhaustion (Blass and Ott, 2021). Then, combining CAR-T cells and ICB may be one of the ways to improve the role of CAR-T cells in solid tumors (Blass and Ott, 2021). It was found that metformin could upregulate the oxidative phosphorylation and energy metabolism of CAR-T cells, promote their proliferation, and simultaneously inhibit the oxidative and glycolytic metabolism of cancer cells, reducing tumor hypoxia. Thus, Liu Zhuang's group designed a hydrogel scaffold based on sodium alginate to load metformin and CAR-T cells (CAR-T@Met/gel) (Figure 6) (Chao et al., 2023). CAR-T@Met/gel showed the strongest tumor recurrence prevention effect in the post-surgical tumor models of gastric and pancreatic cancers, and could significantly reduce the tumor volume. Meanwhile, CAR-T@Met/gel has an excellent antitumor response against post-surgical solid tumors with high safety. This strategy provides a modular platform technology for addressing the critical challenge of the ineffectiveness of CAR-T cell therapy against solid tumors and has the potential for clinical translation.

NK infusion is considered a promising cancer therapy, but the acidic TME and neutrophil extracellular traps (NETs) greatly weaken its therapeutic effect (Vivier et al., 2008; Dagher and Posey, 2023; Vivier et al., 2024). Wenjie Chen et al. developed a dual pH-responsive hydrogel cross-linked with a tumor acidity neutralizer (mesoporous bioactive glass nanoparticles) and a NET lyase (deoxyribonuclease I, DNase I), and used it in combination with NK infusion to prevent postoperative tumor recurrence (Figure 7) (Cheng et al., 2022). This hydrogel can be injected into the surgical margin and form an adherent gel with a rapid hemostatic effect. At the same time, it

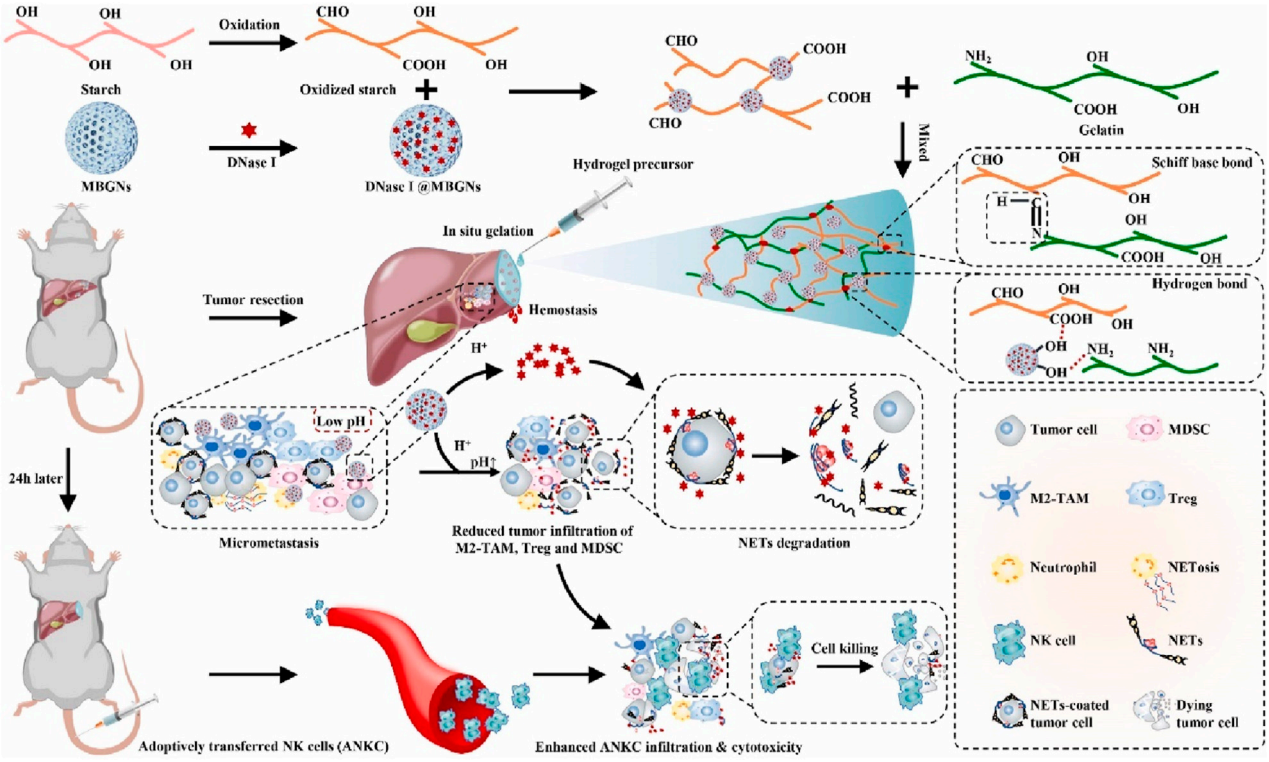

FIGURE 7
The scheme illustrates an *in situ* injectable dual pH-responsive hydrogel for enhancing adoptive NK cell therapy to prevent post-resection HCC recurrence. Reprinted with permission from Ref (Cheng et al., 2022). Copyright 2022 Elsevier.

neutralizes the acidic environment of TME to reduce tumor infiltration of immunosuppressive cells and releases DNase I under pH response to lyse NET. This combination therapy significantly enhances the therapeutic effect of NK infusion, inhibits postoperative tumor recurrence, and does not produce systemic toxicity.

In addition, more and more evidence show that LDDS can be tailored according to the patient's condition to promote personalized tumor treatment (Lu Y. et al., 2022). Tumor cells are the main targets of anti-tumor immune responses, but TME will produce a series of immunosuppressive mechanisms during malignant progression to promote tumor immune escape (Saleh and Elkord, 2020). Obtaining relevant biological information through resected surgical specimens can guide the preparation of personalized hydrogel LDDS (Lu Y. et al., 2022). For example, Deng Junjie's research group developed a hydrogel vaccine system based on granulocyte-macrophage colony-stimulating factor (GM-CSF). The hydrogel is prepared by cross-linking the lysate of surgically resected tumor cells at a low temperature (Lu Y. et al., 2022). The personalized GM-CSF released by the hydrogel vaccine system can recruit DCs, which provides a personalized tumor antigen pool. They combine to promote the activation of the individual immune system. Implanting this personalized hydrogel vaccine system into the surgical area activates a strong anti-tumor immune response in the body and eliminates residual tumor cells after surgery. *In vivo* experiments, this personalized hydrogel vaccine system combined with anti-programmed cell death one ligand 1 (αPD-L1) antibody significantly inhibited tumor recurrence and metastasis in a postoperative tumor model of pancreatic cancer mice.

In situ injection has emerged as a promising strategy for postoperative cancer treatment due to its direct delivery of therapeutics to the surgical site. The primary advantages include rapid administration, localized drug accumulation, and minimized systemic toxicity, which collectively enhance therapeutic efficacy while reducing off-target effects (Wang et al., 2023). However, challenges remain. Precise control over drug release kinetics is technically demanding, as uneven distribution or premature degradation may compromise efficacy. Patient-specific factors, including tumor heterogeneity and surgical cavity morphology, may also influence outcomes, highlighting the need for personalized formulations. Addressing these limitations through advanced material engineering and long-term safety studies will be critical to optimizing *in situ* injection for broader clinical adoption.

3 *In situ* implantation

In situ implantable entities encompass various forms, including implantable hydrogel scaffolds and tissue engineering scaffolds (Sun et al., 2011; Al-Jawadi et al., 2018). These biological entities boast numerous remarkable advantages, regarding biological safety, which lack immunogenicity and adverse reactions towards the human body, and will not trigger human immune rejection reactions, thereby greatly ensuring patient safety (Sun et al., 2011; Al-Jawadi et al., 2018). They exhibit excellent biocompatibility and can coexist harmoniously with human tissues without causing inflammation or other adverse physiological responses (Al-Jawadi

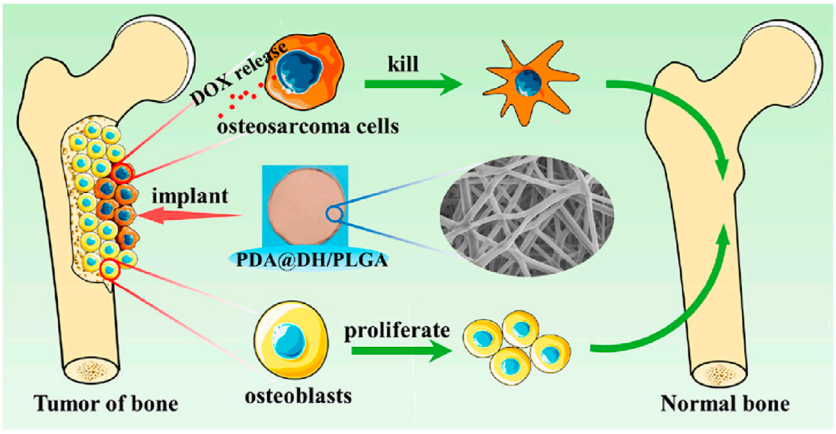

FIGURE 8
The scheme illustrates a polydopamine (PDA)-coated composite (PDA@DH/PLGA) for simultaneously repairing bone defects and preventing tumor recurrence. Reprinted with permission from Ref (Lu et al., 2021). Copyright 2021 American Chemical Society.

et al., 2018). Simultaneously, they also possess excellent biodegradability. After fulfilling their specific therapeutic functions, they can be gradually decomposed and metabolized within the body and will not remain for a long time to cause potential harm to the human body (Al-Jawadi et al., 2018).

Numerous studies have demonstrated that implantable biological entities have been widely utilized in clinical treatments, particularly playing an important role in promoting wound healing and tissue regeneration (Balaure et al., 2019). Wound healing is a complex physiological process. Implantable biological entities can provide a suitable microenvironment for wounds, promote cell proliferation and differentiation, and accelerate the closure and repair of wounds. In terms of tissue regeneration, implantable biological entities can act as scaffolds to guide the growth and development of new tissues and restore the functions of damaged tissues.

3.1 Combination of chemotherapy

Currently, a variety of implantable biological entities have been applied in post-tumor treatment (Bagó et al., 2016; Zhang H. et al., 2021). For instance, Zhiwei Yang et al. prepared a polydopamine (PDA)-coated composite (PDA@DH/PLGA) (Lu et al., 2021). PDA@DH/PLGA achieved controlled drug release, inhibited the growth of tumor cells in the early stage, promoted the proliferation of normal cells in the later stage, and greatly enhanced the bioactivity. The PDA@DH/PLGA scaffold is expected to be a potential candidate for simultaneously repairing bone defects and preventing tumor recurrence (Figure 8).

3.2 Combination of PTT and PDT

The recurrence of head and neck squamous cell carcinoma (HNSCC) following surgical resection remains a significant challenge in cancer treatment (Mahvi et al., 2018; Chow and Longo, 2020). Advanced HNSCC shows a low response rate to ICB, whereas PTT can enhance the infiltration of immune cells, making tumors more receptive to cancer immunotherapy. Our group designed and constructed a novel multifunctional nanocomposite (TB/αPD-1@AuNCs/OBC) consisting of oxidized bacterial cellulose (OBC), thrombin (TB), and gold nanocages (AuNCs) containing anti-programmed death receptor 1 (αPD-1) antibody (αPD-1@AuNCs), enabling the combination of therapies to achieve remarkable postoperative antitumor immunity and control local tumor recurrence (Figure 9) (Zhou et al., 2021). The TB/αPD-1@AuNCs/OBC + L could generate ROS to induce pyroptosis and release intracellular contents, which triggered T-cell-mediated robust tumor eradication due to the enhanced DC process and presentation of tumor-specific antigens.

The TB/αPD-1@AuNCs + L displayed potent photothermal therapeutic effect, which activated potent antitumor immunity combined ICB therapy to prevent tumor recurrence. Meanwhile, the TB/αPD-1@AuNCs/OBC could be adapted in 'real-world practice' and might a promising candidate for HNSCC treatment. Furthermore, Mingqiang Li's group developed an implantable 3D printed hydrogel scaffold (Gel-SA-CuO) that inhibits postoperative tumor recurrence by combining glutathione (GSH) depletion-induced ferroptosis and photothermal-augmented chemodynamic therapy (Dang et al., 2022). They used 3D printing technology to prepare a hydrogel scaffold containing CuO nanoparticles, which allows for controlled and sustained release of CuO during the biodegradation process. CuO nanoparticles function as a reservoir for releasing Cu^{2+} to generate intracellular ROS and also serve as a photothermal agent to generate heat. The heat generated by photothermal conversion further enhances the efficiency of the Fenton-like reaction. Moreover, the scaffolds induce ferroptosis through GSH depletion and inactivation of GPX4. The results indicated that Gel-SA-CuO offered a novel treatment strategy for the inhibition of postoperative tumor recurrence.

3.3 Combination of immunotherapy

Colorectal cancer (CRC) is a commonly occurring malignant tumor in the digestive tract, and surgery is the first-line treatment for

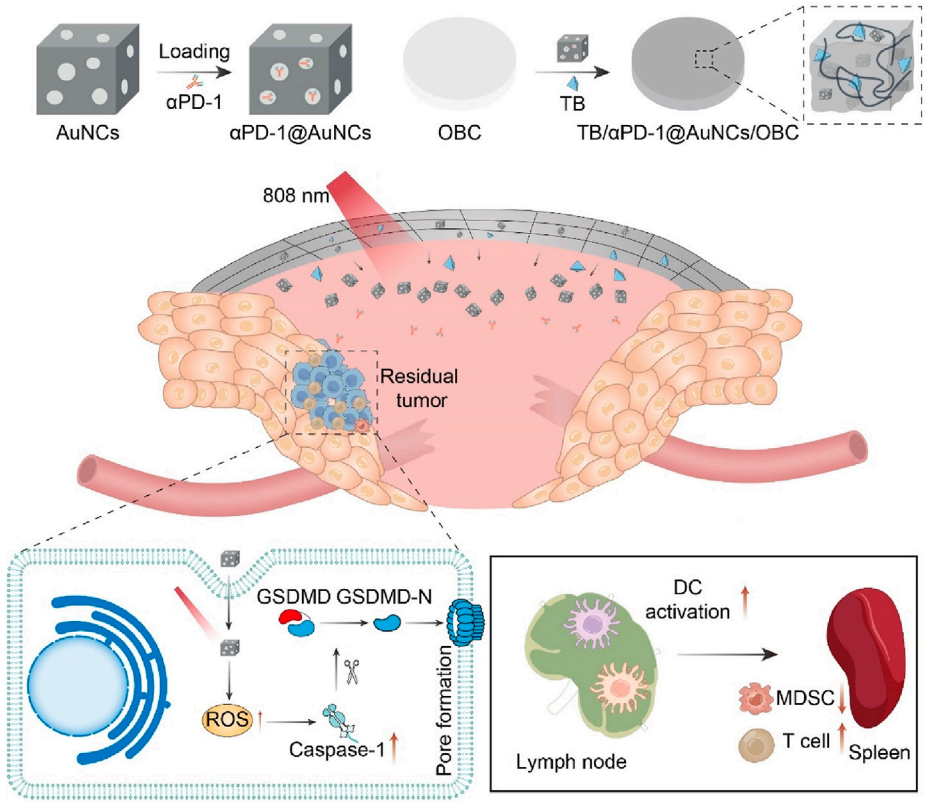

FIGURE 9
Schematic illustration of the versatile OBC-based membrane for achieving a therapeutic effect in antitumor immunotherapy towards HNSCC postoperative treatment.

it (Fakih, 2015; Biller and Schrag, 2021; Moorman et al., 2024). However, for advanced CRC, the efficacy of surgical resection is limited, and the recurrence and metastasis of tumors after surgery lead to high morbidity and mortality (Fakih, 2015). Postoperative *in situ* immunotherapy presents a promising option for preventing tumor recurrence and metastasis, and material-based local immunotherapy has potential in cancer treatment. Xuesi Chen et al. proposed a biopolymer implant fabricated with 4-arm poly (ethylene glycol) amine (4-arm PEG-NH2) and oxidized dextran (ODEX), and co-loaded with resiquimod (R848) and anti-OX40 antibody (aOX40) for CRC post-surgical treatment (Figure 10) (Ji et al., 2020). The research team demonstrated a straightforward post-surgical CRC immunotherapy strategy by placing pre-formed therapeutic biopolymer immune implants in the tumor resection cavity. The sequential activation of innate and adaptive immunity, along with immune memory effects from the gradual release of R848 and aOX40, not only resulted in complete clearance of residual tumors but also inhibited the growth of distant tumors and provided resistance to tumor re-challenge.

3.4 Combination of immune cell therapy

In situ implantable biological entities do indeed include various forms, such as implantable hydrogel scaffolds and tissue engineering scaffolds (Zhang et al., 2023). These entities can provide scaffolding functions for immune cells (Singh and Peppas, 2014). Specifically: Implantable hydrogel scaffolds have good biocompatibility and adjustable physicochemical properties, which can provide a suitable living environment and attachment sites for immune cells (Singh and Peppas, 2014). Tissue engineering scaffolds can simulate the structure and function of the extracellular matrix, guide the migration, proliferation, and differentiation of immune cells, and promote the effective recruitment and activation of immune cells (Singh and Peppas, 2014).

For instance, the team led by Tae-Don Kim proposed a 3D multi-polymer scaffold (3D-ENHANCE) constructed based on HA (Figure 11) (Ahn et al., 2020). This scaffold features a unique porous niche-like structure that is highly conducive to cell amplification. It provides a cytokine-free microenvironment for the expansion of NK cells *in vitro*, significantly enhancing the tumor immunotherapeutic efficacy of NK cells. After in-depth research, it was found that 3D-ENHANCE can be rapidly degraded within 18 days. This characteristic avoids the potential risks of long-term residual in the body. At the same time, it also significantly inhibits the recurrence and metastasis of tumors after breast cancer surgery. In the treatment of breast cancer, after surgical resection of the tumor, there is often a risk of residual tumor cells. The application of the 3D-ENHANCE scaffold provides a new solution to reduce this risk.

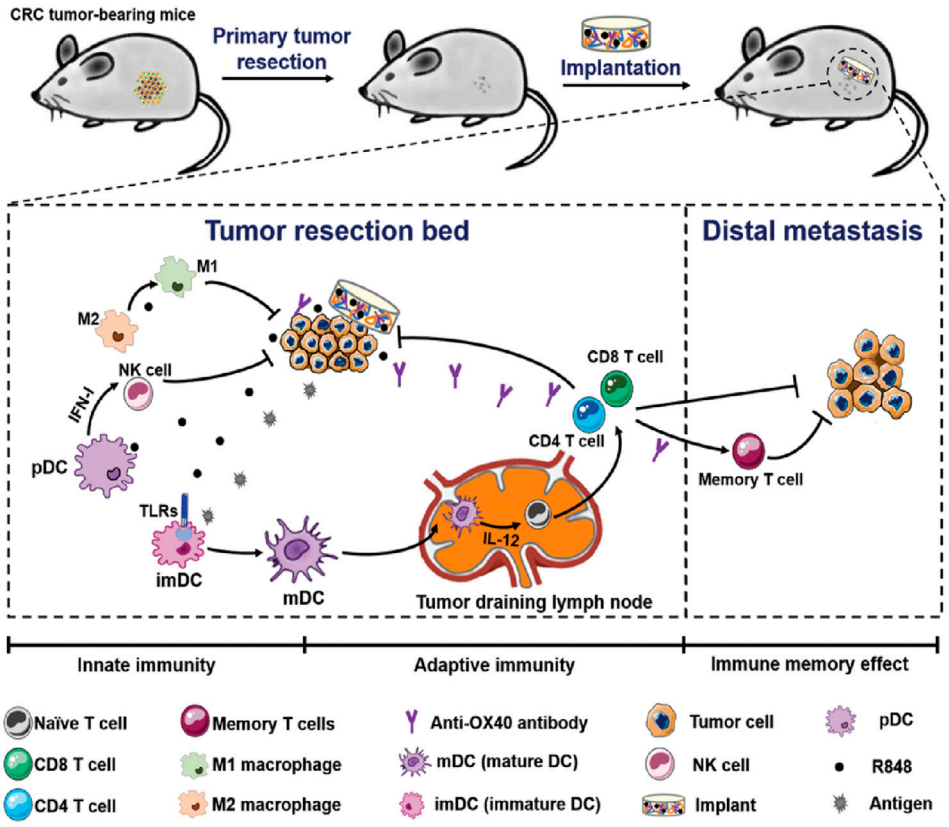

FIGURE 10
Schematic illustration of the biopolymer immune implant BI(R848 + aOX40) for preventing CRC postoperative tumor relapse and metastasis. Reprinted with permission from Ref (Ji et al., 2020). Copyright 2020 WILEY.

4 *In situ* spraying

The *in situ* spraying drug delivery system presents several remarkable advantages (Chen et al., 2018; Shao et al., 2018; Chu et al., 2021; Li et al., 2021). It often employs a multi-in-one spray bottle to blend liquid gels with multiple functional components and then sprays them onto the wound surface (Chen et al., 2018; Shao et al., 2018; Chu et al., 2021; Li et al., 2021). Taking advantage of the unique physiological environment of the wound, it rapidly organizes and forms a film covering the wound, which is highly suitable for relatively large wound surfaces after tumor resection. This system can extensively cover the entire wound area, playing roles in hemostasis, antibacterial activities, promoting wound healing, and slowly releasing drugs.

In previous studies, Yu Xuefeng's research group designed a degradable black phosphorus nano-spray photothermal hydrogel (Shao et al., 2018). After being sprayed on the tumor surgical area, this spray hydrogel can quickly form a film. While eliminating residual tumor cells in the surgical area through PTT, it also takes into account the bactericidal effect of PTT, reducing the occurrence of common clinical complications such as wound infection. The biocompatibility and degradability of this photothermal spray hydrogel are excellent, and it can be gradually degraded in the body, facilitating its further transformation towards clinical applications.

In addition, Gu Zhen's team developed an immunotherapy spray (Figure 12) (Chen et al., 2018). After spraying on the surgical site, it can form a bioactive gel. The immunotherapy antibody embedded in it can be slowly released to awaken the body's immune system and control postoperative local tumor recurrence and the occurrence of potential distant tumor metastasis. This immunotherapy spray is a two-in-one storage spray device. One storage bottle contains fibrinogen and calcium carbonate nanoparticles loaded with αCD47 antibody, and the other storage bottle contains TB solution. After spraying on the surgical site, TB in the solution quickly acts in the environment of micro-bleeding in the surgical area, making the entire gel adhere to the surface of the surgical area. At the same time, the low pH value in the TME will gradually interact with calcium carbonate nanoparticles and release αCD47 antibody, thereby activating the immune system and clearing residual tumor cells in the surgical area. Later, this research group further tested the *in vivo* effect of the spray gel through a postoperative model of melanoma mice. According to the *in vivo* imaging results, it can be seen that after receiving spray treatment, tumor cells in more than 50% of mice are completely inhibited, significantly improving the survival period of mice.

Approximately 12% of malignant gliomas express the IDH1 gene, and the R132H mutation accounts for 92.7% of IDH1 gene mutations (Choi et al., 2018). IDH1 is a very important enzyme in the tricarboxylic acid cycle. Isocitrate is

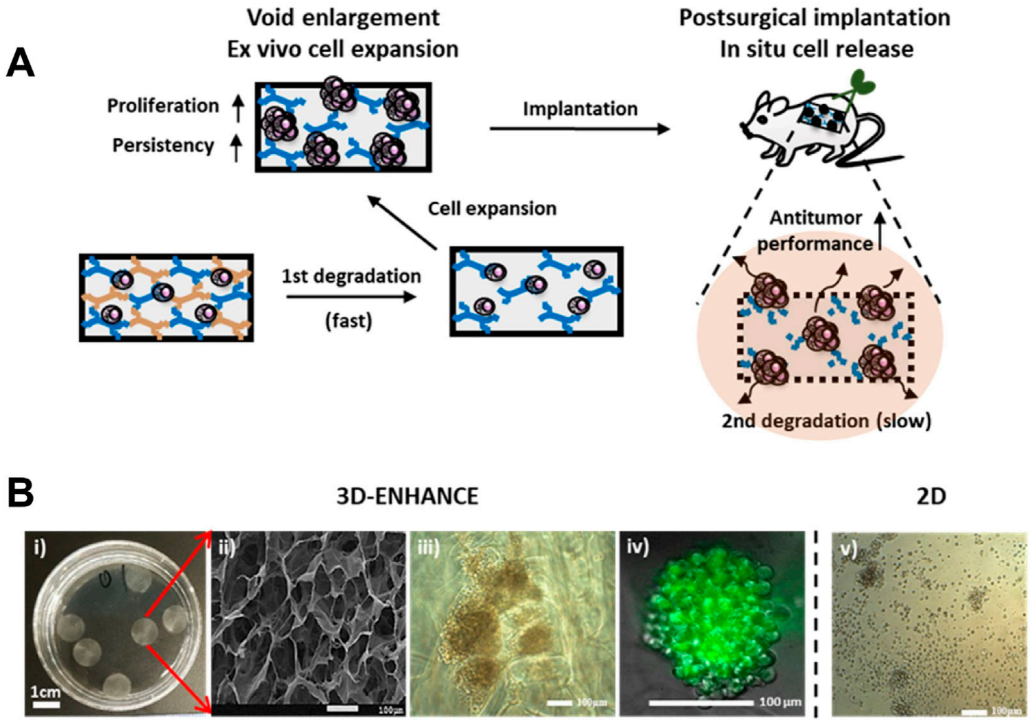

FIGURE 11
(A) Schematic illustration of the 3D-ENHANCE loaded with NK cells for preventing postoperative tumor relapse. **(B)** Macroporous architecture of 3D-ENHANCE. i) Photograph of 3D-ENHANCE. ii) The scanning electronic microscopic image for 3D – ENHANCE. iii) Bright field image of NK cell clusters formed in 3D-ENHANCE. iv) Live cell image of NK cell cluster formed in 3D-ENHANCE. v) Bright field image of NK cell cultured in the 2D manner. Reprinted with permission from Ref (Ahn et al., 2020). Copyright 2020 Elsvier.

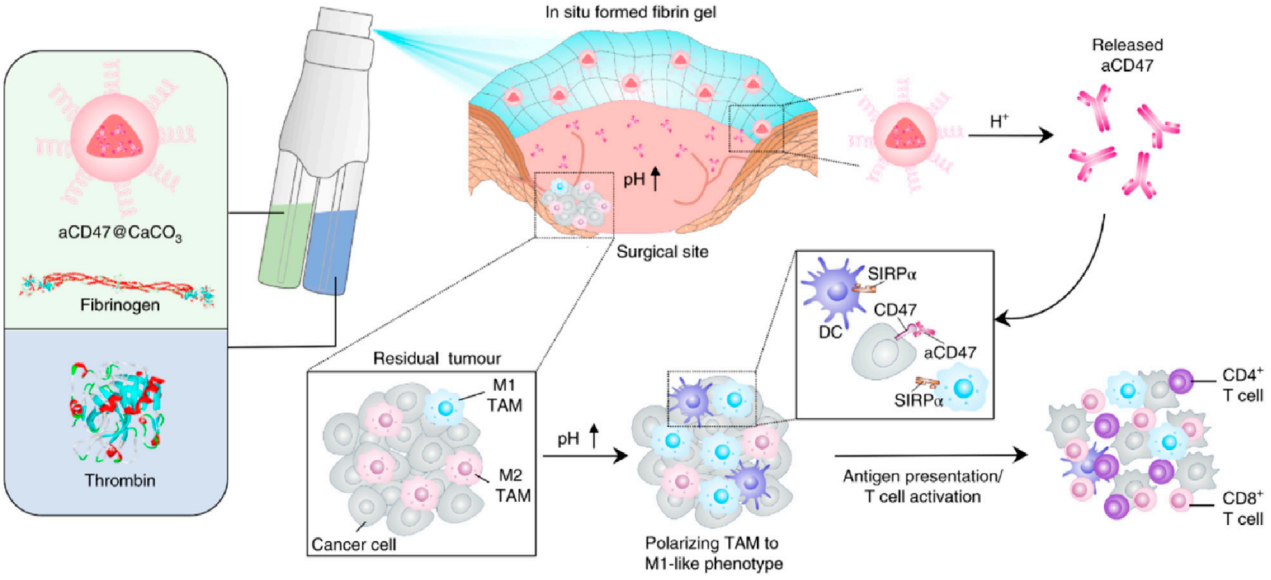

FIGURE 12
Schematic illustration of the *in situ* sprayed bioresponsive fibrin gel containing aCD47@$CaCO_3$ nanoparticles for preventing postoperative tumor local recurrence. Reprinted with permission from Ref (Chen et al., 2018). Copyright 2018 Springer Nature.

converted into α-ketoglutaric acid under the catalysis of IDH1, thereby forming nicotinamide adenine dinucleotide phosphate (NADPH). NADPH is a sacrificial agent for intracellular ROS (McBrayer et al., 2018). Therefore, when the IDH1 gene has an R132H mutation, the expression level of NAPDH will be significantly reduced, thereby increasing the sensitivity of IDH1 cells to oxidation. In addition, mutated IDH1 mainly obtains energy through glycolysis (Fu et al., 2015). Therefore, by reducing the glucose level in the postoperative environment and increasing the generation of ROS, it is expected to inhibit the recurrence of IDH1 (R132H) glioma. Based on this, Huang Peng's team developed a spray gel combining starvation therapy/chemodynamic therapy to inhibit residual IDH1 (R132H) glioma cells after surgery (Li et al., 2021). This team first mineralized glucose oxidase and further loaded it into fibrin gel. When this gel material is sprayed on the surgical area, glucose oxidase can catalyze the oxidation reaction of glucose to produce hydrogen peroxide, which increases the level of ROS while reducing the glucose level in the surgical area environment. The increased ROS further kills the residual IDH1 (R132H) glioma cells, and finally significantly inhibits the recurrence of IDH1 (R132H) glioma. Yao He et al. developed a multifunctional flavonoid-silica nanocomposite (FSiNCs) with good aqueous solubility and fluorescent properties using a facile microwave-assisted synthetic method (Chu et al., 2021). *In vitro* experiments showed that FSiNCs have concentration-dependent cytotoxicity towards cultured cancer cells and normal cells, with higher toxicity towards cancer cells. The developed FSiNCs@Fibrin gel shows potential in preventing post-surgical tumor recurrence and bacterial infections, suggesting its potential for clinical translation in the treatment of post-surgical cancer recurrence and infections.

5 Avoid complications after cancer surgery

Postoperative complications of tumors are significant factors that affect the recovery and quality of life of patients (Nathan et al., 2016). Common complications include bleeding, infection, poor wound healing, lymphedema, organ dysfunction, deep vein thrombosis, intestinal obstruction, nerve injury, pain, and tumor recurrence or metastasis (Savioli et al., 2020). These complications are related to various factors such as surgical trauma, decreased immune function, and residual tumor cells (Eto et al., 2017). The LDDS emerges as a novel therapeutic strategy, providing new ideas for resolving postoperative complications.

Postoperative infection is the most prevalent complication following tumor surgery, and it is attributed to multiple factors (Sun and Kim, 2021). Initially, surgery can impair the skin and mucosal barriers of patients, offering an entry point for bacterial intrusion (Xia et al., 2022). Secondly, tumor patients typically have a lower immunity, making it challenging for them to effectively combat infections. Furthermore, the inappropriate use of antibiotics before and after surgery may result in the emergence of bacterial resistance, consequently augmenting the risk of infection. Thus, Hsiu-Mei Li's group developed a novel multifunctional mesoporous bioactive glass (Fe-MBG–SS–CPT-FA@TC) that integrates chemotherapeutic, magnetothermal, chemodynamic, and antibacterial properties for targeted tumor therapy and postoperative infection prevention (Wei et al., 2024). Tetracycline (TC) was employed as the antibacterial agent, which was loaded into the pores of the multifunctional mesoporous bioactive glass (Fe-MBG). This allows for a sustained release of the antibiotic in the affected area following surgery to prevent bacterial infections. The study indicates that the sustained release of tetracycline from Fe-MBG–SS–CPT-FA@TC generate an antibacterial environment within the postoperative bone cavity. This can decrease the risk of infection. Additionally, the release of tetracycline can be controlled through the porous structure of Fe-MBG to meet various therapeutic needs. These characteristics indicate that Fe-MBG–SS–CPT-FA@TC is not only an effective material for tumor treatment but also possesses excellent antibacterial properties, which contribute to enhance surgical success rates and better quality of postoperative recovery for patients. Meanwhile, by introducing thrombin and fibrinogen, Yao He's group resulted that FSiNCs@Fibrin gel was formed *in situ* at the tumor surgical bed to prevent postoperative tumor recurrence (Figure 13a). Compared with free counterparts, the locally released FSiNCs had an 18-fold enhancement in antibacterial effect and a 12-fold increase in antitumor effect *in vivo*. In addition, the previously mentioned LDDS combined with PTT can also inhibit the growth of bacteria and achieve the effect of preventing postoperative infection.

Postoperative inflammatory response is a common and crucial complication that cannot be ignored after tumor surgery (McSorley et al., 2016). During the surgical procedure for tumors, the body undergoes trauma, and the damaged tissues will initiate a series of immune reactions, consequently resulting in inflammation (Barhoum et al., 2023). This inflammatory response is typically a natural reaction of the body to the surgical wound. However, if it is not adequately controlled, it may adversely affect the patient's recovery. Surgical trauma can aggravate the colonization of residual tumor cell "seeds" in the pre-metastatic niches (PMNs) "soil" at distant sites, thereby promoting postoperative metastasis. The inflammatory response plays a dual role after surgery by reshaping the local immune environment and resuscitating autologous cancer cells succumbing to oncolysis (ACCO) (Li et al., 2022). This helps to eradicate the residual tumor "seeds" and simultaneously intercept the "seed-soil" crosstalk, normalizing the distant lung and leading to the regression of the pre-existing PMNs "soil". Lian Li designed an injection hydrogel *in situ* that can respond to the enriched ROS at the trauma site, enabling the local delivery and on-demand release of ACCO and anti-inflammatory agents (Figure 13b) (Li et al., 2022). They presented an innovative approach that effectively suppresses postoperative tumor recurrence and metastasis by combining oncolysis immunization and inflammation alleviation. Through the use of a trauma-responsive hydrogel scaffold, it achieves effective regulation of the inflammatory microenvironment, offering new perspectives for postoperative tumor treatment.

Postoperative bleeding is a common complication following tumor surgery, and it can happen at various stages after the operation, bringing potential risks to the patient's recovery (Ohta et al., 2019). During the surgical procedure, although doctors will make every effort to take all kinds of measures to control the bleeding, it is sometimes hard to entirely prevent the occurrence

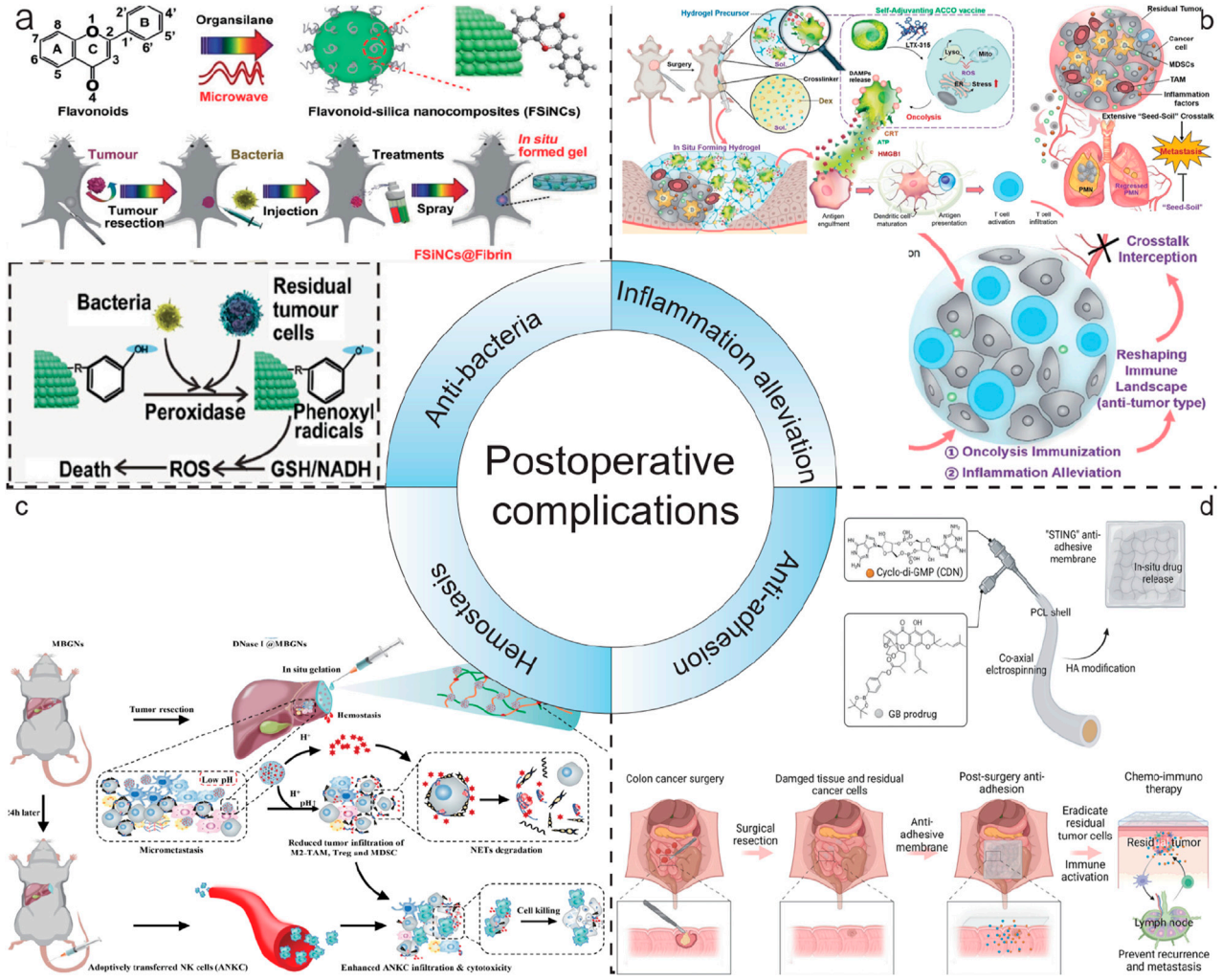

FIGURE 13
Schematic illustration of LDDS in postoperative complications. **(a)** Schematic illustration of FSiNCs-based nanohydrogel LDDS for anti-bacteria. Reprinted with permission from Ref (Chu et al., 2021). Copyright 2022 WILEY. **(b)** Schematic illustration of a trauma-inflammationresponsive and alleviating hydrogel scaffold LDDS for inflammation alleviation. Reprinted with permission from Ref (Li et al., 2022). Copyright 2022 American Chemical Society. **(c)** Schematic illustration of GODM-gel LDDS for swift hemostasis. Reprinted with permission from Ref (Cheng et al., 2022). Copyright 2022 Elsevier. **(d)** Schematic illustration of the fabrication process and the mechanism of action of the dual-drug loaded electrospun membrane LDDS for anti-adhesion. Reprinted with permission from Ref (Wang R. et al., 2024). Copyright 2024 WILEY.

of postoperative bleeding due to factors such as the location and size of the tumor, as well as the complexity of the surgery. Wenjie Chen reported a novel, dual pH-responsive adhesive hemostatic hydrogel (GODM-gel) (Figure 13c) (Cheng et al., 2022). GODM-gel offered rapid adhesion upon injection at the surgical margin, forming a stable gel that achieves swift hemostasis. Both *in vitro* and *in vivo* experiments demonstrated that the GODM-gel possessed superior adhesive strength and burst pressure compared to conventional hemostatic agents, such as fibrin glue, indicating its exceptional hemostatic capabilities in surgical procedures.

Tissue adhesion following tumor surgery is one of the common postoperative complications (Wang J. et al., 2024). After a tumor operation, the normal separating structure between the body's tissues and organs is disrupted. In the healing process, tissues that should have been independent are joined by fibrous tissue, resulting in tissue adhesion. This connection can lead to various problems and requires careful management. Post-surgery tissue adhesion also limits the possibility of reoperation, affecting long-term survival of cancer patients (Wang J. et al., 2024). To address CRC recurrence and post-surgery tissue adhesion, Qingsong Yu's group developed a novel stimulator of interferon genes (STING) membrane using coaxial electrospinning technology and hyaluronic acid modification (Figure 13d) (Wang R. et al., 2024). The membrane co-loads a ROS responsive prodrug of gambogic acid (GB) and a potent STING agonist (CDN), enabling sustained and sequential drug release. Localized delivery of GB and CDN can selectively induce efficient immunogenic cell death of cancer cells and activate the systemic anticancer immunity by stimulating the cGAMP synthase/STING pathway. The "STING" membrane not only prevents tumor recurrence through synergistic chemoimmunotherapy but also avoids post-surgery tissue adhesion, facilitating clinical intervention for CRC.

6 Conclusion and outlook

This review comprehensively summarizes the significant potential demonstrated by the current nanotechnology-based LDDS. It not only has a positive impact on the future development of tumor surgery, providing more effective adjuvant treatment modalities, but also significantly reduces the recurrence and metastasis of postoperative tumors, lowering the risk of tumor recurrence. Furthermore, LDDS shows outstanding capabilities in the treatment of various complications after surgery. It effectively alleviates the suffering of patients and improves their quality of life. Simultaneously, LDDS enhances the therapeutic effect. It contributes to prolonging the survival period of patients, providing them with more hope for survival.

However, in this field, there are still several issues. These issues require careful consideration and resolution:

1. Stability and Long-Term Storage: The LDDS need be stable and capable of long-term storage under various environmental conditions without losing its activity. This involves resistance to temperature, humidity, and light. Moreover, it requires maintaining the completeness of the system's structure and function during storage.
2. Biocompatibility: The LDDS requires excellent biocompatibility. This is to minimize toxicity and immune reactions towards normal tissues.
3. Biosafety: The LDDS must demonstrate good biosafety. In other words, it should not lead to unexpected side effects or long-term adverse consequences within the body.
4. Drug Release Kinetics: The LDDS is required to have the ability to control the release rate of the drug. It also needs to control the release duration of the drug to ensure optimal therapeutic efficacy within the treatment window.
5. Clinical Translation: Translating laboratory research into clinical applications is a complex process. It requires overcoming multiple obstacles, such as obtaining regulatory approval, conducting cost - effectiveness analysis, and designing clinical trials.

In summary, LDDS are playing an increasingly crucial role in the treatment of postoperative complications of tumors. This system has the ability to release drugs directly at the surgical site after tumor resection, which effectively reduces the risk of tumor recurrence. Simultaneously, it exhibits remarkable efficacy in controlling postoperative complications, such as infection, inflammation, and adhesion. It not only improves the therapeutic outcome but also enhances the patients' quality of life and decreases the incidence of postoperative complications. With the continuous progress of materials science and biomedical engineering, the future design of LDDS will be more intelligent and individualized to meet the diverse needs of clinical treatment.

Author contributions

J-JZ: Writing – original draft, Writing – review and editing. Y-CF: Writing – review and editing. M-LZ: Writing – review and editing. QG: Writing – review and editing. X-BZ: Writing – review and editing.

Funding

The author(s) declare that no financial support was received for the research and/or publication of this article.

Acknowledgments

We wish to thank the help of the FreePik to modify Figure 1.

Conflict of interest

The authors declare that the research was conducted in the absence of any commercial or financial relationships that could be construed as a potential conflict of interest.

Generative AI statement

The author(s) declare that no Generative AI was used in the creation of this manuscript.

Publisher's note

References

Abbas, M., Zou, Q., Li, S., and Yan, X. (2017). Self-assembled peptide- and protein-based nanomaterials for antitumor photodynamic and photothermal therapy. *Adv. Mater.* 29 (12). doi:10.1002/adma.201605021

Ahn, Y. H., Ren, L., Kim, S. M., Seo, S.-H., Jung, C.-R., Kim, D. S., et al. (2020). A three-dimensional hyaluronic acid-based niche enhances the therapeutic efficacy of human natural killer cell-based cancer immunotherapy. *Biomaterials* 247, 119960. doi:10.1016/j.biomaterials.2020.119960

Ajithkumar, T., Parkinson, C., Fife, K., Corrie, P., and Jefferies, S. (2015). Evolving treatment options for melanoma brain metastases. *Lancet Oncol.* 16 (13), e486–e497. doi:10.1016/S1470-2045(15)00141-2

Alamdari, S. G., Amini, M., Jalilzadeh, N., Baradaran, B., Mohammadzadeh, R., Mokhtarzadeh, A., et al. (2022). Recent advances in nanoparticle-based photothermal therapy for breast cancer. *J. Control. Release* 349, 269–303. doi:10.1016/j.jconrel.2022.06.050

Al-Jawadi, S., Capasso, P., and Sharma, M. (2018). The road to market implantable drug delivery systems: a review on US FDA's regulatory framework and quality control requirements. *Pharm. Dev. Technol.* 23 (10), 953–963. doi:10.1080/10837450.2018.1509348

Bagó, J. R., Pegna, G. J., Okolie, O., Mohiti-Asli, M., Loboa, E. G., and Hingtgen, S. D. (2016). Electrospun nanofibrous scaffolds increase the efficacy of stem cell-mediated

therapy of surgically resected glioblastoma. *Biomaterials* 90, 116–125. doi:10.1016/j.biomaterials.2016.03.008

Balaure, P. C., Holban, A. M., Grumezescu, A. M., Mogosanu, G. D., Balseanu, T. A., Stan, M. S., et al. (2019). *In vitro* and *in vivo* studies of novel fabricated bioactive dressings based on collagen and zinc oxide 3D scaffolds. *Int. J. Pharm.* 557, 199–207. doi:10.1016/j.ijpharm.2018.12.063

Barhoum, A., Altintas, Z., Devi, K. S. S., and Forster, R. J. (2023). Electrochemiluminescence biosensors for detection of cancer biomarkers in biofluids: principles, opportunities, and challenges. *Nano Today* 50, 101874. doi:10.1016/j.nantod.2023.101874

Bian, S., Lu, W., Zhou, L., and Jin, T. (2024). Advances in upconversion nanomaterials for tumor phototherapy. *Mater. Today Commun.* 41, 110301. doi:10.1016/j.mtcomm.2024.110301

Biller, L. H., and Schrag, D. (2021). A review of the diagnosis and treatment of metastatic colorectal cancer-reply. *Jama* 325 (7), 2405. doi:10.1001/jama.2021.6027

Blass, E., and Ott, P. A. (2021). Advances in the development of personalized neoantigen-based therapeutic cancer vaccines. *Nat. Rev. Clin. Oncol.* 18 (4), 215–229. doi:10.1038/s41571-020-00460-2

Bray, F., Laversanne, M., Sung, H., Ferlay, J., Siegel, R. L., Soerjomataram, I., et al. (2024). Global cancer statistics 2022: GLOBOCAN estimates of incidence and mortality worldwide for 36 cancers in 185 countries. *CA A Cancer J. Clin.* 74 (3), 229–263. doi:10.3322/caac.21834

Bu, L.-L., Yan, J., Wang, Z., Ruan, H., Chen, Q., Gunadhi, V., et al. (2019). Advances in drug delivery for post-surgical cancer treatment. *Biomaterials* 219, 119182. doi:10.1016/j.biomaterials.2019.04.027

Budczies, J., Kazdal, D., Menzel, M., Beck, S., Kluck, K., Altbürger, C., et al. (2024). Tumour mutational burden: clinical utility, challenges and emerging improvements. *Nat. Rev. Clin. Oncol.* 21 (10), 725–742. doi:10.1038/s41571-024-00932-9

Byun, D. J., Wolchok, J. D., Rosenberg, L. M., and Girotra, M. (2017). Cancer immunotherapy — immune checkpoint blockade and associated endocrinopathies. *Nat. Rev. Endocrinol.* 13 (4), 195–207. doi:10.1038/nrendo.2016.205

Cannon, R. B., Houlton, J. J., Mendez, E., and Futran, N. D. (2017). Methods to reduce postoperative surgical site infections after head and neck oncology surgery. *Lancet Oncol.* 18 (7), e405–e413. doi:10.1016/S1470-2045(17)30375-3

Cao, Y., Zhong, X., Wu, N., Wan, L., Tang, R., He, H., et al. (2024). An ultrasound-responsive and *in situ* gelling hydrogel nanocomposite for boosting anti PD-L1 immunotherapy via remodeling aberrant ECM of post-surgical residual cancer. *Adv. Funct. Mater.* 34 (44). doi:10.1002/adfm.202404941

Carvajal, R. D., Sacco, J. J., Jager, M. J., Eschelman, D. J., Olofsson Bagge, R., Harbour, J. W., et al. (2023). Advances in the clinical management of uveal melanoma. *Nat. Rev. Clin. Oncol.* 20 (2), 99–115. doi:10.1038/s41571-022-00714-1

Centeno, P. P., Pavet, V., and Marais, R. (2023). The journey from melanocytes to melanoma. *Nat. Rev. Cancer* 23 (6), 372–390. doi:10.1038/s41568-023-00565-7

Chan, J. D., Lai, J., Slaney, C. Y., Kallies, A., Beavis, P. A., and Darcy, P. K. (2021). Cellular networks controlling T cell persistence in adoptive cell therapy. *Nat. Rev. Immunol.* 21 (12), 769–784. doi:10.1038/s41577-021-00539-6

Changalvaie, B., Han, S., Moaseri, E., Scaletti, F., Truong, L., Caplan, R., et al. (2019). Indocyanine green J aggregates in polymersomes for near-infrared photoacoustic imaging. *ACS Appl. Mater. and Interfaces* 11 (50), 46437–46450. doi:10.1021/acsami.9b14519

Chao, Y., Wei, T., Li, Q., Liu, B., Hao, Y., Chen, M., et al. (2023). Metformincontaining hydrogel scaffold to augment CAR-T therapy against post-surgical solid Q12 tumors. *Biomaterials*. 295, 122052. doi:10.1016/j.biomaterials.2023.122052

Chen, Q., Wang, C., Zhang, X., Chen, G., Hu, Q., Li, H., et al. (2018). *In situ* sprayed bioresponsive immunotherapeutic gel for post-surgical cancer treatment. *Nat. Nanotechnol.* 14 (1), 89–97. doi:10.1038/s41565-018-0319-4

Cheng, Y., Gong, Y., Chen, X., Zhang, Q., Zhang, X., He, Y., et al. (2022). Injectable adhesive hemostatic gel with tumor acidity neutralizer and neutrophil extracellular traps lyase for enhancing adoptive NK cell therapy prevents post-resection recurrence of hepatocellular carcinoma. *Biomaterials* 284, 121506. doi:10.1016/j.biomaterials.2022.121506

Choi, S., Yu, Y., Grimmer, M. R., Wahl, M., Chang, S. M., and Costello, J. F. (2018). Temozolomide-associated hypermutation in gliomas. *Neuro-Oncology* 20 (10), 1300–1309. doi:10.1093/neuonc/noy016

Chow, L. Q. M., and Longo, D. L. (2020). Head and neck cancer. *N. Engl. J. Med.* 382 (1), 60–72. doi:10.1056/nejmra1715715

Chu, B., Wu, S., Yang, Y., Song, B., Wang, H., and He, Y. (2021). Multifunctional flavonoid-silica nanohydrogel enables simultaneous inhibition of tumor recurrence and bacterial infection in post-surgical treatment. *Small* 18 (5), e2104578. doi:10.1002/smll.202104578

Cramer, J. D., Burtness, B., Le, Q. T., and Ferris, R. L. (2019). The changing therapeutic landscape of head and neck cancer. *Nat. Rev. Clin. Oncol.* 16 (11), 669–683. doi:10.1038/s41571-019-0227-z

Cronin, K. A., Scott, S., Firth, A. U., Sung, H., Henley, S. J., Sherman, R. L., et al. (2022). Annual report to the nation on the status of cancer, part 1: National cancer statistics. *Cancer* 128 (24), 4251–4284. doi:10.1002/cncr.34479

Dagher, O. K., and Posey, A. D. (2023). Forks in the road for CAR T and CAR NK cell cancer therapies. *Nat. Immunol.* 24 (12), 1994–2007. doi:10.1038/s41590-023-01659-y

Dang, W., Chen, W.-C., Ju, E., Xu, Y., Li, K., Wang, H., et al. (2022). 3D printed hydrogel scaffolds combining glutathione depletion-induced ferroptosis and photothermia-augmented chemodynamic therapy for efficiently inhibiting postoperative tumor recurrence. *J. Nanobiotechnology* 20 (1), 266. doi:10.1186/s12951-022-01454-1

Della Pelle, G., Delgado López, A., Salord Fiol, M., and Kostevšek, N. (2021). Cyanine dyes for photo-thermal therapy: a comparison of synthetic liposomes and natural erythrocyte-based carriers. *Int. J. Mol. Sci.* 22 (13), 6914. doi:10.3390/ijms22136914

Dhas, Y., Biswas, N., Jones, L. D., and Ashili, S. (2024). Repurposing metabolic regulators: antidiabetic drugs as anticancer agents. *Mol. Biomed.* 5 (1), 40. doi:10.1186/s43556-024-00204-z

Erthal, L. C. S., Shi, Y., Sweeney, K. J., Gobbo, O. L., and Ruiz-Hernandez, E. (2023). Nanocomposite formulation for a sustained release of free drug and drug-loaded responsive nanoparticles: an approach for a local therapy of glioblastoma multiforme. *Sci. Rep.* 13 (1), 5094. doi:10.1038/s41598-023-32257-5

Eto, K., Hiki, N., Kumagai, K., Shoji, Y., Tsuda, Y., Kano, Y., et al. (2017). Prophylactic effect of neoadjuvant chemotherapy in gastric cancer patients with postoperative complications. *Gastric Cancer* 21 (4), 703–709. doi:10.1007/s10120-017-0781-y

Fakih, M. G. (2015). Metastatic colorectal cancer: current state and future directions. *J. Clin. Oncol.* 33 (16), 1809–1824. doi:10.1200/JCO.2014.59.7633

Fiorica, F., Ursino, S., Carau, B., Api, P., Cavallo, M., Padovani, R., et al. (2006). Radiotherapy plus concomitant and adjuvant temozolomide for unresectable glioblastoma: a retrospective analysis of our experience. *Radiotherapy Oncol.* 81, S297.

Fu, X., Chin, R. m, Vergnes, L., Hwang, H., Deng, G., Xing, Y., et al. (2015). 2-Hydroxyglutarate inhibits ATP synthase and mTOR signaling. *Cell Metab.* 22 (3), 508–515. doi:10.1016/j.cmet.2015.06.009

Guan, X., Sun, L., Shen, Y., Jin, F., Bo, X., Zhu, C., et al. (2022). Nanoparticle-enhanced radiotherapy synergizes with PD-L1 blockade to limit post-surgical cancer recurrence and metastasis. *Nat. Commun.* 13 (1), 2834. doi:10.1038/s41467-022-30543-w

Hargadon, K. M., Johnson, C. E., and Williams, C. J. (2018). Immune checkpoint blockade therapy for cancer: an overview of FDA-approved immune checkpoint inhibitors. *Int. Immunopharmacol.* 62, 29–39. doi:10.1016/j.intimp.2018.06.001

He, X., and Xu, C. (2020). Immune checkpoint signaling and cancer immunotherapy. *Cell Res.* 30 (8), 660–669. doi:10.1038/s41422-020-0343-4

Hiller, J. G., Perry, N. J., Poulogiannis, G., Riedel, B., and Sloan, E. K. (2017). Perioperative events influence cancer recurrence risk after surgery. *Nat. Rev. Clin. Oncol.* 15 (4), 205–218. doi:10.1038/nrclinonc.2017.194

Hu, Q., Li, H., Archibong, E., Chen, Q., Ruan, H., Ahn, S., et al. (2021). Inhibition of post-surgery tumour recurrence via a hydrogel releasing CAR-T cells and anti-PDL1-conjugated platelets. *Nat. Biomed. Eng.* 5 (9), 1038–1047. doi:10.1038/s41551-021-00712-1

Huang, L., Zhang, Y., Li, Y., Meng, F., Li, H., Zhang, H., et al. (2021). Time-programmed delivery of sorafenib and anti-CD47 antibody via a double-layer-gel matrix for postsurgical treatment of breast cancer. *Nano-Micro Lett.* 13 (1), 141. doi:10.1007/s40820-021-00647-x

Huang, Y., Fu, Z., Wang, H., Liu, Z., Gao, M., Luo, Y., et al. (2024). Calcium peroxide-based hydrogels enable biphasic release of hydrogen peroxide for infected wound healing. *Adv. Sci.* 11 (40), e2404813. doi:10.1002/advs.202404813

Jassim, A., Rahrmann, E. P., Simons, B. D., and Gilbertson, R. J. (2023). Cancers make their own luck: theories of cancer origins. *Nat. Rev. Cancer* 23 (10), 710–724. doi:10.1038/s41568-023-00602-5

Ji, G., Zhang, Y., Si, X., Yao, H., Ma, S., Xu, Y., et al. (2020). Biopolymer immune implants' sequential activation of innate and adaptive immunity for colorectal cancer postoperative immunotherapy. *Adv. Mater.* 33 (3), e2004559. doi:10.1002/adma.202004559

Jiang, W., Wang, Y., Wargo, J. A., Lang, F. F., and Kim, B. Y. S. (2020). Considerations for designing preclinical cancer immune nanomedicine studies. *Nat. Nanotechnol.* 16 (1), 6–15. doi:10.1038/s41565-020-00817-9

Joshi, S. S., and Badgwell, B. D. (2021). Current treatment and recent progress in gastric cancer. *CA A Cancer J. Clin.* 71 (3), 264–279. doi:10.3322/caac.21657

Labrie, M., Brugge, J. S., Mills, G. B., and Zervantonakis, I. K. (2022). Therapy resistance: opportunities created by adaptive responses to targeted therapies in cancer. *Nat. Rev. Cancer* 22 (6), 323–339. doi:10.1038/s41568-022-00454-5

Lasser, S. A., Ozbay Kurt, F. G., Arkhypov, I., Utikal, J., and Umansky, V. (2024). Myeloid-derived suppressor cells in cancer and cancer therapy. *Nat. Rev. Clin. Oncol.* 21 (2), 147–164. doi:10.1038/s41571-023-00846-y

Li, C., Wan, Y., Zhang, Y., Fu, L. H., Blum, N. T., Cui, R., et al. (2021). *In situ* sprayed starvation/chemodynamic therapeutic gel for post-surgical treatment of IDH1 (R132H) glioma. *Adv. Mater.* 34 (5), e2103980. doi:10.1002/adma.202103980

Li, J., Zhang, P., Zhou, M., Liu, C., Huang, Y., and Li, L. (2022). Trauma-responsive scaffold synchronizing oncolysis immunization and inflammation alleviation for post-operative suppression of cancer metastasis. *ACS Nano* 16 (4), 6064–6079. doi:10.1021/acsnano.1c11562

Li, Q., Geng, S., Luo, H., Wang, W., Mo, Y.-Q., Luo, Q., et al. (2024a). Signaling pathways involved in colorectal cancer: pathogenesis and targeted therapy. *Signal Transduct. Target. Ther.* 9 (1), 266. doi:10.1038/s41392-024-01953-7

Li, X., Lovell, J. F., Yoon, J., and Chen, X. (2020). Clinical development and potential of photothermal and photodynamic therapies for cancer. *Nat. Rev. Clin. Oncol.* 17 (11), 657–674. doi:10.1038/s41571-020-0410-2

Li, Z. Z., Zhong, N. N., Cao, L. M., Cai, Z. M., Xiao, Y., Wang, G. R., et al. (2024b). Nanoparticles targeting lymph nodes for cancer immunotherapy: strategies and influencing factors. *Small* 20 (19), e2308731. doi:10.1002/smll.202308731

Lian, B., Si, L., Chi, Z. H., Sheng, X. N., Kong, Y., Wang, X., et al. (2022). Toripalimab (anti-PD-1) versus high-dose interferon-α2b as adjuvant therapy in resected mucosal melanoma: a phase II randomized trial. *Ann. Oncol.* 33 (10), 1061–1070. doi:10.1016/j.annonc.2022.07.002

Lim, M., Xia, Y., Bettegowda, C., and Weller, M. (2018). Current state of immunotherapy for glioblastoma. *Nat. Rev. Clin. Oncol.* 15 (7), 422–442. doi:10.1038/s41571-018-0003-5

Lin, Q., Liu, H.-M., Wu, L.-Z., Yu, D.-D., Hua, C.-Y., Zou, Y., et al. (2024). Effect and underlying mechanism of a photochemotherapy dual-function nanodrug delivery system for head and neck squamous cell carcinoma. *J. Transl. Med.* 22 (1), 1043. doi:10.1186/s12967-024-05855-8

Liu, C., Ma, Y., Guo, S., He, B., and Jiang, T. (2021). Topical delivery of chemotherapeutic drugs using nano-hybrid hydrogels to inhibit post-surgical tumour recurrence. *Biomaterials Sci.* 9 (12), 4356–4363. doi:10.1039/d0bm01766c

Liu, S., Ding, F., Xu, W., Miu, L., Tang, Y., Xu, D., et al. (2024). Biotin-new indocyanine green conjugate: synthesis, *in vitro* photocytotoxicity and *in vivo* biodistribution. *Chem. Biol. and Drug Des.* 103 (3), e14495. doi:10.1111/cbdd.14495

Liu, Y., Li, C., Xia, H., Bi, J., Guan, R., Du, X., et al. (2022a). An injectable superior depot of Telratolimod inhibits post-surgical tumor recurrence and distant metastases. *Acta Biomater.* 141, 132–139. doi:10.1016/j.actbio.2022.01.013

Liu, Y., Wang, Y., Song, S., and Zhang, H. (2022b). Cascade-responsive nanobomb with domino effect for anti-tumor synergistic therapies. *Natl. Sci. Rev.* 9 (3), nwab139. doi:10.1093/nsr/nwab139

López-Cantillo, G., Urueña, C., Camacho, B. A., and Ramírez-Segura, C. (2022). CAR-T cell performance: how to improve their persistence? *Front. Immunol.* 13. doi:10.3389/fimmu.2022.878209

Lu, Q., Ye, H., Wang, K., Zhao, J., Wang, H., Song, J., et al. (2022a). Bioengineered platelets combining chemotherapy and immunotherapy for postsurgical melanoma treatment: internal core-loaded doxorubicin and external surface-anchored anti-PD-L1 antibody backpacks. *Nano Lett.* 22 (7), 3141–3150. doi:10.1021/acs.nanolett.2c00907

Lu, Y., Wan, Y., Gan, D., Zhang, Q., Luo, H., Deng, X., et al. (2021). Enwrapping polydopamine on doxorubicin-loaded lamellar hydroxyapatite/poly(lactic-co-glycolic acid) composite fibers for inhibiting bone tumor recurrence and enhancing bone regeneration. *ACS Appl. Bio Mater.* 4 (8), 6036–6045. doi:10.1021/acsabm.1c00297

Lu, Y., Wu, C., Yang, Y., Chen, X., Ge, F., Wang, J., et al. (2022b). Inhibition of tumor recurrence and metastasis via a surgical tumor-derived personalized hydrogel vaccine. *Biomaterials Sci.* 10 (5), 1352–1363. doi:10.1039/d1bm01596f

Luke, J. J., Flaherty, K. T., Ribas, A., and Long, G. V. (2017). Targeted agents and immunotherapies: optimizing outcomes in melanoma. *Nat. Rev. Clin. Oncol.* 14 (8), 463–482. doi:10.1038/nrclinonc.2017.43

Luo, M., Dorothy Winston, D., Niu, W., Wang, Y., Zhao, H., Qu, X., et al. (2022). Bioactive therapeutics-repair-enabled citrate-iron hydrogel scaffolds for efficient post-surgical skin cancer treatment. *Chem. Eng. J.* 431, 133596. doi:10.1016/j.cej.2021.133596

Mahalingam, P., and Newsom-Davis, T. (2023). Cancer immunotherapy and the management of side effects. *Clin. Med.* 23 (1), 56–60. doi:10.7861/clinmed.2022-0589

Mahvi, D. A., Liu, R., Grinstaff, M. W., Colson, Y. L., and Raut, C. P. (2018). Local cancer recurrence: the realities, challenges, and opportunities for new therapies. *Ca-a Cancer J. Clin.* 68 (6), 488–505. doi:10.3322/caac.21498

Maxwell, M., Yan, D., Rivest, B., Boone, A., Cardia, J., and Noessner, E. (2024). INTASYL self-delivering RNAi decreases TIGIT expression, enhancing NK cell cytotoxicity: a potential application to increase the efficacy of NK adoptive cell therapy against cancer. *Cancer Immunol. Immunother.* 73 (12), 239. doi:10.1007/s00262-024-03835-x

Mcbrayer, S. K., Mayers, J. R., Dinatale, G. J., Shi, D. D., Khanal, J., Chakraborty, A. A., et al. (2018). Transaminase inhibition by 2-hydroxyglutarate impairs glutamate biosynthesis and redox homeostasis in glioma. *Cell* 175 (1), 101–116.e25. doi:10.1016/j.cell.2018.08.038

Mclaughlin, M., Patin, E. C., Pedersen, M., Wilkins, A., Dillon, M. T., Melcher, A. A., et al. (2020). Inflammatory microenvironment remodelling by tumour cells after radiotherapy. *Nat. Rev. Cancer* 20 (4), 203–217. doi:10.1038/s41568-020-0246-1

Mcsorley, S. T., Watt, D. G., Horgan, P. G., and Mcmillan, D. C. (2016). Postoperative systemic inflammatory response, complication severity, and survival following surgery for colorectal cancer. *Ann. Surg. Oncol.* 23 (9), 2832–2840. doi:10.1245/s10434-016-5204-5

Mi, D., Li, J., Wang, R., Li, Y., Zou, L., Sun, C., et al. (2023). Postsurgical wound management and prevention of triple-negative breast cancer recurrence with a pryoptosis-inducing, photopolymerizable hydrogel. *J. Control. Release* 356, 205–218. doi:10.1016/j.jconrel.2023.02.042

Mimansa, Z. M. A., Verma, D. K., Das, R., Agrewala, J. N., and Shanavas, A. (2024). Shielding against breast tumor relapse with an autologous chemo-photo-immune active Nano–Micro-Sera based fibrin implant. *Nanoscale* 16 (29), 14006–14019. doi:10.1039/d4nr01076k

Moorman, A. R., Benitez, E. K., Cambuli, F., Jiang, Q., Mahmoud, A., Lumish, M., et al. (2024). Progressive plasticity during colorectal cancer metastasis. Nature

Nathan, H., Yin, H., and Wong, S. L. (2016). Postoperative complications and long-term survival after complex cancer resection. *Ann. Surg. Oncol.* 24 (3), 638–644. doi:10.1245/s10434-016-5569-5

Ohta, H., Miyake, T., Shimizu, T., Sonoda, H., Ueki, T., Kaida, S., et al. (2019). The impact of pharmacological thromboprophylaxis and disease-stage on postoperative bleeding following colorectal cancer surgery. *World J. Surg. Oncol.* 17 (1), 110. doi:10.1186/s12957-019-1653-1

Ossio, R., Roldán-Marín, R., Martínez-Said, H., Adams, D. J., and Robles-Espinoza, C. D. (2017). Melanoma: a global perspective. *Nat. Rev. Cancer* 17 (7), 393–394. doi:10.1038/nrc.2017.43

Pan, Y., Cheng, J., Zhu, Y., Zhang, J., Fan, W., and Chen, X. (2024). Immunological nanomaterials to combat cancer metastasis. *Chem. Soc. Rev.* 53 (12), 6399–6444. doi:10.1039/d2cs00968d

Patel, S. P., Othus, M., Chen, Y., Wright, G. P., Yost, K. J., Hyngstrom, J. R., et al. (2023). Neoadjuvant–adjuvant or adjuvant-only pembrolizumab in advanced melanoma. *N. Engl. J. Med.* 388 (9), 813–823. doi:10.1056/NEJMoa2211437

Pérez-Ruiz, E., Melero, I., Kopecka, J., Sarmento-Ribeiro, A. B., García-Aranda, M., and De Las Rivas, J. (2020). Cancer immunotherapy resistance based on immune checkpoints inhibitors: targets, biomarkers, and remedies. *Drug Resist. Updat.* 53, 100718. doi:10.1016/j.drup.2020.100718

Reardon, D. A., Rich, J. N., Friedman, H. S., and Bigner, D. D. (2006). Recent advances in the treatment of malignant astrocytoma. *J. Clin. Oncol.* 24 (8), 1253–1265. doi:10.1200/JCO.2005.04.5302

Roca, A., Camara, B., Bognini, J. D., Nakakana, U. N., Somé, A. M., Beloum, N., et al. (2023). Effect of intrapartum azithromycin vs placebo on neonatal sepsis and death: a randomized clinical trial. *Jama* 329 (9), 716–724. doi:10.1001/jama.2022.24388

Saleh, R., and Elkord, E. (2020). Acquired resistance to cancer immunotherapy: role of tumor-mediated immunosuppression. *Seminars Cancer Biol.* 65, 13–27. doi:10.1016/j.semcancer.2019.07.017

Savioli, F., Edwards, J., Mcmillan, D., Stallard, S., Doughty, J., and Romics, L. (2020). The effect of postoperative complications on survival and recurrence after surgery for breast cancer: a systematic review and meta-analysis. *Crit. Rev. Oncology/ Hematology*, 155, 103075. doi:10.1016/j.critrevonc.2020.103075

Schaff, L. R., and Mellinghoff, I. K. (2023). Glioblastoma and other primary brain malignancies in adults: a review. *Jama* 329 (7), 574–587. doi:10.1001/jama.2023.0023

Schoenfeld, A. J., and Hellmann, M. D. (2020). Acquired resistance to immune checkpoint inhibitors. *Cancer Cell* 37 (4), 443–455. doi:10.1016/j.ccell.2020.03.017

Schröder, W., Gisbertz, S. S., Voeten, D. M., Gutschow, C. A., Fuchs, H. F., and Van Berge Henegouwen, M. I. (2021). Surgical therapy of esophageal adenocarcinoma—current standards and future perspectives. *Cancers* 13 (22), 5834. doi:10.3390/cancers13225834

Shain, A. H., and Bastian, B. C. (2016). From melanocytes to melanomas. *Nat. Rev. Cancer* 16 (6), 345–358. doi:10.1038/nrc.2016.37

Shao, J., Ruan, C., Xie, H., Li, Z., Wang, H., Chu, P. K., et al. (2018). Black-phosphorus-incorporated hydrogel as a sprayable and biodegradable photothermal platform for postsurgical treatment of cancer. *Adv. Sci.* 5 (5), 1700848. doi:10.1002/advs.201700848

Shi, J., Kantoff, P. W., Wooster, R., and Farokhzad, O. C. (2016). Cancer nanomedicine: progress, challenges and opportunities. *Nat. Rev. Cancer* 17 (1), 20–37. doi:10.1038/nrc.2016.108

Siemer, S., Westmeier, D., Barz, M., Eckrich, J., Wünsch, D., Seckert, C., et al. (2019). Biomolecule-corona formation confers resistance of bacteria to nanoparticle-induced killing: implications for the design of improved nanoantibiotics. *Biomaterials* 192, 551–559. doi:10.1016/j.biomaterials.2018.11.028

Singh, A., and Peppas, N. A. (2014). Hydrogels and scaffolds for immunomodulation. *Adv. Mater.* 26 (38), 6530–6541. doi:10.1002/adma.201402105

Sterner, R. C., and Sterner, R. M. (2021). CAR-T cell therapy: current limitations and potential strategies. *Blood Cancer J.* 11 (4), 69. doi:10.1038/s41408-021-00459-7

Sun, F., Zhou, H., and Lee, J. (2011). Various preparation methods of highly porous hydroxyapatite/polymer nanoscale biocomposites for bone regeneration. *Acta Biomater.* 7 (11), 3813–3828. doi:10.1016/j.actbio.2011.07.002

Sun, Y., and Kim, K. G. (2021). Analysis of effect on infection factors and nursing care of postoperative incision in gynecological cancer patients. *BioMed Res. Int.* 2021, 1–5. doi:10.1155/2021/2996216

Tan, A. C., Ashley, D. M., López, G. Y., Malinzak, M., Friedman, H. S., and Khasraw, M. (2020). Management of glioblastoma: state of the art and future directions. *CA A Cancer J. Clin.* 70 (4), 299–312. doi:10.3322/caac.21613

Taranto, D., Kloosterman, D. J., and Akkari, L. (2024). Macrophages and T cells in metabolic disorder-associated cancers. *Nat. Rev. Cancer* 24 (11), 744–767. doi:10.1038/s41568-024-00743-1

Tohme, S., Simmons, R. L., and Tsung, A. (2017). Surgery for cancer: a trigger for metastases. *Cancer Res.* 77 (7), 1548–1552. doi:10.1158/0008-5472.CAN-16-1536

Vivier, E., Rebuffet, L., Narni-Mancinelli, E., Cornen, S., Igarashi, R. Y., and Fantin, V. R. (2024). Natural killer cell therapies. *Nature* 626 (8000), 727–736. doi:10.1038/s41586-023-06945-1

Vivier, E., Tomasello, E., Baratin, M., Walzer, T., and Ugolini, S. (2008). Functions of natural killer cells. *Nat. Immunol.* 9 (5), 503–510. doi:10.1038/ni1582

Wan, Y., Fu, L. H., Li, C., Lin, J., and Huang, P. (2021). Conquering the hypoxia limitation for photodynamic therapy. *Adv. Mater.* 33 (48), e2103978. doi:10.1002/adma.202103978

Wang, H., Li, X., Tse, B. W.-C., Yang, H., Thorling, C. A., Liu, Y., et al. (2018). Indocyanine green-incorporating nanoparticles for cancer theranostics. *Theranostics* 8 (5), 1227–1242. doi:10.7150/thno.22872

Wang, J., Wang, Y., Li, J., Ying, J., Mu, Y., Zhang, X., et al. (2024a). Neutrophil extracellular traps-inhibiting and fouling-resistant polysulfoxides potently prevent postoperative adhesion, tumor recurrence, and metastasis. *Adv. Mater.* 36 (31), e2400894. doi:10.1002/adma.202400894

Wang, J., Yang, P., Hou, D., Yan, Y., Yue, K., Zhong, W., et al. (2022). Bacteria-inspired transformable nanoparticle targets and covers residual tumor against bladder cancer recurrence. *Nano Today* 45, 101551. doi:10.1016/j.nantod.2022.101551

Wang, K.-N., Li, Z.-Z., Cai, Z.-M., Cao, L.-M., Zhong, N.-N., Liu, B., et al. (2024b). The applications of flexible electronics in dental, oral, and craniofacial medicine. *npj Flex. Electron.* 8 (1), 33. doi:10.1038/s41528-024-00318-y

Wang, M., Bergès, R., Malfanti, A., Préat, V., and Bastiancich, C. (2023). Local delivery of doxorubicin prodrug via lipid nanocapsule–based hydrogel for the treatment of glioblastoma. *Drug Deliv. Transl. Res.* 14 (12), 3322–3338. doi:10.1007/s13346-023-01456-y

Wang, R., Hu, Q., Huang, S., Fang, Y., Kong, X., Kaur, P., et al. (2024c). Zwitterionic injectable hydrogel-combined chemo- and immunotherapy medicated by monomolecular micelles to effectively prevent the recurrence of tumor post operation. *ACS Appl. Mater. and Interfaces* 16 (3), 4071–4088. doi:10.1021/acsami.3c17017

Wang, S., Shen, H., Mao, Q., Tao, Q., Yuan, G., Zeng, L., et al. (2021). Macrophage-mediated porous magnetic nanoparticles for multimodal imaging and postoperative photothermal therapy of gliomas. *ACS Appl. Mater. and Interfaces* 13 (48), 56825–56837. doi:10.1021/acsami.1c12406

Wei, T.-Y., Wu, Z.-Y., Lee, Z.-H., Tsou, M.-H., Lee, C.-C., and Lin, H.-M. (2024). Folic acid-enhanced magnetic mesoporous bioactive glass against infections in targeted tumor therapy with tetracycline precision loading. *Microporous Mesoporous Mater.* 370, 113033. doi:10.1016/j.micromeso.2024.113033

Wu, A., and Lim, M. (2023). Advancing combination therapy for recurrent glioblastoma. *Nat. Med.* 29 (6), 1318–1319. doi:10.1038/s41591-023-02350-3

Wu, H., Song, L., Chen, L., Zhang, W., Chen, Y., Zang, F., et al. (2018). Injectable magnetic supramolecular hydrogel with magnetocaloric liquid-conformal property prevents post-operative recurrence in a breast cancer model. *Acta Biomater.* 74, 302–311. doi:10.1016/j.actbio.2018.04.052

Xia, X., Zhang, Z., Zhu, C., Ni, B., Wang, S., Yang, S., et al. (2022). Neutrophil extracellular traps promote metastasis in gastric cancer patients with postoperative abdominal infectious complications. *Nat. Commun.* 13 (1), 1017. doi:10.1038/s41467-022-28492-5

Xie, L., Liu, R., Wang, D., Pan, Q., Yang, S., Li, H., et al. (2023). Golden buckwheat extract–loaded injectable hydrogel for efficient postsurgical prevention of local tumor recurrence caused by residual tumor cells. *Molecules* 28 (14), 5447. doi:10.3390/molecules28145447

Xiong, J., Yan, J., Li, C., Wang, X., Wang, L., Pan, D., et al. (2021). Injectable liquid metal nanoflake hydrogel as a local therapeutic for enhanced postsurgical suppression of tumor recurrence. *Chem. Eng. J.* 416, 129092. doi:10.1016/j.cej.2021.129092

Xiong, Y., Rao, Y., Hu, J., Luo, Z., and Chen, C. (2023). Nanoparticle-based photothermal therapy for breast cancer noninvasive treatment. Advanced materials.

Xu, H., Han, Y., Zhao, G., Zhang, L., Zhao, Z., Wang, Z., et al. (2020). Hypoxia-responsive lipid–polymer nanoparticle-combined imaging-guided surgery and multitherapy strategies for glioma. *ACS Appl. Mater. and Interfaces* 12 (47), 52319–52328. doi:10.1021/acsami.0c12971

Yang, A., Bai, Y., Dong, X., Ma, T., Zhu, D., Mei, L., et al. (2021a). Hydrogel/nanoadjuvant-mediated combined cell vaccines for cancer immunotherapy. *Acta Biomater.* 133, 257–267. doi:10.1016/j.actbio.2021.08.014

Yang, L.-L., Li, H., Liu, D., Li, K., Li, S., Li, Y., et al. (2023). Photodynamic therapy empowered by nanotechnology for oral and dental science: progress and perspectives. *Nanotechnol. Rev.* 12 (1). doi:10.1515/ntrev-2023-0163

Yang, X., Gao, L., Wei, Y., Tan, B., Wu, Y., Yi, C., et al. (2021b). Photothermal hydrogel platform for prevention of post-surgical tumor recurrence and improving breast reconstruction. *J. Nanobiotechnology* 19 (1), 307. doi:10.1186/s12951-021-01041-w

Zeng, Y.-Y., Gu, Q., Li, D., Li, A.-X., Liu, R.-M., Liang, J.-Y., et al. (2024). Immunocyte membrane-derived biomimetic nano-drug delivery system: a pioneering platform for tumour immunotherapy. *Acta Pharmacol. Sin.* 45, 2455–2473. doi:10.1038/s41401-024-01355-z

Zhang, H., Xu, S. D., Zhang, J. S., Wang, Z. F., Liu, D. X., Guo, L., et al. (2021a). Plasma-activated thermosensitive biogel as an exogenous ROS carrier for post-surgical treatment of cancer. *Biomaterials.* 276. doi:10.1016/j.biomaterials.2021.121057

Zhang, J., Chen, C., Li, A., Jing, W., Sun, P., Huang, X., et al. (2021b). Immunostimulant hydrogel for the inhibition of malignant glioma relapse post-resection. *Nat. Nanotechnol.* 16 (5), 538–548. doi:10.1038/s41565-020-00843-7

Zhang, L., Dong, Y., Liu, Y., Liu, X., Wang, Z., Wan, J., et al. (2023). Multifunctional hydrogel/platelet-rich fibrin/nanofibers scaffolds with cell barrier and osteogenesis for guided tissue regeneration/guided bone regeneration applications. *Int. J. Biol. Macromol.* 253, 126960. doi:10.1016/j.ijbiomac.2023.126960

Zhang, P., Li, B., Wang, Z., Li, J., Wang, F., Kong, J., et al. (2024a). Durable attenuation of tumor pH–platelet linkage reinstates bioorthogonal targeting of residual tumors post-debulking. *ACS Nano* 18 (5), 4520–4538. doi:10.1021/acsnano.3c11536

Zhang, W., Chen, S., Bai, Z., Gan, M., Chen, M., Zhang, Y., et al. (2024b). Photodynamic therapy for oral squamous cell carcinoma: current status, challenges, and prospects. *Int. J. Nanomedicine* 19, 10699–10710. doi:10.2147/IJN.S481901

Zhang, X., Wang, J., Chen, Z., Hu, Q., Wang, C., Yan, J., et al. (2018). Engineering PD-1-presenting platelets for cancer immunotherapy. *Nano Lett.* 18 (9), 5716–5725. doi:10.1021/acs.nanolett.8b02321

Zhang, Y., Wang, T., Zhuang, Y., He, T., Wu, X., Su, L., et al. (2021c). Sodium alginate hydrogel-mediated cancer immunotherapy for postoperative *in situ* recurrence and metastasis. *ACS Biomaterials Sci. and Eng.* 7 (12), 5717–5726. doi:10.1021/acsbiomaterials.1c01216

Zhang, Z., Smith, L., Li, W., Jiang, L., Zhou, F., Davies, G.-L., et al. (2022). Polydopamine-coated nanocomposite theranostic implants for localized chemotherapy and MRI imaging. *Int. J. Pharm.* 615, 121493. doi:10.1016/j.ijpharm.2022.121493

Zhao, H., Song, Q., Zheng, C., Zhao, B., Wu, L., Feng, Q., et al. (2020). Implantable bioresponsive nanoarray enhances postsurgical immunotherapy by activating pyroptosis and remodeling tumor microenvironment. *Adv. Funct. Mater.* 30 (51). doi:10.1002/adfm.202005747

Zhao, J., Chen, A. X., Gartrell, R. D., Silverman, A. M., Aparicio, L., Chu, T., et al. (2019). Immune and genomic correlates of response to anti-PD-1 immunotherapy in glioblastoma. *Nat. Med.* 25 (3), 462–469. doi:10.1038/s41591-019-0349-y

Zhao, Y., Pan, Y., Zou, K., Lan, Z., Cheng, G., Mai, Q., et al. (2023). Biomimetic manganese-based theranostic nanoplatform for cancer multimodal imaging and twofold immunotherapy. *Bioact. Mater.* 19, 237–250. doi:10.1016/j.bioactmat.2022.04.011

Zhen, X., Li, Y., Yuan, W., Zhang, T., Li, M., Huang, J., et al. (2024). Biointerface-engineered hybrid nanovesicles for targeted reprogramming of tumor microenvironment. Advanced materials,

Zhou, J., Ma, X., Li, H., Chen, D., Mao, L., Yang, L., et al. (2021). Inspired heat shock protein alleviating prodrug enforces immunogenic photodynamic therapy by eliciting pyroptosis. *Nano Res.* 15 (4), 3398–3408. doi:10.1007/s12274-021-3946-2

Zhou, J.-J., Li, X.-H., He, P.-Y., Qi, F.-Y., Ullah, M. W., Li, S.-J., et al. (2022). Implantable versatile oxidized bacterial cellulose membrane for postoperative HNSCC treatment via photothermal-boosted immunotherapy. *Nano Res.* 16 (1), 951–963. doi:10.1007/s12274-022-4811-7

Zou, P., Lin, R., Fang, Z., Chen, J., Guan, H., Yin, J., et al. (2023). Implanted, wireless, self-powered photodynamic therapeutic tablet synergizes with ferroptosis inducer for effective cancer treatment. *Adv. Sci.* 10 (36), e2302731. doi:10.1002/advs.202302731

frontiers | Frontiers in Oncology

TYPE Original Research
PUBLISHED 19 May 2025
DOI 10.3389/fonc.2025.1580828

OPEN ACCESS

EDITED BY
Xinyu Wang,
Philadelphia College of Osteopathic Medicine (PCOM), United States

REVIEWED BY
Yinu Wang,
Northwestern University, United States
Paula Dobosz,
Poznan University of Medical Sciences, Poland
Yoo Hyung Kim,
Seoul National University Hospital, Republic of Korea

*CORRESPONDENCE
Jinhe Zhang
64331671@qq.com

RECEIVED 21 February 2025
ACCEPTED 23 April 2025
PUBLISHED 19 May 2025

CITATION
Ling L, Zhang J, Zhang X, Wang P, Ma M and Yin B (2025) Iodine-131 induces ferroptosis and synergizes with sulfasalazine in differentiated thyroid cancer cells via suppressing *SLC7A11*.
Front. Oncol. 15:1580828.
doi: 10.3389/fonc.2025.1580828

Iodine-131 induces ferroptosis and synergizes with sulfasalazine in differentiated thyroid cancer cells via suppressing *SLC7A11*

Li Ling[1], Jinhe Zhang[2*], Xiao Zhang[2], Peiqi Wang[2], Mingjun Ma[2] and Bingling Yin[1]

[1]Graduate School, Guangzhou University of Chinese Medicine, Guangzhou, Guangdong, China, [2]Department of Nuclear Medicine, General Hospital of Southern Theater Command, Guangzhou, Guangdong, China

Iodine-131 (^{131}I) plays a key role in the treatment of differentiated thyroid cancer (DTC). Ferroptosis represents a form of regulated cell death that is distinct from necrosis and apoptosis, constituting a unique mode of programmed cell death. In this study, we aimed to ascertain the potential of ^{131}I to trigger ferroptosis in DTC and to assess the synergistic therapeutic impact of combining ^{131}I with sulfasalazine (SAS), a ferroptosis inducer, in the context of DTC. The FTC-133 and TPC-1 cell lines were employed to evaluate the impact of ^{131}I and SAS on cellular functions. Ferrostatin-1 (Fer-1) reversed the cell viability and colony formation ability inhibited by ^{131}I. ^{131}I led to an elevation in the levels of malondialdehyde (MDA), reactive oxygen species (ROS), and lipid peroxidation. DTC cells exposed to ^{131}I displayed characteristic ferroptotic ultrastructure, featuring shrunken mitochondria with increased membrane density. Concurrently, there was a reduction in the content of glutathione (GSH), as well as a downregulation of the expression levels of glutathione peroxidase 4 (*GPX4*) and solute carrier family 7 member 11 (*SLC7A11*) in the cells treated with ^{131}I. The CI values for the combination of SAS and ^{131}I in DTC cells were less than 1, demonstrating that SAS synergized with ^{131}I. Moreover, the combination of SAS and ^{131}I significantly increased the MDA levels and lipid peroxidation, decreased the GSH levels, and suppressed the expression of SLC7A11 and GPX4, while *SLC7A11* knockdown significantly enhanced ferroptosis-related markers in DTC cells. Animal experiments demonstrated that SAS synergized with ^{131}I resulted in notable decreases in tumor volume and weight. Furthermore, immunohistochemical analyses revealed that the combination of ^{131}I and SAS significantly downregulated the expression of GPX4 and SLC7A11 *in vivo*. Taken together, our results suggest that ^{131}I may induce lipid peroxidation and ferroptosis, and demonstrate the potential for a synergistic therapeutic effect when ^{131}I is combined with SAS in the treatment of DTC.

KEYWORDS

differentiated thyroid cancer, ferroptosis, Iodine-131, sulfasalazine, SLC7A11 (xCT)

Introduction

Thyroid cancer is the most prevalent type of endocrine cancer globally. In 2022, it ranked as the seventh most frequently diagnosed cancer worldwide, with its incidence steadily increasing annually (1, 2). The predominant subtype, differentiated thyroid cancer (DTC), generally demonstrates favorable prognosis following standard treatments including surgery and radioactive iodine (RAI) therapy (3). RAI is primarily utilized for three clinical purposes: remnant ablation, adjuvant therapy, and therapeutic intervention in metastatic disease (4, 5).

Ferroptosis, a regulated form of cell death distinct from necrosis and apoptosis in morphology, biochemistry, and genetics, was first conceptualized by Dixon et al. in 2012 (6). This iron-dependent process is driven by lipid peroxidation and has been implicated in both physiological processes and pathological conditions ranging from ischemia-reperfusion injury to neurodegenerative diseases (7–10). Although ferroptosis functions as a natural tumor-suppressive mechanism, its activity is often suppressed in cancer cells (11–13). Given this tumor-suppressive paradox, reactivating ferroptosis represents a promising therapeutic strategy for diverse malignancies. Studies have confirmed that conventional cancer therapies, including radiotherapy, can induce ferroptosis (14, 15). However, the ability of ^{131}I—a widely used internal radiotherapy agent in DTC—to trigger ferroptosis remains underexplored.

GPX4, a central inhibitor of ferroptosis, suppresses lipid peroxidation by catalyzing the reduction of lipid hydroperoxides to lipid alcohols using glutathione (GSH) as a cofactor (16). *SLC7A11* (*xCT*) is a cystine/glutamate antiporter that plays a crucial role in transporting cystine into cells, which is essential for the production of cysteine—a rate-limiting precursor for GSH synthesis (17). Consequently, pharmacological inhibition of *SLC7A11* promotes ferroptosis through dual mechanisms: depleting intracellular GSH and indirectly impairing *GPX4*-mediated lipid repair (18). Recent studies demonstrated that ionizing radiation triggers ferroptosis by downregulating SLC7A11 expression in solid tumors (15). Sulfasalazine (SAS), an FDA-approved drug for inflammatory bowel disease, has recently been repurposed as a ferroptosis inducer that directly inhibits SLC7A11 activity, thereby accelerating lipid peroxidation (19). Notably, SAS exhibits radiosensitizing effects by synergistically reducing GSH levels to amplify radiation-induced ferroptosis (20, 21). Moreover, *SLC7A11* overexpression in thyroid cancer tissues suggests its inhibition could offer therapeutic benefits (22–25). Integrating the dual roles of *SLC7A11* in ferroptosis regulation and thyroid cancer progression, we hypothesize that combining SAS with ^{131}I may synergistically enhance treatment efficacy through concerted *SLC7A11* inhibition.

This study aims to investigate the involvement of ferroptosis in ^{131}I-induced cell death in DTC and evaluate the therapeutic potential of combining SAS with ^{131}I.

Materials and methods

Cell culture and reagents

The normal thyroid cell lines Nthy-ori3-1, kindly provided by the Department of Nuclear Medicine, First Affiliated Hospital of Guangdong Pharmaceutical University, and the human thyroid cancer cell lines TPC-1 and FTC-133, obtained from Zhongqiao Xinzhou Biological Co., Ltd. (Shanghai, China), were cultured in RPMI-1640 medium supplemented with 10% fetal bovine serum (BI, Shanghai, China) and 1% penicillin/streptomycin (BI, Shanghai, China). Cells were maintained at 37°C in a humidified 5% CO_2 atmosphere. Ferrostatin-1 (HY-100579) and sulfasalazine (HY-14655) were procured from MedChemExpress (Monmouth Junction, NJ, USA). Z-VAD-FMK (T7020) and necrostatin-1 (T1847) were obtained from TargetMol (Boston, MA, USA). Sodium iodide-131 ($Na^{131}I$) was purchased from HTA Co., Ltd. (Beijing, China).

CCK-8 assay

Cell viability of FTC-133 and TPC-1 cells treated with ^{131}I, Ferrostatin-1 (Fer-1), Z-VAD-FMK, necrostatin-1, or SAS was quantified using a CCK-8 assay kit (GIPBIO, Montclair, NJ, USA). Cells were seeded into 96-well plates at a density of 5,000 cells/well and treated with compounds according to experimental protocols. After treatment, the medium in each well was replaced with 100 μL of fresh RPMI-1640 containing 10 μL CCK-8 reagent. Following a 3-hour incubation at 37°C under light-protected conditions, absorbance was measured at 450 nm using a microplate reader (Thermo Fisher Scientific, Waltham, MA, USA). Cell viability (%) was calculated using the formula:

$$\text{Viability}\ (\%) = [(OD_{treated} - OD_{blank})/(OD_{untreated} - OD_{blank})] \times 100\,\%$$

OD_{blank} refers to wells containing medium without cells

Colony-formation assay

Cells were seeded in 6-well plates at a density of 700 cells/well. The combination group and Fer-1 monotherapy group were pre-treated with 1 μM Fer-1 for 4 hours; subsequently, the combination group and ^{131}I monotherapy group were exposed to ^{131}I (50 μCi/mL). Cells were cultured in a humidified 5% CO_2 incubator at 37°C until visible colonies formed. Colonies were fixed with 4% paraformaldehyde (PFA) and stained with 0.5% crystal violet (Biosharp, Hefei, Anhui, China) for 30 minutes at room

temperature. Colonies in each well were imaged and quantified using ImageJ software (National Institutes of Health, Bethesda, MD, USA).

Transmission electron microscopy

Cells cultured in 100-mm dishes were exposed to 131I (50 μCi/mL) for 48 h. After treatment, cells were fixed with 2.5% glutaraldehyde and 2% paraformaldehyde in 0.1 M phosphate buffer (pH 7.4) at 4°C overnight. Subsequently, cells were washed three times with phosphate buffer and post-fixed in 2% osmium tetroxide at room temperature for 1 hour. Following dehydration through a graded acetone series (50%, 70%, 90%, 100%), cells were stained with 1% uranyl acetate, embedded in Epon 812 resin (SPI Supplies, West Chester, PA, USA), and polymerized at 60°C for 48 hours. Ultrathin sections (70 nm) were prepared using an ultramicrotome (Leica EM UC7, Germany) and examined with a transmission electron microscope (HT7800, Hitachi, Tokyo, Japan).

GSH measurement

Intracellular GSH levels were determined using a GSH assay kit (Solarbio Science & Technology Co., Ltd., Beijing, China) according to the manufacturer's protocol. Briefly, cells were seeded in 6-well at a density of 1×10^5 cells/well and treated according to experimental protocols. After treatment, cells were harvested and divided into two equal aliquots: one for protein quantification via the bicinchoninic acid (BCA) assay and the other for GSH analysis. For GSH detection, cells were lysed by sonication after adding Reagent I from the kit. The lysate was centrifuged at 12,000 × g for 10 minutes at 4°C to collect the supernatant. Reagents II and III were sequentially added to the supernatant, mixed thoroughly, and incubated at 25°C for 5 minutes. Absorbance at 412 nm was measured using a microplate reader (Thermo Fisher Scientific, Waltham, MA, USA).

Malondialdehyde measurement

Intracellular MDA levels were quantified using an MDA assay kit (Beyotime Biotechnology, Shanghai, China) based on the thiobarbituric acid (TBA) reaction. Cells were seeded in 6-well plates at a density of 1×10^5 cells/well and treated according to experimental protocols. After treatment, cells were harvested, lysed, and centrifuged to collect the supernatant. After protein quantification of the lysates, the MDA working solution was added, and the mixture was heated at 100°C for 15 minutes. The samples were then centrifuged at 1,000 × g for 10 minutes at 4°C. Absorbance of the supernatant was measured at 532 nm using a microplate reader (Thermo Fisher Scientific, Waltham, MA, USA).

ROS detection

Intracellular reactive oxygen species (ROS) levels were detected using the fluorescent probe 2',7'-dichlorodihydrofluorescein diacetate (DCFH-DA). Cells were seeded in 6-well plates at a density of 1×10^5 cells/well. After cell adhesion, the combination group and Fer-1 monotherapy group were pre-treated with 1 μM Fer-1 for 4 hours; subsequently, the combination group and ^{131}I monotherapy group were exposed to ^{131}I (50 μCi/mL) for 48 h. After treatment, cells were incubated with 10 μM DCFH-DA (prepared in serum-free RPMI-1640) under light-protected conditions for 30 minutes. After washing three times with phosphate-buffered saline (PBS), fluorescence images were acquired using a fluorescence microscope (Axio Observer 7, Carl Zeiss AG, Oberkochen, Germany).

Lipid peroxidation measurement

Cells (2×10^3 cells/well) were seeded in 24-well plates and treated according to experimental groups. Lipid peroxidation levels were quantified using the C11-BODIPY 581/591 fluorescent probe (Beyotime Biotechnology Co., Ltd., Shanghai, China) according to the manufacturer's protocol. Briefly, cells were incubated with 5 μM C11-BODIPY 581/591 under light-protected conditions for 30 minutes. Fluorescence intensity was measured using a microplate reader (Fluoroskan Microplate Reader, Thermo Fisher Scientific, Waltham, MA, USA) (reduced form: Ex/Em 581/591 nm; oxidized form: Ex/Em 488/510 nm). The results were expressed as the ratio of oxidized to reduced fluorescence intensity.

Reverse transcription-quantitative polymerase chain reaction

Total RNA was isolated from FTC-133 and TPC-1 cells using TRIzol™ reagent (Thermo Fisher Scientific, Waltham, MA, USA). Complementary DNA (cDNA) was synthesized from 1 μg RNA using SuperScript™ II Reverse Transcriptase (Vazyme Biotech Co., Ltd., Nanjing, Jiangsu, China). RT-qPCR amplification was conducted on a LineGene Pro Real-Time PCR System (Bioer Technology, Hangzhou, China) with the following cycling conditions: 95°C for 5 min, followed by 40 cycles of 95°C for 10 s and 60°C for 30 s. mRNA expression levels were normalized to the endogenous control gene *GAPDH*. Primer sequences were as follows:

Homo-GPX4-F: 5'-ACATGGTTAACCTGGACAAGT ACCG-3'
Homo-GPX4-R: 5'-GGTCGACGAGCTGAGTGTAG TTTAC-3'
Homo-SLC7A11-F: 5'-TGGAAGTCTTTGGTCCATTACC AGC-3'
Homo-SLC7A11-R: 5'-GGTTCCAGAATGTAGCGTCCA AATG-3'

Homo-GAPDH-F: 5'-ACAGCCTCAAGATCATCAGCA-3'
Homo-GAPDH-R: 5'-ATGAGTCCTTCCACGATACCA-3'.

Western blotting

Proteins were extracted from FTC-133 and TPC-1 cells of each experimental group using RIPA lysis buffer (Biosharp Life Sciences, Anhui, China). Protein concentrations were determined using a BCA Protein Assay Kit (Thermo Fisher Scientific, Waltham, MA, USA). Equal amounts of protein (40 μg per lane) were separated by SDS-PAGE and transferred onto polyvinylidene difluoride (PVDF) membranes (Merck Millipore, Burlington, MA, USA). Membranes were blocked with 5% non-fat milk for 1 h at room temperature, followed by overnight incubation at 4°C with primary antibodies. After washing, membranes were incubated with HRP-conjugated secondary antibodies for 1 h. Protein bands were visualized using an Enhanced Chemiluminescent (ECL) Substrate Kit (Abbkine Scientific Co., Ltd., Wuhan, Hubei, China) and imaged on a ChemiDoc MP Imaging System (Bio-Rad Laboratories, Hercules, CA, USA). Antibody details: Anti-SLC7A11 (1:1,000; HUABIO, Hangzhou, Zhejiang, China), Anti-GPX4 (1:1,000; Cell Signaling Technology, Danvers, MA, USA), Anti-GAPDH (1:10,000; HUABIO, Hangzhou, Zhejiang, China), HRP-conjugated Goat Anti-Rabbit IgG (1:10,000; HUABIO, Hangzhou, Zhejiang, China).

siRNA transfection

SLC7A11-targeting siRNAs were synthesized by IGE Biotechnology Co., Ltd. (Guangzhou, Guangdong, China). Transient transfection was performed using siRNA-Mate Transfection Reagent (GenePharma Co., Ltd., Shanghai, China) following the manufacturer's instructions. FTC-133 cells were transfected with siRNA-*SLC7A11*-1(5'-GAAGAUAAGUUAUGAACUA-3'). TPC-1 cells were transfected with siRNA-*SLC7A11*-2 (5'-GGAAGAGA UUCAAGUAUUA-3'). Cells were harvested 48 h post-transfection for downstream analyses.

Animal experiment

All animal experiments were conducted in accordance with the National Guidelines for Experimental Animal Welfare (the Ministry of Science and Technology of People's Republic Laboratory Animals 2006-09-30) at the Animal Experiment Center of General Hospital of Southern Theater Command (Guangzhou, China). The animal experiments were approved by the Institutional Animal Care and Use Committee of General Hospital of Southern Theater Command. Sixteen BALB/C nude mice (3-4 weeks, 16-18 g) purchased from Guangzhou Ruige Biological Technology Co., Ltd (Guangzhou, China) were used for the TPC-1 cell xenografts. One week after adaptive feeding, the mice were randomly divided into four groups: control group (nude mice were administered an equivalent volume of saline as the other group), ^{131}I group (nude mice were administered 7.4 MBq of ^{131}I once every three days), SAS group (nude mice received 8 mg/kg SAS daily) and combination group (nude mice were administered 7.4 MBq of ^{131}I once every three days and received 8 mg/kg SAS daily). After three courses of ^{131}I treatment, mice were euthanized by cervical dislocation. Tumor size was calculated in accordance with the following formula: tumor volume = $1/2 \times A \times B^2$, where A and B represent the longest and shortest tumor diameters, respectively.

Immunohistochemistry

Tumor tissues removed from mice models were fixed in 4% buffered formalin and embedded in paraffin. After the tumor tissue was sectioned into 5 μm thickness, hematoxylin-eosin staining was performed on the sections. For the purpose of immunohistochemical staining, the primary antibodies, including GPX4 (1:500, CST, USA) and SLC7A11 (1:500, HUABIO, Hangzhou, China), were incubated at 4°C overnight. Images were scanned using 3DHISTECH (PANNORAMIC MIDI, Budapest, Hungary).

Statistical analysis

Quantitative data are presented as mean ± standard deviation (SD) derived from at least three independent biological replicates. Intergroup differences were analyzed by Student's unpaired t-test (two groups) or one-way analysis of variance (ANOVA) with Tukey's *post hoc* test (three or more groups). All analyses were performed using SPSS v26.0 (IBM Corp., Armonk, NY, USA). Statistical significance was defined as follows: $p < 0.05$ (*), $p < 0.01$ (**), and $p < 0.001$ (***); nonsignificant (ns) indicates $p \geq 0.05$.

Results

Fer-1 alleviates cell viability and colony formation ability suppressed by ^{131}I in DTC cells

Ionizing radiation has been shown to trigger ferroptosis in cancer cells (14). Given that ^{131}I emits both β- and γ-radiation, we hypothesized it could induce ferroptosis in DTC cells. To test this hypothesis, we first examined the effects of the ferroptosis inhibitor Fer-1 on FTC-133 and TPC-1 cells exposed to grade doses of ^{131}I. Fer-1 significantly attenuated ^{131}I-induced cytotoxicity, manifested by increased cell viability (Figure 1A). Colony formation assays corroborated these findings, demonstrating that Fer-1 alleviated ^{131}I-mediated suppression of clonogenic capacity in both cell lines (Figure 1B). To elucidate the contribution of ferroptosis to

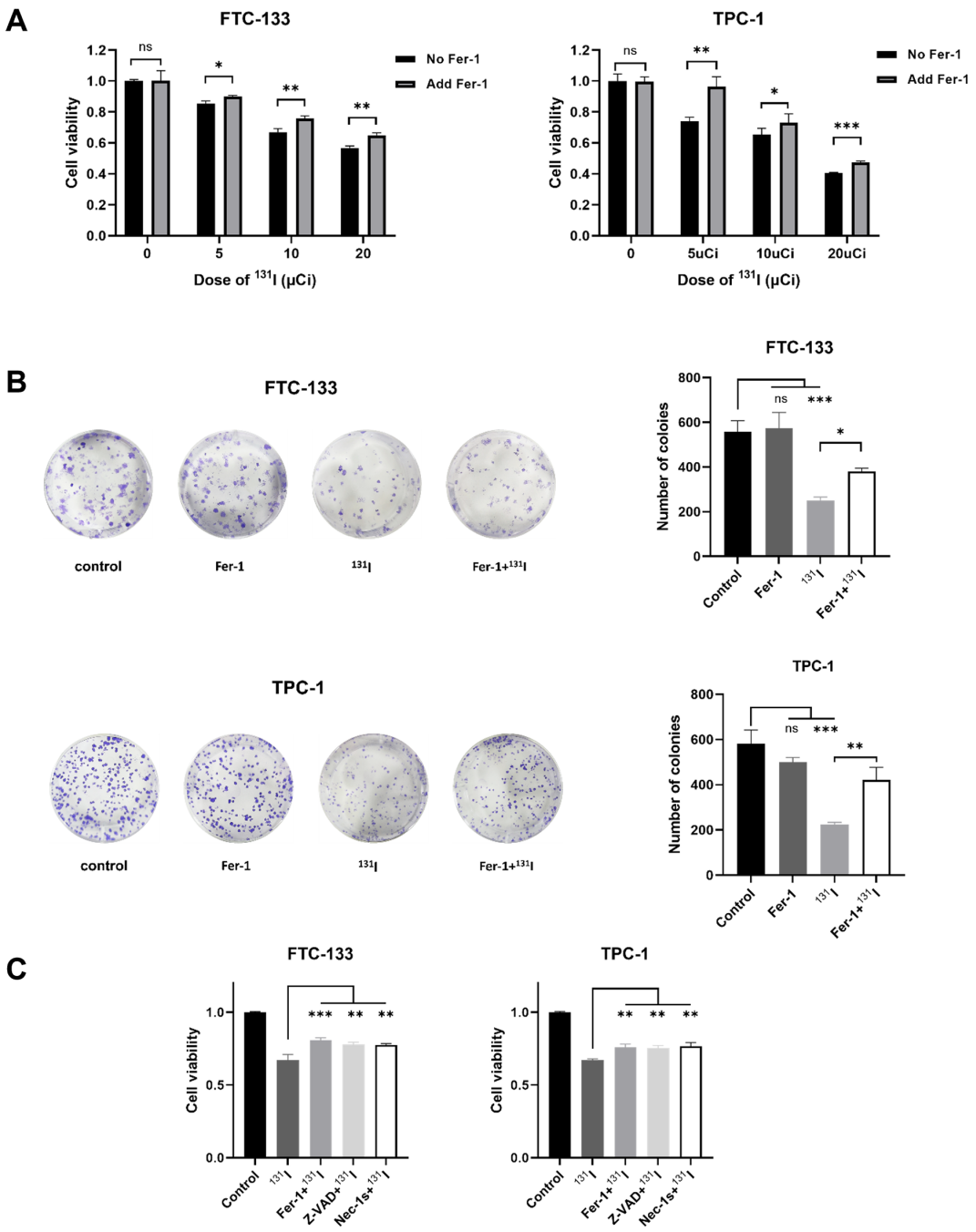

FIGURE 1
Fer-1 alleviates cell viability and colony formation ability suppressed by ^{131}I in DTC cells. **(A)** Cell viability of FTC-133 and TPC-1 cells that were pretreated with 1 μM Fer-1 for 4 h followed by treatment of 5, 10, 20 μCi ^{131}I for 48 h. **(B)** Colony formation ability of FTC-133 and TPC-1 cells that were pretreated with 1 μM Fer-1 for 4 h followed by treatment of 50 μCi ^{131}I. **(C)** Cell viability of FTC-133 and TPC-1 cells that were pretreated with 1 μM Fer-1, 5 μM Necrostatin-1s or 10 μM Z-VAD-fmk for 4 h followed by treatment of 10 μCi ^{131}I for 48 h. Images are representative of at least three independent experiments.

^{131}I-induced cell death, we performed comparative analyses of Fer-1 with apoptosis inhibitor ZVAD-FMK and necroptosis inhibitor necrostatin-1 (Nec-1s). All three inhibitors partially restored viability in ^{131}I-treated DTC cells (Figure 1C), indicating co-activation of ferroptotic, apoptotic, and necroptotic pathway. Based on these findings, we focused subsequent investigations on ferroptosis mechanisms in ^{131}I-treated DTC cells.

Biochemical hallmarks of ferroptosis are observed in ^{131}I-treated DTC cells

We systematically evaluated ferroptosis-associated biochemical alterations in DTC cells following ^{131}I exposure. GSH levels were first quantified in FTC-133 and TPC-1 cells, revealing significant depletion upon ^{131}I treatment (Figure 2A). Consistent with

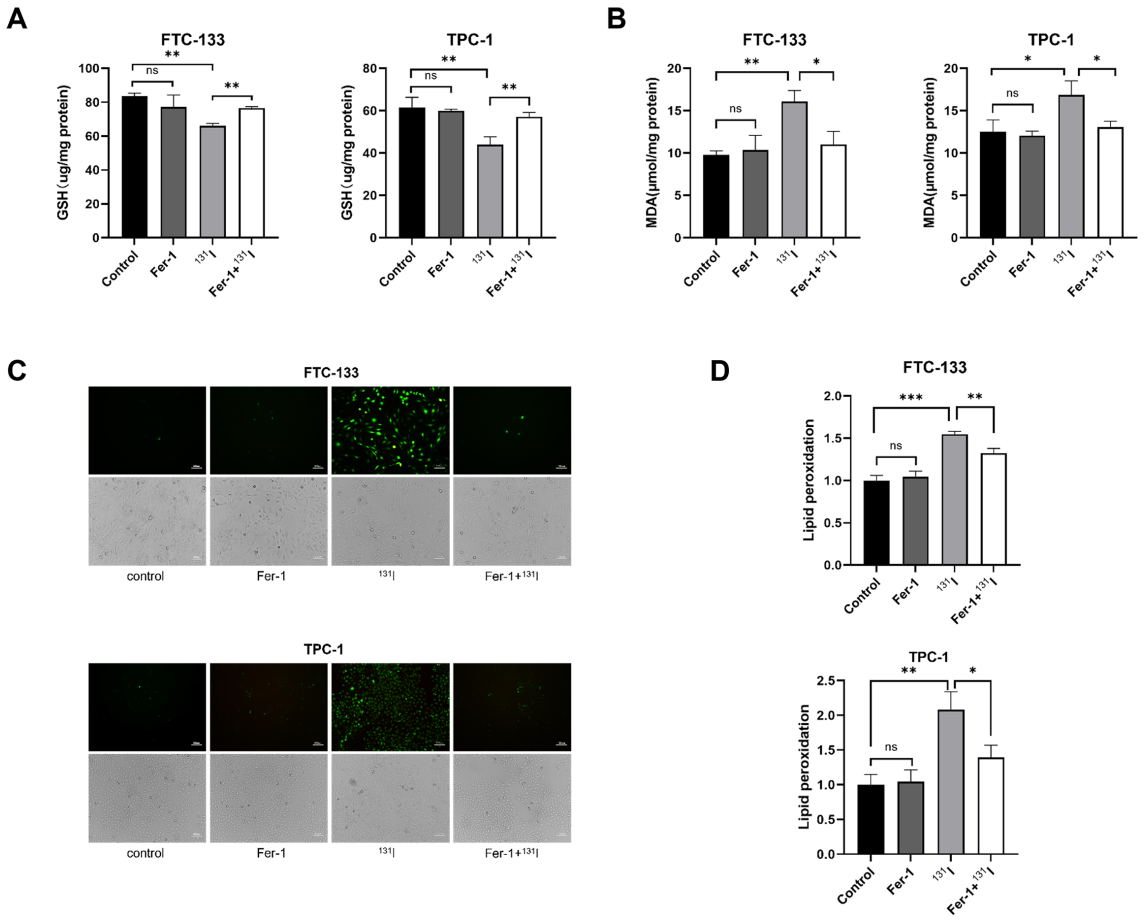

FIGURE 2
Ferroptosis morphological and genetic signatures are observed in ^{131}I-treated DTC cells. **(A)** The GSH levels of FTC-133 and TPC-1 cells pretreated with 1 μM Fer-1 for 4 h followed by treatment of 50 μCi ^{131}I for 48 h. **(B)** The MDA levels of FTC-133 and TPC-1 cells pretreated with 1 μM Fer-1 for 4 h followed by treatment of 50 μCi ^{131}I for 48 h. **(C)** The ROS levels of FTC-133 and TPC-1 cells pretreated with 1 μM Fer-1 for 4 h followed by treatment of 50 μCi ^{131}I for 48 h. Scale bar = 100 μm. **(D)** The lipid peroxidation levels of FTC-133 and TPC-1 cells pretreated with 1 μM Fer-1 for 4 h followed by treatment of 50 μCi ^{131}I for 48 h. Images are representative of at least three independent experiments.

ferroptosis characteristics, MDA-a lipid peroxidation byproduct indicative of ferroptosis (26) - showed marked elevation in ^{131}I-treated cells versus controls (Figure 2B). ROS production and lipid peroxidation were also substantially amplified in both cell lines post-^{131}I exposure (Figures 2C, D). Notably, co-treatment with Fer-1 effectively abrogated ^{131}I-induced perturbations in GSH, MDA, ROS, and lipid peroxidation markers (Figures 2A-D). These data collectively confirm ^{131}I-triggered ferroptosis activation in DTC cells through canonical biochemical pathways.

Ferroptosis morphological and genetic signatures are observed in ^{131}I-treated DTC cells

Ferroptosis is characterized by distinct ultrastructural features that distinguish it from apoptosis and necroptosis. To systematically characterize these morphological changes, we performed TEM on ^{131}I-treated DTC cells. Notably, FTC-133 and TPC-1 cells exposed to ^{131}I displayed pathognomonic ferroptotic ultrastructure, featuring shrunken mitochondria with increased membrane density (27) (Figure 3A).

To e elucidate ferroptosis-related molecular mechanisms, we quantified *GPX4* and *SLC7A11* expression at both transcriptional and translational levels. RT-qPCR analyses revealed that ^{131}I treatment significantly downregulated *GPX4* and *SLC7A11* mRNA levels relative to untreated controls (Figure 3B). Protein expression paralleled transcriptional changes, with marked reductions in GPX4 and SLC7A11 observed by western blot (Figures 3C, D). These results collectively demonstrate that ^{131}I triggers ferroptosis in DTC cells through coordinated suppression of *GPX4* and *SLC7A11* and induces mitochondrial remodeling characteristic of ferroptosis in DTC cells.

SAS synergizes with ^{131}I to promote DTC cells death

Given the observed role of *SLC7A11* suppression in ^{131}I-induced ferroptosis, we investigated whether pharmacological

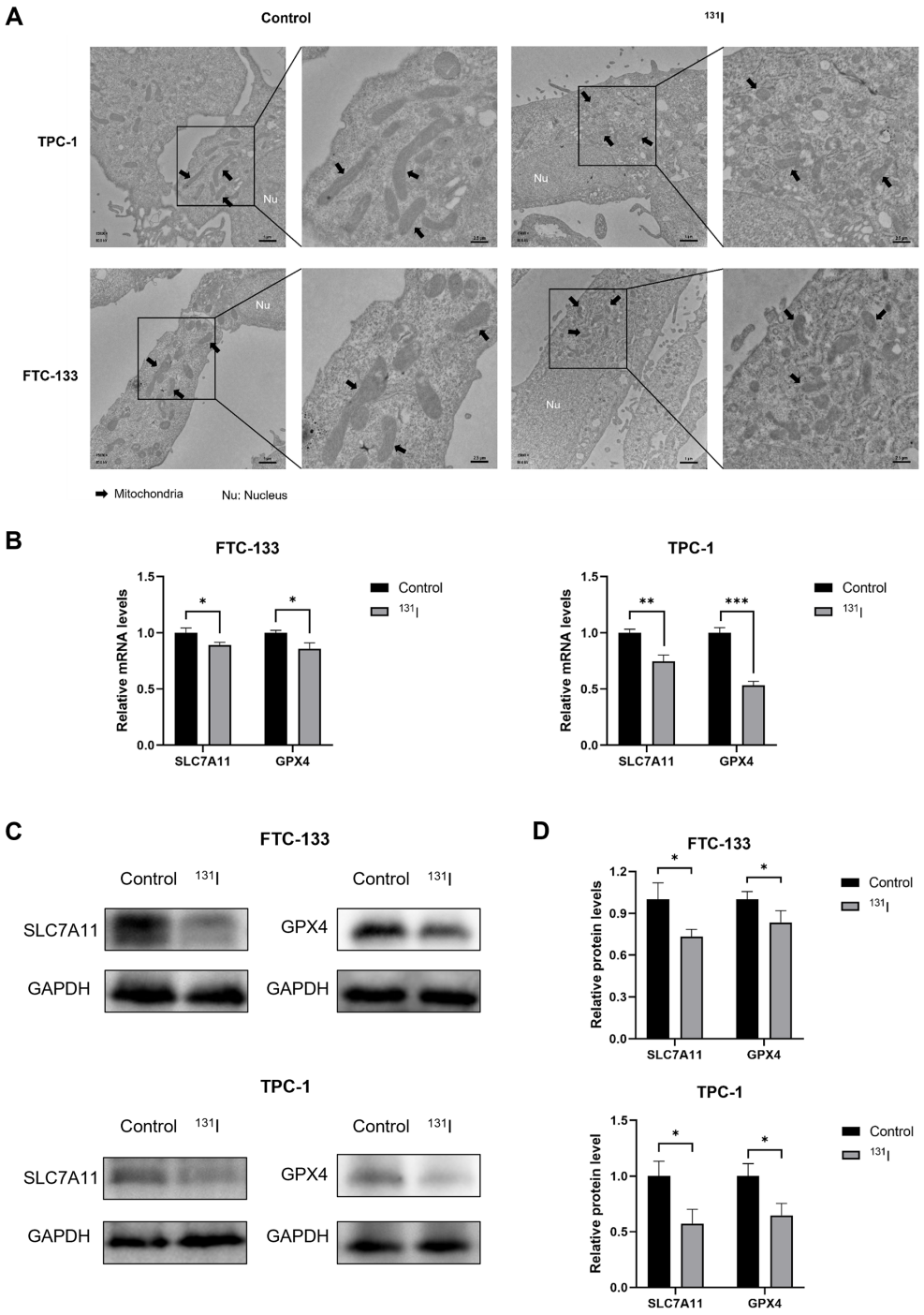

FIGURE 3
Morphological markers and Genetic hallmarks of ferroptosis were observed in ^{131}I -treated DTC cells. **(A)** Transmission electron microscopy images of FTC-133 and TPC-1 cells with or without ^{131}I treatment. Nu, nucleus. Scale bars: left, 1 µm, right, 2.5 µm. **(B)** The relative *SLC7A11* and *GPX4* mRNA expression levels of FTC-133 and TPC-1 cells with or without ^{131}I treatment. **(C)** The relative *SLC7A11* and *GPX4* protein expression levels of FTC-133 and TPC-1 cells with or without ^{131}I. **(D)** The quantitative graph of relative protein expression of *SLC7A11* and *GPX4* using Image J. Images are representative of at least three independent experiments.

SLC7A11 inhibition could enhance ^{131}I efficacy in DTC cells. The system xc^- inhibitor SAS, a class 1 ferroptosis inducer targeting *SLC7A11*, was selected for combination therapy. Dose-response analysis determined IC50 values of 0.42 mM for FTC-133 and 0.48 mM for TPC-1 cells (Figure 4A), prompting selection of sub-IC50 SAS concentrations (0.1 mM) for synergy testing. DTC cells were treated with escalating ^{131}I doses (5, 10, 15, 20, 25 µCi) alone, 0.1 mM SAS monotherapy, or their combination. Combination Index (CI) was calculated using the Chou - Talalay method (28), where CI > 1 indicates antagonism; = 1 additive effect; < 1 synergy.

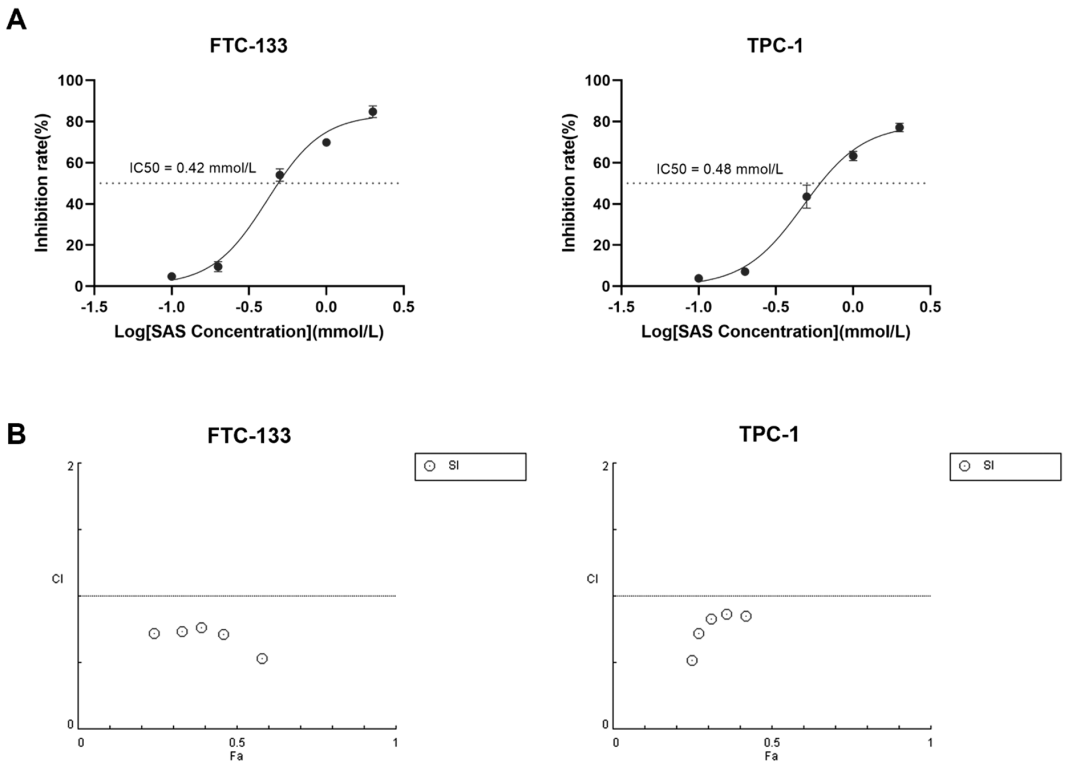

FIGURE 4
SAS synergizes with ^{131}I to promote DTC cells death **(A)** The IC50 of SAS on FTC-133 and TPC-1 cells for 24 h. **(B)** Combination Index of sulfasalazine and ^{131}I on FTC-133 and TPC-1 cells (concentration of SAS when treating alone on the cell: 0.1 mM, 0.2 mM, 0.5 mM, 1 mM, 2 mM, concentration of SAS in combination on cells: 0.1 mM, dose of ^{131}I when treating alone and in combination on cells: 5 μCi, 10 μCi, 15 μCi, 20 μCi, 25 μCi, drug treatment time: 24 h). Images are representative of at least three independent experiments.

Quantitative analysis demonstrated the CI values for the combination of SAS and ^{131}I in DTC cells were less than 1, confirming synergistic effects between SAS and ^{131}I in DTC cells (Figure 4B). Additionally, our findings indicated that the combined use of SAS and ^{131}I also inhibits the activity of normal thyroid cells. However, compared to normal thyroid cells, the combined treatment exhibits a significantly more pronounced inhibitory effect on thyroid cancer cells, suggesting a potential therapeutic advantage in thyroid cancer cells while minimizing the toxic effect on healthy tissue (Supplementary Figure S1).

Combination SAS and ^{131}I enhance ferroptosis in DTC cells

To mechanistically delineate the synergistic effects of SAS and ^{131}I combination therapy in DTC cells, we quantified canonical ferroptosis biomarkers (MDA, GSH and lipid peroxidation) using standardized protocols described above. Intriguingly, the combination group exhibited significantly GSH depletion in FTC-133 and TPC-1 cells compared with the other groups (Figure 5A). And the cotreatment with SAS and ^{131}I resulted in a marked elevation in MDA levels compared to the other treatment groups (Figure 5B). Furthermore, the combination of SAS and ^{131}I resulted in a significant induction of lipid peroxidation, which was significantly higher than that in the other groups (Figure 5C). Moreover, we examined the protein expression levels of GPX4 and SLC7A11 in FTC-133 and TPC-1 cells using Western Blotting. Our results showed that GPX4 and SLC7A11 expression levels were significantly lower in the group treated with the SAS and ^{131}I combination than in those treated with SAS alone, ^{131}I alone, or in the control group. Additionally, GPX4 and SLC7A11 expression levels were significantly downregulated in groups treated with ^{131}I or SAS alone compared to the control group. (Figures 5D, E). The above results indicate that cotreatment with SAS and ^{131}I robustly induces cell death through enhanced lipid peroxidation and activation of ferroptosis.

SLC7A11 knockdown enhances ferroptosis induced by ^{131}I and SAS in DTC cells

Given that the mechanism of action of SAS involves the inhibition of *SLC7A11* activity, and our study has also demonstrated that ^{131}I can downregulate the expression of *SLC7A11*, we posited that their synergistic effects arose from dual targeting of this cystine/glutamate antiporter. To validate this hypothesis, we established *SLC7A11*-knockdown DTC cell models, validated by RT-qPCR and Western blotting (Figures 6A, B). To further elucidate the role of *SLC7A11* in mediating the effects

10.3389/fonc.2025.1580828

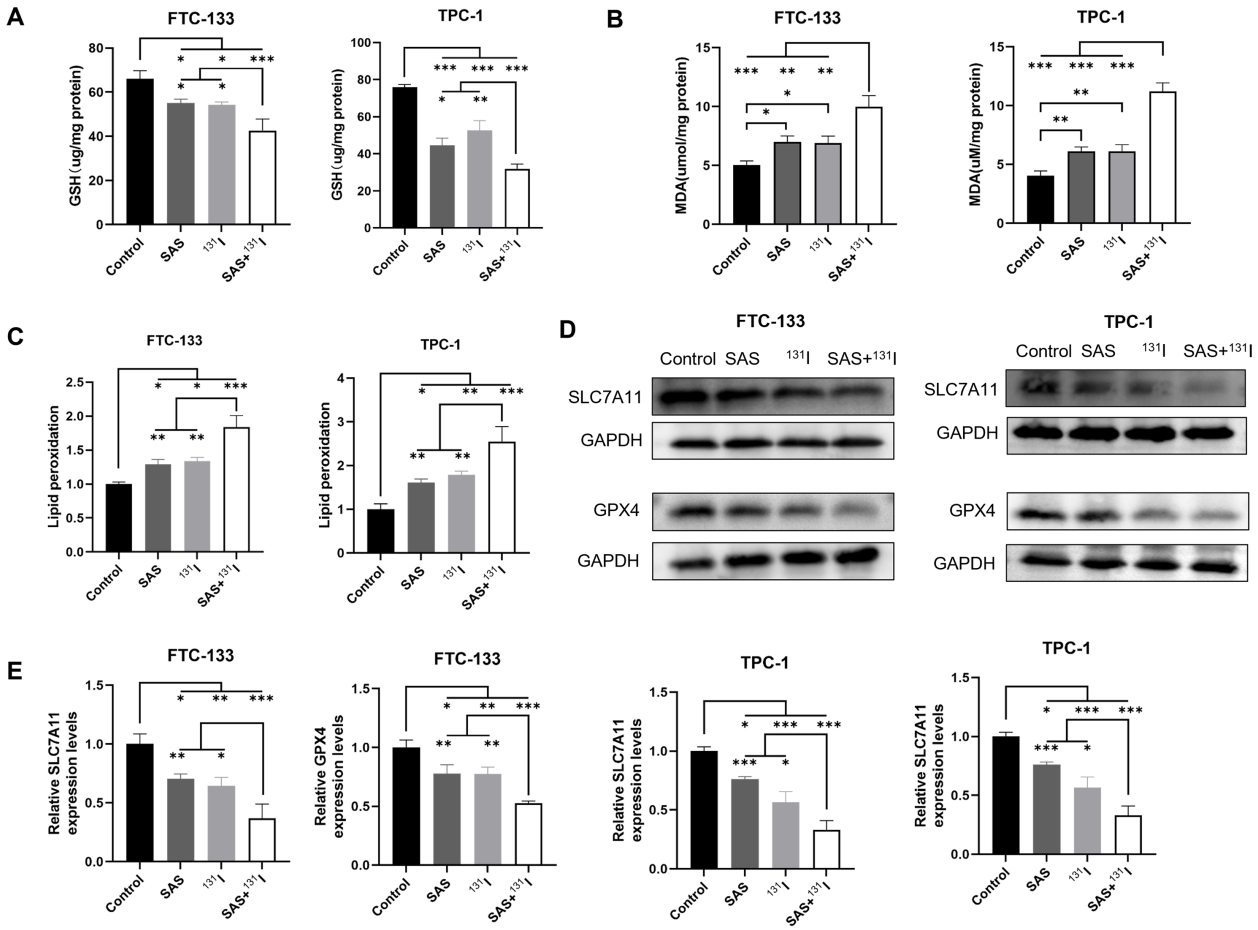

FIGURE 5
Combination SAS and ^{131}I enhance lipid peroxidation and ferroptosis in DTC cells. **(A)** The GSH levels of FTC-133 and TPC-1 cells after 0.1 mmol/L SAS and 50 μCi ^{131}I treatment for 24 h. **(B)** The MDA levels of FTC-133 and TPC-1 cells after 0.1 mM SAS and 50 μCi ^{131}I treatment for 24 h. **(C)** The lipid peroxidation levels of FTC-133 and TPC-1 cells after 0.1 mM SAS and 50 μCi ^{131}I treatment for 24 h. **(D)** The *GPX4* and *SLC7A11* protein expression levels of FTC-133 and TPC-1 cells after 0.1 mM SAS and 50 μCi ^{131}I treatment for 24 h. **(E)** The quantitative graph of relative protein expression of *SLC7A11* and *GPX4* using Image J. Images are representative of at least three independent experiments.

of ^{131}I and SAS on DTC cells, we assessed cell viability, intracellular GSH levels, and lipid peroxidation in *SLC7A11*-knockdown DTC cells. Our results demonstrated that *SLC7A11* knockdown significantly reduced cell viability, irrespective of whether ^{131}I, SAS, or their combination was applied (Figure 6C). Additionally, *SLC7A11* knockdown led to a marked decrease in intracellular GSH levels across all treatment groups, except for the control group (Figure 6D). Moreover, lipid peroxidation levels were significantly elevated in cells treated with ^{131}I alone, SAS alone, or the combination therapy following *SLC7A11* knockdown (Figure 6E). Collectively, these findings highlight the pivotal role of *SLC7A11* in the cytotoxic effects of ^{131}I and SAS on thyroid cancer cells.

SAS synergizes with ^{131}I in DTC xenograft nude mice model

To validate the therapeutic synergy of SAS and ^{131}I *in vivo*, TPC-1 xenograft-bearing nude mice were treated with SAS in combination with ^{131}I. Post-treatment, significant reductions in tumor volume and weight were observed in the combination-treated group compared to the control group (Figures 7A-C). Additionally, treatment with ^{131}I alone also resulted in notable decreases in tumor volume and weight compared to the control group. Immunohistochemical analyses revealed that the combination of ^{131}I and SAS significantly downregulated the expression of GPX4 and SLC7A11 compared to all other group *in vivo* (Figure 7D). Moreover, GPX4 and SLC7A11 expression levels were also reduced in mice treated with ^{131}I alone or SAS alone compared to the control group. Collectively, these findings suggest that SAS synergized with ^{131}I to effectively treat DTC *in vivo*, an effect that is associated with enhanced lipid peroxidation and ferroptosis.

Discussion

Ferroptosis, an iron-dependent form of regulated cell death driven by lipid peroxidation (29), functions as a tumor-suppressive

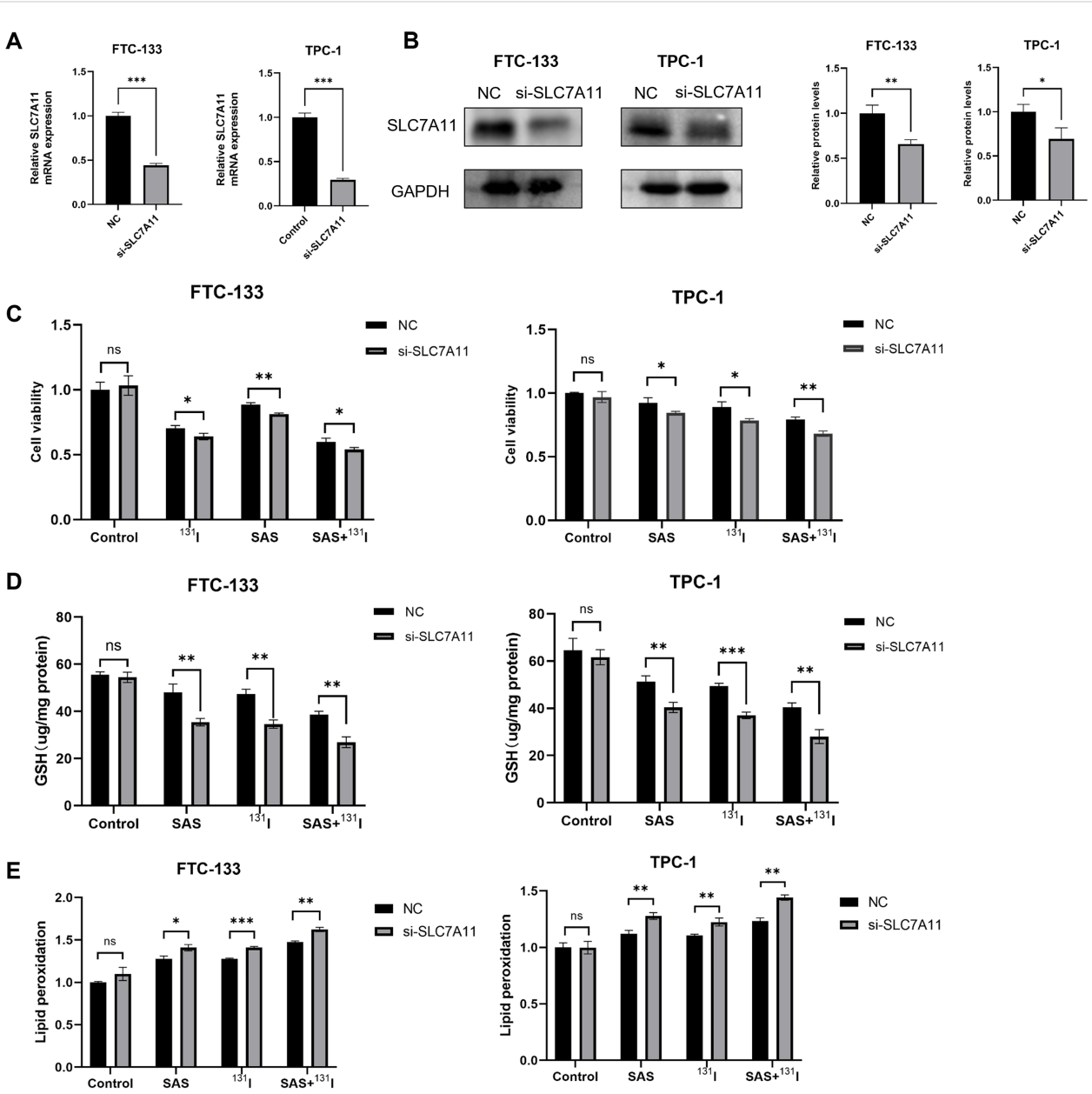

FIGURE 6
SLC7A11 knockdown enhances effects of SAS and ^{131}I on DTC cells. **(A)** Relative expression levels of *SLC7A11* mRNA in FTC-133 and TPC-1 cells with or without knockdown of *SLC7A11*. **(B)** Relative *SLC7A11* protein expression levels in FTC-133 and TPC-1 cells with or without knockdown of *SLC7A11*. **(C)** Cell viability of DTC FTC-133 and TPC-1 cells treated with 0.1 mmol/L sulfasalazine and 10 μCi ^{131}I for 24 h with or without knockdown of *SLC7A11*. **(D)** GSH levels of FTC-133 and TPC-1 cells treated with 0.1 mmol/L sulfasalazine and 50 μCi ^{131}I for 24 h with or without knockdown of *SLC7A11*. **(E)** Lipid peroxidation levels of FTC-133 and TPC-1 cells treated with 0.1 mmol/L sulfasalazine and 50 μCi ^{131}I for 24 h with or without knockdown of *SLC7A11*. Images are representative of at least three independent experiments.

mechanism that is frequently silenced in malignancies (11). Emerging evidence links multiple frontline oncologic therapies—including radiotherapy, endocrine therapy, immune checkpoint blockade, and platinum-based chemotherapy—to ferroptosis potentiation (15, 30–32). The synergistic application of ferroptosis inducer in combination with other therapeutic approaches represents a promising strategy for cancer therapy (33, 34). In this study, we demonstrated that ^{131}I induces lipid peroxidation and ferroptosis in DTC cells and synergizes with SAS in treating DTC cells. Fer-1 alleviated the inhibitory effects of ^{131}I on the viability and clonogenic potential of DTC cells. Through a comprehensive analysis encompassing biochemical, morphological, and genetic perspectives, we have identified that ^{131}I induces ferroptosis in DTC cells. Specifically, ^{131}I treatment results in elevated levels of MDA and ROS, concurrent with a reduction in GSH content within DTC cells. Additionally, ^{131}I induces characteristic morphological changes associated with ferroptosis, including a reduction in mitochondrial volume and contraction of mitochondrial cristae. Furthermore, the expression levels of *SLC7A11* and *GPX4* are downregulated in DTC cells after ^{131}I treatment.

10.3389/fonc.2025.1580828

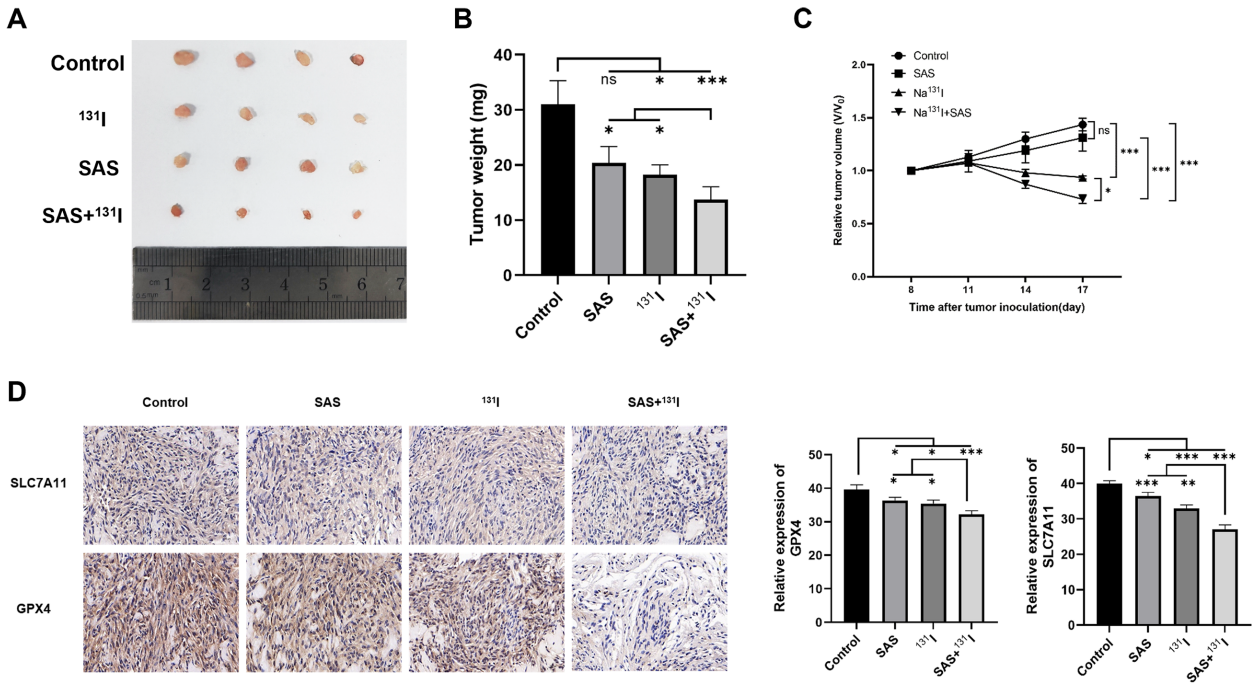

FIGURE 7
SAS synergizes with ^{131}I in DTC xenograft nude mice model. **(A)** Image of tumors isolated from different treatment groups. **(B)** Tumor weights in different treatment groups. **(C)** Curves of relative tumor volume changes in different treatment groups during the treatment period. **(D)** Immunohistochemical analysis of *SLC7A11* and *GPX4*.

As a radionuclide,^{131}I emits β radiation that induces cell death by damaging DNA and eliciting cytotoxicity. The presence of the NIS on the basal membrane of certain tumor cells, such as those in DTC, cholangiocarcinoma and hepatocellular carcinoma, facilitates iodine uptake and forms the basis for radioiodine therapy (35). However, ^{131}I can be used for the radiolabeling of molecules, peptides, antibodies and nanomaterials that selectively binding to cancer cells, thereby targeting cancer cells that do not express NIS. For instance, a ^{131}I-labeled programmed cell death ligand 1 (PD-L1) antibody can target PD-L1 expressed on the cancer cell membrane, inducing ferroptosis in cancer cells (36). Two studies on the synthesis of radiopharmaceuticals using ^{131}I-conjugated PD-L1 antibodies have demonstrated that these radiotherapeutic agents can induce ferroptosis in tumor cells (36, 37). Moreover, Shen et al. employed 3 nm ultrasmall single-crystal iron nanoparticles as a ferroptosis inducer to synergize with ^{131}I-PD-L1 antibodies in treating murine breast cancer cells and embryonic fibroblast cells. These findings support our investigation that ^{131}I can induce lipid peroxidation and ferroptosis in cancer cells. However, given the inability of these cells to uptake ^{131}I, experiments on the therapeutic application of ^{131}I as a solitary agent were not conducted in their research. By contrast, the DTC cells used in the present study are capable of iodine uptake, allowing us to directly observe the role of ferroptosis in tumor cells treated with ^{131}I.

Extensive scholarly research has demonstrated that the induction of ferroptosis enhances the efficacy of radiotherapy in cancer treatment, and can even overcomes the radioresistance of some cancer cells (34, 38–40). SAS has been shown to induce ferroptosis by inhibiting the SLC7A11 transporter, a transmembrane protein responsible for cysteine uptake into cells (41). This inhibition leads to a depletion of GSH, a coenzyme essential for the function of GPX4. Previous studies have identified that SAS exhibits significant radiosensitizing effect both *in vivo* and *in vitro* (14, 20, 42). However, no research has yet explored whether SAS can synergistically treat DTC by enhancing the ferroptosis-inducing effects of ^{131}I. In the current study, we treated DTC cells with a combination of ^{131}I with SAS, and observed that the CI was below 1, indicative of a synergistic interaction. Additionally, cotreatment resulted in the depletion of GSH and the elevation of ROS and MDA levels in DTC cells, along with a marked decrease in the expression of *SLC7A11* and *GPX4*. Our study confirmed that *SLC7A11* is downregulated in DTC cells treated with ^{131}I. Furthermore, SAS induces ferroptosis by inhibiting the activity of *SLC7A11*. Therefore, we propose that *SLC7A11* plays a crucial role in the synergistic effects of ^{131}I and SAS on DTC cells. Accordingly, in this study, we knocked down the expression of *SLC7A11* in TPC-1 and FTC-133 cells and subsequently examined the changes in ferroptosis-related markers following exposure to ^{131}I. The results revealed that, compared with cells without knockdown, cells with *SLC7A11* knockdown exhibited more pronounced ferroptosis-related responses, regardless of whether they were treated with ^{131}I alone, SAS alone, or a combination of both agents. Furthermore, this study also demonstrated that SAS and ^{131}I can exert synergistic antitumor effects through inducing ferroptosis *in vivo*. Overall, we suggest that SAS and ^{131}I can synergistically induce lipid peroxidation and ferroptosis by depleting GSH through the inhibition of *SLC7A11*.

While our study demonstrates the potential of combining ^{131}I and SAS to induce ferroptosis in DTC, we acknowledge that the effects of this combination therapy on normal thyroid cells and GPX4 or SLC7A11 overexpression experiments on DTC cells were not explored. Although ^{131}I is a standard treatment for DTC with a well-established safety profile, and SAS selectively targets ferroptosis in cancer cells, the toxicity of this combination therapy on normal thyroid tissue remains an important consideration. Normal thyroid cells typically express lower levels of GPX4 and SLC7A11 compared to DTC cells, which may reduce their susceptibility to ferroptosis induction (22–25). However, further comparison and *in vivo* studies are required to assess the potential toxicity of ^{131}I and SAS on normal thyroid cells and to investigate effects of GPX4 or SLC7A11 overexpression on DTC cells, ensuring that this combination therapy can be applied safely within a therapeutic window. Additionally, given the crucial role of the NIS in iodine uptake by thyroid cancer cells, future research should focus on whether and how SAS affects NIS expression. This is vital for understanding the synergistic effects of combining ^{131}I and SAS in DTC cells.

Conclusions

Our study highlights that the combination of ^{131}I and SAS can synergistically induce lipid peroxidation and ferroptosis in DTC cells, leading to enhanced therapeutic efficacy. This suggests that targeting ferroptosis pathways, in conjunction with traditional therapies like ^{131}I, may provide a promising approach to improve the treatment of DTC.

Data availability statement

The raw data supporting the conclusions of this article will be made available by the authors, without undue reservation.

Ethics statement

The animal study was approved by Institutional Animal Care and Use Committee of General Hospital of Southern Theater Command (Ethics Approval Number: NBZQZYY2024023). The study was conducted in accordance with the local legislation and institutional requirements.

Author contributions

LL: Conceptualization, Data curation, Methodology, Writing – original draft. JZ: Conceptualization, Supervision, Writing – review & editing. XZ: Formal analysis, Resources, Writing – original draft. PW: Formal analysis, Methodology, Writing – original draft. MM: Software, Writing – original draft. BY: Validation, Visualization, Writing – original draft.

Funding

The author(s) declare that financial support was received for the research and/or publication of this article. This work was supported by Guangzhou Municipal Science and Technology Project (No: 201904010126).

Conflict of interest

The authors declare that the research was conducted in the absence of any commercial or financial relationships that could be construed as a potential conflict of interest.

Generative AI statement

The author(s) declare that no Generative AI was used in the creation of this manuscript.

Publisher's note

Supplementary material

The Supplementary Material for this article can be found online at: https://www.frontiersin.org/articles/10.3389/fonc.2025.1580828/full#supplementary-material

References

1. Bray F, Laversanne M, Sung H, Ferlay J, Siegel RL, Soerjomataram I, et al. Global cancer statistics 2022: GLOBOCAN estimates of incidence and mortality worldwide for 36 cancers in 185 countries. *CA Cancer J Clin*. (2024) 74:229–63. doi: 10.3322/caac.21834

2. Sung H, Ferlay J, Siegel RL, Laversanne M, Soerjomataram I, Jemal A, et al. Global cancer statistics 2020: GLOBOCAN estimates of incidence and mortality worldwide for 36 cancers in 185 countries. *CA Cancer J Clin*. (2021) 71:209–49. doi: 10.3322/caac.21660

3. Boucai L, Zafereo M, Cabanillas ME. Thyroid cancer: A review. *JAMA*. (2024) 331:425–35. doi: 10.1001/jama.2023.26348

4. Ao Z-X, Chen Y-C, Lu J-M, Shen J, Peng L-P, Lin X, et al. Identification of potential functional genes in papillary thyroid cancer by co-expression network analysis. *Oncol Lett*. (2018) 16:4871–8. doi: 10.3892/ol.2018.9306

5. Br H, Ek A, Kc B, Gm D, Sj M, Ye N, et al. 2015 American thyroid association management guidelines for adult patients with thyroid nodules and differentiated

thyroid cancer: the american thyroid association guidelines task force on thyroid nodules and differentiated thyroid cancer. *Thyroid Off J Am Thyroid Assoc*. (2016) 26. doi: 10.1089/thy.2015.0020

6. Dixon SJ, Lemberg KM, Lamprecht MR, Skouta R, Zaitsev EM, Gleason CE, et al. Ferroptosis: an iron-dependent form of non-apoptotic cell death. *Cell*. (2012) 149:1060–72. doi: 10.1016/j.cell.2012.03.042

7. Li Y, Feng D, Wang Z, Zhao Y, Sun R, Tian D, et al. Ischemia-induced ACSL4 activation contributes to ferroptosis-mediated tissue injury in intestinal ischemia/reperfusion. *Cell Death Differ*. (2019) 26:2284–99. doi: 10.1038/s41418-019-0299-4

8. Cai W, Liu L, Shi X, Liu Y, Wang J, Fang X, et al. Alox15/15-hpETE aggravates myocardial ischemia-reperfusion injury by promoting cardiomyocyte ferroptosis. *Circulation*. (2023) 147:1444–60. doi: 10.1161/CIRCULATIONAHA.122.060257

9. Luoqian J, Yang W, Ding X, Tuo Q-Z, Xiang Z, Zheng Z, et al. Ferroptosis promotes T-cell activation-induced neurodegeneration in multiple sclerosis. *Cell Mol Immunol*. (2022) 19:913–24. doi: 10.1038/s41423-022-00883-0

10. Chu J, Li J, Sun L, Wei J. The role of cellular defense systems of ferroptosis in Parkinson's disease and Alzheimer's disease. *Int J Mol Sci*. (2023) 24. doi: 10.3390/ijms241814108

11. Jiang L, Kon N, Li T, Wang S-J, Su T, Hibshoosh H, et al. Ferroptosis as a p53-mediated activity during tumour suppression. *Nature*. (2015) 520:57–62. doi: 10.1038/nature14344

12. Li D, Wang Y, Dong C, Chen T, Dong A, Ren J, et al. CST1 inhibits ferroptosis and promotes gastric cancer metastasis by regulating GPX4 protein stability via OTUB1. *Oncogene*. (2023) 42. doi: 10.1038/s41388-022-02537-x

13. Zhou Q, Liu T, Qian W, Ji J, Cai Q, Jin Y, et al. HNF4A-BAP31-VDAC1 axis synchronously regulates cell proliferation and ferroptosis in gastric cancer. *Cell Death Dis*. (2023) 14:356. doi: 10.1038/s41419-023-05868-z

14. Lei G, Zhang Y, Koppula P, Liu X, Zhang J, Lin SH, et al. The role of ferroptosis in ionizing radiation-induced cell death and tumor suppression. *Cell Res*. (2020) 30:146–62. doi: 10.1038/s41422-019-0263-3

15. Lang X, Green MD, Wang W, Yu J, Choi JE, Jiang L, et al. Radiotherapy and immunotherapy promote tumoral lipid oxidation and ferroptosis via synergistic repression of SLC7A11. *Cancer Discov*. (2019) 9:1673–85. doi: 10.1158/2159-8290.CD-19-0338

16. Bersuker K, Hendricks JM, Li Z, Magtanong L, Ford B, Tang PH, et al. The CoQ oxidoreductase FSP1 acts parallel to GPX4 to inhibit ferroptosis. *Nature*. (2019) 575:688–92. doi: 10.1038/s41586-019-1705-2

17. Koppula P, Zhuang L, Gan B. Cystine transporter SLC7A11/xCT in cancer: ferroptosis, nutrient dependency, and cancer therapy. *Protein Cell*. (2021) 12:599–620. doi: 10.1007/s13238-020-00789-5

18. Yang WS, SriRamaratnam R, Welsch ME, Shimada K, Skouta R, Viswanathan VS, et al. Regulation of ferroptotic cancer cell death by GPX4. *Cell*. (2014) 156:317–31. doi: 10.1016/j.cell.2013.12.010

19. Gout PW, Buckley AR, Simms CR, Bruchovsky N. Sulfasalazine, a potent suppressor of lymphoma growth by inhibition of the x(c)- cystine transporter: a new action for an old drug. *Leukemia*. (2001) 15:1633–40. doi: 10.1038/sj.leu.2402238

20. Nagane M, Kanai E, Shibata Y, Shimizu T, Yoshioka C, Maruo T, et al. Sulfasalazine, an inhibitor of the cystine-glutamate antiporter, reduces DNA damage repair and enhances radiosensitivity in murine B16F10 melanoma. *PloS One*. (2018) 13: e0195151. doi: 10.1371/journal.pone.0195151

21. Rodman SN, Spence JM, Ronnfeldt TJ, Zhu Y, Solst SR, O'Neill RA, et al. Enhancement of radiation response in breast cancer stem cells by inhibition of thioredoxin and glutathione dependent metabolism. *Radiat Res*. (2016) 186:385–95. doi: 10.1667/RR14463.1

22. Shen L, Qian C, Cao H, Wang Z, Luo T, Liang C. Upregulation of the solute carrier family 7 genes is indicative of poor prognosis in papillary thyroid carcinoma. *World J Surg Oncol*. (2018) 16:235. doi: 10.1186/s12957-018-1535-y

23. Chen H, Peng F, Xu J, Wang G, Zhao Y. Increased expression of GPX4 promotes the tumorigenesis of thyroid cancer by inhibiting ferroptosis and predicts poor clinical outcomes. *Aging*. (2023) 15:230–45. doi: 10.18632/aging.204473

24. Sekhar KR, Hanna DN, Cyr S, Baechle JJ, Kuravi S, Balusu R, et al. Glutathione peroxidase 4 inhibition induces ferroptosis and mTOR pathway suppression in thyroid cancer. *Sci Rep*. (2022) 12:19396. doi: 10.1038/s41598-022-23906-2

25. Ji F-H, Fu X-H, Li G-Q, He Q, Qiu X-G. FTO prevents thyroid cancer progression by SLC7A11 m6A methylation in a ferroptosis-dependent manner. *Front Endocrinol*. (2022) 13:857765. doi: 10.3389/fendo.2022.857765

26. Yang WS, Stockwell BR. Ferroptosis: death by lipid peroxidation. *Trends Cell Biol*. (2016) 26:165–76. doi: 10.1016/j.tcb.2015.10.014

27. Stockwell BR, Friedmann Angeli JP, Bayir H, Bush AI, Conrad M, Dixon SJ, et al. Ferroptosis: A regulated cell death nexus linking metabolism, redox biology, and disease. *Cell*. (2017) 171:273–85. doi: 10.1016/j.cell.2017.09.021

28. Tc C. Drug combination studies and their synergy quantification using the Chou-Talalay method. *Cancer Res*. (2010) 70. doi: 10.1158/0008-5472.CAN-09-1947

29. Stockwell BR. Ferroptosis turns 10: Emerging mechanisms, physiological functions, and therapeutic applications. *Cell*. (2022) 185:2401–21. doi: 10.1016/j.cell.2022.06.003

30. Wang W, Green M, Choi JE, Gijón M, Kennedy PD, Johnson JK, et al. CD8+ T cells regulate tumour ferroptosis during cancer immunotherapy. *Nature*. (2019) 569:270–4. doi: 10.1038/s41586-019-1170-y

31. Xu Z, Wang X, Sun W, Xu F, Kou H, Hu W, et al. RelB-activated GPX4 inhibits ferroptosis and confers tamoxifen resistance in breast cancer. *Redox Biol*. (2023) 68:102952. doi: 10.1016/j.redox.2023.102952

32. Guo J, Xu B, Han Q, Zhou H, Xia Y, Gong C, et al. Ferroptosis: A novel anti-tumor action for cisplatin. *Cancer Res Treat*. (2018) 50:445–60. doi: 10.4143/crt.2016.572

33. Wang L, Wang C, Li X, Tao Z, Zhu W, Su Y, et al. Melatonin and erastin emerge synergistic anti-tumor effects on oral squamous cell carcinoma by inducing apoptosis, ferroptosis, and inhibiting autophagy through promoting ROS. *Cell Mol Biol Lett*. (2023) 28:36. doi: 10.1186/s11658-023-00449-6

34. Ye LF, Chaudhary KR, Zandkarimi F, Harken AD, Kinslow CJ, Upadhyayula PS, et al. Radiation-induced lipid peroxidation triggers ferroptosis and synergizes with ferroptosis inducers. *ACS Chem Biol*. (2020) 15:469–84. doi: 10.1021/acschembio.9b00939

35. Shen H, Zhu R, Liu Y, Hong Y, Ge J, Xuan J, et al. Radioiodine-refractory differentiated thyroid cancer: molecular mechanisms and therapeutic strategies for radioiodine resistance. *Drug Resist Update Rev Comment Antimicrob Anticancer Chemother*. (2024) 72:101013. doi: 10.1016/j.drup.2023.101013

36. Shao C, Yan X, Pang S, Nian D, Ren L, Li H, et al. Bifunctional molecular probe targeting tumor PD-L1 enhances anti-tumor efficacy by promoting ferroptosis in lung cancer mouse model. *Int Immunopharmacol*. (2024) 130:111781. doi: 10.1016/j.intimp.2024.111781

37. Shen J, Feng K, Yu J, Zhao Y, Chen R, Xiong H, et al. Responsive and traceless assembly of iron nanoparticles and 131I labeled radiopharmaceuticals for ferroptosis enhanced radio-immunotherapy. *Biomaterials*. (2025) 313:122795. doi: 10.1016/j.biomaterials.2024.122795

38. Lei G, Zhang Y, Hong T, Zhang X, Liu X, Mao C, et al. Ferroptosis as a mechanism to mediate p53 function in tumor radiosensitivity. *Oncogene*. (2021) 40:3533–47. doi: 10.1038/s41388-021-01790-w

39. Zeng L, Ding S, Cao Y, Li C, Zhao B, Ma Z, et al. A MOF-based potent ferroptosis inducer for enhanced radiotherapy of triple negative breast cancer. *ACS Nano*. (2023) 17:13195–210. doi: 10.1021/acsnano.3c00048

40. Liu S, Zhang H-L, Li J, Ye Z-P, Du T, Li L-C, et al. Tubastatin A potently inhibits GPX4 activity to potentiate cancer radiotherapy through boosting ferroptosis. *Redox Biol*. (2023) 62:102677. doi: 10.1016/j.redox.2023.102677

41. Ma M-Z, Chen G, Wang P, Lu W-H, Zhu C-F, Song M, et al. Xc- inhibitor sulfasalazine sensitizes colorectal cancer to cisplatin by a GSH-dependent mechanism. *Cancer Lett*. (2015) 368:88–96. doi: 10.1016/j.canlet.2015.07.031

42. Kerkhove L, Geirnaert F, Rifi AL, Law KL, Gutiérrez A, Oudaert I, et al. Repurposing sulfasalazine as a radiosensitizer in hypoxic human colorectal cancer. *Cancers*. (2023) 15:2363. doi: 10.3390/cancers15082363

frontiers | Frontiers in Pharmacology

TYPE Original Research
PUBLISHED 30 May 2025
DOI 10.3389/fphar.2025.1591643

OPEN ACCESS

EDITED BY
Ana Podolski-Renic,
Institute for Biological Research "Siniša Stanković" – National Institute of Republic of Serbia, Serbia

REVIEWED BY
Luis Mas,
Auna Oncosalud, Peru
Kui Zhang,
Sichuan University, China

*CORRESPONDENCE
Jianchun Duan,
duanjianchun79@163.com

RECEIVED 11 March 2025
ACCEPTED 16 May 2025
PUBLISHED 30 May 2025

CITATION
Guo Y, Han S, Guo Q, Zhai J, Ren X, Li S and Duan J (2025) Real-world analysis of immunochemotherapy in recurrent small-cell lung cancer: opportunities for second-line approaches.
Front. Pharmacol. 16:1591643.
doi: 10.3389/fphar.2025.1591643

Real-world analysis of immunochemotherapy in recurrent small-cell lung cancer: opportunities for second-line approaches

Yanrong Guo[1], Songyan Han[1], Qinxiang Guo[1], Jinfang Zhai[1], Xiaohui Ren[1], Shengshu Li[1] and Jianchun Duan[2]*

[1]Department of Respiratory Medicine, Shanxi Province Cancer Hospital, Shanxi Hospital Affiliated to Cancer Hospital, Chinese Academy of Medical Sciences, Cancer Hospital Affiliated to Shanxi Medical University, Taiyuan, China, [2]Department of Medical Oncology, Cancer Hospital, Chinese Academy of Medical Science and Peking Union Medical College, Beijing, China

Background: Small-cell lung cancer (SCLC) has limited therapeutic options beyond first-line treatment, and the efficacy of PD-1/PD-L1-based immunotherapy in this setting remains uncertain. This study evaluates the efficacy and safety of serplulimab-based immunochemotherapy as a second- or later-line treatment for SCLC.

Methods: This retrospective, real-world study included 39 SCLC patients treated with post-initial serplulimab-based immunochemotherapy at Shanxi Provincial Cancer Hospital between May 2022 and November 2023. Primary and secondary endpoints were overall survival (OS) and progression-free survival (PFS), respectively. Cox analyses were conducted to explore factors associated with survival outcomes.

Results: The median follow-up duration was 13.7 months. The OS was 12.00 months (95% CI: 6.87-not reached), and the median PFS was 4.07 months (95% CI: 3.07–7.17), with an objective response rate of 20.51%. Patients who underwent immunotherapy re-challenge showed numerically higher median OS (12.77 vs. 9.17 months) and PFS (5.93 vs. 3.87 months) than those without prior immunotherapy. Patients with an objective response to front-line therapy exhibited a trend toward improved median OS (not reached vs. 6.47 months) and PFS (5.93 vs. 3.17 months). Cox analysis identified ECOG PS of 2, elevated LDH, ProGrp, and NSE, and liver metastasis were associated with worse OS. The most common adverse events were thrombocytopenia, elevated ALT, and hypothyroidism, with a manageable safety profile.

Conclusion: Second- or later-line serplulimab-based immunochemotherapy shows promising antitumor activity and survival benefits for SCLC, regardless of prior immunotherapy exposure. Although limited by sample size and retrospective design, these findings highlight the potential of immunotherapy combinations beyond first-line therapy.

KEYWORDS

small-cell lung cancer, recurrent, immunochemotherapy, second-line, serplulimab-based

1 Introduction

Small-cell lung cancer (SCLC) represents one of the most critical oncological challenges worldwide, accounting for approximately 15% of all lung cancer cases (Gazdar et al., 2017). While anti-PD-1/PD-L1-based immunochemotherapy strategies have improved survival outcomes, achieving response rates of 80%–90% in limited-stage SCLC (LS-SCLC) and 50%–80% in extensive-stage SCLC (ES-SCLC) (Schmittel, 2011), this approach remains restricted to first-line settings. Despite initial responses to first-line therapy, median progression-free survival (PFS) is typically less than 6 months (Sathiyapalan et al., 2022; Zhang et al., 2023), and disease progression or recurrence is almost inevitable. Currently, effective options for subsequent lines of therapy remain limited (Tariq et al., 2021). As the standard second-line treatment, topotecan, a topoisomerase I inhibitor, has demonstrated a survival advantage over best supportive care, with a median overall survival (OS) of 25.9 weeks compared to 13.9 weeks (O'Brien et al., 2006). However, its utility is compromised by significant toxicity, primarily myelosuppression and hematologic adverse events, which impact tolerability for many patients (Goto et al., 2016; Das et al., 2021). In 2020, lurbinectedin received conditional approval from the U.S. Food and Drug Administration (FDA) as the first drug in over 20 years for second-line treatment of SCLC, based on an objective response rate (ORR) of 35%. Unfortunately, subsequent randomized trials failed to demonstrate a survival benefit with lurbinectedin in this setting (Trigo et al., 2020; Baena et al., 2021).

The efficacy of PD-1-targeted immune checkpoint inhibitors (ICIs), such as pembrolizumab and nivolumab, in the later-line setting for SCLC remains controversial. In 2020 and 2021, the FDA withdrew accelerated approvals for these agents as third-line options, citing insufficient evidence of survival benefit (Rudin et al., 2020; Owonikoko et al., 2021; Spigel et al., 2021). Despite this, the recent National Comprehensive Cancer Network (NCCN) guidelines recommend PD-1-targeted ICIs as a second-line treatment for patients who have not previously received immunotherapy (NCCN, 2024). Given the significant survival benefit observed with ICIs in the frontline setting (Horn et al., 2018; Paz-Ares et al., 2019; Cheng et al., 2022), further investigation into their potential role in later lines of treatment is warranted to address the unmet needs in SCLC management.

Serplulimab, an anti-PD-1 monoclonal antibody, has demonstrated promising efficacy in the international phase III ASTRUM-005 trial, showing a median OS benefit of 15.4 months compared to 10.9 months in ES-SCLC patients (Cheng et al., 2022). Based on these results, regulatory authorities such as China's National Medical Products Administration (NMPA), the Indonesian Food and Drug Authority (BPOM), and the European Medicines Agency (EMA) have approved serplulimab in combination with etoposide and platinum as a first-line treatment for ES-SCLC. Several studies have highlighted its therapeutic potential and its cost-effectiveness advantage, particularly for Chinese patients (Shao et al., 2023; Liu et al., 2024). In the absence of alternative options for recurrent SCLC, clinicians may still consider serplulimab-based immunotherapy or re-challenge with immunotherapy. This study aims to leverage real-world data from a single-center retrospective cohort to evaluate the efficacy and safety of serplulimab-based regimens in SCLC patients beyond first-line treatment.

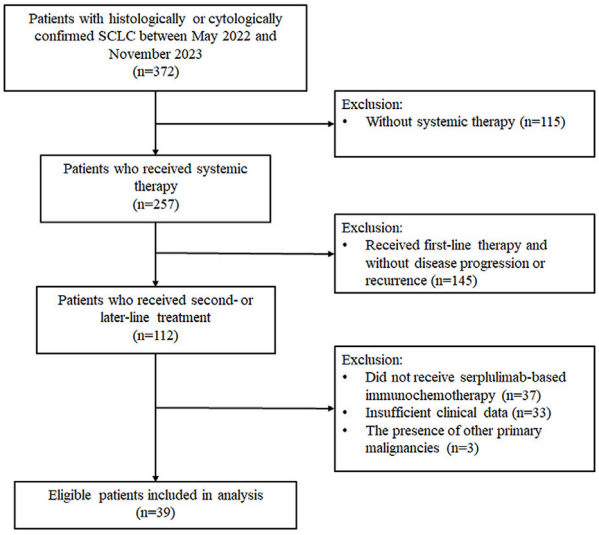

FIGURE 1
Flowchart of patients screening. SCLC, small-cell lung cancer.

2 Subjects and methods

2.1 Patients

This retrospective, real-world study was conducted at the Shanxi Provincial Cancer Hospital, with medical records of patients reviewed by investigators between May 2022 and November 2023. The inclusion criteria were: (1) age ≥ 18 years old; (2) histologically or cytologically confirmed SCLC; (3) disease progression or recurrence after at least one prior regimen; (4) treatment with either a serplulimab-based combination or serplulimab monotherapy as second- or later-line therapy. The exclusion criteria were: (1) insufficient clinical data and (2) the presence of other primary malignancies. This study was approved by the Ethics Committee of the Shanxi Provincial Cancer Hospital (No. KY2024046), with a waiver of written informed consent from patients, and was conducted in accordance with the Declaration of Helsinki. This study was reported following the Strengthening the Reporting of Observational Studies in Epidemiology (STROBE) guidelines (Supplementary Material).

2.2 Data collection and outcome assessment

We gathered a spectrum of demographic and clinicopathological characteristics, including age, sex, body mass index (BMI), smoking status, family tumor history, Eastern Cooperative Oncology Group performance status (ECOG PS), clinical stage, metastasis status, treatment regimens, biomarkers, and toxicity. The antitumor activity of the first line was also collected. Clinical data were collected from the electronic medical database and telephone follow-ups.

TABLE 1 Baseline characteristics of included patients.

Characteristics, n (%)	Patients (N = 39)
Age[a], y	56.56 ± 10.39
Age	
<60 years	21 (53.85)
≥60 years	18 (46.15)
Gender	
Male	34 (87.18)
Female	5 (12.82)
BMI	
<18.5 kg/m^2	2 (5.13)
18.5–24.9 kg/m^2	19 (48.72)
≥25 kg/m^2	18 (46.15)
Family tumor history	
Yes	6 (15.38)
No	33 (84.62)
History of smoking	
Yes	31 (79.49)
No	8 (20.51)
ECOG PS	
1	36 (92.31)
2	3 (7.69)
History of complication	
Yes	11 (28.21)
No	28 (71.79)
Clinical stage	
III	12 (30.77)
IV	27 (69.23)
Baseline NLR	
<3	13 (33.33)
≥3	26 (66.67)
Baseline LDH	
<225 U/I	21 (53.85)
≥225 U/I	18 (46.15)
Baseline ProGrp	
<300 ng/L	30 (76.92)
≥300 ng/L	9 (23.08)
Baseline NSE	
≤16.3 ng/mL	37 (94.87)
>16.3 ng/mL	2 (5.13)
Baseline CEA	
<6 ng/mL	35 (89.74)
≥6 ng/mL	4 (10.26)
Bone metastasis	
Yes	5 (12.82)
No	34 (87.18)
Brain metastasis	
Yes	13 (33.33)
No	26 (66.67)
Liver metastasis	
Yes	7 (17.95)
No	32 (82.05)
Treatment lines	
2	33 (84.62)
≥3	6 (15.38)
Combined chemotherapy regimen[b]	
Taxane-based	22 (56.41)
Platinum-based	27 (69.23)
Others[c]	3 (7.69)
Prior immunotherapy	
Yes	16 (41.03)
No	23 (58.97)
First-line SD/PD	
Yes	13 (33.33)
No	26 (66.67)

[a]data was presented as mean ± standard deviation.
[b]Thirteen patients received both taxane- and platinum-based as the chemotherapy regimen, resulting in an overall percentage greater than 100.
[c]Patients received anlotinib (n = 1), vinorelbine (n = 1), and temozolomide (n = 1) chemotherapy.
BMI, body mass index; ECOG PS, eastern cooperative oncology group performance status; NLR, neutrophil-lymphocyte ratio; LDH, lactate dehydrogenase; ProGrp, Pro Gastrin-Releasing Peptide; NSE, Neuron-Specific Enolase; CEA, carcinoembryonic antigen; SD, stable disease; PD, progressive disease.

The primary endpoint of this study was OS, defined as the time from the first dose of serplulimab-based second- or later-line treatment to death from any cause. The secondary endpoint was PFS, defined as the time from serplulimab-based second or further-line treatment to the first documented disease progression or death from any cause. We also performed subgroup analyses to explore clinicopathological factors that may be associated with treatment efficacy. Additionally, the ORR was calculated as the proportion of patients who achieved a complete response (CR) or partial response (PR) according to the Response Evaluation Criteria in Solid Tumors version 1.1 (RECIST v1.1). The disease control rate (DCR) was calculated as the proportion of patients achieving CR, PR, or stable disease (SD) for at least 4 weeks. Adverse events (AEs) during serplulimab-based treatment were assessed according to the Common Terminology Criteria for Adverse Events (CTCAE) version 5.0 by two independent investigators who reviewed safety events recorded in medical charts. Any discrepancies were resolved by the third investigator.

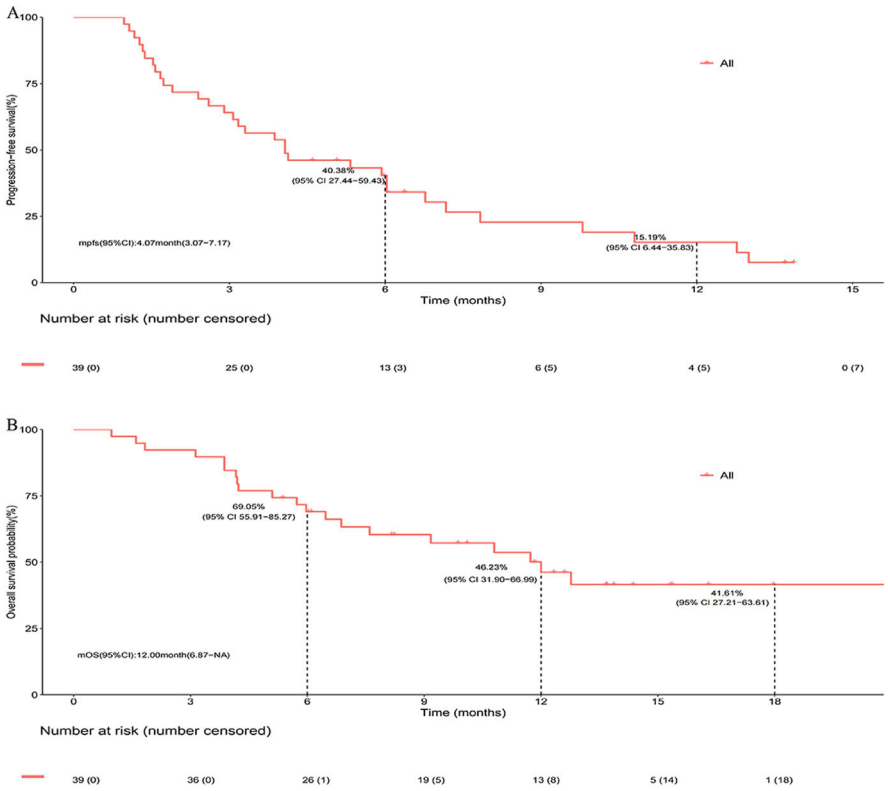

FIGURE 2
Survival of entire cohort following second- or later-line serplulimab-based immunochemotherapy. **(A)** Kaplan-Meier estimates of progress-free survival. **(B)** Kaplan-Meier estimates of overall survival.

2.3 Statistical analysis

Categorical variables were summarized as counts and percentages, while continuous variables were described using mean ± standard deviation or median (range), as appropriate. PFS and OS were estimated with the Kaplan-Meier method, and median values with 95% confidence intervals (CIs) were calculated. Survival and tumor response analyses were further stratified based on first-line tumor response status and prior immunotherapy exposure. To identify survival risk factors, univariate and multivariate Cox proportional-hazards models were applied, with hazard ratios (HR) and corresponding 95% CIs reported. Data management and statistical analyses were performed using R software (version 4.3.2), with statistical significance defined at a two-sided *P*-value of < 0.05.

3 Results

3.1 Baseline characteristics

We reviewed the medical records of 372 SCLC patients treated at the Shanxi Provincial Cancer Hospital between May 2022 and November 2023. Among them, 257 patients received systemic therapy, and 112 had documented second- or later-line treatment. After applying the inclusion and exclusion criteria, 39 patients were included in this retrospective analysis (Figure 1). Most of the included patients (n = 33, 84.62%) received second-line serplulimab-based therapy. The baseline characteristics of these 39 patients are shown in Table 1. The mean age was 56.56 years, with the majority being male (87.18%), smokers (79.49%), having an ECOG PS of 1 (92.31%), and presenting with stage IV disease (69.23%). Sixteen patients (41.03%) had received prior immunotherapy, and 26 patients (66.67%) achieved an objective response to first-line therapy. The majority received immunochemotherapy beyond first-line with taxane- (n = 22, 56.41%) or platinum-based (n = 27, 69.23%) regimens, with 13 of them receiving both taxane- and platinum-based chemotherapy. Additionally, another three patients received serplulimab combined with anlotinib (n = 1), vinorelbine (n = 1), and temozolomide (n = 1), respectively.

3.2 Efficacy and subgroup analysis

After a median follow-up of 13.7 months, the median PFS (mPFS) and median OS (mOS) for the entire cohort were 4.07 months (95% CI, 3.07–7.17) and 12.00 months (95% CI, 6.87-not reached), respectively (Figures 2A,B). In subgroup analysis stratified by prior immunotherapy, patients who underwent immunotherapy re-challenge showed numerically higher mPFS and mOS than those without prior immunotherapy, although the differences were not statistically significant (mPFS: 5.93 vs. 3.87 months, log-rank $P = 0.633$; mOS: 12.77 vs.

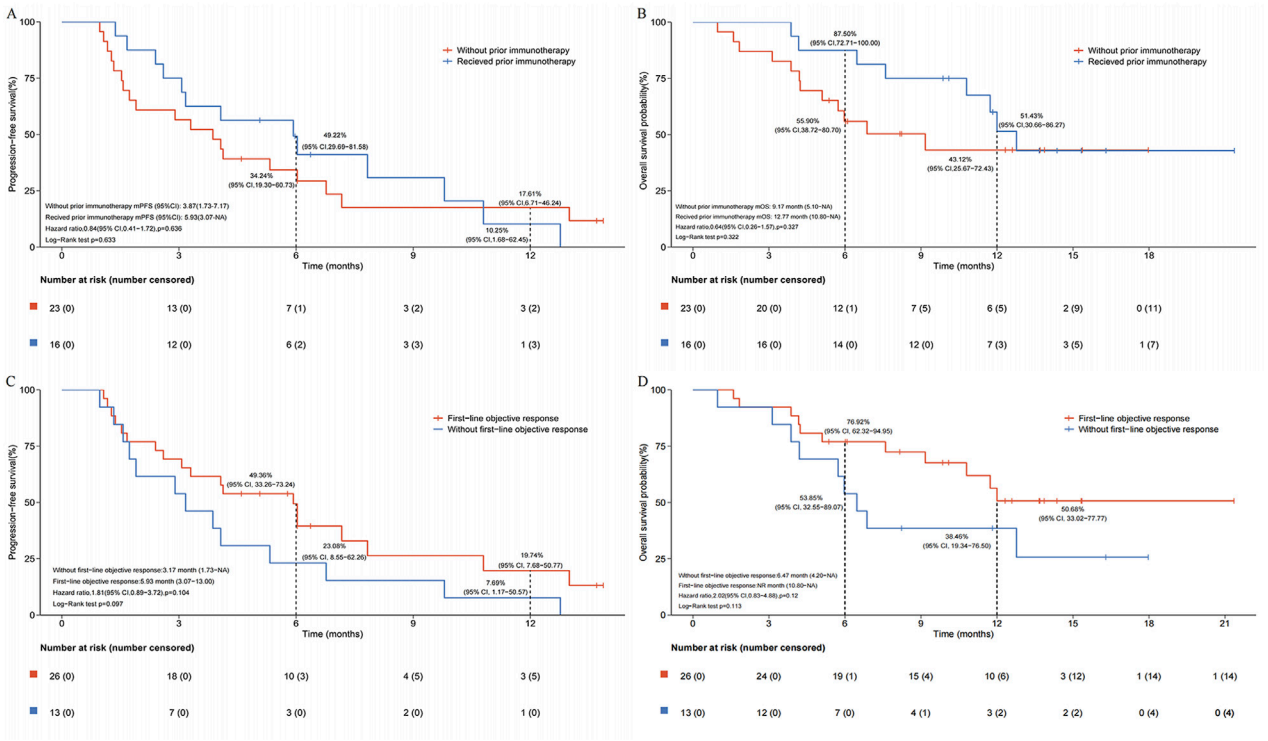

FIGURE 3
Subgroup analysis of survival following second- or later-line serplulimab-based immunochemotherapy. **(A)** Kaplan-Meier estimates of progress-free survival stratified by prior immunotherapy exposure. **(B)** Kaplan-Meier estimates of overall survival stratified by prior immunotherapy exposure. **(C)** Kaplan-Meier estimates of progress-free survival stratified by first-line tumor response status. **(D)** Kaplan-Meier estimates of overall survival stratified by first-line tumor response status.

9.17 months, log-rank $P = 0.322$) (Figures 3A,B). Univariate Cox analysis also confirmed no significant association between prior ICIs use and survival outcomes in subsequent immunotherapy (both $P > 0.05$, Table 2). Patients with an objective response to front-line therapy had numerically longer mPFS (5.93 vs. 3.17 months, log-rank $P = 0.097$, Figure 3C) and mOS (not reached vs. 6.47 months, log-rank $P = 0.113$, Figure 3D) compared to those without an objective response. Univariate Cox analysis also showed that the relationship between first-line tumor response status and survival was not statistically significant (both $P > 0.05$, Table 2).

During immunochemotherapy beyond first-line, 8/39 patients achieved an objective response (all PR), 17/39 achieved SD, and 14/39 had progressive disease. Overall, the ORR was 20.51% (8/39; 95% CI, 9.30–36.46) and DCR was 64.10% (25/39; 95% CI, 47.18–78.80). Additionally, patients with prior immunotherapy showed numerically higher ORR (31.25% vs. 13.04%) and DCR (75.00% vs. 56.52%) compared to those without prior immunotherapy.

Based on clinicopathological characteristics, we conducted an exploratory analysis of factors related to PFS and OS in patients receiving immunochemotherapy beyond first-line using a Cox proportional hazards model (Table 2). Univariate analysis for PFS indicated that females were associated with significantly better PFS (HR, 0.14; 95% CI, 0.03–0.61; $P = 0.009$). In contrast, factors associated with poorer PFS included family history of cancer, ECOG PS of 2, elevated baseline levels of lactate dehydrogenase (LDH), pro-gastrin-releasing peptide (ProGrP), and neuron-specific enolase (NSE) (all $P < 0.05$). On multivariate analysis, the association of PFS with gender and family history of cancer was also confirmed (all $P < 0.05$). For OS, only univariate analysis showed that ECOG PS of 2, elevated baseline levels of LDH, ProGrp, and NSE, and the presence of liver metastasis were associated with worse OS (all $P < 0.05$).

3.3 Safety

Through a comprehensive review of medical records and telephone follow-ups, we identified 47 AEs in 24 patients, resulting in an overall AE incidence of 61.54%. The incidence of grade 1–2 AEs and grade ≥3 AEs were 46.15% and 5.13%, respectively. Additionally, there were 12 AEs in eight patients for which severity could not be assessed due to incomplete documentation and patient refusal to provide further information. The most commonly reported AEs included thrombocytopenia, elevated alanine aminotransferase (ALT), and hypothyroidism (Table 3). All patients tolerated the combination immunotherapy well, and no treatment-related deaths were reported.

4 Discussion

In this retrospective, real-world study, we evaluated the efficacy of serplulimab-based immunochemotherapy as second- or later-line

therapy for patients with SCLC. Our results suggest that this treatment regimen had impressive antitumor activity and encouraging survival outcomes, with 20.51% of patients achieving an ORR, a mPFS of 4.07 months, and a mOS of 12.00 months. Additionally, patients who had received prior immunotherapy and achieved an objective response in front-line therapy showed improved antitumor activity and survival outcomes with serplulimab-based later-line therapy. Most patients (66.67%) included in our study achieved an objective response to first-line therapy, which is consistent with the approximately 70% reported in previous studies (Paz-Ares et al., 2019; Rudin et al., 2020). This consistency enhances the credibility of our findings, even with the limitation of the small sample size included in our cohort.

The role of PD-1/PD-L1-based immunotherapy in second-line treatment for SCLC has been explored in the CheckMate 331 trial (Spigel et al., 2021). In this study, nivolumab monotherapy did not demonstrate an OS benefit, with a median OS of 7.5 months compared to 8.4 months in the topotecan or amrubicin chemotherapy group (HR, 0.86; 95% CI, 0.72–1.04; P = 0.11). Similarly, mPFS showed no advantage with nivolumab monotherapy (1.4 vs. 3.8 months; HR, 1.41; 95% CI, 1.18–1.69). These results suggest that mono-immunotherapy offers limited efficacy for previously treated SCLC patients. However, the trial identified subgroups with low LDH levels and no liver metastases as having better survival benefits from immunotherapy, which is consistent with our findings. Nivolumab also showed limited efficacy as a third-line therapy in SCLC, with the CheckMate 032 trial reporting a median OS of 5.6 months and a median PFS of 1.4 months (Ready et al., 2019). In addition, a pooled analysis of the phase Ib KEYNOTE-028 and phase II KEYNOTE-158 studies showed that pembrolizumab achieved an mOS of 7.7 months and an mPFS of 2.0 months in patients with recurrent or metastatic SCLC who had received two or more prior therapies (Chung et al., 2020). In our study, all patients received serplulimab-based combination regimens, which may have contributed to the relatively longer survival observed in our cohort. This finding aligns with previous reports demonstrating that immunotherapy-chemotherapy combinations achieved median PFS ranging from 3.2 to 4.8 months in patients with previously treated SCLC (Ishii et al., 2021; Liu et al., 2025). The therapeutic synergy likely stems from checkpoint blockade-enhanced T-cell cytotoxicity coupled with chemotherapy-induced immunogenic cell death, which promotes tumor antigen release and dendritic cell maturation. Lurbinectedin, a newly FDA-approved second-line option, is a synthetic alkaloid that covalently binds to DNA, inducing cell death. In a phase II study of lurbinectedin for second-line SCLC, an ORR of 35% and a median duration of response (mDOR) of 5.3 months were observed (Trigo et al., 2020). Additionally, tarlatamab (AMG 757), a bispecific T-cell engager molecule targeting delta-like ligand 3 (DLL3) and CD3, demonstrated preliminary efficacy and safety in recurrent SCLC, with an ORR of 23.4%, median PFS of 3.7 months, and median OS of 13.2 months (Paz-Ares et al., 2023). However, the journey from developing a novel therapy to regulatory approval and clinical application is lengthy and complex. Thus, alongside ongoing drug development, there is a critical need to enhance patient benefits using existing agents. Our study suggests that the immunotherapy-based combination strategies may provide additional clinical benefits for SCLC patients beyond first-line treatment.

Although not statistically significant, our data showed a trend toward improved OS in patients who received immunotherapy rechallenge (12.77 vs. 9.17 months), consistent with previous studies. Campelo et al. (García-Campelo et al., 2023) reported potential survival benefits with atezolizumab rechallenge in patients with progressed ES-SCLC. Other studies have shown that rechallenge with immunochemotherapy can achieve durable antitumor activity and significant survival benefits compared to monotherapy approaches (Li et al., 2022; Zhang et al., 2024). For our treatment regimen, previous research has indicated that serplulimab combined with chemotherapy may provide additive and synergistic effects, reaffirming immunochemotherapy as a viable strategy in both first-line and subsequent lines for SCLC patients (Kataoka et al., 2020; Ishii et al., 2021). Additionally, our study revealed an interesting phenomenon: patients who achieved tumor response in front-line therapy continued to benefit from subsequent immunotherapy. This result may be attributed to several factors (Tang et al., 2016; Xia et al., 2024). First, the initial tumor response may successfully activate the immune microenvironment, allowing for a more robust response to subsequent immunotherapy. Second, the reduction in tumor burden and reshaping of the tumor microenvironment following front-line therapy may enhance the efficacy of subsequent immunotherapy.

Our Cox analysis revealed a significant association between the female gender and longer PFS in the recurrent SCLC setting, indicating that female patients might experience enhanced benefits from immunotherapy. While the correlation between gender and prognosis in SCLC remains inconsistent, most studies suggesting better survival were related to the female gender and largely due to the fewer smokers (Lim et al., 2018; Tas et al., 2024). However, our findings support potential biological differences in immune response between genders. Factors such as sex hormones, genetic polymorphisms, and immune modulation may contribute to these observed differences, and potentially influence the immunotherapy efficacy (Salgado et al., 2015; Lim et al., 2018; Vavala et al., 2021). In addition to LDH, elevated levels of ProGRP and NSE were associated with worse outcomes in our cohort. These markers, which are associated with neuroendocrine differentiation in SCLC, are generally associated with tumor aggressiveness and worse prognosis, consistent with previous research suggesting that they may indicate reduced tumor responsiveness and poorer patient survival outcomes (Shibayama et al., 2001; Li et al., 2023; Muley et al., 2024). Notably, despite extensive biomarker exploration in SCLC, no validated predictive biomarker has emerged to reliably identify patient subsets benefiting from PD-L1/PD-1 inhibitor-based regimens. While PD-L1 expression serves as a key biomarker for immunotherapy selection in non-small cell lung cancer (NSCLC), its predictive utility has not been reliably established in SCLC. For instance, pooled analysis of KEYNOTE-158 and KEYNOTE-028 trials revealed that pembrolizumab exhibited antitumor activity in heavily pretreated SCLC patients regardless of PD-L1 expression status (Chung et al., 2020). Similarly, the CheckMate 331 trial showed no survival benefit of nivolumab over chemotherapy in relapsed SCLC when stratified by PD-L1 combined positive score at a cutoff of 1% (Spigel et al., 2021). The use of tumor mutational

10.3389/fphar.2025.1591643

TABLE 2 Univariate and multivariate Cox analyses of PFS and OS for SCLC patients following second or later-line serplulimab-based immunochemotherapy.

Variable	PFS				OS			
	Univariate analysis		Multivariate analysis		Univariate analysis		Multivariate analysis	
	HR (95%CI)	*P*	HR (95%CI)	*P*	HR (95%CI)	*P*	HR (95%CI)	*P*
Gender*								
Male	Ref.		Ref.					
Female	0.14 (0.03–0.61)	0.009	0.19 (0.04–0.86)	0.031				
Age								
<60 years	Ref.				Ref.			
≥60 years	1.09 (0.54–2.18)	0.814			1.86 (0.76–4.56)	0.175		
BMI								
<18.5 kg/m^2	Ref.				Ref.			
18.5–24.9 kg/m^2	0.57 (0.13–2.52)	0.459			0.46 (0.10–2.14)	0.325		
≥25 kg/m^2	0.53 (0.12–2.35)	0.400			0.38 (0.08–1.8)	0.221		
Family tumor history								
No	Ref.		Ref.		Ref.			
Yes	2.90 (1.12–7.47)	0.028	3.54 (1.26–9.98)	0.017	2.18 (0.72–6.62)	0.168		
History of smoking								
No	Ref.				Ref.			
Yes	1.74 (0.70–4.34)	0.233			1.55 (0.45–5.31)	0.482		
ECOG PS								
1	Ref.		Ref.		Ref.		Ref.	
2	7.22 (1.85–28.25)	0.004	4.35 (0.59–32.31)	0.151	5.24 (1.40–19.58)	0.014	5.10 (0.62–41.70)	0.129
History of complication								
No	Ref.				Ref.			
Yes	0.54 (0.23–1.25)	0.148			0.49 (0.16–1.49)	0.210		
Clinical stage								
III	Ref.				Ref.			
IV	1.76 (0.77–3.99)	0.178			2.13 (0.71–6.38)	0.176		
Baseline NLR								
<3	Ref.				Ref.			
≥3	1.26 (0.59–2.69)	0.552			0.64 (0.26–1.56)	0.325		
Baseline LDH								
<225 U/I	Ref.		Ref.		Ref.		Ref.	
≥225 U/I	2.22 (1.10–4.49)	0.026	1.57 (0.66–3.72)	0.305	3.80 (1.45–9.97)	0.007	2.61 (0.86–7.90)	0.090
Baseline ProGrp								
<300 ng/L	Ref.		Ref.		Ref.		Ref.	
≥300 ng/L	3.69 (1.60–8.48)	0.002	2.21 (0.80–6.14)	0.128	5.66 (2.22–14.38)	<0.001	1.89 (0.55–6.50)	0.312
Baseline NSE								
≤16.3 ng/mL	Ref.		Ref.		Ref.		Ref.	
>16.3 ng/mL	6.58 (1.38–31.29)	0.018	1.10 (0.10–11.67)	0.936	5.60 (1.22–25.73)	0.027	0.65 (0.07–6.51)	0.715
Baseline CEA								
<6 ng/mL	Ref.				Ref.			
≥6 ng/mL	1.28 (0.44–3.68)	0.652			1.34 (0.31–5.83)	0.693		

(Continued on following page)

TABLE 2 (*Continued*) Univariate and multivariate Cox analyses of PFS and OS for SCLC patients following second or later-line serplulimab-based immunochemotherapy.

Variable	PFS				OS			
	Univariate analysis		Multivariate analysis		Univariate analysis		Multivariate analysis	
	HR (95%CI)	*P*	HR (95%CI)	*P*	HR (95%CI)	*P*	HR (95%CI)	*P*
Bone metastasis								
No Yes	Ref. 1.45 (0.50–4.21)	0.496			Ref. 1.72 (0.50–5.92)	0.386		
Brain metastasis								
No Yes	Ref. 1.08 (0.51–2.26)	0.848			Ref. 1.00 (0.40–2.52)	0.995		
Liver metastasis								
No Yes	Ref. 2.15 (0.85–5.44)	0.106			Ref. 3.65 (1.39–9.58)	0.008	Ref. 2.77 (0.85–9.06)	0.091
Prior immunotherapy								
No Yes	Ref. 0.84 (0.41–1.72)	0.636			Ref. 0.64 (0.26–1.57)	0.327		
First-line SD/PD								
No Yes	Ref. 1.81 (0.89–3.72)	0.104			Ref. 2.02 (0.83–4.88)	0.120		

* The relationship between gender and OS, was not analyzed because the model did not converge due to the absence of mortality events in female patients.
PFS, progress-free survival; OS, overall survival; HR, hazard ratio; BMI, body mass index; ECOG PS, eastern cooperative oncology group performance status; NLR, neutrophil-to-lymphocyte ratio; LDH, lactate dehydrogenase; ProGrp, pro-gastrin-releasing peptide; NSE, neuron-specific enolase; CEA, carcinoembryonic antigen; SD, stable disease; PD, progressive disease.

TABLE 3 AEs of SCLC patients following second or later-line serplulimab-based immunochemotherapy.

AEs, n (%)	Total	Grade 1–2	Grade 3–4
Total	24 (61.54)	18 (46.15)	2 (5.13)
Incidence ≥ 5%			
Thrombocytopenia	9 (23.08)	8 (20.51)	1 (2.56)
Elevated ALT	6 (15.38)	5 (12.82)	–
Hypothyroidism	6 (15.38)	2 (5.13)	–
Anemia	5 (12.82)	5 (12.82)	–
Elevated AST	4 (10.26)	2 (5.13)	–
Neutropenia	4 (10.26)	3 (7.69)	1 (2.56)
Pneumonia	2 (5.13)	2 (5.13)	–
Myelosuppression	2 (5.13)	2 (5.13)	–

AEs, adverse events; ALT, alanine aminotransferase; AST, aspartate aminotransferase.

burden (TMB) in SCLC also yielded inconclusive results. A correlation between TMB and tumor response was observed in the CheckMate 032 trial using whole-exome sequencing, but this association was not replicated in the IMpower 133 trial where circulating tumor DNA analysis was employed (Horn et al., 2018; Ready et al., 2020).

As noted, our study is limited by its sample size and geographic scope, which introduces the potential for selection bias and limits the generalizability of our findings to the broader SCLC population. Additionally, as a single-cohort retrospective analysis, our study lacks a control group, restricting us to comparisons with historical data rather than allowing for direct, controlled comparisons with other second- or later-line therapies. This study design further limits our ability to establish causative relationships between treatment regimens and outcomes. The undocumented severity of 12 adverse events in eight patients, attributable to incomplete medical records or patient refusal, may underestimate toxicity risks, underscoring the necessity for enhanced real-time monitoring and standardized reporting in future studies in the real-world research. Moreover, due to the absence of an in-depth biomarker analysis, we were unable to investigate the underlying mechanisms by which patients may benefit from serplulimab-based combination therapy. Future multicenter, prospective studies with larger, more diverse cohorts and biomarker evaluation are essential to validate these findings and to explore potential mechanisms driving response.

In conclusion, this real-world study suggests that immunochemotherapy as a second- or later-line treatment demonstrates promising efficacy and safety in SCLC patients, regardless of prior immunotherapy exposure and first-line tumor response status. Although limited by sample size and study design, the tendency towards extended survival in patients rechallenged with immunotherapy reaffirms immunochemotherapy as a feasible approach for SCLC patients in both first-line and subsequent lines. Our findings underscore the need for further investigation into

tailored immunotherapy approaches that could maximize clinical benefit in SCLC, supporting the rationale for immunochemotherapy beyond first-line treatment.

Data availability statement

The original contributions presented in the study are included in the article/Supplementary Material, further inquiries can be directed to the corresponding author.

Ethics statement

The studies involving humans were approved by the Ethics Committee of the Shanxi Province Cancer Hospital. The studies were conducted in accordance with the local legislation and institutional requirements. The ethics committee/institutional review board waived the requirement of written informed consent for participation from the participants or the participants' legal guardians/next of kin because Informed consent was waived by our Institutional Review Board because of the retrospective nature of our study.

Author contributions

YG: Conceptualization, Data curation, Formal Analysis, Investigation, Writing – original draft. SH: Data curation, Writing – original draft. QG: Data curation, Writing – review and editing. JZ: Data curation, Formal Analysis, Investigation, Writing – review and editing. XR: Data curation, Formal Analysis, Investigation, Writing – review and editing. SL: Data curation, Writing – review and editing. JD: Conceptualization, Formal Analysis, Validation, Writing – review and editing.

Funding

The author(s) declare that financial support was received for the research and/or publication of this article. This work was supported by the Shenzhen Xihepu Biomedical Research Institute-Tumour Immunotherapy Project [CCHRPP-ZL-2023-Q-009].

Conflict of interest

The authors declare that the research was conducted in the absence of any commercial or financial relationships that could be construed as a potential conflict of interest.

Generative AI statement

The author(s) declare that no Generative AI was used in the creation of this manuscript.

Publisher's note

Supplementary material

The Supplementary Material for this article can be found online at: https://www.frontiersin.org/articles/10.3389/fphar.2025.1591643/full#supplementary-material

References

Baena, J., Modrego, A., Zeaiter, A., Kahatt, C., Alfaro, V., Jimenez-Aguilar, E., et al. (2021). Lurbinectedin in the treatment of relapsed small cell lung cancer. *Future Oncol.* 17 (18), 2279–2289. doi:10.2217/fon-2020-1212

Cheng, Y., Han, L., Wu, L., Chen, J., Sun, H., Wen, G., et al. (2022). Effect of first-line serplulimab vs placebo added to chemotherapy on survival in patients with extensive-stage small cell lung cancer: the ASTRUM-005 randomized clinical trial. *JAMA* 328 (12), 1223–1232. doi:10.1001/jama.2022.16464

Chung, H. C., Piha-Paul, S. A., Lopez-Martin, J., Schellens, J. H. M., Kao, S., Miller, W. H., Jr., et al. (2020). Pembrolizumab after two or more lines of previous therapy in patients with recurrent or metastatic SCLC: results from the KEYNOTE-028 and KEYNOTE-158 studies. *J. Thorac. Oncol.* 15 (4), 618–627. doi:10.1016/j.jtho.2019.12.109

Das, M., Padda, S. K., Weiss, J., and Owonikoko, T. K. (2021). Advances in treatment of recurrent small cell lung cancer (SCLC): insights for optimizing patient outcomes from an expert roundtable discussion. *Adv. Ther.* 38 (11), 5431–5451. doi:10.1007/s12325-021-01909-1

García-Campelo, R., Dómine Gómez, M., de Castro, J., Moreno Vega, A., Ponce Aix, S., Arriola, E., et al. (2023). P2.14-04 treatment beyond progression with atezolizumab in extensive-stage SCLC: exploratory analysis from the IMfirst study. *J. Thorac. Oncol.* 18 (11), S372. doi:10.1016/j.jtho.2023.09.656

Gazdar, A. F., Bunn, P. A., and Minna, J. D. (2017). Small-cell lung cancer: what we know, what we need to know and the path forward. *Nat. Rev. Cancer* 17 (12), 725–737. doi:10.1038/nrc.2017.87

Goto, K., Ohe, Y., Shibata, T., Seto, T., Takahashi, T., Nakagawa, K., et al. (2016). Combined chemotherapy with cisplatin, etoposide, and irinotecan versus topotecan alone as second-line treatment for patients with sensitive relapsed small-cell lung cancer (JCOG0605): a multicentre, open-label, randomised phase 3 trial. *Lancet Oncol.* 17 (8), 1147–1157. doi:10.1016/S1470-2045(16)30104-8

Horn, L., Mansfield, A. S., Szczesna, A., Havel, L., Krzakowski, M., Hochmair, M. J., et al. (2018). First-line atezolizumab plus chemotherapy in extensive-stage small-cell lung cancer. *N. Engl. J. Med.* 379 (23), 2220–2229. doi:10.1056/NEJMoa1809064

Ishii, H., Azuma, K., Kawahara, A., Matsuo, N., Tokito, T., and Hoshino, T. (2021). Atezolizumab plus carboplatin and etoposide in small cell lung cancer patients previously treated with platinum-based chemotherapy. *Invest New Drugs* 39 (1), 269–271. doi:10.1007/s10637-020-00983-6

Kataoka, N., Kunimatsu, Y., Tachibana, Y., Sugimoto, T., Sato, I., Tani, N., et al. (2020). Atezolizumab in combination with carboplatin and etoposide for heavily treated small cell lung cancer. *Thorac. Cancer* 11 (9), 2740–2742. doi:10.1111/1759-7714.13588

Li, L., Liu, T., Liu, Q., Mu, S., Tao, H., Yang, X., et al. (2022). Rechallenge of immunotherapy beyond progression in patients with extensive-stage small-cell lung cancer. *Front. Pharmacol.* 13, 967559. doi:10.3389/fphar.2022.967559

Li, L., Zhang, Q., Wang, Y., and Xu, C. (2023). Evaluating the diagnostic and prognostic value of serum TuM2-PK, NSE, and ProGRP in small cell lung cancer. *J. Clin. Lab. Anal.* 37 (7), e24865. doi:10.1002/jcla.24865

Lim, J. H., Ryu, J. S., Kim, J. H., Kim, H. J., and Lee, D. (2018). Gender as an independent prognostic factor in small-cell lung cancer: inha Lung Cancer Cohort study using propensity score matching. *PLoS One* 13 (12), e0208492. doi:10.1371/journal.pone.0208492

Liu, F., Yin, G., Tao, Y., and Pan, Y. (2025). The efficacy of ICIs rechallenge in advanced small cell lung cancer after progression from ICIs plus chemotherapy: a real-world study. *Int. Immunopharmacol.* 152, 114372. doi:10.1016/j.intimp.2025.114372

Liu, Y., Zhu, J., Du, T. Y., Liu, X. H., Xin, Y., Wang, Y., et al. (2024). Navigating first-line therapies for extensive-stage small-cell lung cancer: a frequentist network meta-analysis and systematic review. *Future Oncol.* 20, 2109–2122. doi:10.1080/14796694.2024.2376514

Muley, T., Herth, F. J., Heussel, C. P., Kriegsmann, M., Thomas, M., Meister, M., et al. (2024). Prognostic value of tumor markers ProGRP, NSE and CYFRA 21-1 in patients with small cell lung cancer and chemotherapy-induced remission. *Tumour Biol.* 46 (s1), S219–S232. doi:10.3233/TUB-230016

NCCN (2024). Small cell lung cancer. (version 2, 2025).

O'Brien, M. E., Ciuleanu, T. E., Tsekov, H., Shparyk, Y., Cucevia, B., Juhasz, G., et al. (2006). Phase III trial comparing supportive care alone with supportive care with oral topotecan in patients with relapsed small-cell lung cancer. *J. Clin. Oncol.* 24 (34), 5441–5447. doi:10.1200/JCO.2006.06.5821

Owonikoko, T. K., Park, K., Govindan, R., Ready, N., Reck, M., Peters, S., et al. (2021). Nivolumab and ipilimumab as maintenance therapy in extensive-disease small-cell lung cancer: CheckMate 451. *J. Clin. Oncol.* 39 (12), 1349–1359. doi:10.1200/JCO.20.02212

Paz-Ares, L., Champiat, S., Lai, W. V., Izumi, H., Govindan, R., Boyer, M., et al. (2023). Tarlatamab, a first-in-class DLL3-targeted bispecific T-cell engager, in recurrent small-cell lung cancer: an open-label, phase I study. *J. Clin. Oncol.* 41 (16), 2893–2903. doi:10.1200/JCO.22.02823

Paz-Ares, L., Dvorkin, M., Chen, Y., Reinmuth, N., Hotta, K., Trukhin, D., et al. (2019). Durvalumab plus platinum-etoposide versus platinum-etoposide in first-line treatment of extensive-stage small-cell lung cancer (CASPIAN): a randomised, controlled, open-label, phase 3 trial. *Lancet* 394 (10212), 1929–1939. doi:10.1016/S0140-6736(19)32222-6

Ready, N., Farago, A. F., de Braud, F., Atmaca, A., Hellmann, M. D., Schneider, J. G., et al. (2019). Third-line nivolumab monotherapy in recurrent SCLC: CheckMate 032. *J. Thorac. Oncol.* 14 (2), 237–244. doi:10.1016/j.jtho.2018.10.003

Ready, N. E., Ott, P. A., Hellmann, M. D., Zugazagoitia, J., Hann, C. L., de Braud, F., et al. (2020). Nivolumab monotherapy and nivolumab plus ipilimumab in recurrent small cell lung cancer: results from the CheckMate 032 randomized cohort. *J. Thorac. Oncol.* 15 (3), 426–435. doi:10.1016/j.jtho.2019.10.004

Rudin, C. M., Awad, M. M., Navarro, A., Gottfried, M., Peters, S., Csoszi, T., et al. (2020). Pembrolizumab or placebo plus etoposide and platinum as first-line therapy for extensive-stage small-cell lung cancer: randomized, double-blind, phase III KEYNOTE-604 study. *J. Clin. Oncol.* 38 (21), 2369–2379. doi:10.1200/JCO.20.00793

Salgado, R., Denkert, C., Campbell, C., Savas, P., Nuciforo, P., Aura, C., et al. (2015). Tumor-infiltrating lymphocytes and associations with pathological complete response and event-free survival in HER2-positive early-stage breast cancer treated with lapatinib and trastuzumab: a secondary analysis of the NeoALTTO trial. *JAMA Oncol.* 1 (4), 448–454. doi:10.1001/jamaoncol.2015.0830

Sathiyapalan, A., Febbraro, M., Pond, G. R., and Ellis, P. M. (2022). Chemo-immunotherapy in first line extensive stage small cell lung cancer (ES-SCLC): a systematic review and meta-analysis. *Curr. Oncol.* 29 (12), 9046–9065. doi:10.3390/curroncol29120709

Schmittel, A. (2011). Second-line therapy for small-cell lung cancer. *Expert Rev. Anticancer Ther.* 11 (4), 631–637. doi:10.1586/era.11.7

Shao, T., Zhao, M., Liang, L., and Tang, W. (2023). Serplulimab plus chemotherapy vs chemotherapy for treatment of us and Chinese patients with extensive-stage small-cell lung cancer: a cost-effectiveness analysis to inform drug pricing. *BioDrugs* 37 (3), 421–432. doi:10.1007/s40259-023-00586-6

Shibayama, T., Ueoka, H., Nishii, K., Kiura, K., Tabata, M., Miyatake, K., et al. (2001). Complementary roles of pro-gastrin-releasing peptide (ProGRP) and neuron specific enolase (NSE) in diagnosis and prognosis of small-cell lung cancer (SCLC). *Lung Cancer* 32 (1), 61–69. doi:10.1016/s0169-5002(00)00205-1

Spigel, D. R., Vicente, D., Ciuleanu, T. E., Gettinger, S., Peters, S., Horn, L., et al. (2021). Second-line nivolumab in relapsed small-cell lung cancer: CheckMate 331(☆). *Ann. Oncol.* 32 (5), 631–641. doi:10.1016/j.annonc.2021.01.071

Tang, H., Qiao, J., and Fu, Y. X. (2016). Immunotherapy and tumor microenvironment. *Cancer Lett.* 370 (1), 85–90. doi:10.1016/j.canlet.2015.10.009

Tariq, S., Kim, S. Y., Monteiro de Oliveira Novaes, J., and Cheng, H. (2021). Update 2021: management of small cell lung cancer. *Lung* 199 (6), 579–587. doi:10.1007/s00408-021-00486-y

Tas, F., Ozturk, A., and Erturk, K. (2024). Female patients with small cell lung cancer have better survival than males with extensive but not limited disease. *Oncol. Res. Treat.* 47 (9), 401–409. doi:10.1159/000540244

Trigo, J., Subbiah, V., Besse, B., Moreno, V., Lopez, R., Sala, M. A., et al. (2020). Lurbinectedin as second-line treatment for patients with small-cell lung cancer: a single-arm, open-label, phase 2 basket trial. *Lancet Oncol.* 21 (5), 645–654. doi:10.1016/S1470-2045(20)30068-1

Vavala, T., Catino, A., Pizzutilo, P., Longo, V., and Galetta, D. (2021). Gender differences and immunotherapy outcome in advanced lung cancer. *Int. J. Mol. Sci.* 22 (21), 11942. doi:10.3390/ijms222111942

Xia, X., Yang, Z., Lu, Q., Liu, Z., Wang, L., Du, J., et al. (2024). Reshaping the tumor immune microenvironment to improve CAR-T cell-based cancer immunotherapy. *Mol. Cancer* 23 (1), 175. doi:10.1186/s12943-024-02079-8

Zhang, J., Sun, Y., and Gao, Q. A. (2024). PD-(L)1 inhibitors plus anlotinib: a superior option for second-line treatment of extensive-stage small cell lung cancer. *J. Clin. Oncol.* 42 (16_Suppl. l), e20117. doi:10.1200/JCO.2024.42.16_suppl.e20117

Zhang, T., Li, W., Diwu, D., Chen, L., Chen, X., and Wang, H. (2023). Efficacy and safety of first-line immunotherapy plus chemotherapy in treating patients with extensive-stage small cell lung cancer: a Bayesian network meta-analysis. *Front. Immunol.* 14, 1197044. doi:10.3389/fimmu.2023.1197044

frontiers | Frontiers in Pharmacology

TYPE Mini Review
PUBLISHED 05 June 2025
DOI 10.3389/fphar.2025.1572195

OPEN ACCESS

EDITED BY
Xinyu Wang,
Philadelphia College of Osteopathic Medicine (PCOM), United States

REVIEWED BY
Dianzheng Zhang,
Philadelphia College of Osteopathic Medicine (PCOM), United States

*CORRESPONDENCE
Xiaoyan Qi,
674338436@qq.com
Min Yan,
ymvip7778@163.com

RECEIVED 06 February 2025
ACCEPTED 23 May 2025
PUBLISHED 05 June 2025

CITATION
Li C, Qi X and Yan M (2025) Chemotherapy-induced immunogenic cell death in combination with ICIs: a brief review of mechanisms, clinical insights, and therapeutic implications.
Front. Pharmacol. 16:1572195.
doi: 10.3389/fphar.2025.1572195

Chemotherapy-induced immunogenic cell death in combination with ICIs: a brief review of mechanisms, clinical insights, and therapeutic implications

Chengwei Li[1], Xiaoyan Qi[2]* and Min Yan[1,3]*

[1]Department of Integrated Traditional Chinese and Western Medicine, Shandong Public Health Clinical Center, Shandong University, Jinan, China, [2]Department of Oncology, Zibo Central Hospital, Zibo, China, [3]Department of Respiratory Medicine, Shandong Public Health Clinical Center, Shandong University, Jinan, China

The combination of chemotherapy and immune checkpoint inhibitors (ICIs) represents a promising strategy for enhancing the efficacy of tumor immunotherapy. This review elaborates on its mechanisms and clinical significances. Chemotherapy-induced immunogenic cell death (ICD) serves as the foundation of this therapeutic synergy, involving the release of damage-associated molecular patterns (DAMPs) such as calreticulin, ATP, and HMGB1, which enhance immune activation in the presence of ICIs. Clinical trials have demonstrated that this combination approach markedly improves clinical outcomes across multiple tumor types, including non-small cell lung cancer, melanoma, bladder cancer, and triple-negative breast cancer. In clinical practice, this combination is increasingly adopted as a first-line or advanced-stage treatment, often guided by personalized medicine approaches. However, several challenges persist, including the management of treatment-related toxicity, high costs, and the identification of predictive biomarkers.

KEYWORDS

cancer therapy, ICIS, chemotherapy, immunotherapy, clinical applications

1 Introduction

Tumor immunotherapy has fundamentally transformed the therapeutic landscape of cancer treatment (Yasinjan et al., 2023; Rui et al., 2023; da Silva et al., 2019). Immune checkpoint inhibitors (ICIs), including anti-PD-1 and anti-PD-L1 antibodies, have shown substantial effectiveness in certain patient populations (Dall'Olio et al., 2022; Naimi et al., 2022). These agents function by blocking inhibitory signals on T cells, thereby enhancing the immune system's ability to target and eliminate tumor cells. However, not all patients respond favorably, and resistance to ICIs continues to pose a significant clinical challenge (Sun and Xu, 2020; Sharma and Allison, 2015; Hughes et al., 2016).

Chemotherapy, a longstanding cornerstone in cancer treatment, utilizes various drugs that primarily target rapidly proliferating cells, including cancer cells (Knezevic and Clarke, 2020; Jiang et al., 2024). These agents exert their effects by inducing DNA damage (Bai et al., 2024), arresting cell cycle progression (Sun et al., 2021a), and triggering cell death.

TABLE 1 Clinical trial outcomes of combination chemotherapy and ICIs in tumor immunotherapy.

Cancer type	Trial	Combination	Outcome
Melanoma	CheckMate 067	Ipilimumab + Nivolumab vs. Ipilimumab or Nivolumab alone	Highest response rate and extended OS
Melanoma	Phase II Pembrolizumab Trial	Pembrolizumab + Dacarbazine	56% response rate, median OS 23.5 months, median PFS 8.9 months
Bladder Cancer	IMvigor130	Atezolizumab + Cisplatin/Gemcitabine	Improved OS and PFS in PD-L1-positive tumors; 12-month OS rate of 71%
Bladder Cancer	KEYNOTE-361	Pembrolizumab + Chemotherapy (Gemcitabine/Docetaxel + Carboplatin/Cisplatin)	Positive trend in improving PFS and response rates
Triple-Negative Breast Cancer	KEYNOTE-522	Pembrolizumab + Chemotherapy (Carboplatin/Paclitaxel + Epirubicin/Doxorubicin)	Improved EFS and pCR, 91% EFS at 18 months
Non-Small Cell Lung Cancer	KEYNOTE-189	Pembrolizumab + Platinum-based agent + Pemetrexed	Median PFS 8.8 months vs. 4.9 months (chemotherapy only), 12-month OS 69.2% vs. 49.4%
Non-Small Cell Lung Cancer	IMpower130	Atezolizumab + Nab-paclitaxel + Carboplatin	Improved OS and PFS, 18-month OS 64% vs. 52%, median PFS 7 months vs. 5.5 months
Head and Neck Cancer	KEYNOTE-048	Pembrolizumab + Chemotherapy (Cisplatin/Carboplatin + Fluorouracil)	Improved OS in PD-L1-positive tumors
Gastric and Esophageal Cancer	KEYNOTE-590	Pembrolizumab + Chemotherapy (Fluorouracil + Cisplatin)	Improved PFS and OS compared to chemotherapy alone

Specifically, chemotherapy-induced ICD serves as the pivotal process enabling the immune system to recognize and attack tumor cells more effectively when combined with ICIs. ICD is marked by the exposure and release of immunostimulatory signals—particularly calreticulin, ATP, and HMGB1—which collectively enhance T cell-mediated immune responses (Bian et al., 2022; Obeid et al., 2007; Kroemer et al., 2013).

The synergistic potential of combining chemotherapy and ICIs is promising. This dual approach can amplify the immune system's antitumor response (Qian et al., 2022; Galluzzi et al., 2020). Chemotherapy triggers ICD, leading to tumor antigen release and TME modulation, which subsequently activates antigen-presenting cells and promotes T cells recruitment to the tumor site. ICIs can block T cells' inhibitory signals, further boosting their antitumor efficiency (Zouein et al., 2022). This combinatorialstrategy helps overcome the limitations of monotherapies, providing a more comprehensive and potent anticancer approach. It holds the promise of improved patient outcomes, particularly for those who do not respond adequately to either ICIs or chemotherapy alone (Roskoski, 2024; Li et al., 2022).

In addition to inducing immunogenic cell death, chemotherapy exerts multiple immunomodulatory effects within the tumor microenvironment. For instance, chemotherapeutic agents like cyclophosphamide and gemcitabine have been demonstrated to selectively deplete immunosuppressive cells, including regulatory T cells (Tregs) and myeloid-derived suppressor cells (MDSCs). This depletion alleviats local immune suppression and promoting effector T-cell infiltration and activity. Moreover, chemotherapy can enhance antigen presentation by upregulating major histocompatibility complex (MHC) class I molecules on tumor cells, thus improving tumor recognition by cytotoxic T lymphocytes (CTLs) (Galluzzi et al., 2015). These multifaceted immunological alterations, when combined with ICIs, foster a more permissive immune landscape that significantly enhances antitumor efficacy relative to monotherapy (Pfirschke et al., 2016).

2 Clinical trial outcomes of the combination of chemotherapy and ICIs in tumor immunotherapy

2.1 Melanoma

In the treatment of melanoma, combining chemotherapy with ICIs has emerged as a promising strategy. The CheckMate 067 trial compared the effects of ipilimumab and nivolumab combination therapy to ipilimumab or nivolumab alone in patients with melanoma (Wan et al., 2021; Choueiri Toni et al., 2023; Owonikoko et al., 2021). The results were noteworthy, with the combination regimen yielding the highest response rate and the longest OS observed. The median OS didn't achieve the combination group, while patients receiving ipilimumab alone had a median OS of 19.9 months and 36.9 months in the nivolumab-alone group. These findings indicate that the combination of ipilimumab and nivolumab exerts a synergistic effect, intensifying the antitumor immune response and substantially improving survival outcomes.

In addition, pembrolizumab combined with chemotherapy has been tested in melanoma patients. A phase II trial examined the use of pembrolizumab alongside dacarbazine in metastatic melanoma patients. The outcomes suggest that this combination achieved a 56% response rate, with a median OS of 23.5 months and a median PFS of 8.9 months. These results suggest that integratingchemotherapy with ICIs may represent an effective therapeutic approach for melanoma, capable of improving both response rates and survival.

2.2 Bladder cancer

In the treatment of bladder cancer, combining chemotherapy with ICIs has shown notable advantages. The IMvigor130 trial investigated the addition of atezolizumab to chemotherapy (cisplatin and gemcitabine) vs. chemotherapy alone in patients with metastatic or locally advanced urothelial carcinoma (Funt et al., 2022; Galsky et al., 2024; Balar et al., 2017). The results showed a notable improvement in OS and FPS among patients with PD-L1-positive tumors. The combination therapy group experienced a median PFS of 8.2 months, while the chemotherapy-only group had a median PFS of 6.3 months. Additionally, the 12-month OS rate was 71% in the combination group, compared to 62% in those treated with chemotherapy alone.

The KEYNOTE-361 trial trial assessed the efficacy of pembrolizumab combined with chemotherapy (gemcitabine or docetaxel plus carboplatin or cisplatin) compared to chemotherapy alone in patients with urothelial carcinoma. While the combination therapy did not meet its primary endpoint for OS, it showed a positive trend toward improvoved PFS and response rates (Suzuki et al., 2023; Kelley et al., 2023; Sharma et al., 2024; Nakamura et al., 2023).

2.3 Triple-negative breast cancer

In triple-negative breast cancer (TNBC), the combination of chemotherapy and ICIs has produced encouraging results. For instance, the KEYNOTE-522 trial assessed the use of pembrolizumab combined with chemotherapy (carboplatin and paclitaxel followed by epirubicin or doxorubicin and cyclophosphamide) vs. chemotherapy alone in early-stage TNBC patients (Rizzo et al., 2022; Pusztai et al., 2024; Dent et al., 2024; Zhao et al., 2023). The trial demonstrated significant improvements in both event-free survival (EFS) and pathological complete response (pCR) for the combination treatment. Specifically, patients receiving the combination therapy achieved an 18-month event-free survival (EFS) rate of 91%, significantly higher than the 85% observed in those treated with chemotherapy alone. Additionally, the combination group achieved a pCR rate of 65%, which was higher than the 51% observed with chemotherapy alone. These results suggest that incorporating ICIs into chemotherapy could enhance outcomes for patients with TNBC, potentially lowering recurrence rates and boosting survival. This combination approach may offer a promising strategy for patients with this aggressive breast cancer subtype. A summary of key clinical trials is presented in Table 1.

2.4 Non-small cell lung cancer

In non-small cell lung cancer (NSCLC), combining chemotherapy with ICIs has led to significant improvements in patient outcomes. The KEYNOTE-189 trial evaluated pembrolizumab in combination with chemotherapy (a platinum-based agent and pemetrexed) versus chemotherapy alone in patients with metastatic nonsquamous NSCLC (Gandhi et al., 2018; Wu et al., 2022; Yang et al., 2022; Huang et al., 2024). The findings were compelling, showing a marked improvement in progression-free survival (PFS) among patients receiving the combination therapy. In the combination group, the median PFS in the combination group was 8.8 months, significantly longer than the 4.9 months observed in the chemotherapy-alone group. This data highlights a significant delay in disease progression and offering patients more time with stable disease and improved quality of life. Additionally, the overall survival (OS) benefit was impressive, with 12-month OS rates of 69.2% in the combination group vs. 49.4% in the chemotherapy-alone group. These results indicate not only delayed disease progression but also a clinically meaningful extension in overall survival.

The IMpower130 trial further confirmed the efficacy of this combination in NSCLC. This trial compared atezolizumab combined with chemotherapy (nab-paclitaxel and carboplatin) to chemotherapy alone for the treatment of advanced nonsquamous NSCLC (Zhang et al., 2023; Felip et al., 2021; Horn et al., 2018; Park et al., 2023). The oresults confirmed that the combination therapy significantly enhanced OS and PFS. The 18-month OS rate was 64% in the combination set vs. 52% in the chemotherapy-alone set, while the median PFS was 7 months in the combination set, vs. 5.5 months in the chemotherapy-only set, while.

2.5 Other tumor types

The combination of ICIs and chemotherapy has also been investigated in several other malignancies, including head and neck, gastric, and esophageal cancers. In head and neck cancer, the KEYNOTE-048 trial assessed the effect of pembrolizumab combined with chemotherapy (cisplatin or carboplatin plus fluorouracil) in comparison to chemotherapy alone or with cetuximab in patients with recurrent or metastatic head and neck squamous cell carcinoma (Burtness et al., 2022; Harrington et al., 2022; Burtness et al., 2019). The study demonstrated that the addition of pembrolizumab to chemotherapy significantly improved OS in patients with PD-L1-positive tumors compared to chemotherapy alone.

Similarly, the KEYNOTE-590 trial evaluated pembrolizumab combined with chemotherapy (fluorouracil and cisplatin) versus chemotherapy alone in patients with gastroesophageal junction or esophageal cancer (Kojima et al., 2022; Sun et al., 2021b; Kato et al., 2019). This combination treatment significantly enhanced both PFS and OS compared to chemotherapy alone.

2.6 Real-world applications

For certain malignancies, such as NSCLC, the combination of pembrolizumab and chemotherapy has been established as a standard first-line treatment. This regimen has demonstrated superior PFS and OS compared to chemotherapy alone (Gandhi et al., 2018). Similarly, in melanoma, the combination of chemotherapy with ICIs such as ipilimumab and nivolumab may also be incorporated into treatment regimen (Larkin et al., 2015). For patients with advanced-stage cancers, particularly those with limited treatment options and poor prognoses after prior therapies, combining chemotherapy with ICIs may improve quality of life and delay disease progression. For instance, in TNBC and bladder

cancer, the addition of pembrolizumab or atezolizumab to chemotherapy has shown promising benefits for patients (Emens et al., 2021).

In clinical practice, there is an increasing emphasis on personalized medicine approach. Physicians increasingly tailor treatment strategies according to tumor-specific characteristics, including biomarker expression profiles. Tumors with high PD-L1 expression may respond better to the combination therapy, while those with lower expression may require alternative strategies. Genomic profiling plays a crucial role in identifying mutations or alterations that may be more responsive to this combined treatment, thereby allowing for a more individualized and potentially more effective therapeutic approach (Xu et al., 2024; Malone et al., 2020).

2.7 Selected failed or negative trials

Although numerous clinical trials have demonstrated the efficacy of chemotherapy combined with ICIs, several studies have reported limited or negligible benefits. For instance, the KEYNOTE-361 trial evaluated pembrolizumab in combination with chemotherapy versus chemotherapy alone in advanced urothelial carcinoma. Despite showing a trend toward improved PFS, it failed to meet the primary endpoints for OS or PFS statistically (Powles et al., 2021). Potential reasons for this failure include a heterogeneous patient population with variable PD-L1 expression, suboptimal selection of chemotherapy agents for immune synergy, and insufficient biomarker-based stratification.

Another example is the IMvigor211 study in metastatic urothelial cancer, where atezolizumab failed to demonstrate OS superiority compared to chemotherapy in patients with high PD-L1 expression (Powles et al., 2018). Although early-phase trials yielded promising results, phase III studies failed to replicate these benefits, underscoring the variability of immune responses and the critical need for improved patient selection strategies. These failed trials highlight the importance of biomarker-guided patient selection, appropriate chemotherapy pairing, and understanding of tumor immunobiology to enhance future trial success. It is worth noting that the chemotherapeutic agents used in these successful combinations are recognized for their ability to robustly induce ICD, significantly contributing to the observed clinical benefits.

3 Analysis of clinical trial success factors

A comparative analysis of clinical trials highlights notable similarities and differences in treatment outcomes but alsoreveals several critical factors underlying the varying degrees of success observed when combining chemotherapy with immune checkpoint inhibitors (ICIs).

3.1 Commonalities and individualities across tumor types

Clinical trials spanning diverse cancer types (e.g., NSCLC, melanoma, bladder cancer, TNBC) consistently demonstrate that high PD-L1 expression is positively associated with superior clinical outcomes, as evidenced by studies such as KEYNOTE-189 and IMvigor130. Nevertheless, tumor-intrinsic characteristics significantly influence the therapeutic benefit. Melanoma and NSCLC typically exhibit more robust responses to chemotherapy-ICI combinations, This heightened responsiveness is likely attributable to their relatively higher tumor mutational burdens (TMB) and intrinsic immunogenicity, which enhance the potential for immune recognition and attack. In sharp contrast, bladder cancer demonstrates variable responses to such combinations. This variability indicates that the complexity and heterogeneity of the tumor microenvironment may profoundly impact the tumor's responsiveness to chemotherapy-ICI regimens, as illustrated by the findings of KEYNOTE-361 (Reck et al., 2016; Galsky et al., 2024).

3.2 Why some treatments worked and others did not

Successful clinical trials, including KEYNOTE-189 (NSCLC) and KEYNOTE-522 (TNBC) typically employed regimens integrating chemotherapy agents with proven immunogenic potential (e.g., platinum compounds, taxanes). These regimens were highly effective in enhancing antigen presentation, depleting immunosuppressive populations (e.g., Tregs, MDSCs), and robustly inducing ICD, thereby potentiating the effect of ICIs. Conversely, trials with limited success or failures—such as KEYNOTE-361 in bladder cancer—commonly exhibited inadequate patient stratification, suboptimal chemotherapy drug selection, or less favorable immune modulation. These included insufficient patient stratification, suboptimal selection of chemotherapy drugs, and ineffective immune modulation. Such deficiencies impeded the creation of an optimal immune microenvironment, which is essential for the successful activity of ICIs (Gandhi et al., 2018; Felip et al., 2021; Pusztai et al., 2024).

3.3 Factors influencing superior outcomes

The selection of chemotherapy selection plays a pivotal role in determining treatment efficacy. Platinum-based chemotherapy regimens (KEYNOTE-189, IMpower130) consistently yield improved clinical outcomes due to their potent immunomodulatory effects, including robust ICD induction and enhanced CTL infiltration into tumors. Timing and dosing are equally critical: administering chemotherapy concurrently with or shortly before ICIs maximizes immune priming and antigen release, fosteringa favorable immune environment that significantly enhances therapeutic efficacy. A key determinant of success in chemotherapy-ICI combinations is the ability of chemotherapeutic agents to induce ICD. Agents such as anthracyclines, oxaliplatin, and cyclophosphamide are well documented to elicit strong ICD responses (Zitvogel et al., 2010). The combination of pembrolizumab and certain chemotherapy drugs (KEYNOTE-361) in bladder cancer illustrates such a

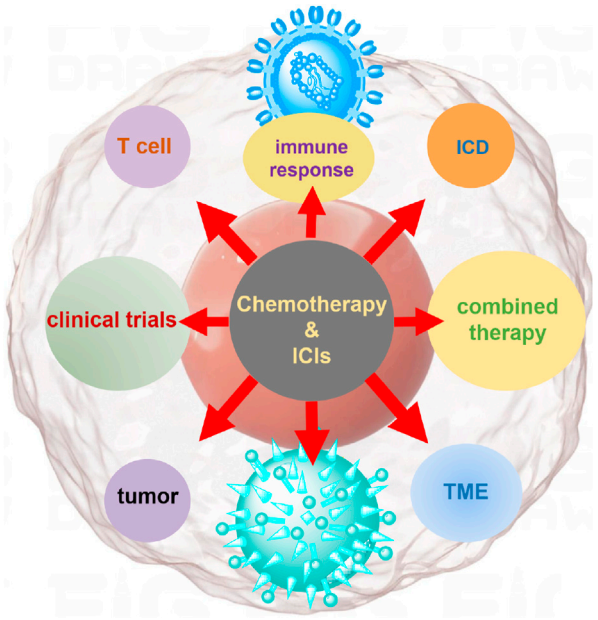

FIGURE 1
Mechanistic illustration of chemotherapy in conjunction with ICIs for tumor treatment. Chemotherapy induces ICD, leading to the release of tumor-associated antigens and DAMPs, such as ATP, calreticulin, and HMGB1. These signals activate dendritic cells (DCs), which process and present tumor antigens to $CD8^+$ T cells. Chemotherapy also modulates the tumor microenvironment by reducing immunosuppressive populations such as Tregs and MDSCs. Meanwhile, immune checkpoint inhibitors (e.g., anti-PD-1, anti-PD-L1) block inhibitory signals between tumor cells and T cells, restoring T cell cytotoxic function. The combination of chemotherapy and ICIs enhances T cell activation, tumor infiltration, and tumor cell killing, providing a synergistic anti-tumor immune response.

scenario, indicating that not all chemotherapy agents synergize equally well with ICIs (Galluzzi et al., 2015; Pfirschke et al., 2016).

4 Mechanisms of action

The synergistic effect of chemotherapy and ICIs relies on a multifaceted mechanism network that collectively boost the antitumor immune response. As a cornerstone of cancer treatment, chemotherapy influences the immune system through various pathways. A pivotal mechanism is the induction of immunogenic cell death: chemotherapy-induced damage to cancer cells leads to the release of tumor antigens and DAMPs (Galluzzi et al., 2017; Kroemer et al., 2022). Tumor antigens are captured and processed by antigen-presenting cells (APCs), while DAMPs act as "danger signals" that alert the immune system. This dual activation primes APCs to mature and migrate to lymph nodes, where they initiate a cascade of immune responses—including the activation of CTLs—to recognize and eliminate tumor cells. Moreover, chemotherapy can modify the TME, which is inherentlyimmunosuppressive, filled with factors that dampen immune cell activity. A core fundamental mechanism driving the efficacy of chemotherapy in this combination is its ability to induce ICD, characterized by the release of DAMPs—including calreticulin, ATP, and HMGB1. Calreticulin promotes dendritic cell phagocytosis of dying cancer cells, ATP serves as a chemoattractant and immunomodulator for dendritic cells, and HMGB1 enhances antigen presentation and T-cell priming (Szulc and Woźniak, 2024; Li et al., 2024; Zhou et al., 2019; Kepp et al., 2014). By reducing immunosuppressive elements and releasing these immunostimulatory signals, chemotherapy transforms the TME into a more "inflammatory" state, thereby enhancing the responsiveness of ICIs and enabling a robust antitumor immune response.

ICIs are pivotal in amplifying the antitumor immune response. T cells express inhibitory receptorslike PD-1 on their surface, while tumor cells in the TME (tumor microenvironment) often overexpress ligands such as PD-L1 (Wei et al., 2018; Kuzume et al., 2020). When PD-L1 on tumor cells interacts with PD-1 on T cells, it transmitsan inhibitory signal that suppresses T cell activity, suppressing effective tumor attack. ICIs, such as anti-PD-L1 or anti-PD-1 antibodies, block this interaction, essentially releasing the inhibitory "brakes" on T cells, enabling them to restore their antitumor activity.

When used in combination, ICIs and chemotherapy work synergistically (Hodi et al., 2010; Peggs and Quezada, 2010). Chemotherapy initiates a cascade by inducing ICD and alters the TME, thereby creating favorable conditions for immune activation. The activation of APCs and the release of tumor antigens prime naïve T cells and recruit them to the tumor site. Concurrently, ICIs prevent these T cells from being inhibited by the immune evasion strategies employed by tumors, allowing them to mount a stronger attack against tumor cells. This integrated approach offers a promising strategy to overcome the limitations of each treatment on its own and enhance the overall effectiveness of cancer therapy (Brahmer et al., 2015; Horn et al., 2017). As illustrated in Figure 1, the synergistic mechanism of chemotherapy-induced ICD in combination with ICIs. By promoting the exposure and release of damage-associated molecular patterns (DAMPs)—such as calreticulin, ATP, and HMGB1—chemotherapy enhances dendritic cell (DC) activation and T cell priming. This process creates a highly immunogenic TME that, when paired with ICIs, amplifies the anti-tumor immune response through sustained T cell-mediated tumor elimination.

5 Conclusion

In conclusion, the combination of chemotherapy and ICIs represents a highly promising strategy in tumor treatment. Mechanistically, chemotherapy induces immunogenic cell death and reprograms the tumor microenvironment, while ICIs block inhibitory signals on T cells, working synergistically to enhance the antitumor immune response. Clinical trials across diverse tumor types, including NSCLC, melanoma, bladder cancer, and TNBC, have demonstrated improved patient outcomes such as enhanced progression - free survival and overall survival. In clinical practice, this combination is increasingly utilized as a first-line or advanced treatment option, with a growing emphasis on personalized medicine. However, several challenges warrant attention, including toxicity management, cost considerations, and the identification of predictive biomarkers to guide patient selection. Future research should prioritize optimizing treatment protocols to

further enhance the efficacy and safety of this combination, ultimately providing better treatment options for cancer patients. The analysis of unsuccessful trials underscore the necessity for meticulous trial design, including patient selection based on predictive biomarkers, appropriate chemotherapy regimens that promote ICD, and strategic treatment sequencing. These elements are indispensable for optimizing the therapeutic potential of chemotherapy and ICI combinations.

Author contributions

CL: Data curation, Writing – original draft, Writing – review and editing. XQ: Validation, Writing – review and editing. MY: Writing – original draft, Writing – review and editing.

Funding

The author(s) declare that no financial support was received for the research and/or publication of this article.

Conflict of interest

The authors declare that the research was conducted in the absence of any commercial or financial relationships that could be construed as a potential conflict of interest.

Generative AI statement

The author(s) declare that no Generative AI was used in the creation of this manuscript.

Publisher's note

References

Bai, B., Ma, Y., Liu, D., Zhang, Y., Zhang, W., Shi, R., et al. (2024). DNA damage caused by chemotherapy has duality, and traditional Chinese medicine may be a better choice to reduce its toxicity. *Front. Pharmacol.* 15, 1483160. doi:10.3389/fphar.2024.1483160

Balar, A. V., Galsky, M. D., Rosenberg, J. E., Powles, T., Petrylak, D. P., Bellmunt, J., et al. (2017). Atezolizumab as first-line treatment in cisplatin-ineligible patients with locally advanced and metastatic urothelial carcinoma: a single-arm, multicentre, phase 2 trial. *Lancet* 389 (10064), 67–76. doi:10.1016/S0140-6736(16)32455-2

Bian, X., Jiang, H., Meng, Y., Li, Y.-p., Fang, J., and Lu, Z. (2022). Regulation of gene expression by glycolytic and gluconeogenic enzymes. *Trends Cell Biol.* 32 (9), 786–799. doi:10.1016/j.tcb.2022.02.003

Brahmer, J., Reckamp Karen, L., Baas, P., Crinò, L., Eberhardt Wilfried, E. E., Poddubskaya, E., et al. (2015). Nivolumab versus docetaxel in advanced squamous-cell non–small-cell lung cancer. *N. Engl. J. Med.* 373 (2), 123–135. doi:10.1056/NEJMoa1504627

Burtness, B., Harrington, K. J., Greil, R., Soulières, D., Tahara, M., de Castro, G., et al. (2019). Pembrolizumab alone or with chemotherapy versus cetuximab with chemotherapy for recurrent or metastatic squamous cell carcinoma of the head and neck (KEYNOTE-048): a randomised, open-label, phase 3 study. *Lancet* 394 (10212), 1915–1928. doi:10.1016/S0140-6736(19)32591-7

Burtness, B., Rischin, D., Greil, R., Soulières, D., Tahara, M., de Castro, Jr G., et al. (2022). Pembrolizumab alone or with chemotherapy for recurrent/metastatic head and neck squamous cell carcinoma in KEYNOTE-048: subgroup analysis by programmed death ligand-1 combined positive score. *J. Clin. Oncol.* 40 (21), 2321–2332. doi:10.1200/JCO.21.02198

Choueiri Toni, K., Powles, T., Albiges, L., Burotto, M., Szczylik, C., Zurawski, B., et al. (2023). Cabozantinib plus nivolumab and ipilimumab in renal-cell carcinoma. *N. Engl. J. Med.* 388 (19), 1767–1778. doi:10.1056/NEJMoa2212851

Dall'Olio, F. G., Marabelle, A., Caramella, C., Garcia, C., Aldea, M., Chaput, N., et al. (2022). Tumour burden and efficacy of immune-checkpoint inhibitors. *Nat. Rev. Clin. Oncol.* 19 (2), 75–90. doi:10.1038/s41571-021-00564-3

da Silva, J. L., Dos Santos, A. L. S., Nunes, N. C. C., de Moraes Lino da Silva, F., Ferreira, C. G. M., and de Melo, A. C. (2019). Cancer immunotherapy: the art of targeting the tumor immune microenvironment. *Cancer Chemother. Pharmacol.* 84 (2), 227–240. doi:10.1007/s00280-019-03894-3

Dent, R., Cortés, J., Pusztai, L., McArthur, H., Kümmel, S., Bergh, J., et al. (2024). Neoadjuvant pembrolizumab plus chemotherapy/adjuvant pembrolizumab for early-stage triple-negative breast cancer: quality-of-life results from the randomized KEYNOTE-522 study. *JNCI J. Natl. Cancer Inst.* 116 (10), 1654–1663. doi:10.1093/jnci/djae129

Emens, L. A., Molinero, L., Loi, S., Rugo, H. S., Schneeweiss, A., Diéras, V., et al. (2021). Atezolizumab and nab-paclitaxel in advanced triple-negative breast cancer: biomarker evaluation of the IMpassion130 study. *JNCI J. Natl. Cancer Inst.* 113 (8), 1005–1016. doi:10.1093/jnci/djab004

Felip, E., Altorki, N., Zhou, C., Csőszi, T., Vynnychenko, I., Goloborodko, O., et al. (2021). Adjuvant atezolizumab after adjuvant chemotherapy in resected stage IB–IIIA non-small-cell lung cancer (IMpower010): a randomised, multicentre, open-label, phase 3 trial. *Lancet* 398 (10308), 1344–1357. doi:10.1016/S0140-6736(21)02098-5

Funt, S. A., Lattanzi, M., Whiting, K., Al-Ahmadie, H., Quinlan, C., Teo, M. Y., et al. (2022). Neoadjuvant atezolizumab with gemcitabine and cisplatin in patients with muscle-invasive bladder cancer: a multicenter, single-arm, phase II trial. *J. Clin. Oncol.* 40 (12), 1312–1322. doi:10.1200/JCO.21.01485

Galluzzi, L., Buqué, A., Kepp, O., Zitvogel, L., and Kroemer, G. (2017). Immunogenic cell death in cancer and infectious disease. *Nat. Rev. Immunol.* 17 (2), 97–111. doi:10.1038/nri.2016.107

Galluzzi, L., Buqué, A., Kepp, O., Zitvogel, L., and Kroemer, G. (2015). Immunological effects of conventional chemotherapy and targeted anticancer agents. *Cancer Cell* 28 (6), 690–714. doi:10.1016/j.ccell.2015.10.012

Galluzzi, L., Humeau, J., Buqué, A., Zitvogel, L., and Kroemer, G. (2020). Immunostimulation with chemotherapy in the era of immune checkpoint inhibitors. *Nat. Rev. Clin. Oncol.* 17 (12), 725–741. doi:10.1038/s41571-020-0413-z

Galsky, M. D., Guan, X., Rishipathak, D., Rapaport, A. S., Shehata, H. M., Banchereau, R., et al. (2024). Immunomodulatory effects and improved outcomes with cisplatin-versus carboplatin-based chemotherapy plus atezolizumab in urothelial cancer. *Cell Rep. Med.* 5 (2), 101393. doi:10.1016/j.xcrm.2024.101393

Gandhi, L., Rodríguez-Abreu, D., Gadgeel, S., Esteban, E., Felip, E., De Angelis, F., et al. (2018). Pembrolizumab plus chemotherapy in metastatic non–small-cell lung cancer. *N. Engl. J. Med.* 378 (22), 2078–2092. doi:10.1056/nejmoa1801005

Harrington, K. J., Burtness, B., Greil, R., Soulières, D., Tahara, M., de Castro, G., et al. (2022). Pembrolizumab with or without chemotherapy in recurrent or metastatic head and neck squamous cell carcinoma: updated results of the phase III KEYNOTE-048 study. *J. Clin. Oncol.* 41 (4), 790–802. doi:10.1200/JCO.21.02508

Hodi, F. S., O'Day Steven, J., McDermott David, F., Weber, R. W., Sosman Jeffrey, A., Haanen John, B., et al. (2010). Improved survival with ipilimumab in patients with metastatic melanoma. *N. Engl. J. Med.* 363 (8), 711–723.

Horn, L., Mansfield, A. S., Szczęsna, A., Havel, L., Krzakowski, M., Hochmair Maximilian, J., et al. (2018). First-line atezolizumab plus chemotherapy in extensive-stage small-cell lung cancer. *N. Engl. J. Med.* 379 (23), 2220–2229. doi:10.1056/NEJMoa1809064

Horn, L., Spigel, D. R., Vokes, E. E., Holgado, E., Ready, N., Steins, M., et al. (2017). Nivolumab versus docetaxel in previously treated patients with advanced non–small-cell lung cancer: two-year outcomes from two randomized, open-label, phase III trials

(CheckMate 017 and CheckMate 057). *J. Clin. Oncol.* 35 (35), 3924–3933. doi:10.1200/JCO.2017.74.3062

Huang, S., Huang, Z., Huang, X., Luo, R., Liang, W., and Qin, T. (2024). Comparative long-term outcomes of pembrolizumab plus chemotherapy versus pembrolizumab monotherapy as first-line therapy for metastatic non-small-cell lung cancer: a systematic review and network meta-analysis. *Front. Immunol.* 15, 1375136. doi:10.3389/fimmu.2024.1375136

Hughes, P. E., Caenepeel, S., and Wu, L. C. (2016). Targeted therapy and checkpoint immunotherapy combinations for the treatment of cancer. *Trends Immunol.* 37 (7), 462–476. doi:10.1016/j.it.2016.04.010

Jiang, H., Gong, Q., Zhang, R., and Yuan, H. (2024). Tetrazine-based metal-organic frameworks. *Coord. Chem. Rev.* 499, 215501. doi:10.1016/j.ccr.2023.215501

Kato, K., Shah, M. A., Enzinger, P., Bennouna, J., Shen, L., Adenis, A., et al. (2019). KEYNOTE-590: phase III study of first-line chemotherapy with or without pembrolizumab for advanced esophageal cancer. *Future Oncol.* 15 (10), 1057–1066. doi:10.2217/fon-2018-0609

Kelley, R. K., Ueno, M., Yoo, C., Finn, R. S., Furuse, J., Ren, Z., et al. (2023). Pembrolizumab in combination with gemcitabine and cisplatin compared with gemcitabine and cisplatin alone for patients with advanced biliary tract cancer (KEYNOTE-966): a randomised, double-blind, placebo-controlled, phase 3 trial. *Lancet* 401 (10391), 1853–1865. doi:10.1016/S0140-6736(23)00727-4

Kepp, O., Laura, S., Ilio, V., Erika, V., Sandy, A., Patrizia, A., et al. (2014). Consensus guidelines for the detection of immunogenic cell death. *OncoImmunology* 3 (9), e955691. doi:10.4161/21624011.2014.955691

Knezevic, C. E., and Clarke, W. (2020). Cancer chemotherapy: the case for therapeutic drug monitoring. *Ther. Drug Monit.* 42 (1), 6–19. doi:10.1097/FTD.0000000000000701

Kojima, T., Hara, H., Tsuji, A., Yasui, H., Muro, K., Satoh, T., et al. (2022). First-line pembrolizumab + chemotherapy in Japanese patients with advanced/metastatic esophageal cancer from KEYNOTE-590. *Esophagus* 19 (4), 683–692. doi:10.1007/s10388-022-00920-x

Kroemer, G., Galassi, C., Zitvogel, L., and Galluzzi, L. (2022). Immunogenic cell stress and death. *Nat. Immunol.* 23 (4), 487–500. doi:10.1038/s41590-022-01132-2

Kroemer, G., Galluzzi, L., Kepp, O., and Zitvogel, L. (2013). Immunogenic cell death in cancer therapy. *Annu. Rev. Immunol.* 31, 51–72. doi:10.1146/annurev-immunol-032712-100008

Kuzume, A., Chi, S., Yamauchi, N., and Minami, Y. (2020). Immune-checkpoint blockade therapy in lymphoma. *Int. J. Mol. Sci.* 21, 5456. doi:10.3390/ijms21155456

Larkin, J., Chiarion-Sileni, V., Gonzalez, R., Grob Jean, J., Cowey, C. L., Lao Christopher, D., et al. (2015). Combined nivolumab and ipilimumab or monotherapy in untreated melanoma. *N. Engl. J. Med.* 373 (1), 23–34. doi:10.1056/NEJMoa1504030

Li, C., Kaur, A., Pavlidaki, A., Spenlé, C., Rajnpreht, I., Donnadieu, E., et al. (2024). Targeting the MAtrix REgulating MOtif abolishes several hallmarks of cancer, triggering antitumor immunity. *Proc. Natl. Acad. Sci. U. S. A.* 121, e2404485121. doi:10.1073/pnas.2404485121

Li, K., Yu, H., Bao, Z., Xu, L., Zhang, H., Wang, T., et al. (2022). Combination of photosensitizer and immune checkpoint inhibitors for improving the efficacy of tumor immunotherapy. *Int. J. Pharm.* 629, 122384. doi:10.1016/j.ijpharm.2022.122384

Malone, E. R., Oliva, M., Sabatini, P. J. B., Stockley, T. L., and Siu, L. L. (2020). Molecular profiling for precision cancer therapies. *Genome Med.* 12 (1), 8. doi:10.1186/s13073-019-0703-1

Naimi, A., Mohammed, R. N., Raji, A., Chupradit, S., Yumashev, A. V., Suksatan, W., et al. (2022). Tumor immunotherapies by immune checkpoint inhibitors (ICIs); the pros and cons. *Cell Commun. Signal.* 20 (1), 44. doi:10.1186/s12964-022-00854-y

Nakamura, R., Hasegawa, G., Ohashi, K., Hashimoto, T., Ikeda, Y., Hara, N., et al. (2023). Primary lung cancer treatable with radical resection after complete remission with pembrolizumab therapy following gemcitabine and carboplatin chemotherapy for multiple metastases of bladder cancer. *IJU Case Rep.* 6 (1), 85–88. doi:10.1002/iju5.12550

Obeid, M., Tesniere, A., Ghiringhelli, F., Fimia, G. M., Apetoh, L., Perfettini, J.-L., et al. (2007). Calreticulin exposure dictates the immunogenicity of cancer cell death. *Nat. Med.* 13 (1), 54–61. doi:10.1038/nm1523

Owonikoko, T., Park, K., Govindan, R., Ready, N., Reck, M., Peters, S., et al. (2021). Nivolumab and ipilimumab as maintenance therapy in extensive-disease small-cell lung cancer: CheckMate 451. *J. Clin. Oncol.* 39, 1349–1359. JCO.20.02212. doi:10.1200/JCO.20.02212

Park, S., Kim, T. M., Han, J.-Y., Lee, G.-W., Shim, B. Y., Lee, Y.-G., et al. (2023). Phase III, randomized study of atezolizumab plus bevacizumab and chemotherapy in patients with *EGFR*- or *ALK*-mutated non-small-cell lung cancer (ATTLAS, KCSG-LU19-04). *J. Clin. Oncol.* 42 (11), 1241–1251. doi:10.1200/JCO.23.01891

Peggs, K., and Quezada, S. (2010). Ipilimumab: attenuation of an inhibitory immune checkpoint improves survival in metastatic melanoma. *Expert Rev. Anticancer Ther.* 10, 1697–1701. doi:10.1586/era.10.144

Pfirschke, C., Engblom, C., Rickelt, S., Cortez-Retamozo, V., Garris, C., Pucci, F., et al. (2016). Immunogenic chemotherapy sensitizes tumors to checkpoint blockade therapy. *Immunity* 44 (2), 343–354. doi:10.1016/j.immuni.2015.11.024

Powles, T., Csļëszi, T., Ìñzgİroǿülu, M., Matsubara, N., Gİczi, L., Cheng, S. Y. S., et al. (2021). Pembrolizumab alone or combined with chemotherapy versus chemotherapy as first-line therapy for advanced urothelial carcinoma (KEYNOTE-361): a randomised, open-label, phase 3 trial. *Lancet Oncol.* 22 (7), 931–945. doi:10.1016/S1470-2045(21)00152-2

Powles, T., Durİn, I., van der Heijden, M. S., Loriot, Y., Vogelzang, N. J., De Giorgi, U., et al. (2018). Atezolizumab versus chemotherapy in patients with platinum-treated locally advanced or metastatic urothelial carcinoma (IMvigor211): a multicentre, open-label, phase 3 randomised controlled trial. *Lancet* 391 (10122), 748–757. doi:10.1016/S0140-6736(17)33297-X

Pusztai, L., Denkert, C., O'Shaughnessy, J., Cortes, J., Dent, R., McArthur, H., et al. (2024). Event-free survival by residual cancer burden with pembrolizumab in early-stage TNBC: exploratory analysis from KEYNOTE-522☆. *Ann. Oncol.* 35 (5), 429–436. doi:10.1016/j.annonc.2024.02.002

Qian, X., Hu, W., and Yan, J. (2022). Nano-Chemotherapy synergize with immune checkpoint inhibitor- A better option? *Front. Immunol.* 13, 963533. doi:10.3389/fimmu.2022.963533

Reck, M., Rodrİguez-Abreu, D., Robinson Andrew, G., Hui, R., Csļëszi, T., Fİlrİİp, A., et al. (2016). Pembrolizumab versus chemotherapy for PD-L1ق. . .Positive Nonق. . .Small-cell lung cancer. *N. Engl. J. Med.* 375 (19), 1823–1833. doi:10.1056/nejmoa1606774

Rizzo, A., Cusmai, A., Acquafredda, S., Giovannelli, F., Rinaldi, L., Misino, A., et al. (2022). KEYNOTE-522, IMpassion031 and GeparNUEVO: changing the paradigm of neoadjuvant immune checkpoint inhibitors in early triple-negative breast cancer. *Future Oncol.* 18 (18), 2301–2309. doi:10.2217/fon-2021-1647

Roskoski, R. (2024). Combination immune checkpoint and targeted protein kinase inhibitors for the treatment of renal cell carcinomas. *Pharmacol. Res.* 203, 107181. doi:10.1016/j.phrs.2024.107181

Rui, R., Zhou, L., and He, S. (2023). Cancer immunotherapies: advances and bottlenecks. *Front. Immunol.* 14, 1212476. doi:10.3389/fimmu.2023.1212476

Sharma, P., and Allison, J. (2015). Immune checkpoint targeting in cancer therapy: toward combination strategies with curative potential. *Cell* 161, 205–214. doi:10.1016/j.cell.2015.03.030

Sharma, P., Stecklein, S. R., Yoder, R., Staley, J. M., Schwensen, K., O'Dea, A., et al. (2024). Clinical and biomarker findings of neoadjuvant pembrolizumab and carboplatin plus docetaxel in triple-negative breast cancer: NeoPACT phase 2 clinical trial. *JAMA Oncol.* 10 (2), 227–235. doi:10.1001/jamaoncol.2023.5033

Sun, C., and Xu, S. (2020). Advances in personalized neoantigen vaccines for cancer immunotherapy. *Biosci. Trends* 14 (5), 349–353. doi:10.5582/bst.2020.03267

Sun, J.-M., Shen, L., Shah, M. A., Enzinger, P., Adenis, A., Doi, T., et al. (2021b). Pembrolizumab plus chemotherapy versus chemotherapy alone for first-line treatment of advanced oesophageal cancer (KEYNOTE-590): a randomised, placebo-controlled, phase 3 study. *Lancet* 398 (10302), 759–771. doi:10.1016/S0140-6736(21)01234-4

Sun, Y., Liu, Y., Ma, X., and Hu, H. (2021a). The influence of cell cycle regulation on chemotherapy. *Int. J. Mol. Sci.* 22, 6923. doi:10.3390/ijms22136923

Suzuki, R., Hamada, K., Ohkuma, R., Homma, M., Tsurui, T., Iriguchi, N., et al. (2023). Case Report: combined pembrolizumab, 5-fluorouracil, and cisplatin therapy were remarkably effective in p16-positive squamous cell carcinoma of unknown primary. *Front. Oncol.* 13, 1231986. doi:10.3389/fonc.2023.1231986

Szulc, A., and Woźniak, M. (2024). Targeting pivotal hallmarks of cancer for enhanced therapeutic strategies in triple-negative breast cancer treatment—*in vitro*, *in vivo* and clinical trials literature review. *Cancers* 16, 1483. doi:10.3390/cancers16081483

Wan, X., Zeng, X., Peng, L., Peng, Y., Liu, Q., Yi, L., et al. (2021). Cost-effectiveness analysis of nivolumab plus ipilimumab for advanced non-small-cell lung cancer. *Front. Pharmacol.* 12. doi:10.3389/fphar.2021.580459

Wei, S. C., Duffy, C. R., and Allison, J. P. (2018). Fundamental mechanisms of immune checkpoint blockade therapy. *Cancer Discov.* 8 (9), 1069–1086. doi:10.1158/2159-8290.CD-18-0367

Wu, M., Qin, S., Wang, L., Tan, C., Peng, Y., Zeng, X., et al. (2022). Cost-effectiveness of pembrolizumab plus chemotherapy as first-line therapy for advanced oesophageal cancer. *Front. Pharmacol.* 13, 881787. doi:10.3389/fphar.2022.881787

Xu, W., Jia, A., Lei, Z., Wang, J., Jiang, H., Wang, S., et al. (2024). Stimuli-responsive prodrugs with self-immolative linker for improved cancer therapy. *Eur. J. Med. Chem.* 279, 116928. doi:10.1016/j.ejmech.2024.116928

Yang, Z., Chen, Y., Wang, Y., Hu, M., Qian, F., Zhang, Y., et al. (2022). Pembrolizumab plus chemotherapy versus chemotherapy monotherapy as a first-line treatment in elderly patients (≥75 Years old) with non-small-cell lung cancer. *Front. Immunol.* 13, 807575. doi:10.3389/fimmu.2022.807575

Yasinjan, F., Xing, Y., Geng, H., Guo, R., Yang, L., Liu, Z., et al. (2023). Immunotherapy: a promising approach for glioma treatment. *Front. Immunol.* 14, 1255611. doi:10.3389/fimmu.2023.1255611

Zhang, C., Liu, Y., Tan, J., Tian, P., and Li, W. (2023). Cost-effectiveness evaluation based on two models of first-line atezolizumab monotherapy and chemotherapy for advanced non-small cell lung cancer with high-PDL1 expression. *Front. Oncol.* 13, 1093469. doi:10.3389/fonc.2023.1093469

Zhao, H., Yu, J., Zhang, R., Chen, P., Jiang, H., and Yu, W. (2023). Doxorubicin prodrug-based nanomedicines for the treatment of cancer. *Eur. J. Med. Chem.* 258, 115612. doi:10.1016/j.ejmech.2023.115612

Zhou, J., Wang, G., Chen, Y., Wang, H., Hua, Y., and Cai, Z. (2019). Immunogenic cell death in cancer therapy: present and emerging inducers. *J. Cell. Mol. Med.* 23 (8), 4854–4865. doi:10.1111/jcmm.14356

Zitvogel, L., Kepp, O., Senovilla, L., Menger, L., Chaput, N., and Kroemer, G. (2010). Immunogenic tumor cell death for optimal anticancer therapy: the calreticulin exposure pathway. *Clin. Cancer Res.* 16 (12), 3100–3104. doi:10.1158/1078-0432.CCR-09-2891

Zouein, J., Haddad, F. G., Eid, R., and Kourie, H. R. (2022). The combination of immune checkpoint inhibitors and chemotherapy in advanced non-small-cell lung cancer: the rational choice. *Immunotherapy* 14 (2), 155–167. doi:10.2217/imt-2021-0014

frontiers | Frontiers in Oncology

TYPE Clinical Trial
PUBLISHED 10 June 2025
DOI 10.3389/fonc.2025.1577468

OPEN ACCESS

EDITED BY
Xinyu Wang,
Philadelphia College of Osteopathic Medicine (PCOM), United States

REVIEWED BY
Sutapa Mukherjee,
Chittaranjan National Cancer Institute (CNCI), India
Zhang Yang,
Fujian Medical University Union Hospital, China

*CORRESPONDENCE
Rick Fontenot
rick@lanternpharma.com

†These authors have contributed equally to this work

RECEIVED 15 February 2025
ACCEPTED 12 May 2025
PUBLISHED 10 June 2025

CITATION
Fontenot R, Biyani N, Bhatia K, Ewesuedo R, Chamberlain M and Sharma P (2025) Clinical outcomes of DNA-damaging agents and DNA damage response inhibitors combinations in cancer: a data-driven review.
Front. Oncol. 15:1577468.
doi: 10.3389/fonc.2025.1577468

Clinical outcomes of DNA-damaging agents and DNA damage response inhibitors combinations in cancer: a data-driven review

Rick Fontenot[1*†], Neha Biyani[1†], Kishor Bhatia[1], Reggie Ewesuedo[1], Marc Chamberlain[1,2] and Panna Sharma[1,2]

[1]Lantern Pharma Inc., Dallas, TX, United States, [2]Starlight Therapeutics, Plano, TX, United States

The combination of DNA-damaging agents (DDAs) and DNA damage response inhibitors (DDRis) has been extensively studied to improve therapeutic outcomes. While both groups of agents show promise individually, DDAs are limited by tumor resistance, and DDRis are limited by specific genetic context. Combining DDAs with DDRis may overcome these challenges and enhance patient outcomes. This review systematically analyzes clinical trials investigating the combination of DDAs and DDRis by dividing them into two sections: PARP and non-PARP inhibitors. An evaluation was conducted on 221 DDA-DDRi combination-arm trials involving 22 DDAs and 46 DDRis. DDAs were classified into eight subclasses, and DDRis into 14 distinct subclasses based on their mechanisms of action and specific targets, respectively. 89 of the 221 combination-arm trials had interpretable outcomes and were selected for further analysis. These were assigned outcome scores based on predefined criteria, reflecting their clinical effectiveness, safety, and benefit across different tumor types and patient populations. Our analysis emphasizes the patterns in treatment effectiveness, safety, and emerging trends across various cancer types and discusses the potential of biomarkers to guide treatment selection and improve patient outcomes. This review outlines an understanding of the recent state of DDA-DDRi combinations, offering critical insights for refining future cancer treatment strategies.

KEYWORDS

DNA-damaging agents, DNA damage response inhibitors, PARP inhibitors, combination therapy, clinical trials, DNA repair pathways, cancer treatment, biomarkers

1 Introduction

DNA-damaging agents (DDAs), including chemotherapy and radiotherapy, have long been central to cancer treatment. They rely on their ability to induce irreparable genetic damage in rapidly dividing tumor cells (1). However, the efficacy of DDAs is frequently hampered by the activation of DNA damage response (DDR) mechanisms in cancer cells, which enable DNA repair and promote cell survival (2). This has spurred the development of DDR inhibitors (DDRis) designed to target these repair mechanisms, thereby enhancing the cytotoxic effects of DDAs (2, 4).

The DDR network is a complex, interconnected system with redundant pathways that provide compensatory and alternative repair mechanisms (5, 6). This redundancy presents therapeutic opportunities, exemplified by poly (ADP-ribose) polymerase inhibitors (PARPis), which exploit synthetic lethality to selectively kill cancer cells with defective DNA repair, as in cancers with BRCA mutations (3). PARPi approvals for treating ovarian, breast, and prostate cancers marked a significant advancement in personalized cancer therapy (7–11). However, the clinical utility of PARPis is confined mainly to specific genetic contexts, highlighting the need for broader treatment strategies (3). This need has driven the development of next-generation DDRis targeting diverse components of the DDR network.

Inhibitors of ATM, ATR, WEE1, and DNA-PK, for instance, disrupt distinct aspects of the DDR pathway, including cell cycle checkpoint regulation, DNA damage signaling, and repair processes (5, 12, 13). These agents offer potential therapeutic benefits across a broader range of tumor types, independent of specific genetic alterations like homologous recombination (HR) deficiencies, offering a more inclusive approach to overcoming resistance to DNA-damaging therapies (12). However, as monotherapies, DDRis often demonstrate limited efficacy due to rapid adaptation and developing resistance mechanisms in cancer cells (14).

The combination of DDRis and DDAs offers a compelling strategy to overcome these limitations. By simultaneously inducing DNA damage and inhibiting its repair, this approach can circumvent resistance mechanisms observed with monotherapy and expand the therapeutic potential beyond traditional DDA applications (2, 15). Numerous clinical trials are investigating these combination strategies across various cancer types and treatment regimens. The success of these combinations is influenced by factors such as tumor type, genetic profile, and the specific agents used. A critical challenge lies in identifying predictive biomarkers that can stratify patients based on their likelihood of response, enabling personalized treatment strategies and minimizing unnecessary toxicity (13, 16).

This review systematically analyzes the results of 221 DDAs-DDRis combination-arm clinical trials, encompassing 22 DDAs and 46 DDRis, without employing statistical methods. DDAs were grouped into eight subclasses according to their mechanisms of action, while DDRis were classified into 14 subclasses based on their specific targets. From the 221 initial combination-arm trials, 89 with interpretable outcomes were selected for in-depth analysis. These 89 trials were scored based on predefined criteria evaluating clinical effectiveness, safety, and benefit across diverse tumor types and patient populations, incorporating biomarker data where available. Given the prominent role of PARPis, the review is divided into PARP-focused and non-PARP-focused sections. By analyzing successful and challenging regimens, this work aims to provide a comprehensive overview of the field and inform future research on refining these combined therapies.

2 Methods

The identification of relevant clinical trials and assembly of trial details and outcomes relied on accessing and organizing information from clinicaltrials.gov in conjunction with internally developed python scripts as well as steps of manual review and annotations to ensure details of each trial, drug, and results are reliable and accurate. Figure 1 includes an overview of the workflow, and detailed descriptions of workflow sections follow.

2.1 Clinical trial data acquisition and processing

A queryable database of clinical trial information was needed to identify applicable trials and the relevant information associated with each trial. Pytrials (https://pytrials.readthedocs.io/en/latest/) provides a python query tool using the Clinicaltrials.gov API (https://clinicaltrials.gov/data-api/api); however, the API does not include relevant sections such as the trial's detailed description, patient inclusion criteria, PMID references discussing trial results, and many more fields available on the clinicaltrials.gov page for each trial. Furthermore, the interventions returned by the API require further processing to properly extract and separate drug names.

In addition to the API clinicaltrials.gov allows users to download a JSON file including all fields for all trials. Data can be downloaded from this link: https://clinicaltrials.gov/search by clicking on the download button and selecting JSON with all available fields.

The nested trials inside the downloaded JSON are text rather than standardized dictionaries and do not all have the same fields or formats. A custom python script with additional processing was created to transform the JSON file into a standardized data table containing all fields available for each trial.

While the clincaltrials.gov page and JSON for each trial include a list of treatments in the "interventions" section, in many cases, it is not a complete list of drugs in the trial or synonyms the drug name is referenced to throughout the trial documents. Scripts using natural language processing and regular expressions tools were created to extract all drug names from the Interventions, ARM-Groups, and ARM-Interventions fields and compiled into a complete list for each trial in the newly created database.

The clinicaltrials.gov pages and downloads do not specifically include a field or label indicating whether the trial is a drug combination trial, so a rules-based script was created to flag

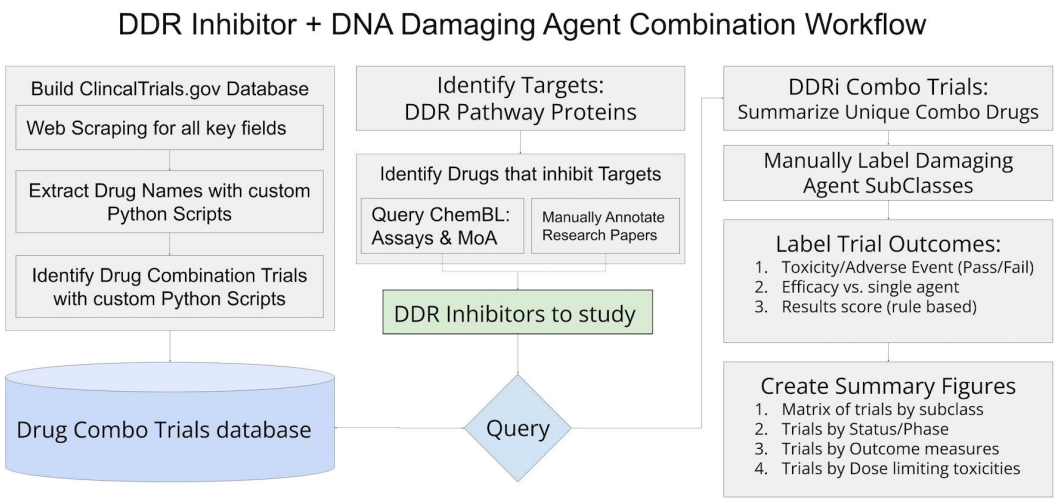

FIGURE 1
Workflow diagram of methods utilized to assemble data and results for this study.

which trials are drug combination trials. If a trial includes more than one drug, it is not necessarily a drug combination trial as the drugs may be administered as monotherapies for comparison in different arms of the trial. A rules-based script using natural language processing and regular expressions was created to flag trials with the words "combination" or "combined" used in either the trials title or brief summary and more than one unique drug in the trial drugs list created as described above. These flagged trials were included in a drug combinations specific view of the database for downstream querying and analysis. In total 490,490 clinical trials were processed, and 31,576 trials were identified as drug combination trials.

2.2 DNA damage repair inhibitor and DNA damaging agent identification

Identification of drugs that inhibit DDR pathways was accomplished by two methods, assay research and reviews of public conference presentations. A list of 120 proteins involved in the HR, NHEJ, alt-NHEJ, NER, MMR, BER, ICL, and TLS DNA damage repair pathways was compiled from literature (5, 17–31) to query the ChemBL database (https://www.ebi.ac.uk/chembl/). The query searched for inhibition assays for each protein in the compiled list and joined the drug names and drug name synonyms for each study with a significant percentage inhibition of the applicable protein and its associated repair pathway to retain the subclass of DNA damage repair inhibitors.

The list of 46 DDRis identified was used to query the drug combination clinical trials database view, resulting in 1,549 trials for initial review. A list of all unique drug names included in these trials resulted in 731 drugs that were manually annotated as DDA vs. other classes of drugs. Twenty-two DDAs across eight different DNA-damaging subclasses were identified as having at least one trial in combination with a DDRi. After filtering initially identified trials to the applicable drug class combinations, 221 trials with a DDRi and DDA in combination were identified for full review, with 89 of the trials being complete with at least one public source of the trial outcomes.

During the trial review phase, additional trials were removed as not relevant to this study if the DDA is only in a comparator arm while the DDRi drug was in a separate experimental arm rather than a test in combination.

In trials with multiple arms containing a DDRi + DDA combination, each arm was evaluated separately during reviews. This format allows for the analysis of counts based on specific drug combinations rather than a trial study ID.

2.3 Assigning numerical scores based on trial outcomes

Each applicable trial with results was manually reviewed to summarize outcomes from both outcome measures reported on clinicaltrials.gov tables as well as publicly available research papers summarizing results. For the purposes of visualization figures to graphically summarize which combinations of drug classes and specific drugs have demonstrated positive outcomes vs. negative or inconclusive outcomes, a numerical score was assigned to each trial. This numerical score is utilized to color code figures for a high-level representation of outcomes covering multiple trials as introduction prior to presenting details on specific individual trials or drug classes.

Initially three categories of numerical scores assigned are based on the following criteria during the manual annotation of outcomes process:

2.3.1 Toxicity score

Trials that were discontinued due to significant adverse events or toxicities that prevented trial completion were graded as a

negative outcome and assigned a numerical score of 1 representing the occurrence of discontinuation due to toxicity. Trials that were able to complete the study without trial limiting adverse events were graded as positive and assigned a score of 0, representing the lack of discontinuation. Although trials that received a score of 0 reported adverse events of varying severity, the current scoring system does not differentiate between the levels of severity of these adverse events, and no additional scoring was implemented to address this.

2.3.2 Overall efficacy score

In trials where outcomes were measured as defined endpoints, the most used efficacy endpoints included partial response (PR), complete response (CR), objective response rate (ORR), disease control rate (DCR), median progression-free survival (mPFS), and overall survival (mOS), disease (SD), duration of response (DoR). Combination-trial arms achieving predefined efficacy endpoints were graded as positive outcome and assigned a numerical score of 1 (positive efficacy); those failing to meet endpoints were graded as negative and assigned a numerical score of 0 (lack of required efficacy). For trials lacking pre-defined endpoints but reporting efficacy outcomes, results were compared to standard-of-care expectations for the relevant indications and scored in the same manner as trials with defined endpoints. No reported outcomes: Completed combination-arm trial lacking any reported efficacy outcomes (e.g., some maximum tolerated dose [MTD] studies, which often focus on dose-limiting toxicity [DLT] and determining the recommended phase 2 dose [RP2D] rather than direct efficacy) were classified as having no available outcome data.

2.3.3 Biomarker response score

In addition to the overall efficacy score, which is based on all trial participants, combination trial arms that reported differential efficacy outcomes for a subpopulation with specific biomarkers were also graded. Combination trial arms with a biomarker-defined patient subpopulation achieving the trials' predefined efficacy endpoints or meeting standard-of-care expectations were graded as positive and assigned a score of 1. Combination trial arms where the biomarker-defined patient subpopulation did not exceed response rate of the overall trial participant group, or did not have outcomes reported for a biomarker patient subpopulation were graded as neutral and assigned a numerical score of 0.

2.3.4 Outcome score

For use in summary visualizations and figures, these three individual categorical scores were then combined into an overall Outcome Score calculated as:

$$Outcome\ \ Score = Overall\ \ Efficacy\ \ Score + \frac{Biomarker\ \ response\ \ Score}{2}$$

Outcome Score values can be interpreted as:

Score 0: The combination-arm trial had a negative outcome where either the trial was discontinued due to adverse events or toxicities, or when the outcome was negative due to a lack of efficacy.

Score 0.5: The combination-arm trial was not discontinued due to adverse events or toxicities. While efficacy was not demonstrated for the overall participant group, there was a biomarker defined subpopulation that demonstrated efficacy.

Score 1.0: The combination-arm trial was not discontinued due to adverse events or toxicities and demonstrated efficacy for the studied participant group, but there were no outcomes reported for biomarker defined subgroups or the defined biomarker subgroup did not demonstrate efficacy above the other patients in the trial-arm.

Score 1.5: The combination-arm trial was not discontinued due to adverse events or toxicities and demonstrated efficacy for both the studied participant group, as well as an additional improvement in efficacy for a biomarker defined subgroup of participants.

3 Results

3.1 Clinical trial status of DDRis and DDAs: trends, development stages, and trial distribution

To assess the clinical landscape of DDAs-DDRis combinations, we analyzed clinical trials involving 22 unique DDAs in combination with 46 distinct DDRis. As a first step 22 DDAs were classified based on their mechanism of DNA damage into eight distinct DNA-damaging subclasses: alkylating agents, interstrand cross-linkers (ICLs), topoisomerase inhibitors, DNA intercalators, (dual-action agents) DNA intercalation & topoisomerase inhibition, ribonucleotide reductase inhibitors, G-quadruplex stabilizers, and multiple agents (Table 1A). Multiple agents denote a combination of multiple distinct therapeutic regimens, with at least one of these regimens including a DDA, with the possible addition of other agents like paclitaxel or pemetrexed. 46 DDRis were categorized into 14 subclasses based on their specific targets: ATR, AURK, CHK1/2, DNA-PK, PARP, PKMYT1, PLK, PLK+WEE1 (dual-targeting agents), PRMT5, RAD52, TP53, USP1, WEE1, and WRN (Table 1B).

Next, we analyzed clinical trials investigating combinations of these 22 DDAs and 46 DDRis. Each unique DDA-DDRi pairing within a trial was treated as an individual combination-arm trial. This means that if a single trial evaluated multiple treatment arms with different combinations of the DDA-DDRi, each arm was counted separately. The process yielded 221 combination-arm trials for analysis, listed in Supplementary Tables S1, S2 (32–95), and S3.

Clinical trial data, seen in Figure 2, reveals a distinct trend in investigating DDAs-DDRis combinations by plotting the number of tested combinations across all trial phases and recruitment statuses wherein PARPis have been more extensively studied in combination

10.3389/fonc.2025.1577468

TABLE 1A List of DDAs and their Subclasses.

Damaging Drug Name	Damaging class
cyclophosphamide	alkylating agent
dacarbazine	alkylating agent
lurbinectedin	alkylating agent
temozolomide	alkylating agent
trabectedin	alkylating agent
mitomycin c	alkylating agent
doxorubicin	DNA intercalation
daunorubicin	DNA intercalation & topoisomerase inhibitor
epirubicin	DNA intercalation & topoisomerase inhibitor
idarubicin	DNA intercalation & topoisomerase inhibitor
mitoxantrone	DNA intercalation & topoisomerase inhibitor
cytarabine	DNA intercalation, topoisomerase inhibitor
pidnarulex	G-quadruplex stabilizer
carboplatin	Interstrand cross linker
cisplatin	Interstrand cross linker
oxaliplatin	Interstrand cross linker
gemcitabine	Ribonucleotide reductase inhibitor
hydroxyurea	Ribonucleotide reductase inhibitor
ep0057	topoisomerase inhibitor
etoposide	topoisomerase inhibitor
irinotecan	topoisomerase inhibitor
topotecan	topoisomerase inhibitor

TABLE 1B List of DDRi Drugs, Their Subclasses, and affected DNA Damage Response Pathways.

Drug Name	DDRi Subclass	DNA damage response affected by DDRi Subclass
berzosertib	ATR	DNA damage checkpoint
elimusertib	ATR	DNA damage checkpoint
gartisertib	ATR	DNA damage checkpoint
sc0245	ATR	DNA damage checkpoint
tuvusertib	ATR	DNA damage checkpoint
alisertib	AURK	DNA damage checkpoint
chiauranib	AURK	DNA damage checkpoint
ilorasertib	AURK	DNA damage checkpoint
azd7762	CHK1/2	DNA damage checkpoint
prexasertib	CHK1/2	DNA damage checkpoint
rabusertib	CHK1/2	DNA damage checkpoint
sra737	CHK1/2	DNA damage checkpoint
azd7648	DNA-PK	DSBR
peposertib	DNA-PK	DSBR
samotolisib	DNA-PK	DSBR
vx-984	DNA-PK	DSBR
azd5305	PARP	SSBR
cep-9722	PARP	SSBR
e7016	PARP	SSBR
e7449	PARP	SSBR
fluzoparib	PARP	SSBR
nesuparib	PARP	SSBR
niraparib	PARP	SSBR
nms-03305293	PARP	SSBR
olaparib	PARP	SSBR
pamiparib	PARP	SSBR
rucaparib	PARP	SSBR
senaparib	PARP	SSBR
talazoparib	PARP	SSBR
veliparib	PARP	SSBR
venadaparib	PARP	SSBR
rp-6306	PKMYT1	DNA damage checkpoint
bal0891	PLK	DNA damage checkpoint
onvansertib	PLK	DNA damage checkpoint
rigosertib sodium	PLK	DNA damage checkpoint
adavosertib	PLK+WEE1	DNA damage checkpoint
volasertib	PLK+WEE1	DNA damage checkpoint
amg 193	PRMT5	DNA damage checkpoint
gossypol	RAD52	DSBR
idasanutlin	TP53	DNA damage checkpoint
navtemadlin	TP53	DNA damage checkpoint
siremadlin	TP53	DNA damage checkpoint
ro7623066	USP1	TLS and FA
azenosertib	WEE1	DNA damage checkpoint
debio 0123	WEE1	DNA damage checkpoint
hro761	WRN	DSBR and SSBR

SSBR, Single-Strand Break Repair, DSBR, Double-Strand Break Repair, TLS, Translesion Synthesis, FA, Fanconi Anemia.

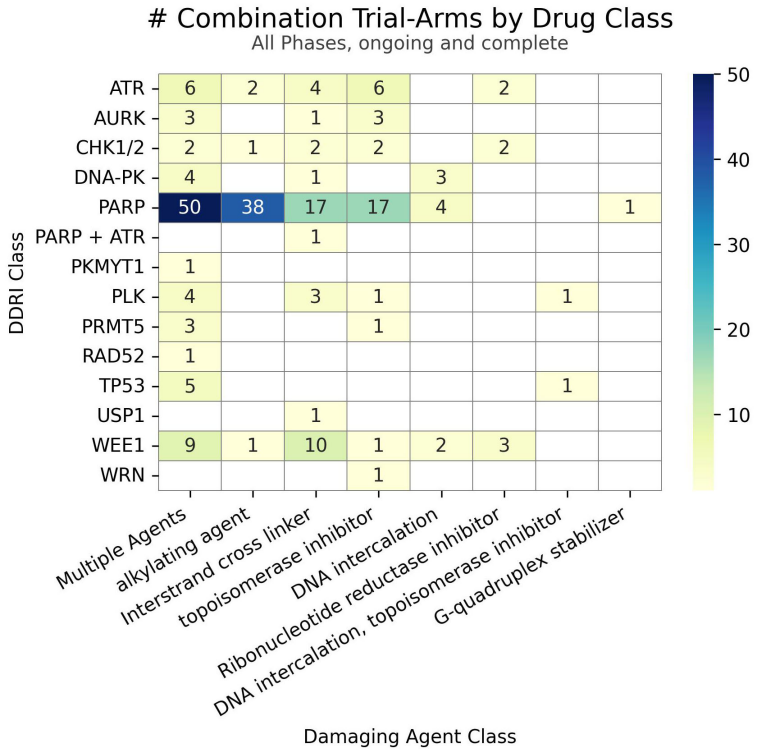

FIGURE 2
The number of combinations tested in trials for each class of DDRi (y-axis) versus DDA (x-axis). Unique drug combinations with multiple trials/phases are counted in the totals. Each drug combination is counted separately under the appropriate drug class totals for trials with multiple arms of interest.

with DDAs. Specifically, 127 combination arms have explored PARPi-DDA combinations, representing 57% of DDAs-DDRis combinations. At the same time, 94 trials have focused on non-PARP inhibitors (non-PARPis) and DDAs combinations, representing 43% of DDAs-DDRis combinations. Among DNA-damaging mechanisms investigated in DDRis combination-arm trials, multiple-agent regimens appeared the most frequently in 88 combination-arm trials. Among single-DDAs combinations with DDRis, alkylating agents were the most commonly investigated (42 combination-arm trials), followed by ICLs (40 combination-arm trials) and topoisomerase inhibitors (32 combination-arm trials). ICL agents, such as carboplatin, cisplatin, and oxaliplatin, are the most frequently utilized DDAs in multi-agent combination studies. The carboplatin and paclitaxel regimen (n=23) is the most commonly used DDAs-DDRis combination in multiple-agent combination arm trials, followed by the cisplatin and gemcitabine regimen (n=7), as shown in Figure 3.

A detailed discussion about multiple agent combination-arm trials is beyond the scope of this article; however, essential information is provided in tables and relevant sections where applicable. Our analysis of the distribution of combination agents by clinical development stage within the PARPi and non-PARPi spaces revealed distinct trends as shown in Figure 4. A greater diversity of combination trials was observed in the PARPi space (Figure 4A). Specifically, among single DDA classes combined with PARPis, alkylating agents were the most frequently investigated in 38 combination-arm trials, followed by ICLs and topoisomerase inhibitors each in 17 combination-arm trials. Conversely, in the non-PARPi space (Figure 3B), ICLs (23 combination-arm trials) and topoisomerase inhibitors (15 combination-arm trials) were more extensively evaluated than alkylating agents (4 combination-arm trials). Alkylating agent combination arms represent 30% of PARPis combination-arm trials compared to 4% of non-PARPi combination arms. In contrast, ICLs were more frequently used in non-PARPi combination-arm trials (24%) than in PARPi combination-arm trials (13%). This indicates a distinct difference in combination strategies, where PARPi primarily combines with alkylating agents, whereas non-PARPi favors a combination with ICL agents.

221 DDAs-DDRis combination-arm clinical trials were distributed as follows: Phase 1 (117), phase 1/2 (49), phase 2 (52), with one in phase 2/3 and two in phase 3. PARPi combination-arm clinical trials were distributed as follows: Phase 1 (62), phase 1/2 (27), phase 2 (35), one in phase 2/3, and two in phase 3. Non-PARPi combination-arm clinical trials were predominantly distributed in Phase 1 (55), followed by phase 1/2 (22) and phase 2 (17), as shown in Figures 5A–D.

3.2 Clinical outcome scoring of selected DDAs-DDRis combination trials in PARPi and non-PARPi spaces

To assess the clinical outcomes of DDAs-DDRis combinations, 89 of the 221 identified combination-arm trials with interpretable

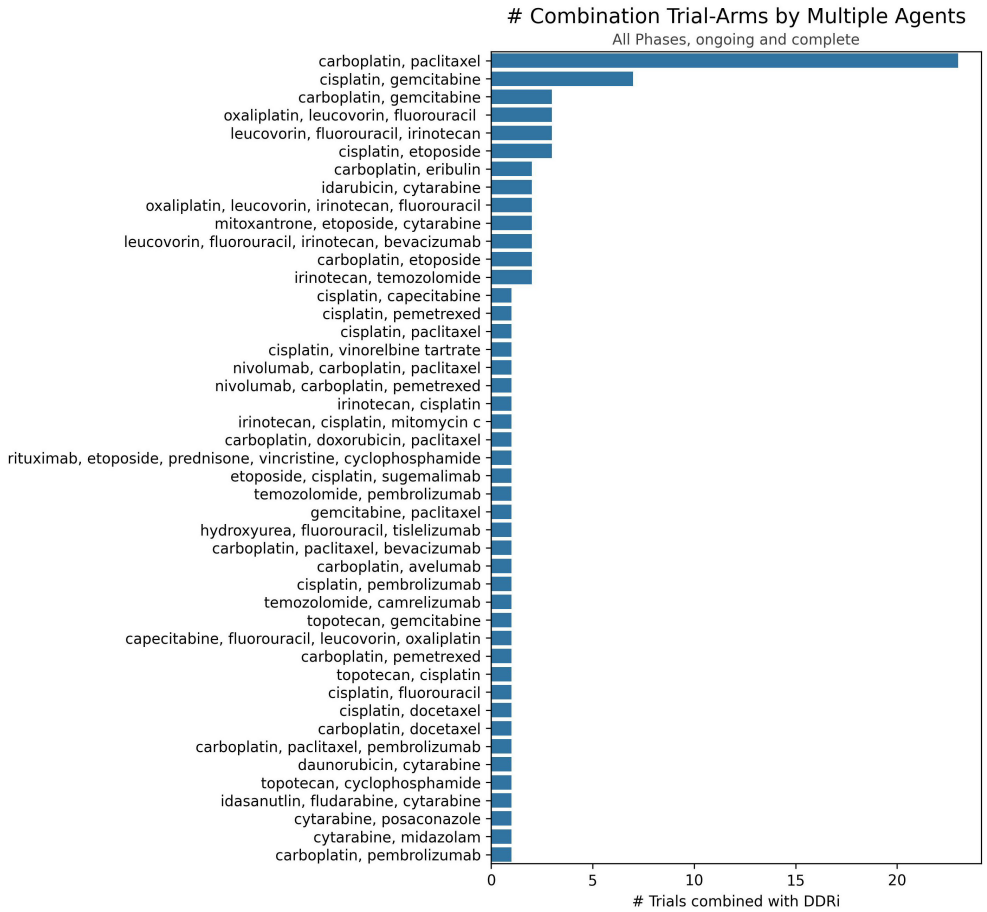

FIGURE 3
Number of trials investigating specific multiple-agent regimens in combination with DDRis. The x-axis represents the number of trials, and the y-axis lists the specific multiple-agent regimens.

outcomes were scored using a pre-defined scale (0, 0.5, 1, and 1.5; described in Methods) and listed in Supplementary Table S1. Zero scores indicate no efficacy or toxicity (failure); 0.5 indicates a positive response in a biomarker-selected population only; 1 indicates positive overall efficacy with no reported biomarker response; and 1.5 indicates both positive overall efficacy and a positive biomarker response. Table 2 presents the score distribution across PARPi and non-PARPi spaces. A comparison of PARP and non-PARP inhibitor trials (n=57 and n=32, respectively) reveals distinct outcome distributions. PARP inhibitor trials showed a higher proportion of failures (35.1% scoring 0) compared to non-PARP inhibitor trials (28.1% scoring 0). Conversely, non-PARP inhibitor trials exhibited a higher proportion of positive efficacy without a reported biomarker response (40.6% scoring 1) compared to PARP inhibitor trials (28.1% scoring 1). The proportion of trials showing both positive efficacy and a biomarker response (score 1.5) was relatively similar between the two classes (26.3% for PARP inhibitors and 25.0% for non-PARP inhibitors). PARP inhibitors also demonstrated a higher percentage of trials with positive biomarker response only (10.5% scoring 0.5) compared to non-PARP inhibitors (6.2%).

3.3 PARPis combinations: clinical trial outcomes with diverse DDAs

Of the initial 221 DDA-DDRi combination-arm trials, 127 in PARPi combination with DDAs and 57 had interpretable outcomes selected for further analysis and scored using pre-defined criteria (0, 0.5, 1, and 1.5, as described in methods). This analysis focused on eight PARPis, including five FDA approved drugs: olaparib (7), niraparib (8), rucaparib (9), talazoparib (10), and pamiparib (96) investigated in combination with DDAs (Supplementary Table S1, Figure 5). Supplementary Table S1 provides key highlights of these trials, including specific regimens, trial phases, overall outcomes, adverse effects, and the score`s distribution.

Among the FDA approved PARPi inhibitors, veliparib and olaparib are the most widely studied in combinations with DDAs (Figure 6A).

Multiple agents, including carboplatin with paclitaxel, demonstrated positive outcomes when tested in combination with three PARPis-olaparib, talazoparib, and veliparib (Figure 6A). Among the seven multiple-agent regimens combined with veliparib (as shown in Figure 6), six (85%) showed overall

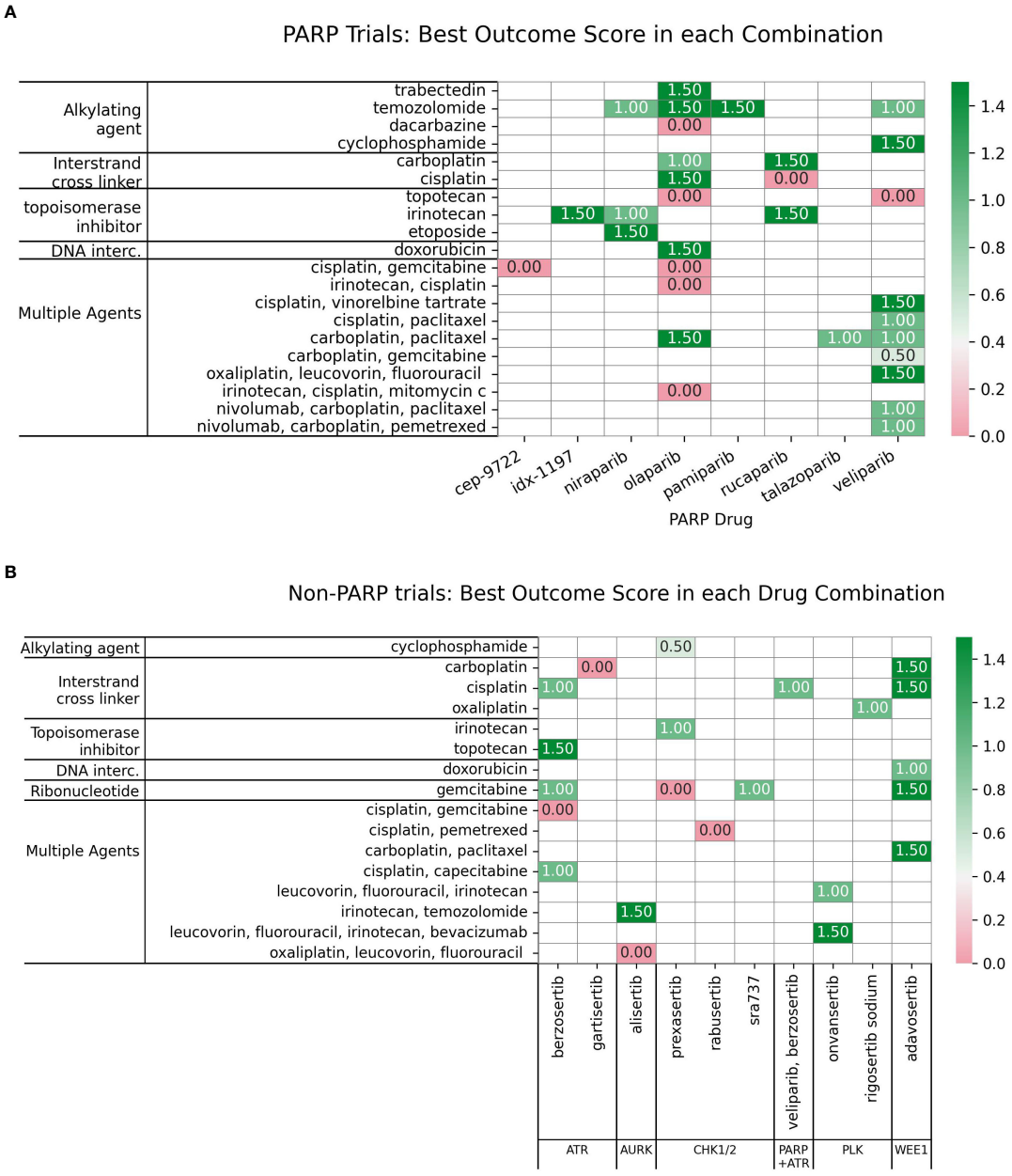

FIGURE 4
Number of trials distributed by clinical trial phase for each subclass of DDAs in combinations with **(A)** PARP inhibitors or **(B)** non-PARP DDR inhibitors. The x-axis represents the clinical trial phase, and the y-axis lists the number of combination-arm trials.

positive outcomes. Although the remaining regimen was not positive in the overall cohort, it did show efficacy in a biomarker-defined subpopulation. In trials investigating 22 PARPi-alkylating agent combinations and shown in Figure 6B, 45.5% (10 trials) showed no efficacy/toxicity (score 0). The remaining trials were evenly distributed across positive outcomes: 18.2% (4 trials each) demonstrated a biomarker-specific response (score 0.5), overall efficacy without biomarker information (score 1), and both overall efficacy and a positive biomarker response (score 1.5). This mixed outcome profile highlights the challenges and variability in achieving both efficacy and biomarker responses. While alkylating agents, particularly temozolomide (TMZ), showed promise in uterine leiomyosarcoma (uLMS) (31) and relapsed small cell lung carcinoma (SCLC) (97), not all combinations were successful (e.g., veliparib/cyclophosphamide in TNBC (98), and veliparib/TMZ in hepatocellular carcinoma (99). Dose-limiting toxicities, including myelosuppression, were also observed (100). Biomarker-driven approaches, such as ERCC1 expression in metastatic melanoma (101) and an 8-gene signature in sarcomas CDKN2A, PIK3R1, SLFN11, ATM, APEX2, BLM, XRCC2, MAD2L2 that may help predict better outcomes (102, 103), offer potential for tailoring therapies.

For PARPi-ICL combinations (n=6), the outcome distribution was: 3 trials (50%) scored 0, indicating failure/no efficacy/toxicity; 1

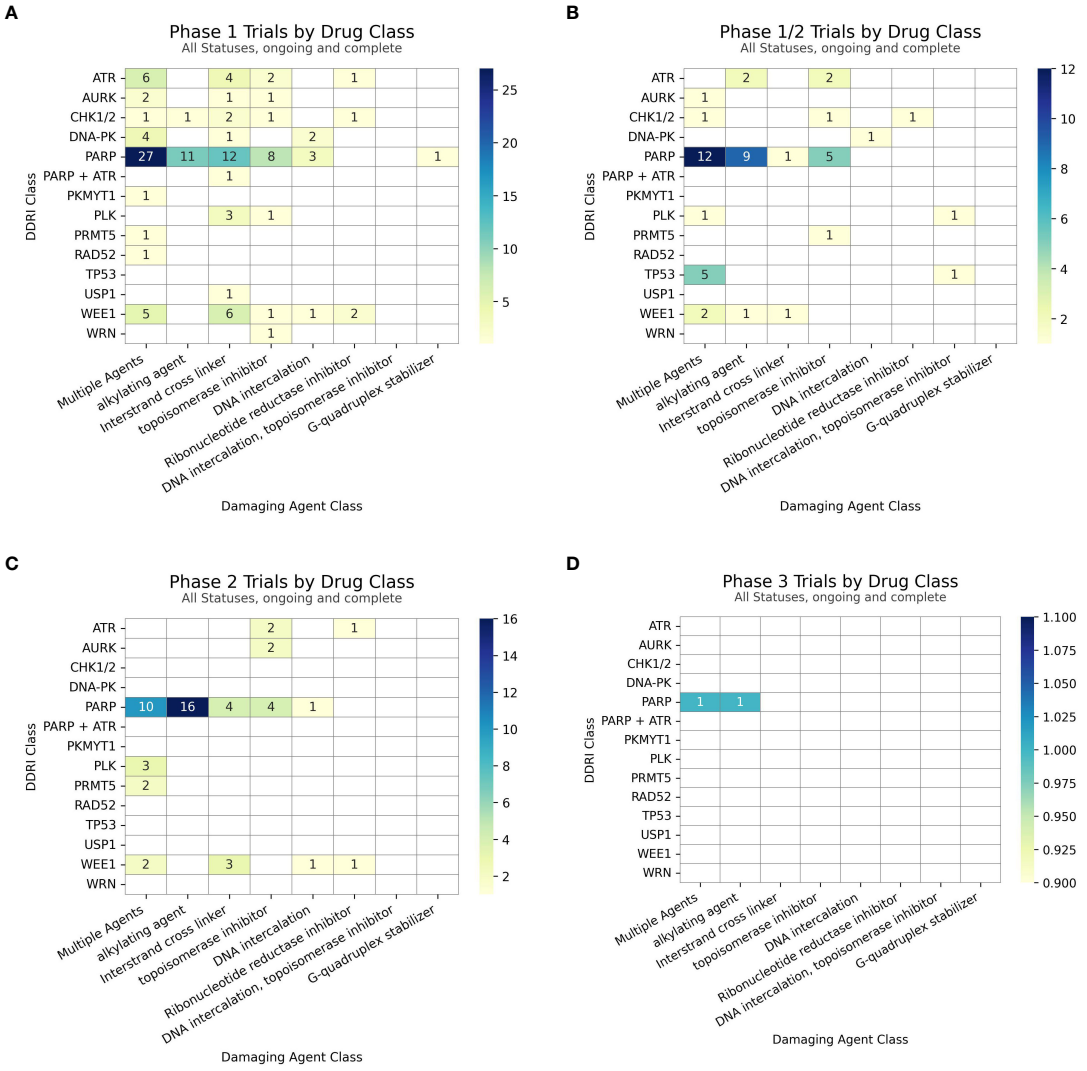

FIGURE 5
(A) Count of Phase 1 trial arms **(B)** Count of Phase 1/2 trial arms **(C)** Count of Phase 2 (inclusive of Phase 1/2) trial arms and **(D)** Count of Phase 3 trial arms with subtotals for combinations within each DDRi + DDA subclass.

TABLE 2 Distribution of scores across the PARP and non-PARP spaces.

DDRi Broad Class	Total number of trials	Number of trials by Outcome			
		Outcome Score			
		0	0.5	1.0	1.5
PARP Inhibitors	57	20	6	16	15
Non-PARP Inhibitors	32	9	2	13	8

The table summarizes the allocation of scores (0, 0.5, 1, and 1.5) for the outcomes of selected trials based on their classification within the PARP and non-PARP categories.

trial (16.7%) scored 1, reflecting positive overall efficacy without a reported biomarker response; and 2 trials (33.3%) scored 1.5, indicating both positive efficacy and a positive biomarker response (Figure 6B). Combinations of PARPi with ICL agents, such as platinum compounds, demonstrate synergy (104, 105), particularly in BRCA-mutated tumors, but overlapping myelotoxicity remains a significant challenge (Figure 7).

In contrast, PARPi-topoisomerase inhibitor combinations (n=6) showed a different profile: 2 trials (33.3%) scored 0; 1 trial (16.7%) scored 1; and 3 trials (50%) scored 1.5. This suggests a trend towards positive efficacy and biomarker responses, although failures were also observed (Figure 6B) Notably, BRCA mutation status has emerged as a key predictor of improved outcomes with these combinations. PARPi combinations with topoisomerase

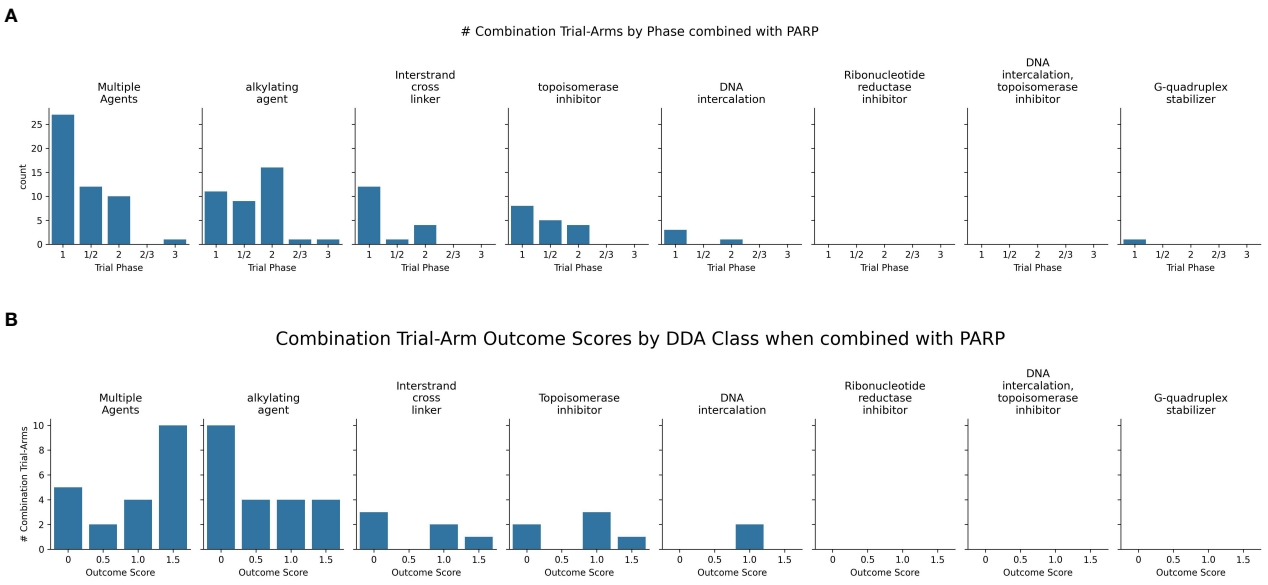

FIGURE 6
(A) Charts the highest combination trial-arm efficacy scores for PARPis combined with different DDA subclasses, illustrating which combinations have shown positive outcomes in at least one study. **(B)** Distribution of combination-arm trial's outcome scores by DDA subclasses for PARPis in combinations. The x-axis represents the specific outcome score, and the y-axis lists the number of combination-arm trials.

inhibitors (e.g., irinotecan, etoposide) have yielded mixed results, showing promise in some indications like platinum-resistant ovarian (106) and HRD-positive gastric cancers, especially with specific genetic mutations (107); however, significant hematological toxicities (108, 109) have also limited the development of certain combinations.

These results indicate distinct outcome profiles for different PARPi-DDA combinations. In contrast, PARPi-ICL combinations in this small sample show a mix of responses; PARPi-topoisomerase inhibitor combinations trend toward more positive efficacy and biomarker responses. PARPi-alkylating agent combinations show a more balanced distribution of positive and negative outcomes.

3.4 Non-PARPis combinations: clinical trial outcomes with diverse DDAs

Newer non-PARP DDRi targeting ATR, WEE1, and CHK1 also show promise in combination with DDAs (Supplementary Table S2, Figure 8).

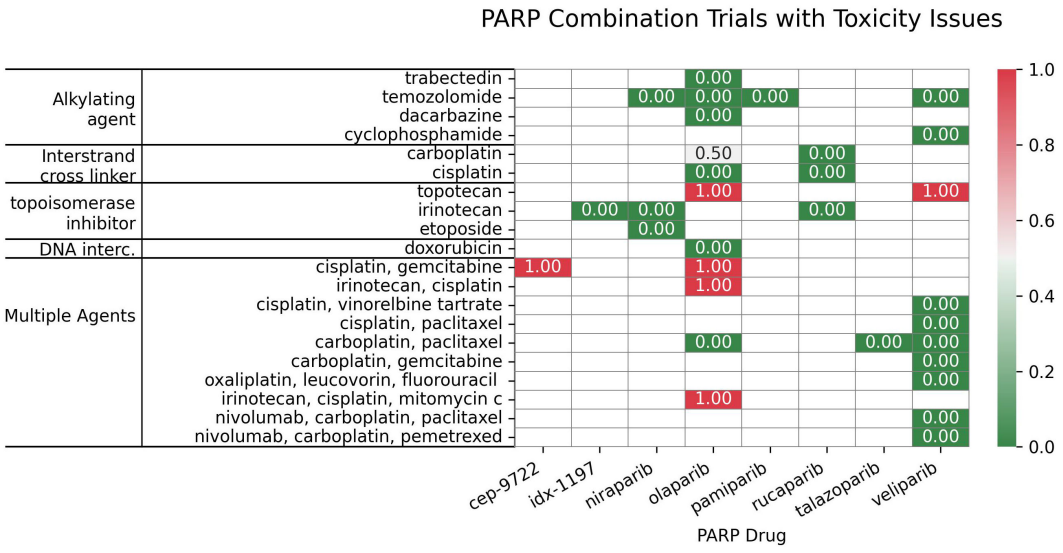

FIGURE 7
Distribution of the PARP inhibitors in combination with subclasses of DNA-damaging agents, categorized based on their toxicity scores.

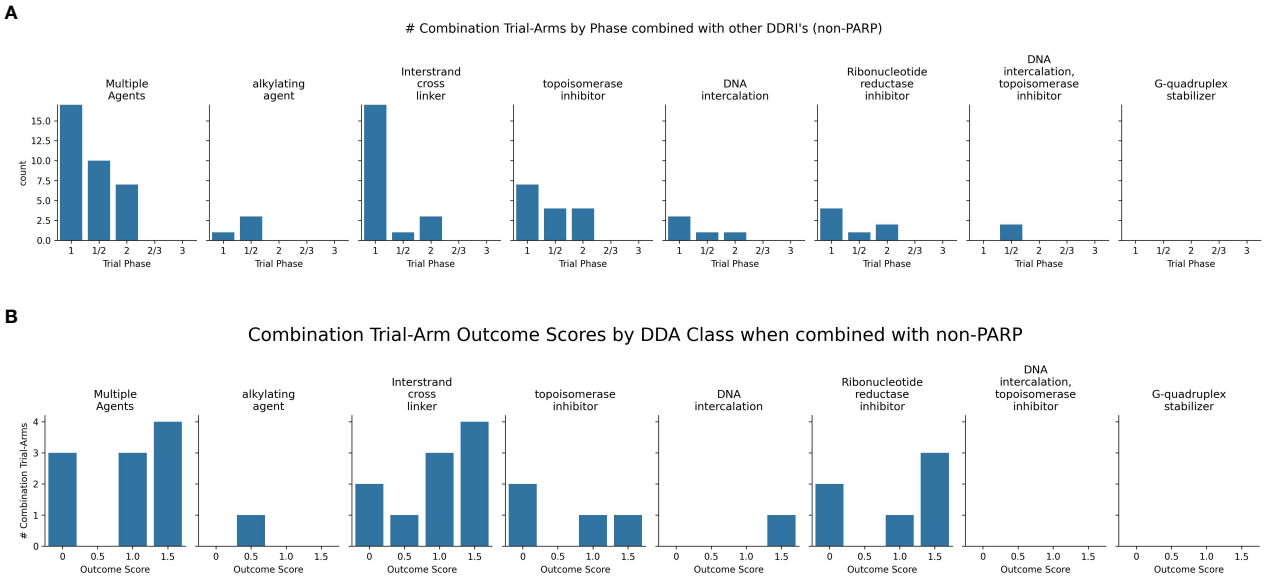

FIGURE 8
(A) Charts the highest combination trial-arm efficacy scores for non-PARPis combined with different DDA subclasses, illustrating which combinations have shown positive outcomes in at least one study. **(B)** Distribution of combination-arm trial's outcome scores by DDA subclasses for non-PARPis. The x-axis represents the specific outcome score, and the y-axis lists the number of combination-arm trials.

As shown in Figure 8B, non-PARPi combinations were evaluated more extensively with ICLs (n=10) than with alkylating agents (n=1). The one trial investigating alkylating agents combined with non-PARPis scored 0.5 (100%), indicating a positive biomarker response only. Among the ten ICL-NonPARPi combinations, 80% (8 trials) showed some level of positive outcome (scores 0.5, 1, or 1.5), with 40% (4 trials) demonstrating positive overall efficacy without biomarker information and 30% (3 trials) demonstrating both positive efficacy and a positive biomarker response. 20% (2 trials) showed no efficacy (score 0). For the four topoisomerase inhibitor combinations with non-PARPis, the distribution was: 2 trials (50%) scored 0; 1 trial (25%) scored 1; and one trial (25%) scored 1.5. These results suggest that ICL-NonPARPi combinations demonstrate a more varied response, with a mix of failures and positive efficacy outcomes. Topoisomerase-NonPARPi combinations show a mixed outcome profile, with 50% of trials showing no efficacy and 50% showing some positive outcome (score 1 or 1.5). Clinically, berzosertib (ATR inhibitor) has shown promise with topotecan in relapsed neuroendocrine cancers (110) and also improving outcomes with gemcitabine in platinum-resistant HGSOC (111) and Non-Small Cell Lung Cancer (NSCLC) with high TMB/LOH (112). The same trial showed a negative outcome score when used in combination with gemcitabine + cisplatin, which did not yield an established RP2D due to toxicity concerns (113). As revealed in Figure 8, WEE1 inhibitor adavosertib consistently achieved a score of 1.5 across 3 combination -arm trials when combined with ICL-inducing agents, demonstrating a potent synergistic interaction and suggesting a promising synthetic lethal strategy. Adavosertib demonstrated benefit in TP53-mutated patients with platinum agents or gemcitabine (114); specifically achieving a 43% overall response rate in platinum-resistant or refractory epithelial ovarian cancer when combined with carboplatin (115). Further details on these trials, including specific outcomes, can be found in Supplementary Table S2. These findings highlight the potential of non-PARP DDRis, mainly when combined with platinum-based chemotherapy and emphasize the importance of identifying genetic vulnerabilities like TP53 mutations.

4 Discussion

This analysis of DDRi combinations with DDAs reveals distinct outcome profiles depending on the specific DDRi class (PARP vs. non-PARP) and the DDA employed. While this review aimed to provide a comprehensive overview using a defined scoring system (0 for failure/no efficacy/toxicity to 1.5 for positive efficacy and biomarker response, as detailed in the Results section and summarized in Supplementary Tables S1, S2, Figures 6–8), the dynamic nature of this field and the focus on interpretable outcomes means that it may not be fully exhaustive of all published studies. Future research will provide additional insights.

For PARPi combinations, the outcome distribution varied considerably across DDA subclasses. In 22 PARPi-alkylating agent combination trials, a substantial proportion (45.5%, 10 trials) showed no efficacy/toxicity (score 0), highlighting a key challenge with this combination strategy. The remaining trials exhibited a more balanced distribution across positive outcomes, with similar proportions demonstrating a biomarker-specific response (score 0.5), overall efficacy without biomarker information (score 1), and combined efficacy and biomarker response (score 1.5), each at 18.2% (4 trials). This heterogeneity underscores the influence of tumor biology and emphasizes the need for careful patient selection. While specific

examples like olaparib/TMZ in uLMS (98) and SCLC (97) demonstrate promising efficacy, other combinations and tumor types did not show similar benefits, and dose-limiting toxicities were observed. This highlights the importance of biomarker-driven approaches, as exemplified by studies using ERCC1 expression (101) and 8-gene signatures (102, 103), to personalize treatment strategies.

In contrast, the limited data for PARPi-ICL combinations (n=6) revealed a distinct profile: (50%) showed no efficacy/toxicity (score 0), while 3 trials showed other positive outcome scores. This small sample size prevents definitive conclusions; however, it suggests that while synergy with platinum agents is theoretically sound (especially in BRCA-mutated tumors), clinical outcomes are not uniformly positive, and overlapping myelotoxicity remains a critical challenge. PARPi-topoisomerase inhibitor combinations (n=6) indicated a more promising trend, with a higher proportion of trials showing both positive efficacy and biomarker responses (50%, score 1.5), although failures were also observed (33.3%, score 0). This suggests that this combination strategy may be particularly promising in certain contexts, particularly in HRD-positive tumors. Furthermore, ongoing investigation of next-generation PARP1-selective inhibitors, e.g., NMS-03305293 (116) and AZD5305 (117), in combination with DDAs, aims to address toxicity and improve the therapeutic index.

Optimizing the delivery and tolerability of DNA-damaging agents can be a critical parallel strategy to enhancing their efficacy in combination with DDR inhibitors. Liposomal doxorubicin, for example, offers a more favorable pharmacokinetic profile and reduced cardiotoxicity, expanding its therapeutic window and making it a more suitable partner in regimens where cumulative cardiac risk is a limiting factor (118, 119). These advancements in formulation can help address the challenges of maximizing the therapeutic index of DNA-damaging agents for successful combination strategies with DDRis. In our analysis, all identified trials using doxorubicin in combination with DDRi employed a liposomal or pegylated liposomal formulation. Notably, the two PARP inhibitor trials—NCT03161132 (120, 121) and NCT00819221 (122)—demonstrated strong performance, receiving maximum scores of 1.5 for overall efficacy and biomarker relevance. Conventional doxorubicin was not studied in combination with DDRis. Nonetheless, these observations highlight the promise of novel formulation strategies to improve tolerability and expand the therapeutic potential of DDR-based combination therapies.

Non-PARPi combinations exhibited a different pattern. They were more extensively evaluated with ICLs (n=10) than alkylating agents (n=1), possibly reflecting a strategic focus on exploiting platinum-induced DNA damage. These ICL-NonPARPi combinations demonstrated promising activity, with the majority of trials (80%, 8 trials) showing some level of positive outcome. The distribution of these positive outcomes—40% (4 trials) demonstrating overall efficacy without biomarker information (score 1) and 30% (3 trials) demonstrating both efficacy and a positive biomarker response (score 1.5)—highlights the need for further investigation to understand the factors contributing to varied responses and to develop strategies for patient selection. The single trial evaluating alkylating-NonPARPi combinations prevents any meaningful conclusions. Topoisomerase-NonPARPi combinations (n=4) showed a mixed outcome profile, with 50% of trials showing no efficacy and 50% showing some positive outcome (score 1 or 1.5).

Comparing PARPi and non-PARP DDRi combinations, it is evident that different DDAs elicit distinct responses. While PARPi combinations show a more balanced distribution of outcomes across DDA subclasses (with the exception of the small ICL dataset), non-PARPi combinations appear to be more focused on ICLs, with a more varied range of responses. This highlights the importance of considering the specific DDR pathway targeted by the inhibitor and the type of DNA damage induced by the DDA when designing combination strategies. As the field evolves, refining these strategies and identifying new targets within the DDR network and combination agents is crucial. Advancing promising DDRi–DDA combinations will require further validation through large-scale clinical trials in well-defined patient populations, supported by the development of robust predictive biomarkers. Optimizing treatment sequencing and dosing will also be key to maximizing clinical benefits (2). Preclinical studies should continue elucidating synergistic mechanisms in diverse cancer models and investigating resistance mechanisms. Future research should focus on the rational selection of DDRi-DDA combinations based on tumor-specific DDR defects and explore multi-DDR targeting strategies to achieve deeper and more durable responses (123, 124). A data-driven approach with a higher level of automation could be highly beneficial for scientists and clinicians in determining and designing optimal combination trials.

Data availability statement

The original contributions presented in the study are included in the article/Supplementary Material. Further inquiries can be directed to the corresponding author.

Ethics statement

Ethical approval was not required for the study involving humans in accordance with the local legislation and institutional requirements. Written informed consent to participate in this study was not required from the participants or the participants' legal guardians/next of kin in accordance with the national legislation and the institutional requirements.

Author contributions

RF: Conceptualization, Data curation, Methodology, Project administration, Visualization, Writing – original draft, Writing – review & editing. NB: Conceptualization, Investigation, Methodology, Project administration, Supervision, Validation, Writing – original draft, Writing – review & editing. KB: Conceptualization, Supervision, Writing – review & editing. RE: Supervision, Writing –

review & editing. MC: Supervision, Writing – review & editing. PS: Funding acquisition, Supervision, Writing – review & editing.

Funding

The author(s) declare that financial support was received for the research and/or publication of this article. RF, NB, RE, MC, KB and PS have been salaried employees of or consultants to the pharmaceutical company Lantern Pharma Inc. ("Lantern"). MC and PS are officers of Lantern's subsidiary, Starlight Therapeutics Inc. The research reported on in this manuscript was funded by Lantern Pharma Inc. Employees, consultants and contractors of Lantern Pharma Inc. were involved in writing this article and in the design, collection, analysis, and interpretation of data reported on herein. The specific roles of these authors are articulated in the 'author contributions' section.

Conflict of interest

RF, NB, RE, MC, KB and PS have been salaried employees of or consultants to the pharmaceutical company Lantern Pharma Inc. ("Lantern"). MC and PS are officers of Lantern's subsidiary, Starlight Therapeutics Inc.

The remaining authors declare that the research was conducted in the absence of any commercial or financial relationships that could be construed as a potential conflict of interest.

This study received funding from Lantern Pharma Inc. Lantern Pharma Inc. was involved in the writing of this article, design, collection, analysis, and interpretation of data.

Generative AI statement

The author(s) declare that no Generative AI was used in the creation of this manuscript.

Publisher's note

Supplementary material

The Supplementary Material for this article can be found online at: https://www.frontiersin.org/articles/10.3389/fonc.2025.1577468/full#supplementary-material

SUPPLEMENTARY TABLE 1
This table summarizes DDAs- PARPi combination-arm trials, including study ID, drugs, cancer types, phase, status, efficacy, biomarkers, toxicity-related discontinuations, adverse effects, treatment regimens, and trial dates/enrollment and scores, as defined in the method section. Abbreviations: partial response (PR), dose-limiting toxicity (DLT), recommended phase 2 dose (RP2D), stable disease (SD), objective response rate (ORR), disease control rate (DCR), median progression-free survival (mPFS), overall survival (mOS), adverse events (AEs), complete response (CR), duration of response (DoR), twice daily (BID), maximum tolerated dose (MTD), pharmacokinetics (PK), small-cell lung cancer (SCLC), triple-negative breast cancer (TNBC), non-small-cell lung cancer (NSCLC), glioblastoma (GBM), and pancreatic ductal adenocarcinoma (PDAC).

SUPPLEMENTARY TABLE 2
This table summarizes DDAs-NonPARPi combination-arm trials, including study ID, drugs, cancer types, phase, status, efficacy, biomarkers, toxicity-related discontinuations, adverse effects, treatment regimens, and trial dates/enrollment and scores, as defined in the method section. Abbreviations: partial response (PR), dose-limiting toxicity (DLT), recommended phase 2 dose (RP2D), stable disease (SD), objective response rate (ORR), disease control rate (DCR), median progression-free survival (mPFS), overall survival (mOS), adverse events (AEs), complete response (CR), duration of response (DoR), twice daily (BID), maximum tolerated dose (MTD), pharmacokinetics (PK), small-cell lung cancer (SCLC), non-small-cell lung cancer (NSCLC), primary platinum-resistant ovarian cancer (PROC), extrapulmonary small cell neuroendocrine carcinoma (EP-SCNC).

SUPPLEMENTARY TABLE 3
A list of combination-arm clinical trials without outcomes.

References

1. Larsen BD, Benada J, Yung PYK, Bell RAV, Pappas G, Urban V, et al. Cancer cells use self-inflicted DNA breaks to evade growth limits imposed by genotoxic stress. *Science*. (2022) 376:476–83. doi: 10.1126/science.abi6378

2. O'Connor MJ. Targeting the DNA damage response in cancer. *Mol Cell*. (2015) 60:547–60. doi: 10.1016/j.molcel.2015.10.040

3. Lord CJ, Ashworth A. PARP inhibitors: Synthetic lethality in the clinic. *Science*. (2017) 355:1152–8. doi: 10.1126/science.aam7344

4. Goldstein M, Kastan MB. The DNA damage response: implications for tumor responses to radiation and chemotherapy. *Annu Rev Med*. (2015) 66:1–15. doi: 10.1146/annurev-med-081313-121208

5. Li Q, Qian W, Zhang Y, Hu L, Chen S, Xia Y. A new wave of innovations within the DNA damage response. *Signal Transduct Target Ther*. (2023) 8:338. doi: 10.1038/s41392-023-01548-8

6. Pearl LH, Schierz AC, Ward SE, Al-Lazikani B, Pearl FMG. Therapeutic opportunities within the DNA damage response. *Nat Rev Cancer*. (2015) 15:166–80. doi: 10.1038/nrc3891

7. Deeks ED. Olaparib: first global approval. *Drugs*. (2015) 75:231–40. doi: 10.1007/s40265-015-0345-6

8. Scott LJ. Niraparib: first global approval. *Drugs*. (2017) 77:1029–34. doi: 10.1007/s40265-017-0752-y

9. Syed YY. Rucaparib: first global approval. *Drugs*. (2017) 77:585–92. doi: 10.1007/s40265-017-0716-2

10. Hoy SM. Talazoparib: first global approval. *Drugs*. (2018) 78:1939–46. doi: 10.1007/s40265-018-1026-z

11. Lee A. Fuzuloparib: first approval. *Drugs*. (2021) 81:1221–6. doi: 10.1007/s40265-021-01541-x

12. Pilié PG, Tang C, Mills GB, Yap TA. State-of-the-art strategies for targeting the DNA damage response in cancer. *Nat Rev Clin Oncol*. (2019) 16:81–104. doi: 10.1038/s41571-018-0114-z

13. Cleary JM, Aguirre AJ, Shapiro GI, D'Andrea AD. Biomarker-guided development of DNA repair inhibitors. *Mol Cell*. (2020) 78:1070–85. doi: 10.1016/j.molcel.2020.04.035

14. Li H, Liu Z-Y, Wu N, Chen Y-C, Cheng Q, Wang J. PARP inhibitor resistance: the underlying mechanisms and clinical implications. *Mol Cancer*. (2020) 19:107. doi: 10.1186/s12943-020-01227-0

15. Helleday T, Petermann E, Lundin C, Hodgson B, Sharma RA. DNA repair pathways as targets for cancer therapy. *Nat Rev Cancer*. (2008) 8:193–204. doi: 10.1038/nrc2342

16. Smith AD, Roda D, Yap TA. Strategies for modern biomarker and drug development in oncology. *J Hematol Oncol*. (2014) 7:70. doi: 10.1186/s13045-014-0070-8

17. Helleday T, Lo J, van Gent DC, Engelward BP. DNA double-strand break repair: From mechanistic understanding to cancer treatment. *DNA Repair*. (2007) 6:923–35. doi: 10.1016/j.dnarep.2007.02.006

18. Lieber MR, Ma Y, Pannicke U, Schwarz K. Mechanism and regulation of human non-homologous DNA end-joining. *Nat Rev Mol Cell Biol*. (2003) 4:712–20. doi: 10.1038/nrm1202

19. McVey M, Lee SE. MMEJ repair of double-strand breaks (director's cut): deleted sequences and alternative endings. *Trends Genet*. (2008) 24:529–38. doi: 10.1016/j.tig.2008.08.007

20. Krokan H, Standal R, Slupphaug G. DNA glycosylases in the base excision repair of DNA. *Biochem J*. (1997) 325:1–16. doi: 10.1042/bj3250001

21. Shilkin ES, Boldinova EO, Stolyarenko AD, Goncharova RI, Chuprov-Netochin RN, Smal MP, et al. Translesion DNA synthesis and reinitiation of DNA synthesis in chemotherapy resistance. *Biochem (Mosc)*. (2020) 85:869–82. doi: 10.1134/s0006297920080039

22. Li G-M. Mechanisms and functions of DNA mismatch repair. *Cell Res*. (2008) 18:85–98. doi: 10.1038/cr.2007.115

23. Räschle M, Knipscheer P, Knipsheer P, Enoiu M, Angelov T, Sun J, et al. Mechanism of replication-coupled DNA interstrand crosslink repair. *Cell*. (2008) 134:969–80. doi: 10.1016/j.cell.2008.08.030

24. Sale JE, Lehmann AR, Woodgate R. Y-family DNA polymerases and their role in tolerance of cellular DNA damage. *Nat Rev Mol Cell Biol*. (2012) 13:141–52. doi: 10.1038/nrm3289

25. Wang M, Chen S, Ao D. Targeting DNA repair pathway in cancer: Mechanisms and clinical application. *MedComm*. (2021) 2:654–91. doi: 10.1002/mco2.103

26. Caracciolo D, Riillo C, Martino MTD, Tagliaferri P, Tassone P. Alternative non-homologous end-joining: error-prone DNA repair as cancer's Achilles' Heel. *Cancers*. (2021) 13:1392. doi: 10.3390/cancers13061392

27. Hashimoto S, Anai H, Hanada K. Mechanisms of interstrand DNA crosslink repair and human disorders. *Genes Environ*. (2016) 38:9. doi: 10.1186/s41021-016-0037-9

28. Lieber MR. The mechanism of human nonhomologous DNA end joining*. *J Biol Chem*. (2008) 283:1–5. doi: 10.1074/jbc.r700039200

29. Kusakabe M, Onishi Y, Tada H, Kurihara F, Kusao K, Furukawa M, et al. Mechanism and regulation of DNA damage recognition in nucleotide excision repair. *Genes Environ*. (2019) 41:2. doi: 10.1186/s41021-019-0119-6

30. Harrigan JA, Wilson DM, Prasad R, Opresko PL, Beck G, May A, et al. The Werner syndrome protein operates in base excision repair and cooperates with DNA polymerase β. *Nucleic Acids Res*. (2006) 34:745–54. doi: 10.1093/nar/gkj475

31. Sallmyr A, Rassool FV. Up-regulated WRN and DNA ligase IIIα Are involved in alternative NHEJ repair pathway of DNA double strand breaks (DSB) in chronic myeloid leukemia (CML). *Blood*. (2007) 110:1016. doi: 10.1182/blood.v110.11.1016.1016

32. Kummar S, Wade JL, Oza AM, Sullivan D, Chen AP, Gandara DR, et al. Randomized phase II trial of cyclophosphamide and the oral poly (ADP-ribose) polymerase inhibitor veliparib in patients with recurrent, advanced triple-negative breast cancer. *Invest N Drugs*. (2016) 34:355–63. doi: 10.1007/s10637-016-0335-x

33. Khan OA, Gore M, Lorigan P, Stone J, Greystoke A, Burke W, et al. A phase I study of the safety and tolerability of olaparib (AZD2281, KU0059436) and dacarbazine in patients with advanced solid tumours. *Br J Cancer*. (2011) 104:750–5. doi: 10.1038/bjc.2011.8

34. Foster JC, Freidlin B, Kunos CA, Korn EL. Single-arm phase II trials of combination therapies: A review of the CTEP experience 2008–2017. *JNCI: J Natl Cancer Inst*. (2020) 112:128–35. doi: 10.1093/jnci/djz193

35. Study Details | Veliparib and Temozolomide in Treating Patients With Recurrent Glioblastoma. ClinicalTrials.gov. Available at: https://clinicaltrials.gov/study/NCT01026493?term=NCT01026493&rank=1.

36. Cecchini M, Zhang JY, Wei W, Sklar J, Lacy J, Zhong M, et al. Quantitative DNA repair biomarkers and immune profiling for temozolomide and olaparib in metastatic colorectal cancer. *Cancer Res Commun*. (2023) 3:1132–9. doi: 10.1158/2767-9764.crc-23-0045

37. Su JM, Thompson PA, Adesina A, Li X-N, Kilburn LB, Onar-Thomas A, et al. A phase I clinical trial of veliparib and temozolomide in children with recurrent central nervous system tumors: A Pediatric Brain Tumor Consortium report. *J Clin Oncol*. (2013) 31:2036–6. doi: 10.1200/jco.2013.31.15_suppl.2036

38. Stradella A, Johnson M, Goel S, Park H, Lakhani N, Arkenau H, et al. Phase 1b study to assess the safety, tolerability, and clinical activity of pamiparib in combination with temozolomide in patients with locally advanced or metastatic solid tumors. *Cancer Med*. (2024) 13:e7385. doi: 10.1002/cam4.7385

39. Hussain M, Carducci MA, Slovin S, Cetnar J, Qian J, McKeegan EM, et al. Targeting DNA repair with combination veliparib (ABT-888) and temozolomide in patients with metastatic castration-resistant prostate cancer. *Invest N Drugs*. (2014) 32:904–12. doi: 10.1007/s10637-014-0099-0

40. Kummar S, Ji J, Morgan R, Lenz H-J, Puhalla SL, Belani CP, et al. A phase I study of veliparib in combination with metronomic cyclophosphamide in adults with refractory solid tumors and lymphomas. *Clin Cancer Res*. (2012) 18:1726–34. doi: 10.1158/1078-0432.ccr-11-2821

41. Pishvaian MJ, Slack RS, Jiang W, He AR, Hwang JJ, Hankin A, et al. A phase 2 study of the PARP inhibitor veliparib plus temozolomide in patients with heavily pretreated metastatic colorectal cancer. *Cancer*. (2018) 124:2337–46. doi: 10.1002/cncr.31309

42. Xu J, Keenan TE, Overmoyer B, Tung NM, Gelman RS, Habin K, et al. Phase II trial of veliparib and temozolomide in metastatic breast cancer patients with and without BRCA1/2 mutations. *Breast Cancer Res Treat*. (2021) 189:641–51. doi: 10.1007/s10549-021-06292-7

43. Halford SER, Cruickshank G, Dunn L, Erridge S, Godfrey L, Herbert C, et al. Results of the OPARATIC trial: A phase I dose escalation study of olaparib in combination with temozolomide (TMZ) in patients with relapsed glioblastoma (GBM). *J Clin Oncol*. (2017) 35:2022–2. doi: 10.1200/jco.2017.35.15_suppl.2022

44. Piotrowski A, Puduvalli V, Wen P, Campian J, Colman H, Pearlman M, et al. Actr-39. Pamiparib in combination with radiation therapy (rt) and/or temozolomide (tmz) in patients with newly diagnosed or recurrent/refractory (r/r) glioblastoma (gbm); phase 1b/2 study update. *Neuro-Oncol*. (2019) 21:vi21–2. doi: 10.1093/neuonc/noz175.081

45. Chugh R, Ballman KV, Helman LJ, Patel S, Whelan JS, Widemann B, et al. SARC025 arms 1 and 2: A phase 1 study of the poly(ADP-ribose) polymerase inhibitor niraparib with temozolomide or irinotecan in patients with advanced Ewing sarcoma. *Cancer*. (2021) 127:1301–10. doi: 10.1002/cncr.33349

46. Kurzrock R, Galanis E, Johnson DR, Kansra V, Wilcoxen K, Mcclure T, et al. A phase I study of niraparib in combination with temozolomide (TMZ) in patients with advanced cancer. *J Clin Oncol*. (2014) 32:2092–2. doi: 10.1200/jco.2014.32.15_suppl.2092

47. Heilig CE, Teleanu M, Bhatti IA, Richter S, Siveke JT, Wagner S, et al. Randomized phase II study of trabectedin/olaparib compared to physician's choice in subjects with previously treated advanced or recurrent solid tumors harboring DNA repair deficiencies (2022). Available online at: https://oncologypro.esmo.org/meeting-resources/esmo-congress-2022/randomized-phase-ii-study-of-trabectedin-olaparib-compared-to-physician-s-choice-in-subjects-with-previously-treated-advanced-or-recurrent-solid-tu (Accessed January 23, 2025).

48. van der Noll R, Jager A, Ang JE, Marchetti S, Mergui-Roelvink MWJ, Lolkema MP, et al. Phase I study of continuous olaparib capsule dosing in combination with carboplatin and/or paclitaxel (Part 1). *Invest N Drugs*. (2020) 38:1117–28. doi: 10.1007/s10637-019-00856-7

49. Forster M. ORCA-2: A phase I study of olaparib in addition to cisplatin-based concurrent chemoradiotherapy for patients with high risk locally advanced (LA) squamous cell carcinoma of the head and neck (HNSCC) (2021). Available online at: https://cslide.ctimeetingtech.com/esmo2021/attendee/confcal_4/presentation/list?q=866P (Accessed January 23, 2025).

50. Lee J-M, Hays JL, Chiou VL, Annunziata CM, Swisher EM, Harrell MI, et al. Phase I/Ib study of olaparib and carboplatin in women with triple negative breast cancer. *Oncotarget*. (2017) 8:79175–87. doi: 10.18632/oncotarget.16577

51. Miller K, Tong Y, Jones DR, Walsh T, Danso MA, Ma CX, et al. Cisplatin with or without rucaparib after preoperative chemotherapy in patients with triple negative breast cancer: Final efficacy results of Hoosier Oncology Group BRE09-146. *J Clin Oncol*. (2015) 33:1082–2. doi: 10.1200/jco.2015.33.15_suppl.1082

52. Wilson RH, Evans TJ, Middleton MR, Molife LR, Spicer J, Dieras V, et al. A phase I study of intravenous and oral rucaparib in combination with chemotherapy in patients with advanced solid tumours. *Br J Cancer*. (2017) 116:884–92. doi: 10.1038/bjc.2017.36

53. Balmaña J, Tung NM, Isakoff SJ, Graña B, Ryan PD, Saura C, et al. Phase I trial of olaparib in combination with cisplatin for the treatment of patients with advanced breast, ovarian and other solid tumors. *Ann Oncol*. (2014) 25:1656–63. doi: 10.1093/annonc/mdu187

54. Awada A, Campone M, Varga A, Aftimos P, Frenel J-S, Bahleda R, et al. An open-label, dose-escalation study to evaluate the safety and pharmacokinetics of CEP-9722 (a PARP-1 and PARP-2 inhibitor) in combination with gemcitabine and cisplatin in patients with advanced solid tumors. *Anti-Cancer Drugs*. (2016) 27:342–8. doi: 10.1097/cad.0000000000000336

55. Giaccone G, Rajan A, Kelly RJ, Gutierrez M, Kummar S, Yancey M, et al. A phase I combination study of olaparib (AZD2281; KU-0059436) and cisplatin (C) plus gemcitabine (G) in adults with solid tumors. *J Clin Oncol*. (2010) 28:3027–7. doi: 10.1200/jco.2010.28.15_suppl.3027

56. Stodtmann S, Eckert D, Joshi R, Nuthalapati S, Ratajczak CK, Menon R, et al. Exposure-response model with time-varying predictors to estimate the effects of veliparib in combination with carboplatin/paclitaxel and as monotherapy: Veliparib

phase 3 study in BRCA-mutated advanced breast cancer (BROCADE3) trial. *J Clin Pharmacol*. (2022) 62:1236–46. doi: 10.1002/jcph.2061

57. Yarchoan M, Myzak MC, Johnson BA, Jesus-Acosta AD, Le DT, Jaffee EM, et al. Olaparib in combination with irinotecan, cisplatin, and mitomycin C in patients with advanced pancreatic cancer. *Oncotarget*. (2017) 8:44073–81. doi: 10.18632/oncotarget.17237

58. Mego M, Svetlovska D, Reckova M, Kalavska K, Obertova J, Palacka P, et al. Phase II study of gemcitabine, carboplatin and veliparib in multiple relapsed/refractory germ cell tumors (GCTs). *J Clin Oncol*. (2021) 39:e17009. doi: 10.1200/jco.2021.39.15_suppl.e17009

59. Clarke JM, Patel JD, Robert F, Kio EA, Thara E, Camidge DR, et al. Veliparib and nivolumab in combination with platinum doublet chemotherapy in patients with metastatic or advanced non-small cell lung cancer: A phase 1 dose escalation study. *Lung Cancer*. (2021) 161:180–8. doi: 10.1016/j.lungcan.2021.09.004

60. Gray HJ, Bell-McGuinn K, Fleming GF, Cristea M, Xiong H, Sullivan D, et al. Phase I combination study of the PARP inhibitor veliparib plus carboplatin and gemcitabine in patients with advanced ovarian cancer and other solid Malignancies. *Gynecol Oncol*. (2018) 148:507–14. doi: 10.1016/j.ygyno.2017.12.029

61. Malhotra MK, Pahuja S, Kiesel BF, Appleman LJ, Ding F, Lin Y, et al. A phase 1 study of veliparib (ABT-888) plus weekly carboplatin and paclitaxel in advanced solid Malignancies, with an expansion cohort in triple negative breast cancer (TNBC) (ETCTN 8620). *Breast Cancer Res Treat*. (2023) 198:487–98. doi: 10.1007/s10549-023-06889-0

62. Turk AA, Leal T, Chan N, Wesolowski R, Spencer KR, Malhotra J, et al. NCI9782: A phase 1 study of talazoparib in combination with carboplatin and paclitaxel in patients with advanced solid tumors. *J Clin Oncol*. (2019) 37:e14640. doi: 10.1200/jco.2019.37.15_suppl.e14640

63. Han HS, Diéras V, Robson M, Palácová M, Marcom PK, Jager A, et al. Veliparib with temozolomide or carboplatin/paclitaxel versus placebo with carboplatin/paclitaxel in patients with BRCA1/2 locally recurrent/metastatic breast cancer: randomized phase II study. *Ann Oncol*. (2018) 29:154–61. doi: 10.1093/annonc/mdx505

64. Mizugaki H, Yamamoto N, Nokihara H, Fujiwara Y, Horinouchi H, Kanda S, et al. A phase 1 study evaluating the pharmacokinetics and preliminary efficacy of veliparib (ABT-888) in combination with carboplatin/paclitaxel in Japanese subjects with non-small cell lung cancer (NSCLC). *Cancer Chemother Pharmacol*. (2015) 76:1063–72. doi: 10.1007/s00280-015-2876-7

65. Oza AM, Cibula D, Benzaquen AO, Poole C, Mathijssen RHJ, Sonke GS, et al. Olaparib combined with chemotherapy for recurrent platinum-sensitive ovarian cancer: a randomised phase 2 trial. *Lancet Oncol*. (2015) 16:87–97. doi: 10.1016/s1470-2045(14)71135-0

66. Ramalingam SS, Blais N, Mazieres J, Reck M, Jones CM, Juhasz E, et al. Randomized, placebo-controlled, phase II study of veliparib in combination with carboplatin and paclitaxel for advanced/metastatic non–small cell lung cancer. *Clin Cancer Res*. (2017) 23:1937–44. doi: 10.1158/1078-0432.ccr-15-3069

67. Nishio S, Takekuma M, Takeuchi S, Kawano K, Tsuda N, Tasaki K, et al. Phase 1 study of veliparib with carboplatin and weekly paclitaxel in Japanese patients with newly diagnosed ovarian cancer. *Cancer Sci*. (2017) 108:2213–20. doi: 10.1111/cas.13381

68. Rivkin SE, Moon J, Iriarte DS, Bailey E, Sloan HL, Goodman GE, et al. Phase Ib with expansion study of olaparib plus weekly (Metronomic) carboplatin and paclitaxel in relapsed ovarian cancer patients. *Int J Gynecol Cancer*. (2019) 29:325–33. doi: 10.1136/ijgc-2018-000035

69. Pishvaian MJ, Wang H, Parenti S, He AR, Hwang JJ, Ley L, et al. Final report of a phase I/II study of veliparib (Vel) in combination with 5-FU and oxaliplatin (FOLFOX) in patients (pts) with metastatic pancreatic cancer (mPDAC). *J Clin Oncol*. (2019) 37:4015–5. doi: 10.1200/jco.2019.37.15_suppl.4015

70. Jelinek MJ, Foster NR, Zoroufy AJ, Souza JAD, Schwartz GK, Munster PN, et al. A phase I/II trial adding poly(ADP-ribose) polymerase (PARP) inhibitor veliparib to induction carboplatin-paclitaxel (Carbo-Tax) in patients with head and neck squamous cell carcinoma (HNSCC) Alliance A091101. *J Clin Oncol*. (2018) 36:6031–1. doi: 10.1200/jco.2018.36.15_suppl.6031

71. Rodler ET, Gralow J, Kurland BF, Griffin M, Yeh R, Thompson JA, et al. Phase I: Veliparib with cisplatin (CP) and vinorelbine (VNR) in advanced triple-negative breast cancer (TNBC) and/or BRCA mutation-associated breast cancer. *J Clin Oncol*. (2014) 32:2569–9. doi: 10.1200/jco.2014.32.15_suppl.2569

72. Thaker PH, Salani R, Brady WE, Lankes HA, Cohn DE, Mutch DG, et al. A phase I trial of paclitaxel, cisplatin, and veliparib in the treatment of persistent or recurrent carcinoma of the cervix: an NRG Oncology Study (NCT01281852). *Ann Oncol*. (2017) 28:505–11. doi: 10.1093/annonc/mdw635

73. Tsang ES, Dhawan MS, Pacaud R, Thomas S, Grabowsky J, Wilch L, et al. Synthetic lethality beyond BRCA: A phase I study of rucaparib and irinotecan in metastatic solid tumors with homologous recombination-deficiency mutations beyond BRCA1/2. *JCO Precis Oncol*. (2024) 8:e2300494. doi: 10.1200/po.23.00494

74. Gottardo NG, Endersby R, Billups C, Orr B, Hansford JR, Hassall T, et al. MDB-65. Results from the sj-eliot phase 1 clinical trial evaluating prexasertib (ly2606368) in combination with cyclophosphamide or gemcitabine for children and adolescents with refractory or recurrent medulloblastoma. *Neuro-Oncol*. (2024) 26:0–0. doi: 10.1093/neuonc/noae064.514

75. Moore KN, Chambers SK, Hamilton EP, Chen L, Oza AM, Ghamande SA, et al. Adavosertib with chemotherapy in patients with primary platinum-resistant ovarian, fallopian tube, or peritoneal cancer: an open-label, four-arm, phase II study. *Clin Cancer Res*. (2021) 28:158. doi: 10.1158/1078-0432.ccr-21-0158

76. Gonzalez-Ochoa E, Milosevic M, Corr B, Abbruzzese JL, Girda E, Miller RW, et al. A phase I study of the Wee1 kinase inhibitor adavosertib (AZD1775) in combination with chemoradiation in cervical, upper vaginal, and uterine cancers. *Int J Gynecol Cancer*. (2023) 33:1208–14. doi: 10.1136/ijgc-2023-004491

77. Burris HA, Berlin J, Arkenau T, Cote GM, Lolkema MP, Ferrer-Playan J, et al. A phase I study of ATR inhibitor gartisertib (M4344) as a single agent and in combination with carboplatin in patients with advanced solid tumours. *Br J Cancer*. (2024) 130:1131–40. doi: 10.1038/s41416-023-02436-2

78. Keenan TE, Li T, Vallius T, Guerriero JL, Tayob N, Kochupurakkal B, et al. Clinical efficacy and molecular response correlates of the WEE1 inhibitor adavosertib combined with cisplatin in patients with metastatic triple-negative breast cancer. *Clin Cancer Res*. (2021) 27:983–91. doi: 10.1158/1078-0432.ccr-20-3089

79. Mittra A, Coyne GHO, Do KT, Piha-Paul SA, Kummar S, Takebe N, et al. Safety and tolerability of veliparib, an oral PARP inhibitor, and M6620 (VX-970), an ATR inhibitor, in combination with cisplatin in patients with refractory solid tumors. *J Clin Oncol*. (2019) 37:3067–7. doi: 10.1200/jco.2019.37.15_suppl.3067

80. Ohnuma T, Holland JF, Goel S, Wilck E, Lehrer D, Ghalib MH, et al. Final results of a phase I dose-escalation study of ON 01910.Na in combination with oxaliplatin in patients with advanced solid tumors. *J Clin Oncol*. (2011) 29:e13584. doi: 10.1200/jco.2011.29.15_suppl.e13584

81. Shapiro GI, Wesolowski R, Devoe C, Lord S, Pollard J, Hendriks BS, et al. Phase 1 study of the ATR inhibitor berzosertib in combination with cisplatin in patients with advanced solid tumours. *Br J Cancer*. (2021) 125:520–7. doi: 10.1038/s41416-021-01406-w

82. Goff LW, Azad NS, Stein S, Whisenant JG, Koyama T, Vaishampayan U, et al. Phase I study combining the aurora kinase a inhibitor alisertib with mFOLFOX in gastrointestinal cancer. *Invest N Drugs*. (2019) 37:315–22. doi: 10.1007/s10637-018-0663-0

83. Dubois SG, Mosse YP, Fox E, Kudgus RA, Reid JM, McGovern R, et al. Phase 2 trial of alisertib in combination with irinotecan and temozolomide for patients with relapsed or refractory neuroblastoma. *Clin Cancer Res*. (2018) 24:1381. doi: 10.1158/1078-0432.ccr-18-1381

84. Pellini B, Li J, Schell MJ, Melendez M, Tanvetyanon T, Creelan BC, et al. A phase II trial of AZD1775 plus carboplatin-paclitaxel in squamous cell lung cancer (SqCLC). *J Clin Oncol*. (2024) 42:8545–5. doi: 10.1200/jco.2024.42.16_suppl.8545

85. Wehler T, Thomas M, Schumann C, Bosch-Barrera J, Segarra NV, Dickgreber NJ, et al. A randomized, phase 2 evaluation of the CHK1 inhibitor, LY2603618, administered in combination with pemetrexed and cisplatin in patients with advanced nonsquamous non-small cell lung cancer. *Lung Cancer*. (2017) 108:212–6. doi: 10.1016/j.lungcan.2017.03.001

86. Javed SR, Lord S, Badri SE, Harman R, Holmes J, Kamzi F, et al. CHARIOT: a phase I study of berzosertib with chemoradiotherapy in oesophageal and other solid cancers using time to event continual reassessment method. *Br J Cancer*. (2024) 130:467–75. doi: 10.1038/s41416-023-02542-1

87. Ahn DH, Barzi A, Ridinger M, Samuëlsz E, Subramanian RA, Croucher PJP, et al. Onvansertib in combination with FOLFIRI and bevacizumab in second-line treatment of KRAS-mutant metastatic colorectal cancer: A phase ib clinical study. *Clin Cancer Res*. (2024) 30:OF1–9. doi: 10.1158/1078-0432.ccr-23-3053

88. Conroy R. Onvansertib Yields Positive Activity in SCLC and Pancreatic Cancer (2023). Available online at: https://www.cancernetwork.com/view/onvansertib-yields-positive-activity-in-sclc-and-pancreatic-cancer (Accessed January 23, 2025).

89. Kato H, de Souza P, Kim S-W, Lickliter JD, Naito Y, Park K, et al. Safety, pharmacokinetics, and clinical activity of adavosertib in combination with chemotherapy in Asian patients with advanced solid tumors: phase ib study. *Target Oncol*. (2020) 15:75–84. doi: 10.1007/s11523-020-00701-5

90. Oza AM, Estevez-Diz M, Grischke E-M, Hall M, Marmé F, Provencher D, et al. A biomarker-enriched, randomized phase II trial of adavosertib (AZD1775) plus paclitaxel and carboplatin for women with platinum-sensitive TP53-mutant ovarian cancer. *Clin Cancer Res*. (2020) 26:4767–76. doi: 10.1158/1078-0432.ccr-20-0219

91. Jones R, Plummer R, Moreno V, Carter L, Roda D, Garralda E, et al. A phase I/II trial of oral SRA737 (a chk1 inhibitor) given in combination with low-dose gemcitabine in patients with advanced cancer. *Clin Cancer Res*. (2022) 29:331–40. doi: 10.1158/1078-0432.ccr-22-2074

92. Slotkin EK, Mauguen A, Ortiz MV, Cruz FSD, O'Donohue T, Kinnaman MD, et al. A phase I/II study of prexasertib in combination with irinotecan in patients with relapsed/refractory desmoplastic small round cell tumor and rhabdomyosarcoma. *J Clin Oncol*. (2022) 40:11503–3. doi: 10.1200/jco.2022.40.16_suppl.11503

93. Study Details | Berzosertib + Topotecan in Relapsed Platinum-Resistant Small-Cell Lung Cancer (DDRiver SCLC 250). ClinicalTrials.gov. Available at: https://clinicaltrials.gov/study/NCT04768296?cond=NCT04768296.

94. Merck Advances Development Programs in Oncology Focusing on Novel Mechanisms and Pathways | Business Wire (2022). Available online at: https://www.businesswire.com/news/home/20220602005775/en/Merck-Advances-Development-Programs-in-Oncology-Focusing-on-Novel-Mechanisms-and-Pathways (Accessed January 23, 2025).

95. Takahashi N, Hao Z, Villaruz LC, Zhang J, Ruiz J, Petty WJ, et al. Berzosertib plus topotecan vs topotecan alone in patients with relapsed small cell lung cancer. *JAMA Oncol*. (2023) 9:1669–77. doi: 10.1001/jamaoncol.2023.4025

96. Markham A. Pamiparib: first approval. *Drugs*. (2021) 81:1343–8. doi: 10.1007/s40265-021-01552-8

97. Meador CB, Digumarthy S, Yeap BY, Farago AF, Heist RS, Marcoux JP, et al. Phase I/II investigator-initiated study of olaparib and temozolomide in SCLC: Updated analysis and CNS outcomes. *J Clin Oncol*. (2022) 40:8565–5. doi: 10.1200/jco.2022.40.16_suppl.8565

98. Ingham M, Allred JB, Chen L, Das B, Kochupurakkal B, Gano K, et al. Phase II study of olaparib and temozolomide for advanced uterine leiomyosarcoma (NCI protocol 10250). *J Clin Oncol*. (2023) 41:4154–63. doi: 10.1200/jco.23.00402

99. Gabrielson A, Tesfaye AA, Marshall JL, Pishvaian MJ, Smaglo B, Jha R, et al. Phase II study of temozolomide and veliparib combination therapy for sorafenib-refractory advanced hepatocellular carcinoma. *Cancer Chemother Pharmacol*. (2015) 76:1073–9. doi: 10.1007/s00280-015-2852-2

100. Su JM, Thompson P, Adesina A, Li X-N, Kilburn L, Onar-Thomas A, et al. A phase I trial of veliparib (ABT-888) and temozolomide in children with recurrent CNS tumors: a Pediatric Brain Tumor Consortium report†. *Neuro-Oncol*. (2014) 16:1661–8. doi: 10.1093/neuonc/nou103

101. Middleton MR, Friedlander P, Hamid O, Daud A, Plummer R, Falotico N, et al. Randomized phase II study evaluating veliparib (ABT-888) with temozolomide in patients with metastatic melanoma. *Ann Oncol*. (2015) 26:2173–9. doi: 10.1093/annonc/mdv308

102. Grignani G, D'Ambrosio L, Pignochino Y, Palmerini E, Zucchetti M, Boccone P, et al. Trabectedin and olaparib in patients with advanced and non-resectable bone and soft-tissue sarcomas (TOMAS): an open-label, phase 1b study from the Italian Sarcoma Group. *Lancet Oncol*. (2018) 19:1360–71. doi: 10.1016/s1470-2045(18)30438-8

103. Merlini A, Centomo ML, Ferrero G, Chiabotto G, Miglio U, Berrino E, et al. DNA damage response and repair genes in advanced bone and soft tissue sarcomas: An 8-gene signature as a candidate predictive biomarker of response to trabectedin and olaparib combination. *Front Oncol*. (2022) 12:844250. doi: 10.3389/fonc.2022.844250

104. Perez J, Soto M, Quevedo C, Alonso C, Cepeda V, Fuertes M, et al. Poly(ADP-ribose) polymerase-1 inhibitor 3-aminobenzamide enhances apoptosis induction by platinum complexes in cisplatin-resistant tumor cells. *Med Chem*. (2006) 2:47–53. doi: 10.2174/157340606775197697

105. Matulonis UA, Monk BJ. PARP inhibitor and chemotherapy combination trials for the treatment of advanced Malignancies: does a development pathway forward exist? *Ann Oncol*. (2017) 28:443–7. doi: 10.1093/annonc/mdw697

106. Zhou H, Liu Q, Zhang D, Li Q, Cao D, Cheng N, et al. Efficacy and safety of an oral combination therapy of niraparib and etoposide in platinum resistant/refractory ovarian cancer: a single arm, prospective, phase II study. *Int J Gynecol Cancer*. (2024) 34:1761–7. doi: 10.1136/ijgc-2024-005386

107. Ryu M-H, Kim H-D, Oh D-Y, Lee K-W, Rha SY, Kim ST, et al. Association between homologous recombination deficiency (HRD) gene mutations and the efficacy of venadaparib in combination with irinotecan as third- or fourth-line treatment in patients with metastatic gastric cancer (mGC). *J Clin Oncol*. (2024) 42:e16057. doi: 10.1200/jco.2024.42.16_suppl.e16057

108. Samol J, Ranson M, Scott E, Macpherson E, Carmichael J, Thomas A, et al. Safety and tolerability of the poly(ADP-ribose) polymerase (PARP) inhibitor, olaparib (AZD2281) in combination with topotecan for the treatment of patients with advanced solid tumors: a phase I study. *Invest N Drugs*. (2012) 30:1493–500. doi: 10.1007/s10637-011-9682-9

109. Kummar S, Chen A, Ji J, Zhang Y, Reid JM, Ames M, et al. Phase I study of PARP inhibitor ABT-888 in combination with topotecan in adults with refractory solid tumors and lymphomas. *Cancer Res*. (2011) 71:5626–34. doi: 10.1158/0008-5472.can-11-1227

110. Takahashi N, Desai PA, Sciuto L, Nichols S, Steinberg SM, Thomas A. Targeting genomic instability in extrapulmonary small cell neuroendocrine cancers: A phase II study with ATR inhibitor berzosertib and topotecan. *J Clin Oncol*. (2022) 40:8518–8. doi: 10.1200/jco.2022.40.16_suppl.8518

111. Konstantinopoulos PA, Cheng S-C, Hendrickson AEW, Penson RT, Schumer ST, Doyle LA, et al. Berzosertib plus gemcitabine versus gemcitabine alone in platinum-resistant high-grade serous ovarian cancer: a multicentre, open-label, randomised, phase 2 trial. *Lancet Oncol*. (2020) 21:957–68. doi: 10.1016/s1470-2045(20)30180-7

112. Plummer R, Dean E, Arkenau H-T, Redfern C, Spira AI, Melear JM, et al. A phase 1b study evaluating the safety and preliminary efficacy of berzosertib in combination with gemcitabine in patients with advanced non-small cell lung cancer. *Lung Cancer*. (2022) 163:19–26. doi: 10.1016/j.lungcan.2021.11.011

113. Middleton MR, Dean E, Evans TRJ, Shapiro GI, Pollard J, Hendriks BS, et al. Phase 1 study of the ATR inhibitor berzosertib (formerly M6620, VX-970) combined with gemcitabine ± cisplatin in patients with advanced solid tumours. *Br J Cancer*. (2021) 125:510–9. doi: 10.1038/s41416-021-01405-x

114. Leijen S, van Geel RMJM, Pavlick AC, Tibes R, Rosen L, Razak ARA, et al. Phase I study evaluating WEE1 inhibitor AZD1775 as monotherapy and in combination with gemcitabine, cisplatin, or carboplatin in patients with advanced solid tumors. *J Clin Oncol*. (2016) 34:4371–80. doi: 10.1200/jco.2016.67.5991

115. Leijen S, van Geel RMJM, Sonke GS, de Jong D, Rosenberg EH, Marchetti S, et al. Phase II study of WEE1 inhibitor AZD1775 plus carboplatin in patients with TP53-mutated ovarian cancer refractory or resistant to first-line therapy within 3 months. *J Clin Oncol*. (2016) 34:4354–61. doi: 10.1200/jco.2016.67.5942

116. Montagnoli A, Rainoldi S, Ciavolella A, Ballinari D, Caprera F, Ceriani L, et al. Abstract 1223: NMS-P293, a novel potent and selective PARP-1 inhibitor with high antitumor efficacy and tolerability. *Cancer Res*. (2016) 76:1223–3. doi: 10.1158/1538-7445.am2016-1223

117. Illuzzi G, Staniszewska AD, Gill SJ, Pike A, McWilliams L, Critchlow SE, et al. Preclinical characterization of AZD5305, a next generation, highly selective PARP1 inhibitor and trapper. *Clin Cancer Res*. (2022) 28:4724–36. doi: 10.1158/1078-0432.ccr-22-0301

118. O'Brien MER, Wigler N, Inbar M, Rosso R, Grischke E, Santoro A, et al. Reduced cardiotoxicity and comparable efficacy in a phase IIItrial of pegylated liposomal doxorubicin HCl(CAELYXTM/Doxil®) versus conventional doxorubicin forfirst-line treatment of metastatic breast cancer. *Ann Oncol*. (2004) 15:440–9. doi: 10.1093/annonc/mdh097

119. Barenholz Y. Doxil® — The first FDA-approved nano-drug: Lessons learned. *J Control Release*. (2012) 160:117–34. doi: 10.1016/j.jconrel.2012.03.020

120. Perez-Fidalgo JA, Tavira B, Peña CJ, Guerra E, Martínez-Pretel JJ, García Y, et al. Role of the receptor for advanced glycation end products (RAGE) in blood as a potential biomarker for progression to olaparib: A *post hoc* analysis of patients with platinum-resistant ovarian cancer (PROC) treated in the ROLANDO-GEICO 1601 trial. *J Clin Oncol*. (2024) 42:5566–6. doi: 10.1200/jco.2024.42.16_suppl.5566

121. Perez-Fidalgo JA, Cortés A, Guerra E, García Y, Iglesias M, Sarmiento UB, et al. Olaparib in combination with pegylated liposomal doxorubicin for platinum-resistant ovarian cancer regardless of BRCA status: a GEICO phase II trial (ROLANDO study) ☆. *ESMO Open*. (2021) 6:100212. doi: 10.1016/j.esmoop.2021.100212

122. Conte GD, Sessa C, von Moos R, Viganò L, Digena T, Locatelli A, et al. Phase I study of olaparib in combination with liposomal doxorubicin in patients with advanced solid tumours. *Br J Cancer*. (2014) 111:651–9. doi: 10.1038/bjc.2014.345

123. Ohmoto A, Yachida S. Current status of poly(ADP-ribose) polymerase inhibitors and future directions. *OncoTargets Ther*. (2017) 10:5195–208. doi: 10.2147/ott.s139336

124. Zhang H, Kreis J, Schelhorn S-E, Dahmen H, Grombacher T, Zühlsdorf M, et al. Mapping combinatorial drug effects to DNA damage response kinase inhibitors. *Nat Commun*. (2023) 14:8310. doi: 10.1038/s41467-023-44108-y

frontiers | Frontiers in Pharmacology

TYPE Original Research
PUBLISHED 23 July 2025
DOI 10.3389/fphar.2025.1608832

OPEN ACCESS

EDITED BY
Xinyu Wang,
Philadelphia College of Osteopathic Medicine (PCOM), United States

REVIEWED BY
Sayed-Rzgar Hosseini,
Indiana State University, United States
Yanglan Gan,
Donghua University, China

*CORRESPONDENCE
Tiantian Li,
litiantian@jspgh.com
Ximei Luo,
luoximei@uestc.edu.cn

RECEIVED 09 April 2025
ACCEPTED 30 June 2025
PUBLISHED 23 July 2025

CITATION
Kang X, Liu X, Zou Q, Li T and Luo X (2025) CDFA: Calibrated deep feature aggregation for screening synergistic drug combinations. *Front. Pharmacol.* 16:1608832. doi: 10.3389/fphar.2025.1608832

CDFA: Calibrated deep feature aggregation for screening synergistic drug combinations

Xiaorui Kang[1], Xiaoyan Liu[2], Quan Zou[1,3], Tiantian Li[4]* and Ximei Luo[3,5]*

[1]Faculty of Applied Sciences, Macao Polytechnic University, Macau, China, [2]Faculty of Computing, Harbin Institute of Technology, Harbin, Heilongjiang, China, [3]Institute of Fundamental and Frontier Sciences, University of Electronic Science and Technology of China, Chengdu, Sichuan, China, [4]Editorial Office, Geriatric Hospital of Nanjing Medical University, Nanjing, Jiangsu, China, [5]Yangtze Delta Region Institute (Quzhou), University of Electronic Science and Technology of China, Quzhou, Zhejiang, China

Introduction: Drug combination therapy represents a promising strategy for addressing complex diseases, offering the potential for improved efficacy while mitigating safety concerns. However, conventional wet-lab experimentation for identifying optimal drug combinations is resource-intensive due to the vast combinatorial search space. To address this challenge, computational methods leveraging machine learning and deep learning have emerged to effectively navigate this space.

Methods: In this study, we introduce a Calibrated Deep Feature Aggregation (CDFA) framework for screening synergistic drug combinations. Concretely, CDFA utilizes a novel cell line representation based on the protein information and gene expression capturing complementary biological determinants of drug response. Besides, a novel feature aggregation network is proposed based on the Transformer to model the intricate interactions between drug pairs and cell lines through multi-head attention mechanisms, enabling discovery of non-linear synergy patterns. Furthermore, a method is introduced to quantify and calibrate the uncertainties associated with CDFA's predictions, enhancing the reliability of the identified synergistic drug combinations.

Results: Experiments results have demonstrated that CDFA outperforms existing state-of-the-art deep learning models.

Discussion: The superior performance of CDFA stems from its biologically informed cell line representation, its ability to capture complex non-linear drug-cell interactions via attention mechanisms, and its enhanced reliability through uncertainty calibration. This framework provides a robust computational tool for efficient and reliable drug combination screening.

KEYWORDS

drug combination, deep learning, feature fusion, transformer, synergistic drug

1 Introduction

Drug combination therapy has emerged as a mainstay in the clinical treatment of various cancers (Meng et al., 2023), including lung cancer (Nair et al., 2023; Cui et al., 2024), ovarian cancer (Kong et al., 2023), and pancreatic cancer (Jaaks et al., 2022). Compared with monotherapy, combination therapies often demonstrate enhanced efficacy, reduced drug resistance, and decreased toxicity. However, it is crucial to recognize that not all drug

combinations yield synergistic effects; in fact, some combinations may even exhibit antagonistic effects (Wang T. et al., 2023). For instance, the concomitant administration of antibiotics inhibiting DNA synthesis and those targeting protein synthesis can stimulate bacterial growth (Bollenbach et al., 2009). Therefore, the precise identification of synergistic drug pairs for specific cell types is essential to harness the full potential of combination therapy (Wang T. et al., 2022).

Traditional laboratory experiments to screen for synergistic drug combinations from the vast pharmacological space are often time-consuming and resource-intensive. Moreover, drug combination trials can sometimes result in side effects or harmful reactions in patients. With the growing availability of high-throughput screening data (Jiang et al., 2024; Liu et al., 2021), computational methods have emerged as efficient preclinical strategies for identifying synergistic drug combinations (Cao et al., 2024).

With the accumulation of data and the advancement of related technologies in recent decades, classical machine learning (ML)-based approaches and deep learning (DL) techniques have been employed to model drug combination trials, showing promising results by leveraging a variety of drug and cell line features. As drug combination effect prediction can be formulated as a regression or a multi-class classification task, the early ML-based methods often used the classical machine learning, such as logistic regression (LR) (H et al., 2014), support vector machine (SVM), random forests (RF) (Breiman, 2001), and extreme gradient boosting (XGboost). As early as 2014, Huang H et al. used a logistic regression model to systematically predict the drug combinations based on clinical side-effect (H et al., 2014). Pavel Sidorov et al. predicted Synergism of Cancer Drug Combinations by using NCI-ALMANAC Data based on RF and XGboost models (Sidorov et al., 2019). These methods laid the groundwork for more advanced approaches. Recently, deep learning (DL) models have shown excellent performance in bio-sequence analysis, gene regulation, and other areas, for extracting various data features and fusing heterogeneous data (Wang T. et al., 2024; Zhu et al., 2025). As the data about drugs continues to expand, most ML-based work has shifted towards deep learning (DL) models, driven by significant advancements in neural network architectures. One notable early DL model is DeepSynergy (Preuer et al., 2018), which integrates genomic data and drug information to identify drug combinations by a fully connected neural networks. Building on this foundation, newer DL models have emerged, leveraging advanced architectures like Transformers (Wang T. et al., 2024), Graph Neural Networks (GNNs) (Zhang et al., 2024), and Auto-Encoders (Zhu et al., 2025). For instance, CCSynergy (Hosseini and Zhou, 2023), GTextSy (Yan and Zheng, 2024), MMGCSyn (Zhang et al., 2025) and MatchMaker (Kuru et al., 2022) are integrated DNN with drug and cell line features. Based on Transformers models, DeepTraSynergy (Rafiei et al., 2023) and TranSynergy (Liu and Xie, 2021) were developed to learn drug representations and incorporate auxiliary knowledge through a novel neural network design. MRHGNN (Chen et al., 2025) and DeepDDS (Wang JX. et al., 2022) employ various GNNs to extract drug features by modeling drugs as graphs, capturing their structural properties. Moreover, recent research has introduced hypergraph neural networks to model complex relationships between cell lines and drug pairs (Wang W. et al., 2024; Liu et al., 2022).

In addition to neural network design, the fusion mechanism plays a crucial role in drug combination synergy prediction models. Recent studies have focused on effectively combining drug and cell line information to improve predictive accuracy. In parallel, advances in biological sequence classification have demonstrated the benefits of integrating multiple types of information. For instance, the SBSM-Pro model (Wang YZ. et al., 2024) introduces a novel multiple kernel learning strategy to combine sequence similarity measures, significantly enhancing classification performance. Similarly, DFFNDDS (Xu et al., 2023) employs two distinct neural networks to fuse drug features and cell line information from both bit-wise and vector-wise perspectives. DualSyn (Chen et al., 2024) introduces two modules to capture high-order and global information, enhancing the model's ability to understand complex interactions. SynergyX (Guo et al., 2024) utilizes mutual-attention and self-attention mechanisms to model drug-cell and drug-drug interactions, providing a more nuanced understanding of these relationships. CircRDRP (Wang Y. et al., 2024) uses a graph neural network model to predict the association of circRNA with drug resistance by combining disease context characteristics and deep learning techniques. MMSyn (Pang et al., 2024) and AttenSyn (Wang TS. et al., 2023) leverage attention mechanisms to integrate multiple drug and cell line features, allowing the model to focus on the most relevant aspects of the data. CLCDA (Wang YT. et al., 2023) is a collaborative deep learning-based model for predicting potential associations between circRNA and disease. Despite these significant contributions, many of these approaches still rely on late fusion mechanisms, where drug and cell line features are combined at a later stage in the model. This can limit the model's ability to fully capture the intricate interactions between drugs and cell lines. To address the limitations of late fusion mechanisms, this study proposes the Calibrated Deep Feature Aggregation (CDFA) framework–a Transformer-based architecture that enables early-stage integration of proteomic features and gene expression profiles to capture intricate drug-drug-cell interactions. The design incorporates dedicated uncertainty calibration to ensure probabilistic reliability. Experimental validation demonstrates CDFA's fusion efficacy: comprehensive testing across two benchmark datasets (spanning diverse cell lines and tissue types) confirms both the structural effectiveness and superior generalization of our approach.

2 Materials and methods

2.1 Synergy datasets

We assessed our method using two publicly available datasets: O'Neil (O'Neil et al., 2016) and NCI-ALMANAC (Holbeck et al., 2017). The O'Neil dataset comprised 23,062 drug combination samples involving 38 drugs and 39 human cancer cell lines. The NCI-ALMANAC dataset was relatively larger, containing 304,549 data points across 104 drugs and 60 cell lines. The synergy value for each sample is represented by the Loewe and combination scores for O'Neil and NCI-ALMANAC, respectively. The characteristics of the cell lines were represented by 651 gene expression values obtained from the COSMIC database (Forbes et al., 2015). Following established preprocessing steps (Liu et al., 2022), the final datasets included 18,950 and 74,139 drug-drug-cell line combinations for O'Neil and NCI-ALMANAC, respectively. Figure 1 depicts the distribution of synergy scores for both datasets. Notably, the left side of the distribution, centered around 30, constitutes more than half of the dataset. These values correspond to the negative pairs that exhibit either

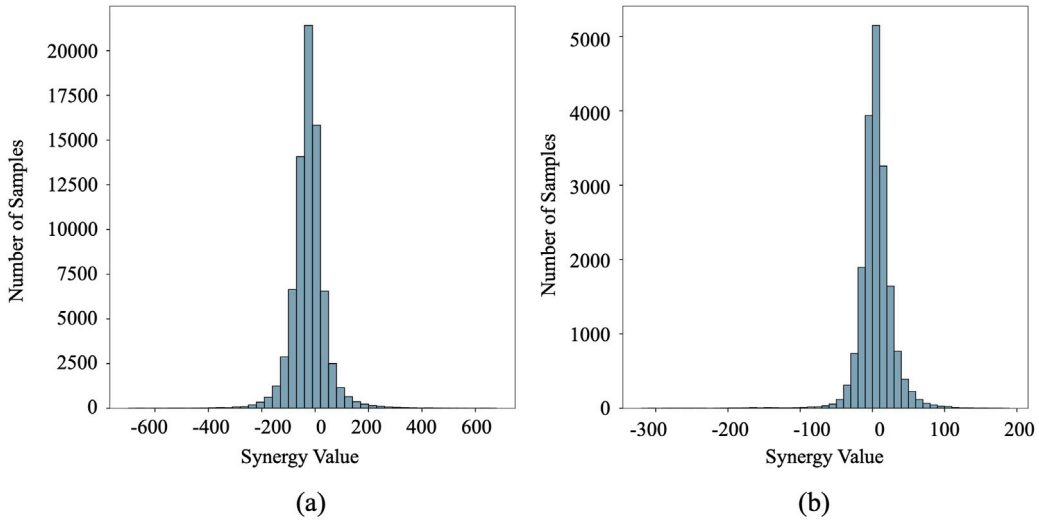

FIGURE 1
The distribution of synergy scores in the O'Neil and NCI-ALMANAC datasets. The vertical axis represents sample frequency counts, while the horizontal axis displays synergy scores. **(a)** O'Neil dataset. **(b)** NCI-ALMANAC dataset.

additive or antagonistic effects, indicating that a significant portion of the drug combinations do not show a synergistic benefit over the individual effects of the drugs. This observation underscores the complexity of identifying truly synergistic drug pairs and highlights the importance of systematic screening and computational approaches to optimize drug combination therapies.

To train and evaluate the model, we began by randomly selecting 90% of drug pairs and cell lines from each dataset to conduct three different experimental settings: random setting, cold cell line setting, and cold drug pair setting. The remaining 10% of the samples were set aside as an independent test set to evaluate generalization performance. For the random splitting setting, we divided the samples into five equal subsets. One subset served as the test set, while the remaining four were further split into training and validation sets in a 9:1 ratio. In the cold cell line setting, all the unique cell lines were divided into five equal groups randomly. The related samples which contain the cell line from one of these groups were used for testing, while the remaining samples were split into a 9:1 ratio as the training set and validation set. This ensured that the test set included only cell lines not present in the training set. For the cold drug pair setting, drug pairs were similarly partitioned into five equal groups. Four groups were used for training, with the test set containing only those drug pairs not seen during training. This ensured that the model was tested on an entirely new pair of drugs.

2.2 Problem formulation

In this study, we formulate the synergy prediction problem as a regression task. Let $X_{train} = \{d_1^i, d_2^i, c^i\}_{i-1}^N$ denote the set of the training samples where d_1^i, d_2^i denote the drug pair and c^i is the cell lines, and N denotes the number of training samples. Also, the corresponding synergy effect is represented by the label $Y_{train} = \{y^i\}_{i=1}^N$. The paper aims at learning a drug combination function $f(\cdot)$, given a drug pair and a cell line, $f(\cdot)$ can generate the target value $\hat{y}$.

2.3 Drug and cell line representations

A variety of molecular representations have been employed for drug combination prediction tasks. Fingerprints, such as ECFP and MHFP, are commonly used to encode compound structures. In this study, we adopted the MinHashed Atom-Pair fingerprint extended to four bonds (MAP4) as our molecular representation. MAP4 offers a versatile approach to representing diverse chemical structures.

Gene expression profiles have been commonly employed to represent cell lines in drug combination prediction tasks. In this study, we utilized gene expression data extracted from COSMIC, represented as 651-dimensional vectors (g), where each element corresponds to the expression level of a specific gene. In the most of the deep learning-based models treat the gene expression g as a vector which does not satisfy the biomedical meaning which each gene expression should be treated separately. In the bio-mechanism of drug synergy, only a part of genes contributes to the synergy effect. So, we treat the 651-dimensional vectors (g) as a matrix $H = \{h_j\}_{j=1}^{651} \in R^{1\times 651}$. In the following work, we use the CNN to extract the important genes to simulate the bio-mechanism.

2.4 Feature encoder

The weighted gene expression representation of a cell line is fed into a cell line feature encoder to learn abstract cell line representations. This encoder comprises three convolutional layers interleaved with pooling layers. The initial convolutional layer transforms the input into feature maps, which are subsequently downsampled using max-pooling. This process is repeated three times.

The MAP4 vector representing a drug is input into a drug feature encoder to extract high-level abstract features. The encoder consists of two fully connected (FC) layers followed by Gaussian Error Linear Units (GELU) (Hendrycks and Gimpel, 2016) and

batch normalization. The resulting features serve as essential inputs for subsequent fusion operations. The formulation of the drug feature encoder can be summarized as follows (Equation 1):

$$F_o^i = BN\left(GELU\left(FC^{1024}\left(BN\left(GELU\left(FC^{2048}\left(x_o^i\right)\right)\right)\right)\right)\right) \quad (1)$$

where x_o^i is one of the input features and F_o^i denotes the corresponding generated feature. BN represents 1day batch normalization. $FC^n(\cdot)$ represents an FC layer with n neurons. During the feature extraction stage, we project drug features and cell line feature into the same dimension to obtain higher-quality information for use in the subsequent modules.

We refer to these generated drug pair features as $(F_{d_1}, F_{d_2}) \in R^D$ and cell line feature as $F_c \in R^{L\times D}$.

2.5 Deep feature aggregation module

Given the drug pair features $(F_{d_1}, F_{d_2}) \in R^D$ and extracted feature of weight gene expression of cell line $F_c \in R^{L\times D}$, we first use a global max pooling operation to obtain the global cell line feature as $G_c \in R^D$. We treat the drug pair features and global cell line feature as whole global features $G = \{F_{d_1}, F_{d_2}, G_c\} \in R^{3\times D}$ and the F_c as the local cell line feature. The deep feature aggregation module can be decomposed into two parts: 1) global feature fusion, and 2) global to local feature fusion. Details are discussed as follows:

Global feature fusion: This process aims to integrate drug and early cell line features, followed by reinforcing the fused global features back into the local cell features. We employ a transformer encoder for global feature fusion. The core idea of the transformer encoder is the attention mechanism. An attention function maps queries (Q), keys (K), and values (V) to an output o as follows (Equation 2):

$$Attention(Q, K, V) = softmax\left(\frac{QK^T}{\sqrt{d}}\right)V \quad (2)$$

where $\sqrt{d}$ is the dimensionality of the query vector.

The multi-head attention mechanism consists of multiple attention heads, with each head conducting a linear transformation on the input vectors before performing the attention operation. Each attention head has its own set of trainable parameters, allowing it to potentially model an independent relationship between the input vectors. This is achieved by utilizing different parameters in the linear transformation step.

Then, for the h head, three weight matrices $W^{Qh}, W^{Kh}, W^{Vh} \in R_{d_f\times d_p}$ are used to project Q, K, and V, respectively, to a lower dimension d_p; then, an attention function is performed (Equation 3).

$$A^h = Attention\left(Q^h, K^h, V^h\right) \quad (3)$$

wherein $Q^h = QW^{Qh}, K^h = KW^{Kh}, V^h = VW^{Vh}$.

Then, the output of the multi-head attention mechanism is the linear transformation of the concatenation of the output vectors acquired from the attention heads (Equation 4):

$$MultiHead(Q, K, V) = Concat\left(A^1, A^2, \cdots, A^H\right)W^O \quad (4)$$

where H is the number of heads and W^O is a trainable weight matrix.

Besides the attention mechanism, the transformer encoder also contains the residual and feed-forward neural network. Formally, the global feature fusion can be defined as follows (Equation 5):

$$A_G = LN(G + MultiHead(G, G, G))$$
$$F_G = LN(A_G + FFN(A_G)) \quad (5)$$

where $LN(\cdot)$ and $FFN(\cdot)$ represent layer normalization and feed-forward neural network, respectively.

Global to local cell line feature fusion: Inspired by recent findings that drugs can influence the synergistic or antagonistic effects of drug combinations through modulating key gene expression (Wu et al., 2023), we incorporate a global-to-local cell line feature fusion network to simulate drug-induced gene regulation effects. The local cell line feature is enhanced through multi-head attention where global features (F_G)are incorporated using a Transformer decoder. This enables adaptive re-weighting of gene expressions based on cross-tissue biological patterns, with layer normalization and residual connections stabilizing feature refinement. This process can be mathematically expressed as follows (Equation 6):

$$F_G = LN(F_c + \text{MultiHead}(F_c, F_c, F_c))$$
$$C_G = LN(F_c + \text{MultiHead}(F_c, F_G, F_G))$$
$$F_c = LN(C_c + FFN(C_c)) \quad (6)$$

2.6 Synergy prediction module

The final synergy value of a drug combination is predicted using the output of the global feature fusion network (F_G) and the global-to-local cell line feature fusion network (F_c). Specifically, F_G is flattened into a 1D vector, and global max pooling is applied to F_c to obtain another 1D vector. These vectors are then fed into separate multi-layer fully connected layers to refine their abstract features. Finally, the refined features are concatenated and passed through a final FC layer to predict the synergy value $\hat{y}$.

Given a training dataset, that contains N samples with ground-truth synergy scores y and the corresponding values $\hat{y}$ predicted by our method, we can train the deep learning model in an end-to-end fashion using the mean squared error (MSE) loss as the loss function.

2.7 Uncertainty quantification

We use an ensemble method to further enhance generalization and quantify the uncertainty of the CDFA. Specifically, we trained M distinct model replicas. Each replica shares the same neural network architecture and settings but uses a different initial random seed for parameter initialization. This ensures that while the models are structurally identical, they develop unique parameter values during training, leading to diverse predictions and a more robust uncertainty estimation. For every input drug combination, each model generates a predicted synergy value,

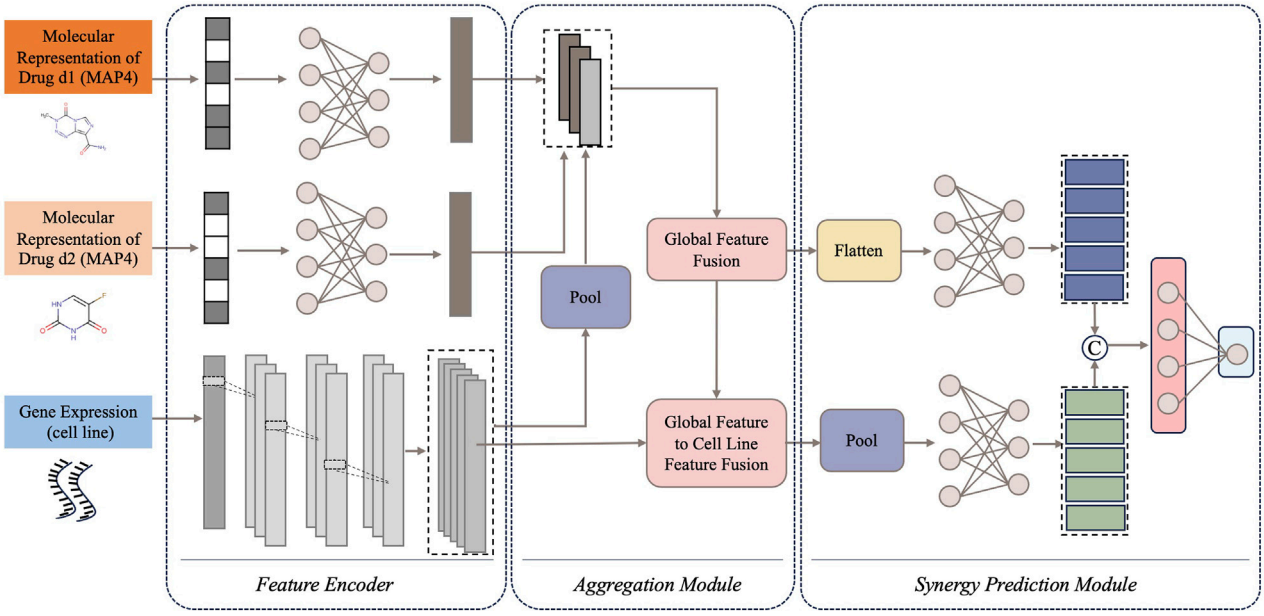

FIGURE 2
The overview network of CDFA. Data flows sequentially from input to output through three core components: (1) feature encoders for drug pairs and cell lines, (2) feature aggregation module, and (3) synergy prediction module.

denoted as $\hat{y}_k^{(d_1^i, d_2^i, c^i)}$. The final synergy prediction, $\mu(d_1^i, d_2^i, c^i)$, is determined by averaging these individual predictions. Meanwhile, the uncertainty associated with this prediction, $\sigma(d_1^i, d_2^i, c^i)$, is quantified by calculating the standard deviation of the individual predictions from the ensemble.

2.8 Uncertainty recalibration

Calibration errors (Mervin et al., 2021) in probability estimates compromise reliability by creating discrepancies between predicted and true probabilities. Specifically, they refer to the discrepancy between the model's predicted confidence and the actual observed frequency of correctness at that confidence level. For example, if a model assigns 80% confidence to a set of predictions, but only 70% of them are correct, this indicates a calibration error in that confidence range. Such miscalibration reduces the effectiveness of uncertainty estimates as indicators of trustworthiness in predictions.

To address this issue, a common strategy is to learn a recalibration function that adjusts the predicted uncertainties to better align with the true underlying probabilities. The recalibration function is often a non-linear uncertainty scaling function, learned using a hold-out validation dataset to create a calibration map, and is often assessed using metrics like Expected Calibration Error (ECE). In our method, we adopt a simple yet effective single-parameter scaling approach that adjusts only the uncertainty component $\boldsymbol{\sigma}(\cdot)$. We achieve this by multiplying $\boldsymbol{\sigma}(\cdot)$ with a scaling factor $\boldsymbol{r}$, while keeping the predicted synergy value $\boldsymbol{\mu}(\cdot)$ unchanged. This choice is motivated by the fact that $\boldsymbol{\mu}(\cdot)$, as the model's point estimate, already captures the optimal synergy prediction and should not be altered during post-hoc calibration. Instead, we rescale $\boldsymbol{\sigma}(\cdot)$ by a positive scalar factor $\boldsymbol{r}$, resulting in the recalibrated output $\boldsymbol{\mu}(\cdot), \boldsymbol{r\sigma}(\cdot)$. The scaling factor r is optimized using Brent's method (Brent, 1971) to ensure that the recalibrated uncertainties accurately reflect the true probability of correctness. The objective is to minimize the miscalibration, quantified by ECE, on a separate validation set. This optimization ensures that the adjusted uncertainties more accurately reflect the true likelihood of correct predictions across confidence levels. The result is an uncertainty estimate that is better aligned with the model's empirical behavior and more trustworthy for downstream decision-making.

3 Results

3.1 Overview of the CDFA framework

CDFA is an ensemble deep learning framework for predicting the potential synergy effects of drug combinations based on the drugs' molecular information and the cells' gene expression. The overall architecture of CDFA is shown in Figure 2. It consists of three main components: the feature encoders for the drug pair and cell line, the feature aggregation module, and the synergy prediction module. First, MAP4 is used to represent diverse chemical structures of the paired drugs. Gene expression profiles are employed to represent cell lines in drug combination prediction tasks. Then, feature encoders are used to extract these three types of features separately. A novel feature aggregation network is involved based on the Transformer which tries to capture the intricate interactions between drug pairs and cell lines. Finally, the aggregated features are connected to another synergy prediction module. The subsequent sections of this section provide detailed evidence of the superiority of this computational framework.

TABLE 1 Performance comparison on the O'Neil dataset. Bold values indicate the best performance.

	Randon split			Cold cell line setting			Cold drug pair setting		
	RMSE	R2	PCC	RMSE	R2	PCC	RMSE	R2	PCC
CDFA	**13.522**	**0.651**	**0.808**	19.597	0.25	0.53	**15.976**	**0.511**	**0.717**
PermuteDDS	13.721	0.641	0.801	19.668	0.243	0.522	16.152	0.501	0.709
HypergraphSynergy	14.727	0.586	0.775	**19.537**	**0.252**	0.533	17.346	0.42	0.656
DeepSynergy	14.87	0.584	0.765	23.89	0.195	0.426	17.28	0.433	0.663
ComboFM	16.86	0.451	0.702	20.82	0.142	0.396	18.62	0.376	0.635
DTF	14.73	0.594	0.775	21.11	0.132	**0.535**	17.37	0.429	0.671
Celebi's method	16.34	0.5	0.708	20.6	0.179	0.473	19.1	0.309	0.572
MatchMaker	17.4948	0.4162	0.6466	28.5376	−0.7616	0.3628	17.7172	0.399	0.6332
GTextSyn	16.231	0.497	0.709	20.866	0.144	0.457	18.186	0.367	0.625
MMGCSyn	17.138	0.439	0.69	25.754	−0.342	0.316	18.837	0.317	0.605

TABLE 2 Performance comparison on the NCI-ALMANAC dataset. Bold values indicate the best performance.

	Randon split			Cold cell line setting			Cold drug pair setting		
	RMSE	R2	PCC	RMSE	R2	PCC	RMSE	R2	PCC
CDFA	**41.893**	**0.552**	**0.746**	53.819	0.259	0.536	**50.522**	0.346	**0.593**
PermuteDDS	43.053	0.527	0.726	54.128	0.242	0.519	51.58	0.318	0.569
HypergraphSynergy	43.89	0.508	0.719	**53.398**	0.273	**0.538**	52.609	0.291	0.543
DeepSynergy	44.44	0.491	0.701	54.56	0.23	0.322	53.5	0.262	0.526
ComboFM	48.27	0.399	0.651	54.67	0.245	0.531	53.89	0.267	0.526
DTF	47.03	0.43	0.678	54.73	0.223	0.517	53.47	0.263	0.531
Celebi's method	47.31	0.423	0.653	53.49	0.259	0.516	55.83	0.196	0.456
MatchMaker	51.7316	0.3168	0.5642	64.6824	**0.3644**	−0.0652	55.7034	0.2028	0.4588
GTextSyn	47.425	0.426	0.657	56.369	0.187	0.479	55.511	0.208	0.483
MMGCSyn	47.793	0.417	0.659	60.353	0.067	0.454	54.523	**0.519**	0.236

3.2 Comparison with existing models

To evaluate CDFA's performance, we compared it with nine existing drug combination synergy prediction models: HypergraphSynergy, DeepSynergy, DTF, CombFM, Celebi's method, PermuteDDS, MatchMaker, GTextSyn and MMGCSyn. We employed three common regression evaluation metrics to assess the performance of these methods: root mean squared error (RMSE), coefficient of determination (R^2), and Pearson's Correlation Coefficient (PCC).

As Table 1 shows, we compared CDFA's performance with several models using the O'Neil dataset across three different experimental setups. In the random split scenario, where data is divided without specific constraints, the CDFA model outshone others with the lowest RMSE at 13.522, alongside the highest R^2 at 0.651 and PCC at 0.808. When tested on unseen cell lines (cold cell line setting), HypergraphSynergy led with the highest R^2 of 0.252 and the lowest RMSE of 19.537. However, CDFA maintained a competitive edge despite not leading in every metric. For the cold drug pair setting, where models predict outcomes for drug combinations not encountered during training, CDFA performed exceptionally well, achieving the lowest RMSE (15.976), highest R^2 (0.511), and a PCC of 0.717, demonstrating its strength in handling unseen drug pairs.

As shown in Table 2, the consistent superiority of CDFA has also been demonstrated on the NCI-ALMANAC dataset. In the random split setup, CDFA exhibited the best performance with the lowest RMSE of 41.893, highest R^2 of 0.552, and highest PCC of 0.746. Under the cold cell line condition, HypergraphSynergy performed best with an RMSE of 53.398, R^2 of 0.273, and PCC of 0.538. In the cold drug pair scenario, CDFA once again stood out, achieving the lowest RMSE (50.522), sub-optimal R^2 (0.346), and highest PCC (0.593), underscoring its effectiveness in predicting responses for novel drug combinations.

TABLE 3 Performance comparison on the independent test datasets. Bold values indicate the best performance.

	Randon split			Cold cell line setting		
	RMSE	R2	PCC	RMSE	R2	PCC
CDFA	**15.111**	**0.660**	0.818	**42.307**	**0.508**	**0.713**
PermuteDDS	15.144	0.659	**0.821**	43.338	0.484	0.696
HypergraphSynergy	16.710	0.585	0.788	43.730	0.474	0.693
DeepSynergy	16.840	0.578	0.765	45.325	0.435	0.670
ComboFM	16.080	0.541	0.754	46.370	0.457	0.685
DTF	16.150	0.548	0.752	49.860	0.372	0.700
Celebi's method	16.500	0.529	0.728	45.860	0.469	0.688
MatchMaker	20.725	0.361	0.6466	51.259	0.2778	0.5282
GTextSyn	18.931	0.466	0.686	48.026	0.366	0.612
MMGCSyn	19.834	0.412	0.647	48.312	0.358	0.619

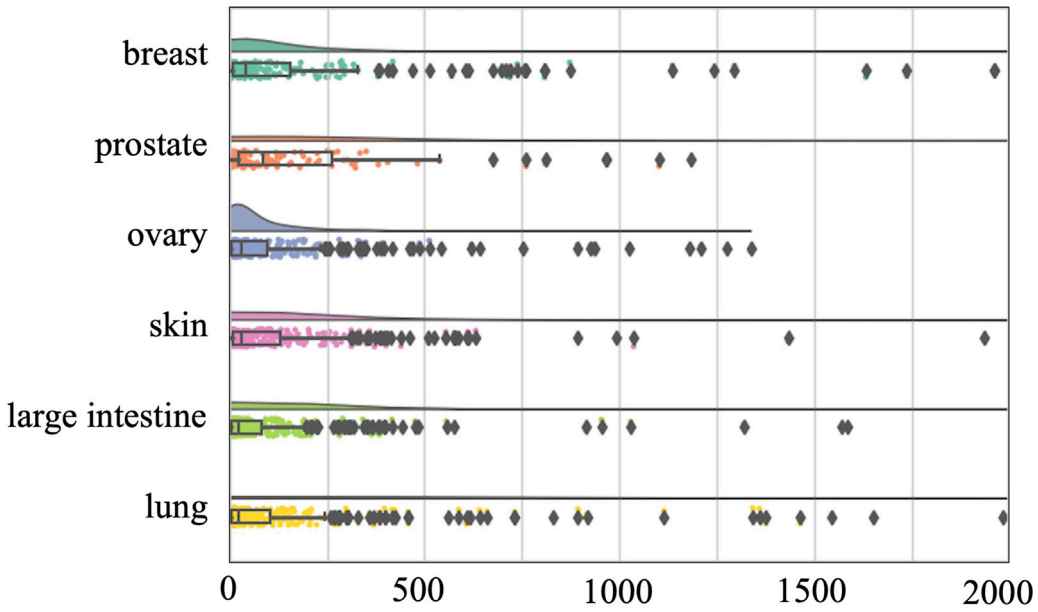

FIGURE 3
Raincloud plots of MSE for O'Neil independent test dataset. The horizontal axis quantifies mean squared error (MSE) between true synergy scores and model predictions.

The 10% of the samples of the O'Neil and NCI-ALMANAC datasets were set aside as an independent test set to evaluate these models' generalization performance. In the independent test data section of the O'Neil and NCI-ALMANAC datasets, the superior performance of CDFA has been once again proven. As Table 3 shows, it illustrates the performance of various methods when applied to the independent test datasets. For the O'Neil dataset, CDFA demonstrates superior accuracy with the lowest RMSE of 15.111 and the highest R^2 of 0.660. PermuteDDS trails closely behind with similarly strong results, showing almost no difference from CDFA. On the NCI-ALMANAC dataset, CDFA retains its leadership by achieving the best RMSE at 42.307 and the highest R^2 value at 0.508, confirming its robustness in both precision and explanatory capability. Although PermuteDDS performs well, it still lags slightly behind CDFA across all metrics. The remaining methods exhibit higher RMSE figures and lower R^2 values, suggesting they are less precise and less effective compared to our method.

Overall, CDFA consistently demonstrated strong performance, particularly excelling in the random split and cold drug pair settings. However, the poor performance of all methods in the cold cell line setting suggests that future research should focus on improving models' ability to generalize to new cell lines.

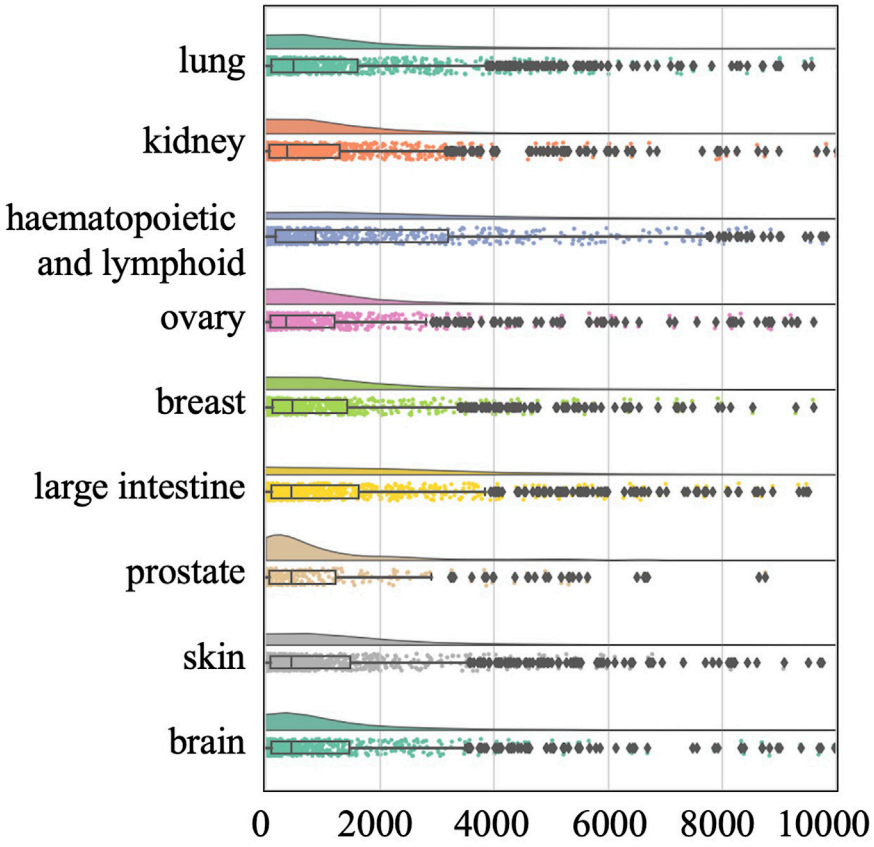

FIGURE 4
Raincloud plots of MSE for NCI-ALMANAC independent test dataset. The horizontal axis quantifies mean squared error (MSE) between true synergy scores and model predictions.

3.3 Tissue-specific analysis

Both previous studies and our own experiments have consistently demonstrated that model performance deteriorates significantly under the cold cell-line scenario, where test cell lines are entirely disjoint from those seen during training. This setting introduces substantial biological variability, making it difficult to disentangle whether performance degradation arises from tissue-specific effects or from the challenge of generalizing to unseen cell-line profiles.

To avoid this confounding factor, we also conducted a tissue-specific analysis on the O'Neil and NCI-ALMANAC datasets. The O'Neil dataset is built on testing 38 drugs on 39 cell lines representing multiple cancer types from six tissue origins. The NCI-ALMANAC dataset covers 104 drugs in 60 cell lines from nine tissue origins. As illustrated in Figures 3, 4, our analysis employs raincloud plots to visualize the distribution of MSE for the two independent test datasets. These plots combine box plots with kernel density estimates ('clouds') to visualize both the shape and central tendency of the error distributions, with outliers indicated by diamond markers.

Our analysis reveals that although the MSE values of the median, second quartile, and third quartile are low, almost all tissues included by the two datasets have MSE values exceeding 500 and 2000, respectively. This suggests that while there is a small number of higher error values across most tissues, the central tendency of the error distribution may be relatively low. This pattern indicates that the model can achieve efficient prediction across different tissues. Our analysis confirms that the presence of high-error predictions—though limited in quantity—reveals significant variability in model performance. Such findings highlight the need for further investigation into the factors contributing to these higher errors and suggest that improvements in model accuracy and consistency are necessary for more reliable predictions across different tissue types.

3.4 Uncertainty results

Figure 5 displays the calibration curves of CDFA under various settings for both the O'Neil and NCI-ALMANAC datasets. The figures are organized from left to right, representing random splits, cold cell line settings, and cold drug pair settings, respectively. The first row showcases the O'Neil dataset, whereas the second row pertains to the NCI-ALMANAC dataset. The space between the calibration curves and the diagonal line represents the miscalibration area, which quantifies the extent of uncertainty calibration. As illustrated in Figure 5, CDFA's recalibration algorithm successfully shifts the calibration curves closer to the

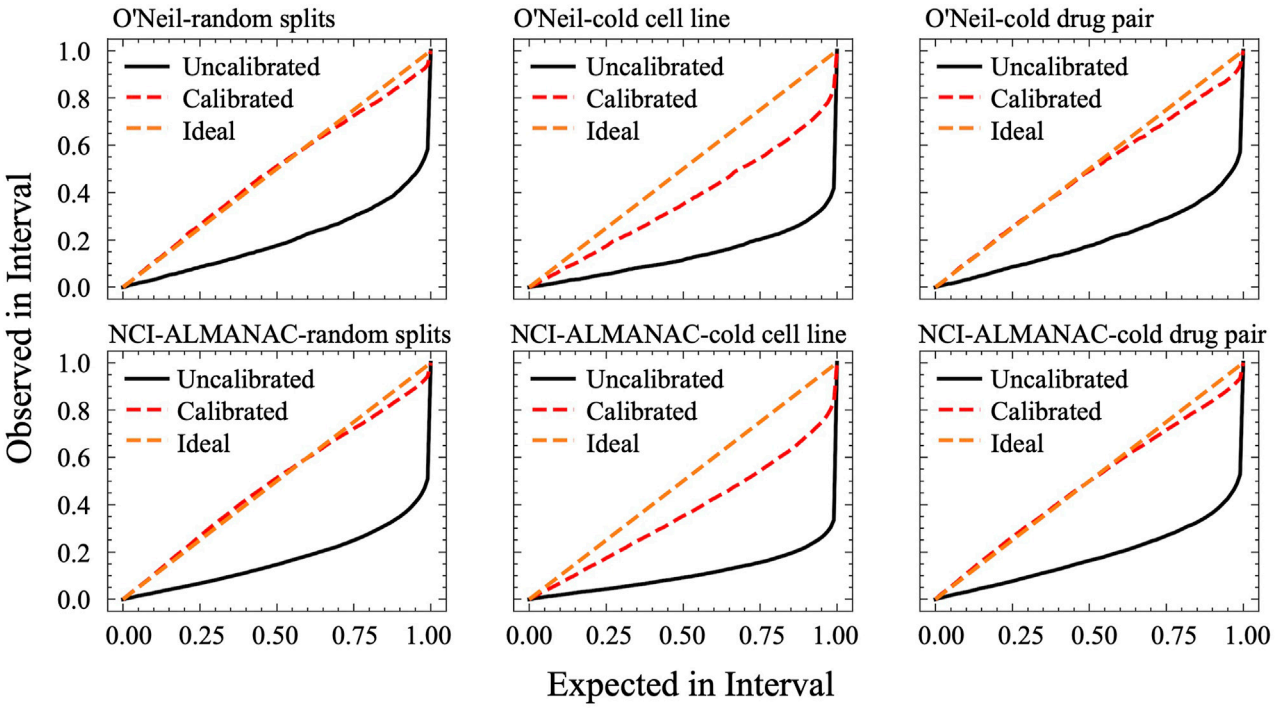

FIGURE 5
Calibration curves of CDFA. On the x-axis, it plots the expected confidence level, while the y-axis shows the observed proportion of correct predictions. A perfectly calibrated model lies on the diagonal line, where the observed proportion of correct outcomes exactly matches the stated confidence at every interval.

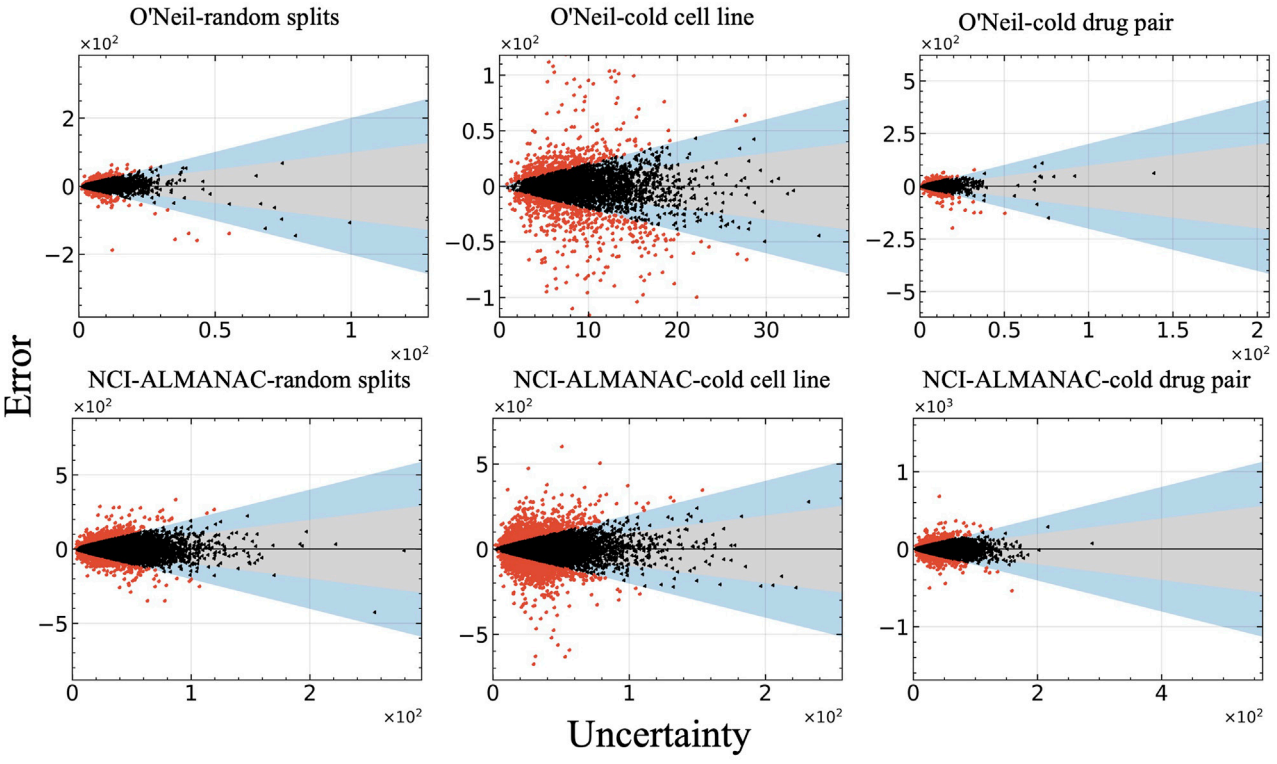

FIGURE 6
Relationship between model error and uncertainty of all test datasets. The vertical axis represents the prediction errors, while the horizontal axis displays uncertainty measured as the standard deviation (std).

diagonal line, thereby reducing the miscalibration area and improving the reliability of the predictions.

Figure 6 illustrates the relationship between prediction error and uncertainty, with uncertainty measured as the standard deviation (std). In this figure, red points indicate errors that do not fall within two standard deviations, while black and blue points represent errors that fall within one and two standard deviations, respectively. It is evident that the majority of the observed errors lie within two standard deviations, reflecting a reasonable alignment between the model's predicted uncertainty and its actual prediction error.

4 Conclusion

This study introduces an ensemble deep learning framework for predicting the potential synergy effects of drug combinations, showcasing superior performance relative to existing methods. A key innovation is the dual-level feature fusion mechanism, which integrates deep semantic features from various network modules, enhancing the model's ability to capture complex interactions. The model leverages convolutional processing of the gene expression matrix to identify key gene signals relevant to drug response. Combined with a Transformer-based attention mechanism, this architecture enables context-aware re-weighting of gene importance under specific drug–cell interactions. This design emulates biological processes where only a subset of genes contribute significantly to the synergistic effect of drug combinations. Furthermore, the model's prediction errors demonstrate robust generalization across tissues, as reflected in the consistent error distributions observed across different tissue types. Isolated high-error samples may correspond to biologically unique or complex cell lines, offering potential avenues for future investigation. Uncertainty estimation is integrated into the model, providing a critical safeguard against biased or overconfident predictions. This feature is especially valuable in guiding both the refinement of known synergies and the exploration of novel drug combinations. Additionally, the uncertainty estimation is integrated into the model, providing a critical safeguard against biased or overconfident predictions. This feature is especially valuable in guiding both the refinement of known synergies and the exploration of novel drug combinations. The uncertainty quantification and recalibration processes ensure that the model's predictions are not only accurate but also reliable, offering a balanced approach to decision-making. While the experimental results demonstrate excellent performance on two datasets, further investigation is needed to assess the model's robustness and generalization capabilities, particularly in scenarios involving new cell lines. Enhancing the interpretability of the model is another important area for future research, as it can provide deeper insights into the mechanisms underlying drug synergy and facilitate broader acceptance.

Data availability statement

The datasets presented in this study can be found in online repositories. The names of the repository/repositories and accession number(s) can be found in the article/supplementary material. All codes of CDFA can be accessed from https://github.com/TracyHIT/CDFA.

Author contributions

XK: Formal Analysis, Data curation, Writing – original draft. XyL: Writing – review and editing. QZ: Formal Analysis, Data curation, Writing – review and editing, Funding acquisition. TL: Writing – original draft. XmL: Formal Analysis, Data curation, Writing – review and editing, Funding acquisition.

Funding

The author(s) declare that financial support was received for the research and/or publication of this article. This research was funded by the National Science and Technology Major Project (Grant No. 2022ZD0117700), and the National Natural Science Foundation of China (Grant No.62371347 and 62271174). The submission code of Macao Polytechnic University is fca.c4de.e9f0.1.

Acknowledgments

We sincerely appreciate the dedicated efforts of Ximei Luo and XK in primary data collection and analysis, with valuable assistance from QZ. Special thanks go to TL and XK for leading the manuscript writing, as well as Xiaoyan Liu for her meticulous proofreading and constructive suggestions. We also extend our gratitude to all colleagues and collaborators who provided insightful discussions and technical support throughout this research.

Finally, we thank the reviewers for their insightful comments, which helped improve the quality of this manuscript.

Conflict of interest

The authors declare that the research was conducted in the absence of any commercial or financial relationships that could be construed as a potential conflict of interest.

Generative AI statement

The author(s) declare that no Generative AI was used in the creation of this manuscript.

Publisher's note

References

Bollenbach, T., Quan, S., Chait, R., and Kishony, R. (2009). Nonoptimal microbial response to antibiotics underlies suppressive drug interactions. *Cell* 139 (4), 707–718. doi:10.1016/j.cell.2009.10.025

Breiman, L. (2001). Random forests. *Mach. Learn.* 45, 5–32. doi:10.1023/a:1010933404324

Brent, R. P. (1971). An algorithm with guaranteed convergence for finding a zero of a function. *Comput. J.* 14 (4), 422–425. doi:10.1093/comjnl/14.4.422

Cao, C., Wang, C., Dai, Q., Zou, Q., and Wang, T. (2024). CRBPSA: circrna-rbp interaction sites identification using sequence structural attention model. *BMC Biol.* 22, 260. doi:10.1186/s12915-024-02055-0

Chen, M. J., Zhang, M., Yan, G. Y., Wang, G. H., and Qu, C. Q. (2025). MRHGNN: enhanced multimodal relational hypergraph neural network for synergistic drug combination forecasting. *IEEE Trans. Neural Netw. Learn Syst.*, 1–13. doi:10.1109/TNNLS.2025.3553385

Chen, Z. H., Li, Z. M., Shen, X. Z., Liu, Y. S., Lin, X., Zeng, D. J., et al. (2024). DualSyn: a dual-level feature interaction method to predict synergistic drug combinations. *Expert Syst. Appl.* 257, 125065. doi:10.1016/j.eswa.2024.125065

Cui, X., Lin, Q., Chen, M., Wang, Y., Wang, Y., Wang, Y., et al. (2024). Long-read sequencing unveils novel somatic variants and methylation patterns in the genetic information system of early lung cancer. *Comput. Biol. Med.* 171, 108174. doi:10.1016/j.compbiomed.2024.108174

Forbes, S. A., Beare, D., Gunasekaran, P., Leung, K., Bindal, N., Boutselakis, H., et al. (2015). COSMIC: exploring the world's knowledge of somatic mutations in human cancer. *Nucleic Acids Res.* 43 (D1), D805–D811. doi:10.1093/nar/gku1075

Guo, Y., Hu, H. T., Chen, W. B., Yin, H., Wu, J., Hsieh, C. Y., et al. (2024). SynergyX: a multi-modality mutual attention network for interpretable drug synergy prediction. *Briefings Bioinforma.* 25 (2), 15. doi:10.1093/bib/bbae015

Hendrycks, D., and Gimpel, K. (2016). "Gaussian error linear units (gelus)," in *arXiv preprint arXiv:160608415*.

Holbeck, S. L., Camalier, R., Crowell, J. A., Govindharajulu, J. P., Hollingshead, M., Anderson, L. W., et al. (2017). The national cancer institute ALMANAC: a comprehensive screening resource for the detection of anticancer drug pairs with enhanced therapeutic activity. *Cancer Res.* 77 (13), 3564–3576. doi:10.1158/0008-5472.CAN-17-0489

Hosseini, S. R., and Zhou, X. B. (2023). CCSynergy: an integrative deep -learning framework enabling context -aware prediction of anti -cancer drug synergy. *Brief. Bioinform* 24 (1), bbac588. doi:10.1093/bib/bbac588

Huang, H., Zhang, P., Qu, X. A., Sanseau, P., and Yang, L. (2014). Systematic prediction of drug combinations based on clinical side-effects. *Sci. Rep.* 4 (1), 7160. doi:10.1038/srep07160

Jaaks, P., Coker, E. A., Vis, D. J., Edwards, O., Carpenter, E. F., Leto, S. M., et al. (2022). Effective drug combinations in breast, Colon and pancreatic cancer cells. *Nature* 603 (7899), 166–173. doi:10.1038/s41586-022-04437-2

Jiang, T., Guo, H. Z., Liu, Y. D., Li, G. Y., Cui, Z., Cui, X. R., et al. (2024). A comprehensive genetic variant reference for the Chinese population. *Sci. Bull.* 69 (24), 3820–3825. doi:10.1016/j.scib.2024.06.017

Kong, S., Moharil, P., Handly-Santana, A., Boehnke, N., Panayiotou, R., Gomerdinger, V., et al. (2023). Synergistic combination therapy delivered *via* layer-by-layer nanoparticles induces solid tumor regression of ovarian cancer. *Bioeng. Transl. Med.* 8 (2), e10429. doi:10.1002/btm2.10429

Kuru, H. I., Tastan, O., and Cicek, A. E. (2022). MatchMaker: a deep learning framework for drug synergy prediction. *IEEE-ACM Trans. Comput. Biol. Bioinform* 19 (4), 2334–2344. doi:10.1109/TCBB.2021.3086702

Liu, Q., and Xie, L. (2021). TranSynergy: mechanism-Driven interpretable deep neural network for the synergistic prediction and pathway deconvolution of drug combinations. *PLoS Comput. Biol.* 17 (2), e1008653. doi:10.1371/journal.pcbi.1008653

Liu, X., Song, C. Z., Liu, S. C., Li, M. L., Zhou, X. H., and Zhang, W. (2022). Multi-way relation-enhanced hypergraph representation learning for anti-cancer drug synergy prediction. *Bioinformatics* 38 (20), 4782–4789. doi:10.1093/bioinformatics/btac579

Liu, Y. D., Jiang, T., Gao, Y., Liu, B., Zang, T. Y., and Wang, Y. D. (2021). Psi-caller: a lightweight short read-based variant caller with high speed and accuracy. *Front. Cell Dev. Biol.* 9, 11. doi:10.3389/fcell.2021.731424

Meng, P., Wang, G. H., Guo, H. Z., and Jiang, T. (2023). Identifying cancer driver genes using a two-stage random walk with restart on a gene interaction network. *Comput. Biol. Med.* 158, 106810. doi:10.1016/j.compbiomed.2023.106810

Mervin, L. H., Johansson, S., Semenova, E., Giblin, K. A., and Engkvist, O. (2021). Uncertainty quantification in drug design. *Drug Discov. Today* 26 (2), 474–489. doi:10.1016/j.drudis.2020.11.027

Nair, N. U., Greninger, P., Zhang, X. H., Friedman, A. A., Amzallag, A., Cortez, E., et al. (2023). A landscape of response to drug combinations in non-small cell lung cancer. *Nat. Commun.* 14 (1), 3830. doi:10.1038/s41467-023-39528-9

O'Neil, J., Benita, Y., Feldman, I., Chenard, M., Roberts, B., Liu, Y. P., et al. (2016). An unbiased oncology compound screen to identify novel combination strategies. *Mol. Cancer Ther.* 15 (6), 1155–1162. doi:10.1158/1535-7163.MCT-15-0843

Pang, Y., Chen, Y. H., Lin, M. J., Zhang, Y. H., Zhang, J. Q., and Wang, L. (2024). MMSyn: a new multimodal deep learning framework for enhanced prediction of synergistic drug combinations. *J. Chem. Inf. Model* 64 (9), 3689–3705. doi:10.1021/acs.jcim.4c00165

Preuer, K., Lewis, R. P. I., Hochreiter, S., Bender, A., Bulusu, K. C., and Klambauer, G. (2018). DeepSynergy: predicting anti-cancer drug synergy with deep learning. *Bioinformatics* 34 (9), 1538–1546. doi:10.1093/bioinformatics/btx806

Rafiei, F., Zeraati, H., Abbasi, K., Ghasemi, J. B., Parsaeian, M., and Masoudi-Nejad, A. (2023). DeepTraSynergy: drug combinations using multimodal deep learning with transformers. *Bioinformatics* 39 (8), btad438. doi:10.1093/bioinformatics/btad438

Sidorov, P., Naulaerts, S., Arley-Bonnet, J., Pasquier, E., and Ballester, P. J. (2019). Predicting synergism of cancer drug combinations using NCI-ALMANAC data. *Front. Chem.* 7, 13. doi:10.3389/fchem.2019.00509

Wang, J. X., Liu, X. J., Shen, S. Y., Deng, L., and Liu, H. (2022b). DeepDDS: deep graph neural network with attention mechanism to predict synergistic drug combinations. *Briefings Bioinforma.* 23 (1), bbab390. doi:10.1093/bib/bbab390

Wang, T., Renteria, M. E., and Peng, J. (2022a). Editorial: data mining and statistical methods for knowledge discovery in diseases based on multimodal omics. *Front. Genet.* 13, 895796. doi:10.3389/fgene.2022.895796

Wang, T., Shu, H., Hu, J. L., Wang, Y. T., Chen, J., Peng, J. J., et al. (2024a). Accurately deciphering spatial domains for spatially resolved transcriptomics with stCluster. *Brief. Bioinform* 25 (4), bbae329. doi:10.1093/bib/bbae329

Wang, T., Yang, J., Xiao, Y., Wang, J., Wang, Y., Zeng, X., et al. (2023a). DFinder: a novel end-to-end graph embedding-based method to identify drug–food interactions. *Bioinformatics* 39 (1), btac837. doi:10.1093/bioinformatics/btac837

Wang, T. S., Wang, R. H., and Wei, L. Y. (2023b). AttenSyn: an attention-based deep graph neural network for anticancer synergistic drug combination prediction. *J. Chem. Inf. Model* 64 (7), 2854–2862. doi:10.1021/acs.jcim.3c00709

Wang, W., Yuan, G., Wan, S., Zheng, Z., Liu, D., Zhang, H., et al. (2024b). A granularity-level information fusion strategy on hypergraph transformer for predicting synergistic effects of anticancer drugs. *Briefings Bioinforma.* 25 (1), bbad522. doi:10.1093/bib/bbad522

Wang, Y., Shen, W., Shen, Y., Feng, S., Wang, T., Shang, X., et al. (2024d). Integrative graph-based framework for predicting circRNA drug resistance using disease contextualization and deep learning. *IEEE J. Biomed. health Inf.* 1–12. doi:10.1109/JBHI.2024.3457271

Wang, Y. T., Liu, X. M., Shen, Y. W., Song, X. R., Wang, T., Shang, X. Q., et al. (2023c). Collaborative deep learning improves disease-related circRNA prediction based on multi-source functional information. *Briefings Bioinforma.* 24 (2), bbad069. doi:10.1093/bib/bbad069

Wang, Y. Z., Zhai, Y. X., Ding, Y. J., and Zou, Q. (2024c). SBSM-Pro: support bio-sequence machine for proteins. *Sci. China-Information Sci.* 67 (11), 212106. doi:10.1007/s11432-024-4171-9

Wu, L., Gao, J., Zhang, Y., Sui, B., Wen, Y., Wu, Q., et al. (2023). A hybrid deep forest-based method for predicting synergistic drug combinations. *Cell Rep. methods.* 3 (2), 100411. doi:10.1016/j.crmeth.2023.100411

Xu, M. D., Zhao, X. W., Wang, J. Y., Feng, W., Wen, N. F., Wang, C. Y., et al. (2023). DFFNDDS: prediction of synergistic drug combinations with dual feature fusion networks. *J. Cheminformatics* 15 (1), 33. doi:10.1186/s13321-023-00690-3

Yan, S. Y., and Zheng, D. (2024). A deep neural network for predicting synergistic drug combinations on cancer. *Interdiscip. Sci.* 16 (1), 218–230. doi:10.1007/s12539-023-00596-6

Zhang, T., Zhang, X., Wu, Z., Ren, J., Zhao, Z., Zhang, H., et al. (2024). VGAE-CCI: variational graph autoencoder-based construction of 3D spatial cell-cell communication network. *Brief. Bioinform* 26 (1), bbae619. doi:10.1093/bib/bbae619

Zhang, Y. Q., Yuan, H., Liu, Y. H., Xiong, S. W., Zhou, Z. G., Xu, Y. G., et al. (2025). MMGCSyn: explainable synergistic drug combination prediction based on multimodal fusion. *Futur Gener. Comp. Syst.* 168, 107784. doi:10.1016/j.future.2025.107784

Zhu, P. F., Shu, H., Wang, Y. T., Wang, X. F., Zhao, Y., Hu, J. L., et al. (2025). MAEST: accurately spatial domain detection in spatial transcriptomics with graph masked autoencoder. *Brief. Bioinform* 26 (2), bbaf086. doi:10.1093/bib/bbaf086

frontiers | Frontiers in Pharmacology

TYPE Original Research
PUBLISHED 15 September 2025
DOI 10.3389/fphar.2025.1633978

OPEN ACCESS

EDITED BY
Xinyu Wang,
Philadelphia College of Osteopathic Medicine (PCOM), United States

REVIEWED BY
Ali Hafez El-Far,
Damanhour University, Egypt
Mariana Magalhães,
University of Coimbra, Portugal

*CORRESPONDENCE
G. Ulrich-Merzenich,
Gudrun.ulrich-merzenich@ukbonn.de

RECEIVED 23 May 2025
ACCEPTED 12 August 2025
PUBLISHED 15 September 2025

CITATION
Shcherbakova A, Nguyen L, Koptina A, Backlund A, Banerjee S, Romanov E and Ulrich-Merzenich G (2025) Phytochemical combinations of lichen *Evernia prunastri* (L.) Ach. reduce drug resistance to temozolomide but not to paclitaxel *in vitro*. *Front. Pharmacol.* 16:1633978. doi: 10.3389/fphar.2025.1633978

Phytochemical combinations of lichen *Evernia prunastri* (L.) Ach. reduce drug resistance to temozolomide but not to paclitaxel *in vitro*

A. Shcherbakova[1,2], L. Nguyen[1,3], A. Koptina [1,3], A. Backlund [3], S. Banerjee[4], E. Romanov[2] and G. Ulrich-Merzenich[1]*

[1]Medical Clinic III, Synergy and Experimental Medicine Research Group, University Hospital Bonn (UKB), Bonn, Germany, [2]Institute of Forestry and Nature Management, Volga State University of Technology, Yoshkar-Ola, Russia, [3]Pharmacognosy, Department of Pharmaceutical Biosciences, Uppsala University, Uppsala, Sweden, [4]Medicinal Plants Innovation Center, Mae Fah Luang University, Chiang Rai, Thailand

Introduction: Temozolomide (TMZ) and Paclitaxel (PXT), crucial anti-cancer drugs for glioblastoma (GBM) and primary breast cancer (BC), respectively, face drug resistance. Therefore, we investigated the adjuvant potential of characterized extracts of the lichens *Evernia prunastri* (L.) Ach. (Epr), *Cladonia arbuscula* (Wallr.) Flot (Car) and their metabolites, evernic acid (EA) and usnic acid (UA) alone or in combination with TMZ and PTX for their immunomodulatory and chemosensitivity increasing potential.

Methods: TMZ-resistant U-87 cells, MCF7 BC-cells, and normal human skin fibroblasts (HSKF) were treated with hexane (Hex), dichloromethane (DCM), and acetonitrile (ACN) extracts of Epr (EprDCM, EprACN), Car (CarHex, CarACN), and with EA and UA to measure cell metabolic activity. Molecular mechanisms were predicted using ChemGPS-NP and validated by Western blot, RNA sequencing, quantitative RT-PCR, and Wnt inhibitory factor 1 (WIF1) protein expression. Combinatory effects were calculated by Combination Index (CI) and Zero Interaction Potency methods (ZIP).

Results: Extracts and selected metabolites reduced concentration-dependent cellular metabolic activity in U-87 and MCF7 cells. EprACN and EA (U-87 cells: IC_{50} 30 µg/mL), safe to HSKF, regulated key proteins in MAP kinases pathways, supporting predictions made by ChemGPS-NP. The combination EA-TMZ showed additive effects (TMZ-reduction: 3.4 fold), reduced transcription of Wnt pathway members, and increased in U-87 cells protein releases of WiF1, the central inhibitor of Wnt-signaling. Further gene expression data (GE) suggest involvement of IL-17 receptor and BDNF.

Discussion: The combination EA-TMZ interacts with the Wnt pathway regulation associated with sensitizing U-87 cells, without increasing GEs of pro-inflammatory cytokines. EA deserves further investigation as an adjuvant.

KEYWORDS

lichens, glioblastoma, synergy, Wnt signaling, prediction, resistance

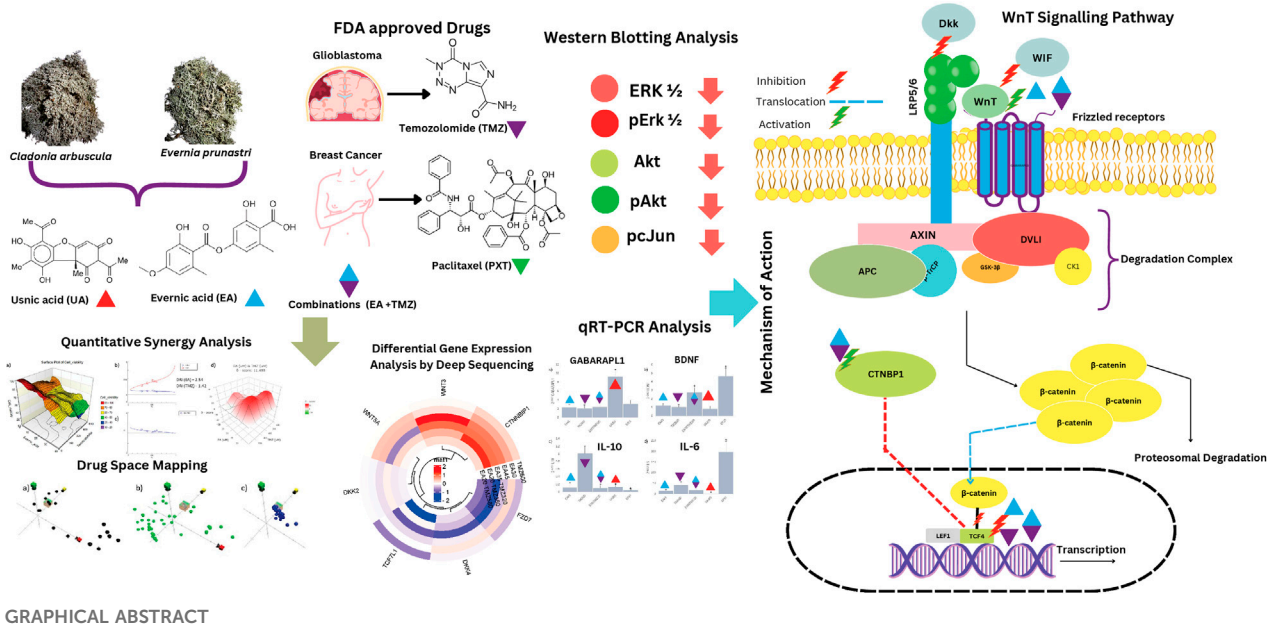

GRAPHICAL ABSTRACT

1 Introduction

Breast cancer (BC) is the most common cancer worldwide and ranks fifth among cancer-related deaths (Zhang et al., 2023). Projections indicate a significant increase in the global burden, with cases expected to rise by nearly 40% and deaths by 68% by 2050 if current trends continue (Liao, 2025). Brain and central nervous system cancer ranks approximately 12th in incidence and 8th in mortality in Europe based on age-standardized rates (DeCordova et al., 2020). Glioblastoma (GBM), classified as a WHO Grade 4 CNS tumor according to the 2021 WHO Classification of Tumors of the Central Nervous System, represents the most aggressive form of brain cancer (Louis et al., 2021). The 5- and 10-year survival rates still remain at 5% and 2.6%, respectively (Ma et al., 2022; Alcantara Llaguno et al., 2009). The current standard of care for GBM follows the Stupp protocol, established in 2005, which includes maximal safe surgical resection, concurrent chemoradiotherapy, and adjuvant temozolomide (TMZ) (Jezierzański et al., 2024).

The poor treatment prognosis, notably GBM, has been linked to its diverse molecular profiles, resulting in distinct phenotypes also associated with TMZ-resistance (DeCordova et al., 2020). Several fundamental mechanisms contribute to GBM's treatment resistance and incurability. The blood-brain barrier represents a critical obstacle, preventing most systemic chemotherapeutic agents from reaching therapeutic concentrations in brain tissue (Zuccarini et al., 2018). Glioblastoma stem cells (GSCs) constitute another major resistance mechanism, exhibiting enhanced DNA repair capacity, resistance to apoptosis, metabolic reprogramming, and self-renewal capacity that maintains the tumor cell population (Nowak et al., 2021; Guan et al., 2020). Methylation of the O6-methylguanine-DNA methyltransferase (MGMT) promoter plays a critical role in TMZ-resistance. Tumors with an unmethylated MGMT promoter are significantly more resistant to TMZ, and prolonged treatment may induce loss of MGMT methylation, further contributing to acquired resistance (Li et al., 2021).

Recently, Weighted Gene Co-Expression Network Analysis (WGCNA) was used to capture the molecular heterogeneity of GBM patients on the molecular level. Authors constructed an immune-related prognostic model to predict patient sensitivity to checkpoint inhibitor blockade therapy (Ma et al., 2022). The high-risk group (non-survival) was associated with epithelial-mesenchymal transition (EMT), high immune cell infiltration, immune activation, a low mutation number, and high methylation, while the low-risk group had an adverse status (Ma et al., 2022).

BC is also extremely variable in morphology and at the molecular level, necessitating combinatorial therapy modalities depending on the molecular subtype, which is defined by hormone receptor (HR) status and human epidermal growth factor receptor-2 (HER2) expression (Li et al., 2017; Kashyap et al., 2022). These include HR-positive/HER2-negative (HR+/HER2-), HR+/HER2+, HR-/HER2+, and triple-negative breast

Abbreviations: TMZ, Temozolomide; PXT, Paclitaxel; GBM, glioblastoma; BC, breast cancer; EprDCM, dichloromethane extract from *E. prunastri*; EprACN–acetonitrile extract from *E. prunastri*; CarHex, hexane extract from *C. arbuscula*; CarACN–acetonitrile extract from *C. arbuscula*; EA, evernic acid; UA, usnic acid; TMZ320EA35, combination of TMZ (320 μM = 62.13 μg/mL) with EA (35 μM = 11.63 μg/mL); TMZ380EA20, TMZ (380 μM = 73.78 μg/mL) with EA (20 μM = 6.65 μg/mL); TMZ580EA20, TMZ (580 μM = 112.61 μg/mL) with EA (20 μM = 6.65 μg/mL).

cancer (TNBC), which lacks estrogen receptor, progesterone receptor, and HER2 expression (Li et al., 2017). TNBC is particularly aggressive, accounting for approximately 10%–15% of all breast cancers but contributing to a disproportionately high percentage of breast cancer-related deaths globally, estimated at around 40% (Rosińska et al., 2024). The 5-year relative survival rate for TNBC, combining all stages, is approximately 77%, with significantly lower rates for distant metastatic disease (Baranova et al., 2022).

The current standard of care in breast cancer varies by subtype and stage. Early-stage breast cancer typically involves surgical resection, adjuvant or neoadjuvant chemotherapy, radiation therapy, hormone therapy for hormone receptor-positive tumors, and targeted therapy for HER2-positive tumors (Bravo et al., 2023; Grant et al., 2024).

The Wnt pathway is implicated in both BC and GBM, significantly contributing to treatment resistance (Zhong and Virshup, 2020), even though precise regulatory mechanisms remain unclear (Kashyap et al., 2022). Crosstalk between Wnt signaling and other pathways contributes to cancer development and spread, including resistance to pathway inhibitors (Zhong and Virshup, 2020). This understanding drives the development of novel combination therapies to minimize toxicity and resistance (Zhong and Virshup, 2020). Therefore, exploring unexamined plant extracts or phytocompounds contributes to discovering safe, effective, and novel combination therapies (Ulrich-Merzenich et al., 2017).

TMZ and paclitaxel (PTX), key chemotherapeutics for GBM and BC, respectively, are under investigation for combination therapies (Tan et al., 2020). TMZ, a DNA alkylating agent, induces cell death by causing base mismatches and DNA strand breaks (Tan et al., 2020). Ongoing 583 clinical trials worldwide explore treatments for GBM (https://clinicaltrials.gov/), including immune checkpoint inhibitors paired with CNS-penetrant or potent inhibitors (Gueble et al., 2022). Despite multimodal treatments, GBM patients face a low median survival of 12.1–16.6 months (Neff et al., 2022; Minea et al., 2024; Fekete et al., 2023), emphasizing the urgency for novel treatment strategies (Tan et al., 2020).

Taxanes, like PTX, used in BC treatment, were derived from the Pacific yew's bark (Wani et al., 1971). PTX induces cell death by stabilizing microtubules, causing G2/M arrest and initiating apoptosis (Manthey et al., 1992). Resistance to PTX and other anti-cancer drugs (Das et al., 2021; Bukowsk et al., 2020) is common for BC, just as resistance in GBM to TMZ (Lee, 2016). The resistance of BC to PTX is thought to be a consequence of a disequilibrium in various signaling pathways, mutations in certain genes, and epigenetic deregulations (Abu et al., 2019). In particular, the genes of the ATP-binding cassette (ABC) superfamily of drug efflux, including P-glycoprotein (P-gp), are involved in the resistance to PTX by leading to an overexpression of P-gp in BC-cells (Abu et al., 2019). In MCF7 cells, aberrantly regulated expression of FOXM1 and KIF20A was associated with PTX-resistance (Abu et al., 2019; Khongkow et al., 2016). Further, the overexpression of miR-200c-3p contributed to the resistance of BC cells to PTX by an aberrant regulation of SOX2 (Abu et al., 2019).

This diversity of resistance mechanisms promotes a search for natural compounds as adjuvants (Persano et al., 2022). Therapies triggering multiple pathways (and specifically addressing crucial survival pathways) may be more promising (Sestito et al., 2018).

Lichens have been utilized in traditional medicine for ages (Crawford and Ranković, 2015). They are symbiotic organisms consisting of a fungus (mycobiont) and either algae or cyanobacteria (photobiont) (Schwendener, 2011). They are a promising source for novel organic small molecules and synergistic therapeutic strategies. *Evernia prunastri* L. and *Cladonia arbuscula* (Wallr.) Fot. were selected based on their published bioactivity. Evernic acid (EA), the main metabolite of *E. prunastri* L., has shown antimicrobial, cytotoxic, neuroprotective, and anti-inflammatory properties in prior studies (Fernández-Moriano et al., 2017; Lee et al., 2021; Gökalsın and Sesal, 2016; Shcherbakova et al., 2019). However, its role in cancer therapy remains largely unexplored. Usnic acid (UA), a prominent secondary metabolite isolated from *C. arbuscula* (Wallr.) Fot., has shown potent antiproliferative effects in several cancer types. Notably, UA exhibited promising cytotoxicity against T-47D breast cancer cells, Capan-2 pancreatic cancer cells (Einarsdottir et al., 2010), and MCF7 breast cancer cells as well (Bačkorová et al., 2011; Galanty et al., 2017; Kiliç et al., 2019; Brisdelli et al., 2013).

We investigated extracts from *E. prunastri* L. (Parmeliaceae) and *C. arbuscula* (Wallr.) Fot. (Cladoniaceae) along with their major metabolites, evernic acid (EA) and usnic acid (UA), for their potential to reduce metabolic activity in U-87 glioma and MCF7 breast cancer cells.

Both cell lines were selected as representative *in vitro* models for glioblastoma and breast cancer, respectively, due to their widespread use, well-characterized molecular profiles, and relevance to the mechanisms under investigation. U-87 cells are among the most commonly used GBM models and exhibit key features of primary glioblastoma, such as rapid proliferation, resistance to temozolomide (TMZ) (Xie et al., 2015). Similarly, MCF7 cells are commonly used for BC, characterized by estrogen receptor positivity and moderate sensitivity to chemotherapeutics like paclitaxel (PTX), making them a standard model for studying HR+ BC and mechanisms of taxane resistance (Neve et al., 2006).

U-87 and MCF7 remain widely accepted platforms for early-stage anticancer research. In this study, they were used to evaluate not only the ability of the lichen extracts and their metabolites to influence cancer cell metabolic activity, but also their potential to synergize with standard chemotherapeutics (TMZ or PTX). Extracts and combinations showing efficacy were further assessed for possible mechanisms of action. This included chemographic prediction tools, cytokine response profiling, and evaluation of their potential to modulate cellular pathways involved in drug sensitivity, forming a foundation for future translational investigations.

2 Materials and methods

2.1 Chemicals, media, and assays

Usnic acid (UA) (purity 98%), paclitaxel, resazurin tox kit, insulin (Sigma Aldrich, Germany); evernic acid (EA) (purity 98%), temozolomide (Cayman Chemical, United States); (phospho-AKT rabbit polyclonal antibody (1:2000), ß-actin rabbit polyclonal antibody (1:2000), phospho-p44/42 (Thr202/Tyr204) rabbit polyclonal antibody (1:2000), p44/42 mouse clonal

antibody (1:2000), goat anti-rabbit IgG-HRP conjugated to horseradish peroxidase (1:2000) (Santa Cruz Biotechnology, United States); phospho-c-Jun (Ser73) rabbit polyclonal antibody (1:2000) (Cell Signaling Technology, United States); Minimum Essential Medium (MEM), Roswell Park Memorial Institute (RPMI) 1,640 Medium, Dulbecco's Modified Eagle's Medium (DMEM, fetal bovine serum (FBS), non-essential amino acids (MEM NEAA), sodium pyruvate, penicillin/streptomycin (Gibco™, United States); Human WIF-1 DuoSet ELISA (R&D Systems, United States), RNeasy MiniPlus kit (QIAGEN, Netherlands).

2.2 Lichens material

Samples of *E. prunastri* (L.) Ach. and *C. arbuscula* (L.) Hoffm. were collected in the Mari El Republic of Russia on the campus of the Volga State University of Technology. The lichens were identified by lichenologist G.A. Bogdanov at the Bolshaya Kokshaga Natural Reserve. The voucher specimens of the lichens were deposited at the Institute of Forestry and Nature Management, Volga State University of Technology, Yoshkar-Ola, Russia, with the references Epr_06.2012 (*E. prunastri*) and Car_06.2012 (*C. arbuscula*).

2.3 Extraction and characterisation

Extracts were obtained and characterized as described earlier (Shcherbakova et al., 2021). Air-dried powdered thalli of the lichens were extracted by sequential maceration with hexane, dichloromethane (DCM), or with 60% acetonitrile in water (ACN) at room temperature (RT) for 24 h with each solvent. The extracts were filtered and then concentrated under reduced pressure in a rotary evaporator Rotavapor R (Buchi Labortechnik AG, Flawil, Switzerland). The dry extracts were stored at RT until usage.

2.4 Chemographic prediction of the mode of action

ChemGPS-NP (http://chemgps.bmc.uu.se) provides a multidimensional (8D) map of physicochemical property space. On this map, molecules are positioned based on their estimated physico-chemical properties. Compounds with similar structures and hence properties are positioned on the map in mutual proximity. Thus positions and distances between compounds can be used to predict their biological activities. This method has been specifically validated for anti-cancer modes of action as well as for a broad range of other experimentally demonstrated activities (Buonfiglio et al., 2015). It was used to predict possible modes of action of EA.

2.5 Cell culture and cytotoxicity assay

2.5.1 Cell lines and culture

Human primary glioblastoma (U-87), human breast adenocarcinoma (MCF7), and human skin fibroblast (HSKF) cell lines were purchased via Cell Line Services (CLS) from the German Collection of Microorganisms and Cell Cultures (DSMZ) and Promocell and grown as described earlier (Ammar and Ulrich-Merzenich, 2017). HSKF was included as a non-malignant cell line to assess the general cytotoxicity and selectivity of the tested extracts, metabolites, and compounds, distinguishing between broad cellular effects and specific anti-cancer activity.

2.5.2 Metabolic activity assay as measure for cell viability

Cells (5×10^3 cells/well) were seeded into 96-well plates and treated as described (Ulrich-Merzenich et al., 2017). For the treatment with the CarHex, CarACN, EprDCM, and EprACN extracts, a concentration range of 6.25–100 µg/mL was used. For EA and UA, the tested concentration range was 4.15–66.46 µg/mL and 4.30–68.86 µg/mL, respectively (corresponding to 12.5–200 µM). TMZ was tested in a range of 9.71–155.32 µg/mL (50–800 µM), and PTX in a range of 21.35–341.56 µg/mL (25–400 µM). All treatments were performed for 24 h. Metabolic activity of the cells, as an indirect measure of cell viability, was measured by resazurin fluorometric assay (Sigma) as described (Ulrich-Merzenich et al., 2017). The concentration range was selected based on the published data (Einarsdottir et al., 2010; Kiliç et al., 2019; Brisdelli et al., 2013; Emsen et al., 2018; Bézivin et al., 2004). The 24-h time point was selected for all viability assays to ensure consistency and comparability across all experimental conditions. This time frame is widely used for resazurin-based cytotoxicity assays and is sufficient to capture early drug-induced effects on cell viability, as well as to minimize secondary effects such as nutrient depletion or over-confluence in culture.

2.6 Western blot analysis

Western blot analysis was performed to investigate the expression and phosphorylation levels of Akt, Erk1/2, and c-Jun in U-87 cells treated with EprACN or EA as described (Ulrich-Merzenich et al., 2007) and in Supplementary Material S1. Antibody (Ab) details (pAKT, pErk1/2, Erk 1/2, p-cJun, ß-actin, secondary Abs) are provided in Supplementary Material Table S1.

2.7 Synergy screening

Cells (as described under Section 2.5.2) were treated with 7 different combinations of metabolites/compounds. Concentrations for the combinations were chosen based on the results with the single extracts/metabolites (Chou, 2010) (see also Section 3.1 and Supplementary Material S2). A total of five concentrations were chosen with the following concentration ranges for the different metabolites/drugs: 1) TMZ (9.75–155.32 µg/mL = 50–800 µM) and EprACN (6.25–100 µg/mL); 2) TMZ (9.75–155.32 µg/mL = 50–800 µM) and EA (4.15–66.46 µg/mL = 12.5–200 µM); 3) TMZ (9.75–155.32 µg/mL = 50–800 µM) and UA (4.30–68.86 µg/mL = 12.5–200 µM); 4) PTX (5.34–85.39 µg/mL = 6.25–100 µM) and EprACN (6.25–100 µg/mL); 5) PTX (5.34–85.39 µg/mL = 6.25–100 µM) and EA (4.15–66.46 µg/mL = 12.5–200 µM); 6) PTX

TABLE 1 Effect of lichen extracts, lichen metabolites, and reference drugs on cell viability.

Extract/Compound	IC_{50}, fibroblasts	IC_{50}, U-87	SI_U-87	IC_{50}, MCF7	SI_MCF7
E. prunastri (EprDCM)	29 ± 5 μg/mL	13 ± 3 μg/mL*	2.3 ± 0.19	72 ± 8 μg/mL*	0.4 ± 0.02
E. prunastri (EprACN)	79 ± 6 μg/mL	31 ± 6 μg/mL*	2.6 ± 0.15	107 ± 13 μg/mL	0.7 ± 0.03
C. arbuscula (CarHex)	44 ± 2 μg/mL	35 ± 3 μg/mL*	1.3 ± 0.03	85 ± 14 μg/mL*	0.5 ± 0.02
C. arbuscula (CarACN)	16 ± 2 μg/mL	33 ± 2 μg/mL*	0.5 ± 0.02	67 ± 7 μg/mL*	0.2 ± 0.01
Evernic acid (EA)	>66.46 μg/mL (200 μM)	20.60 ± 2.99 μg/mL 62 ± 9 μM*	3.3 ± 0.13	>66.46 μg/mL (200 μM)	1.0
Usnic acid (UA)	>68.86 μg/mL (200 μM)	69.90 ± 5.16 μg/mL 203 ± 15 μM	1.0 ± 0.02	57.50 ± 9.30 μg/mL 167 ± 27 μM	1.2 ± 0.05
Temozolomide (TMZ)	>155.32 μg/mL (800 μM)	115.13 ± 6.40 μg/mL (593 ± 33 μM)	1.4 ± 0.02	—	
Paclitaxel (PTX)	>341.56 μg/mL (400 μM)	—		116.13 ± 12.81 μg/mL 136 ± 15 μM	3.0 ± 0.1

The effect is represented as an IC_{50} value. SI, selectivity index defining the ratio between IC_{50}s of fibroblasts and cancer cells, as higher the SI as better the selectivity. For experimental details see Material and Methods.

*p-value <0.05 in comparison to TMZ or PTX. Experiments were performed with 3 replicates.

(5.34–85.39 μg/mL = 6.25–100 μM) and UA (4.30–68.86 μg/mL = 12.5–200 μM); 7) TMZ (62.13–124.26 μg/mL = 320–640 μM) and EA (6.65–13.29 μg/mL = 20–40 μM). For details, see Supplementary Material S3. Drug combinations were tested in comparison to their respective controls.

2.7.1 Synergy calculation

Synergism was calculated using the CompuSyn software (https://compusyn.software.informer.com/) based on the Chou and Talalay Combination Index (CI) method (Chou, 2010) and by the web application "SynergyFinder" (v.1) employing the Zero Interaction Potency (ZIP) model (Ianevski et al., 2017). For the CI and the Dose Reduction Index (DRI) calculation, the following ratios of the combined drugs were used: 1) TMZ: EP – 1.5:1 (c:c); 2) TMZ: EA – 8:1 (c:c); 3) TMZ: UA – 8:1 (c:c); 4) PTX: EP – 1:1.2 (c:c); 5) 4) PTX: EA – 1:2 (c:c); 6) 4) PTX: UA – 1:2 (c:c); 7) TMZ: EA – 16:1 (c:c).

2.8 RNA deep sequencing of primary glioblastoma cells (U-87)

2.8.1 Cell culture

U-87 cells (106 cells/well) were seeded in 6-well plates and stimulated for 24 h with the following treatments: 1) EA (9.97 μg/mL = 30 μM); 2) EA (14.95 μg/mL = 45 μM); 3) TMZ (116.49 μg/mL = 600 μM); 4) EA (6.65 μg/mL = 20 μM) + TMZ (73.78 μg/mL = 380 μM); 5) EA (6.65 μg/mL = 20 μM) + TMZ (112.61 μg/mL = 580 μM); 6) EA (11.63 μg/mL = 35 μM) + TMZ (62.13 μg/mL = 320 μM); 7) untreated controls.

2.8.2 RNA isolation and sequencing

RNA was extracted as described (Ulrich-Merzenich et al., 2017) 100 ng/μL was used for RNA sequencing. The RNA sequencing was performed by the NGSCore Facility of the University Hospital Bonn. RNASeq data were deposited into the Gene Expression Omnibus database under accession number GSE245919 (URL: 154 https://www.ncbi.nlm.nih.gov/geo/query/acc.cgi?acc=GSE245919).

2.8.3 Data evaluation

Data evaluation was performed according to the guidelines provided on the Galaxy Training website (https://training.galaxyproject.org/) and with Ingenuity Pathway Analysis (QIAGEN IPA). GeneMANIA (Warde-Farley et al., 2010) was used to construct the network based on data on co-expression, genetic interaction, and pathways (https://genemania.org/).

2.9 Quantitative RT-PCR (qRT-PCR)

The same RNA samples analyzed by RNASeq were used for quantitative reverse transcription (qRT-PCR) as described earlier (Abdel-Aziz et al., 2015). See also Supplementary Material S3, S4.

2.10 Protein Wnt-inhibitory factor 1 (WIF1) release

Cells were treated as described under 2.5.2. Treatment was either with EA (6.65, 13.29, and 19.94 μg/mL = 20, 40, and 60 μM) or TMZ (58.25, 87.37, and 116.49 μg/mL = 300, 450, and 600 μM) alone or in combinations. The WIF1 release was determined by Human WIF-1 DuoSet ELISA (R&D Systems).

2.11 Statistical analysis

All values are expressed as mean ± SEM of three independent experiments. Experiments were performed with at least 3 replicates for each condition, if not otherwise mentioned. Statistical analyses were performed with SigmaStat (v.4.0) (http://www.systat.de/SigmaStat4_PR.html) and Origin 2018 software (https://www.originlab.com/origin) packages.

10.3389/fphar.2025.1633978

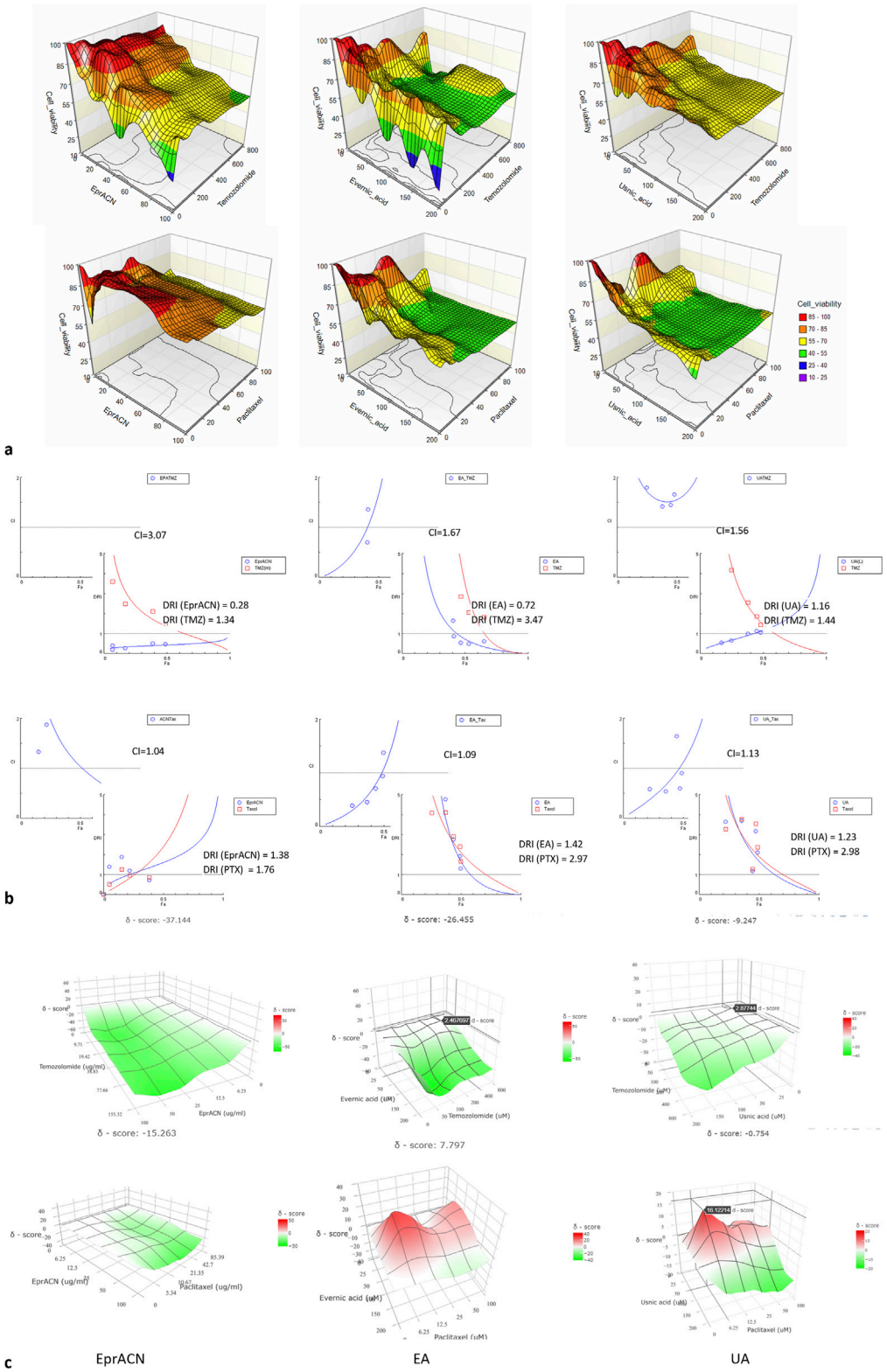

FIGURE 1
Synergy assessments **(a)** Surface plots illustrating the cell viability expressed as a percentage of the control (Z-axes) depending on the treatment with the combination of TMZ or PTX (X-axes) and EprACN or EA or UA (Y-axes) at different concentrations. **(b)** Plots indicating the relation of CI and DRI to Fa. The CI < 1 denotes synergy, CI = 1 addition, and CI > 1 antagonism. **(c)** Surface plots illustrating the δ-score (Z-axes) indicating synergy (red), additive effect (white), or antagonism (green) for the combinations of TMZ or PTX (Y-axes) with EprACN, EA, or UA (X-axes) at various concentrations. Experiments were performed with 3 replicates.

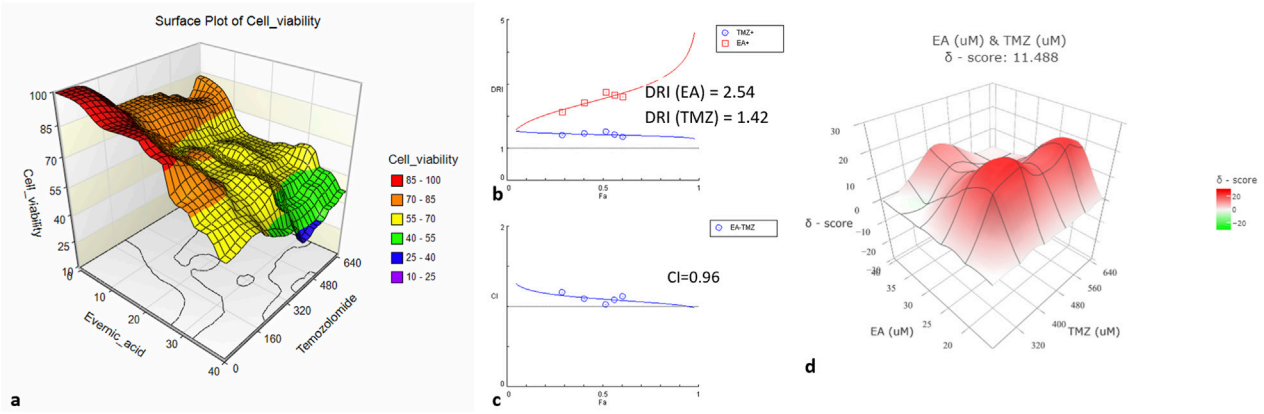

FIGURE 2
U-87 cell viability and synergy calculations for the combinations of TMZ with EA at a ratio of 1:16. **(a)** Surface plot illustrating the cell viability as a percentage of the control (Z-axes) with the combination of TMZ (X-axes) and EA (Y-axes) at different concentrations. **(b)** The plot illustrates the relation of DRI to Fa. **(c)** The plot illustrates the CI according to Fa. **(d)** The surface plot illustrates the δ-score (Z-axes) indicating synergy for TMZ (Y-axes) with EA (X-axes) combination at different concentrations. Experiments were performed with 3 replicates.

3 Results

3.1 Effects of lichen extracts and metabolites on cancer cells and fibroblasts

The ability of the lichen extracts, metabolites, and reference drugs to reduce the metabolic activity of TMZ-resistant U-87 and MCF7 cell lines and normal human skin fibroblasts (HSKF) is displayed in Table 1 and Supplementary Material S2.

The IC_{50} of TMZ against U-87 cells was high, confirming resistance to TMZ (Lee, 2016). All lichen extracts and metabolites significantly reduced the metabolic activity of U-87 cells. EprDCM had the highest potency, however, it also affected HSKF at a similar concentration, showing undesirable off-target action. EprACN, CarHex, and CarACN showed comparable reduction in U-87 cell metabolic activity. CarACN showed a high effect on HSKF, while EprACN demonstrated favorable specificity with a high selectivity index (SI) for U-87.

EA and UA did not significantly affect the metabolic activity of HSKF at concentrations up to 66.46 µg/mL and 68.86 µg/mL (equivalent to 200 µM), respectively. In U-87 cells, EA demonstrated greater activity and more favorable response comparing to UA. The results indicated that while the compounds were effective against cancer cell lines, they exhibited reduced activity toward HSKF cells, suggesting a degree of selectivity toward malignant cells.

The lichen extracts did not reduce the metabolic activity of MCF7 with the SI value below 1, indicating a lack of selectivity. Both EA and UA showed activity against MCF7 cells, but their SI was comparatively lower than that of PTX, leading to the discontinuation of further experiments with MCF7 cells. In the next step, combinations were investigated.

3.2 Combinatorial effects of lichen metabolites with TMZ or PTX

Figure 1a demonstrates the effects of combining TMZ or PTX with EprACN, EA, or UA on the metabolic activity of U-87 and MCF7 cells. The combination Index (CI) and the Dose Reduction Index (DRI) are shown in Figure 1b and the δ-score in Figure 1c.

The combination of EprACN with TMZ exhibited antagonism (CI = 3.07) and with PTX additive effects (CI = 1.04) (Figure 1b). Despite the additive effect of EprACN-PTX, metabolic activity remained above 50%. Consequently, combinations involving EprACN were not pursued. The UA-TMZ combination also displayed limited modulation of the metabolic activity (Figure 1a), and was therefore excluded from further investigations.

Although the EA-TMZ combination demonstrated antagonism, EA increased the sensitivity of U-87 cells to TMZ by 3.4 times (DRI = 3.4). Synergistic effects were observed at Fa < 0.5 (Figure 1b) with a CI of 0.97 for the combination of EA (8.31 µg/mL = 25 µM) and TMZ (77.66 µg/mL = 400 µM) at a 1:4 ratio (Figure 1c), resulting in approximately 50% reduction in metabolic activity (Figure 1a).

Effects of the EA-PTX and UA-PTX combinations were similar, with enhanced effectiveness leading to up to 60% in metabolic activity reduction (Figure 1a). These combinations had a primarily additive effect (Figure 1b, CI ≈ 1), transitioning to synergistic effects at concentrations of EA (4.15–33.23 µg/mL = 12.5–100 µM) – PTX (5.34–85.39 µg/mL = 6.25–100 µM) and UA (4.30–34.43 µg/mL = 12.5–100 µM) – PTX (5.34–85.39 µg/mL = 6.25–100 µM) (Figure 1c, δ-score > 0).

Since synergistic effects are influenced not only by drug concentrations but also by their ratio (Ammar and Ulrich-Merzenich, 2017), further research focused on the ratio (1:16) that demonstrated synergy (Figure 2).

At a ratio of 1:16, the TMZ-EA combination reached the maximum reduction of metabolic activity (75%). The IC_{50} of the drug combination was lower than the IC_{50} values of the single drugs (Figure 2a). Both metabolites showed a dose reduction (DRI > 1), and the CI value indicated additive effects (Figures 2 b,c). The δ-score demonstrated synergistic effects (Figure 2d). These promising results led to the investigation of the potential mechanisms underlying EA's action (Figure 3).

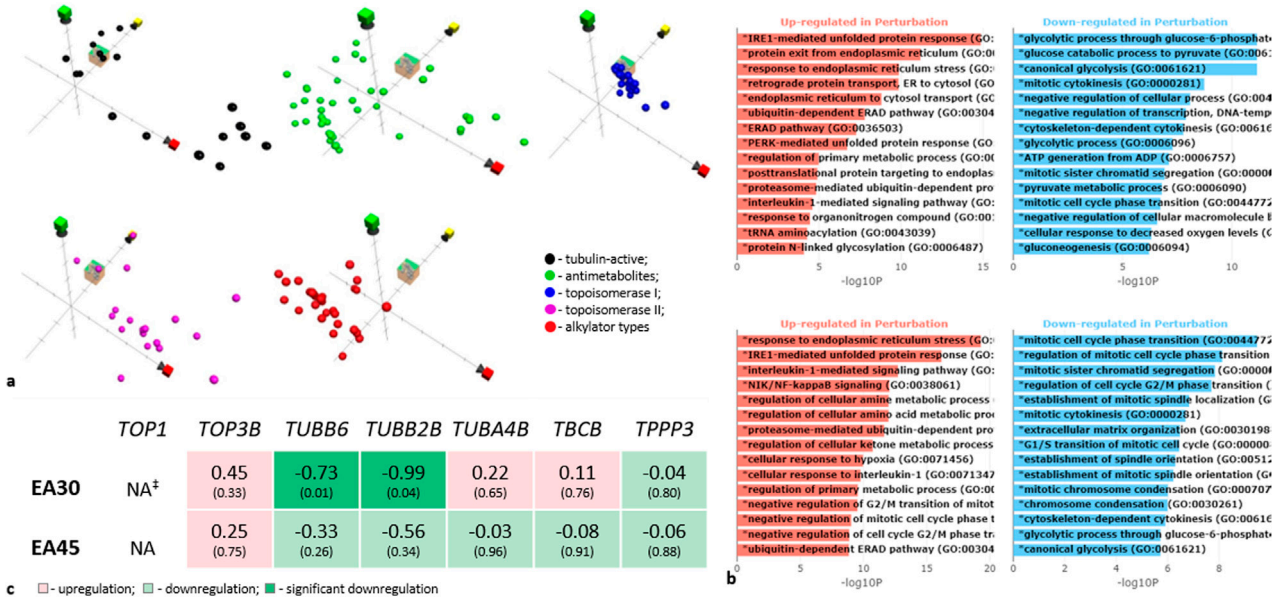

		TOP1	TOP3B	TUBB6	TUBB2B	TUBA4B	TBCB	TPPP3
EA30	NA‡	0.45 (0.33)	-0.73 (0.01)	-0.99 (0.04)	0.22 (0.65)	0.11 (0.76)	-0.04 (0.80)
EA45	NA	0.25 (0.75)	-0.33 (0.26)	-0.56 (0.34)	-0.03 (0.96)	-0.08 (0.91)	-0.06 (0.88)

FIGURE 3
Investigation of the mechanism of action of *Evernia prunastri* ingredients. **(a)** Position in chemical property space of EA (cube), compared to reference sets of compounds in ChemGPS. The axis markers: red–size-related properties, yellow–conjugation and aromaticity-related properties, and green–lipophilicity and solubility-related properties. **(b)** Gene ontology enrichment analysis bar plot based on RNA deep sequencing data. Y-axis indicates significantly enriched GO biological processes, X-axis shows -$\log_{10}$ (p-values). Upper panel -EA 30 μM (9.97 μg/mL), lower panel -EA 45 μM (14.95 μg/ml). For details see Supplementary Material S5. **(c)** Gene sequencing data for tubulin-encoding genes. ‡NA: the gene is "not available" or the gene was excluded from analysis because it contained an extreme count outlier–large counts (during the gene expression analysis in Galaxy). Experiments were performed with 3 replicates.

3.3 Mechanistic insights into EA's mode of action

In a first step, we used ChemGPs for a chemographic prediction of EA's mode of action. The Euclidean distance calculation over all eight dimensions of the ChemGPS-NP chemical property space suggests that EA's most probable mode of action is either topoisomerase I inhibition or disturbance of tubulin activity (Figure 3a). EA shares chemical properties with topoisomerase I (TOP1) inhibitors. Few TOP-1 inhibitors are semi-synthetic derivatives of the plant alkaloid camptothecin, stabilizing TOP1-DNA cleavable complexes (Top1cc) (Thomas and Pommier, 2019/06). In a second step, we compared the prediction with the RNAseq data analyses of the experiments. Here, the level of TOP1 was insignificant (Figure 3c). Thus, EA may interact with TOP1 either by blocking the DNA-helix or by disrupting, e.g., electrostatic interactions on the surface of TOP1 by binding to the active site.

Tubulin-active compounds bind to the tubulin microtubules, affecting their dynamics (Janke and Magiera, 2020). Although we did not examine the polymerization of microtubules and their dynamics, we evaluated the transcription of tubulins. EA decreased transcription of the β-tubulins *TUBB6* and *TUBB2B* (Figure 3c). Since microtubules consist of α-β tubulin heterodimers (Janke and Magiera, 2020), a downregulation of β-isotypes may change the microtubule formations and prevent cell division. The Gene Ontology analysis of genes regulated by EA demonstrated an involvement of mitotic cell cycle phase transition, mitotic sister chromatid segregation, the establishment of mitotic spindle localization, mitotic cytokinesis, and mitotic chromosome condensation in such an activity (Figure 3b). This supports the prediction for EA to be a tubulin-active compound (see also Supplementary Material S5 for results of the Expression of genes coding tubulin-related proteins and Supplementary Material S6 for results of the Gene Ontology analysis).

Western blot analyses revealed that EA, along with EprACN, also modulates key signaling pathways. Figures 4a,b depict the modulation of Erk1/2, c-Jun, and Akt by EprACN and EA over 6, 12, and 24 h. EprACN and EA initially stimulated ERK1/2 formation at 6 h, followed by a downregulation after 12 h and 24 h compared to the control. Higher concentrations of EprACN and EA decreased the ERK phosphorylation at all times. They also downregulated c-Jun phosphorylation after 24 h, with a transient increase observed at 6 h. EprACN downregulated Akt phosphorylation after 6 h, whereas EA insignificantly upregulated it. Significant downregulation was observed after 12 h with EprACN (30 μg/mL), with no further change at 24 h, and with EA (13.29 μg/mL = 40 μM) after 24 h. The RNAseq data of the MAPK and PI3K pathways members' expression, shown in Figure 4c, demonstrated no significant effect on their transcription.

3.4 Multitarget mechanisms of EA-TMZ synergy

Expanding the RNA Seq analyses, we compared significantly regulated genes from the GE-analyses for all treatments using Venn diagrams (Figure 5a) to identify unique genes for the combinations. A network built using these genes revealed the canonical Wnt pathway as a pathway regulated by these genes (Figure 5b). The canonical Wnt signaling pathway significantly contributes to the

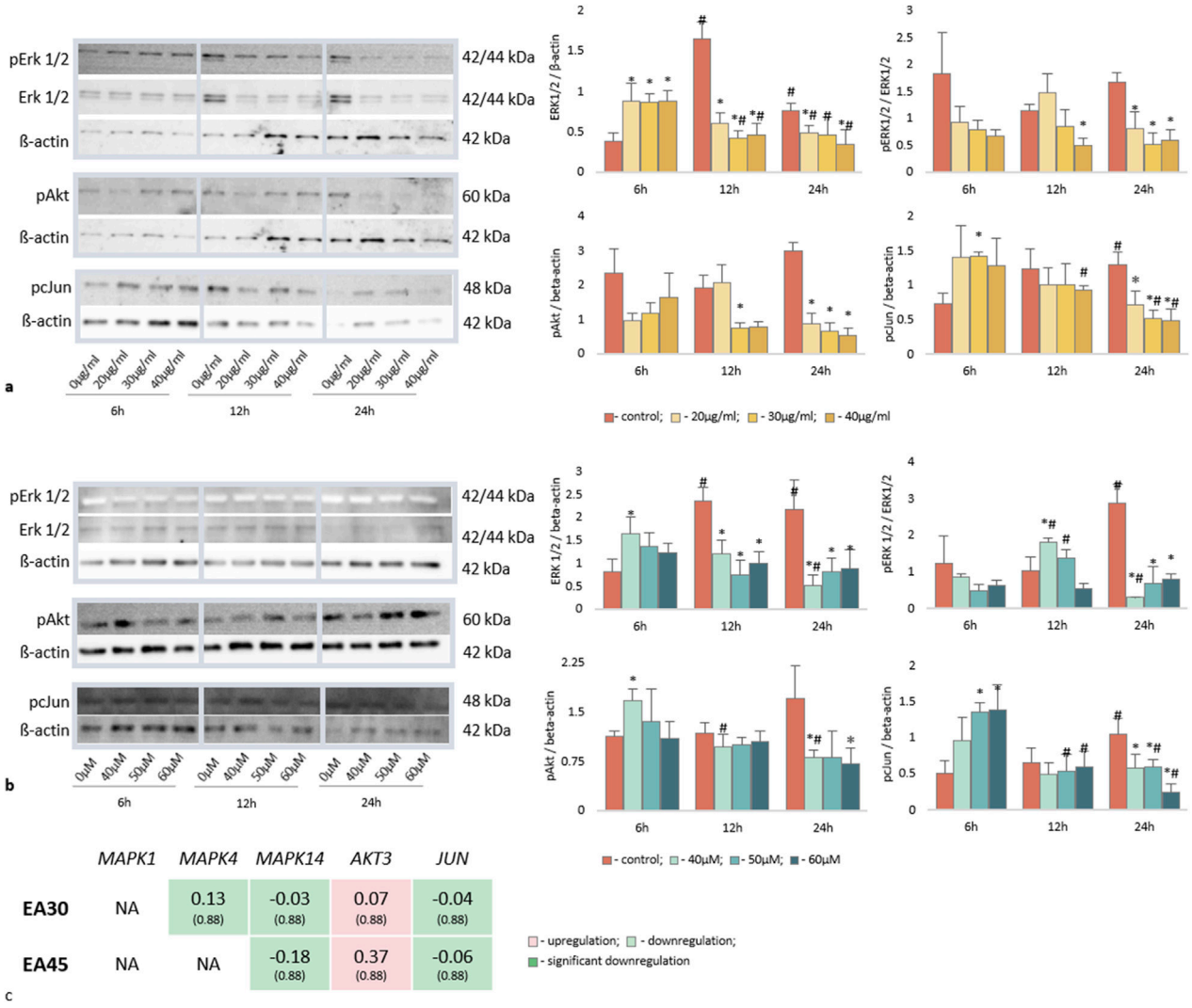

FIGURE 4
Western blot for key proteins of the MAP Kinase and mTOR pathways expressed in U-87 cells treated with **(a)** EprACN (0, 20, 30, 40 µg/mL) and **(b)** EA (0, 40, 50, 60 µM) over a time period of 6, 12, and 24 h. **(c)** Gene expression of MAPK and PI3K pathways at 24 h #p-value <0.05: time-dependent comparison to control, *p-value <0.05: concentration-dependent protein expression over time. Experiments were performed with 3 replicates.

development of resistance to chemo- and radiotherapy in GBM (Zhong and Virshup, 2020). Figure 5c illustrates the expressed genes involved in Wnt signaling upon treatment.

Particularly, EA35TMZ320 significantly downregulated the upstream member *WNT5A*, whereas other treatments did not show a significant effect. Conversely, *WNT3*, a ligand of LRP5/6 (Low-density lipoprotein receptor-related protein 5/6), exhibited significant undesirable upregulation by EA45, whereas *DKK2* and *DKK4*, which are inhibitors of LRP5/6, remained unaffected by any treatment.

All combinations significantly downregulated *FZD7* transcription, which encodes a transmembrane receptor crucial for Wnt downstream. Activation of this receptor by Wnts inhibits the β-catenin degradation complex. Additionally, *CTNNBIP1*, an intracellular member known to prevent β-catenin activity, showed significant upregulation of gene expression by EA20TMZ380.

TCF7L1, an intranuclear member of the pathway involved in cell cycle regulation and proliferation, was significantly downregulated by TMZ600, EA45, EA35TMZ320, and EA20TMZ580.

Figure 5d summarizes the interaction of affected targets within the Wnt pathway. The combinations regulated the transcription of more targets compared to single metabolites.

After analyzing the GE of members of the Wnt-signaling pathway under treatment, we wanted to know whether Wnt-signaling is affected on the protein level. Therefore, we measured the Wnt inhibitory factor 1 (WIF1). WIF1 binds to Wnt-proteins, thereby inhibiting the activation of the Wnt-signaling (see also Supplementary Material S7).

Figure 5e shows the release of WIF1 protein by U-87 cells treated with TMZ and EA alone or in combination. Both single metabolites and combinations significantly increased the WIF1 release compared to the control. Combinations demonstrated a dose-dependent increase in WIF1 release, with

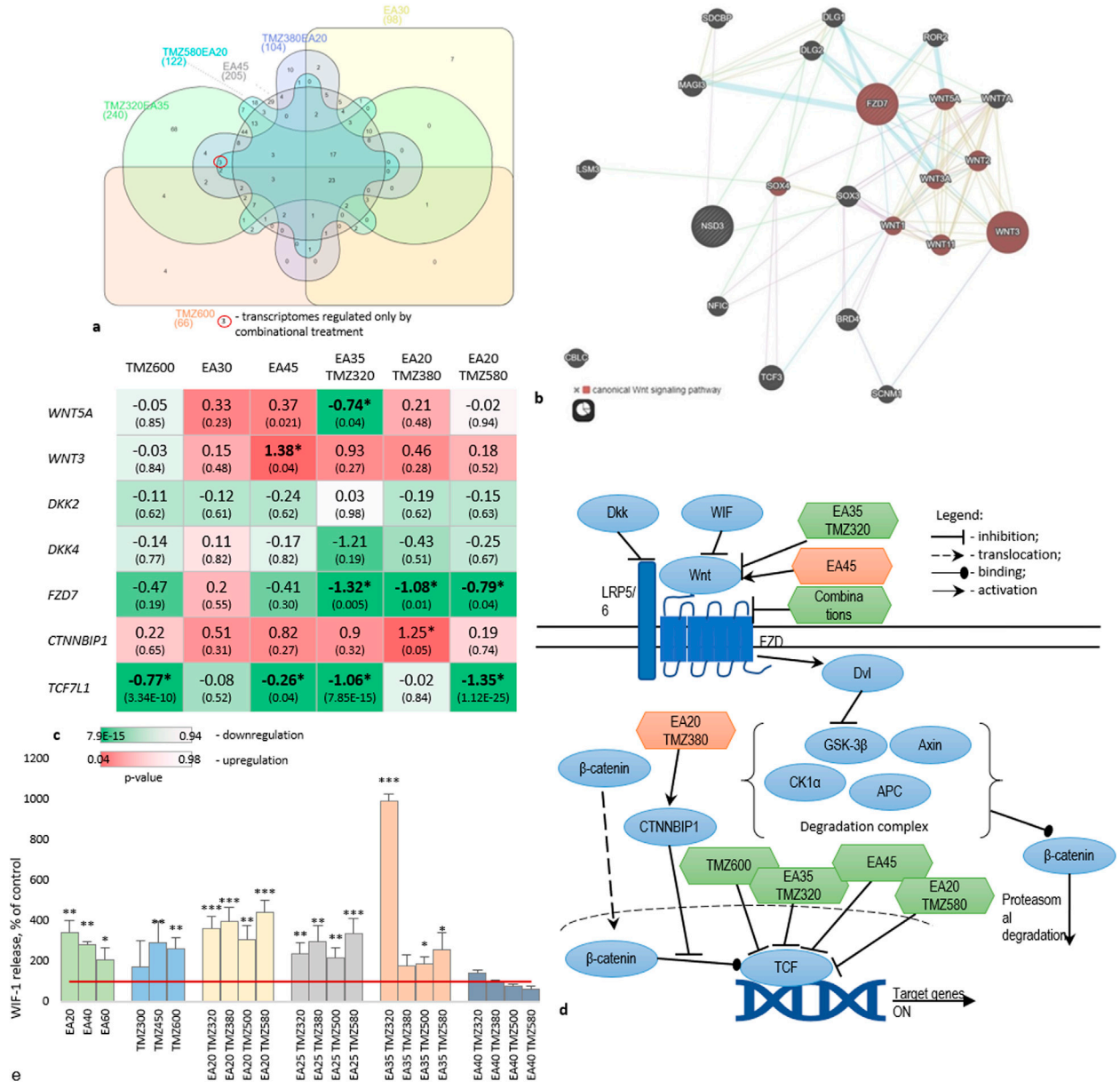

	TMZ600	EA30	EA45	EA35 TMZ320	EA20 TMZ380	EA20 TMZ580
WNT5A	-0.05 (0.85)	0.33 (0.23)	0.37 (0.021)	**-0.74*** (0.04)	0.21 (0.48)	-0.02 (0.94)
WNT3	-0.03 (0.84)	0.15 (0.48)	**1.38*** (0.04)	0.93 (0.27)	0.46 (0.28)	0.18 (0.52)
DKK2	-0.11 (0.62)	-0.12 (0.61)	-0.24 (0.62)	0.03 (0.98)	-0.19 (0.62)	-0.15 (0.63)
DKK4	-0.14 (0.77)	0.11 (0.82)	-0.17 (0.82)	-1.21 (0.19)	-0.43 (0.51)	-0.25 (0.67)
FZD7	-0.47 (0.19)	0.2 (0.55)	-0.41 (0.30)	**-1.32*** (0.005)	**-1.08*** (0.01)	**-0.79*** (0.04)
CTNNBIP1	0.22 (0.65)	0.51 (0.31)	0.82 (0.27)	0.9 (0.32)	1.25* (0.05)	0.19 (0.74)
TCF7L1	**-0.77*** (3.34E-10)	-0.08 (0.52)	**-0.26*** (0.04)	**-1.06*** (7.85E-15)	-0.02 (0.84)	**-1.35*** (1.12E-25)

FIGURE 5
Regulation of Wnt signaling during treatment of U-87 cells with TMZ, EA, and their combinations. **(a)** Venn-diagram (https://www.interactivenn.net/) on significantly regulated genes obtained from the transcriptome analyses. **(b)** Network depicting a possible pathway uniquely regulated by the combinations, obtained from GeneMania (https://genemania.org/). **(c)** Gene expression of Wnt signaling members. Data are presented as logFC. Cell colors represent p-values. **(d)** Schematic representation of the proposed pathway regulated by combinations. **(e)** Level of WIF1 protein release into the culture medium. *p < 0.05, **p < 0.01, ***: p < 0.001. The red line indicates the control. Experiments were performed with 3 replicates.

the highest activity for EA35TMZ320. The effect of TMZ and EA on the WIF1 release showed a concentration-dependent inverse pattern: higher TMZ concentration increases the effect, while higher EA concentration reduces it. Significant up-regulations were observed by the following combinations: EA20TMZ500, EA20TMZ580, EA25TMZ580, EA35TMZ320, EA35TMZ380, and EA30TMZ500. However, EA35TMZ320 showed the highest influence on the WIF1 release.

The Wnt pathway is a regulatory system interacting directly or indirectly with other signaling pathways, including the NF-kB pathway, as a central pathway in inflammation (Guo et al., 2024). This pathway is essential for connecting inflammation and cancer, as well as for tumor growth and resistance (Guo et al., 2024). For BC, it was shown that NF-kB signaling boosts the growth potential of BC cells and facilitates the spread of tumors (Guo et al., 2024). Therefore, we were interested in the influence of our metabolites and their combinations with TMZ on inflammation. At the same time, we were interested in EA's reported neuroprotective and anti-inflammatory properties (Lee et al., 2021). Figure 6 shows the influence of the single metabolites and the combinations on the GE of *GABRs*, *BDNF*, and major cytokines regulating inflammatory processes (*IL6*, *IL10*, and

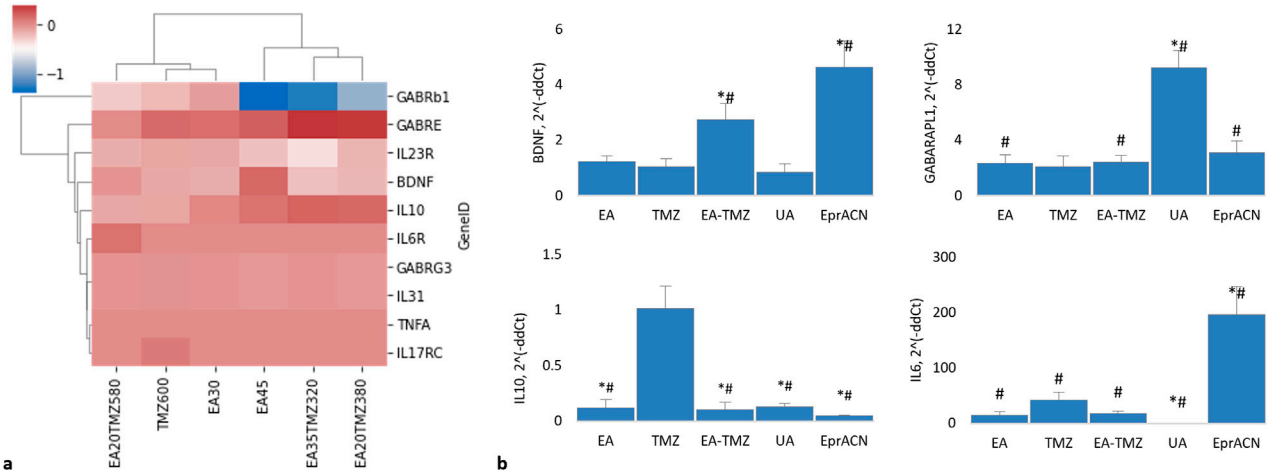

FIGURE 6
Expression of genes encoding brain-related proteins and cytokines. **(a)** Clustered HeatMap of RNAseq data showing the expression levels of various genes. None of the genes were found to be significantly regulated ($p > 0.05$). Genes include GABRB1: gamma-aminobutyric acid receptor (GABR) subunit beta 1; GABRE: GABR subunit epsilon; GABRG3: GABR subunit gamma 3; BDNF: brain-derived neurotrophic factor; IL10: interleukin 10; IL6R: interleukin 6 receptor; TNFa: tumor necrosis factor a; IL23R: interleukin 23 receptor; IL31: interleukin 31; IL17RC: interleukin 17 receptor. **(b)** Histograms showing mRNA levels based on qRT-PCR data. Concentrations: EA – 45 μM, TMZ – 600 μM, EA-TMZ – 35–320 μM, UA – 200 μM, and EprACN – 30 μg/mL. GABARAPL1: GABAA receptor-associated protein-like 1. *$p < 0.05$ comparing to TMZ, #$p < 0.05$ comparing to untreated control. Experiments were performed with 3 replicates.

TNFA) based on RNA deep sequencing (Figure 6a) and RT-PCR (Figure 6b).

The pro-inflammatory cytokine *TNFA* was neither detected by RNA deep sequencing nor by qRT-PCR. The anti-inflammatory *IL10,* detected by deep sequencing, was not significantly influenced. The RNAseq data showed no regulation of *IL6*. However, qRT-PCR data showed a significantly amplified expression of *IL6* for the single treatment with EprACN or with TMZ, whereas UA downregulated the GE.

RNAseq analysis showed no significant differences in the expression of *GABA* receptor subunits. However, *GABRB1* was downregulated by EA45 ($p = 0.07$), while *GABARAPL1* was desirably upregulated for all treatments, with the highest expression seen with UA.

RNAseq analysis further revealed insignificant influences of all treatments on *BDNF* transcription. However, in qRT-PCR investigations, *BDNF* was upregulated by EA-TMZ and EprACN and downregulated by UA.

IL10 gene expression was significantly downregulated by all treatments except TMZ, while *IL6* gene expression was significantly increased by EprACN and decreased by UA.

4 Discussion

The effectiveness of standard chemotherapeutics such as temozolomide (TMZ) in glioblastoma (GBM) and paclitaxel (PTX) in breast cancer (BC) is often limited by developing resistance and eventual treatment failure (Das et al., 2021; Lee, 2016). Therefore, we investigated the adjuvant potential of characterized extracts of *E. prunastri* and *C. arbuscula* and their metabolites evernic acid (EA) and usnic acid (UA) alone or in combination with TMZ and PTX for their immunomodulatory and chemosensitivity-increasing potential. HSKF served to evaluate general cytotoxicity and selectivity, even though these cells do not fully replicate the physiological environment or cellular characteristics of normal brain or mammary tissue. U-87 and MCF7 cells have their limitation, too. U-87 cells differ genetically from primary GBM tumors and do not fully recapitulate the intratumoral heterogeneity, stem cell populations, or invasive behavior observed in patient-derived GBM (Xie et al., 2015; Allen et al., 2016). Likewise, MCF7 cells, while representative of HR+ BC, do not model the full spectrum of BC subtypes, particularly TNBC or HER2+ disease, and lack the tumor microenvironment components that influence drug response *in vivo* (Neve et al., 2006; Holliday and Speirs, 2011). Both models are grown in two-dimensional monolayers, which do not capture the complexity of tumor-stroma interactions, hypoxia, or immune modulation present in human tumors. Despite these limitations, the use of U-87 and MCF7 in this study provides a well-established platform for assessing the antiproliferative and resistance-modulating effects of lichen-derived metabolites with findings that can inform subsequent validation in more complex models such as patient-derived cells, organoids, or *in vivo* systems.

The initial experiments revealed a reduction in cellular metabolic activity in U-87 and MCF7 cells after treated with the lichen extracts and their metabolites. However, they were less effective against MCF7 cells compared to PTX. Therefore, experiments with MCF7 cells were discontinued, even though UA had exhibited activity against MCF7 cells in earlier studies (Bačkorová et al., 2011; Hawrył et al., 2020).

For extracts of *E. prunastri,* IC_{50} values of 90.1 μg/mL and 81.8 μg/mL were reported (Bézivin et al., 2004), which is in the range of our results. Effects of EA against MCF7 and U-87 have not been reported earlier. However, previous reports suggest its activity

against A-172 and T98G glioblastoma cell lines (Studzińska-Sroka et al., 2021), supporting our findings.

The extracts of *C. arbuscula* were not further investigated due to their non-selective effect. Further experiments focused on the TMZ-resistant U-87 cells (IC_{50} > 500 μM) (Lee, 2016) and the combination of TMZ and EA, since this combination yielded the most promising reduction in cellular metabolic activity, while showing minimal effect on HSKF.

To substantiate the antiproliferative effects, we performed Western blot (WB) analyses of members of the central MAPK families. They play a central role by regulating the cell cycle engine and other proliferation-related proteins (Bézivin et al., 2004; Studzińska-Sroka et al., 2021; Zhang and Liu, 2002). In addition, we measured AKT. In the context of cancer, Akt signaling promotes tumor cell survival, proliferation, growth, and metabolism by activating its downstream effectors. Both the PI3K/Akt and the MEK/ERK pathways cooperate in tumor growth and are involved in the development of therapeutic resistance in GBM cells (Singh et al., 2023).

WB analyses revealed that EprACN and EA reduced the expression and phosphorylation of ERK1/2 over time, explaining the observed decrease in the metabolic activity in U-87 cells and revealing an antiproliferative activity, as in most cells, sustained ERK activation is required to induce cell cycle entry. In Glioma, an aberrant activity of the RAS/MAPK/ERK pathway appears to play a crucial role in the development of gliomas (Stachyra and Grzybowska-Szatkowska, 2025). Even a large proportion of resistance mechanisms are associated with reactivation of the RTK/Raf/Ras/MEK/ERK pathway. Co-treatment with inhibitors targeting these pathways is meanwhile regarded as a compelling strategy to overcome resistance mechanisms in GBM (Yakubov et al., 2025).

Another member of the MAPK-pathway, the so-called proto-oncogene c-Jun, is also central to cancer-altered signalling: an upregulated c-Jun was described for variable tumor cells, specifically in brain tumors, contributing to its malignancy (Blau et al., 2012). Blau et al. demonstrated that the accumulation of c-Jun in tumors is regulated more translationally than transcriptionally (Blau et al., 2012) corresponding to our data with the regulation of c-Jun at the protein but not at the mRNA level.

EprACN and EA downregulated pAkt in a time- and dose-dependent manner corresponding to the reduction in metabolic activity in U-87 cells. This is particularly relevant, given that overexpression and high phosphorylation of Akt correlate with a poor prognosis in glioblastoma patients (Shahcheraghi et al., 2020). Increased pAkt activates transcription factors by phosphorylating GSK3β, leading to its inactivation and subsequent translocation of β-catenin into the nucleus. Both pathways, when activated independently, may contribute to resistance (Manoranjan et al., 2020). Conversely, β-catenin also induces the expression of Akt1 and Akt2 and the phosphorylation of Akt (Zhong and Virshup, 2020). Transcription of *WNT3* was contradictorily upregulated by EA, indicating a limitation as a single treatment at higher concentrations. Nevertheless, the downregulation of Akt by EprACN and EA may contribute to the enhanced sensitivity of U-87 cells to TMZ.

In our combinatory study, GE-profiling of U-87 cells revealed the modulation of multiple components within the Wnt/β-catenin pathway. Combination EA35TMZ320 reduced the transcription of WNT5A, an upstream intracellular member (Yu et al., 2007; Chen et al., 2021) known to play a pro-tumor role in glioma (Zuccarini et al., 2018; Chen et al., 2021) to induce the migration of GBM cells (Lee, 2016) to increase cell proliferation (Yu et al., 2007; Chen et al., 2021) and to correlate with higher WHO histological glioma classification grades (Alkailani et al., 2022). A Wnt5a knockdown inhibited the activity of the GSK3β/β-catenin pathway related to glioma-derived endothelial cell angiogenesis (Chen et al., 2021).

Frizzleds (FZDs) are transmembrane receptors (Alkailani et al., 2022) inhibiting the β-catenin degradation complex (Shahcheraghi et al., 2020). In glioma, FZD7 is upregulated, correlating with poor patient outcomes (Zuccarini et al., 2018). The significant downregulation of *FZD7* GE by all combinations is promising. Alike EA20TMZ380 significantly upregulated the GE of *CTNNBIP1*, which prevents the interaction of β-catenin and TCF (transcription factors) family members. Negative regulation of CTNNBIP1 correlates with higher grades of glioma (Tong et al., 2015).

To support the transcriptional findings, we measured the release of Wnt inhibitory factor (WIF1) protein via ELISA. WIF1 binds to Wnt-proteins, thereby inhibiting Wnt pathway signalling. Both single metabolites and combinations increased the release of WIF1 protein. In contrast, the combination of high concentrations of EA (40 μM) and TMZ (≥380 μM) reduced WIF1 releases, supporting the dose-dependent effects observed in the GE analyses, where higher concentrations induced an upregulation of *WNT3*. This inverse dose-dependent WIF1 regulation underscores the importance of optimized dosing to balance pathway modulation.

Cross-talks between signaling pathways are known to play a role in resistance development f. e. Wnt/ß-catenin signaling activates NF-kB in the cytoplasm, whereas Dvl inhibits NF-kB signaling in the nucleus (Guo et al., 2024). Even more in breast cancer, NF-kB has been confirmed to be a crucial link between resistance signaling pathways (Zhao et al., 2021). Activated NF-kB promotes the production of Wnt, ß-catenin, and ß-TrCP, which can lead to cytokine storms up to death (Guo et al., 2024; Jang et al., 2021). We did not measure NF-kB, but the gene expression of *IL6*, a product of NF-kB, which can activate, via STAT3, cell survival, proliferation, and inflammation (Guo et al., 2024). The resolution of inflammation is regarded as a novel host-focused option to complement existing therapies for glioma (Bazan et al., 2021). IL6 is frequently upregulated in GBM, where it activates JAK/STAT3 signaling to promote tumor cell survival, proliferation, and therapy resistance, and contributes to an immunosuppressive milieu (West et al., 2018). IL10 primarily exerts immunosuppressive effects in the GBM microenvironment by inhibiting effective anti-tumor immune responses and, in some contexts, directly enhancing glioma proliferation via JAK–STAT3 activation (Widodo et al., 2021). EprACN and TMZ increased the transcription of *IL6* (RT-PCR), and *IL10* transcripts were detectable. However, we previously observed that plant ingredients and acetylsalicylic acid stimulated the GE of *IL6* and *IL10* under non-stress conditions, which turned into an anti-inflammatory response under inflammatory conditions. Such cytokine regulations may keep the immune-regulatory system active and influence the cytokine release dynamics (Ulrich-Merzenich et al., 2017). This hypothesis aligns with Ahmad

et al.'s proposition that the simultaneous expression of IL6 and IL10 in tumor tissues improves the survival of breast cancer patients, although underlying mechanisms remain unclear (Ahmad et al., 2018).

We did not observe changes in the GE of *IL4* and *IL8*. However, both exert their most critical actions via crosstalk with immune and endothelial cells. In a tumor-cell-only model, the roles of IL4 and IL8 would likely appear less central compared to their significance in the complex *in vivo* GBM microenvironment (Brat et al., 2005; Losur et al., 2024).

Furthermore, the IL-17B/ IL-17RB pathway has been implicated in tumorigenesis and resistance to anticancer therapies (Briukhovetska et al., 2021). The IL-17A/F, binding to the IL17RC receptor, demonstrated pro-tumoral effects (Briukhovetska et al., 2021). Although its precise role in tumor resistance remains unclear. Our RNAseq data revealed exclusive expression of RNA encoding *IL17RC* in resistant U-87 cells treated with high TMZ concentrations, suggesting that the IL-17 pathway may contribute to the development of resistance in U-87 cells, a finding warranting further study.

Brain-derived neurotrophic factor (BDNF), an endogenous signaling molecule, is involved in the carcinogenesis of glioma (Zheng and Chen, 2020), especially in tumor growth and metastasis in neuroblastoma (Chen et al., 2016), whereas a precursor of BDNF (proBDNF) plays a role in the modulation of cell apoptosis (Xiong et al., 2013). In our study, EA35TMZ320 and EprACN30 induced significant over-expression of *BDNF* without activating GE of the PI3K and MAPK pathway members. We hypothesize that such an effect does not induce cell growth or counteract the reduction in metabolic activity seen in U-87 cells upon different treatments.

GABAA forms a heterotetrameric complex (Huang et al., 2022). The expression of subunits α, β, and γ-subfamilies correlates with the malignancy grade of gliomas (Smits et al., 2012). Patients with high GABAA receptor-associated protein (GABARAPL1) expression levels were reported to have a lower risk for metastasis (Le Grand et al., 2011). In MCF7 cells, GABARAPL was demonstrated to inhibit Dvl2 (disheveled segment polarity protein 2), an inhibitor of the β-catenin degradation complex (Boyer-Guittaut et al., 2014). While TMZ, EA, and TMZ-EA did not affect the GE of Dvl2, TMZ and EA upregulated the GE of *GABARAPL1*. Thus, we suggest that the downregulation of the Wnt signaling cascade observed in our study is likely a direct effect on Wnt signaling members rather than through GABARAPL1.

5 Summary and conclusion

This study demonstrates the potential of lichen-derived metabolites, particularly evernic acid (EA), to modulate key pathways associated with TMZ resistance in U-87 cells, suggesting a promising multitarget mechanism for future investigation. EA reduced the metabolic activity of TMZ-resistant U-87 cells, synergizing with TMZ to reduce viability by 75% at optimized ratios. The prediction of ChemGPS that EA acts on tubulin activity was supported by deep sequencing. Mechanistically, EA suppressed GE of oncogenic Wnt/β-catenin signaling while upregulating the protein expression of WIF1 as a central inhibitor of Wnt-signaling. Combinatorial EA-TMZ treatment further modulated MAPK/PI3K pathways, inhibiting ERK1/2, c-Jun, and Akt phosphorylation, which are critical for glioblastoma survival and resistance.

The discovery of IL17RC overexpression in resistant cells underscores a novel pathway implicated in TMZ resistance, warranting further exploration.

Even though present studies lack an *in vivo* validation, findings form a base for subsequent validation in more complex models. Future studies should clarify EA's direct role in tubulin dynamics, its influence on the IL-17 pathway, on established mechanisms of drug resistance, such as MGMT promoter methylation status, DNA repair pathways, or efflux transporter activity in primary patient-derived cells, as well as *in vivo*, for example, in genetically engineered glioma models (GEGMs) or orthotopic animal models including pharmacodynamic and pharmacokinetic evaluations to explore clinical translation of EA-TMZ combinations. Integrating computational tools like ChemGPS-NP with multi-omics approaches will accelerate the development of natural product-based therapies to address refractory cancers. This work advances the paradigm of combinatorial, mechanism-driven strategies to disrupt resistance-associated pathways and enhance chemosensitivity in oncology.

Data availability statement

The datasets presented in this study can be found in online repositories. The names of the repository/repositories and accession number(s) can be found in the article/Supplementary Material.

Ethics statement

Ethical approval was not required for the studies on humans in accordance with the local legislation and institutional requirements because humans were not involved in the study. Only commercially available established cell lines were used. Ethical approval was not required for the studies on animals in accordance with the local legislation and institutional requirements because animals were not involved in the study. Only commercially available established cell lines were used.

Author contributions

AS: Conceptualization, Software, Investigation, Formal Analysis, Writing – review and editing, Resources, Visualization, Writing – original draft. LN: Formal Analysis, Writing – review and editing, Investigation, Visualization, Validation. AK: Writing – review and editing, Methodology, Conceptualization. AB: Conceptualization, Methodology, Writing – review and editing, Software. SB: Methodology, Conceptualization, Writing – review and editing, Software. ER: Writing – review and editing, Resources. GU-M: Supervision, Conceptualization, Writing – review and editing, Software, Methodology, Funding acquisition, Data curation, Writing – original draft.

Funding

The author(s) declare that financial support was received for the research and/or publication of this article. A. Shcherbakova was supported by the German Academic Exchange Service (DAAD) with a long-term scholarship at Bonn University (Medical Clinic III, University Hospital Bonn, Germany) in 2014/15, a short-term scholarship in 2019, by a grant from the President of the Russian Federation for Young Scientists [number MK5290.2012.4] and a grant for international mobility from the Volga State University of Technology at Uppsala University in 2013. Institutional funding was provided for the experimental research at UKB. This publication was supported by the Open Access Publication Fund of the University of Bonn.

Acknowledgments

Part of the work on extract preparation was undertaken in the laboratory of Ulf Göransson, Uppsala University (Shcherbakova et al., 2021). The authors thank Bernd Merzenich for his skillful language editing of the manuscript.

Conflict of interest

The authors declare that the research was conducted in the absence of any commercial or financial relationships that could be construed as a potential conflict of interest.

The author(s) declared that they were an editorial board member of Frontiers, at the time of submission. This had no impact on the peer review process and the final decision.

Generative AI statement

The author(s) declare that no Generative AI was used in the creation of this manuscript.

Any alternative text (alt text) provided alongside figures in this article has been generated by Frontiers with the support of artificial intelligence and reasonable efforts have been made to ensure accuracy, including review by the authors wherever possible. If you identify any issues, please contact us.

Publisher's note

All claims expressed in this article are solely those of the authors and do not necessarily represent those of their affiliated organizations, or those of the publisher, the editors and the reviewers. Any product that may be evaluated in this article, or claim that may be made by its manufacturer, is not guaranteed or endorsed by the publisher.

Supplementary material

The Supplementary Material for this article can be found online at: https://www.frontiersin.org/articles/10.3389/fphar.2025.1633978/full#supplementary-material

References

Abdel-Aziz, H., Schneider, M., Neuhuber, W., Kassem, A. M., Khailah, S., Müller, J., et al. (2015). GPR84 and TREM-1 signaling contribute to the pathogenesis of reflux esophagitis. *Mol. Med.* 21, 1011–1024. doi:10.2119/molmed.2015.00098

Abu, S. T. M., Samec, M., Liskova, A., Kubatka, P., and Büsselberg, D. (2019). Paclitaxel's mechanistic and clinical effects on breast cancer. *Biomolecules* 9, 789. doi:10.3390/biom9120789

Ahmad, N., Ammar, A., Storr, S. J., Green, A. R., Rakha, E., Ellis, I. O., et al. (2018). IL-6 and IL-10 are associated with good prognosis in early stage invasive breast cancer patients. *Cancer Immunol. Immunother.* 67 (4), 537–549. doi:10.1007/s00262-017-2106-8

Alcantara Llaguno, S. R., Chen, J., and Parada, L. F. (2009). Signaling in malignant astrocytomas: role of neural stem cells and its therapeutic implications. *Clin. Cancer Res.* 15 (23), 7124–7129. doi:10.1158/1078-0432.CCR-09-0433

Alkailani, M. I., Aittaleb, M., and Tissir, F. (2022). WNT signaling at the intersection between neurogenesis and brain tumorigenesis. *Front. Mol. Neurosci.* 15, 1017568. doi:10.3389/fnmol.2022.1017568

Allen, M., Bjerke, M., Edlund, H., Nelander, S., and Westermark, B. (2016). Origin of the U87MG glioma cell line: good news and bad news. *Sci. Transl. Med.* 8 (354), 354re3. doi:10.1126/scitranslmed.aaf6853

Ammar, R., and Ulrich-Merzenich, G. (2017). Curcumin synergizes with the endocannabinoid reuptake inhibitor OMDM-2 in human MCF-7 breast cancer and U-87 glioblastoma cells. *Synergy.* 5, 7–14. doi:10.1016/j.synres.2017.11.001

Bačkorová, M., Bačkor, M., Mikeš, J., Jendželovský, R., Fedoročko, P., Backorova, M., et al. (2011). Variable responses of different human cancer cells to the lichen compounds parietin, atranorin, usnic acid and gyrophoric acid. *Toxicol Vitro.* 25(1), 37–44. doi:10.1016/j.tiv.2010.09.004

Baranova, A., Krasnoselskyi, M., Starikov, V., Kartashov, S., Zhulkevych, I., Vlasenko, V., et al. (2022). Triple-negative breast cancer: current treatment strategies and factors of negative prognosis. *J. Med. Life* 15 (2), 153–161. doi:10.25122/jml-2021-0108

Bazan, N. G., Reid, M. M., Flores, V. A. C., Gallo, J. E., Lewis, W., and Belayev, L. (2021). Multiprong control of glioblastoma multiforme invasiveness: blockade of pro-inflammatory signaling, anti-angiogenesis, and homeostasis restoration. *Cancer Metastasis Rev.* 40 (3), 643–647. doi:10.1007/s10555-021-09987-x

Bézivin, C., Tomasi, S., Rouaud, I., Delcros, J. G. G., Boustie, J., Bezivin, C., et al. (2004). Cytotoxic activity of compounds from the lichen: Cladonia convoluta. *Planta Med.* 70, 874–877. doi:10.1055/s-2004-827240

Blau, L., Knirsh, R., Ben-Dror, I., Oren, S., Kuphal, S., Hau, P., et al. (2012). Aberrant expression of c-Jun in glioblastoma by internal ribosome entry site (IRES)-mediated translational activation. *Proc. Natl. Acad. Sci.* 109 (42), E2875–E2884. doi:10.1073/pnas.1203659109

Boyer-Guittaut, M., Poillet, L., Liang, Q., Bôle-Richard, E., Ouyang, X., Benavides, G. A., et al. (2014). The role of GABARAPL1/GEC1 in autophagic flux and mitochondrial quality control in MDA-MB-436 breast cancer cells. *Autophagy* 10 (6), 986–1003. doi:10.4161/auto.28390

Brat, D. J., Bellail, A. C., and Van Meir, E. G. (2005). The role of interleukin-8 and its receptors in gliomagenesis and tumoral angiogenesis. *Neuro Oncol.* 7 (2), 122–133. doi:10.1215/S1152851704001061

Bravo, P., Dois, A., Villarroel, L., González-Agüero, M., Fernández-González, L., Sánchez, C., et al. (2023). Factors influencing the implementation of shared decision-making in breast cancer care: protocol for a mixed-methods study. *BMJ Open* 13 (7), e074111. doi:10.1136/bmjopen-2023-074111

Brisdelli, F., Perilli, M., Sellitri, D., Piovano, M., Garbarino, J. A., Nicoletti, M., et al. (2013). Cytotoxic activity and antioxidant capacity of purified lichen metabolites: an *in vitro* study. *Phytotherapy Res.* 27 (3), 431–437. doi:10.1002/ptr.4739

Briukhovetska, D., Dörr, J., Endres, S., Libby, P., Dinarello, C. A., and Kobold, S. (2021). Interleukins in cancer: from biology to therapy. *Nat. Rev. Cancer* 21 (8), 481–499. doi:10.1038/s41568-021-00363-z

Bukowski, K., Kciuk, M., and Kontek, R. (2020). Mechanisms of multidrug resistance in cancer chemotherapy. *Int. J. Mol. Sci.* 21 (9), 3233. doi:10.3390/ijms21093233

Buonfiglio, R., Engkvist, O., Várkonyi, P., Henz, A., Vikeved, E., Backlund, A., et al. (2015). Investigating pharmacological similarity by charting chemical space. *J. Chem. Inf. Model* 55 (11), 2375–2390. doi:10.1021/acs.jcim.5b00375

Chen, B., Liang, Y., He, Z., An, Y., Zhao, W., and Wu, J. (2016). Autocrine activity of BDNF induced by the STAT3 signaling pathway causes prolonged TrkB activation and promotes human non-small-cell lung cancer proliferation. *Sci. Rep.* 6 (1), 30404. doi:10.1038/srep30404

Chen, Z. F., Liu, J., Huang, Z., Zheng, Y., Deng, S., et al. (2021). Dual role of WNT5A in promoting endothelial differentiation of glioma stem cells and angiogenesis of glioma derived endothelial cells. *Oncogene* 40 (32), 5081–5094. doi:10.1038/s41388-021-01922-2

Chou, T. C. (2010). Drug combination studies and their synergy quantification using the Chou-Talalay method. *Cancer Res.* 70 (2), 440–446. doi:10.1158/0008-5472.CAN-09-1947

Crawford, S. D. (2015). "Lichens used in traditional medicine," in *Lichen secondary metabolites: bioactive properties and pharmaceutical potential*. Editor B. Ranković (Cham, Switzerland: Springer International Publishing), 27–80. doi:10.1007/978-3-319-13374-4_2

Das, T., Anand, U., Pandey, S. K., Ashby, C. R., Assaraf, Y. G., Chen, Z. S., et al. (2021). Therapeutic strategies to overcome taxane resistance in cancer. *Drug Resist. Updat.* 55, 100754. doi:10.1016/j.drup.2021.100754

DeCordova, S., Shastri, A., Tsolaki, A. G., Yasmin, H., Klein, L., Singh, S. K., et al. (2020). Molecular heterogeneity and immunosuppressive microenvironment in glioblastoma. *Front. Immunol.* 11, 1402. doi:10.3389/fimmu.2020.01402

Einarsdottir, E., Groeneweg, J., Bjornsdottir, G. G., Harethardottir, G., Omarsdottir, S., Ingolfsdottir, K., et al. (2010). Cellular mechanisms of the anticancer effects of the lichen compound usnic acid. *Planta Med.* 76 (10), 969–974. doi:10.1055/s-0029-1240851

Emsen, B., Aslan, A., Türkez, H., Taghizadehghalehjoughi, A., and Kaya, A. (2018). The anti-cancer efficacies of diffractaic, lobaric, and usnic acid: *in vitro* inhibition of glioma. *J. Cancer Res. Ther.* 14, 941–951. doi:10.4103/0973-1482.177218

Fekete, B., Werlenius, K., Tisell, M., Pivodic, A., Smits, A., Jakola, A. S., et al. (2023). What predicts survival in glioblastoma? A population-based study of changes in clinical management and outcome. *Front. Surg.* 10, 1249366. doi:10.3389/fsurg.2023.1249366

Fernández-Moriano, C., Divakar, P. K., Crespo, A., and Gómez-Serranillos, M. P. (2017). Protective effects of lichen metabolites evernic and usnic acids against redox impairment-mediated cytotoxicity in central nervous system-like cells. *Food Chem. Toxicol.* 105, 262–277. doi:10.1016/j.fct.2017.04.030

Galanty, A., Koczurkiewicz, P., Wnuk, D., Paw, M., Karnas, E., Podolak, I., et al. (2017). Usnic acid and atranorin exert selective cytostatic and anti-invasive effects on human prostate and melanoma cancer cells. *Toxicol Vitro* 40, 161–169. doi:10.1016/j.tiv.2017.01.008

Gökalsın, B., and Sesal, N. C. (2016). Lichen secondary metabolite evernic acid as potential quorum sensing inhibitor against *Pseudomonas aeruginosa*. *World J. Microbiol. Biotechnol.* 32 (9), 150. doi:10.1007/s11274-016-2105-5

Grant, S. J., Kay, S., Lacey, J., Kumar, S., Kerin-Ayres, K., Stehn, J., et al. (2024). Feasibility study of a multimodal prehabilitation programme in women receiving neoadjuvant therapy for breast cancer in a major cancer hospital: a protocol. *BMJ Open* 14 (3), e080239. doi:10.1136/bmjopen-2023-080239

Guan, R., Zhang, X., and Guo, M. (2020). Glioblastoma stem cells and Wnt signaling pathway: molecular mechanisms and therapeutic targets. *Chin. Neurosurg. J.* 6 (1), 25. doi:10.1186/s41016-020-00207-z

Gueble, S. E., Vasquez, J. C., and Bindra, R. S. (2022). The role of PARP inhibitors in patients with primary malignant central nervous system tumors. *Curr. Treat. Options Oncol.* 23 (11), 1566–1589. doi:10.1007/s11864-022-01024-5

Guo, Q., Jin, Y., Chen, X., Ye, X., Shen, X., Lin, M., et al. (2024). NF-κB in biology and targeted therapy: new insights and translational implications. *Signal Transduct. Target Ther.* 9 (1), 53. doi:10.1038/s41392-024-01757-9

Hawrył, A., Hawrył, M., Hajnos-Stolarz, A., Abramek, J., Bogucka-Kocka, A., and Komsta, Ł. (2020). HPLC fingerprint analysis with the antioxidant and cytotoxic activities of selected lichens combined with the chemometric calculations. *Molecules* 25 (18), 4301. doi:10.3390/molecules25184301

Holliday, D. L., and Speirs, V. (2011). Choosing the right cell line for breast cancer research. *Breast Cancer Res.* 13 (4), 215. doi:10.1186/bcr2889

Huang, Q., Chen, L., Liang, J., Huang, Q., and Sun, H. (2022). Neurotransmitters: potential targets in glioblastoma. *Cancers (Basel)* 14 (16), 3970. doi:10.3390/cancers14163970

Ianevski, A., He, L., Aittokallio, T., and Tang, J. (2017). SynergyFinder: a web application for analyzing drug combination dose – response matrix data. *Bioinformatics* 33 (15), 2413–2415. doi:10.1093/bioinformatics/btx162

Jang, J., Song, J., Sim, I., Kwon, Y. V., and Yoon, Y. (2021). Wnt-signaling inhibitor Wnt-C59 suppresses the cytokine upregulation in multiple organs of lipopolysaccharide-induced endotoxemic mice via reducing the interaction between β-catenin and NF-κB. *Int. J. Mol. Sci.* 22 (12), 6249. doi:10.3390/ijms22126249

Janke, C., and Magiera, M. M. (2020). "The tubulin code and its role in controlling microtubule properties and functions. Vol. 21," in *Nature reviews molecular cell biology*. Berlin, Germany: Nature Research, 307–326.

Jezierzański, M., Nafalska, N., Stopyra, M., Furgoł, T., Miciak, M., Kabut, J., et al. (2024). Temozolomide (TMZ) in the treatment of glioblastoma multiforme—a literature review and clinical outcomes. *Curr. Oncol.* 31 (7), 3994–4002. doi:10.3390/curroncol31070296

Kashyap, D., Pal, D., Sharma, R., Garg, V. K., Goel, N., Koundal, D., et al. (2022). Global increase in breast cancer incidence: risk factors and preventive measures. *Biomed. Res. Int.* 2022, 9605439–16. doi:10.1155/2022/9605439

Khongkow, P., Gomes, A. R., Gong, C., Man, E. P. S., Tsang, J. W. H., Zhao, F., et al. (2016). Paclitaxel targets FOXM1 to regulate KIF20A in mitotic catastrophe and breast cancer paclitaxel resistance. *Oncogene* 35 (8), 990–1002. doi:10.1038/onc.2015.152

Kiliç, N., Islakoğlu, Y. Ö., Büyük, İ., Gür-Dedeoğlu, B., and Cansaran-Duman, D. (2019). Determination of usnic acid responsive miRNAs in breast cancer cell lines. *Anticancer Agents Med. Chem.* 19 (12), 1463–1472. doi:10.2174/1871520618666181112120142

Le Grand, J., Chakrama, F., Seguin-Py, S., Fraichard, A., Delage-Mourroux, R., Jouvenot, M., et al. (2011). GABARAPL1 (GEC1): original or copycat? *Autophagy* 7, 1098–1107. doi:10.4161/auto.7.10.15904

Lee, S. Y. (2016). Temozolomide resistance in glioblastoma multiforme. *Genes Dis.* 3 (3), 198–210. doi:10.1016/j.gendis.2016.04.007

Lee, S., Suh, Y. J., Yang, S., Hong, D. G., Ishigami, A., Kim, H., et al. (2021). Neuroprotective and anti-inflammatory effects of evernic acid in an MPTP-induced Parkinson's disease model. *Int. J. Mol. Sci.* 22 (4), 2098. doi:10.3390/ijms22042098

Li, J., Xia, Y., Wu, Q., Zhu, S., Chen, C., Yang, W., et al. (2017). Outcomes of patients with inflammatory breast cancer by hormone receptor- and HER2-defined molecular subtypes: a population-based study from the SEER program. *Oncotarget* 8 (30), 49370–49379. doi:10.18632/oncotarget.17217

Li, H., Liu, S., Jin, R., Xu, H., Li, Y., Chen, Y., et al. (2021). Pyrvinium pamoate regulates MGMT expression through suppressing the Wnt/β-catenin signaling pathway to enhance the glioblastoma sensitivity to temozolomide. *Cell Death Discov.* 7 (1), 288. doi:10.1038/s41420-021-00654-2

Liao, L. (2025). Inequality in breast cancer: global statistics from 2022 to 2050. *Breast* 79, 103851. doi:10.1016/j.breast.2024.103851

Losurdo, A., Di Muzio, A., Cianciotti, B. C., Dipasquale, A., Persico, P., Barigazzi, C., et al. (2024). T cell features in glioblastoma may guide therapeutic strategies to overcome microenvironment immunosuppression. *Cancers (Basel)* 16 (3), 603. doi:10.3390/cancers16030603

Louis, D. N., Perry, A., Wesseling, P., Brat, D. J., Cree, I. A., Figarella-Branger, D., et al. (2021). The 2021 WHO classification of tumors of the central nervous system: a summary. *Neuro Oncol.* 23 (8), 1231–1251. doi:10.1093/neuonc/noab106

Ma, S., Wang, F., Wang, N., Jin, J., Ba, Y., Ji, H., et al. (2022). Multiomics data analysis and identification of immune-related prognostic signatures with potential implications in prognosis and immune checkpoint blockade therapy of glioblastoma. *Front. Neurol.* 20, 886913. doi:10.3389/fneur.2022.886913

Manoranjan, B., Chokshi, C., Venugopal, C., Subapanditha, M., Savage, N., Tatari, N., et al. (2020). A CD133-AKT-Wnt signaling axis drives glioblastoma brain tumor-initiating cells. *Oncogene* 39 (7), 1590–1599. doi:10.1038/s41388-019-1086-x

Manthey, C. L., Brandes, M. E., Perera, P. Y., and Vogel, S. N. (1992). Taxol increases steady-state levels of lipopolysaccharide-inducible genes and protein-tyrosine phosphorylation in murine macrophages. *J. Immunol.* 149 (7), 2459–2465. doi:10.4049/jimmunol.149.7.2459

Minea, R. O., Thein, T. Z., Yang, Z., Campan, M., Ward, P. M., Schönthal, A. H., et al. (2024). NEO212, temozolomide conjugated to NEO100, exerts superior therapeutic activity over temozolomide in preclinical chemoradiation models of glioblastoma. *Neurooncol Adv.* 6 (1), vdae095. doi:10.1093/noajnl/vdae095

Neff, C., Chavez, G., Proescholdt, C., Kruchko, C., Cioffi, G., Waite, K., et al. (2022). EPID-06. improvements in survival for glioblastoma in the post-stupp protocol era. *Neuro Oncol.* 24 (Suppl. ment_7), vii110. doi:10.1093/neuonc/noac209.416

Neve, R. M., Chin, K., Fridlyand, J., Yeh, J., Baehner, F. L., Fevr, T., et al. (2006). A collection of breast cancer cell lines for the study of functionally distinct cancer subtypes. *Cancer Cell* 10 (6), 515–527. doi:10.1016/j.ccr.2006.10.008

Nowak, B., Rogujski, P., Janowski, M., Lukomska, B., and Andrzejewska, A. (2021). Mesenchymal stem cells in glioblastoma therapy and progression: how one cell does it all. *Biochimica Biophysica Acta (BBA) - Rev. Cancer* 1876 (1), 188582. doi:10.1016/j.bbcan.2021.188582

Persano, F., Gigli, G., and Leporatti, S. (2022). Natural compounds as promising adjuvant agents in the treatment of gliomas. *Int. J. Mol. Sci.* 23 (6), 3360. doi:10.3390/ijms23063360

Rosińska, M., Dubiański, R., Konieczna, A., Poleszczuk, J., Pawlik, H., Nowecki, Z. I., et al. (2024). Retrospective observational study to determine the epidemiology and treatment patterns of patients with triple-negative breast cancer. *Cancers (Basel)* 16 (6), 1087. doi:10.3390/cancers16061087

Schwendener, S. (2011). Untersuchungen über den Flechtenthallus. In: *Beiträge zur wissenschaftlichen Botanik*. Ann Arbor, MI: University of Michigan. p. 127–195.

Sestito, S., Runfola, M., Tonelli, M., Chiellini, G., and Rapposelli, S. (2018). New multitarget approaches in the war against glioblastoma: a mini-perspective. *Front. Pharmacol.* 9, 874. doi:10.3389/fphar.2018.00874

Shahcheraghi, S. H., Tchokonte-Nana, V., Lotfi, M., Lotfi, M., Ghorbani, A., and Sadeghnia, H. R. (2020). Wnt/beta-catenin and PI3K/Akt/mTOR signaling pathways in glioblastoma: two main targets for drug design: a review. *Curr. Pharm. Des.* 26 (15), 1729–1741. doi:10.2174/1381612826666200131100630

Shcherbakova, A., Strömstedt, A. A., Göransson, U., Gnezdilov, O., Turanov, A., Boldbaatar, D., et al. (2021). Antimicrobial and antioxidant activity of Evernia prunastri extracts and their isolates. *World J. Microbiol. Biotechnol.* 37 (8), 129. doi:10.1007/s11274-021-03099-y

Shcherbakova, A., Nyugen, L., and Ulrich-Merzenich, G. (2019). The Lichen compounds evernic acid and usnic acid synergize with Temozolomide in the glioblastoma cellline U-87. *Oncol. Res. Treat.* 42 (S4), 275–276.

Singh, K., Han, C., Fleming, J. L., Becker, A. P., McElroy, J., Cui, T., et al. (2023). TRIB1 confers therapeutic resistance in GBM cells by activating the ERK and Akt pathways. *Sci. Rep.* 13 (1), 12424. doi:10.1038/s41598-023-32983-w

Smits, A., Jin, Z., Elsir, T., Pedder, H., Nistér, M., Alafuzoff, I., et al. (2012). GABA-A channel subunit expression in human glioma correlates with tumor histology and clinical outcome. *PLoS One* 7 (5), e37041. doi:10.1371/journal.pone.0037041

Stachyra, P., and Grzybowska-Szatkowska, L. (2025). Signaling pathways in gliomas. *Genes (Basel)* 16 (5), 600. doi:10.3390/genes16050600

Studzińska-Sroka, E., Majchrzak-Celińska, A., Zalewski, P., Szwajgier, D., Baranowska-Wójcik, E., Kaproń, B., et al. (2021). Lichen-derived compounds and extracts as biologically active substances with anticancer and neuroprotective properties. *Pharmaceuticals* 14 (12), 1293. doi:10.3390/ph14121293

Tan, A. C., Ashley, D. M., López, G. Y., Malinzak, M., Friedman, H. S., and Khasraw, M. (2020). Management of glioblastoma: state of the art and future directions. *CA Cancer J. Clin.* 70 (4), 299–312. doi:10.3322/caac.21613

Thomas, A., and Pommier, Y. (2019/06/21. 2019). Targeting topoisomerase I in the era of precision medicine. *Clin. Cancer Res.* 25 (22), 6581–6589. doi:10.1158/1078-0432.CCR-19-1089

Tong, Y. Q., Liu, B., Zheng, H. Y., Gu, J., Liu, H., Li, F., et al. (2015). MiR-215, an activator of the CTNNBIP1/β-catenin pathway, is a marker of poor prognosis in human glioma. *Oncotarget* 6 (28), 25024–25033. doi:10.18632/oncotarget.4622

Ulrich-Merzenich, G., Zeitler, H., Panek, D., Bokemeyer, D., and Vetter, H. (2007). Vitamin C promotes human endothelial cell growth via the ERK-signaling pathway. *Eur. J. Nutr.* 46 (2), 87–94. doi:10.1007/s00394-006-0636-5

Ulrich-Merzenich, G., Hartbrod, F., Kelber, O., Müller, J., Koptina, A., and Zeitler, H. (2017). Salicylate-based phytopharmaceuticals induce adaptive cytokine and chemokine network responses in human fibroblast cultures. *Phytomedicine* 34, 202–211. doi:10.1016/j.phymed.2017.08.002

Wani, M. C., Taylor, H. L., Wall, M. E., Coggon, P., and McPhail, A. T. (1971). Plant antitumor agents. VI. The isolation and structure of taxol, a novel antileukemic and antitumor agent from Taxus brevifolia. *J. Am. Chem. Soc.* 93 (9), 2325–2327. doi:10.1021/ja00738a045

Warde-Farley, D., Donaldson, S. L., Comes, O., Zuberi, K., Badrawi, R., Chao, P., et al. (2010). The GeneMANIA prediction server: biological network integration for gene prioritization and predicting gene function. *Nucleic Acids Res.* 38 (Suppl. l_2), W214–W220. doi:10.1093/nar/gkq537

West, A., Tsui, V., Stylli, S., Nguyen, H., Morokoff, A., Kaye, A., et al. (2018). The role of interleukin-6-STAT3 signalling in glioblastoma. *Oncol. Lett.* 16, 4095–4104. doi:10.3892/ol.2018.9227

Widodo, S. S., Dinevska, M., Furst, L. M., Stylli, S. S., and Mantamadiotis, T. (2021). IL-10 in glioma. *Br. J. Cancer* 125 (11), 1466–1476. doi:10.1038/s41416-021-01515-6

Xie, Y., Bergström, T., Jiang, Y., Johansson, P., Marinescu, V. D., Lindberg, N., et al. (2015). The human glioblastoma cell culture resource: validated cell models representing all molecular subtypes. *EBioMedicine* 2 (10), 1351–1363. doi:10.1016/j.ebiom.2015.08.026

Xiong, J., Zhou, L., Lim, Y., Yang, M., Zhu, Y. H., Li, Z. W., et al. (2013). Mature BDNF promotes the growth of glioma cells *in vitro*. *Oncol. Rep.* 30 (6), 2719–2724. doi:10.3892/or.2013.2746

Yakubov, R., Kaloti, R., Persaud, P., McCracken, A., Zadeh, G., and Bunda, S. (2025). It's all downstream from here: RTK/Raf/MEK/ERK pathway resistance mechanisms in glioblastoma. *J. Neurooncol* 172 (2), 327–345. doi:10.1007/s11060-024-04930-w

Yu, J. M., Jun, E. S., Jung, J. S., Suh, S. Y., Han, J. Y., Kim, J. Y., et al. (2007). Role of Wnt5a in the proliferation of human glioblastoma cells. *Cancer Lett.* 257 (2), 172–181. doi:10.1016/j.canlet.2007.07.011

Zhang, W., and Liu, H. T. (2002). MAPK signal pathways in the regulation of cell proliferation in mammalian cells. *Cell Res.* 12 (1), 9–18. doi:10.1038/sj.cr.7290105

Zhang, M. I., Lucas, E., Rol, M. L., Carvalho, A. L., Basu, P., et al. (2023). CanScreen5, a global repository for breast, cervical and colorectal cancer screening programs. *Nat. Med.* 29 (5), 1135–1145. doi:10.1038/s41591-023-02315-6

Zhao, H., Wu, L., Yan, G., Chen, Y., Zhou, M., Wu, Y., et al. (2021). Inflammation and tumor progression: signaling pathways and targeted intervention. *Signal Transduct. Target Ther.* 6 (1), 263. doi:10.1038/s41392-021-00658-5

Zheng, B., and Chen, T. (2020). MiR-489-3p inhibits cell proliferation, migration, and invasion, and induces apoptosis, by targeting the BDNF-mediated PI3K/AKT pathway in glioblastoma. *Open Life Sci.* 15 (1), 274–283. doi:10.1515/biol-2020-0024

Zhong, Z., and Virshup, D. M. (2020). Wnt signaling and drug resistance in cancer. *Mol. Pharmacol.* 97 (2), 72–89. doi:10.1124/mol.119.117978

Zuccarini, M., Giuliani, P., Ziberi, S., Carluccio, M., Iorio, P. D., Caciagli, F., et al. (2018). The role of Wnt signal in glioblastoma development and progression: a possible new pharmacological target for the therapy of this tumor. *Genes* 9, 105. doi:10.3390/genes9020105

frontiers | Frontiers in Pharmacology

TYPE Review
PUBLISHED 17 October 2025
DOI 10.3389/fphar.2025.1569502

OPEN ACCESS

EDITED BY
Ana Podolski-Renic,
Institute for Biological Research "Siniša Stanković"–National Institute of Republic of Serbia, Serbia

REVIEWED BY
Shreyans Gandhi,
King's College Hospital NHS Foundation Trust, United Kingdom
Michelle Teo,
UCSI University, Malaysia
John Weldon,
Towson University, United States

*CORRESPONDENCE
Stephen E. Braun,
sbraun@tulane.edu

RECEIVED 31 January 2025
ACCEPTED 15 September 2025
PUBLISHED 17 October 2025

CITATION
Rashad Y, Alt EU, Izadpanah R, Qin X and Braun SE (2025) Clinically approved immunotoxins targeting hematological cancers: "the best of both worlds". *Front. Pharmacol.* 16:1569502. doi: 10.3389/fphar.2025.1569502

Clinically approved immunotoxins targeting hematological cancers: "the best of both worlds"

Yasmine Rashad[1,2], Eckhard U. Alt[1], Reza Izadpanah[1], Xuebin Qin[2,3] and Stephen E. Braun [1,4,5]*

[1]Applied Stem Cell Laboratory, Department of Medicine, Heart and Vascular Institute, Tulane University School of Medicine, New Orleans, LA, United States, [2]Department of Immunology and Microbiology, Tulane University School of Medicine, New Orleans, LA, United States, [3]Division of Comparative Pathology, Tulane National Primate Research Center, Covington, LA, United States, [4]Division of Immunology, Tulane National Primate Research Center, Covington, LA, United States, [5]Department of Pharmacology, Tulane University School of Medicine, New Orleans, LA, United States

Hematological malignancies contribute significantly to the overall cancer burden. Certain subtypes, such as hairy cell leukemia (HCL), are chronic and characterized by residual disease after first-line therapy, while others, such as blastic plasmacytoid dendritic cell neoplasm (BPDCN), are aggressive and associated with poor prognosis. Although cornerstone interventions such as radiation and chemotherapy are efficiently used to treat some malignant blood neoplasms, these treatments are often limited by resistance, relapse, lack of enduring disease-free survival/complete remission, and systemic toxicity. Immunotoxins were developed to improve tumor targeting and have evolved into recombinant immunotoxins (RITs). These novel bioengineered chimeras genetically combine potent cytotoxins with targeted binding domains. In this review, we analyze three FDA-approved RITs, namely, moxetumomab pasudotox, tagraxofusp, and denileukin diftitox, that utilize bacterial toxins from *Pseudomonas* and *Corynebacterium diphtheriae* to treat refractory/relapsed (R/R) HCL, BPDCN, and adult R/R cutaneous T-cell lymphoma (CTCL), respectively. We reviewed their comprehensive safety profiles, describe complications associated with these fusion proteins, and, finally, discuss potential risk management strategies that may enhance their clinical outcomes. Overall, RITs have demonstrated efficacy, and researchers continue to extend these findings to other indications.

KEYWORDS

hematological malignancies, cancer immunotherapy, recombinant immunotoxins, diphtheria toxin, *Pseudomonas* exotoxin, moxetumomab pasudotox, tagraxofusp, E7777

Introduction

According to the National Cancer Institute registry, in 2023, hematological malignancies accounted for ~9.4% of new cancer cases and were responsible for 9.4% of reported cancer deaths within the United States. The 5-year (2013–2019) estimated survival rate for leukemia was 66.7% (Cancer Statistics, 2024). Although traditional cancer therapies have advanced over the past decades, detectable minimal residual disease (MRD) post-treatment, health vulnerability in old age, systemic adverse effects including bystander cell/tissue toxicity, relapse, and chemo-resistance continue to pose major challenges in blood cancer management. This emphasizes the quest for a highly specific curing therapy, like a "magic bullet."

Chemo-monotherapy is generally effective in some hematological malignancies, such as diffuse large B-cell lymphoma, and some T-cell malignancies, such as acute leukemia. However, chemo-resistance still constrains this approach. For example, acute myeloid leukemia (AML) is characterized by several functional chemo-resistance mechanisms, which include drug efflux pumps (Yeung and Radich, 2017). Accordingly, immunotherapy has been introduced for cancer treatment and aims to enhance the host's immune system in combating malignancies (Farkona et al., 2016).

Recombinant immunotoxins (RITs), a type of immunotherapy, have shown promise in compensating for these unmet qualities of traditional systemic treatments. The recombinant technology provides consistency in combining their two subunits, a tumor-specific targeting moiety genetically fused to a fast-acting modified cytotoxin (Allahyari et al., 2017). Potential RITs are highly stable (protein stability of the chimeric fusion is tested at body temperature), bind with high affinity to tumor-specific antigens (TSAs), and can effectively translocate into the cytosol and become cytotoxic (FitzGerald et al., 2004). These properties of RITs could limit systemic toxicity and drug resistance experienced with conventional modalities while eradicating MRD to achieve a complete response (CR) more rapidly. Thus, they improve the efficiency of targeting residual disease in adult populations and provide other strategies for patients without the option of hematopoietic stem-cell transplant (HSCT).

Hairy cell leukemia (HCL) is an example of a chronic B-cell leukemia characterized by cytopenia (Morton et al., 2006). Purine nucleoside analog (PNA) chemotherapy, using either cladribine or pentostatin, is the current standard of care for *de novo* HCL. Else et al., (2009) reported a CR of 76% in patients treated with cladribine and 82% in those treated with pentostatin in an assessment of 233 patients with HCL. However, these regimens often fail to induce a durable disease-free plateau. Refractory/relapsing disease was also found by Else et al., (2009) at 38% relapse with cladribine and 44% with pentostatin. Despite a high initial CR rate with PNA chemotherapy, MRD is often detected in HCL patients post-treatment. Getta et al. (2015) identified MRD in 27%–50% of a CR patient sample. Second-line therapy is indicated based on CR sustainability and includes retreatment with PNAs or different combinations of chemo-immunotherapy (rituximab with PNA or bendamustine) (Maitre et al., 2019). However, subsequent PNA courses eventually decline the response rates, accumulate toxicity (Kreitman and Pastan, 2020; Seymour et al., 1994; Seymour et al., 1997; Tadmor, 2011), and increase susceptibility to secondary malignancies (Morton et al., 2006; Getta et al., 2016). The risk of infection is also higher as both these PNAs are immunosuppressive, especially cladribine (Kreitman et al., 2021). As a result, the FDA approved moxetumomab pasudotox (MP) for managing refractory/relapsed (R/R) HCL (FDA, 2020). Compellingly, MP may also play a role in eradicating MRD in patients with HCL and may potentially be associated with a reduced relapse rate.

Another hematological malignancy, blastic plasmacytoid dendritic cell neoplasm (BPDCN), was originally categorized by WHO under AML before they identified it as its own individual disease in a 2016 revision (Arber et al., 2016). BPDCN's rare incidence and unclear understanding of its biology challenged the establishment of a specific standard of care. BPDCN is an aggressive cancer with an extremely low incidence rate of <0.5% (Shi and Wang, 2014; Rauh et al., 2012; Yu et al., 2014) that mainly affects adults (~60–70 years). It is less commonly observed in the pediatric population, which has historically shown great outcomes with existing leukemia/lymphoma-based treatment protocols. Unlike younger patients, multiple studies report poorer prognosis in the older population (Shimony et al., 2025). Kharfan-Dabaja et al. (2013) found a median estimated survival of <18 months with chemotherapy in affected adults. Treating BPDCN with chemotherapy resulted in an approximate average of 21.5% early mortality (Pemmaraju et al., 2019). As immunocompetency declines with age, patients likely cannot tolerate immunosuppressive chemotherapy, which could affect their chances of undergoing further treatments, such as HSCT and additional pre-conditioning requirements (Tay et al., 2019). The disease presents with cutaneous lesions but can also occur without dermatological involvement (Rauh et al., 2012; Yu et al., 2014). In these cases, systemic treatment/conditioning with chemotherapy/radiation may be only palliative, which has prompted investigations into the antineoplastic activity of RITs against BPDCN. Currently, tagraxofusp is the only specific treatment for BPDCN approved by the FDA and the European Medicines Agency (Shimony et al., 2025).

The tumor behavior of some mature T-cell lymphomas (TCL), such as cutaneous T-cell lymphoma (CTCL) and peripheral TCL, also shows frequent relapse, refractory disease, and poor prognosis in the later stages. For local manifestations, treatment could include topical creams or light therapy. For extensive skin involvement, current protocols include systemic chemotherapy, such as cyclophosphamide, doxorubicin, vincristine, and prednisone; extracorporeal photopheresis; or radiation. However, the low reported long-term survival average of 25%, along with disease relapse post-HSCT, has encouraged the pursuit of alternative second-line therapies (Hamadani et al., 2014; Khan and Sawas, 2019). Denileukin diftitox (DD), an RIT preparation now reformulated as E7777 (Lymphir), is FDA-approved for treating adult R/R CTCL (Kawai et al., 2021).

In this study, we discuss these three FDA-approved RITs against hematological malignancies—moxetumomab pasudotox (MP), tagraxofusp, and denileukin diftitox (DD)—with an emphasis on the bacterial toxins utilized in these agents. This review encompasses these chimeras' limitations, safety profiles, and suggested improvement capacities. Increased targeting and specific toxicity would be "the best of both worlds."

IT design and development

Toxin moiety: characterization of bacterial-based ITs

William Coley established the preliminary form of immunotherapy using bacterial components for inoperable cancer treatment in the late 1890s. He cured sarcomas with "Coley's toxins"—a mixture of *Streptococcus pyogenes*, *Serratia marcescens*, and bacterial products (McCarthy, 2006). In the late 1800s and early 1900s, Paul Ehrlich developed the concepts of tumor-specific markers and, later, the concept of specific drugs

that target diseased tissue and used the term "magic bullets." He suggested that aberrant cells were common but maintained by host factors. Advances in the understanding of modern immunity have provided some insights into host defenses and changes in cell-surface expression, forming the foundation for tumor-specific targets (Valent et al., 2016).

Subsequently, the immunotoxin technology evolved over several generations, starting from a few research groups in the 1970s and 1980s using different toxins (Moolten et al., 1975; Krolick et al., 1982). The first generation used whole toxins conjugated to antibodies. Then, the second generation eliminated unessential portions of the toxin to mitigate the vascular-leak adverse reactions. Finally, RITs are the latest generation using recombinant DNA to fuse the binding and toxin domains (Allahyari et al., 2017).

RITs refer to genetically fusing the sequences of the antibody's cell-binding fragments to sequences of the modified toxin. This construct allows further alterations to increase binding affinity or cytotoxic activity (Greer et al., 2018; Matthey et al., 2000). The two most commonly used toxins in RIT are *Pseudomonas* exotoxin (PE) and diphtheria toxin (DT). They belong to the same group of ADP-ribosylating toxins and originate from the AB toxin family, consisting of catalytic (A) and binding (B) counterparts. PE and DT are favorable because of their limited non-specific toxicity compared to that of other toxins (including plant toxins). They are also easily cloned and expressed, which makes them cost-effective molecules (Mazor and Pastan, 2020).

Both PE and DT have single-chain polypeptide structures with efficient cytotoxic activity using an analogous mechanism. Each toxin inhibits the function of EF-2 translocase, an elongation factor in protein synthesis, by transferring the ADP-ribose from NAD^+ to the diphthamide residue on EF-2, which then blocks translation and induces apoptosis (Mei et al., 2019; Michalska and Wolf, 2015; Weldon and Pastan, 2011; Zdanovsky et al., 1993). PE and DT follow receptor-mediated endocytosis (Zdanovsky et al., 1993; Shafiee et al., 2019); however, they follow distinct cytosolic translocation pathways. PE (including the PE38 variant used in RIT) requires assistance with cytoplasm translocation using the retrograde pathway from the ER to the cytosol through the ER's protein channels. In contrast, DT bypasses the ER and moves directly through the endosomal membrane (in a pH-dependent manner) into the cytosol (Michael Lord and Roberts, 1998). Additionally, the structural and enzymatic domains for each toxin are in different orientations (Srivastava and Luqman, 2015).

PE in the RIT structure

The native PE precursor molecule is 638 amino-acids (aa), of which the 25 aa signal sequence is cleaved during secretion (Allured et al., 1986). A mature PE molecule is a single polypeptide 613 aa chain: domain Ia (1 aa–252 aa) binds the receptor on target cells, domain II (253 aa–364 aa) enables cytosol translocation, and domain Ib (365 aa–404 aa), along with III (405 aa–613 aa), catalyzes ADP-ribosyl transferase activity.

Generally, in PE-mediated RITs, the recombinant binding domain genetically replaces the minor domain Ia, while domains III, II, and a subunit of Ib are preserved in the chimeric molecule (Hansen et al., 2010). Removal of domain Ia resulted in PE40, a truncated (40 kDa) PE (Wolf and Elsasser-Beile, 2009; Pastan et al., 1992). To further reduce immunogenicity, more residues were deleted from domain Ib, resulting in PE38, a 38 kDa toxin. The PE38 form of *Pseudomonas* protein toxin A has been commonly used in RITs; one such example is MP (Kreitman et al., 2018a). The intracellular processing of MP, schematically illustrated in Figure 1A, is similar after binding, presumptively using the KDEL receptor pathway.

PE cytotoxic pathway

Native PE is cleaved at the 613 aa in the extracellular environment; this is hypothesized to be carried out by host plasma carboxypeptidases, excising lysine and resulting in a motif change to REDL. The REDL motif enables the toxin to bind KDEL receptors at the Golgi apparatus during intracellular trafficking. PE binds at domain Ia to a low-density lipid-related protein (LRP), which is also known as CD91 or the α2-macroglobulin receptor, and is internalized by receptor-mediated endocytosis (Wolf and Elsasser-Beile, 2009).

Intracellularly, two pathways are available for PE to reach the ER, namely, the KDEL receptor-mediated pathway and the lipid-dependent sorting pathway (Wolf and Elsasser-Beile, 2009; Pastan et al., 1992). Using the KDEL receptor-mediated pathway, the PE bound to CD91 translocates intracellularly via clathrin-coated pits. As the complex reaches the endosome, low pH induces the dissociation of LRP from PE, and a conformational change exposes the furin protease motif site (in domain II). PE is cleaved into two units that are still attached by disulfide bonds. These bonds are reduced in the late endosome, resulting in 27 kDa and 37 kDa fragments containing domains II, Ib, and III. The 37 kDa fragment reaches the trans-Golgi-network (TGN), where the REDL motif of PE binds to the KDEL receptor and the toxin is translocated to the ER in retrograde movement. In the cytosol, the 37 kDa fragment catalyzes the ADP-ribosylation by binding NAD^+ and cleaving the bond between the nicotinamide and ribose of the NAD^+ molecule. This stimulates ADP-ribose transfer to diphthamide, which is a post-translationally modified histidine only found on EF-2. Since the main function of EF-2 is to translocate mRNA across the ribosome, inhibition of EF-2 activity halts protein synthesis, induces cell-cycle arrest, and subsequently induces apoptosis.

DT in the RIT structure

DT was discovered by Yersin and Roux in 1888 and has been one of the most investigated bacterial toxins. Its potent cytotoxic properties can induce cell death with as low as a single molecule of DT (Yamaizumi et al., 1978; Kolybo et al., 2013) or a minimal lethal dose of <0.1 μg per kg of body weight in humans (Kolybo et al., 2013). It is a single polypeptide Y-shaped chain consisting of three domains within two subunits totaling 535 aa residues. The C-domain (1 aa–193 aa) resides within the A subunit, while the T-domain (201 aa–384 aa) and the R-domain (385 aa–455 aa) are

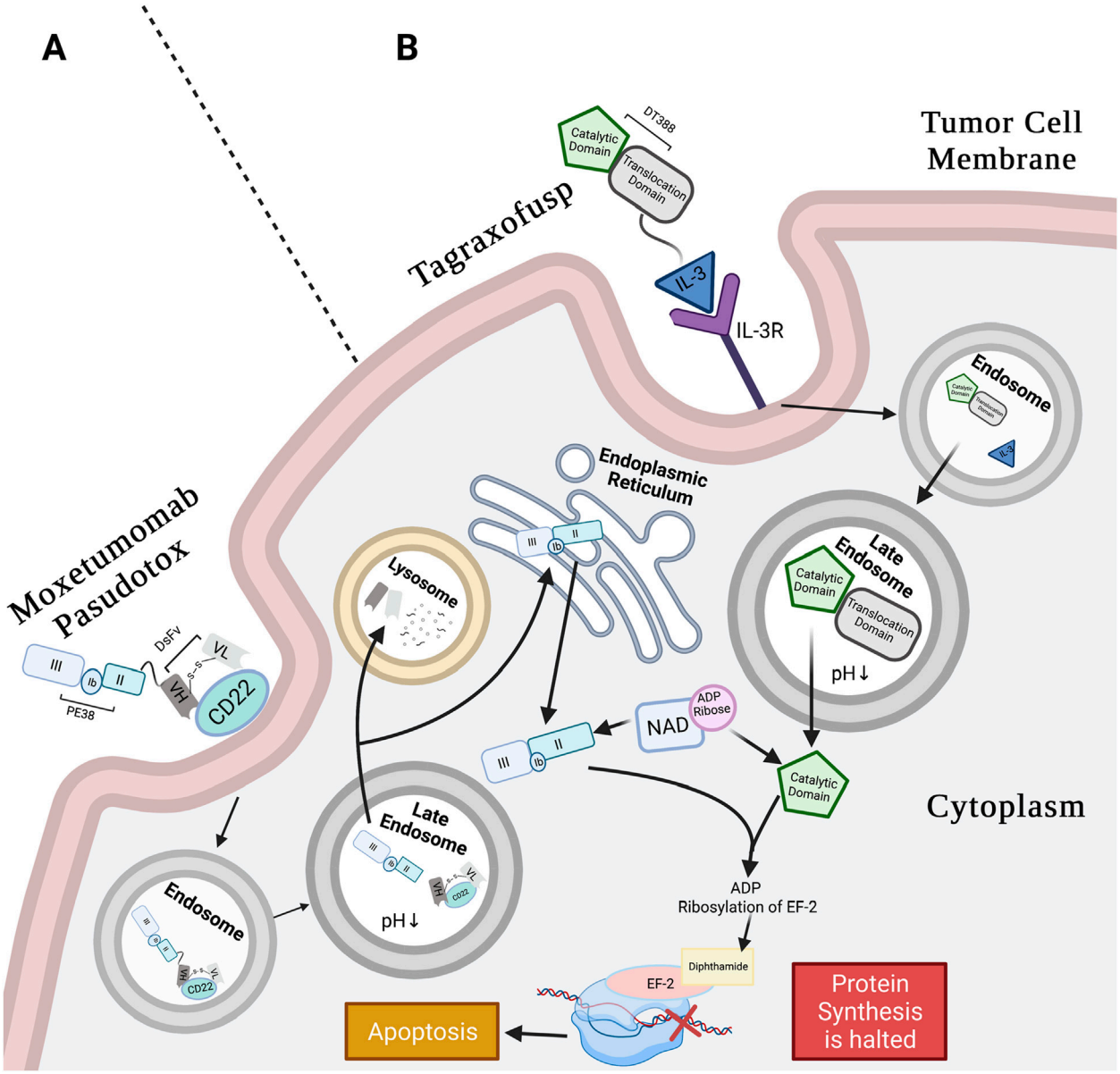

FIGURE 1
Moxetumomab pasudotox's and tagraxofusp's mechanism of action (MoA). **(A)** Moxetumomab pasudotox MoA: anti-CD22 DsFv of RIT binds CD22 on B-tumor cells. The whole conjugate is internalized in clathrin pits via receptor-mediated endocytosis. Pit containing conjugate buds into early endosome and then late endosome, where low pH separates the PE38 from the dsFv, and furin cleavage releases the catalytic payload. Next, the dsFv is degraded in the lysosome, and PE38 moves retrogradely to the ER, likely using the REDL motif and KDEL receptor pathway. The catalytic PE38 payload enters the ER and then the cytosol, where it catalyzes ADP-ribosylation of EF2 diphthamide. This inactivates EF-2 protein synthesis function, leading to apoptosis (Weldon and Pastan, 2011; Kreitman and Pastan, 2011; Abou Dalle and Ravandi, 2019; Pastan et al., 2006). **(B)** Tagraxofusp MoA: IL-3 subunit of tagraxofusp binds with high affinity to CD123 (α-chain of IL-3R) that is highly expressed on BPDCN cell surface and is also internalized through endocytosis. The drug relies on the late endosome for acidification to weaken bonds between the T- and C-domains. Unlike PE38, the C-domain of the RIT is directly translocated to the cytosol to catalyze NAD^+ by transferring the ADP-ribose molecule to diphthamide on EF-2, interfering with EF-2 protein synthesis activity, and inducing apoptosis (Shafiee et al., 2019; Alkharabsheh and Frankel, 2019). Created in BioRender. Rashad, Y. (2025) https://BioRender.com/p1vrc3a.

located within the B subunit. The C-domain is responsible for catalyzing the ADP-ribosylation of EF-2, the T-domain is the transmembrane subunit, and the R-domain is the receptor-binding subunit (Mazor and Pastan, 2020). Only lysogenic corynephage-infected *Corynebacterium diphtheriae* secrete DT or are toxicogenic as the phage carries the *tox* gene that encodes DT (John, 1996).

When using DT in a genetically engineered RIT, the R-domain is substituted with a smaller and more stable targeting molecule, while the functional activity of the T- and C-domains is retained. Once inside the cell, RITs employ the same cytotoxic mechanism as native DT (Shafiee et al., 2019). This is shown in Figure 1B, which shows the pathway of the FDA-approved tagraxofusp, a DT-mediated RIT.

TABLE 1 Bacterial-based immunotoxins targeting hematological malignancies (Allahyari et al., 2017; Pemmaraju et al., 2019; Shafiee et al., 2019; Kim et al., 2020; Weber, 2015).

Immunotoxin	Market drug name	Binding moiety	Toxin moiety	Bacterial toxin	Disease[a]	Clinical progress
DT388 GM-CSF	--	GM-CSF	DAB388	DT	AML	Phase I
A-dmDT390-bisFv (UCHT1)	--	Anti-CD3	DT390	DT	T-cell-derived malignancies including MF-CTCL	Phase II Completed
DAB486IL2	--	IL-2	DT486	DT	NHL and CTCL	Phase II
DAB389IL2	Denileukin diftitox (Ontak)	IL-2	DAB389	DT	CTCL, NHL, CLL, and more diseases	Accelerated FDA approval in February 1999 and full approval in 2006
HA22	Moxetumomab pasudotox (Lumoxiti)	Anti-CD22 dsFv	PE38	PE	HCL	FDA approved in September of 2018
DT388IL3	Tagraxofusp (Elzonris)	IL-3	DT388	DT	BPDCN	FDA approved in December of 2018

[a]NHL, non-Hodgkin lymphoma; MF-CTCL, mycosis fungoides-type cutaneous T-cell lymphoma; CTCL, cutaneous T-cell lymphoma; AML, acute myeloid leukemia; CLL, chronic lymphocytic leukemia.

DT cytotoxic pathway

The native DT cytotoxic pathway begins with the R-domain of DT binding to type 1 transmembrane protein pro-heparin-binding epidermal growth factor (pro-HB-EGF) and CD9 on the mammalian cell surface (Srivastava and Luqman, 2015; Kolybo et al., 2013). Upon binding, cell surface proteolytic enzymes cleave the polypeptide bond between the C- and T-domains, which allows for internalization by endocytosis (some DT particles escape surface furin-mediated cleavage but are later cleaved intracellularly instead by furins in the early endosome lumen). Translocation of the C- and T-domains across the plasma membrane and into the endosome takes place in enclosed clathrin-coated pits. At this point, the C- and T-domains are still linked together by a disulfide bond in the endosome. Upon acidification and the reduction of the disulfide bond, conformational changes in the T-domain cause the hydrophobic regions to project through the endosomal membrane and channel the C-domain into the cytosol, where the enzymatic domain's toxic function is activated. Acidification is crucial for DT intracellular translocation (Antignani and Fitzgerald, 2013). The C-domain binds NAD^+ in the cytosol and transfers ADP-ribose of the NAD to diphthamide on EF-2. This ADP-ribosylation halts EF-2 activity, causing cell death (Shafiee et al., 2019; Srivastava and Luqman, 2015).

Targeting moiety

Candidate targeting molecules (i.e., growth factors, cytokines, monoclonal antibodies (mAbs), or fragments of mAbs) should be able to bind with high affinity to the designated (malignant) mammalian cells and effectively deliver the attached toxin. Targeted TSA should be abundantly and homogenously expressed on the tumor cell surface at moderate-to-high density to avoid off-target or competitive binding. It should also be anchored to the plasma membrane, instead of being freely available, to ensure that the toxins bind the tumor cell and reach the cytoplasm (Brown et al., 2008). The technology to retain the antigen-binding fragment (Fv) and eliminate the constant region (Fc) from the targeting mAb facilitates rapid clearance of the RIT from the circulation. This helps reduce the negative effect of unwanted interactions between the hybrid conjugate and vital cells (Mansfield et al., 1997). Ligand binding to their receptors has also demonstrated a potent ability to deliver the RIT molecule with high specificity to tumor cells. Currently, the investigated ligands include interleukins (IL) 2, IL-3, and granulocyte-macrophage colony-stimulating factor (GM-CSF) (Kim et al., 2020).

After the receptor–ligand binding, internalization is crucial for proper toxin uptake. The DT and PE exploit the receptor-mediated endocytosis pathway to cross the plasma membrane in clathrin-coated vesicles and ultimately induce cytotoxicity through the inhibition of EF-2 activity (Michalska and Wolf, 2015; Murphy, 2011).

Linker

Linkers are vital components in RITs. They play a structural role in attaching the toxin to the binding molecule. Biological linkers enhance the stability and expression of the RIT-targeting domains, particularly those derived from mammalian proteins (i.e., cytokines and growth factors) (Amet et al., 2009; Chen et al., 2013). Chen et al. (2013) reported three main empirical linker classifications in drug delivery applications: rigid, flexible, and cleavable linkers. In protein fusion biologics, linkers can be helical or non-helical (George and Heringa, 2002). Peptide linkers also serve as furin cleavage sites. In toxins, these proteolytic cleaving sites are necessary to activate the catalytic domains' cytotoxic activity (Weldon et al., 2015). Conceivably, a robust linker would preserve the functions of both domains (binding and toxicity) without compromising drug potency.

Clinical pearls of immunotoxins: efficacy and toxic effects

To date, there are three FDA-approved RITs indicated for hematological malignancies: tagraxofusp, MP, and DD. Table 1 summarizes some of the history of bacterial-based toxins and their clinical status.

Moxetumomab pasudotox (Lumoxiti)

MP (HA22) is an FDA-approved RIT targeting CD22 against R/R HCL for adults who previously received ≥2 systemic therapies, including PNA (Kreitman et al., 2012). CD22 is a popular B-cell surface target for RIT against HCL; Olejniczak et al. (2006) utilized flow cytometry and showed that 100% of the nine examined HCL specimens are CD22-positive. Their data also suggest that the CD22 antigen exhibits negligible change following B-cell neoplastic transformation, which makes it a stable targeting marker (Olejniczak et al., 2006). Most importantly, it is not displayed on the B-stem-cell surface (FitzGerald et al., 2004).

The HA22 RIT is composed of anti-CD22 Fv (V_L and V_H domains), cloned from the murine IgG clone RFB4 (Mansfield et al., 1997), genetically linked to PE38 at V_H using recombinant DNA technology, and then produced in *E. coli* (Kreitman et al., 2012). V_L and V_H in HA22 have three aa substitutions (THW) in place of cysteines (SSY) to increase the high binding affinity and cytotoxicity of RFB4 in the RIT (Kreitman and Pastan, 2011). RFB4 is an excellent binding domain in HA22 due to its high selectivity in binding malignant B-cells with no perceptible evidence of binding normal/benign cells (Mansfield et al., 1997). Additional high-affinity mutants are being tested in a phase-I clinical trial (Salvatore et al., 2002).

From bench to bedside: milestones to FDA approval

The clinical phase-I (NCT00586924), stage-1 "dose-escalation" cohort included 28 HCL patients treated with MP at three doses ranging from 5 to 50 μg/kg administered every other day to evaluate drug safety. The treatment continued to a maximum of 16 cycles per patient (with ≤4 weeks between cycles) or until disease progression. This stage revealed 86% response rates throughout dose escalation, including 46% with durable CR, with only one case sustaining CR for less than a year. One patient experienced disease progression after the first treatment cycle and was terminated from the study. Of the 27 remaining eligible patients, 3 had stable disease, 13 had CR, and 11 had PR. Immunogenicity assessment of 26 evaluable patients showed 65% with antitoxin-binding Abs after a median of two cycles and 38% developing neutralizing antibodies (nAbs) blocking <75% of 1 μg/mL of IT after at least two cycles; however, among the patients undergoing 5–16 cycles/patient, five patients showed no nAbs. Only one patient had nAbs after the first cycle. Patients with Abs neutralizing <75% of 1 μg/mL of IT qualified for continued treatment as blood levels of the drug were greater than the Ab levels. No dose-limiting responses were reported (Kreitman et al., 2012; Kreitman et al., 2018b).

In stage 2, this phase study was expanded by recruiting 21 additional participants for the 50 μg/kg dose, which was administered in 3 doses over 4-week cycles given every other day. The results showed MRD eradication in the blood and bone marrow in most CR patients, contributing to enduring CR. At a 50 μg/kg dose, the participants' median duration to reach CR is 42.4 months. The MRD-positive cases of the CR-positive population represented 45% (9 cases), with a median of CR-positive duration of 13.5 months. The MRD-negative population (11 patients) did not reach the median duration of CR. Altogether, this concluded the successful completion of the phase-I trial and unlocked the phase-III clinical trial (Kreitman et al., 2018b).

The phase-III pivotal study (CD-ON-CAT8015-1053) was a third-line, multi-center (in 14 different countries, with the majority of the centers in the United States), open-label efficacy trial. A total of 80 patients were enrolled and treated with 40 μg/kg on days 1, 3, and 5 of every 28-day cycle for a maximum total of six cycles. The results revealed a total of 79% CR and PR, in addition to 80% hematological remissions. Of the population that responded to treatment, 85% tested negative for MRD on immunohistochemistry slides. Overall, the results concluded a durable CR rate along with MRD eradication in R/R HCL patients (Kreitman et al., 2018a). MP was approved by the FDA in September 2018 after successful clinical outcomes (FDA, 2018a).

In November 2022, the manufacturer of MP announced the discontinuation of the product in an official letter to the FDA, citing "very low clinical uptake," with the discontinuation effective from August 2023. They stated that the decision does not reflect the safety and efficacy of the drug but anticipated that the complexity of specialized administration, the need for patient monitoring, and potential prophylactic toxicity may have affected the observed clinical uptake (FDA, 2023).

Immunogenicity assessment

An electrochemiluminescent immunoassay was used to assess for the presence of anti-drug antibodies (ADA)—anti-MP. Of the ADA-positive population, nAbs levels were measured using a cell-based assay. A phase-III study (CD-ON-CAT8015-1053) revealed that 59% of the participants were ADA-positive. These ADA-positive patients proceeded to nAb testing, and 95.7% of them had detectable nAbs. Of the nAb-positive cases, 99% exhibited PE38-binding domain-specific ADA, and 54% had CD22-binding domain-specific ADA. If the participants were baseline ADA-positive, they had reduced systemic drug concentrations (FDA, 2018a). Results from the phase-III clinical study reported that the median CD19 B-cell count in the peripheral blood on day 8 declined by 90% and remained reduced throughout the study. Six months after treatment, PR/CR patients exhibited relatively normal B-cell counts (Kreitman et al., 2018a).

Toxicity and adverse outcomes

Reactions related to infusion account for ≤20% and include diarrhea (≤50%), nausea, edema, headache, anemia, and fever. Renal toxicity and electrolyte alterations were also noted. Other severe effects include capillary leak syndrome (CLS) and hemolytic uremic syndrome (FDA, 2018a).

Recommended administration protocol: dosing and route.

FDA regulations recommend administering 40 μg/kg through a 30-min intravenous (IV) infusion on days 1, 3, and 5 of each 28-day

TABLE 2 Ongoing clinical trial of Tagraxofusp against blood cancers (National Library of Medicine, 2024a).

Indication/disease[a]	Clinical trial ID
Post-transplant maintenance of CD123-positive chronic blood malignancies: AML, MF, CMML	NCT05233618
CD123-positive or BPDCN-IPh-like AML	NCT04342962
(Tagraxofusp + decitabine) CMML	NCT05038592
(Tagraxofusp + gemtuzumab) R/R AML	NCT05716009
Pediatrics R/R CD123-positive hematological malignancies (ALL, AML, AUL, BPDCN, HL, LL, BCL, TCL, MDS, and MPAL)	NCT05476770

[a]CMML, chronic myelomonocytic leukemia; MF, myelofibrosis; BPDCN-IPh-like AML, blastic plasmacytoid dendritic cell neoplasm immunophenotype-like acute myeloid leukemia; ALL, acute lymphoblastic leukemia; AUL, acute undifferentiated leukemia; HL, Hodgkin's lymphoma; LL, lymphoblastic lymphoma; BCL, B-cell lymphoma; TCL, T-cell lymphoma; MDS, myelodysplastic syndrome; MPAL, mixed-phenotype acute leukemia.

cycle. The regimen is to advance for a maximum of six cycles, until disease progression or intolerable toxicity.

Tagraxofusp

Tagraxofusp is an FDA-approved RIT for relapsed or naïve BPDCN, a blood neoplasm that is characterized by IL-3 receptor (CD123) overexpression (El et al., 2020). The RIT is composed of recombinant human IL-3 fused to a truncated DT by a His-Met dipeptide linker and is expressed in *E. coli* (FDA, 2018b). IL-3 binds to the CD123 marker on the tumor cell surface (Economides et al., 2019). IL-3R is a potent target associated with low-to-no myelosuppression susceptibility due to the receptor's low expression on benign blood cells (Fanny et al., 2013). Tagraxofusp is currently being investigated for post-transplant maintenance of CD123-positive chronic blood malignancies such as AML (clinicaltrial.gov ID: NCT05233618), among other indications summarized in Table 2.

From bench to bedside: milestones to FDA approval

Preliminary pharmacological studies measured the *in vitro* and *in vivo* cytolytic activity. Researchers demonstrated tagraxofusp's ability to increase apoptosis and reduce cell proliferation using MTT assays and flow cytometry with AV/7AAD staining in model cell lines (CAL-1 and GEN 2.2) and primary BPDCN (collected from 12 patients) cells. They designed various treatment conditions for the MTT assays to assess for toxicity at different concentrations, as monotherapy versus co-administration with other toxins or chemotherapeutics, at 18 h versus 48 h post-treatment. The experimental results of Fanny et al. (2013) reported the notable potency of the drug as a single agent. They confirmed the superior benefit of tagraxofusp to chemotherapy in seven out of eight tested chemotherapeutic agents. Fanny et al. (2013) also showed a reduction in the viability of BPDCN cell lines (92%) and primary cells (80%) at low drug concentrations.

Tagraxofusp showed an increase in survival rate after a single treatment cycle *in vivo*, following intraperitoneal injection into NSG mice 7 days after BPDCN tumor induction (Fanny et al., 2013). Non-clinical toxicology studies were conducted in cynomolgus monkeys to determine the sufficient human-equivalent dose (FDA, 2018b).

To translate these outcomes clinically, a pilot study was conducted for initial clinical validation. Nine participants were evaluable out of 11 recruited. Results revealed a 78% positive response to treatment. A larger multi-center, four-staged, multi-cohort, open-label, single-arm, phase-I/II clinical trial (study STML-401-0114) in adults (≥18 years old), along with three pharmacometrics reports, provided sufficient pharmacological assessment for FDA review.

In the pivotal cohort, 54% of patients entered the CR/complete remission composite (CRc). Notably, no pediatric population was recruited throughout the trial. However, tagraxofusp is indicated for children (≥2 years old) because three pediatric cases treated with the drug showed a biological profile comparable to that observed in adult BPDCN patients (FDA, 2018b).

In STML-401-0114 (clinicaltrial.gov ID: NCT02113982), tagraxofusp was administered for 5 days with a cycle length of 21 days each throughout all four stages of the trial. The results from all stages were interpreted upon reaching the primary clinical endpoint of CR and CRc percentages.

Stage 1 (dose-escalation) aimed to examine the maximum dose tolerance (dose range 7 μg–16 μg per kg of body weight daily for 5 days). Twenty-three patients with BPDCN or refractory/relapsed (R/R) AML were included. The maximum tolerated dose was determined to be 12 μg per kg of body weight daily for 5 days and was used in the subsequent study stages. Therefore, this dose was used in stages 2–4 (FDA, 2018b).

Stage 2 included the same patient criteria, BPDCN or R/R AML, but a larger sample size of 58 cases. A different population was recruited in the "pivotal cohort" stage 3, where 13 patients with untreated newly diagnosed BPDCN were included. In stage 4, referred to as "continued access," 16 additional participants were enrolled (FDA, 2018b).

One of the centers in the clinical trial included 47 BPDCN patients—32 of whom were untreated, and 15 were relapsed patients. Conclusions from this trial reported a 90% treatment response rate, with the majority achieving CR—59% at 18 months and 52% at 24 months, even in the BPDCN-naïve group. The overall response rate for the refractory group was 67%, with a median overall survival of 8.5 months. Additionally, 45% of the cases advanced to HSCT (Pemmaraju et al., 2019). Tagraxofusp was approved by the FDA for clinical use on December 21, 2018 (Olejniczak et al., 2006; FDA, 2018b; Elzonris, 2020).

Pemmaraju et al. (2022) reported an update in July 2022 on the positive long-term effects of tagraxofusp (with a median follow-up

of 34 months), in patients previously enrolled in clinical trials. Overall, rapid treatment response and durable CR + CRc were noted. Results from this recent assessment showed a 75% objective response rate, including 57% CR + CRc. A total of 51% of patients achieving CR + CRc were advanced to either autologous or allogenic stem-cell transplant. The median overall survival of those who achieved CR + CRc and received stem-cell transplants is 38.4 months, and 72% of the patients were in remission for a year or longer after transplant. A total of 37% of patients in CR + CRc who received transplant had major reductions in baseline bone marrow blasts (12%–94%). Furthermore, 4 out of 18 patients with CR + CRc did not undergo transplant, 2 of whom had 27- and 52-month response durations. A novel finding was also reported in the R/R BPDCN patient population, where a 58% response rate was reported after 1–2 treatment cycles (Pemmaraju et al., 2022).

Immunogenicity assessment

The established vaccination protocol recommends that children (≥6 years old) and infants receive diphtheria vaccination (Centers for Disease Control and Prevention, 2022). In light of this, of the four clinical trials in the tagraxofusp FDA approval summary, pre-existing Abs against DT were detected in 96% of the patients prior to tagraxofusp treatment, 21% of which were neutralizing Abs (nAbs). At the end of cycle two, the antibody titer and frequency of patients with ADA (99%) increased, with 85% having nAbs. After cycle three, 68% of the patients also expressed anti-IL-3 Abs. The study conclusions suggest higher susceptibility to adverse effects in the group with pre-existing Abs at baseline (FDA, 2018b).

Toxicity and adverse outcomes

CLS was reported in 55% of the participating patients (FDA, 2018b), including several fatalities (Pemmaraju et al., 2019; FDA, 2018b; Elzonris, 2020), and affected 46% as either grade-1 or grade-2 adverse events. Hepatotoxicity was also reported in 40% of the patients. Other chemistry and hematology abnormalities include thrombocytopenia, hypocalcemia, low sodium levels, and hyperglycemia. Hypersensitivity reactions were considered for precautionary measures as they accounted for a 10% incidence rate in the trials (FDA, 2018b).

In the 2022 update by Pemmaraju et al. (2022) on the long-term effects of tagraxofusp, they reported nine grade-5 and three treatment-related CLS events. To resolve these events, tagraxofusp treatment was paused, albumin was administered to all participants with CLS, and steroids were administered to some CLS patients. Nine patients continued receiving additional doses of tagraxofusp after CLS resolution and did not report recurrence (Pemmaraju et al., 2022).

The major hazardous condition of CLS was listed as a boxed warning (Elzonris, 2020). An *in vivo* study using a rat model showed that the prophylactic use of 15-deoxyspergualin (DSG), an inhibitor of NF-kB, reduced vascular leak syndrome when co-administered with a ricin-based IT. Siegall et al. (1994) suggested that prophylactic DSG administration not only allowed for dose escalation that is necessary for successful treatment with IT, but it also did not decline or affect the conjugate's anti-tumor activity. Further studies may be extended to evaluate whether similar results may be reproduced using DSG with tagraxofusp and other bacterial-based RITs (Siegall et al., 1994). Moreover, severe outcomes during the clinical trial period warranted avid monitoring for dose-modification as needed (Elzonris, 2020; Pemmaraju et al., 2022).

Recommended administration protocol: dosing and route

The FDA-recommended dosage of tagraxofusp is 12 μg per kg of body weight to be administered intravenously on days 1–5 of a 21-day cycle. The regimen is to continue with repeat cycles until disease progression or unacceptable toxicity is reached (Elzonris, 2020).

Denileukin diftitox

In 1999, DAB389IL2 (DD) was the first FDA-approved RIT marketed as "Ontak." In 2009, Ontak was reformulated as E7777 (Lymphir) with further purification to reduce protein aggregates and thereby increase the number of active monomers; however, it retained the same amino acid sequence as DD. In March 2024, the FDA approved E7777 as a new drug for R/R CTCL based on the results from a phase-III multicenter clinical trial, as detailed in Figure 2. E7777 combines human IL-2 with DT and mainly targets IL-2Rα (CD25) on tumor cells. Interestingly, E7777 has also been reported to function against tumors with lower CD25 expression due to its binding to all types of IL-2R, not exclusively CD25 (IL-2Rα). Foss et al. (2022) reported that E7777 showed ~two times higher specific bioactivity than Ontak (Ghelani et al., 2020).

From bench to bedside: milestones to FDA approval

Lymphir (E7777) reemerged as a new FDA drug. The approval was supported by the clinical safety and efficacy assessment in NCT01871727 (study 302). Progression-free survival (PFS), quality of life, and time to progression (TTP) were also investigated. The established efficacy endpoints were the objective response rate (ORR) per independent review committee (IRC) based on Global Response Scoring (GRS) as a primary endpoint and the time to response (TTR) and duration of response (DOR) as secondary endpoints. Other endpoints included safety, drug tolerance, and immunogenicity.

The study was conducted in 20 centers across the United States and Australia from May 2013 to December 2021. Two stages were undertaken: the lead-in and the main study. Participants were recruited based on a histopathological CTCL diagnosis and no history of Ontak treatment. Of the 112 recruited patients (median age: 64 years old and average: 62.9 years old) with CTCL stages I–III at baseline, 98 were enrolled and received treatment. Sixty-nine of those patients (five from lead-in and 64 from the main study) plus two additional patients with visceral disease (n = 71) were selected for primary efficacy analysis based on ORR for investigator review. Thirty-four of the 69 patients had previously been treated with ≥1 targeted therapies. Results from this clinical trial showed 6 out of 71 with CR, 24 out of 71 with PR, and 33 out of 71 with stable disease. CR was reported if no detectable evidence of the disease was

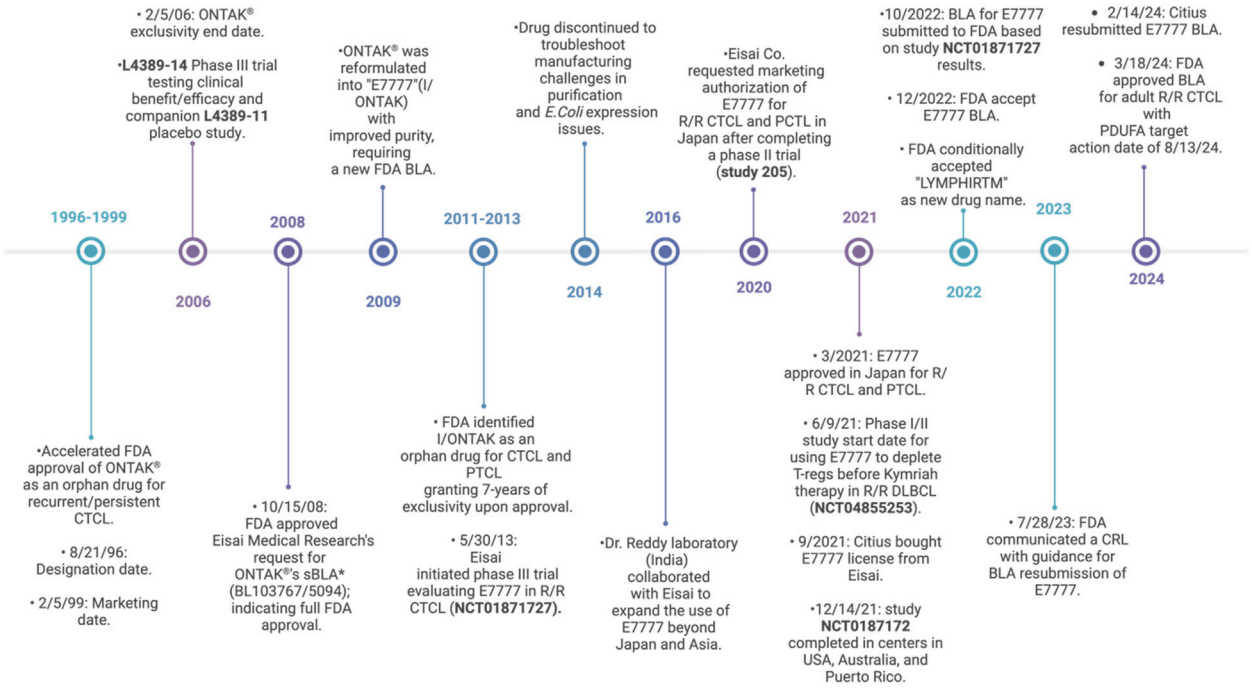

FIGURE 2
Timeline of clinical status from DD to E7777 (DD-cxdl). Peripheral T-cell lymphoma (PTCL), biologics license application (BLA), supplemental biologics license application (sBLA), complete response letter (CRL), and Prescription Drug User Fee Act (PDUFA) (FDA, 2024; FDA, 2008; Co, 2024; Mahdi et al., 2023; Allen, 2024; LaHucik, 2024; Wang et al., 2017; Eisai, 2024; Shiiba et al., 2022; National Library of Medicine, 2024b; Citiuspharma, 2024; Wrigley, 2022; Conroy, 2022; PR Newswire, 2023; Sava, 2024; Salsburg, 2024).

found, and PR was determined based on disease regression and the absence of newly detected sites.

Approximately 70% of patients who responded to E7777 treatment did so after one to two cycles, with a median TTR of 1.41 months. DOR was 6 or 12 months for 13 and 5 participants, respectively (Foss et al., 2022; Inc. E, 2022).

Immunogenicity assessment

Immunogenicity was tested based on anti-E7777 and anti-IL2 Abs. The samples were collected on day 1 of cycles 1, 2, 3, and 5. In the lead-in phase (dose escalation study), 100% of the patients were reported to have anti-E7777 Abs; comparably, 37.5%, 87.5%, 100%, and 83.3% of the patients had anti-IL-2 Abs on day 1 of the four cycles. In the main study (objective response rate), 85.7%, 91.7%, and 95.7% of the patients were reported to have anti-E7777 Abs on day 1 of cycles 1, 2, and 3, while only 5.5%, 52.3%, and 88.6% of the patients, respectively, had anti-IL-2 Abs at the start of each cycle (Inc. E, 2022).

In a Japanese phase-II clinical trial, an immunogenicity panel of anti-E7777 and anti-IL2 antibodies was tested for neutralizing activity. The samples were collected pre-treatment; on the first day of cycles 1, 2, 3, 5, and 8; and upon treatment completion. Post-treatment, 74.3% of the patients had positive anti-E7777 Abs. Anti-IL2 and neutralizing Abs increased from 5.4% to 0% at baseline to over 54.3% and 57.1%, respectively. After administration of E7777 in each cycle, the antibodies against E7777 rapidly cleared the drug from the serum.

Toxicity and adverse outcomes

Safety assessments in Study 302 were not new to E7777 as they were similar to those reported previously with Ontak. Adverse effects included grade-I/II CLS in some patients; other adverse effects were mild, including ~28% experiencing either chills, higher ALT levels, or peripheral edema; ~32% experiencing fatigue; and ~40% experiencing nausea (Foss et al., 2022).

Recommended administration protocol: dosing and route

Study 302 conducted dose-escalation analysis in the lead-in phase (6 μg/kg–15 μg/kg) and optimized the recommended dosage of 9 μg/kg/day administered for five consecutive days through an IV infusion over 60 min (±10 min) for up to eight cycles (median of six cycles) or until disease progression or unacceptable toxicity. The cycles were scheduled 21 days apart (Foss et al., 2022; Inc. E, 2022).

Improvement capacities and risk management

Efforts to reduce immunogenicity are evident throughout the evolution of ITs, such as isolating the catalytic moiety of toxins, utilizing fragments of humanized Abs, and introducing DNA recombination technology. Among the newer mitigation

strategies are B- and T-cell epitope mutations, SVP-R, and PEGylation (Mazor et al., 2018a; Mazor et al., 2018b; Zheng et al., 2020).

Since multiple studies have demonstrated that nAbs inhibit RIT function, nullifying B-cell epitopes that are naturally associated with nAbs has been suggested to decrease immunogenicity. Mapping and eliminating B-cell epitopes is a promising strategy (Mazor et al., 2018a). An example of this is LMB-100 (PE24 RIT currently in clinical stages), which is deimmunized from human B-cell epitopes (Mazor et al., 2018b). However, a more cost-effective technique was described to target and eliminate only amino acids with a key role in B-cell responses; this was tested in hopes of mitigating immunogenicity in DT-mediated RITs, where pre-existing ADAs from vaccination are detected (Schmohl et al., 2015).

Similarly, T-cell epitope modification was tested. Unlike B-cells, which naturally undergo affinity maturation, T-cell specificity is not altered upon epitope identification. Thus, elimination of T-cell epitopes is suggested to limit ADA formation (Mazor et al., 2018a). Mazor et al. (2014) studied PE38 and reported the presence of eight main T-cell epitopes. They deleted three epitopes and introduced point mutations in key residues of the remaining five epitopes, resulting in the modified LMB-T18 RIT (targeting CD22). Preclinical trials showed high cytotoxic and antitumor activity and a 93% reduction in T-cell epitopes. Furthermore, no new T-cell epitopes emerged as a result of the mutations. LMB-T18 immunogenicity was also tested against patient sera, and a significant decrease in antibody binding activity was reported (Mazor et al., 2014).

In another study, researchers explored the use of synthetic vaccine particles encapsulating rapamycin (SVP-R) for deimmunization purposes. The efficacy of this strategy was evaluated in an LMB-100 mouse model. Results reported durable effects, specificity, and transferable immune tolerance, preventing ADA and nAbs formation against the RIT. It further showed success in mice with baseline nAbs (Mazor et al., 2018b).

Chemical PEGylation (polyethylene glycol) is a technology that is long-established to improve pharmacokinetics/dynamic capacities in drug delivery in general. In the world of RITs, PEG reduces immunogenicity, improves the short half-life of some RITs, and enhances their cytotoxic efficiency. Zheng et al. (2020) published a study in March 2020, concluding that site-specific PEGylation of anti-mesothelin RITs increases their anti-tumor function and improves the drug's half-life. As noted with different generations of RITs, mutations to improve and enhance product half-life are paramount because they induce more durable remission that is achieved over a shorter period (Zahaf and Schmidt, 2017).

Conclusion

Immunotherapy with chimeric bacterial toxins as anti-neoplastic agents is showing clinical promise against hematological malignancies (Johannes and Decaudin, 2005). The RITs use the enzymatic domain of a bacterial toxin and the binding of the antibody to target tumor cells (Greer et al., 2018). Generally, the intracellular toxins from PE and DT have been used because they are extremely effective in mammalian cells (Johannes and Decaudin, 2005; Frankel et al., 2002). Other properties influencing the choice of the toxin include the orientation and structure of the enzymatic domain, purification yields, target antigen expression, and off-target toxicity.

More recently, investigations of RITs targeting solid tumors have gained momentum. Pre-clinically, in a BALB/c mouse model, a study tested E7777 in combination with anti-PD-1 against liver and colon cancer; they reported anti-tumor activity and increased overall survival (Ghelani et al., 2020; Mahdi et al., 2023). In a phase-I clinical trial with LMB-100 against mesothelioma and mesothelin-positive cancers, RIT monotherapy application against solid cancers had dose-limiting toxicity and generated anti-drug antibodies (Hassan et al., 2020). Efforts to evaluate LMB-100 combined with other treatments are under investigation (Skorupan et al., 2024).

As with other immunotherapies, RITs have been more effective in hematological diseases than in solid tumors. Blood cancers usually show milder antibody neutralization against either the toxin or Fv, thereby sustaining higher tolerance for extended treatment sessions. In addition, since blood cancers share the same reservoir of immune cells, RIT access to target cells provides increased immune suppression. Comparably, in solid tumors, RIT dose escalation is limited, secondary to rapid immunogenicity with nAbs forming only weeks after treatment (Pemmaraju et al., 2022). Additionally, usually reduced anti-tumor interaction is observed due to lower tumor penetration into solid tumors, considering their physiological structure. The increase in heterogeneity of solid tumors could also affect RIT treatment efficiency (Pirker, 1988).

RITs have historically encountered challenges within the pharmaceutical industry. Biologics that require complex drug development face difficulties in manufacturing and intellectual property management, which increase production costs. At times, companies have even obtained intellectual property with no intention to implement the drug, effectively abandoning its development (Holzman, 2009). Over the years, these challenges have limited the clinical adoption of RITs.

Other technical issues in RIT development have proven challenging. High levels of purified and active protein can be difficult to achieve. Pharmaceutical companies have explored multiple expression systems from bacteria, yeast, and mammalian cells to cell-free protein synthesis. Although mammalian systems offer advantages, they are costly as their yield is limited (Zhu et al., 2017). Bacterial production can reduce investment and production costs for simple proteins, but it does not add post-translational modifications. For example, in the previously FDA-approved preparations of DD (Ontak), expression in *E. Coli* led to struggles with purifying the active drug from misfolded and aggregated proteins. Difficulties with quality control and production, along with the drug's safety profile, decreased commercial viability. Increased cost and low demand eventually led to Ontak's discontinuation (Foss et al., 2022). The refined manufacturing and purification process in the reformulated drug Lymphir (E7777) resulted in higher purity of the active protein monomer with a better safety profile (Kawai et al., 2021).

Additionally, patients could undergo further screening to categorize them with more optimal TSA characteristics, such as low ADA, high TSA expression and density, or low antigen shedding, to ensure favorable outcomes.

Overall, RITs show a growing potential against many hematological malignancies, such as BPDCN, R/R HCL, and R/R CTCL, and can potentially be repurposed for other hematological

indications. However, this is a growing field, and researchers continue to investigate other risk management strategies to maximize the benefit from this treatment.

Author contributions

YR: Conceptualization, Formal analysis, Investigation, Validation, Writing – original draft, Writing – review and editing. EA: Funding acquisition, Writing – review and editing. RI: Supervision, Writing – review and editing. XQ: Conceptualization, Supervision, Writing – review and editing. SB: Formal analysis, Funding acquisition, Investigation, Supervision, Validation, Writing – review and editing.

Funding

The author(s) declare that financial support was received for the research and/or publication of this article. Research reported in this publication was supported by the Department of Pharmacology and the Applied Stem Cell Laboratory in the Tulane University School of Medicine and the National Center for Research Resources and the Office of Research Infrastructure Programs (ORIP) at the NIH through grant P51 OD011104 (TNPRC). The content is solely the responsibility of the authors and does not necessarily represent the official views of the supporting agencies. The funders had no role in study design, data collection and interpretation, or the decision to submit the work for publication.

Conflict of interest

The authors declare that the research was conducted in the absence of any commercial or financial relationships that could be construed as a potential conflict of interest.

The author(s) declared that they were an editorial board member of Frontiers, at the time of submission. This had no impact on the peer review process and the final decision.

Generative AI statement

The author(s) declare that no Generative AI was used in the creation of this manuscript.

Any alternative text (alt text) provided alongside figures in this article has been generated by Frontiers with the support of artificial intelligence and reasonable efforts have been made to ensure accuracy, including review by the authors wherever possible. If you identify any issues, please contact us.

Publisher's note

References

Abou Dalle, I., and Ravandi, F. (2019). Moxetumomab pasudotox for the treatment of relapsed and/or refractory hairy cell leukemia. *Expert Rev. Hematol.* 12 (9), 707–714. doi:10.1080/17474086.2019.1643231

Alkharabsheh, O., and Frankel, A. E. (2019). Clinical activity and tolerability of SL-401 (Tagraxofusp): recombinant diphtheria toxin and Interleukin-3 in hematologic malignancies. *Biomedicines* 7 (1), 6. doi:10.3390/biomedicines7010006

Allahyari, H., Heidari, S., Ghamgosha, M., Saffarian, P., and Amani, J. (2017). Immunotoxin: a new tool for cancer therapy. *Tumour Biol.* 39 (2), 1010428317692226. doi:10.1177/1010428317692226

Allen, I. (2024). Citius pharmaceuticals completes enrollment in the pivotal phase 3 study of its cancer immunotherapy I/ONTAK for the treatment of cutaneous T-Cell lymphoma. *Citius Pharma*. Available online at: https://www.sec.gov/Archives/edgar/data/1506251/000121390021063614/ea151726ex99-1_citiuspharrm.htm (Accessed February 25, 2024).

Allured, V. S., Collier, R. J., Carroll, S. F., and McKay, D. B. (1986). Structure of exotoxin A of Pseudomonas aeruginosa at 3.0-Angstrom resolution. *Proc. Natl. Acad. Sci. U. S. A.* 83 (5), 1320–1324. doi:10.1073/pnas.83.5.1320

Amet, N., Lee, H. F., and Shen, W. C. (2009). Insertion of the designed helical linker led to increased expression of tf-based fusion proteins. *Pharm. Res.* 26 (3), 523–528. doi:10.1007/s11095-008-9767-0

Antignani, A., and Fitzgerald, D. (2013). Immunotoxins: the role of the toxin. *Toxins (Basel)* 5 (8), 1486–1502. doi:10.3390/toxins5081486

Arber, D. A., Orazi, A., Hasserjian, R., Thiele, J., Borowitz, M. J., Le Beau, M. M., et al. (2016). The 2016 revision to the world Health Organization classification of myeloid neoplasms and acute leukemia. *Blood, J. Am. Soc. Hematol.* 127 (20), 2391–2405. doi:10.1182/blood-2016-03-643544

Brown, J. G., Entwistle, J., Glover, N., and MacDonald, G. C. (2008). *Preclinical safety evaluation of immunotoxins. Preclinical safety evaluation of biopharmaceuticals A sciencebased approach to facilitating clinical trials*. Hoboken, NJ: John Wiley and Sons, 649–668.

Cancer Statistics (2024). Cancer statistics. Available online at: https://seer.cancer.gov/statfacts/html/leuks.html (Accessed January, 2024).

Centers for Disease Control and Prevention (2022). *Diphtheria, tetanus, and pertussis vaccine recommendations*. Centers for Disease Control and Prevention. Available online at: https://www.cdc.gov/vaccines/vpd/dtap-tdap-td/hcp/recommendations.html.

Chen, X., Zaro, J. L., and Shen, W. C. (2013). Fusion protein linkers: property, design and functionality. *Adv. Drug Deliv. Rev.* 65 (10), 1357–1369. doi:10.1016/j.addr.2012.09.039

Citiuspharma (2024). Engineered IL-2-diphtheria toxin fusion protein denileukin diftitox for the treatment of rare forms of cancer. Available online at: https://citiuspharma.com/pipeline/I-ONTAK/default.aspx.

Co, E. G. (2024). FDA grants full approval to ONTAK® (denileukin diftitox) for use in patients with cutaneous T-Cell lymphoma (CTCL). *News Release*. Available online at: https://www.eisai.com/news/news200856.html (Accessed February 24, 2024).

Conroy, R. (2022). FDA accepts BLA for denileukin diftitox in cutaneous persistent/recurrent T-Cell lymphoma. *CancerNetwork*. Available online at: https://www.cancernetwork.com/view/fda-accepts-bla-for-denileukin-diftitox-in-cutaneous-persistent-recurrent-t-cell-lymphoma (Accessed February 26, 2024).

Economides, M. P., McCue, D., Lane, A. A., and Pemmaraju, N. (2019). Tagraxofusp, the first CD123-targeted therapy and first targeted treatment for blastic plasmacytoid dendritic cell neoplasm. *Expert Rev. Clin. Pharmacol.* 12 (10), 941–946. doi:10.1080/17512433.2019.1662297

Eisai (2024). Eisai submits marketing authorization application in Japan for anticancer agent denileukin diftitox (genetic recombinant) for cutaneous t-cell lymphoma and peripheral t-cell lymphoma. Available online at: https://www.eisai.com/news/2020/pdf/enews202015pdf.pdf (Accessed February 25, 2024).

El, A. H., Dupont, E., Paul, S., and Khoury, J. D. (2020). CD123 as a biomarker in hematolymphoid malignancies: principles of detection and targeted therapies. *Cancers (Basel)* 12 (11), 3087. doi:10.3390/cancers12113087

Else, M., Dearden, C. E., Matutes, E., Garcia-Talavera, J., Rohatiner, A. Z. S., Johnson, S. A. N., et al. (2009). Long-term follow-up of 233 patients with hairy cell leukaemia, treated initially with pentostatin or cladribine, at a median of 16 years from diagnosis. *Br. J. Haematol.* 145 (6), 733–740. doi:10.1111/j.1365-2141.2009.07668.x

Elzonris (2020). The largest prospective BPDCN study (N=84) of treatment-naive and previously treated patients. *Elzonris*. Available online at: https://elzonris.com/hcp/study-design.

Fanny, D., Frankel, A. E., Seilles, E., Biichle, S., Deconninck, E., Bonnefoy, F., et al. (2013). Preclinical studies of SL-401, a targeted therapy directed to the interleukin-3 receptor (IL3-R), in blastic plasmacytoid dendritic cell neoplasm (BPDCN): potent activity in BPDCN cell lines, primary tumor, and in an *in vivo* model. *Blood* 122 (21), 3942. doi:10.1182/blood.V122.21.3942.3942

Farkona, S., Diamandis, E. P., and Blasutig, I. M. (2016). Cancer immunotherapy: the beginning of the end of cancer? *BMC Med.* 14, 73. doi:10.1186/s12916-016-0623-5

FDA (2008). Letter response to BLA. Available online at: https://www.accessdata.fda.gov/drugsatfda_docs/appletter/2008/103767s5094ltr.pdf (Accessed February 28th, 2024).

FDA (2018a). FDA highlights of lumoxiti prescribing information. Available online at: https://www.accessdata.fda.gov/drugsatfda_docs/label/2018/761104s000lbl.pdf.

FDA (2018b). Tagraxofusp-erzs FDA approval summary review. Available online at: https://www.accessdata.fda.gov/drugsatfda_docs/nda/2018/761116Orig1s000SumR.pdf.

FDA (2020). FDA approves moxetumomab pasudotox-tdfk for hairy cell leukemia. Available online at: https://www.fda.gov/drugs/resources-information-approved-drugs/fda-approves-moxetumomab-pasudotox-tdfk-hairy-cell-leukemia (Accessed April, 2020).

FDA (2023). AstraZeneca's letter to the FDA about discontinuing lumoxiti. *Lett. Novemb. 18th*. Available online at: https://www.fda.gov/media/164425/download (Accessed February 7, 2024).

FDA (2024). FDA. Available online at: https://www.accessdata.fda.gov/scripts/opdlisting/oopd/detailedIndex.cfm?cfgridkey=99396 (Accessed February 28th, 2024).

FitzGerald, D. J., Kreitman, R., Wilson, W., Squires, D., and Pastan, I. (2004). Recombinant immunotoxins for treating cancer. *Int. J. Med. Microbiol.* 293 (7-8), 577–582. doi:10.1078/1438-4221-00302

Foss, F. M., Kim, Y. H., Prince, H., Kuzel, T. M., Yannakou, C. K., Ooi, C. E., et al. (2022). Efficacy and safety of E7777 (improved purity denileukin diftitox [ONTAK]) in patients with relapsed or refractory cutaneous T-cell lymphoma: results from pivotal study 302. *Blood* 140 (Suppl. 1), 1491–1492. doi:10.1182/blood-2022-166916

Frankel, A. E., Rossi, P., Kuzel, T. M., and Foss, F. (2002). Diphtheria fusion protein therapy of chemoresistant malignancies. *Curr. Cancer Drug Targets* 2 (1), 19–36. doi:10.2174/1568009023333944

George, R. A., and Heringa, J. (2002). An analysis of protein domain linkers: their classification and role in protein folding. *Protein Eng.* 15 (11), 871–879. doi:10.1093/protein/15.11.871

Getta, B. M., Park, J. H., and Tallman, M. S. (2015). Hairy cell leukemia: past, present and future. *Best. Pract. Res. Clin. Haematol.* 28 (4), 269–272. doi:10.1016/j.beha.2015.10.015

Getta, B. M., Woo, K. M., Devlin, S., Park, J. H., Abdel-Wahab, O., Saven, A., et al. (2016). Treatment outcomes and secondary cancer incidence in young patients with hairy cell leukaemia. *Br. J. Haematol.* 175 (3), 402–409. doi:10.1111/bjh.14207

Ghelani, A., Bates, D., Conner, K., Wu, M. Z., Lu, J., Hu, Y. L., et al. (2020). Defining the threshold IL-2 signal required for induction of selective Treg cell responses using engineered IL-2 muteins. *Front. Immunol.* 11, 1106. doi:10.3389/fimmu.2020.01106

Greer, J. P., Arber, D. A., Glader, B. E., List, A. F., Means, R. M., and Rodgers, G. M. (2018). *Wintrobe's clinical hematology*. Lippincott Williams and Wilkins.

Hamadani, M., Abu Kar, S. M., Usmani, S. Z., Savani, B. N., Ayala, E., and Kharfan-Dabaja, M. A. (2014). Management of relapses after hematopoietic cell transplantation in T-cell Non-Hodgkin lymphomas. *Semin. Hematol.* 51 (1), 73–86. doi:10.1053/j.seminhematol.2013.11.005

Hansen, J. K., Weldon, J. E., Xiang, L., Beers, R., Onda, M., and Pastan, I. (2010). A recombinant immunotoxin targeting CD22 with low immunogenicity, low nonspecific toxicity, and high antitumor activity in mice. *J. Immunother.* 33 (3), 297–304. doi:10.1097/CJI.0b013e3181cd1164

Hassan, R., Alewine, C., Mian, I., Spreafico, A., Siu, L. L., Gomez-Roca, C., et al. (2020). Phase 1 study of the immunotoxin LMB-100 in patients with mesothelioma and other solid tumors expressing mesothelin. *Cancer* 126 (22), 4936–4947. doi:10.1002/cncr.33145

Holzman, D. C. (2009). Whatever happened to immunotoxins? Research, and hope, are still alive. *J. Natl. Cancer Inst.* 101 (9), 624–625. doi:10.1093/jnci/djp110

Inc. E (2022). A trial of E7777 in persistent and recurrent cutaneous T-Cell lymphoma. Available online at: https://clinicaltrials.gov/study/NCT01871727 (Accessed June 12, 2024).

Johannes, L., and Decaudin, D. (2005). Protein toxins: intracellular trafficking for targeted therapy. *Gene Ther.* 12 (18), 1360–1368. doi:10.1038/sj.gt.3302557

John, R. M. (1996). "Corynebacterium Diphtheriae," in *Medical microbiology*. Editor S. B 4th ed.

Kawai, H., Ando, K., Maruyama, D., Yamamoto, K., Kiyohara, E., Terui, Y., et al. (2021). Phase II study of E7777 in Japanese patients with relapsed/refractory peripheral and cutaneous T-cell lymphoma. *Cancer Sci.* 112 (6), 2426–2435. doi:10.1111/cas.14906

Khan, S., and Sawas, A. (2019). Antibody-Directed therapies: toward a durable and tolerable treatment platform for CTCL. *Front. Oncol.* 9, 645. doi:10.3389/fonc.2019.00645

Kharfan-Dabaja, M. A., Lazarus, H. M., Nishihori, T., Mahfouz, R. A., and Hamadani, M. (2013). Diagnostic and therapeutic advances in blastic plasmacytoid dendritic cell neoplasm: a focus on hematopoietic cell transplantation. *Biol. Blood Marrow Transpl.* 19 (7), 1006–1012. doi:10.1016/j.bbmt.2013.01.027

Kim, J. S., Jun, S. Y., and Kim, Y. S. (2020). Critical issues in the development of immunotoxins for anticancer therapy. *J. Pharm. Sci.* 109 (1), 104–115. doi:10.1016/j.xphs.2019.10.037

Kolybo, D., Labyntsev, A., Korotkevich, N., Komisarenko, S., Romaniuk, S., and Oliinyk, O. (2013). Immunobiology of diphtheria. Recent approaches for the prevention, diagnosis, and treatment of disease. *Biotechnol. Acta* 6 (4), 043–062. doi:10.15407/biotech6.04.043

Kreitman, R. J., and Pastan, I. (2011). Antibody fusion proteins: anti-CD22 recombinant immunotoxin moxetumomab pasudotox. *Clin. Cancer Res.* 17 (20), 6398–6405. doi:10.1158/1078-0432.CCR-11-0487

Kreitman, R. J., and Pastan, I. (2020). Development of recombinant immunotoxins for hairy cell leukemia. *Biomolecules* 10 (8), 1140. doi:10.3390/biom10081140

Kreitman, R. J., Tallman, M. S., Robak, T., Coutre, S., Wilson, W. H., Stetler-Stevenson, M., et al. (2012). Phase I trial of anti-CD22 recombinant immunotoxin moxetumomab pasudotox (CAT-8015 or HA22) in patients with hairy cell leukemia. *J. Clin. Oncol.* 30 (15), 1822–1828. doi:10.1200/JCO.2011.38.1756

Kreitman, R. J., Dearden, C., Zinzani, P. L., Delgado, J., Karlin, L., Robak, T., et al. (2018a). Moxetumomab pasudotox in relapsed/refractory hairy cell leukemia. *Leukemia* 32 (8), 1768–1777. doi:10.1038/s41375-018-0210-1

Kreitman, R. J., Tallman, M. S., Robak, T., Coutre, S., Wilson, W. H., Stetler-Stevenson, M., et al. (2018b). Minimal residual hairy cell leukemia eradication with moxetumomab pasudotox: phase 1 results and long-term follow-up. *Blood, J. Am. Soc. Hematol.* 131 (21), 2331–2334. doi:10.1182/blood-2017-09-803072

Kreitman, R. J., Dearden, C., Zinzani, P. L., Delgado, J., Robak, T., le Coutre, P. D., et al. (2021). Moxetumomab pasudotox in heavily pre-treated patients with relapsed/refractory hairy cell leukemia (HCL): long-term follow-up from the pivotal trial. *J. Hematol. Oncol.* 14 (1), 35. doi:10.1186/s13045-020-01004-y

Krolick, K. A., Uhr, J. W., Slavin, S., and Vitetta, E. S. (1982). *In vivo* therapy of a murine B cell tumor (BCL1) using antibody-ricin A chain immunotoxins. *J. Exp. Med.* 155 (6), 1797–1809. doi:10.1084/jem.155.6.1797

LaHucik, K. (2024). Citius buys out license to Ontak replacement from dr. Reddy's for $40M. Available online at: https://www.fiercepharma.com/drug-delivery/citius-buys-out-license-to-ontak-replacement-from-dr-reddy-s-for-40m (Accessed February 24, 2024).

Mahdi, H. S., Woodall-Jappe, M., Singh, P., and Czuczman, M. S. (2023). Targeting regulatory T cells by E7777 enhances CD8 T-cell–mediated anti-tumor activity and extends survival benefit of anti-PD-1 in solid tumor models. *Front. Immunol.* 14, 1268979. doi:10.3389/fimmu.2023.1268979

Maitre, E., Cornet, E., and Troussard, X. (2019). Hairy cell leukemia: 2020 update on diagnosis, risk stratification, and treatment. *Am. J. Hematol.* 94 (12), 1413–1422. doi:10.1002/ajh.25653

Mansfield, E., Amlot, P., Pastan, I., and FitzGerald, D. J. (1997). Recombinant RFB4 immunotoxins exhibit potent cytotoxic activity for CD22-bearing cells and tumors. *Blood* 90 (5), 2020–2026. doi:10.1182/blood.v90.5.2020

Matthey, B., Engert, A., and Barth, S. (2000). Recombinant immunotoxins for the treatment of Hodgkin's disease. *Int. J. Mol. Med.* 6 (5), 509–523. doi:10.3892/ijmm.6.5.509

Mazor, R., and Pastan, I. (2020). Immunogenicity of immunotoxins containing pseudomonas Exotoxin A: causes, consequences, and mitigation. *Front. Immunol.* 11, 1261. doi:10.3389/fimmu.2020.01261

Mazor, R., Eberle, J. A., Hu, X., Vassall, A. N., Onda, M., Beers, R., et al. (2014). Recombinant immunotoxin for cancer treatment with low immunogenicity by identification and silencing of human T-cell epitopes. *Proc. Natl. Acad. Sci. U. S. A.* 111 (23), 8571–8576. doi:10.1073/pnas.1405153111

Mazor, R., King, E. M., and Pastan, I. (2018a). Strategies to reduce the immunogenicity of recombinant immunotoxins. *Am. J. Pathol.* 188 (8), 1736–1743. doi:10.1016/j.ajpath.2018.04.016

Mazor, R., King, E. M., Onda, M., Cuburu, N., Addissie, S., Crown, D., et al. (2018b). Tolerogenic nanoparticles restore the antitumor activity of recombinant immunotoxins by mitigating immunogenicity. *Proc. Natl. Acad. Sci. U. S. A.* 115 (4), E733–E742. doi:10.1073/pnas.1717063115

McCarthy, E. F. (2006). The toxins of William B. Coley and the treatment of bone and soft-tissue sarcomas. *Iowa Orthop. J.* 26, 154–158.

Mei, X., Chen, J., Wang, J., and Zhu, J. (2019). Immunotoxins: targeted toxin delivery for cancer therapy. *Pharm. Fronts* 1 (01), e33–e45. doi:10.1055/s-0039-1700507

Michael Lord, J., and Roberts, L. M. (1998). Toxin entry: retrograde transport through the secretory pathway. *J. cell Biol.* 140 (4), 733–736. doi:10.1083/jcb.140.4.733

Michalska, M., and Wolf, P. (2015). Pseudomonas Exotoxin A: optimized by evolution for effective killing. *Front. Microbiol.* 6, 963. doi:10.3389/fmicb.2015.00963

Moolten, F. L., Capparell, N. J., Zajdel, S. H., and Cooperband, S. R. (1975). Antitumor effects of antibody-diphtheria toxin conjugates. II. Immunotherapy with conjugates directed against tumor antigens induced by simian virus 40. *J. Natl. Cancer Inst.* 55 (2), 473–477. doi:10.1093/jnci/55.2.473

Morton, L. M., Wang, S. S., Devesa, S. S., Hartge, P., Weisenburger, D. D., and Linet, M. S. (2006). Lymphoma incidence patterns by WHO subtype in the United States, 1992-2001. *Blood* 107 (1), 265–276. doi:10.1182/blood-2005-06-2508

Murphy, J. R. (2011). Mechanism of diphtheria toxin catalytic domain delivery to the eukaryotic cell cytosol and the cellular factors that directly participate in the process. *Toxins* 3 (3), 294–308. doi:10.3390/toxins3030294

National Library of Medicine (2024a). Accessed February 2024. Available online at: https://www.clinicaltrials.gov/search?intr=tagraxofusp&page=1.

National Library of Medicine (2024b). A trial of E7777 in persistent and recurrent cutaneous T-Cell lymphoma. Available online at: https://www.clinicaltrials.gov/study/NCT01871727?intr=NCT01871727&rank=1 (Accessed February 25, 2024).

Olejniczak, S. H., Stewart, C. C., Donohue, K., and Czuczman, M. S. (2006). A quantitative exploration of surface antigen expression in common B-cell malignancies using flow cytometry. *Immunol. Invest* 35 (1), 93–114. doi:10.1080/08820130500496878

Pastan, I., Chaudhary, V., and FitzGerald, D. J. (1992). Recombinant toxins as novel therapeutic agents. *Annu. Rev. Biochem.* 61, 331–354. doi:10.1146/annurev.bi.61.070192.001555

Pastan, I., Hassan, R., Fitzgerald, D. J., and Kreitman, R. J. (2006). Immunotoxin therapy of cancer. *Nat. Rev. Cancer* 6 (7), 559–565. doi:10.1038/nrc1891

Pemmaraju, N., Lane, A. A., Sweet, K. L., Stein, A. S., Vasu, S., Blum, W., et al. (2019). Tagraxofusp in blastic plasmacytoid dendritic-cell neoplasm. *N. Engl. J. Med.* 380 (17), 1628–1637. doi:10.1056/NEJMoa1815105

Pemmaraju, N., Sweet, K. L., Stein, A. S., Wang, E. S., Rizzieri, D. A., Vasu, S., et al. (2022). Long-Term benefits of tagraxofusp for patients with blastic plasmacytoid dendritic cell neoplasm. *J. Clin. Oncol.* 40 (26), 3032–3036. doi:10.1200/JCO.22.00034

Pirker, R. (1988). Immunotoxins against solid tumors. *J. Cancer Res. Clin. Oncol.* 114 (4), 385–393. doi:10.1007/BF02128183

PR Newswire (2023). *Citius pharmaceuticals, Inc. Receives regulatory guidance from the U.S. food and Drug Administration (FDA) regarding the planned resubmission of the BLA for LYMPHIR™*. Citius Pharmaceuticals, Inc. Available online at: https://www.prnewswire.com/news-releases/citius-pharmaceuticals-inc-receives-regulatory-guidance-from-the-us-food-and-drug-administration-fda-regarding-the-planned-resubmission-of-the-bla-for-lymphir-301921591.html (Accessed February 26, 2024).

Rauh, M. J., Rahman, F., Good, D., Silverman, J., Brennan, M. K., Dimov, N., et al. (2012). Blastic plasmacytoid dendritic cell neoplasm with leukemic presentation, lacking cutaneous involvement: case series and literature review. *Leuk. Res.* 36 (1), 81–86. doi:10.1016/j.leukres.2011.07.033

Salsburg, G. (2024). Citius pharmaceuticals announces FDA acceptance of the BLA resubmission of LYMPHIR™ (denileukin diftitox) for the treatment of adults with relapsed or refractory cutaneous T-Cell lymphoma. *Citius Pharma News* Available online at: https://citiuspharma.com/investors/news-media/news/release-details/2024/Citius-Pharmaceuticals-Announces-FDA-Acceptance-of-the-BLA-Resubmission-of-LYMPHIR-Denileukin-Diftitox-for-the-Treatment-of-Adults-with-Relapsed-or-Refractory-Cutaneous-T-Cell-Lymphoma/default.aspx (Accessed August 23, 2024).

Salvatore, G., Beers, R., Margulies, I., Kreitman, R. J., and Pastan, I. (2002). Improved cytotoxic activity toward cell lines and fresh leukemia cells of a mutant anti-CD22 immunotoxin obtained by antibody phage display. *Clin. Cancer Res.* 8 (4), 995–1002. doi:10.1158/1078-0432.CCR-01-0450

Sava, J. (2024). Denileukin diftitox BLA resubmitted for CTCL after addressing FDA concerns. Available online at: https://www.targetedonc.com/view/denileukin-diftitox-bla-resubmitted-for-ctcl-after-addressing-fda-concerns (Accessed February 26, 2024).

Schmohl, J. U., Todhunter, D., Oh, S., and Vallera, D. A. (2015). Mutagenic deimmunization of diphtheria toxin for use in biologic drug development. *Toxins (Basel)* 7 (10), 4067–4082. doi:10.3390/toxins7104067

Seymour, J. F., Kurzrock, R., Freireich, E. J., and Estey, E. H. (1994). 2-chlorodeoxyadenosine induces durable remissions and prolonged suppression of CD4+ lymphocyte counts in patients with hairy cell leukemia. *Blood* 83 (10), 2906–2911. doi:10.1182/blood.v83.10.2906.2906

Seymour, J. F., Talpaz, M., and Kurzrock, R. (1997). Response duration and recovery of CD4+ lymphocytes following deoxycoformycin in interferon-alpha-resistant hairy cell leukemia: 7-year follow-up. *Leukemia* 11 (1), 42–47. doi:10.1038/sj.leu.2400513

Shafiee, F., Aucoin, M. G., and Jahanian-Najafabadi, A. (2019). Targeted diphtheria toxin-based therapy: a review article. *Front. Microbiol.* 10, 2340. doi:10.3389/fmicb.2019.02340

Shi, Y., and Wang, E. (2014). Blastic plasmacytoid dendritic cell neoplasm: a clinicopathologic review. *Arch. Pathol. Lab. Med.* 138 (4), 564–569. doi:10.5858/arpa.2013-0101-RS

Shiiba, H., Takechi, A., Asakura, S., Kawaguchi, T., and Sato, M. (2022). Preclinical and clinical researches of Denileukin Diftitox (genetical Recombination)(Remitoro®), a novel agent for T-cell lymphoma. *Nihon Yakurigaku zasshi Folia Pharmacol. Jpn.* 157 (5), 376–382. doi:10.1254/fpj.22032

Shimony, S., Luskin, M. R., Gangat, N., LeBoeuf, N. R., Feraco, A. M., and Lane, A. A. (2025). Blastic Plasmacytoid Dendritic Cell Neoplasm (BPDCN): 2025 update on diagnosis, pathophysiology, risk assessment, and management. *Am. J. Hematol.* 100 (8), 1408–1422. doi:10.1002/ajh.27737

Siegall, C. B., Liggitt, D., Chace, D., Tepper, M. A., and Fell, H. P. (1994). Prevention of immunotoxin-mediated vascular leak syndrome in rats with retention of antitumor activity. *Proc. Natl. Acad. Sci. U. S. A.* 91 (20), 9514–9518. doi:10.1073/pnas.91.20.9514

Skorupan, N., Peer, C. J., Zhang, X., Choo-Wosoba, H., Ahmad, M. I., Lee, M. J., et al. (2024). Tofacitinib to prevent anti-drug antibody formation against LMB-100 immunotoxin in patients with advanced mesothelin-expressing cancers. *Front. Oncol.* 14, 1386190. doi:10.3389/fonc.2024.1386190

Srivastava, S., and Luqman, S. (2015). Immune-O-Toxins as the magic bullet for therapeutic purposes. *Biomed. Res. Ther.* 2 (1), 2–15. doi:10.7603/s40730-015-0002-4

Tadmor, T. (2011). Purine analog toxicity in patients with hairy cell leukemia. *Leuk. Lymphoma* 52 (Suppl. 2), 38–42. doi:10.3109/10428194.2011.565097

Tay, J., Daly, A., Jamani, K., Labelle, L., Savoie, L., Stewart, D., et al. (2019). Patient eligibility for hematopoietic stem cell transplantation: a review of patient-associated variables. *Bone Marrow Transpl.* 54 (3), 368–382. doi:10.1038/s41409-018-0265-7

Valent, P., Groner, B., Schumacher, U., Superti-Furga, G., Busslinger, M., Kralovics, R., et al. (2016). Paul Ehrlich (1854-1915) and his contributions to the foundation and birth of translational medicine. *J. Innate Immun.* 8 (2), 111–120. doi:10.1159/000443526

Wang, Z., Zheng, Q., Zhang, H., Bronson, R. T., Madsen, J. C., Sachs, D. H., et al. (2017). Ontak-like human IL-2 fusion toxin. *J. Immunol. Methods* 448, 51–58. doi:10.1016/j.jim.2017.05.008

Weber, G. F. (2015). *Molecular therapies of cancer*. Springer.

Weldon, J. E., and Pastan, I. (2011). A guide to taming a toxin--recombinant immunotoxins constructed from Pseudomonas exotoxin A for the treatment of cancer. *FEBS J.* 278 (23), 4683–4700. doi:10.1111/j.1742-4658.2011.08182.x

Weldon, J. E., Skarzynski, M., Therres, J. A., Ostovitz, J. R., Zhou, H., Kreitman, R. J., et al. (2015). Designing the furin-cleavable linker in recombinant immunotoxins based on Pseudomonas exotoxin A. *Bioconjug Chem.* 26 (6), 1120–1128. doi:10.1021/acs.bioconjchem.5b00190

Wolf, P., and Elsasser-Beile, U. (2009). Pseudomonas exotoxin A: from virulence factor to anti-cancer agent. *Int. J. Med. Microbiol.* 299 (3), 161–176. doi:10.1016/j.ijmm.2008.08.003

Wrigley, N. (2022). BLA submitted to the FDA for denileukin diftitox in cutaneous Persistent/Recurrent T-Cell lymphoma. *CancerNetwork*. Available online at: https://www.cancernetwork.com/view/bla-submitted-to-the-fda-for-denileukin-diftitox-in-cutaneous-persistent-recurrent-t-cell-lymphoma (Accessed February 25, 2024).

Yamaizumi, M., Mekada, E., Uchida, T., and Okada, Y. (1978). One molecule of diphtheria toxin fragment A introduced into a cell can kill the cell. *Cell* 15 (1), 245–250. doi:10.1016/0092-8674(78)90099-5

Yeung, C. C. S., and Radich, J. (2017). Predicting chemotherapy resistance in AML. *Curr. Hematol. Malig. Rep.* 12 (6), 530–536. doi:10.1007/s11899-017-0378-x

Yu, S., Kwon, M. J., Kim, K., Koo, D. H., Woo, H. Y., and Park, H. (2014). A rare case of acute leukemic presentation of blastic plasmacytoid dendritic cell neoplasm without cutaneous lesions. *Ann. Lab. Med.* 34 (2), 148–151. doi:10.3343/alm.2014.34.2.148

Zahaf, N. I., and Schmidt, G. (2017). Bacterial toxins for cancer therapy. *Toxins (Basel)* 9 (8), 236. doi:10.3390/toxins9080236

Zdanovsky, A. G., Chiron, M., Pastan, I., and FitzGerald, D. J. (1993). Mechanism of action of Pseudomonas exotoxin. Identification of a rate-limiting step. *J. Biol. Chem.* 268 (29), 21791–21799. doi:10.1016/s0021-9258(20)80612-7

Zheng, Z., Okada, R., Kobayashi, H., Nagaya, T., Wei, J., Zhou, Q., et al. (2020). Site-Specific PEGylation of Anti-Mesothelin recombinant immunotoxins increases half-life and antitumor activity. *Mol. Cancer Ther.* 19 (3), 812–821. doi:10.1158/1535-7163.MCT-19-0890

Zhu, S., Liu, Y., Wang, P. C., Gu, X., and Shan, L. (2017). Recombinant immunotoxin therapy of glioblastoma: smart design, key findings, and specific challenges. *Biomed. Res. Int.* 2017, 7929286. doi:10.1155/2017/7929286

frontiers | Frontiers in Pharmacology

TYPE Original Research
PUBLISHED 31 October 2025
DOI 10.3389/fphar.2025.1631505

OPEN ACCESS

EDITED BY
Ana Podolski-Renic,
Institute for Biological Research "Siniša Stanković" – National Institute of Republic of Serbia, Serbia

REVIEWED BY
Harsh Goel,
All India Institute of Medical Sciences, India
Petar Popovic,
University of Belgrade, Serbia

*CORRESPONDENCE
Nigar Huseynova,
nigarhuseynova@bsu.edu.az
Yusuf Baran,
ybaran@gmail.com

RECEIVED 19 May 2025
ACCEPTED 19 September 2025
PUBLISHED 31 October 2025

CITATION
Huseynova N, Baran Z, Khalilov R, Mammadova A and Baran Y (2025) Chemosensitizing effect of apigenin on T-ALL cell therapy.
Front. Pharmacol. 16:1631505.
doi: 10.3389/fphar.2025.1631505

Chemosensitizing effect of apigenin on T-ALL cell therapy

Nigar Huseynova[1]*, Züleyha Baran[2], Rovshan Khalilov[1], Afat Mammadova[3] and Yusuf Baran[4]*

[1]Department of Biophysics and Biochemistry, Baku State University, Baku, Azerbaijan, [2]Department of Pharmacology, Laboratory of Molecular Pharmacology, Anadolu University, Eskişehir, Türkiye, [3]Department of Botany and Plant Physiology, Baku State University, Baku, Azerbaijan, [4]Department of Molecular Biology and Genetics, Laboratory of Cancer Genetics, İzmir Institute of Technology, İzmir, Türkiye

T-cell acute lymphoblastic leukemia (T-ALL) is an aggressive hematological malignancy with limited therapeutic options and frequent treatment-associated toxicities. L-asparaginase, a cornerstone in T-ALL therapy, is often restricted by hypersensitivity reactions and systemic side effects, highlighting the need for safer strategies to enhance its efficacy. This study investigated the potential of apigenin, a naturally occurring flavonoid with antioxidant and pro-apoptotic properties, to act as a chemosensitizer for L-asparaginase in MOLT-4 T-ALL cells. Cytotoxicity was assessed using the MTT assay, apoptosis by Annexin V/PI staining, cell cycle distribution by flow cytometry, and mitochondrial membrane potential by JC-1 staining. Both apigenin and L-asparaginase produced dose- and time-dependent cytotoxicity, with combination treatment resulting in reduced IC_{50} values. Apoptotic analysis showed significantly higher apoptosis in the combination-treated groups than in single-agent groups. Cell cycle analysis revealed that apigenin induced S-phase arrest and L-asparaginase induced G1-phase arrest, while the combination disrupted cell cycle progression at multiple checkpoints. JC-1 assay further demonstrated enhanced mitochondrial depolarization, with up to a 29.2-fold increase in cytoplasmic-to-mitochondrial fluorescence ratio in combination therapy compared to L-asparaginase alone. These findings indicate that apigenin potentiates L-asparaginase-induced cytotoxicity through mitochondrial dysfunction and intrinsic apoptotic signaling. The combined use of apigenin and L-asparaginase may provide a novel strategy to improve therapeutic efficacy in T-ALL while potentially reducing the toxicity associated with high-dose L-asparaginase monotherapy.

KEYWORDS

apigenin, L-asparaginase, T-ALL, combination therapy, chemosensitization

Introduction

Leukemia is a collection of cancers originating from abnormal cells in the body's hematopoietic tissues, characterized by poor differentiation and aggressive behavior (Feng Li, 2024; Shafat et al., 2017; Yang et al., 2021). According to Sung et al., 2021, leukemia ranked as the 13th most common cause of cancer-related mortality worldwide, accounting for ~3.1% (305,405 cases) of all cancer deaths. Among its subtypes, acute lymphoblastic leukemia (ALL) is a particularly aggressive form that arises from the lymphoid lineage, resulting in overproduction of immature lymphocytes and disruption of normal hematopoiesis. ALL is most prevalent in children, progresses rapidly, and requires prompt intervention (Ekpa et al., 2023; Pui et al., 2004; Rujkijyanont and Inaba, 2024).

T -cell acute lymphoblastic leukemia (T-ALL) is a rarer subtype, comprising 15%–20% of pediatric and 25%–30% of adult ALL cases, and is historically associated with inferior survival compared with B-ALL (Möricke et al., 2016; Raetz and Teachey, 2016). Despite improvements in chemotherapy protocols, outcomes for T-ALL, especially in relapsed and high-risk groups, remain poor (Durinck et al., 2015; Van Vlierberghe and Ferrando, 2012). The mainstay of treatment for ALL is combination chemotherapy that includes asparaginase, anthracyclines, cytarabine, cyclophosphamide, and intrathecal methotrexate (Hayashi et al., 2024; Juluri et al., 2022). While this regimen has improved survival to 80%–85%, management of resistant or recurrent disease is still challenging (Chen et al., 2013; Youns et al., 2010).

L-asparaginase is a crucial and highly effective drug for treating T-ALL (Egler et al., 2016; Ishida H, 2024; Tong and Rizzari, 2023). Its selective action is based on the inability of leukemic lymphoblasts to upregulate asparagine synthetase, leaving them vulnerable to extracellular asparagine depletion. However, dosing and administration are complicated by hypersensitivity, hepatotoxicity, coagulopathy, and pancreatitis, with hypersensitivity being the main cause of treatment interruption (Baruchel et al., 2020). Maintaining serum asparaginase activity (SAA) ≥0.1 IU/mL is required for therapeutic efficacy, but achieving this threshold while limiting toxicity is difficult (van der Sluis et al., 2016). Thus, strategies that enhance L-asparaginase efficacy while minimizing toxicity are urgently needed.

A major barrier in ALL therapy is the toxicity of chemotherapeutics to normal tissues, which restricts both dosing and treatment duration. Therefore, a promising approach is to combine conventional chemotherapy with natural, low-toxicity agents that enhance therapeutic efficacy while protecting healthy cells (Gilad et al., 2021). Plants are rich in bioactive compounds with anticancer potential, particularly polyphenols. These secondary metabolites influence multiple stages of carcinogenesis and are generally safe, affordable, and accessible (Kang et al., 2012; Kilani-Jaziri et al., 2012; Russo et al., 2010). Flavonoids, widely found in fruits, vegetables, teas, and herbal medicines, exhibit diverse pharmacological activities, including antioxidant, anti-inflammatory, hepatoprotective, immunoregulatory, and anticancer properties (Hasnat et al., 2024).

Among flavonoids, apigenin—a dietary flavone abundant in fruits, vegetables, and herbs—has attracted particular interest. It displays antioxidant, anti-inflammatory, and anticancer effects (Telange et al., 2017). Mechanistic studies show that apigenin arrests HL-60 myeloid leukemia cells at G2/M and TF-1 erythroid leukemia cells at G0/G1, partly through inhibition of the PI3K/AKT pathway and activation of caspases (A. Mahbub et al., 2017). Importantly, apigenin has low toxicity in normal cells, supporting its potential as an adjuvant to chemotherapy. It has also been shown to sensitize cancer cells to chemotherapeutic agents such as 5-fluorouracil, doxorubicin, chlorambucil, imatinib, and cyclophosphamide (Bokulić et al., 2011).

However, flavonoid–drug interactions can be context dependent. While many studies confirm their chemosensitizing potential, others report antagonistic effects. For example, apigenin has been shown to attenuate vincristine-induced apoptosis in hematological malignancy models (Goto et al., 2012). This variability highlights the need for rationally designed studies to define specific drug–flavonoid interactions in leukemia.

In this study, we investigated the potential of apigenin to sensitize T-ALL cells to L-asparaginase. By evaluating their combined effects on cell viability, apoptosis, mitochondrial function, and cell-cycle regulation, we aimed to identify a strategy to enhance L-asparaginase efficacy while reducing its dose-related toxicities, thereby improving therapeutic outcomes in T-ALL.

Materials and methods

Chemicals

L-Asparaginase from *E. coli* (A3809-1KU) and apigenin were purchased from Sigma (United States). A stock solution of L-asparaginase was prepared at 1 mg/mL using distilled water and stored at −20 °C. With dimethyl sulfoxide (DMSO), a stock solution of apigenin was made at a concentration of 2.5 mg/mL and stored at −20 °C.

The sterile DMSO was obtained from the Merck Group (Germany) and stored at room temperature. Fetal Bovine Serum (FBS) and RPMI 1640 media (1X) were sourced from Gibco (United Kingdom). Dulbecco's Phosphate-buffered saline (PBS) (1X) was acquired from Capricorn Scientific (Germany), while Penicillin-Streptomycin (100X) was purchased from Euroclone (Italy). 3-(4,5-Dimethylthiazol-2-yl)-2,5-Diphenyltetrazolium Bromide (MTT) powder was obtained from Invitrogen (United States), and a stock solution was prepared in 1X PBS at a final concentration of 5 mg/mL. Trypan blue powder was obtained from Sigma Aldrich (United States), and a stock solution was prepared at a final concentration of 0.4% in 1X PBS. The FITC Annexin V Apoptosis Detection Kit I, used for apoptosis assays, was purchased from BD Biosciences (United States). The MitoProbe™ JC-1 Assay Kit for flow cytometry was acquired from Invitrogen (United States). Propidium iodide (PI) powder was sourced from AppliChem (Germany), and a 1 mg/mL stock solution was prepared in distilled water and stored at 4 °C. Triton X-100 was also purchased from AppliChem (Germany), while RNase A (DNase- and protease-free, 10 mg/mL) was obtained from Thermo Scientific (United States).

Abbreviations: ALL, Acute Lymphoblastic Leukemia; ANOVA, Analysis of Variance; ATCC, American Type Culture Collection (inferred from context, not explicitly stated but common for cell lines); B-ALL, B-cell Acute Lymphoblastic Leukemia; CDK2, Cyclin-dependent Kinase 2; CCCP, Carbonyl Cyanide 3-Chlorophenylhydrazone; CI, Combination Index; DMSO, Dimethyl Sulfoxide; DNA, Deoxyribonucleic Acid; ER, Endoplasmic Reticulum; FACS, Fluorescence-Activated Cell Sorting; FBS, Fetal Bovine Serum; FITC, Fluorescein Isothiocyanate; G1, Gap 1 Phase; G2, Gap 2 Phase; JC-1, 5,5′,6,6′-Tetrachloro-1,1′,3,3′-tetraethylbenzimidazolylcarbocyanine iodide; MMP, Mitochondrial Membrane Potential (appears as ΔΨm); MTT, 3-(4,5-Dimethylthiazol-2-yl)-2,5-Diphenyltetrazolium Bromide; PBS, Phosphate-Buffered Saline; PI, Propidium Iodide; PKB, Protein Kinase B (another name for AKT); PMSF, Phenylmethylsulfonyl Fluoride (not mentioned, but often used with protease-free conditions—could be excluded if not present); qPCR, Quantitative Polymerase Chain Reaction (not in your document, but often associated with gene expression studies—omit if not present); RNA, Ribonucleic Acid; RNase, Ribonuclease; SAA, Serum Asparaginase Activity; SDS, Sodium Dodecyl Sulfate (not used in your text); SD, Standard Deviation; T-ALL, T-cell Acute Lymphoblastic Leukemia; ΔΨm, Mitochondrial Membrane Potential.

Cell line

The human T-ALL cell line, MOLT-4 cells, was purchased from Icell Bioscience (Shanghai, China). The cell line used in this study was previously cryopreserved at −80 °C to maintain its viability and integrity before use. After thawing, cells were expanded under standard culture conditions, and experiments were performed using cells at the 3rd–4th passage to ensure stable growth and viability. The cells were grown in RPMI 1640 medium with 10% FBS, 1% L-glutamine, and 1% penicillin-streptomycin solution, and kept at 37 °C in a room with 5% CO_2.

Cell viability assay

Cell viability was determined using the 3-(4,5)-2,5-diphenyl-tetrazolium bromide (MTT) assay. MOLT-4 cells (1 × 10⁴ cells per well) were placed in 96-well plates and given different amounts of L-asparaginase and apigenin, either by themselves or with a control, for 24 and 48 h at 37 °C in a 5% CO2 environment. At the conclusion of each incubation period, 20 μL of freshly prepared MTT solution (5 mg/mL) was added to each well and incubated for 4 h at 37 °C in a 5% CO_2 environment. The absorbance was measured at 570 and 670 nm using a microplate reader (Thermo Scientific, Multiskan GO, Finland). The obtained absorbance values reflect cellular metabolic activity, which indirectly indicates viability and cytotoxicity. The values of IC25, IC50, and IC75 were determined based on the percentages of cell proliferation inhibition at different apigenin and L-asparaginase concentrations and were graphed.

Apoptotic assay

MOLT-4 cells (6×10^5 cells per well) were seeded into 6-well plates and exposed to varying concentrations of L-asparaginase (0.5, 1.0, and 1.5 μg/mL) and apigenin (5, 10, and 15 μg/mL), either individually or in combination, for 24 and 48 h at 37 °C in a 5% CO_2 incubator. Apoptotic cells were evaluated using an Annexin V-FITC/propidium iodide (PI) apoptosis detection kit, following the manufacturer's protocol. Quantification of apoptotic populations was performed using a flow cytometer (BD FACS Canto, United States) with two-channel analysis, and data were processed with CellQuest software (BD Biosciences).

Determination of mitochondrial membrane potential

The MitoProbe™ JC-1 Assay Kit, which is used for flow cytometry, was used to check the mitochondrial transmembrane potential with a JC-1 dye test. MOLT-4 cells (6×10^5 cells/well) were seeded into 6-well plates and were incubated with the indicated combined doses of apigenin and L-asparaginase (5μg/mL–0.5 μg/mL, 10μg/mL–1.0 μg/mL, and 15μg/mL–1.5 μg/mL) for 48 h in a 5% CO_2 atmosphere. The experimental design included two untreated control groups and one negative control group, which contained cells exposed only to the solvent vehicles (distilled water and DMSO at their highest applied concentrations). After 48 h of incubation in a 5% CO_2 atmosphere, carbonyl cyanide 3-chlorophenylhydrazone (CCCP; 2 μL, 50 mM), a compound that disrupts mitochondrial membrane potential, was added to one of the control groups to reach a final concentration of 50 μM and was maintained at 37 °C in a 5% CO_2 atmosphere for 5 min. JC-1 dye (20 μL, 200 μM) was then added 20 min before the termination of the experiment and incubated at 37 °C in a 5% CO_2 atmosphere. After incubation, the cells were collected and washed with PBS. Fluorescence intensity was ultimately measured using flow cytometry (BD FACS Canto, United States). In the JC-1 assay, P6 represents polarized mitochondria (healthy cells, red fluorescence), while P7 represents depolarized mitochondria (apoptotic cells, green fluorescence).

Cell cycle analysis

MOLT-4 cells (6×10^5 cells per well) were cultured in 6-well plates and exposed to various concentrations of apigenin and L-asparaginase, administered either separately or in combination. Two control groups were used: one group had cells treated with distilled water and DMSO at high levels, and the other group had cells that were not treated with any drugs at all. After 48 h of incubation in a 5% CO_2 atmosphere, the cells were fixed with ethanol (80%) at −20 °C, then permeabilized with Triton X-100 in PBS (200 μL, 0.1%) and treated with RNase A (4 μL, 200 μg/mL) to remove RNA. Cells were stained with PI solution (20 μL, 1 mg/mL) and analyzed by flow cytometry (BD FACS Canto, United States). The percentage of cells in the G1, S, and G2 phases was measured to see how well apigenin and L-asparaginase, either separately or together, could stop the cell cycle by comparing the treated groups to the control groups.

Isobologram and combination index analysis

The combination effects of L-asparaginase and apigenin were evaluated using the improved isobologram method and the combination index (CI) approach, as implemented in the CompuSyn software. Combination Index (CI) values were computed to evaluate the interaction between L-asparaginase and apigenin, with CI < 1 indicating a synergistic effect, CI = 1 representing an additive effect, and CI > 1 suggesting antagonism. These values were derived using the median-effect principle according to the Chou–Talalay method (Chou, 2010).

Statistical analysis

Statistical analysis and graph generation were carried out using GraphPad Prism 10.0. A paired t-test was applied to assess differences between the control and experimental groups. Additionally, a two-way ANOVA was used to analyze the overall experimental data.

Results

Apigenin and L-asparaginase inhibit leukemia cell viability

The MTT assay was employed to evaluate the cytotoxic effects of apigenin and L-asparaginase, both individually and in combination,

10.3389/fphar.2025.1631505

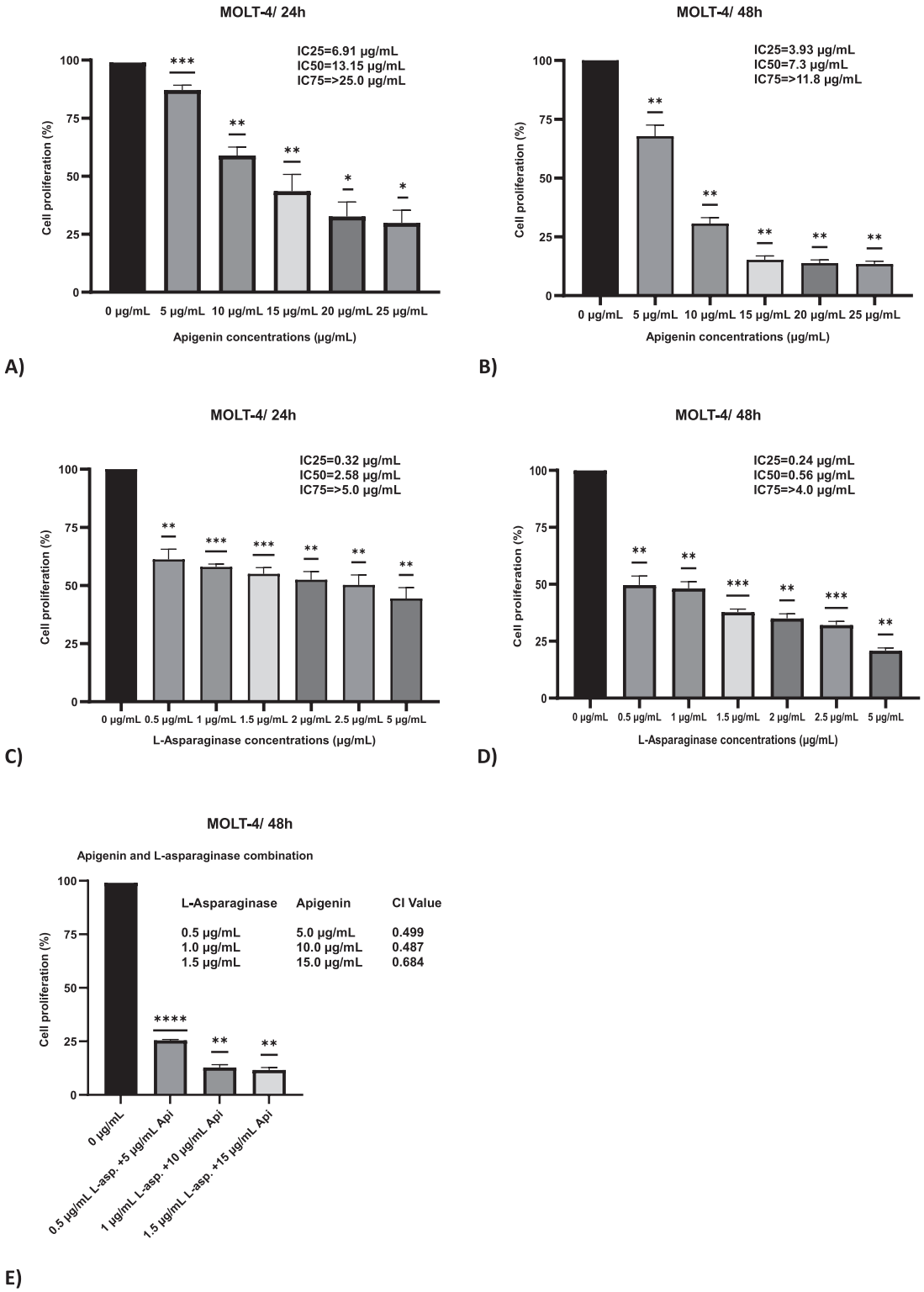

FIGURE 1
The effect of apigenin and L-asparaginase on the proliferation of MOLT-4 cells at 48 and 24 h. **(A)** Apigenin 24 h; **(B)** Apigenin 48 h; **(C)** L-asparaginase 24 h; **(D)** L-asparaginase 48 h; **(E)** Percentage proliferation data for apigenin + L-asparaginase combinations at 48 h. These data were used to calculate the Combination Index (CI), reported in the Results. Data represent mean ± SD of three independent experiments (*P < 0.01, **P < 0.05, vs. the control).

on MOLT-4 cells following 24 and 48 h of incubation. For apigenin alone, there was a dose-dependent decrease in cell viability, which was stronger at 48 h than at 24 h (Figures 1A,B). The IC50 of apigenin was 13.15 μg/mL at 24 h but decreased to 7.3 μg/mL at 48 h, indicating that cytotoxic activity increased over time. Additionally, at 48 h, the IC25 and IC75 values were 3.93 μg/mL and 11.8 μg/mL, respectively, indicating a gradual dose-dependent response. Time-dependent cytotoxicity was evident at higher concentrations (≥15 μg/mL) of this compound.

An additional delay during the 48 h period further increased efficacy, with a dose-dependent inhibition of cell growth observed following treatment with L-asparaginase alone. The IC50 was 2.58 μg/mL at 24 h and decreased to 0.56 μg/mL at 48 h, representing a 4.6-fold reduction (Figures 1C,D). Moreover, at 48 h, the IC25 and IC75 values were 0.24 μg/mL and 4.0 μg/mL.

Combination index (CI) values below 1 at all tested concentrations, calculated using 48-h MTT assay viability data, indicated a synergistic interaction between apigenin and L-asparaginase. The CI values were 0.499 for the combination of 0.5 μg/mL L-asparaginase with 5 μg/mL apigenin, and 0.487 for 1 μg/mL L-asparaginase with 10 μg/mL apigenin, indicating strong synergy. At the highest tested dose—1.5 μg/mL L-asparaginase combined with 15 μg/mL apigenin—a slightly reduced synergistic effect was noted, with a CI value of 0.684 (Figure 1E).

Cell cycle effects of L-asparaginase and/or apigenin in MOLT-4 cells

MOLT-4 cells were treated with apigenin and L-asparaginase alone and in combination for 48 h. The results suggested that either of the two compounds caused a concentration-dependent alteration of cell cycle progression, and at the cell cycle indices, they had a more prominent synergistic effect (Figure 2).

L-asparaginase treatment primarily led to G1-phase cell cycle arrest with a dose-dependent increase in the accumulation of cells in G1 phase. The percentage of G1 cells increased from 46.74% in the untreated control to 66.05% in the presence of 0.5 μg/mL. This effect was also more pronounced in higher concentrations, e.g., 1.5 μg/mL for 71.41% of cells in G1. As a result, the fraction of cells in S and G2 phases decreased. The S-phase cells decreased to 25.38% and the G2-phase cells were reduced to 3.22% at the 1.5 μg/mL value of L-asparaginase.

Contrasting results were obtained with apigenin treatment, where S phase arrest was shown in a higher percentage of cells at higher concentrations. The percentage of S-phase cells remained comparable to the control (47.35%), with 46.25% at 10 μg/mL, but increased further to 51.21% at 15 μg/mL. Conversely, G1-phase cells were reduced (15 μg/mL, 42.92%), and G2-phase cells were slightly reduced (15 μg/mL, 5.90%).

Using apigenin and L-asparaginase together at doses that were very effective in killing cells showed clear changes in how the cells progressed through their cycle. The number of cells in the G1 phase rose to 59.34%, while the number of cells in the S phase slowly dropped to 34.84% when treated with 0.5 μg/mL L-asparaginase and 5 μg/mL apigenin. G2 phase were also stable at 5.82%. Finally, the number of S-phase cells went up a lot to 45.62% compared to when

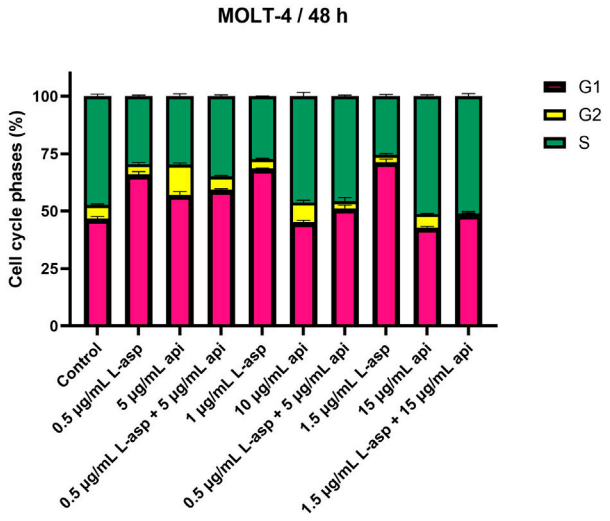

FIGURE 2
Apigenin and L-asparaginase induce cell-cycle arrest alone or in combination. After treatment with agents for 48 h, MOLT-4 cells were stained with PI and analyzed for cell cycle distribution using flow cytometry. Data represent mean ± SD of three independent experiments (*P < 0.01, **P < 0.05, vs. the control).

1 μg/mL L-asparaginase was used with 10 μg/mL apigenin; however, the number of G1-phase cells dropped to 51.19%. The G2 phase fell to 3.20%. The maximum extent of S-phase reached only 51.07% in L-asparaginase at 1.5 μg/mL and apigenin at 15 μg/mL, while the proportion of G1 phase cells was decreased down to 48.71% and G2 phase cells were almost absent, comprising only 0.23% of cells.

Apoptotic assay

The apoptotic impact of apigenin and L-asparaginase, both individually and in combination, was assessed using Annexin V-FITC/PI dual staining followed by flow cytometry at 24- and 48-h post-treatment. Based on cytotoxicity results from the MTT assay, L-asparaginase was used at concentrations of 0.5, 1.0, and 1.5 μg/mL, while apigenin was applied at 5, 10, and 15 μg/mL. These same concentrations were combined to evaluate potential synergistic effects on apoptosis.

The X-axis of the dot plots represents Annexin V-FITC staining, while the Y-axis denotes PI staining. Apoptotic cells were quantified as the sum of Q2 (late apoptosis) and Q4 (early apoptosis), while necrotic cells (Q1) were identified but not included in the apoptosis analysis (Figure 3A). Quadrant Q3 indicated the proportion of viable MOLT-4 cells, which was recorded as 90.9% at 24 h and 93.3% at 48 h in the control group. At 24 h, apigenin alone induced apoptosis in a dose-dependent manner, with 13.1%, 29.3%, and 63.4% apoptotic cells at 5, 10, and 15 μg/mL, respectively, while L-asparaginase alone caused 31.0%, 32.0%, and 31.4% apoptosis at 0.5, 1.0, and 1.5 μg/mL, respectively. Combination treatments significantly increased apoptotic activity, reaching 38.1% for 0.5 μg/mL L-asparaginase +5 μg/mL apigenin, 65.2% for 1.0 μg/mL + 10 μg/mL, and 77.8% for 1.5 μg/mL + 15 μg/mL, suggesting additive or synergistic interactions even at early time points.

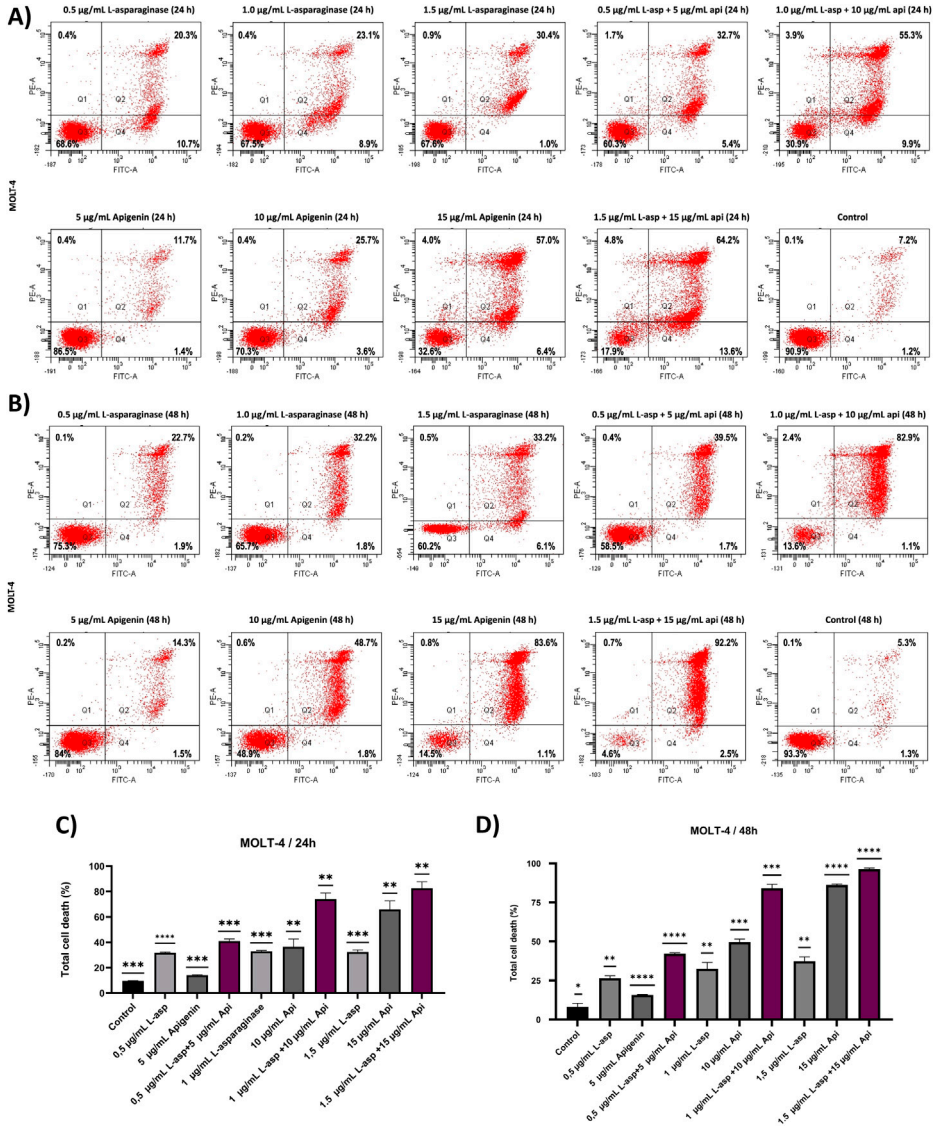

FIGURE 3
The apoptotic effect of apigenin and L-asparaginase alone and in combination on the proliferation of MOLT-4 cells at 24- and 48 h. **(A)** Apigenin and L-asparaginase alone and in combination at 24 h; **(B)** Apigenin and L-asparaginase alone and in combination at 48 h; **(C)** Quantification of total cell death in MOLT-4 cells treated with apigenin, L-asparaginase, or their combination for 24 h. **(D)** Quantification of total cell death in MOLT-4 cells treated with apigenin, L-asparaginase, or their combination for 48 h Data represent mean ± SD of three independent experiments (*P < 0.01, **P < 0.05, vs. the control).

After 48 h, apoptosis levels increased across all conditions: apigenin alone caused 15.8%, 50.5%, and 84.7% apoptosis at 5, 10, and 15 µg/mL, respectively, while L-asparaginase alone induced 24.6%, 34.0%, and 39.3% at 0.5, 1.0, and 1.5 µg/mL (Figure 3B). Notably, the combined treatments produced striking apoptosis rates of 41.2%, 84.0%, and 94.7% for 0.5 + 5, 1.0 + 10, and 1.5 + 15 µg/mL, respectively, reinforcing a robust time- and dose-dependent synergistic effect consistent with enhanced intrinsic apoptotic signaling and mitochondrial dysfunction as reported in similar studies (Aithal et al., 2019; Naponelli et al., 2024; W. Wang et al., 2000) The statistical analysis of three independently performed experiments is shown in Figures 3C,D, where the Y-axis represents the overall cell death rate calculated as the sum of Q1 (necrotic), Q2 (late apoptotic), and Q4 (early apoptotic) cell populations.

Determination of mitochondrial membrane potential

The mitochondrial membrane potential (ΔΨm) of MOLT-4 cells was evaluated after 48 h of treatment with apigenin and L-asparaginase, individually and in combination at different concentrations, using JC-1 dye-based flow cytometry. The percentages of P6 and P7 for each condition were reported alongside the results obtained from CCCP treatment (Figure 4B). CCCP, a well-established disruptor of mitochondrial membrane potential, was used to verify the sensitivity of the JC-1 dye in detecting changes in mitochondrial polarization in MOLT-4 cells. The data from the CCCP-treated group served as a reference for normalizing the values obtained from the untreated control samples.

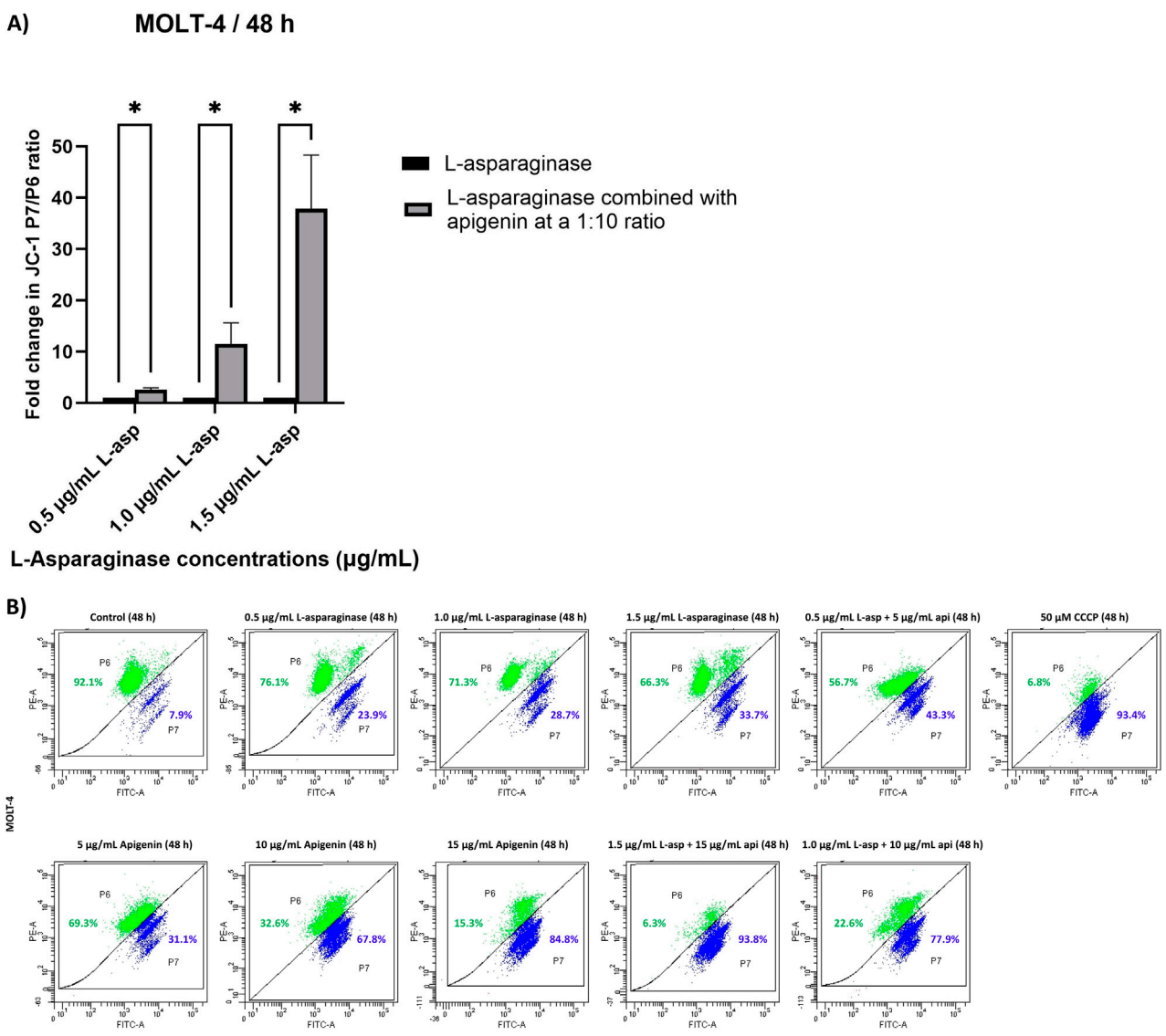

FIGURE 4
(A) Quantitative analysis of JC-1 red/green fluorescence ratio in MOLT-4 cells treated with L-asparaginase alone or in combination with apigenin for 48 h; **(B)** The effect of apigenin and L-asparaginase alone and in combination on the loss of mitochondria membrane potential of MOLT-4 cells at 48 h; Data represent mean ± SD of three independent experiments (*P < 0.01, **P < 0.05, vs. the control).

And drug-exposed groups. The calculated and normalized P7/P6 ratios of apigenin and L-asparaginase combination-treated groups were compared to the corresponding L-asparaginase-only groups to determine the relative fold change in the cytoplasmic/mitochondrial JC-1 ratio. This comparison was specifically chosen in accordance with the study's aim to evaluate the chemosensitizing effect of apigenin on L-asparaginase-induced mitochondrial depolarization.

In comparison to the respective L-asparaginase-only groups (0.5, 1.0, and 1.5 µg/mL), the combination of 0.5 µg/mL L-asparaginase with 5 µg/mL apigenin produced only a modest change in the cytoplasmic-to-mitochondrial JC-1 ratio (2.4-fold increase over L-asparaginase alone). However, a substantial rise in this ratio was observed with the 1.0 µg/mL L-asparaginase +10 µg/mL apigenin combination (8.7-fold increase), and an even greater enhancement was recorded with the 1.5 µg/mL L-asparaginase +15 µg/mL apigenin treatment (29.2-fold increase relative to 1.5 µg/mL L-asparaginase) (Figure 4A).

Discussion

Flavonoids are often mentioned to be able to sensitize malignant cells to classical anticancer drugs and potentiate their cytotoxicity, thus revealing their potential use as adjunctive agents for the treatment of neoplastic diseases including leukemia. It has been reported that flavonoids, specifically apigenin, can enhance the anticancer activity of chemotherapeutic agents (Mahbub et al., 2015; Mahbub et al., 2017; Mahbub et al., 2022). Consistent with these reports, our study demonstrates that apigenin augments the activity of L-asparaginase against T-ALL cells, supporting its role as a chemosensitizer.

Apigenin, a naturally occurring flavonoid, showed time-dependent inhibitory effects on leukemic cell viability, consistent with its reported ability to induce apoptosis through oxidative stress, mitochondrial membrane depolarization, and caspase activation (Rooprai et al., 2021; Shukla and Gupta, 2010). These findings also align with its recognized role as a chemosensitizing agent that enhances the responsiveness of cancer cells to therapy (Mahbub et al., 2022).

When combined, apigenin and L-asparaginase demonstrated clear synergistic interactions. This effect is likely driven by complementary mechanisms: L-asparaginase deprives cells of an essential amino acid, while apigenin lowers the apoptotic threshold by modulating mitochondrial pathways and apoptotic regulators. Together, these actions amplify cell death signals, as has been described for apigenin–flavonoid combinations in previous reports (B. Wang and Zhao, 2017).

Such synergy is particularly relevant in the clinical context, as it suggests the possibility of lowering effective L-asparaginase doses while maintaining efficacy, thereby reducing treatment-related toxicity. These observations are consistent with earlier findings that flavonoids, including apigenin, can potentiate the anticancer activity of standard chemotherapeutics (Asnaashari et al., 2023; Nozhat et al., 2021).

Cell-cycle analyses further highlight the complementary actions of both agents. L-asparaginase primarily induced G1 arrest, consistent with its role in limiting asparagine availability essential for DNA replication and protein synthesis (Takahashi et al., 2017) whereas apigenin promoted S-phase accumulation, a phenomenon linked to oxidative stress–mediated DNA damage and inhibition of cyclin-dependent regulators (Shi et al., 2015). Their combination produced mixed G1 and S-phase arrest, suggesting a dual blockade at multiple checkpoints. Such dual-phase interference may prevent adaptive resistance, a frequent obstacle in leukemia therapy (Ghelli Luserna di Rora' et al., 2017; Simabuco et al., 2018).

Apoptosis assays further support the hypothesis that apigenin enhances L-asparaginase efficacy. Mechanistically, flavonoids such as apigenin are known to destabilize mitochondrial membranes, upregulate pro-apoptotic proteins, and inhibit survival pathways including PI3K/AKT and mTOR, thereby amplifying intrinsic apoptotic signaling (Naponelli et al., 2024; Zughaibi et al., 2021). The strong apoptotic responses in the combination groups are consistent with these mechanisms, underscoring apigenin's role as a chemosensitizer.

Interestingly, while L-asparaginase alone maintained relatively consistent apoptotic activity over time, apigenin's effects were highly dose- and time-responsive, reinforcing its role as a dynamic enhancer of cell death when used in combination. The combination's superiority was further substantiated by the inclusion of both early and late apoptotic events (Q4 and Q2), while excluding necrosis (Q1), ensuring that the measured responses specifically reflect programmed cell death.

Altogether, these results suggest that co-administration of apigenin may allow for the use of lower L-asparaginase doses while maintaining or enhancing therapeutic efficacy, which could potentially minimize L-asparaginase-associated toxicity in clinical applications.

The mitochondrial depolarization observed with JC-1 staining further reinforces this interpretation. While L-asparaginase alone induces apoptosis largely through ER stress and protein synthesis inhibition (Hawkins et al., 2004), apigenin directly targets mitochondria by modulating Bax/Bcl-2 balance and cytochrome c release (Çetinkaya and Baran, 2023; Huseynova et al., 2024). The pronounced mitochondrial dysfunction in the combination groups reflects a convergence of these mechanisms, leading to amplified intrinsic apoptosis.

Taken together, these findings suggest that apigenin enhances the therapeutic potential of L-asparaginase in T-ALL cells by acting on complementary pathways involving cell-cycle arrest and mitochondrial-mediated apoptosis. By enabling dose reduction of L-asparaginase without loss of efficacy, this strategy could help overcome toxicity-related limitations in clinical settings. Future work should focus on elucidating the precise molecular targets of this synergy and validating these effects *in vivo* to assess translational potential.

Conclusion

This study highlights the potential of combining natural flavonoids with conventional chemotherapeutic agents to enhance anticancer efficacy. Specifically, the flavonoid apigenin significantly potentiated the cytotoxic, apoptotic, and mitochondrial-disrupting effects of L-asparaginase in leukemic cells. The combination treatment led to greater reductions in cell viability, increased rates of programmed cell death, and enhanced mitochondrial membrane depolarization compared to either agent alone, suggesting a synergistic interaction.

Mechanistically, the results suggest that apigenin may sensitize cancer cells to chemotherapy by modulating mitochondrial function and apoptotic signaling pathways. Additionally, distinct cell cycle arrest patterns induced by each agent contributed to their combined effectiveness, potentially limiting cancer cell adaptability and resistance.

These findings support the growing interest in using plant-derived bioactive compounds as adjuvants in cancer therapy. The observed synergy between apigenin and L-asparaginase provides a promising foundation for future research and highlights the potential for reduced dosing and improved therapeutic outcomes in leukemia and possibly other malignancies. Further studies, including *in vivo* models and clinical evaluation, are warranted to fully explore and validate this combination strategy.

Data availability statement

The original contributions presented in the study are included in the article/supplementary material, further inquiries can be directed to the corresponding authors.

Author contributions

NH: Formal Analysis, Funding acquisition, Project administration, Supervision, Writing – original draft, Writing – review and editing. ZB: Resources, Writing – review and editing. RK: Resources, Writing – review and editing. AM:

Resources, Writing – review and editing. YB: Conceptualization, Funding acquisition, Supervision, Writing – review and editing.

Funding

The author(s) declare that financial support was received for the research and/or publication of this article. This research was supported by the Türkiye Scholarships Program under Research Scholarship Grant No. 23AZ002939. The funding body had no role in study design, data collection and analysis, decision to publish, or preparation of the manuscript.

Conflict of interest

The authors declare that the research was conducted in the absence of any commercial or financial relationships that could be construed as a potential conflict of interest.

Generative AI statement

The author(s) declare that no Generative AI was used in the creation of this manuscript.

Any alternative text (alt text) provided alongside figures in this article has been generated by Frontiers with the support of artificial intelligence and reasonable efforts have been made to ensure accuracy, including review by the authors wherever possible. If you identify any issues, please contact us.

Publisher's note

References

Aithal, A. P., Bairy, L. K., Seetharam, R. N., and Rao, M. K. G. (2019). Human bone marrow-derived mesenchymal stromal cells in combination with silymarin regulate hepatocyte growth factor expression and genotoxicity in carbon tetrachloride induced hepatotoxicity in wistar rats. *J. Cell. Biochem.* 120 (8), 13026–13036. doi:10.1002/jcb.28573

Asnaashari, S., Amjad, E., and Sokouti, B. (2023). Synergistic effects of flavonoids and paclitaxel in cancer treatment: a systematic review. *Cancer Cell Int.* 23 (1), 211. doi:10.1186/s12935-023-03052-z

Baruchel, A., Brown, P., Rizzari, C., Silverman, L., Van Der Sluis, I., Wolthers, B. O., et al. (2020). Increasing completion of asparaginase treatment in childhood acute lymphoblastic leukaemia (ALL): summary of an expert panel discussion. *ESMO Open* 5 (Issue 5), e000977. doi:10.1136/esmoopen-2020-000977

Bokulić, A., Garaj-Vrhovac, V., Brajša, K., Durić, K., Glojnarić, I., and Šitum, K. (2011). The effect of apigenin on cyclophosphamide and doxorubicin genotoxicity *in vitro* and *in vivo*. *J. Environ. Sci. Health - Part A Toxic/Hazardous Subst. Environ. Eng.* 46 (5), 526–533. doi:10.1080/10934529.2011.551744

Çetinkaya, M., and Baran, Y. (2023). Therapeutic potential of luteolin on cancer. *Vaccines (Basel).* 11 (3), 554. doi:10.3390/vaccines11030554

Chen, Y. J., Wu, C. S., Shieh, J. J., Wu, J. H., Chen, H. Y., Chung, T. W., et al. (2013). Baicalein triggers mitochondria-mediated apoptosis and enhances the antileukemic effect of vincristine in childhood acute lymphoblastic leukemia CCRF-CEM cells. *Evid. Based Complement. Altern. Med.* 2013, 124747. doi:10.1155/2013/124747

Chou, T.-C. (2010). Drug combination studies and their synergy quantification using the chou-talalay method. *Cancer Res.* 70 (2), 440–446. doi:10.1158/0008-5472.CAN-09-1947

Durinck, K., Goossens, S., Peirs, S., Wallaert, A., Van Loocke, W., Matthijssens, F., et al. (2015). Novel biological insights in T-cell acute lymphoblastic leukemia. *Exp. Hematol.* 43 (Issue 8), 625–639. doi:10.1016/j.exphem.2015.05.017

Egler, R. A., Ahuja, S. P., and Matloub, Y. (2016). L-asparaginase in the treatment of patients with acute lymphoblastic leukemia. *J. Pharmacol. Pharmacother.* 7 (Issue 2), 62–71. doi:10.4103/0976-500X.184769

Ekpa, Q. L., Akahara, P. C., Anderson, A. M., Adekoya, O. O., Ajayi, O. O., Alabi, P. O., et al. (2023). A review of acute lymphocytic leukemia (ALL) in the pediatric population: evaluating current trends and changes in guidelines in the past decade. *Cureus* 15, e49930. doi:10.7759/cureus.49930

Feng Li, H., Wang, H., Ye, T., Guo, P., Lin, X., Hu, Y., et al. (2024). Recent advances in material technology for leukemia treatments. *Adv. Mater.* 36 (26), e2313955. doi:10.1002/adma.202313955

Ghelli Luserna di Rora', A., Iacobucci, I., and Martinelli, G. (2017). The cell cycle checkpoint inhibitors in the treatment of leukemias. *J. Hematol. & Oncol.* 10 (1), 77. doi:10.1186/s13045-017-0443-x

Gilad, Y., Gellerman, G., Lonard, D. M., and O'Malley, B. W. (2021). Drug combination in cancer treatment—From cocktails to conjugated combinations. *Cancers* 13 (4), 669. doi:10.3390/cancers13040669

Goto, H., Yanagimachi, M., Goto, S., Takeuchi, M., Kato, H., Yokosuka, T., et al. (2012). Methylated chrysin reduced cell proliferation, but antagonized cytotoxicity of other anticancer drugs in acute lymphoblastic leukemia. *Anticancer Drugs* 23 (4), 417–425. doi:10.1097/CAD.0b013e32834fb731

Hasnat, H., Shompa, S. A., Islam, Md. M., Alam, S., Richi, F. T., Emon, N. U., et al. (2024). Flavonoids: a treasure house of prospective pharmacological potentials. *Heliyon* 10 (6), e27533. doi:10.1016/j.heliyon.2024.e27533

Hawkins, D. S., Park, J. R., Thomson, B. G., Felgenhauer, J. L., Holcenberg, J. S., Panosyan, E. H., et al. (2004). Asparaginase pharmacokinetics after intensive polyethylene glycol-conjugated L-Asparaginase therapy for children with relapsed acute lymphoblastic leukemia. *Clin. Cancer Res.* 10 (16), 5335–5341. doi:10.1158/1078-0432.CCR-04-0222

Hayashi, H., Makimoto, A., and Yuza, Y. (2024). Treatment of pediatric acute lymphoblastic leukemia: a historical perspective. *Cancers* 16 (4), 723. doi:10.3390/cancers16040723

Huseynova, N., Çetinkaya, M., Baran, Z., Khalilov, R., Mammadova, A., and Baran, Y. (2024). Flavonoids as chemosensitizers in leukemias. *Adv. Exp. Med. Biol.* 1479, 205–234. doi:10.1007/5584_2024_828

Ishida, H., Imamura, T., Kobayashi, R., Hashii, Y., Deguchi, T., Miyamura, T., et al. (2024). Differential impact of asparaginase discontinuation on outcomes of children with T-cell acute lymphoblastic leukemia and T-cell lymphoblastic lymphoma. *Cancer Meedicine* 13 (12), e7246. doi:10.1002/cam4.7246

Juluri, K. R., Siu, C., and Cassaday, R. D. (2022). Asparaginase in the treatment of acute lymphoblastic leukemia in adults: current evidence and place in therapy. *Blood Lymphatic Cancer Targets Ther.* 12, 55–79. doi:10.2147/BLCTT.S342052

Kang, S. H., Jeong, S. J., Kim, S. H., Kim, J. H., Jung, J. H., Koh, W., et al. (2012). Icariside II induces apoptosis in U937 acute myeloid leukemia cells: role of inactivation of STAT3-related signaling. *PLoS ONE* 7 (4), e28706. doi:10.1371/journal.pone.0028706

Kilani-Jaziri, S., Frachet, V., Bhouri, W., Ghedira, K., Chekir-Ghedira, L., and Ronot, X. (2012). Flavones inhibit the proliferation of human tumor cancer cell lines by inducing apoptosis. *Drug Chem. Toxicol.* 35 (1), 1–10. doi:10.3109/01480545.2011.564180

Mahbub, A., Le Maitre, C., Haywood-Small, S., Cross, N., and Jordan-Mahy, N. (2015). Polyphenols act synergistically with doxorubicin and etoposide in leukaemia cell lines. *Cell Death Discov.* 1 (1), 15043–12. doi:10.1038/cddiscovery.2015.43

Mahbub, A., Le Maitre, C., Haywood-Small, S., Cross, N., and Jordan-Mahy, N. (2017). Dietary polyphenols influence antimetabolite agents: methotrexate, 6-mercaptopurine and 5-fluorouracil in leukemia cell lines. *Oncotarget* 8 (62), 104877–104893. doi:10.18632/oncotarget.20501

Mahbub, A. A., Le Maitre, C. L., Cross, N. A., and Jordan-Mahy, N. (2022). The effect of apigenin and chemotherapy combination treatments on apoptosis-related genes and proteins in acute leukaemia cell lines. *Sci. Rep.* 12 (1), 8858. doi:10.1038/s41598-022-11441-z

Möricke, A., Zimmermann, M., Valsecchi, M. G., Stanulla, M., Biondi, A., Mann, G., et al. (2016). Dexamethasone vs prednisone in induction treatment of pediatric ALL:

results of the randomized trial AIEOP-BFM ALL 2000. *Blood* 127 (17), 2101–2112. doi:10.1182/blood-2015-09-670729

Naponelli, V., Rocchetti, M. T., and Mangieri, D. (2024). Apigenin: molecular mechanisms and therapeutic potential against cancer spreading. *Int. J. Mol. Sci.* 25 (10), 5569. doi:10.3390/ijms25105569

Nozhat, Z., Heydarzadeh, S., Memariani, Z., and Ahmadi, A. (2021). Chemoprotective and chemosensitizing effects of apigenin on cancer therapy. *Cancer Cell Int.* 21 (1), 574. doi:10.1186/s12935-021-02282-3

Pui, C.-H., Relling, M. V., and Downing, J. R. (2004). Acute lymphoblastic leukemia. *N. Engl. J. Med.* 350 (15), 1535–1548. doi:10.1056/NEJMra023001

Raetz, E. A., and Teachey, D. T. (2016). T-cell acute lymphoblastic leukemia. *Hematology* 2016 (1), 580–588. doi:10.1182/asheducation-2016.1.580

Rooprai, H. K., Christidou, M., Murray, S. A., Davies, D., Selway, R., Gullan, R. W., et al. (2021). Inhibition of invasion by polyphenols from citrus fruit and berries in human malignant glioma cells *in vitro*. *Anticancer Res.* 41 (2), 619–633. doi:10.21873/anticanres.14813

Rujkijyanont, P., and Inaba, H. (2024). Diagnostic and treatment strategies for pediatric acute lymphoblastic leukemia in low- and middle-income countries. *Leukemia* 38 (8), 1649–1662. doi:10.1038/s41375-024-02277-9

Russo, M., Spagnuolo, C., Volpe, S., Mupo, A., Tedesco, I., and Russo, G. L. (2010). Quercetin induced apoptosis in association with death receptors and fludarabine in cells isolated from chronic lymphocytic leukaemia patients. *Br. J. Cancer* 103 (5), 642–648. doi:10.1038/sj.bjc.6605794

Shafat, M. S., Gnaneswaran, B., Bowles, K. M., and Rushworth, S. A. (2017). The bone marrow microenvironment – home of the leukemic blasts. *Blood Rev.* 31 (Issue 5), 277–286. doi:10.1016/j.blre.2017.03.004

Shi, M.-D., Shiao, C.-K., Lee, Y.-C., and Shih, Y.-W. (2015). Apigenin, a dietary flavonoid, inhibits proliferation of human bladder cancer T-24 cells *via* blocking cell cycle progression and inducing apoptosis. *Cancer Cell Int.* 15 (1), 33. doi:10.1186/s12935-015-0186-0

Shukla, S., and Gupta, S. (2010). "Apigenin and cancer chemoprevention," in *Bioactive foods in promoting health* (Elsevier), 663–689.

Simabuco, F. M., Morale, M. G., Pavan, I. C. B., Morelli, A. P., Silva, F. R., and Tamura, R. E. (2018). p53 and metabolism: from mechanism to therapeutics. *Oncotarget* 9 (Issue 34), 23780–23823. doi:10.18632/oncotarget.25267

Sung, H., Ferlay, J., Siegel, R. L., Laversanne, M., Soerjomataram, I., Jemal, A., et al. (2021). Global cancer statistics 2020: GLOBOCAN estimates of incidence and mortality worldwide for 36 cancers in 185 countries. *CA Cancer J. Clin.* 71 (03), 209–249. doi:10.3322/caac.21660

Takahashi, H., Inoue, J., Sakaguchi, K., Takagi, M., Mizutani, S., and Inazawa, J. (2017). Autophagy is required for cell survival under L-asparaginase-induced metabolic stress in acute lymphoblastic leukemia cells. *Oncogene* 36 (30), 4267–4276. doi:10.1038/onc.2017.59

Telange, D. R., Patil, A. T., Pethe, A. M., Fegade, H., Anand, S., and Dave, V. S. (2017). Formulation and characterization of an apigenin-phospholipid phytosome (APLC) for improved solubility, *in vivo* bioavailability, and antioxidant potential. *Eur. J. Pharm. Sci.* 108, 36–49. doi:10.1016/j.ejps.2016.12.009

Tong, W. H., and Rizzari, C. (2023). Back to the future: the amazing journey of the therapeutic anti-leukemia enzyme asparaginase Erwinia chrysanthemi. *Haematologica* 108 (Issue 10), 2606–2615. doi:10.3324/haematol.2022.282324

van der Sluis, I. M., Vrooman, L. M., Pieters, R., Baruchel, A., Escherich, G., Goulden, N., et al. (2016). Consensus expert recommendations for identification and management of asparaginase hypersensitivity and silent inactivation. *Haematologica* 101 (3), 279–285. doi:10.3324/haematol.2015.137380

Van Vlierberghe, P., and Ferrando, A. (2012). The molecular basis of T cell acute lymphoblastic leukemia. *J. Clin. Investigation* 122 (Issue 10), 3398–3406. doi:10.1172/JCI61269

Wang, B., and Zhao, X.-H. (2017). Apigenin induces both intrinsic and extrinsic pathways of apoptosis in human colon carcinoma HCT-116 cells. *Oncol. Rep.* 37 (2), 1132–1140. doi:10.3892/or.2016.5303

Wang, W., Heideman, L., Chung, C. S., Pelling, J. C., Koehler, K. J., and Birt, D. F. (2000). Cell-cycle arrest at G2/M and growth inhibition by apigenin in human colon carcinoma cell lines. *Mol. Carcinog.* 28 (2), 102–110. doi:10.1002/1098-2744(200006)28:2<102::AID-MC6>3.0.CO;2-2

Yang, X., Chen, H., Man, J., Zhang, T., Yin, X., He, Q., et al. (2021). Secular trends in the incidence and survival of all leukemia types in the United States from 1975 to 2017. *J. Cancer* 12 (8), 2326–2335. doi:10.7150/jca.52186

Youns, M., Fu, Y.-J., Zu, Y.-G., Kramer, A., Konkimalla, V. B., Radlwimmer, B., et al. (2010). Sensitivity and resistance towards isoliquiritigenin, doxorubicin and methotrexate in T cell acute lymphoblastic leukaemia cell lines by pharmacogenomics. *Naunyn-Schmiedeberg's Archives Pharmacol.* 382 (3), 221–234. doi:10.1007/s00210-010-0541-6

Zughaibi, T. A., Suhail, M., Tarique, M., and Tabrez, S. (2021). Targeting PI3K/Akt/mTOR pathway by different flavonoids: a cancer chemopreventive approach. *Int. J. Mol. Sci.* 22 (22), 12455. doi:10.3390/ijms222212455

frontiers | Frontiers in Oncology

TYPE Original Research
PUBLISHED 12 December 2025
DOI 10.3389/fonc.2025.1634503

OPEN ACCESS

EDITED BY
Milica Pešić,
University of Belgrade, Serbia

REVIEWED BY
Ana Podolski-Renic,
National Institute of Republic of Serbia, Serbia
Marija Mojić,
Univerzitet u Beogradu, Serbia

*CORRESPONDENCE
Wonyoung Choi
wonyoungchoi@ncc.re.kr
Sun-Young Kong
ksy@ncc.re.kr

†These authors share first authorship

RECEIVED 24 May 2025
REVISED 20 November 2025
ACCEPTED 24 November 2025
PUBLISHED 12 December 2025

CITATION
Choi W, Lee GY and Kong S-Y (2025) Activation of the STING pathway potentiates the antitumor efficacy of doxorubicin in soft-tissue sarcoma.
Front. Oncol. 15:1634503.
doi: 10.3389/fonc.2025.1634503

Activation of the STING pathway potentiates the antitumor efficacy of doxorubicin in soft-tissue sarcoma

Wonyoung Choi[1,2*†], Gi Yeon Lee[3†] and Sun-Young Kong[3,4,5*]

[1]Center for Clinical Trials, National Cancer Center, Goyang, Republic of Korea, [2]Division of Cancer Biology, National Cancer Center, Goyang, Republic of Korea, [3]Division of Rare and Refractory Cancer, National Cancer Center, Goyang, Republic of Korea, [4]Department of Cancer Biomedical Science, National Cancer Center Graduate School of Cancer Science and Policy, Goyang, Republic of Korea, [5]Department of Laboratory Medicine, National Cancer Center, Goyang, Republic of Korea

Background: Systemic treatment of soft-tissue sarcoma (STS) relies on cytotoxic chemotherapy, with doxorubicin being the key therapeutic agent. However, immune activation is required for optimal antitumor effects of doxorubicin. This study investigated whether activation of the STING pathway enhances doxorubicin's antitumor effect in STS.

Methods: STS cell lines were treated with doxorubicin to evaluate the activation of STING pathway. Deletion of *Sting1* gene was employed to validate its role in mediating doxorubicin's effects. In a syngeneic mouse model of STS, doxorubicin was administered alone or in combination with a STING agonist ADU-S100. Tumor-infiltrating $CD45^+$ cells were magnetically sorted for RNA sequencing to identify genes and pathways linked to STING activation. The upregulated genes were analyzed for their association with survival in the Cancer Genome Atlas Sarcoma (TCGA-SARC) patient cohort.

Results: Doxorubicin induced cytosolic DNA leakage in STS cell lines, triggering the activation of STING pathway. Deletion of *Sting1* attenuated doxorubicin-induced upregulation of proinflammatory cytokines in cells. In the syngeneic mouse model of STS, doxorubicin suppressed tumor growth, an effect significantly enhanced by coadministration of ADU-S100. RNA sequencing of tumor-infiltrating $CD45^+$ cells revealed upregulation of immune pathways linked with STING signaling. In TCGA-SARC cohort, patients with higher expression of genes upregulated in the cells from STING-activated tumors exhibited improved survival, whereas those with lower expression showed poorer overall survival.

Conclusion: Activation of STING pathway by ADU-S100 enhances the antitumor efficacy of doxorubicin in STS. Combining doxorubicin with STING agonists may be a promising therapeutic strategy worth exploring in future clinical trials.

KEYWORDS

soft-tissue sarcoma, STING pathway, immunostimulation, chemotherapy, doxorubicin

1 Introduction

Soft-tissue sarcoma (STS) is a rare cancer, accounting for only 1% of all malignancies, with an annual incidence of 2.49 per 100,000 person-years in Korea and a global age-standardized incidence rate of 1.16 in every 100,000 people (1, 2). About 11.9% of patient with STS present with distant metastasis at the time of diagnosis (3), and up to 40% eventually develop metastatic disease (4). Despite the heterogeneity of STS, which encompasses over 100 distinct subtypes of mesenchymal tumors, systemic treatments for metastatic diseases are mostly selected without consideration of the subtype (5). Moreover, the scarcity of actionable oncogenic alterations and relatively low tumor mutational burden in STS limits the efficacy of targeted therapies and reduces the clinical benefits of immune checkpoint inhibitors (6, 7). Due to these challenges, cytotoxic chemotherapy remains the cornerstone of systemic treatment, with doxorubicin being the first-line drug-of-choice for STS (8, 9). Doxorubicin intercalates into DNA, interfering with the topoisomerase activity. However, recent findings have highlighted the pivotal role of the immune system in mediating its antitumor effects (10–12). As such, the activation of proinflammatory cascades and stimulation of interferon (IFN) signaling pathways may augment the antitumor activity of doxorubicin.

The stimulator of interferon genes (STING) pathway is a key innate immune mechanism that detects cytosolic DNA and activates downstream signaling, resulting in the production of type I IFN and other immunostimulatory cytokines (13). This pathway is regulated by cyclic GMP-AMP synthase (cGAS), which interacts with cytosolic DNA and generates the cyclic dinucleotide cGAMP. This secondary messenger binds to and activates STING located on the endoplasmic reticulum. Upon activation, STING translocates to the Golgi apparatus, initiating a signaling cascade that activates TANK-binding kinase 1 (TBK1) and subsequently the transcription factor IRF3. This leads to the production of type I IFNs and other proinflammatory cytokines, which are crucial for antiviral defense, cancer immunosurveillance, and immune-mediated inflammation (14). In this context, the STING pathway has emerged as a promising target for antitumor immunotherapy (15).

Clinical responses to doxorubicin remain limited in patients with metastatic STS, with an objective response rate of 14%–18% and a median progression-free survival of 4–6 months (4, 9). Given this significant unmet clinical need, we investigated whether costimulation of the STING pathway could enhance the antitumor effects of doxorubicin in STS. Toward this end, we utilized ADU-S100, a synthetic cyclic dinucleotide that activates the STING pathway and has been tested in clinical trials (16, 17). Our findings provide a proof-of-concept for the therapeutic potential of STING agonists in STS treatment.

2 Materials and methods

2.1 Cell culture

Mouse sarcoma cell lines CCRF S-180 II, and WEHI-164, and human sarcoma cell lines HT-1080 (RRID: CVCL_0317), were obtained from the Korean Cell Line Bank (KCLB, Seoul, Korea), and MES-SA (RRID: CVCL_1400) was obtained from the American Type Culture Collection (ATCC, Manassas, VA, USA). All cell lines were authenticated by short tandem repeat (STR) profiling within the past three years to confirm their identity. The STR profiling was performed by the Genomics Core Facility of National Cancer Center, and results were compared against reference profiles. Prior to experimental use, all cell lines were routinely tested and confirmed to be free of mycoplasma contamination using a PCR-based mycoplasma detection assay.

CCRF S-180 II cells were cultured in DMEM supplemented with 10% fetal bovine serum (FBS). WEHI-164 and HT-1080 cells were cultured in RPMI 1640 medium supplemented with 10% FBS. MES-SA cells were cultured in McCoy's 5A medium. All culture media were supplemented with penicillin (100 U/ml), and streptomycin (100 mg/ml). Cell lines used in this study were all authenticated by DNA fingerprinting and were routinely tested for Mycoplasma.

2.2 Cell viability assay and determination of IC_{50} values

Cell viability following doxorubicin treatment was assessed using the CellTiter-Glo® 2.0 Cell Viability Assay (Promega, Madison, WI, USA) according to the manufacturer's instructions. Briefly, cells were seeded in 96-well plates (2×10^3 cells per well) and allowed to adhere overnight. The next day, cells were treated with serial dilutions of doxorubicin for 48 hours. Following treatment, an equal volume of CellTiter-Glo reagent was added to each well, and luminescence was measured using a microplate reader (Infinite 200 Pro, Tecan, Switzerland). Relative cell viability was normalized to untreated controls. IC_{50} values were calculated by nonlinear regression analysis using a four-parameter logistic model in GraphPad Prism (version 8.3.1). All experiments were performed in six replicates and repeated independently at least three times.

2.3 Immunofluorescent staining

Cells were seeded onto 8-well Lab-Tek II chamber slide (Thermo Fisher Scientific, #154534) and allowed to adhere overnight. Doxorubicin of IC_{50} doses for each cell line or DMSO (vehicle) was applied for 48 hours. After treatment, cells were washed three times with cold PBS and fixed with cold methanol at -20°C for 10 minutes. Blocking was performed with 1% bovine serum albumin (BSA) in PBS for 1 hour. For γ-H2AX staining, cells were incubated with a primary antibody against γ-H2AX (Ser139) (Cell Signaling #2577, 1:800 dilution) at 4°C overnight. After washing twice with PBS, cells were incubated with a goat anti-rabbit Alexa Fluor 594 secondary antibody (Thermo Fisher Scientific, #A-11012, 1:500) for 1 hour at room temperature in the dark. For PicoGreen staining, Quant-iT PicoGreen dsDNA reagent (Thermo Fisher Scientific, 3µl/mL) was applied at 37°C

for 1 hour. Nuclei were counterstained with Hoechst 33342 (1:500 dilution) for 10 minutes at room temperature, and fluorescent images were captured using a confocal microscope. Staining intensities were calculated using ImageJ software.

2.4 Gene expression analysis by RT-qPCR

RNA was isolated from cultured cells using TRIzol (Thermo Fisher Scientific), and complementary DNA was synthesized from 1μg of total RNA with ReverTra Ace® qPCR RT Master Mix (Toyobo, # FSQ-201) following the manufacturer's protocols. Real-time quantitative PCR was performed using LightCycler 96 Real-Time PCR system (Roche) and Power SYBR Green PCR Master Mix (Applied Biosystems). Gene expression levels were calculated using the ΔΔCt (Delta–Delta Ct) method, with GAPDH serving as the endogenous control.

The sequences of the primers used in this study are listed below (Table 1).

2.5 CRISPR-Cas9 knockout

Sting1-deficient cells were generated using the CRISPR/Cas9 system (18). In brief, the sgRNA sequences were cloned into the LentiCRISPR v2 vector containing the *Streptococcus pyogenes* Cas9 nuclease gene. The sgRNA sequences were designed using a web-based tool (https://crispr.mit.edu) (Table 2). Lentivirus was prepared in HEK293FT cells by co-transfection of the LentiCRISPR v2 vector and the viral packaging vectors pLP1, pLP2, and pLP/VSVG. Viral supernatant was collected 48 hours after transfection. Target cells were transduced with polybrene (8 μg/ml) and selected with puromycin for 2–3 days, starting 48 hours after transduction. Knockout effect was confirmed by immunoblot analysis of whole cell protein extracts. The guide RNA sequences used in this study are listed below.

TABLE 1 The sequences of the primers used for RT-qPCR in this study.

Ccl5	Mouse	Forward	GCTGCTTTGCCTACCTCTCC
		Reverse	TCGAGTGACAAACACGACTGC
Cxcl10	Mouse	Forward	CCAAGTGCTGCCGTCATTTTC
		Reverse	GGCTCGCAGGGATGATTTCAA
Ifnb1	Mouse	Forward	CAGCTCCAAGAAAGGACGAAC
		Reverse	GGCAGTGTAACTCTTCTGCAT
Gapdh	Mouse	Forward	AGGTCGGTGTGAACGGATTTG
		Reverse	TGTAGACCATGTAGTTGAGGTCA
CCL5	Human	Forward	TGCCCACATCAAGGAGTATTT
		Reverse	CTTTCGGGTGACAAAGACG
CXCL10	Human	Forward	GGCCATCAAGAATTTACTGAAAGCA
		Reverse	TCTGTGTGGTCCATCCTTGGAA
IFNB1	Human	Forward	GCTTGGATTCCTACAAAGAAGCA
		Reverse	ATAGATGGTCAATGCGGCGTC
GAPDH	Human	Forward	GGAGCGAGATCCCTCCAAAAT
		Reverse	GGCTGTTGTCATACTTCTCATGG

TABLE 2 The sequences of sgRNA used in this study.

sgSting1	Mouse	5' – CGGCAGTTATTTCGAGACTC – 3'
sgNTC	Mouse	5' – GCGAGGTATTCGGCTCCGCG – 3'

2.6 Immunoblot analysis

Cells were lysed with radio-immunoprecipitation buffer (50 mM Tris-Cl, pH 7.5, 150 mM NaCl, 0.1% SDS, 0.5% sodium deoxycholate and 1 mM EDTA) containing protease and phosphatase inhibitors (1 mM NaF, 1 mM Na3OV4, PMSF, 2 mg/ml leupeptin and pepstatin; all purchased from Sigma) for 30 min at 4°C. The protein concentration was quantified with a Pierce BCA protein assay kit (Thermo Scientific). Blots were incubated with primary antibodies at 4°C overnight. The following antibodies were used for immunoblots: anti-STING (Cell Signaling #13647, 1:1,000) and anti-GAPDH (Cell Signaling #2118, 1:1,000).

2.7 Syngeneic graft and drug treatment

All mouse experiments were performed under approval by the Institutional Animal Care and Use Committee (IACUC) of the National Cancer Center. A total of 3×10^6 WEHI-164 cells were subcutaneously inoculated near the thigh of BALB/c mice. Tumor volume ($0.5 \times \text{length} \times \text{width}^2$) was monitored regularly using a caliper. When the tumor volume reached 200mm^3, mice were received weekly intratumoral injections of doxorubicin (MedChemExpress, HY-15142) at a dose of 5mg/kg body weight and/or twice-weekly intratumoral injections of 25μg of ADU-S100 (InvivoGen, tlrl-nacda2r-01).

2.8 Tumor dissection and sorting of CD45$^+$ cells

Grafted tumors were harvested 7 days after drug treatment and dissociated using the Tumor Dissociation Kit (Miltenyi Biotec, #130-096-730). The dissociated tumor tissue was stained with anti-mouse CD45 microbeads (Mitenyi Biotech, #130-052-301). CD45$^+$ cells were positively selected using QuadroMACS separator LS columns (Miltenyi Biotec, #130-091-051, #130-042-401), according to the manufacturer's protocol. The sorted cells were stained with CD45 (BD, #5562848), and 7-AAD (BD, #344563) antibodies and analyzed by flow cytometry to confirm successful selection.

2.9 RNA sequencing

RNA was isolated using TRIzol (Thermo Fisher Scientific), and total RNA integrity number (RIN) was assessed using TapeStation RNA screentape (Agilent, #5067-5576). Only high-quality RNA samples with a RIN greater than 7.0 were used for library preparation. The cDNA libraries were prepared using the Illumina TruSeq Stranded mRNA Sample Prep Kit (Illumina, Inc., San Diego, CA, USA, #RS-122-2101). Indexed libraries were subsequently sequenced on an Illumina NovaSeq platform (Illumina, Inc., San Diego, CA, USA) using paired-end (2×100 bp) sequencing. After quality filtering with Trimmomatic (v0.38), raw sequencing data were aligned to the reference genome (mm10) using HISAT2 (v2.1.0) (19), and the sequence reads were counted with StringTie (v2.1.3) (20). Differential gene expression was statistically determined using DESeq2 (v1.38.3) (21). Gene ontology analysis was performed using clusterProfiler (v4.14.4) (22). All data analysis and visualization of differentially expressed genes was conducted using R (version 4.4.1). The data have been deposited in NCBI's Gene Expression Omnibus and are accessible through GEO Series accession number GSE287710 (https://www.ncbi.nlm.nih.gov/geo/query/acc.cgi?acc=GSE287710).

2.10 Analysis of TCGA data

TCGA-SARC dataset was accessed using the TCGAbiolinks package (v2.34.0) (23). Survival analysis was conducted using the survival R package (v3.8-3), and Kaplan-Meier plots were visualized using the survminer R package (v0.5.0).

2.11 Sample size and replicates

All *in vitro* experiments were performed with at least three biological replicates (independent experiments) and at least three technical replicates per condition, unless otherwise specified.

3 Result

3.1 Doxorubicin treatment induces upregulation of inflammatory cytokines via cytoplasmic DNA leakage

Cytotoxic agents, such as cisplatin and etoposide, induce the production of inflammatory cytokines via a STING-dependent mechanism (24). To investigate whether doxorubicin exerts a similar effect, we assessed its ability to induce type I IFN signature genes in STS cell lines. Mouse (CCRF S-180 II and WEHI-164), and human (HT1080 and MES-SA) STS cell lines were treated with doxorubicin at their respective IC_{50} concentrations (Supplementary Figure 1). Double-stranded DNA breaks (DSBs) were prominently detected via γH2AX staining (Figure 1A). DSBs can lead to cytoplasmic DNA leakage, which subsequently activates the STING pathway (25). Consistent with this, doxorubicin treatment caused a significant increase in cytoplasmic DNA levels in STS cells (Figure 1B), resulting in the upregulation of STING at the protein level and increased expression of type I IFN signature genes, including *Ccl5*, *Cxcl10*, and *Ifnb1* in mouse sarcoma cells, and CCL5, CXCL10, IFNB1 in human sarcoma cells (Figure 1C, and Supplementary Figures 1B, C). Collectively, these findings indicated that doxorubicin induces the activation of STING pathway via DSB-mediated DNA leakage into the cytoplasm, leading to the upregulation of type I IFN signature genes.

3.2 Knockout of *Sting1* abrogates doxorubicin-mediated upregulation of inflammatory cytokines

To confirm whether the doxorubicin-induced expression of type I IFN signature genes is mediated by the activation of STING pathway, we knocked out *Sting1* in two mouse STS cell lines using the CRISPR-Cas9 method (Figure 2A). The proliferation rates of *Sting1*-knockout (*Sting1*-KO) cell lines were comparable to those of non-target controls, and their responses to doxorubicin were also similar *in vitro* (Figure 2B and Supplementary Figure 2). However, while the doxorubicin-induced upregulation of *Ccl5* and *Cxcl10* was observed in both non-target controls and Sting1-KO cells, their relative expression levels remained significantly attenuated in both *Sting1*-KO cell lines (Figure 2C). These findings corroborate the fact that the activation of STING pathway mediates doxorubicin-induced upregulation of type I IFN signaling. Furthermore, because STING deficiency did not affect the antitumor effect of doxorubicin *in vitro* where immune cells are absent, we sought to investigate the role of STING pathway in mediating the antitumor effect of doxorubicin in an immunocompetent *in vivo* model.

3.3 Addition of STING agonist potentiates the antitumor effect of doxorubicin

Type 1 IFN signaling promotes proinflammatory responses, which is critical for mediating the antitumor effect of doxorubicin *in vivo* (11). Therefore, we investigated whether activating the STING pathway would potentiate the antitumor effects of doxorubicin using an *in vivo* syngeneic model, wherein WEHI-164 cells were grafted into BALB/c mice. For inducing the activation of STING pathway, we used ADU-S100, a STING agonist that has been tested in clinical trials. When the grafted tumors reached a size of 200 mm^3, doxorubicin was administered either alone or in combination with ADU-S100 (Figure 3A). Intratumoral injection of doxorubicin alone suppressed the growth of the grafted tumor. However, its

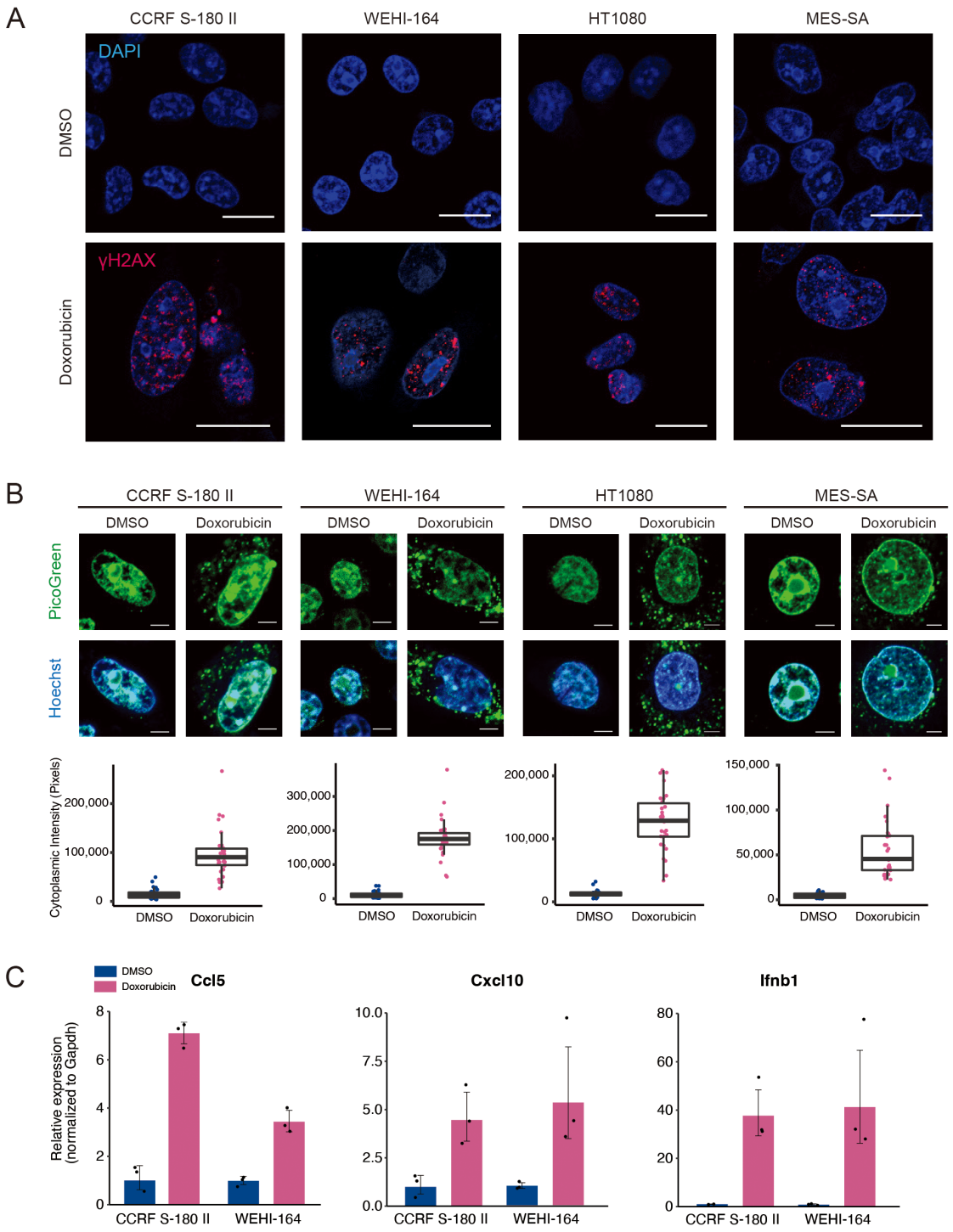

FIGURE 1
Doxorubicin treatment leads to the upregulation of proinflammatory cytokines. **(A)** Immunofluorescence staining of γH2AX after doxorubicin treatment of mouse (CCRF S-180 II and WEHI-164) and human (HT1080 and MES-SA) soft-tissue sarcoma (STS) cell lines. Scale bars, 20 μm. **(B)** PicoGreen staining and quantification after treatment of STS cell lines with doxorubicin. Scale bars, 5 μm. **(C)** RT-qPCR analysis for *Ccl5*, *Cxcl10*, and *Ifnb1* expression in mouse STS cells treated with dimethyl sulfoxide (DMSO) or doxorubicin at their respective IC_{50} doses for 48 hours. All experiments were performed in at least three biological replicates and repeated independently at least three times.

antitumor effect was significantly enhanced by coadministration of ADU-S100 (Figure 3B). To determine whether this enhancement was primarily due to ADU-S100 itself, we repeated the experiment including an additional group treated with ADU-S100 alone. Tumor volumes in the combination group were smaller than those in either monotherapy group, corroborating that STING pathway activation by ADU-S100 enhances the antitumor efficacy of doxorubicin *in vivo* (Supplementary Figure 3).

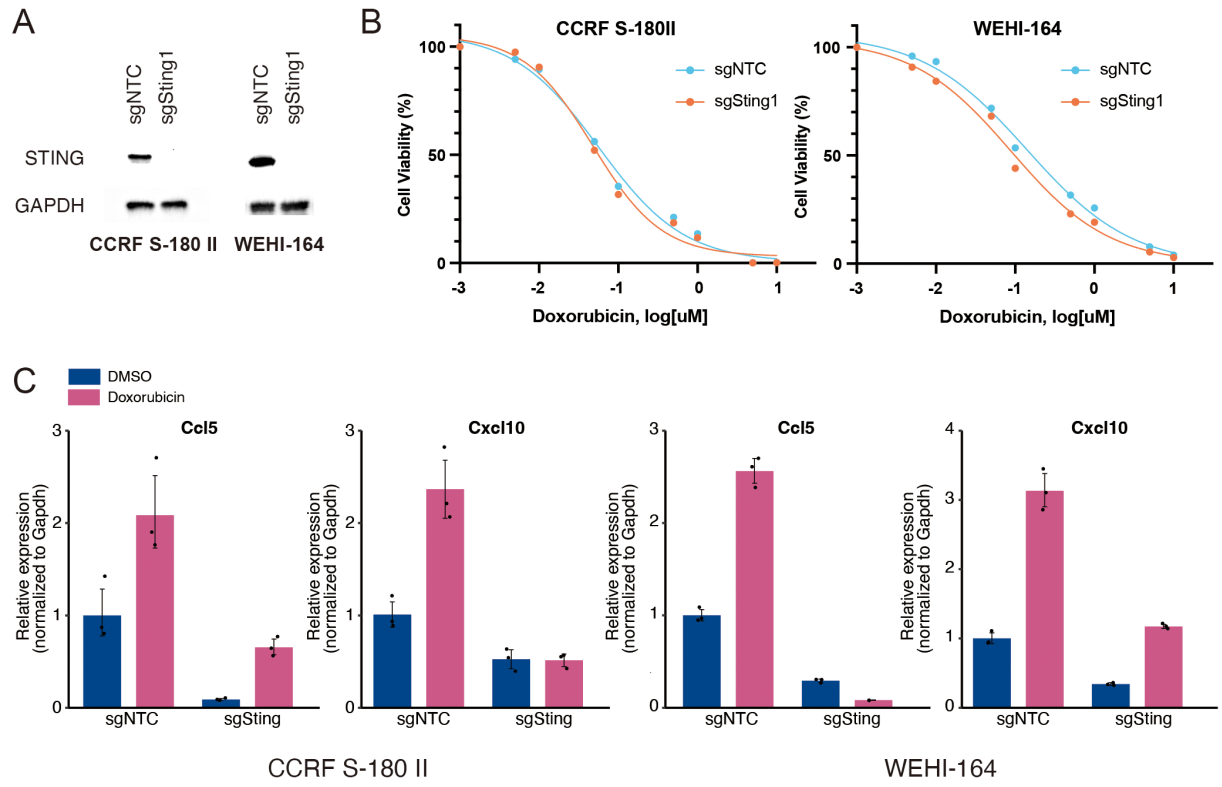

FIGURE 2
Knockout of *Sting1* attenuates doxorubicin-induced upregulation of proinflammatory cytokines. **(A)** Western blotting for STING expression in mouse soft-tissue sarcoma (STS) cells (CCRF S-180 II and WEHI-164) with *Sting1* deletion (sgSting1) and control (sgNTC). **(B)** Dose-response curves for mouse STS cells with sgSting1 and sgNTC treated with doxorubicin. **(C)** RT-qPCR analysis for *Ccl5* and *Cxcl10* expression in mouse STS cells with sgSting1 and sgNTC. All experiments were performed in at least three biological replicates and repeated independently at least three times.

3.4 RNA-sequencing of tumor-infiltrating leukocytes revealed upregulation of innate immune pathway in tumors treated with the STING agonist

Given that activation of the STING pathway induces proinflammatory responses, we sought to identify which type of immune cell signaling within the tumor microenvironment (TME) contributes to the observed antitumor effects. To address this, we harvested tumors treated with the control vehicle, doxorubicin alone, or the doxorubicin and ADU-S100 combination. The tumors were dissociated, and immune cells within the TME were isolated using CD45-linked microbeads and magnetic-activated cell sorting. RNA sequencing was subsequently performed on the $CD45^+$ cell population (Figure 3C). In the analysis of differentially expressed genes (DEGs), doxorubicin treatment alone led to the upregulation of *Cd3*, *Cd8*, and *Pdcd1* in the immune cells within the TME (Figure 3D, right panel). Gene ontology (GO) analysis of the DEGs further supported this finding, showing enrichment of T-cell signaling pathways (Figure 3E, right panel). When comparing the doxorubicin and ADU-S100 combination with either doxorubicin alone or the control vehicle, significant upregulation of genes associated with monocyte/macrophage lineages (*Ly6a*, *Ly6c1*, and *Ly6c2*), and of cytokines or chemokines (*Ccl11*, *Il10*, and *Il6*) that promote immune cell infiltration into the TME was noted (Figure 3D, left and middle panel). GO analysis further confirmed these findings, showing enrichment of innate immune signatures and activation of proinflammatory responses (Figure 3E, left and middle panel).

3.5 Upregulated genes in STING agonist-treated tumors are correlated with improved survival in TCGA-SARC cohort

Comparisons of the upregulated genes in immune cells from tumors treated with doxorubicin and ADU-S100 with those treated with doxorubicin alone or the control vehicle reflected gene signatures consistent with the activation of STING pathway. We subclassified the DEGs that were exclusively upregulated (fold change >2 and raw p-value <0.05) in the doxorubicin plus ADU-S100 group compared with that in the doxorubicin-alone group as "unique gene set (N = 78)." Additionally, genes upregulated in the doxorubicin plus ADU-S100 group compared with that in the control vehicle group, but not overlapping with the upregulated DEGs in the doxorubicin versus control comparison, were combined with the "unique gene set" and collectively termed the "broad gene set (N = 307)" (Figure 4A, and Supplementary

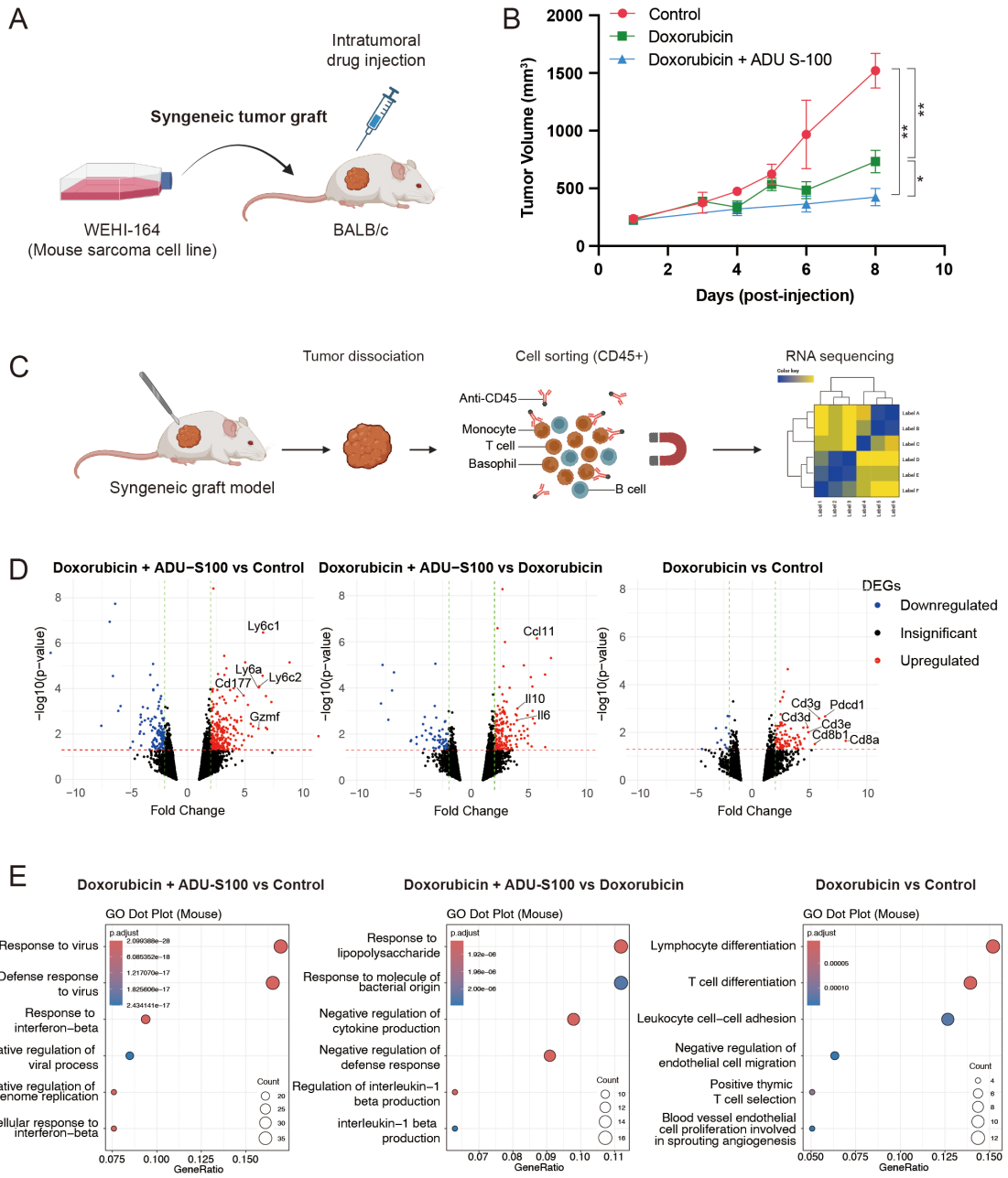

FIGURE 3
STING agonist ADU-S100 enhances the antitumor effect of doxorubicin in a syngeneic graft model of soft-tissue sarcoma (STS). **(A)** Schematic representation of the generation of syngeneic graft model and drug treatment *in vivo*. **(B)** Tumor sizes in grafted BALB/c mice (n = 5 per group) treated with control vehicle, doxorubicin alone, or doxorubicin combined with ADU-S100. *P < 0.05, **P < 0.01. **(C)** Schematic representation of tumor dissociation and immunomagnetic sorting of $CD45^+$ cells for RNA sequencing. **(D)** Volcano plots showing differentially expressed genes (DEGs) in $CD45^+$ cells, comparing (left) doxorubicin + ADU-S100 versus control, (middle) doxorubicin + ADU-S100 versus doxorubicin alone, and (right) doxorubicin versus control. **(E)** Gene ontology analysis of DEGs, comparing (left) doxorubicin + ADU-S100 versus control, (middle) doxorubicin + ADU-S100 versus doxorubicin alone, and (right) doxorubicin versus control. RNA sequencing was performed using biological triplicates for each treatment group.

Tables 1, 2). We sought to explore whether the gene sets reflecting the activation of STING pathway in the TME of our experimental model could predict the clinical outcomes in patients with STS. Using transcriptome data of The Cancer Genome Atlas Sarcoma (TCGA-SARC), we performed single-sample gene set enrichment analysis (ssGSEA) with the "unique gene set," and the "broad gene set." We then compared the overall survival among groups with high (top 25^{th} percentile), moderate (25^{th}–75^{th} percentile), and low (bottom 25^{th} percentile) expression levels. Patients with high expression levels of either the "unique gene set" or the "broad gene set" had significantly longer overall survival compared with those with low expression levels (Figures 4B, C). These findings

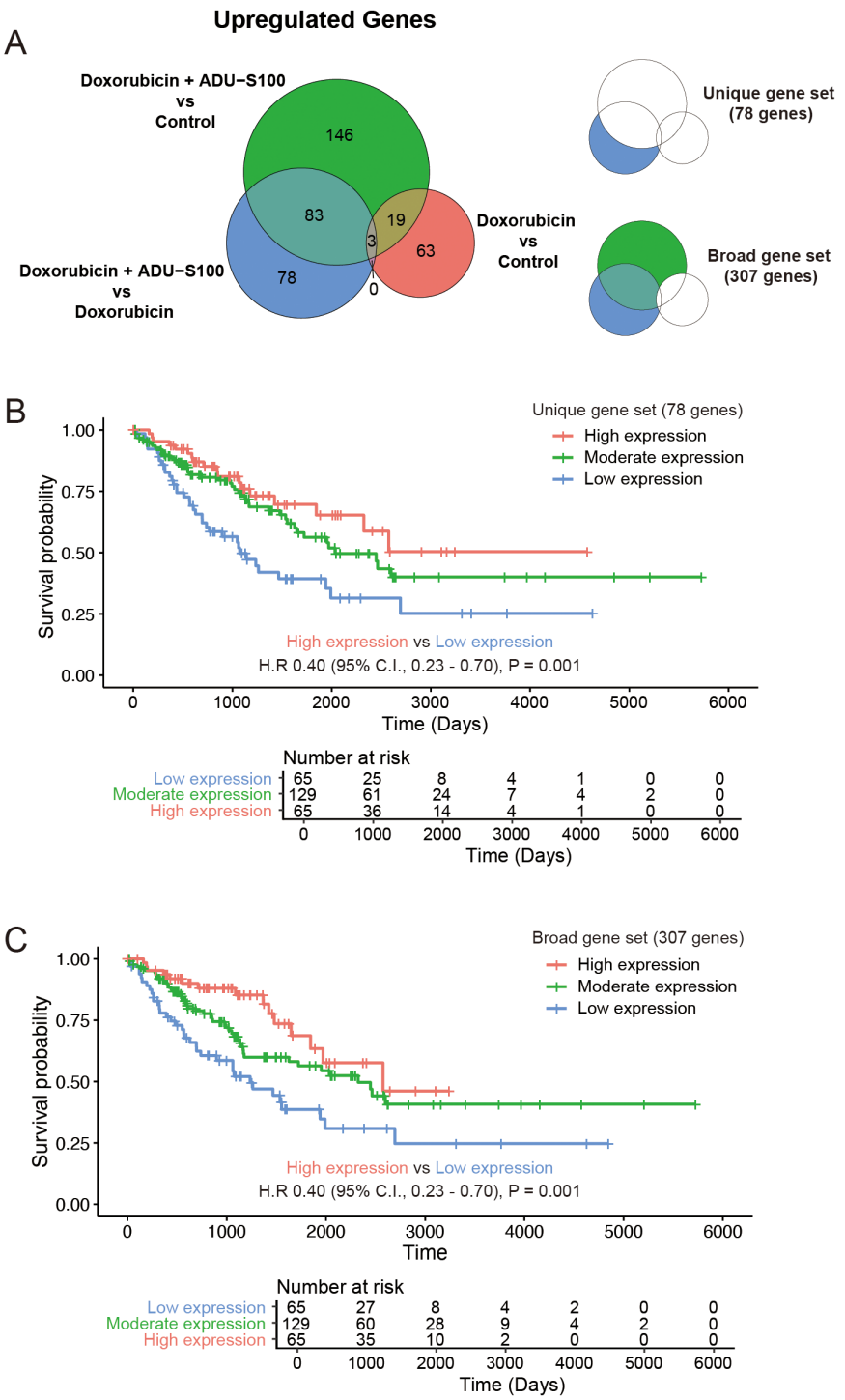

FIGURE 4
Genes upregulated in STING agonist-treated tumors are correlated with improved survival in human soft-tissue sarcoma (STS). **(A)** Venn diagram showing differentially upregulated genes. **(B)** Kaplan–Meier plot of the overall survival in the Cancer Genome Atlas Sarcoma (TCGA-SARC) cohort stratified by the expression status of the "unique gene set." **(C)** Kaplan–Meier plot of the overall survival in TCGA-SARC cohort stratified by the expression status of the "broad gene set.".

indicated that patients with STS exhibiting higher expression of STING activation markers have improved clinical outcome, supporting our experimental model and highlighting the potential of strategies aimed at activating the STING pathway for STS therapy.

4 Discussion

Doxorubicin is a chemotherapeutic agent widely used for the treatment of various malignancies; however, the precise mechanisms for the antitumor effect of doxorubicin remain

incompletely understood (26). Although the ability of doxorubicin to induce DNA damage is the most well-characterized and critical mode of its action, recent studies have highlighted its role in modulating the TME and triggering T-cell responses (27, 28). Furthermore, evidence suggests that antitumor immunity is essential for the therapeutic efficacy of doxorubicin. Mattarollo et al. demonstrated that $CD8^+$ T cells and IFN-γ production are necessary for the therapeutic effects of doxorubicin (10). Additionally, Sistigu et al. demonstrated that a type I IFN signature is essential for the therapeutic efficacy of doxorubicin and that this signature could also predict clinical responses to anthracycline-based chemotherapy in various cohorts of patients with breast cancer (11).

STS is generally considered immunologically "cold," and clinical trials of immune checkpoint inhibitors have yielded unsatisfactory outcomes (29). Combinations of doxorubicin with the anti-PD1 antibody pembrolizumab have also been evaluated in clinical trials but have not demonstrated significant improvements in the overall survival (30, 31). The limited efficacy of doxorubicin and anti-PD1 blockade may be attributed to the absence of robust antitumor immune responses within the TME. As this represents a significant challenge for many solid tumors, strategies aimed at converting "cold" tumors into "hot" tumors have come under extensive research focus (32). Given these unmet clinical needs, our model of combining a STING agonist with doxorubicin offers a novel therapeutic approach for STS.

Using our experimental model, we demonstrated that the doxorubicin-induced upregulation of proinflammatory cytokines is mediated via activation of the STING pathway, which is triggered by cytoplasmic DNA leakage resulting from DSBs. Furthermore, using a syngeneic graft model of STS, we showed that enhancing this pathway by combining the STING agonist ADU-S100 with doxorubicin could potentiate the antitumor activity via the upregulation of innate immune response signaling.

ADU-S100, a synthetic cyclic dinucleotide that activates the STING pathway, has been evaluated in clinical trials. During the course of our research, results from two phase 1 trials were published: one investigating ADU-S100 as a monotherapy in a dose-escalation study and the other examining the efficacy of its combination with spartalizumab, an anti-PD1 antibody (16, 17). Both studies demonstrated that ADU-S100 was well tolerated, but the clinical efficacy was limited both as a monotherapy and when used in combination with anti-PD1 therapy. However, novel STING agonists are under active investigation in numerous ongoing clinical trials (33). Additionally, in contrast to cyclic dinucleotides, which are primarily administered via an intratumoral injection, small molecules that directly bind to STING and enable systemic administration have been characterized (34, 35). Innovative approaches, such as antibody-drug conjugates of STING agonists and targeted protein upregulation of STING, have been also reported and are expected to be evaluated in clinical studies (36, 37).

Our study had several limitations. First, our model relied on a single syngeneic graft model using a murine STS cell line. However, in our in silico analysis of TCGA-SARC cohort with the genes upregulated in STING agonist-treated tumors, patients with higher expression of genes upregulated in STING agonist-treated tumors showed improved overall survival. This finding supports the notion that enhancing STING signaling could potentially lead to improved clinical outcomes in human STS. Second, while we utilized intratumoral injection to ensure localized delivery of doxorubicin to the tumor microenvironment and minimize systemic exposure, this route is not routinely used in clinical practice. We did not evaluate alternative routes such as intravenous or intraperitoneal administration, which would be essential for future translational studies assessing the clinical feasibility of this therapeutic strategy. Third, we did not include a monotherapy group receiving ADU-S100 alone. The absence of this group precludes definitive conclusions regarding the additive or synergistic nature of the combination treatment. While our study focused on evaluating the combinatorial effects, we acknowledge that without the ADU-S100-only group, the individual contribution of STING activation remains uncertain. These issues should be addressed in future studies to refine the therapeutic relevance of this approach. Fourth, the STING agonist ADU-S100, used in our experiments, has shown limited efficacy in clinical trials, raising questions about the feasibility of combining this class of drugs for human patients with STS. Nonetheless, given recent advancements in strategies to enhance STING activity, our study provides proof-of-concept data to justify exploring this combination in future clinical trials.

In conclusion, we demonstrate that the activation of STING pathway enhances the antitumor efficacy of doxorubicin in STS. Given the limited advancements in systemic treatment of STS, including targeted therapies and immune checkpoint inhibitors, incorporating the activation STING pathway into standard chemotherapy regimens may offer a promising strategy to improve clinical outcomes for this challenging disease.

Data availability statement

The datasets presented in this study can be found in online repositories. The names of the repository/repositories and accession number(s) can be found below: https://www.ncbi.nlm.nih.gov/geo/query/acc.cgi?acc=GSE287710, GSE287710.

Ethics statement

Ethical approval was not required for the study involving humans in accordance with the local legislation and institutional requirements. Written informed consent to participate in this study was not required from the participants or the participants' legal guardians/next of kin in accordance with the national legislation and the institutional requirements. The animal study was approved by IACUC of the National Cancer Center. The study was conducted in accordance with the local legislation and institutional requirements.

Author contributions

WC: Writing – original draft, Formal Analysis, Investigation, Visualization, Writing – review & editing, Conceptualization, Funding acquisition. GL: Validation, Investigation, Formal Analysis, Writing – review & editing. S-YK: Writing – review & editing, Supervision, Project administration.

Funding

The author(s) declare that financial support was received for the research and/or publication of this article. This work was supported by a National Research Foundation of Korea (NRF) grant funded by the Korean government (MSIT) (No. 2021R1F1A1062942 to WC) and a National Cancer Center Research Grant (No. NCC-2031560-1 to WC).

Conflict of interest

The authors declare that the research was conducted in the absence of any commercial or financial relationships that could be construed as a potential conflict of interest.

Generative AI statement

The author(s) declare that no Generative AI was used in the creation of this manuscript.

Any alternative text (alt text) provided alongside figures in this article has been generated by Frontiers with the support of artificial intelligence and reasonable efforts have been made to ensure accuracy, including review by the authors wherever possible. If you identify any issues, please contact us.

Publisher's note

Supplementary material

The Supplementary Material for this article can be found online at: https://www.frontiersin.org/articles/10.3389/fonc.2025.1634503/full#supplementary-material.

References

1. Kim HS, Nam CM, Jang SY, Choi SK, Han M, Kim S, et al. Characteristics and treatment patterns of patients with advanced soft tissue sarcoma in korea. *Cancer Res Treat*. (2019) 51:1380–91. doi: 10.4143/crt.2018.476

2. Zhou J, Xu S, Long Y, He R, Cai J, Ding N, et al. Global burden of soft tissue sarcomas in 204 countries and territories from 1990 to 2021: data from the global burden of disease study 2021. *BMC Public Health*. (2025) 25:1519. doi: 10.1186/s12889-025-22782-5

3. Liu H, Zhang H, Zhang C, Liao Z, Li T, Yang T, et al. Pan-soft tissue sarcoma analysis of the incidence, survival, and metastasis: A population-based study focusing on distant metastasis and lymph node metastasis. *Front Oncol*. (2022) 12:890040. doi: 10.3389/fonc.2022.890040

4. Savina M, Le Cesne A, Blay JY, Ray-Coquard I, Mir O, Toulmonde M, et al. Patterns of care and outcomes of patients with METAstatic soft tissue SARComa in a real-life setting: the METASARC observational study. *BMC Med*. (2017) 15:78. doi: 10.1186/s12916-017-0831-7

5. Antonescu CR, Board WHOCoTE, World Health O and International Agency for Research on C. *Soft tissue and bone tumours. 5th edition*. Lyon: International Agency for Research on Cancer (2020).

6. Cancer Genome Atlas Research Network, Electronic address edsc and Cancer Genome Atlas Research N. Comprehensive and integrated genomic characterization of adult soft tissue sarcomas. *Cell*. (2017) 171:950–65 e28. doi: 10.1016/j.cell.2017.10.014

7. Gounder MM, Agaram NP, Trabucco SE, Robinson V, Ferraro RA, Millis SZ, et al. Clinical genomic profiling in the management of patients with soft tissue and bone sarcoma. *Nat Commun*. (2022) 13:3406. doi: 10.1038/s41467-022-30496-0

8. Judson I, Verweij J, Gelderblom H, Hartmann JT, Schoffski P, Blay JY, et al. Doxorubicin alone versus intensified doxorubicin plus ifosfamide for first-line treatment of advanced or metastatic soft-tissue sarcoma: a randomised controlled phase 3 trial. *Lancet Oncol*. (2014) 15:415–23. doi: 10.1016/S1470-2045(14)70063-4

9. Tap WD, Wagner AJ, Schoffski P, Martin-Broto J, Krarup-Hansen A, Ganjoo KN, et al. Effect of doxorubicin plus olaratumab vs doxorubicin plus placebo on survival in patients with advanced soft tissue sarcomas: the ANNOUNCE randomized clinical trial. *JAMA*. (2020) 323:1266–76. doi: 10.1001/jama.2020.1707

10. Mattarollo SR, Loi S, Duret H, Ma Y, Zitvogel L, Smyth MJ. Pivotal role of innate and adaptive immunity in anthracycline chemotherapy of established tumors. *Cancer Res*. (2011) 71:4809–20. doi: 10.1158/0008-5472.CAN-11-0753

11. Sistigu A, Yamazaki T, Vacchelli E, Chaba K, Enot DP, Adam J, et al. Cancer cell-autonomous contribution of type I interferon signaling to the efficacy of chemotherapy. *Nat Med*. (2014) 20:1301–9. doi: 10.1038/nm.3708

12. Li J, Jia Z, Wang R, Xiao B, Cai Y, Zhu T, et al. Activated interferon response from DNA damage in multiple myeloma cells contributes to the chemotherapeutic effects of anthracyclines. *Front Oncol*. (2024) 14:1357996. doi: 10.3389/fonc.2024.1357996

13. Ishikawa H, Barber GN. STING is an endoplasmic reticulum adaptor that facilitates innate immune signalling. *Nature*. (2008) 455:674–8. doi: 10.1038/nature07317

14. Kwon J, Bakhoum SF. The cytosolic DNA-sensing cGAS-STING pathway in cancer. *Cancer Discov*. (2020) 10:26–39. doi: 10.1158/2159-8290.CD-19-0761

15. Jiang M, Chen P, Wang L, Li W, Chen B, Liu Y, et al. cGAS-STING, an important pathway in cancer immunotherapy. *J Hematol Oncol*. (2020) 13:81. doi: 10.1186/s13045-020-00916-z

16. Meric-Bernstam F, Sweis RF, Hodi FS, Messersmith WA, Andtbacka RHI, Ingham M, et al. Phase I dose-escalation trial of MIW815 (ADU-S100), an intratumoral STING agonist, in patients with advanced/metastatic solid tumors or lymphomas. *Clin Cancer Res*. (2022) 28:677–88. doi: 10.1158/1078-0432.CCR-21-1963

17. Meric-Bernstam F, Sweis RF, Kasper S, Hamid O, Bhatia S, Dummer R, et al. Combination of the STING agonist MIW815 (ADU-S100) and PD-1 inhibitor spartalizumab in advanced/metastatic solid tumors or lymphomas: an open-label, multicenter, phase ib study. *Clin Cancer Res*. (2023) 29:110–21. doi: 10.1158/1078-0432.CCR-22-2235

18. Sanjana NE, Shalem O, Zhang F. Improved vectors and genome-wide libraries for CRISPR screening. *Nat Methods*. (2014) 11:783–4. doi: 10.1038/nmeth.3047

19. Kim D, Paggi JM, Park C, Bennett C, Salzberg SL. Graph-based genome alignment and genotyping with HISAT2 and HISAT-genotype. *Nat Biotechnol*. (2019) 37:907–15. doi: 10.1038/s41587-019-0201-4

20. Pertea M, Pertea GM, Antonescu CM, Chang TC, Mendell JT, Salzberg SL. StringTie enables improved reconstruction of a transcriptome from RNA-seq reads. *Nat Biotechnol*. (2015) 33:290–5. doi: 10.1038/nbt.3122

21. Love MI, Huber W, Anders S. Moderated estimation of fold change and dispersion for RNA-seq data with DESeq2. *Genome Biol*. (2014) 15:550. doi: 10.1186/s13059-014-0550-8

22. Yu G, Wang LG, Han Y, He QY. clusterProfiler: an R package for comparing biological themes among gene clusters. *OMICS*. (2012) 16:284–7. doi: 10.1089/omi.2011.0118

23. Colaprico A, Silva TC, Olsen C, Garofano L, Cava C, Garolini D, et al. TCGAbiolinks: an R/Bioconductor package for integrative analysis of TCGA data. *Nucleic Acids Res*. (2016) 44:e71. doi: 10.1093/nar/gkv1507

24. Ahn J, Xia T, Konno H, Konno K, Ruiz P, Barber GN. Inflammation-driven carcinogenesis is mediated through STING. *Nat Commun*. (2014) 5:5166. doi: 10.1038/ncomms6166

25. Miller KN, Victorelli SG, Salmonowicz H, Dasgupta N, Liu T, Passos JF, et al. Cytoplasmic DNA: sources, sensing, and role in aging and disease. *Cell*. (2021) 184:5506–26. doi: 10.1016/j.cell.2021.09.034

26. Kciuk M, Gielecinska A, Mujwar S, Kolat D, Kaluzinska-Kolat Z, Celik I, et al. Doxorubicin-an agent with multiple mechanisms of anticancer activity. *Cells*. (2023) 12. doi: 10.3390/cells12040659

27. Park JY, Jang MJ, Chung YH, Kim KY, Kim SS, Lee WB, et al. Doxorubicin enhances CD4(+) T-cell immune responses by inducing expression of CD40 ligand and 4-1BB. *Int Immunopharmacol*. (2009) 9:1530–9. doi: 10.1016/j.intimp.2009.09.008

28. Zirakzadeh AA, Kinn J, Krantz D, Rosenblatt R, Winerdal ME, Hu J, et al. Doxorubicin enhances the capacity of B cells to activate T cells in urothelial urinary bladder cancer. *Clin Immunol*. (2017) 176:63–70. doi: 10.1016/j.clim.2016.12.003

29. Saerens M, Brusselaers N, Rottey S, Decruyenaere A, Creytens D, Lapeire L. Immune checkpoint inhibitors in treatment of soft-tissue sarcoma: A systematic review and meta-analysis. *Eur J Cancer*. (2021) 152:165–82. doi: 10.1016/j.ejca.2021.04.034

30. Pollack SM, Redman MW, Baker KK, Wagner MJ, Schroeder BA, Loggers ET, et al. Assessment of doxorubicin and pembrolizumab in patients with advanced anthracycline-naive sarcoma: A phase 1/2 nonrandomized clinical trial. *JAMA Oncol*. (2020) 6:1778–82. doi: 10.1001/jamaoncol.2020.3689

31. Livingston MB, Jagosky MH, Robinson MM, Ahrens WA, Benbow JH, Farhangfar CJ, et al. Phase II study of pembrolizumab in combination with doxorubicin in metastatic and unresectable soft-tissue sarcoma. *Clin Cancer Res*. (2021) 27:6424–31. doi: 10.1158/1078-0432.CCR-21-2001

32. Zabransky DJ, Yarchoan M, Jaffee EM. Strategies for heating up cold tumors to boost immunotherapies. *Annu Rev Cancer Biol*. (2023) 7:149–70. doi: 10.1146/annurev-cancerbio-061421-040258

33. Hines JB, Kacew AJ, Sweis RF. The development of STING agonists and emerging results as a cancer immunotherapy. *Curr Oncol Rep*. (2023) 25:189–99. doi: 10.1007/s11912-023-01361-0

34. Ramanjulu JM, Pesiridis GS, Yang J, Concha N, Singhaus R, Zhang SY, et al. Design of amidobenzimidazole STING receptor agonists with systemic activity. *Nature*. (2018) 564:439–43. doi: 10.1038/s41586-018-0705-y

35. Pan BS, Perera SA, Piesvaux JA, Presland JP, Schroeder GK, Cumming JN, et al. An orally available non-nucleotide STING agonist with antitumor activity. *Science*. (2020) 369:993–9. doi: 10.1126/science.aba6098

36. Cho W, Won S, Choi Y, Yi S, Park JB, Park JG, et al. Targeted protein upregulation of STING for boosting the efficacy of immunotherapy. *Angew Chem Int Ed Engl*. (2023) 62:e202300978. doi: 10.1002/anie.202300978

37. Malli Cetinbas N, Monnell T, Soomer-James J, Shaw P, Lancaster K, Catcott KC, et al. Tumor cell-directed STING agonist antibody-drug conjugates induce type III interferons and anti-tumor innate immune responses. *Nat Commun*. (2024) 15:5842. doi: 10.1038/s41467-024-49932-4

Frontiers in Pharmacology

Explores the interactions between chemicals and living beings

The most cited journal in its field, which advances access to pharmacological discoveries to prevent and treat human disease.

Discover the latest Research Topics

See more →

Frontiers

Avenue du Tribunal-Fédéral 34
1005 Lausanne, Switzerland
frontiersin.org

Contact us

+41 (0)21 510 17 00
frontiersin.org/about/contact